

Muni Raj Maurya · Kishor Kumar Sadasivuni ·
John-John Cabibihan · Shahzada Ahmad ·
Samrana Kazim *Editors*

Shape Memory Composites Based on Polymers and Metals for 4D Printing

Processes, Applications and Challenges

 Springer

Shape Memory Composites Based on Polymers and Metals for 4D Printing

Muni Raj Maurya · Kishor Kumar Sadasivuni ·
John-John Cabibihan · Shahzada Ahmad ·
Samrana Kazim
Editors


Shape Memory Composites Based on Polymers and Metals for 4D Printing


Processes, Applications and Challenges

 Springer

Editors

Muni Raj Maurya
Center for Advanced Materials
Qatar University
Doha, Qatar

Kishor Kumar Sadasivuni 
Center for Advanced Materials
Qatar University
Doha, Qatar

John-John Cabibihan 
Department of Mechanical and Industrial
Engineering
Qatar University
Doha, Qatar

Shahzada Ahmad
UPV/EHU Science Park
Basque Center for Materials, Application
Leioa, Spain

Samrana Kazim
UPV/EHU Science Park
Basque Center for Materials, Application
Leioa, Spain

ISBN 978-3-030-94113-0

ISBN 978-3-030-94114-7 (eBook)

<https://doi.org/10.1007/978-3-030-94114-7>

© The Editor(s) (if applicable) and The Author(s), under exclusive license to Springer Nature Switzerland AG 2022, corrected publication 2022

This work is subject to copyright. All rights are solely and exclusively licensed by the Publisher, whether the whole or part of the material is concerned, specifically the rights of translation, reprinting, reuse of illustrations, recitation, broadcasting, reproduction on microfilms or in any other physical way, and transmission or information storage and retrieval, electronic adaptation, computer software, or by similar or dissimilar methodology now known or hereafter developed.

The use of general descriptive names, registered names, trademarks, service marks, etc. in this publication does not imply, even in the absence of a specific statement, that such names are exempt from the relevant protective laws and regulations and therefore free for general use.

The publisher, the authors and the editors are safe to assume that the advice and information in this book are believed to be true and accurate at the date of publication. Neither the publisher nor the authors or the editors give a warranty, expressed or implied, with respect to the material contained herein or for any errors or omissions that may have been made. The publisher remains neutral with regard to jurisdictional claims in published maps and institutional affiliations.

This Springer imprint is published by the registered company Springer Nature Switzerland AG
The registered company address is: Gewerbestrasse 11, 6330 Cham, Switzerland

Preface

Shape Memory Composites Based on Polymers and Metals for 4D-Printing Processes, Applications, and Challenges covers the physics behind the emerging area of materials science, i.e., engineering of shape-memory composites (SMCs) and 4D printing. The Additive manufacturing technology, also known as 3D printing, is well known. Recently, the advent of innovative and novel 4D printing has added an additional dimension to the existing 3D technique, where the shape of the objects can be altered as a function of time by external stimuli. The backbone of 4D printing requires the use of smart materials, such as shape-memory polymers (SMPs), shape-memory alloys (SMAs), and their composites. Shape-memory materials are active smart materials that have the ability to return from a deformed state to their original shape or vice versa under the external stimulus. The fusion of shape-memory materials with additive manufacturing technology has huge applications in the fields like aerospace, biomedical equipment, morphing structures, deployable structures, biomaterials, smart textiles, 4D printing of active origami structures, and self-healing composite systems. The book covers the elementary knowledge of SMPs/SMAs/composites and additive manufacturing techniques. Different alloy compositions and polymer composites are covered, and their feasibility with 4D printing is discussed in detail. The influence of micro, meso, and nanoscale fillers on the properties of shape-memory materials is presented. The impact of hybrid nanofillers and synergistic composite mixtures which are used extensively or have shown promising outcomes in the field of 4D printing is discussed in the book. These novel SMCs will vary from metal alloys/organic/organic composites for improvement in mechanical properties that are triggered by external sources like a magnetic field, temperature, pH of solvent, humidity, light, and electric current. The various unresolved issues and challenges, regarding the implementation of 4D printing of SMCs and its commercialization scope, are highlighted. This book gives the fundamental knowledge of

shape-memory materials and additive manufacturing techniques and fills the void information on their implementation in 4D-printing technology.

Doha, Qatar

Doha, Qatar

Doha, Qatar

Leioa, Spain

Leioa, Spain

Muni Raj Maurya

Kishor Kumar Sadasivuni

John-John Cabibihan

Shahzada Ahmad

Samrana Kazim

Acknowledgement

This book publication was supported by an NPRP grant from the Qatar National Research Fund under the grant number NPRP12S-0131-190030. The statements made herein are solely the responsibility of the editors.

Contents

1	Advances in 4D Printing of Shape-Memory Materials: Current Status and Developments	1
	Muni Raj Maurya, Kishor Kumar Sadasivuni, Samrana Kazim, J. V. S. K. V. Kalyani, John-John Cabibihan, and Shahzada Ahmad	
2	Characterization Techniques for Shape-Memory Alloys	29
	Praveen K. Jain, Neha Sharma, Rishi Vyas, and Shubhi Jain	
3	Nitinol-Based Shape-Memory Alloys	45
	Mukesh Kumar	
4	Molecular Dynamics Simulations for Nanoscale Insight into the Phase Transformation and Deformation Behavior of Shape-Memory Materials	67
	Natraj Yedla, Sameer Aman Salman, and V. Karthik	
5	Influences of Powder Size (SMAs) Distribution Fe–Mn/625 Alloy Systematic Studies of 4D-Printing Conceivable Applications	81
	S. Shanmugan	
6	Copper-Based Shape-Memory Alloy	93
	Gopal Krushnaji Kulkarni and Girish Sambhaji Gund	
7	Synthesis Techniques of Shape-Memory Polymer Composites	115
	Gautam M. Patel, Vraj Shah, and Miral Vora	
8	Wet Synthesis Methods of Shape-Memory Polymer Composites	155
	Ashok Bhogi and T. Rajani	
9	Recent Progress in Synthesis Methods of Shape-Memory Polymer Nanocomposites	173
	Kalpana Madgula and Venkata Sreenivas Puli	

10	Effect of Nano and Hybrid Fillers on Shape-Memory Polymers Properties	213
	G. V. S. Subbaroy Sarma, Murthy Chavali, Maria P. Nikolova, and Gagan Kant Tripathi	
11	Meso, Micro, and Nano Particulate Filled Shape-Memory Polymers	253
	T. Rajani and Ashok Bhogi	
12	Fiber- and Fabric-Reinforced Shape-Memory Polymers	267
	Murugesan Gowri, Nachimuthu Latha, and Mariappan Rajan	
13	Organic Shape-Memory Polymers and their Foams and Composites in Space	287
	Loredana Santo, Daniele Santoro, and Fabrizio Quadrini	
14	Combination of Shape-Memory Polymers and Metal Alloys	311
	Jyoti Prasad Gogoi, Sunita Barman, Utpal Jyoti Mahanta, Muni Raj Maurya, Sreedevi Paramparambath, Sadiya Waseem, Kishor Kumar Sadasivuni, and John-John Cabibihan	
15	Devices and Sensors Based on Additively Manufactured Shape-Memory of Hybrid Nanocomposites	341
	Vinayak Adimule, Santosh S. Nandi, and B. C. Yallur	
16	Recent Developments on 4D Printings and Applications	361
	Deepalekshmi Ponnamma, M. Sai Bhargava Reddy, Muni Raj Maurya, Omkar Kulkarni, Manikant Paswan, Kishor Kumar Sadasivuni, Mithra M. M. Nair Geetha, and Mariam Ali Al-Maadeed	
17	Modern Approach Towards Additive Manufacturing and 4D Printing: Emerging Industries, Challenges and Future Scope	389
	Pallav Gupta, Anbesh Jamwal, Sumit Gupta, and Vijay Chaudhary	
	Correction to: Characterization Techniques for Shape-Memory Alloys	C1
	Praveen K. Jain, Neha Sharma, Rishi Vyas, and Shubhi Jain	

Contributors

Vinayak Adimule Department of Chemistry, Angadi Institute of Technology and Management (AITM), Belagavi, Karnataka, India

Shahzada Ahmad IKERBASQUE, Basque Foundation for Science, Bilbao, Spain; BCMaterials-Basque Center for Materials, Applications and Nanostructures, Martina Casiano, UPV/EHU Science Park, Barrio Sarriena S/N, Leioa, Spain

Mariam Ali Al-Maadeed Center for Advanced Materials, Qatar University, Doha, Qatar

Sunita Barman Department of Physics, Assam Kaziranga University, Jorhat, India

Ashok Bhogi Department of Humanities and Sciences (Physics), VNR Vignana Jyothi Institute of Engineering and Technology, Hyderabad, Telangana, India

John-John Cabibihan Department of Mechanical and Industrial Engineering, College of Engineering, Qatar University, Doha, Qatar

Vijay Chaudhary Department of Mechanical Engineering, A.S.E.T., Amity University Uttar Pradesh, Noida, India

Murthy Chavali Office of the Dean (Research) & Division of Chemistry, Department of Science, Faculty of Science & Technology, Alliance University, Bengaluru, Karnataka, India

Jyoti Prasad Gogoi Department of Physics, D.K.D. College, Dergaon, Assam, India

Murugesan Gowri Department of Chemistry, V.S.B Engineering College, Tamil Nadu, Karur, India

Girish Sambhaji Gund Department of Physics, M.P.A.S.C. College, Panvel, India

Pallav Gupta Department of Mechanical Engineering, A.S.E.T., Amity University Uttar Pradesh, Noida, India

Sumit Gupta Department of Mechanical Engineering, A.S.E.T., Amity University Uttar Pradesh, Noida, India

Praveen K. Jain Department of Electronics and Communication Engineering, Swami Keshvanand Institute of Technology, Management & Gramothan, Jaipur, India

Shubhi Jain Department of Electronics and Communication Engineering, Swami Keshvanand Institute of Technology, Management & Gramothan, Jaipur, India

Anbesh Jamwal Department of Mechanical Engineering, Alakh Prakash Goyal Shimla University, Shimla, Himachal Pradesh, India

J. V. S. K. V. Kalyani B.V.K. College, Dwarakanagar, Visakhapatnam, India

V. Karthik Department of Metallurgical and Materials Engineering, National Institute of Technology Tiruchirappalli, Tiruchirappalli, Tamil Nadu, India

Samrana Kazim IKERBASQUE, Basque Foundation for Science, Bilbao, Spain; BCMaterials-Basque Center for Materials, Applications and Nanostructures, Martina Casiano, UPV/EHU Science Park, Barrio Sarriena S/N, Leioa, Spain

Gopal Krushnaji Kulkarni Thick and Thin Film Device Laboratory, Department of Physics, Shivaji University, Kolhapur, India

Omkar Kulkarni Department of Mechanical Engineering, National Institute of Technology, Jamshedpur, India

Mukesh Kumar Department of Physics, Faculty of Science, Shree Guru Gobind Singh Tricentenary University Gurgaon, Delhi-NCR, Haryana, India

Nachimuthu Latha Department of Chemistry, Kandaswami Kandari's College, Tamil Nadu, Velur, India

Kalpana Madgula SAS Nanotechnologies LLC, Newark, DE, USA

Utpal Jyoti Mahanta Department of Physics, Sibsagar College, Joysagar, India

Muni Raj Maurya Center for Advanced Materials, Qatar University, Doha, Qatar; Mechanical and Industrial Engineering Department, College of Engineering, Qatar University, Doha, Qatar

Mithra M. M. Nair Geetha Center for Advanced Materials, Qatar University, Doha, Qatar

Santosh S. Nandi Chemistry Section, Department of Engineering Science and Humanities, KLE Dr M. S. Sheshgiri College of Engineering and Technology, Udhyambagh, Belagavi, Karnataka, India

Maria P. Nikolova Department of Material Science and Technology, University of Ruse "A. Kanchev", Ruse, Bulgaria

Sreedevi Paramparambath Center for Advanced Materials, Qatar University, Doha, Qatar

Manikant Paswan Department of Mechanical Engineering, National Institute of Technology, Jamshedpur, India

Gautam M. Patel Department of Industrial Chemistry, Institute of Science and Technology for Advanced Studies and Research (ISTAR), CVM University, V.V. Nagar, Gujarat, India

Deepalekshmi Ponnamma Center for Advanced Materials, Qatar University, Doha, Qatar

Venkata Sreenivas Puli Smart Nanomaterials Solutions LLC, Casselberry, Orlando, FL, USA;
Materials and Manufacturing Directorate, Air Force Research Laboratory, Fairborn, OH, USA

Fabrizio Quadrini Department of Industrial Engineering, University of Rome Tor Vergata, Rome, Italy

Mariappan Rajan Department of Natural Products Chemistry, School of Chemistry, Madurai Kamaraj University, Tamil Nadu, Madurai, India

T. Rajani Department of Humanities and Sciences (Physics), VNR Vignana Jyothi Institute of Engineering and Technology, Hyderabad, Telangana, India

Kishor Kumar Sadasivuni Center for Advanced Materials, Qatar University, Doha, Qatar

M. Sai Bhargava Reddy Center for Nanoscience and Technology, Institute of Science and Technology, Jawaharlal Nehru Technological University, Telangana State, Hyderabad, India

Sameer Aman Salman Department of Metallurgical and Materials Engineering, National Institute of Technology Tiruchirappalli, Tiruchirappalli, Tamil Nadu, India

Loredana Santo Department of Industrial Engineering, University of Rome Tor Vergata, Rome, Italy

Daniele Santoro Department of Industrial Engineering, University of Rome Tor Vergata, Rome, Italy

Vraj Shah Department of Chemistry, School of Sciences, ITM SLS Baroda University, Vadodara, Gujarat, India

S. Shanmugan Research Center for Solar Energy, Department of Physics, Koneru Lakshmaiah Education Foundation, Green Fields, Guntur District, Vaddeswaram, Andhra Pradesh, India

Neha Sharma Department of Physics, Vishwavidyalaya Engineering College, Ambikapur, Surguja, Chhattisgarh, India

G. V. S. Subbaroy Sarma Department of Basic Sciences & Humanities, Vignan's Lara Institute of Technology and Science, Guntur, Andhra Pradesh, India

Gagan Kant Tripathi Office of the Dean (Research) & Division of Chemistry, Department of Science, Faculty of Science & Technology, Alliance University, Bengaluru, Karnataka, India

Miral Vora Industrial Chemistry Department, Faculty of Life, Health and Allied Sciences, ITM Vocational University, Vadodara, Gujarat, India

Rishi Vyas Department of Physics, Swami Keshvanand Institute of Technology, Management & Gramothan, Jaipur, India

Sadiya Waseem Advanced Carbon Products, CSIR-NPL, New Delhi, India

B. C. Yallur Department of Chemistry, M S Ramaiah Institute of Technology, Bangalore, Karnataka, India

Natraj Yedla Department of Metallurgical and Materials Engineering, National Institute of Technology Rourkela, Rourkela, Odisha, India

Abbreviations

3D	Three-dimensional
4D	Four-dimensional
AM	Additive manufacturing
APS	Aminopropyl Triethoxysilane
BA	Butyl Acrylate
BCT	Body-centered tetragonal
BHECA	N-Bis (2-Hydroxyethyl) Cinnamon
CA	Cinnamic corrosive
CAA	Cynnamyliden acid corrosive
CB	Carbon black
CBCM	Controlled behavior of composite material
CC	Cholesteric cellulose
CFR	Carbon fiber-reinforced
CGMD	Coarse grain molecular dynamics
CHEM	Cold hibernated elastic memory
CLIP	Continuous liquid interface production
CMC	Carboxymethyl Cellulose
CNC	Cellulose nanocrystal
CNF	Carbon nanofiber
CNT	Carbon nanotube
CTAB	Cetyltrimethyl ammonium bromide
CTD	Composite technology development
CVD	Chemical vapor deposition
DCM	Dual-component mechanism
DEA	Dielectric elastomer actuator
DEA	Diethanolamine
DFT	Density functional theory
DGEBA	Di-glycidyl ether of bisphenol
DIW	Direct ink writing
DLP	Digital light processing
DMA	Dynamic mechanical analyzer

DMTA	Dynamic mechanical thermal analyzer
DPR	Deployable panel radiator
DSC	Differential scanning calorimeter
DSM	Dual-state mechanism
EAM	Embedded-atom method
ECM	Extracellular mimicked
EMI	Electromagnetic interference
EMM	Epoxy methyl methacrylate
EOC	Ethylene olefin copolymer
ESMA	Electron sample microanalyzer
ER	Electrical resistivity
EU	Experiment Unit
EVA	Ethylene-vinyl acetate
FCC	Face-centered cubic
FDM	Fused deposition method
FEM	Finite-element modeling
FFF	Fused filament fabrication
FGM	Functionally graded material
FRP	Fiber-reinforced polymer
FSMA	Ferromagnetic shape-memory alloy
FWHM	Full width at half maximum
GO	Graphene oxide
HA	Hydroxyapatite
HCP	Hexagonal close-packed
HDI	Hexamethylene diisocyanate
HEA-CA	Ethyleneglycol-1-Acrylate-2-CA
HEMA	Hydroxyethyl methacrylate
HPED	Hydroxy propylethylenediamine
HPGP	Hydrogen peroxide gas plasma
HRTEM	High-resolution electron microscopy
HST	Heat shrinkable tube
ICA	Intracranial aneurysm
IPN	Interpenetrating system
IRT	Interventional radiology technique
ISS	International space station
ITOP	Integrated tissue–organ printer
LDPE	Low-density polyethylene
LRO	Long-range order
LVDT	Linear variable differential transformer
M/NEMS	Micro/nano-electromechanical system
MAI	Macroazoinitiator
MCC	Micro-crystalline cellulose
MD	Molecular dynamics
MEMS	Micro-electromechanical system
MFIS	Magnetic field-induced strain

MJF	Multijet fusion
MMSME	Metamagnetic shape-memory effect
MMT	Montmorillonite
MSMA	Magnetic Shape-memory alloy
MSMS	Multifunctional smart material system
MT	Martensitic transformation
MWCN	Multi-walled carbon nanotube
NaMMT	Sodium montmorillonite
NC	Nanocomposite
NGDE	Neopentyl glycol di glycidyl ether
NIPAM	N-isopropylacrylamide
NMP	N-methyl pyrrolidone
NP	Nanoparticle
NR	Nanorod
NVCL	N-vinylcaprolactam
OBC	Olefin block copolymer
OM	Optical microscope
OSMF	Organic shape-memory foam
OWSMA	One-way shape-memory alloy
OWSME	One-way shape-memory effect
P3BT	Poly-3-Butylthiophene
PAC	Printed active composite
PCL	Poly(ϵ -caprolactone)
PCL-co-PEG	Poly(3-Caprolactone)-Copoly(Ethylene Glycol)
PCLDMA	Polycaprolactone dimethacrylate
PCLM	Methacrylated polycaprolactone
PDA	Polydopamine
PE	Polyethylene
PEBA	Polyether squared amide elastomer
PECU	Poly(ethylene glycol)–poly(ϵ -caprolactone)-based polyurethane
PEEK	Polyether ether ketone
PEG	Poly(ethylene glycol)
PEGDA	Poly(Ethylene Glycol)Diacrylate
PEO	Poly(ethylene oxide)
PET	Poly(Ethylene Terephthalate)
PEU	Polymer (Ester–Urethane)
PFTE	Polytetrafluoroethylene
PHBV	Poly(hydroxybutyrate–Hydroxyvalerate)
PLA	Poly lactic acid
PM	Powder metallurgy
PNC	Polymer nanocomposite
POSS	Polyhedral oligomeric silsesquioxane
PPD	Poly(ω -pentadecalactone)
PTFE	Polytetrafluoroethylene
PTM	Partial-transition mechanism

PU	Polyurethane
PV	Photovoltaic
PVA	Polyvinyl liquor
P μ SL	Projection micro-stereolithography
RF	Radiofrequency
RM	Reaction mixture
ROSHGFs	Randomly oriented short hollow glass fibers
RSP	Rapid solidification processing
SCP	Shape-changing polymer
SEM	Scanning electron micrograph
SHM	Structural health monitoring
SL	Stereolithography
SLM	Selective laser melting
SLP	Sheet lamination process
SLS	Selective laser sintering
SM	Shape-memory
SMC	Shape-memory cycle
SME	Shape-memory effect
SMH	Shape-memory hybrid
SMM	Shape-memory material
SMMA	Shape-memory metallic alloy
SMPC	Shape-memory polymer composite
SMPFED	Shape-memory polymer-based flexible electronic device
SMPLD	Shape-memory polymer light-radiating diode
SMPNC	Shape-memory polymer nanocomposite
SMP	Shape-memory polymer
SMPTFT	Shape-memory polymer dainty film semiconductor
SMPTFT	Shape-memory polymer thin-film transistor
SMPTU	Shape-memory thermoplastic polyurethane
SMPU	Shape-memory polyurethane
SQUID	Superconducting quantum interference device
STD	Substrate distance
TEA	Triethanolamine
TEM	Transmission electron microscopy
TEOS	Tetra ethoxy silane
TGA	Thermogravimetric analysis
TMA	Thermo-mechanical analyzer
TME	Temperature memory effect
TP	Thermoplastic
TPISMPC	Trans-1,4-polyisoprene shape-memory polymer composite
TPU	Thermoplastic polyurethane
TSMP	Three-layered shape-memory polymer
TWSMA	Two-way shape-memory alloy
TWSME	Two-way shape-memory effect
UAV	Unmanned aerial vehicle

UHMWPE	Ultra high molecular weight polyethylene
UPyMA	2-Ureido-4[1H]-Pyrimidinone Motif
UTM	Universal testing machine
VGCF	Vapour growth carbon fiber
WDX	Wavelength dispersive X-ray
XRD	X-ray diffraction

Chapter 1

Advances in 4D Printing of Shape-Memory Materials: Current Status and Developments



**Muni Raj Maurya, Kishor Kumar Sadasivuni, Samrana Kazim,
J. V. S. K. V. Kalyani, John-John Cabibihan, and Shahzada Ahmad**

1.1 Introduction

Additive Manufacturing (AM), typically referred to as rapid prototyping or three-dimensional (3D) printing, was introduced in the late 1980s and since then, it has rapidly emerged as a sustainable, efficient, and intelligent tool. With 3D-printing methods, researchers can fabricate complex designs [1], drug delivery systems [2], remotely actuated robots [3], multi-material designs, and even bio-inspired designs [4, 5]. Moreover, recent developments in novel materials and software tools have synergistically expanded the stage for additive manufacturing. Conventional AM technologies are designed to produce static structures using a single material, which is not capable of fulfilling the demands of dynamic functions needed for applications such as adaptive wind turbines, self-folding packaging, and soft grippers for surgery. This kind of dynamic transformation incorporation in the object fabricated with AM gave the advent to the four dimension printing. This idea of additional dimension

M. R. Maurya · K. K. Sadasivuni (✉)
Center for Advanced Materials, Qatar University, P.O. Box, 2713 Doha, Qatar
e-mail: kishorkumars@qu.edu.qa

M. R. Maurya
Mechanical and Industrial Engineering Department, College of Engineering, Qatar University,
P.O. Box, 2713 Doha, Qatar

S. Kazim · S. Ahmad
IKERBASQUE, Basque Foundation for Science, 48013 Bilbao, Spain

BCMaterials-Basque Center for Materials, Applications and Nanostructures, Martina Casiano,
UPV/EHU Science Park, Barrio Sarriena S/N, 48940 Leioa, Spain

J. V. S. K. V. Kalyani
B.V.K. College, Dwarakanagar, Visakhapatnam 530003, India

J.-J. Cabibihan
Department of Mechanical and Industrial Engineering, College of Engineering, Qatar University,
P.O. Box, 2713 Doha, Qatar

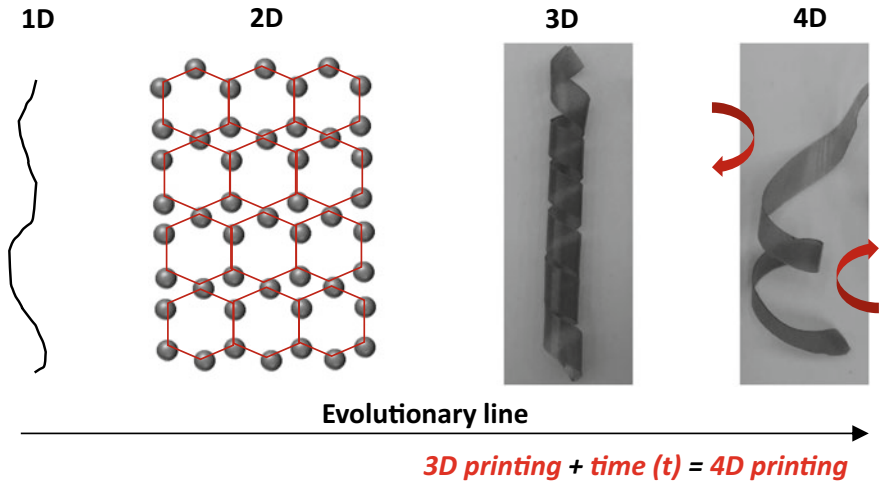


Fig. 1.1 Schematic illustrating the concept of 1D, 2D, 3D, and 4D

introduced a new branch of AM and is known as four-dimensional (4D) printing. The term 4D printing was first introduced by Tibbitts in a 2013 TED talk, where 3D-printed static structures would transform their shape over time. Followed by this, report dealing with 4D-printing was published, demonstrating a printed sheet of active composite getting transformed into complex designs based on the phenomenon of shape-memory effect [6]. Thereafter, 4D printing received the attention of smart material and 3D-printing field research communities [7]. Initially, 4D printing was defined as $4D \text{ printing} = 3D \text{ printing} + \text{time}$ as shown in Fig. 1.1.

The 4D printing needs to be defined properly to have a clear differentiation between 4 and 3D printing. According to Tibbitts et al., 4D printing is a new technique, in which customized material systems or multi-material structures can be printed with the ability to change from one shape to another or can transform over time, directly off the print bed [8]. The transformation over time was described as the fourth dimension, stressing that printed structures are no more dead objects or static; instead, they can transform independently and are active. The 4D printing was suggested as the AM technology where material with varying properties or stimuli-responsive composite material-based physical objects are printed by laying down successive layers appropriately [9]. The printed objects respond to the manually applied stimuli or from the environment, leading to a chemical or physical transformation of the state, over time. Thus, the main difference between the two definitions is that Tibbitts et al. considered the shape changes only, while 4D printing was supposed to induce either a chemical or physical change of state [9]. Later, the concept was evolved, and researchers redefined the definition as 3D-printed objects that show intended targeted property, shape, or functionality transformation with exposure to a predetermined stimulus, such as light [10], water [11], heat [7], and pH [12]. The Gartner hype cycle looks into the evolution of emerging technologies and predicts

their potential for possible practical application in a business ecosystem with a highly competitive advantage over the next few years. Along with other new technologies, such as artificial intelligence, quantum computing, and autonomous mobile robots, 4D printing is in the stage of development triggering and is expected to reach its mainstream in a decade [13].

For effective designing in 4D printing and better results, it is necessary to adopt the following steps:

- Individualization.
- Smart shape-memory lightweight materials.
- Integrated designing.
- Overall product efficiency.

For the successful 4D printing of the objects, these elements are essential and provide technological and economical improvements.

Currently, it is the initial development stage of 4D printing, and within a short time, it has evolved as a vibrant branch of AM and has grabbed the interest of industries and researchers. The extensive ongoing research on the active topic of 4D printing is indicated by the increased number of scientific publications in the past years [14]. Thus, before adopting fully the 4D printing technology, it is important to understand the concept of 3D printing which is one of the essential parts of 4D printing. The section below gives detailed information about the techniques involved in 3D printing.

1.2 3D Printing

Recent advances in 3D-printing techniques have shown a surge for future additive manufacturing, and extensive ongoing research in this area can be gazed at based on the number of publications [14]. There are more than 50 AM technologies that are recognized by the American Society for Testing and Materials (ISO/ASTM 52,900:2015). These common 3D-printing technologies can be classified into seven categories that include direct energy deposition, sheet lamination, binder jetting, material jetting, powder bed fusion, VAT photopolymerization process, and material extrusion. A brief description of their deposition method, materials used, and associated techniques is listed in Table 1.1.

1.2.1 Binder Jetting

The printing of 3D structures by jet deposition of binding agent and powdered material mixture is known as binder jetting. This technology prints materials like ceramics, polymers, and metals. The developers of this technology are 3D Systems (USA), ExOne (USA), and voxeljet (Germany).

Table 1.1 Different additive manufacturing techniques

Process category	Materials	Description	Technologies
Sheet lamination	Paper, Metals	3D object is formed by the bonding of materials layer in form of sheets.	UC, LOM
Material jetting	Waxes, Polymers	3D object is formed by selective deposition of material droplets	MultiJet, PolyJet, MJM, etc.
Binder jetting	Ceramic, metals, Polymers	Powder materials are selectively joined by a liquid bonding agent and are finally cured to achieve the structure.	PBIH, PP, BJ
Vat photopolymerization	Photo-polymers	Ultraviolet light is used to selectively cure (polymerize) the liquid photopolymer in a vat.	DLP, SLA
Material extrusion	Polymer-based materials	Heated nozzle is used to selectively extruded material and get deposited layer by layer	FDM
Direct energy deposition	Metals	Focused thermal energy is used to fuse materials by melting as the material are being deposited.	LDD, DMD, DALM, LMD
Powder bed fusion	Ceramic, Polymers, Metals	Regions of a powder bed are selectively fused by thermal energy.	SHS, DMLS, SLM, SLS, EBM

Note: AM = additive manufacturing; UC = ultrasonic consolidation; LDOM = laminated object manufacturing; MJM = multijet modeling; PP = plaster-based 3D printing; PBIH = powder bed and inkjet head; BJ = binder jetting; SLA = stereolithography; DLP = digital light processing; FDM = fused deposition modeling; LDD = laser direct deposition; DMD = direct metal deposition; DALM = direct additive laser manufacturing; LMD = laser metal deposition; SHS = selective heat sintering; EBM = electron beam melting; DMLS = direct SLS = selective laser sintering; metal laser sintering; and SLM = selective laser melting

1.2.2 Material Jetting

In this, small droplets of filaments are allowed to settle down and be carved by exposing to UV radiation as per the design instruction. The layer resolution by this printing is about 16 μm . For this type of printing, the materials used are wax and photopolymers. The technology was invented by Luxcel (Netherlands), 3D systems (USA), and Stratasys (USA).

1.2.3 Direct Energy Deposition

In this process, direct deposition of the fused material takes place, which is assisted by the focused thermal energy. The suitable materials for this type of feeding mechanism are in the form of wires and powders. The technology was implemented by TRUMPF (Germany), NRC-IMI (Canada), DM3D (USA), and IREPA LASER (France).

1.2.4 Powder Bed Fusion

In this technology, regions of a powder bed are fused based on the time dimension, and the deposition process is assisted by thermal energy. The materials employed for deposition consist of metals, ceramics, and polymers. This technology was developed by the 3D systems (US), Renishaw (UK), ARCAM (Sweden), EOS (Germany), Phoenix Systems (France), and Matsuura Machinery (Japan). The various processes used in the powder bed fusion technology are listed below.

- *Direct metal laser sintering*
This process uses a highly focused laser beam to melt and fuse material in an inert atmosphere to generate desired 3D structures.
- *Electron beam melting*
This technology employs high-intensity electron beam to melt the material power inside the vacuum chamber, and successive cooling of the processed material results in the final shape of the design.
- *Selective heat sintering*
This method incorporates heating of thermoplastic powder inside the thermal print head, followed by layer-by-layer deposition of the processed material.
- *Selective laser melting*
Here, a pool of melted metal powder is created inside an inert gas chamber by using a laser beam. The final product is generated by repeatedly rolling the melt in the form of layers.

- *Selective laser sintering*

In this process, a laser beam is employed to sinter the material powder and then rolled to produce the final shape. The process is similar to the laser melting, except that instead of heating material above the melting point, the material is heated below the melting point to allow particle fusion.

1.2.5 Light Photopolymerization

This process is based on creating objects by selectively curing materials using light. The technique uses materials like photopolymers and was developed by 3D Systems (US), DWS SRL (Italy), EnvisionTEC (Germany), and Lithoz (Australia). The technique employs either digital light processing or stereolithography during the printing of 3D structures.

- Digital light processing

The CAD image of the object is projected layer by layer into the VAT of photopolymer, and with the simultaneous projection of light, the material gets cured to form a desired 3D part.

- Stereolithography

This technique uses a laser source for irradiating UV light in a defined pattern over a liquid photopolymer. With the exposure of light, solidification of resin takes place and desired 3D structure is created.

1.2.6 Extrusion

Material is fed through a heated nozzle whose output is repetitively deposited layer by layer on a printing bed, where material instantly becomes hard to permit next layer deposition. Mainly thermoplastic material and thermosetting polymers are used for the printing process, and technology was implemented by Stratasys (US), 3D Systems (US), and Delta Micro-factory (China).

1.2.7 Sheet Lamination

In this process, sheets of printable material are trimmed and joined layer by layer to create 3D structures. The technique incorporates laminated and ultrasonic additive manufacturing. Materials like metallic sheets, ceramics, and hybrid materials are used in this process. This technology was developed by Fabrisonic (US) and CAM-LEM (US).

- **Laminated object manufacturing**
In this process, the desired geometry of material is cut in the form of sheets by the laser cutter and then bonded layer by layer using plastic, metal, or adhesive paper.
- **Ultrasonic additive manufacturing**
In this process, ultrasonic welding is used for laminating thin metallic sheets to form objects, and excess material is trimmed by an integrated CNC mill.

Among all these methods, material extrusion technologies and VAT photopolymerization process are being mostly utilized. The various material extrusion-based printing methods include fused deposition method (FDM) or fused filament fabrication (FFF) and direct ink writing (DIW). In both these deposition techniques, the 3D structure is printed layer by layer; the major variation is that DIW deposits a viscous ink composed of thermosetting polymers that needs to be cured, whereas in FDM the solid thermoplastic filament is melted in the heated nozzle and doesn't require a further curing step. Using extrusion-based technique, a wide range of materials and composites can be printed into 3D objects, where resolution is governed by the diameter of the nozzle an 100–200 μm [15]. Both FDM and DIW printing methods have limitations in printing multiple materials. The involvement of multiple materials in FDM can result in poor interface bonding due to a mismatch between their printing temperatures, and DIW suffers from the issue of polymer resin compatibility. On the other hand, using inkjet printing, multiple polymer resins can be printed by incorporating multiple nozzles for simultaneous spray, followed by UV curing. As a result, multi-material 3D objects can be fabricated easily with a relatively high resolution. For single-material inkjet printing, the resolution is about 30–40 μm , and for multi-material printing, the typical resolution is 200–400 μm [15]. Another polymer-based 3D-printing method is called VAT photopolymerization. Compared to material extrusion, the VAT photopolymerization process can be operated at higher printing speeds and can achieve better resolutions. The last major group of 3D-printing techniques is multijet fusion (MJF) and selective laser sintering (SLS). SLA and FFF printing techniques are most extensively used followed by DIW, inkjet, and DLP. In the DLP method, the introduction of continuous liquid interface production (CLIP) allows fast printing that can match with production level. Moreover, using optical lens setup, a high resolution of micro and nanoscale can be achieved, and this technique is called Projection Micro-Stereolithography (P μ SL). A schematic illustration of a few conventionally used 3D-printing technologies is shown in Fig. 1.2.

1.3 4D Printing

The advancement in smart material and their incorporation in cost-effective 3D printing have triggered the AM technology to the next level, known as 4D printing. 4D printing is the next-generation version of 3D printing, which has the potential to

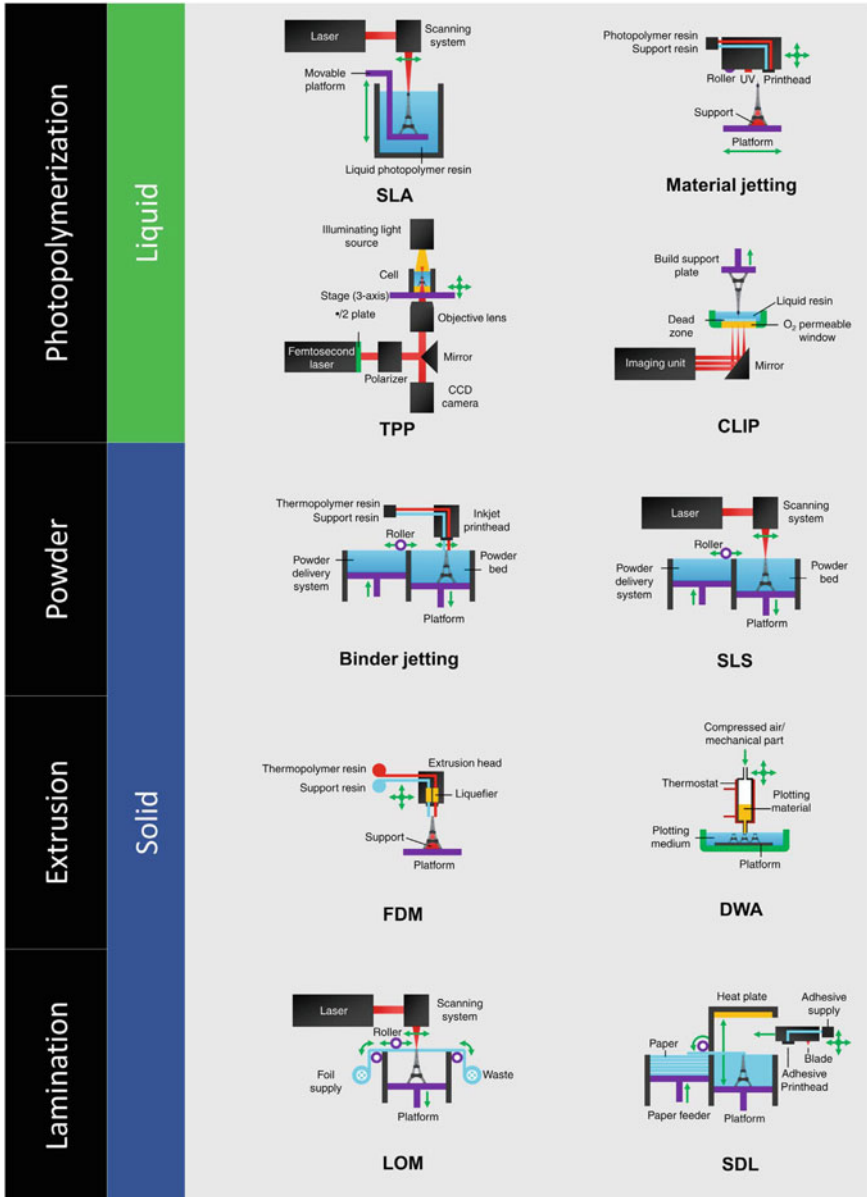


Fig. 1.2 Schematic illustration of conventionally used additive manufacturing techniques. Reproduced from [16], originally published under a CC BY 4.0 license, <https://doi.org/10.1016/j.memsci.2016.10.006>

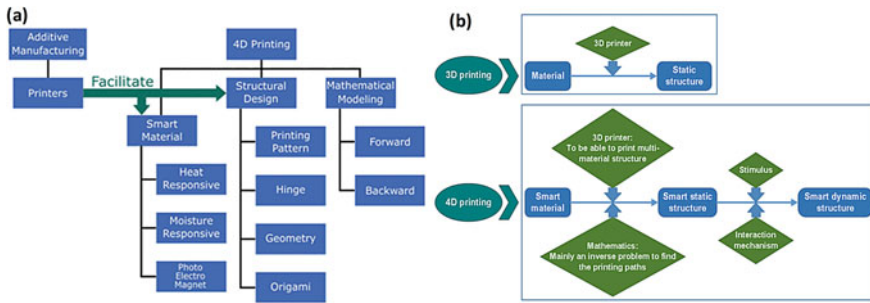


Fig. 1.3 **a** Schematic showing the research features of the 4D printing. Reproduced from [17], originally published under a CC BY 4.0 license. Copyright ©2019 Zhang et al. Published by Informa UK Limited, trading as Taylor & Francis Group. Taylor & Francis. <https://doi.org/10.1080/19475411.2019.1591541>. **b** Schematic for comparison between 4D and 3D printing. Reprinted from [18] Copyright © (2017) with permission from Elsevier Ltd.

realize self-repair, self-assembly, and multifunctionality. 4D printing feeds on technology related to 3D printing, with the extra feature of getting transformed over time under external stimuli [17, 18]. The salient features of the 4D printing are shown in Fig. 1.3a, and the technical difference between the printing process of 4D and 3D printing is illustrated in Fig. 1.3b.

Compared to 3D printing, 4D printing uses smart material with added features like interaction parts, stimulus, and mathematics. These elements facilitate the predictable and targeted progression of 4D-printed objects over time which is listed below:

- *3D-printing resource*: Generally, an appropriate distribution of different materials forming a single composite material is used for 4D-printing objects. The synergistic effect of materials properties, such as thermal expansion coefficient and swelling ratio, results in shifting behavior, transforming to a new desired shape. Therefore, to fabricate the simple and complex geometry of these smart materials, 3D printing is essential.
- *Stimulus-responsive material*: They are the most essential element of 4D printing. The capability of these materials is governed by the properties like self-repair, multifunctionality, self-adaptability, self-sensing, shape memory, responsiveness, and decision.
- *Stimulus*: 4D-printed structures are triggered to transform their shape/functionality/property by applying an external stimulus. Various stimuli like light, heat, different solvent, and even their combination can be used for 4D-printed objects. The stimulus selection depends on the types of smart materials used during 4D printing and desired application.
- *Interaction mechanism*: The interaction mechanism is referred to as a process by which the desired shape of 4D-printed objects is achieved by exposing them to an external stimulus in a defined sequence, over a period. This process is generally required for the materials that don't transform simply by exposing them to external stimulus.

- *Mathematical Modeling*: In 4D printing to achieve the desired functionality or property and change in shape, it is necessary to study the material distribution. Thus, numerical and theoretical models need to be studied to ascertain the relation between elements like material properties, desired final shape, material structure, and stimulus properties.

During the early breakthrough of 4D-printing technology, structures were designed to display one-way transformation, which means that structures need to be programmed (temporary shape setting by human interference) before every single cycle of stimulus. Thus, the need to eliminate the manual interaction to achieve two-way or reversible 4D printing arises. This kind of two-way reversibility can be realized by employing materials that can respond to an external stimulus and attain their parent properties back, by exposing them to another external stimulus. This allows reversibility into 4D-printed parts where the phenomenon is fully dependent on the external stimuli. Further, it eliminates the necessity of reprogramming, which is time-consuming. Moreover, after every recovery, the structure can be reused, which allows its usage over continuous cycles. Conventionally, this type of reversibility is termed “two-way memory” since it allows the two permanent shapes of material. Figure 1.4 illustrates the mechanism of one-way (irreversible) shape memory and two-way (reversible) shape memory with stimuli. Reversibility or repeatability is referred to as the capability of 4D-printed objects to replicate the complete cycle without any significant alteration to the permanent shape or fracture.

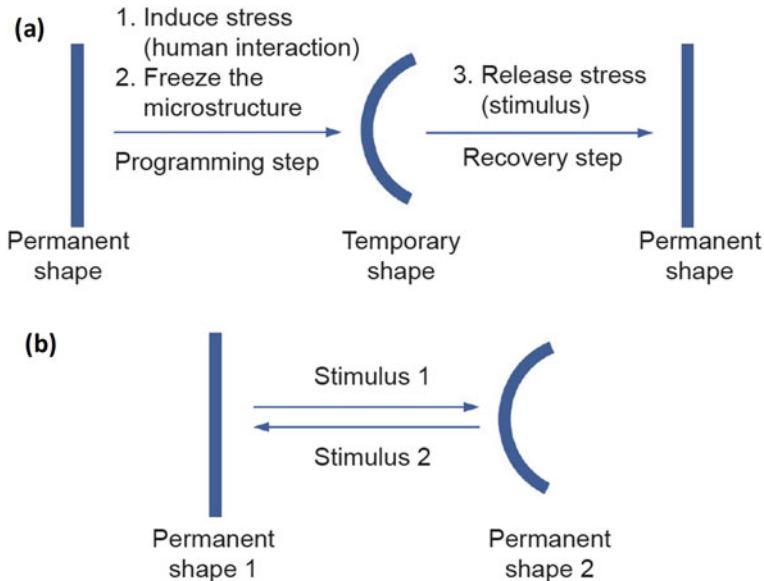


Fig. 1.4 Mechanism of one-way (irreversible) shape memory and two-way (reversible) shape memory with stimuli. Reproduced from [19], originally published under a CC BY 4.0 license, <https://doi.org/10.1016/J.ENG.2017.05.014>

The transformed geometry of the 4D-printed objects can be classified based on the structures and steps involved in the deformation (Fig. 1.5). The single deformation comes in the category of basic shape where a single step or process results in the desired transformation of the object. This includes contraction, topographical change expansion, curving, buckling, helixing, rolling, bending, folding, and twisting. The deformation geometry that involves multiple steps comes in the category of sequential shifting process, where stepwise transformation occurs at specific points of time. Such type of shape-changing behaviors comprises of multiple topographical, multiple helixing, multiple buckling, multiple twisting, multiple rolling, multiple bending, or multiple folding. Further, more complex and complicated geometry changes include curling and waving. Another category is the combined form, whereby printed objects are programmed to have two or more shape-changing behavior within the component.

Materials, those consists of two-way reversible ability are promising candidates for the future development of 4D-printing technology. Under the context, materials with shape-memory effect get the attraction of the researchers. To address such issues, shape-memory alloys (SMAs), shape-memory polymers (SMPs), and their composites are the rational choice for 4D printing to perform desired functions. An understanding of the shape-memory effect and a brief introduction to the concept are provided in the next section.

1.4 Fundamentals of Shape-Memory Effect

Shape-memory materials belong to a particular group of smart materials that can attain their original shape under external stimuli. Shape-memory materials are conventionally subjected to a programming process between different transformation phases which is initiated by the stimuli, and the phenomenon is termed as the shape-memory effect (SME). To achieve 4D printing of shape-memory materials, it is necessary to understand the functioning mechanisms of these materials.

1.4.1 Mechanisms of Shape-Memory Alloys

Shape-memory alloys (SMAs) are one such choice that can be transformed to a new shape upon cooling and while heating attains its original shape.

1.4.1.1 Thermal Shape-Memory Effect

SMA can attain different crystal structures and can exist in different structural phases. SMAs generally exist in three crystal structures (austenite, twinned, and detwinned martensite) having two different phases, which give rise to six possible transformations. As compared to the austenitic phase (stronger phase occurring at a higher

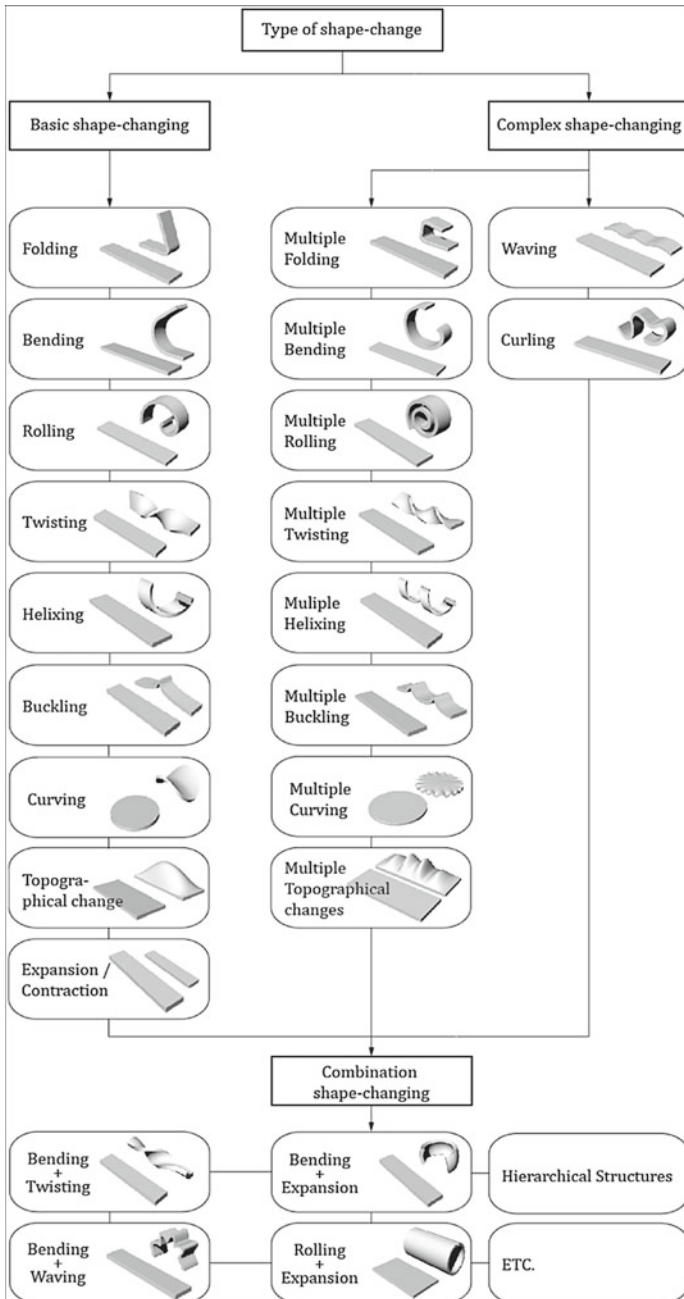


Fig. 1.5 Classification of shape-change geometry and their taxonomy. Reproduced from [20], originally published under a CC BY 4.0 license, Copyright © 2019, Seokwoo Nam et al. <https://doi.org/10.1007/s40964-019-00079-5>

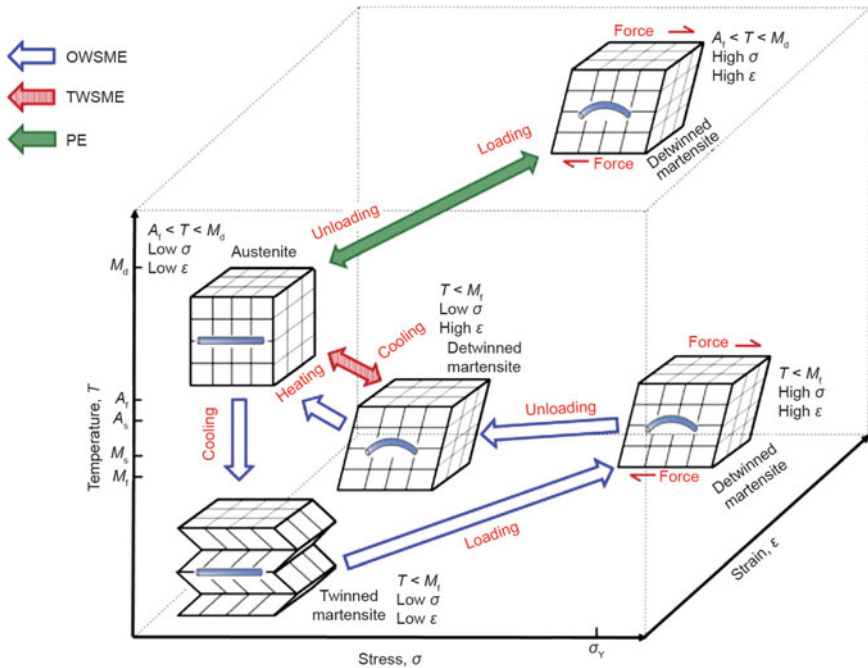


Fig. 1.6 Crystal structures and phases of SMA. Reprinted from [21] Copyright © (2013) with permission from Elsevier Ltd.

temperature), the martensite phase is soft, can be easily deformed, and exists at a lower temperature. Moreover, heating of alloy above its transformation temperature range results in its transformation from martensitic phase to austenite. A remarkable point in austenite phase is metal retains memory and “remembers” pre-deformation shape. There are three categories of SMAs, one-way shape-memory effect, two-way shape-memory effect, and pseudoelasticity as shown in Fig. 1.6.

- *One-way shape-memory effect*

In this process, after removing the external force, the material retains its deformed shape, and upon heating, it comes to its original shape. Above the austenite start temperature (A_s), crystallographic phase reversibility is assisted by the difference in chemical free energy. At higher temperatures, the austenite structure is stable, but at lower temperatures, the martensite structure is more stable. Naturally, SMA exists in the form of a twinned martensite state, and under load, it forms a detwinned martensite structure that remains after unloading. When detwinned martensite material structure is heated above the austenite phase start temperature, it contracts and converts into the austenite phase, resulting in shape recovery. On further heating at a particular temperature (M_d), a stage reaches where martensite cannot be recovered and SMA will be permanently deformed.

- *Two-way shape-memory effect*

In this, the SMA will transform between two phases, which are generally the detwinned martensite phase at low temperatures and the austenite phase at high temperatures. Thus, these alloys can remember shapes at both low/high temperatures, and unlike one-way shape-memory alloy, it does not require any external mechanical stress. This type of functionality is achieved by tailoring one-way shape-memory alloys at the structural level.

- Pseudoelasticity

In the mechanism, when the load is removed between austenite final temperature and M_d , without any heat, the SMA reverts to its original shape completely. This functionality is more like that of elastic solid; hence, it is less important in the context of smart materials.

1.4.2 Mechanisms of Shape-Memory Polymers

Shape-memory polymers (SMPs) contain molecular switches and net points that are either chemical or physical cross-links and behave as switching domains during the thermal transition. Conventional light (photo-responsive), chemical (chemo-responsive), or temperature changes (thermo-responsive) are used as a stimulus.

1.4.2.1 Thermo-Responsive Shape-Memory Polymers

In polymeric materials, the shape-memory effect induced by heat is based on a two-element system in which one element (metric) remains elastic during transformation while the other element (fibers) responds to temperature by a reversible change in the stiffness. To achieve a change in stiffness of polymer, melting glass transition temperature is commonly used. Based on the programming and recovery cycle, the working strategy of thermo-responsive SMPs can be classified into three mechanisms as shown in Fig. 1.7a.

- *Dual-state mechanism (DSM)*

In this, polymers attain a more flexible rubbery stage above the glass transition temperature (T_g) and can be easily deformed. Below T_g , micro-Brownian motion in the polymer is frozen, and as a result, it becomes harder and exists in a glassy state. Thus, by cooling below T_g , the polymer attains a distorted shape and even retained this transformation after removing the applied constraint. On the other hand, micro-Brownian motion can be reactivated by heating above T_g and polymer recovers its shape. Usually, all polymers and their composites show a glass transition phenomenon; therefore, the thermal shape-memory effect is their intrinsic property.

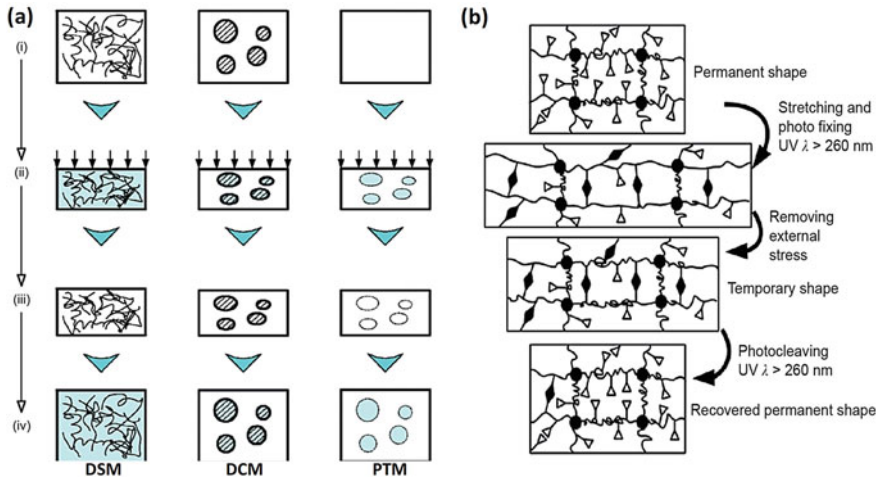


Fig. 1.7 **a** Thermo-responsive SMPs working mechanisms. (i) Original shape at low temperature; (ii) with compressing and heating; (iii) upon constraint removal and cooling; and (iv) Shape recovery upon heating. Reprinted with permission from Springer Nature: Springer Science Business Media B.V.: Journal of Polymer Research [22]. Copyright © 2012. **b** Molecular mechanism of a photo-responsive SMP. Reprinted with permission from Springer Nature: Nature Publishing Group: Nature [23] Copyright © 2005

- *Dual-component mechanism (DCM)*

In this, polymer usually has two or more elastic transition/matrix elements or has soft/hard elements as an inclusion. During programming, the elastic matrix or hard element stores static elastic energy and retains its parent behavior throughout the transformation process. Whereas, upon heating, the stiffness of the soft element changes and is considered as the transition component. At low temperatures, the stiffness of these elements is high and prevents shape recovery. While heating reactivates the stored elastic energy of the transition element and polymer gets soft enough to return to its original shape.

- *Partial-transition mechanism (PTM)*

Unlike DSM or DCM, in this, the polymer is heated within the transition range that lies between the glass transition and melting temperature. During the phenomenon, the softened component serves as a transition element and the un-softened component serves as the elastic element where elastic energy is stored.

1.4.2.2 Chemo-Responsive Shape-Memory Polymers

Here, appropriate chemicals are used to initiate plasticizing behavior in the polymer, which in turn decreases the glass transition temperature of the polymer, and transition can be triggered below T_g . This phenomenon is observed as swelling, softening, and dissolving of the polymer, which depends on the quality of the chemical, ionic strength, and pH value. The chemo-responsive shape-memory effect is widely observed in the hydrogel and gel polymers.

- *Swelling*

The swelling can be exaggerated by allowing alteration in the miscibility and by inducing a change in the degree of cross-linking between solvent molecules and polymeric segments. The swelling amount is inversely proportional to the cross-linking density, which can be tuned by adjusting the pH of the solvent.

- *Softening*

In this, the actuation of the polymer is initiated by gradual softening of the materials, and it attains its original shape. For example, in polyurethane (PU), transformation can be initiated through water or moisture as a stimulus.

- *Dissolving*

This phenomenon is observed in the extreme case of softening, where, due to excess material softening the outer layer, the transition element starts dissolving into the solvent.

1.4.2.3 Photo-Responsive Shape-Memory Polymers

These polymers respond to light, and the corresponding molecular change is reflected in their shape transformation. A cinnamic group-containing polymer was reported by Lendlein et al. with the ability to attain modified transform shape upon exposure to UV light as shown in Fig. 1.7b [23]. The new transformed shape remains stable, and the original shape can be recovered under ambient conditions or by exposing it to lights of different wavelengths.

1.5 Development in Shape-Memory Material-Based 4D Printing

Integration of shape-memory materials in 4D printing has opened the possibility of systems for self-assembly, self-healing, and changes in material properties. SMAs, SMPs, and their composites are widely studied in this regard. The SMAs have a unique characteristic; they can remember their original shape prior to the deformation and return to their original shape after deformation, once they are heated. Only a few

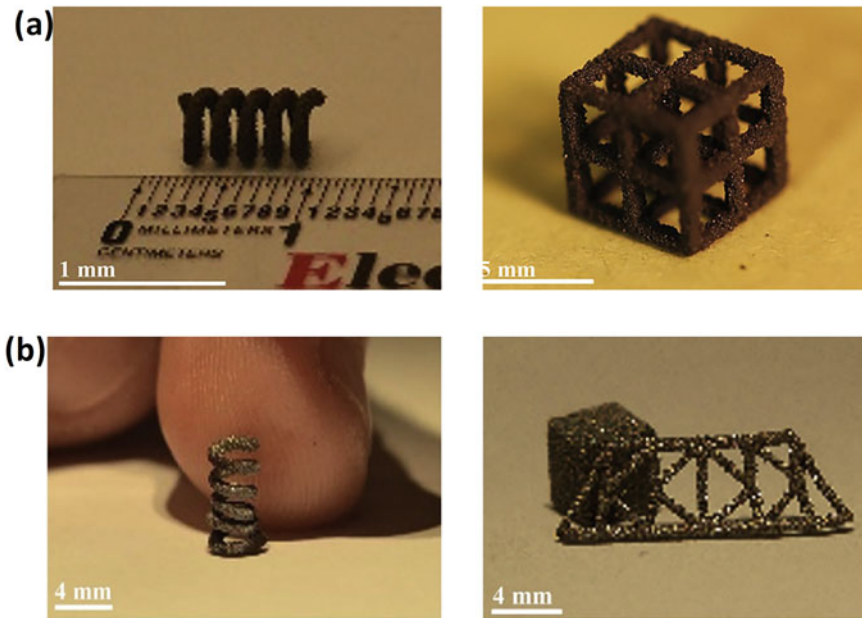


Fig. 1.8 **a** Spark eroded Ni–Mn–Ga 3D-printed parts after curing. **b** Ball-milled Ni–Mn–Ga 3D-printed parts after sintering. Reprinted from [24], Copyright © 2018 with permission from Elsevier B.V.

alloys systems like Au–Cd, In–Ti, Au–Cu, Cu–Al, Cu–Zn, Cu–Al–Be, Fe–Pd, Fe–Pt, Ni–Ti, Ni–Mn–Ga, etc. exhibit shape-memory effect. Recently, Caputo et al. fabricated 4D parts of Ni–Mn–Ga alloy by incorporating predictable changes in 3D printing as a function of time. Ni–Mn–Ga powders-based net-shaped porous structure was produced by binder jetting 3D printing [24]. The fabricated object showed good mechanical strength after curing and sintering. Figure 1.8a, b shows spark eroded Ni–Mn–Ga 3D-printed parts after curing and ball-milled Ni–Mn–Ga 3D-printed parts after sintering.

In particular, SMP materials with the ability to change their shape in response to stimuli have made remarkable progress in the 4D-printing research field. These materials are suitable alternatives for SMAs due to their flexibility, lightweight, biocompatibility, and high-strain capacities. A DLP-printed reversible and free-standing origami geometry was reported by Zhao et al. via swelling and desolvation of film and in acetone (Fig. 1.9a) [25]. Direct 3D printing of liquid crystal elastomer was demonstrated by Yuan et al. that can have high 4D-printing potential [26]. On the other hand, pure SMP exhibits lower modulus and recovery forces, when compared to shape-memory alloys and/or shape-memory ceramics. Due to the high density of cross-linking, most of the polymers suffer from the issue of large stretchability, and this hinders their employment in 4D printing. For efficient high-strength and high-recovery force-related applications, these unreinforced pure

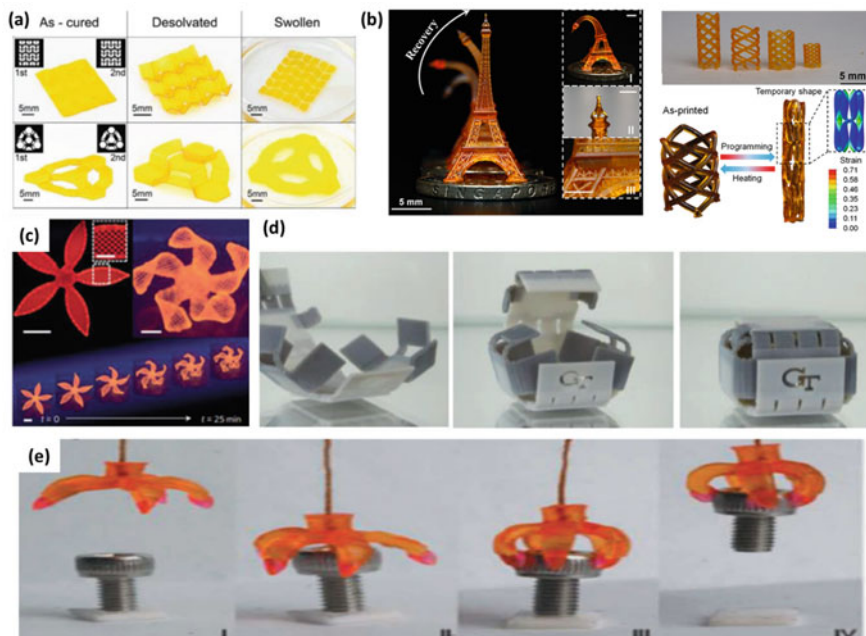


Fig. 1.9 4D-printed structures. **a** The as-cured 3D origami object, the folded desolvated, swollen shape, and flat sheet folded for application as an LED device. Reproduced with permission from [25] Copyright © 2016 WILEY-VCH Verlag GmbH & Co. KGaA, Weinheim. **b** Dimension tunable ability of P μ SL-printed stent. Reproduced from [27], originally published under a CC BY 4.0 license Copyright © 2016 Qi Ge et al., <https://doi.org/10.1038/srep31110>. **c** Biomimetic 4D printing by anisotropic swelling printed by DIW technique. Reprinted with permission from Springer Nature: Nature Publishing Group: Nature Materials [28] Copyright © 2016. **d** 4D-printed box showing the self-locking mechanism. Reproduced from [29], originally published under a CC BY 4.0 license Copyright © 2015 Yiqi Mao et al. <https://doi.org/10.1038/srep13616>. **e** 4D-printed grippers using P μ SL 3D-printing technology. Reproduced from [27], originally published under a CC BY 4.0 license Copyright © 2016 Qi Ge et al., <https://doi.org/10.1038/srep31110>

SMPs are not suitable. To overcome these issues, materials with specific performance are essential to diversify their utilization in various applications. This can be achieved by using the incorporation of various reinforcing fillers within SMPs, where its pristine mechanical properties (high strength and high Young's modulus) can be improved. Under this context, shape-memory polymer composites have emerged as an attractive substitute. The shape-memory polymer composites (SMPCs) have additionally improved high recovery stress and novel functions. In a study by Ge et al., several difunctional acrylate oligomers and benzyl methacrylate were used to improve the stretchability [27]. High-resolution P μ SL was used to print different geometry stents and displayed appreciable recovery (Fig. 1.9b, e). Multi-material printing can assist the complex shape formation and recovery. Figure 1.9c shows a biomimetic 4D-printed programmable bilayer structure reported by Gladman et al. [28]. Viscoelectric composite hydrogel ink was used, and printing was done by the

DIW technique. The anisotropic stiffness in the transverse and longitudinal direction of printed objects enabled the localization of the swelling, resulting in the transformation of structure from 2D to complex 3D structure. A hydrophobic swelling rubber-based 4D printing was reported, where bending deformation was triggered by the Eigenstrain induced in the hinge during hydrogel expansion. A deformed hyperbolic structure was observed when the grid was immersed in the water as stimuli [11]. By altering the spatial distribution materials, the folding angle could be controlled precisely. Thus, multi-material printing gives freedom to have multiple sequential shape transformations and shifting. In a study, Mao et al. controlled the printed object shape-changing sequence and demonstrated sequential folding of the hinges that resulted in the self-locking of the printed box, as shown in Fig. 1.9d [29].

1.6 Challenges in 4D Printing of Shape-Memory Materials

Smart materials should possess desirable properties for employing in the 4D-printing methods. Figure 1.10 shows the properties of the 4D-printing material. 4D printing of shape-memory materials has opened up the possibility of systems for self-assembly, self-healing, and changes in material properties. Currently, 4D-printing technology that is used for printing smart materials has a major challenge with the use of multi-material printing.

The various other challenges for the advancement of next-generation 4D-printing technology are listed below.

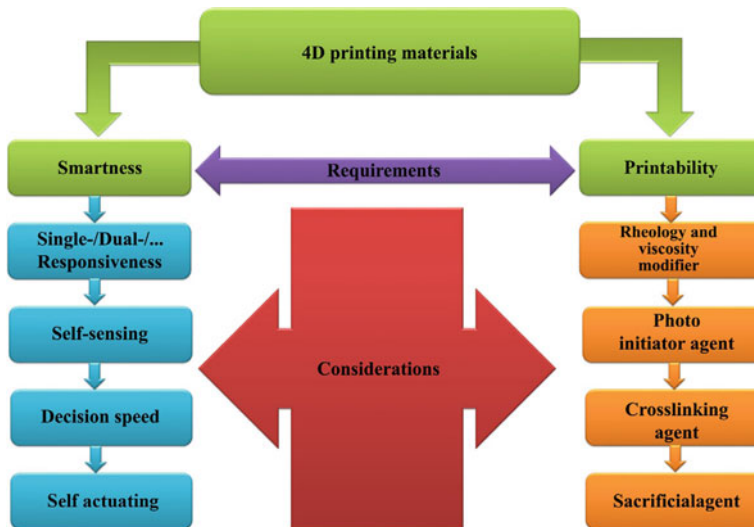


Fig. 1.10 Required properties of the 4D-printing material. Reprinted from [30] Copyright © (2020) with permission from Elsevier Inc.

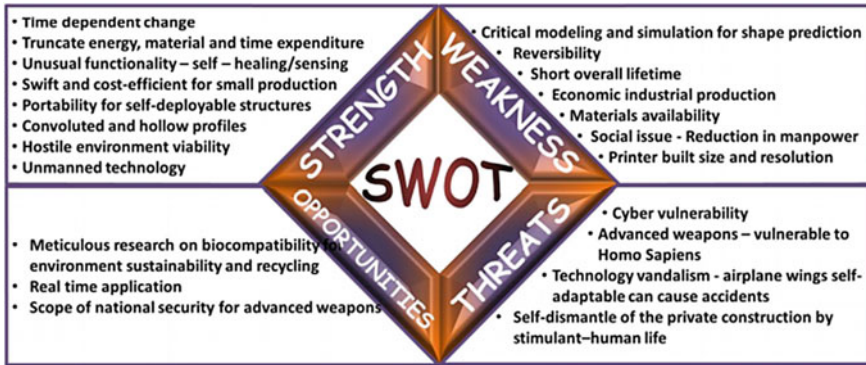


Fig. 1.11 SWOT analysis of 4D printing. Reprinted from [31] Copyright © (2019) with permission from Elsevier B.V.

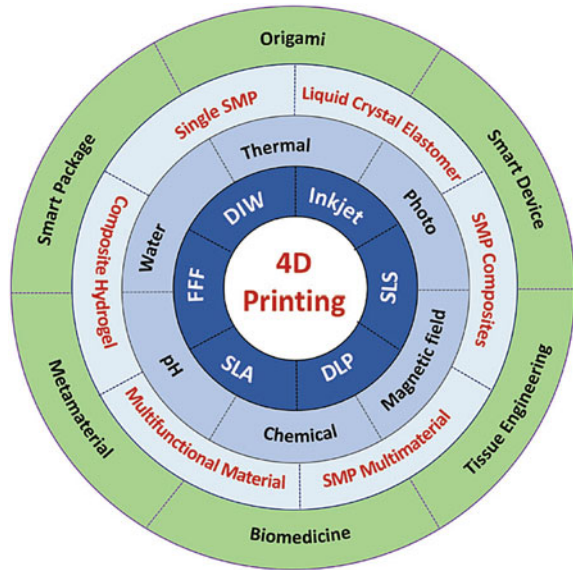
- Integration of 3D printing with other hybrid technologies for 4D printing.
- Develop new advanced properties of materials for 4D printing.
- Improve scale size (e.g., nanoscale) and accuracy of the 4D-printed structure
- Improve resolution and printing speed to reduce cost and energy consumption.

Apart from this, the SWOT analysis of 4D printing is shown in Fig. 1.11.

1.7 Application and Future Prospective

4D printing has opened up the possibility of systems for self-assembly, self-healing, and changes in material properties. Shape-memory materials are active smart materials that can change from a deformed state to their original shape or vice versa under the external stimulus. These materials have attracted researchers due to their wide range of potential applications in various fields like aerospace, biomedical equipment, morphing structures, deployable structures, biomaterials, smart textiles, 4D printing of active origami structures and self-healing composite systems, etc. [32–37]. 4D printing technology will offer benefits to biomedical engineering especially in areas not covered by 3D-printing technologies [38]. Findings have proven to enhance the credibility of technology and it can provide extensive support in the medical field, especially with better smart medical devices of polymer composites, implants, and tools so that medical researchers can explore this with 4D-printing technology to provide improved service to a patient. 4D printing of organic foams provides additional functionalities such as the partial recovery of damages from impacts or volume reduction for long-time storage. For this reason, organic foams have big potential to be used in the aerospace and biomedical field mainly as light actuators, expandable and self-deployable structures, and environmental-sensitive structures. Superelasticity and pseudoplasticity are the most important mechanical properties that exhibit SMAs.

Fig. 1.12 Applications of 4D-printed shape-memory materials. Reproduced with permission from [15]. Copyright © 2018 WILEY-VCH Verlag GmbH & Co. KGaA, Weinheim



The above-mentioned properties make these materials unique for structural applications, automobiles, and actuators in micro-electromechanical systems (MEMSs) [39, 40]. A schematic showing the possible application of 4D-printed shape-memory materials is shown in Fig. 1.12.

The endless application possibility of the 4D-printed shape-memory materials will increase further improvement in the properties listed below:

- Improving structural complexity of printed objects.
- Improve printed programmed cycle capability, and product lifespan.
- Research on self-reacting and self-growing controllable function.
- Improvement in stimulus response.
- Synthesis of novel shape-memory materials with advanced properties.

1.8 Book Chapter's Outlook

The invention of new technology and materials has always been a stringent challenge to scientists and engineers to address its applications in various sectors. 4D printing along with shape-memory materials have opened the possibility of systems for self-assembly, self-healing, and changes in material properties. Integration of these smart materials with 4D printing to perform suitable functions needs systematic analysis of technology and associated material. To understand the material's behavior in a better way and utilize them for specific applications, it is crucial to use characterization techniques for materials testing. Chapter 2 covers the detailed description of conventional techniques that are used in the characterization of shape-memory

alloys and polymers. In this chapter, characterization techniques like Dilatometry to measure the thermal stress, Differential Scanning Calorimetry (DSC) for describing recoverable strain parameters, Electrical Resistivity probe (ER) to study the dependence of various phases on heat treatment, Nano-indentation tool for characterizing the local mechanical properties and to study the pseudoelastic behavior, Dynamic mechanical analyzed (DMA) for mechanical and thermal study, Thermogravimetric Analysis (TGA) to demonstrate the stability of the material, Thermo-Mechanical Analyzer (TMA), etc., are covered in detail.

Metallic alloys consist of shape-memory alloys (SMAs) that demonstrate twin unique properties, i.e., shape-memory effect and pseudoelasticity. With the rise of new technological developments and modern production techniques, demand for new materials with highly functional, specific, and special properties has increased. Thus, to have a more elaborate and clear understanding of the SMA state of the art, key materials in the field of the SMA need to be covered. In this regard, Chap. 3 discusses the processing and performance analysis of Nitinol (Ni–Ti alloys)-based SMA. Other advantages of Nitinol including high power to weight ratio, large deformation, large actuation force, high damping capacity, and high frequency response lead to a faster response in the micron-size actuators. Nitinol has gained significant interest as a micro-electromechanical system (MEMS)-based micro-actuators which are precision control devices that work based on mechanical forces at the microscale level. In the book, Chap. 3, dependency of the transformation and shape-memory behavior of Nitinol on composition, annealing temperature, sputtering pressure, sputtering power, and growth temperature has been explained. Further difficulties arise during the fabrication process of near-equiatom Ni–Ti shape-memory alloy with stable ductility due to the strong tendency of oxidation, and cracking that takes place during co-sputtering has also been explained. The shape-memory effect is due to the microstructural changes occurring at the atomic level. Thus, it is difficult and expensive to monitor through in situ experimental studies. In this scenario, molecular dynamics (MD) simulations provide significant insight into atomic-level details of the structural changes during loading or thermal treatment. Chapter 4 provides a comprehensive review of the usage of MD simulations for a better and deeper understanding of the transformation and deformation behavior of SMAs. The related MD simulations studies like austenite–martensite–austenite transformation, micro-mechanisms of deformation, crack propagation, twinning and de-twinning, shear deformation, superelasticity, pseudoplasticity, nano-indentation, etc., are covered in this chapter. The 4D-printing techniques have been implemented to produce SMAs with complex geometries such as U-shaped parts, layer-structured parts, and lattice-based and hollow structures. Chapter 5 discusses the influence of powder size distribution of Fe–Mn/ Alloy 625 for 4D-printing conceivable applications. In Chap. 6, copper (Cu)-based SMA and their possibilities to be prepared by 4D printing are outlined and emphasized. In addition, viewpoints on current challenges and future research directions for the high performance of 4D-printed Cu-based SMA are also covered. Apart from SMA, shape-memory polymers (SMP)

and their composites are a new class of smart polymer materials gaining wide attention due to their multifunctional applications. The past decade has seen an impressive development in SMPs and shape-memory polymer composites (SMPCs). These materials undergo significant macroscopic deformation upon the application of an external stimulus and provide a cheap, efficient alternative to well-established shape-memory alloys. As a result, it is essential to have a grasp of various synthesis methods of SMPs and SMPCs. Various techniques employing numerous composite materials for synthesis SMPCs have been reported till date. The SMP- and SMPCs-related important literature are covered in the successive book chapters. Chapter 7 discussed the synthesis techniques of SMPCs using different materials such as reinforcement fillers (such as Si-C fiber, Ti-Ni fiber, chopped fiberglass, woven fiberglass, Kevlar fiber, and carbon fiber), carbon nanotubes, polyurethane nanocomposites, and nanoclay. Chapter 8 covers a detailed description of the techniques used in the preparation of shape-memory polymer composites like in situ polymerization, melt mixing, solution mixing, precipitation, sol-gel process, and electrospinning. Apart from the preparation methods, the conventional SMPCs like thermoplastic polymer, thermoset polymer, their composites with cross-linkers and one-step synthesis of phase-segregated block copolymer composites are reviewed. Understanding the relationships between the composition and structure of an SMP and its SM properties as well as its limitations enables one to better define the development areas for high-performance SMPs. Thus, recent progress in synthesis techniques of SMPCs and their proposed applications is presented in Chap. 9. Literature reports that SMPs structure, properties, and functionality can be affected with the addition of various fillers/particulates of different sizes, scaffolds, and fibers. The effect of nano and hybrid fillers on SMPs properties is illustrated in Chap. 10. The addition of different sizes of particulates impacts the phase separation process and material properties of polymer composites. Thus, it is important to have an understanding of the synergetic effect of the particulates doping that enhances various mechanical, optical, magnetic, functional, and shape recovery properties of SMPs. In Chap. 11, emphases are given on the incorporation of particulates such as meso, micro, and nanostructures to polymers, and their behavior is discussed. Further, the fiber and fabric shape materials act as a crucial role in enriching the shape-memory properties. In Chap. 12, we examined the reinforcement of carbon fiber, natural fiber, and conductive fiber in SMPs along with its potential applications. Another class of SMPs is organic shape-memory foams (OSMFs). They have advantages of lightweight, low cost, high shape deformability, high shape recoverability, tailorable switch temperature, and are easy to manufacture. In Chap. 13, literature on OSMFs is reviewed, highlighting synthesis and characterization of different materials, challenges and applications in technical fields, and future expected developments and perspectives. The possibility to manufacture OSMFs by 4D-could open new scenarios for in-space manufacturing and colonization missions. Thus, some conceptual evaluations on 3D- and 4D-printing feasibility are reported. Moreover, a combination of stimuli-responsive metal alloys and polymers significantly change their properties like shape, mechanical properties, optical properties, and electrical properties upon a small variation of environmental conditions. Chap. 14 gives an extensive review of the recent progress of combined

shape-memory polymers and metal alloys composites with design feasibility and fabrication by various methods. The outcome of research, the challenges in this field, and its prospects are highlighted and concluded in this chapter. All these chapters together give a broad and systematic outlook of the SMAs and SPMs, related to their synthesis, characterization, property enhancement, and recent development. These details are very valuable to combine these materials with newly emerging 4D-printing technology. 4D printing of SMAs and SMPs is still in its initial triggering stage. Extensive research is being conducted to explore its application in aerospace, biomedical equipment, morphing structures, smart textiles, self-healing composite systems, etc. To give an overview of the SMP 4D-printing application, one such study is reported in Chap. 15. This study demonstrated the 4D material which can be easily fabricated with different loadings of thiophene-based polymer with localized smart actuation behavior. It encompasses the mechanisms, sensor response, repeatability, and also potential research involved in the development of thiophene polymer in 4D printing and shape-memory polymer thin-film transistors (SMPTFTs). Further Chap. 16 covers the applications of 4D printing in various fields like aerospace, biomedical devices, morphing structures, deployable structures, biomaterials, smart textiles, 4D printing of active origami structures, self-healing composite systems, soft robotics, wearable sensors, transportation, etc. 4D-printing technology is a new branch of research that originated from 3D printing (which involves the printing of complex geometries with smart materials). The development in synthetic smart materials, deformation mechanisms, novel printers, and mathematical modeling has enhanced the research area of 4D printing. In Chap. 17, the progress in additive manufacturing and 4D printing is discussed with the help of bibliometric analysis. Smart materials developed with 4D printing are explained with their morphing mechanisms for Industry 4.0. The chapter also includes a discussion about emerging industries in 4D printing, challenges, and future scope in terms of manufacturing and business perspective.

1.9 Conclusion

The advancement in the smart material and their incorporation in 4D-printing technology have triggered additive manufacturing technology to the next stage, and arguably a valuable technology in the current era. Compared to conventional printing technology, it has transformed the additive manufacturing technology by reducing manual intervention and manufacturing time. 4D-printing technologies are emerging and require a considerable amount of research to convey and deliver up to their actual potential. Additionally, the incorporation of shape-memory materials in 4D printing can be beneficial in numerous ways (reduction in labor, cost, and time).

Acknowledgements This work was supported by an NPRP grant from the Qatar National Research Fund under the grant number NPRP12S-0131-190030. The statements made herein are solely the responsibility of the authors.

References

1. Gu GX, Libonati F, Wettermark SD, Buehler MJ (2017) Printing nature: unraveling the role of nacre's mineral bridges. *J Mech Behav Biomed Mater* 76:135–144. <https://doi.org/10.1016/j.jmbbm.2017.05.007>
2. Firth J, Gaisford S, Basit AW (2018) A new dimension: 4D printing opportunities in pharmaceuticals. In: *3D printing of pharmaceuticals*, pp 153–162. https://doi.org/10.1007/978-3-319-90755-0_8
3. Gul JZ, Sajid M, Rehman MM, Siddiqui GU, Shah I, Kim KH, Lee JW, Choi KH (2018) 3D printing for soft robotics—a review. *Sci Technol Adv Mater* 19:243–262. <https://doi.org/10.1080/14686996.2018.1431862>
4. Gu GX, Takaffoli M, Hsieh AJ, Buehler MJ (2016) Biomimetic additive manufactured polymer composites for improved impact resistance. *Extreme Mech Lett* 9:317–323. <https://doi.org/10.1016/j.eml.2016.09.006>
5. Sullivan TN, Pissarenko A, Herrera SA, Kisailus D, Lubarda VA, Meyers MA (2016) A lightweight, biological structure with tailored stiffness: The feather vane. *Acta Biomater* 41:27–39. <https://doi.org/10.1016/j.actbio.2016.05.022>
6. Ge Q, Qi HJ, Dunn ML (2013) Active materials by four-dimension printing. *Appl Phys Lett* 103:131901. <https://doi.org/10.1063/1.4819837>
7. Quanjin M, Rejab MR, Idris MS, Kumar NM, Abdullah MH, Reddy GR (2020) Recent 3D and 4D intelligent printing technologies: A comparative review and future perspective. *Procedia Comput Sci* 167:1210–1219. <https://doi.org/10.1016/j.procs.2020.03.434>
8. Tibbits S (2014) 4D printing: multi-material shape change. *Archit Des* 84:116–121. <https://doi.org/10.1002/ad.1710>
9. Pei E (2014) 4D Printing: dawn of an emerging technology cycle. *AssemAutom*. <https://doi.org/10.1108/AA-07-2014-062>
10. Yang H, Leow WR, Wang T, Wang J, Yu J, He K, Qi D, Wan C, Chen X (2017) 3D printed photoresponsive devices based on shape-memory composites. *Adv Mater* 29:1701627
11. Raviv D, Zhao W, McKnelly C, Papadopoulou A, Kadambi A, Shi B, Hirsch S, Dikovskiy D, Zyracki M, Olguin C, Raskar (2018) Active printed materials for complex self-evolving deformations. *Sci Rep* 4:1–8. <https://doi.org/10.1038/srep07422>
12. Nadgorny M, Xiao Z, Chen C, Connal LA (2016) Three-dimensional printing of pH-responsive and functional polymers on an affordable desktop printer. *ACS Appl Mater Interfaces* 8:28946–28954. <https://doi.org/10.1021/acsami.6b07388>
13. Gartner Gartner Hype Cycle. <https://www.gartner.com/en/newsroom/press-releases/2018-08-20-gartner-identifies-five-emerging-technology-trends-that-will-blur-the-lines-between-human-and-machine>
14. Ahmed K, Shiblee MN, Khosla A, Nagahara L, Thundat T, Furukawa H (2020) Recent progresses in 4D printing of gel materials. *J Electrochem Soc* 167:037563. <https://doi.org/10.1149/1945-7111/ab6e60>
15. Kuang X, Roach DJ, Wu J, Hamel CM, Ding Z, Wang T, Dunn ML, Qi HJ (2019) Advances in 4D printing: materials and applications. *Adv Funct Mater* 29:1805290. <https://doi.org/10.1002/adfm.201805290>
16. Low ZX, Chua YT, Ray BM, Mattia D, Metcalfe IS, Patterson DA (2017) Perspective on 3D printing of separation membranes and comparison to related unconventional fabrication techniques. *J Membr Sci* 523:596–613. <https://doi.org/10.1016/j.memsci.2016.10.006>
17. Zhang Z, Demir KG, Gu GX (2019) Developments in 4D-printing: a review on current smart materials, technologies, and applications. *Int J Smart Nano Mater* 10:205–224
18. Momeni F, Mehdi Hassani M, NS, Liu X, Ni J (2017) A review of 4D printing. *Mater Des* 122:42–79. <https://doi.org/10.1016/j.matdes.2017.02.068>
19. Lee AY, An J, Chua CK (2017) Two-way 4D printing: a review on the reversibility of 3D-printed shape-memory materials. *Engineering* 3:663–674. <https://doi.org/10.1016/J.ENG.2017.05.014>

20. Nam S, Pei E (2019) A taxonomy of shape-changing behavior for 4D printed parts using shape-memory polymers. *Prog Addit Manuf* 4:167–184. <https://doi.org/10.1007/s40964-019-00079-5>
21. Jani JM, Leary M, Subic A, Gibson MA (2014) A review of shape-memory alloy research, applications and opportunities. *Mater Des* (1980–2015) 56:1078–1113. <https://doi.org/10.1016/j.matdes.2013.11.084>
22. Huang WM, Zhao Y, Wang CC et al (2012) Thermo/chemo-responsive shape-memory effect in polymers: a sketch of working mechanisms, fundamentals and optimization. *J Polym Res* 19:9952. <https://doi.org/10.1007/s10965-012-9952-z>
23. Lendlein A, Jiang H, Jünger O, Langer R (2005) Light-induced shape-memory polymers. *Nature* 434:879–882. <https://doi.org/10.1038/nature03496>
24. Caputo MP, Berkowitz AE, Armstrong A, Müllner P, Solomon CV (2018) 4D printing of net shape parts made from Ni-Mn-Ga magnetic shape-memory alloys. *Addit Manuf* 21:579–588. <https://doi.org/10.1016/j.addma.2018.03.028>
25. Zhao Z, Wu J, Mu X, Chen H, Qi HJ, Fang D (2017) Desolvation induced origami of photocurable polymers by digit light processing. *Macromol Rapid Commun* 38:1600625. <https://doi.org/10.1002/marc.201600625>
26. Yuan C, Roach DJ, Dunn CK, Mu Q, Kuang X, Yakacki CM, Wang TJ, Yu K, Qi HJ (2017) 3D printed reversible shape changing soft actuators assisted by liquid crystal elastomers. *Soft Matter* 13:5558–5568. <https://doi.org/10.1039/C7SM00759K>
27. Ge Q, Sakhaei AH, Lee H, Dunn CK, Fang NX, Dunn ML (2016) Multimaterial 4D printing with tailorable shape-memory polymers. *Sci Rep* 6:1–11. <https://doi.org/10.1038/srep31110>
28. Gladman AS, Matsumoto EA, Nuzzo RG, Mahadevan L, Lewis JA (2016) Biomimetic 4D printing. *Nat Mater* 15:413–418. <https://doi.org/10.1038/nmat4544>
29. Mao Y, Yu K, Isakov MS, Wu J, Dunn ML, Qi HJ (2015) Sequential self-folding structures by 3D printed digital shape-memory polymers. *Sci Rep* 5:1–12. <https://doi.org/10.1038/srep13616>
30. Deshmukh K, Houkan MT, AlMaadeed MA, Sadasivuni KK (2020) Introduction to 3D and 4D printing technology: State of the art and recent trends. *3D 4D Print Polym Nanocomposite Mater* 1:1–24. <https://doi.org/10.1016/B978-0-12-816805-9.00001-6>
31. Rastogi P, Kandasubramanian B (2019) Breakthrough in the printing tactics for stimuli-responsive materials: 4D printing. *Chem Eng J* 366:264–304. <https://doi.org/10.1016/j.cej.2019.02.085>
32. Rayate A, Jain PK (2018) A review on 4D printing material composites and their applications. *Mater Today: Proc* 5:20474–20484. <https://doi.org/10.1016/j.matpr.2018.06.424>
33. Khoo ZX, Teoh JE, Liu Y, Chua CK, Yang S, An J, Leong KF, Yeong WY (2015) 3D printing of smart materials: a review on recent progresses in 4D printing. *Virtual Phys Prototy* 10:103–122. <https://doi.org/10.1080/17452759.2015.1097054>
34. Gao B, Yang Q, Zhao X, Jin G, Ma Y, Xu F (2016) 4D bioprinting for biomedical applications. *Trends Biotechnol* 34:746–756. <https://doi.org/10.1016/j.tibtech.2016.03.004>
35. Zarek M, Layani M, Eliazar S, Mansour N, Cooperstein I, Shukrun E, Szlar A, Cohn D, Magdassi S (2016) 4D printing shape-memory polymers for dynamic jewellery and fashionwear. *Virtual Phys Prototy* 11:263–270. <https://doi.org/10.1080/17452759.2016.1244085>
36. Zhang W, Zhang F, Lan X, Leng J, Wu AS, Bryson TM, Cotton C, Gu B, Sun B, Chou TW (2018) Shape-memory behavior and recovery force of 4D printed textile functional composites. *Compos Sci Technol* 160:224–230. <https://doi.org/10.1016/j.compscitech.2018.03.037>
37. Jian B, Demoly F, Zhang Y, Gomes S (2019) An origami-based design approach to self-reconfigurable structures using 4D printing technology. *Procedia CIRP* 84:159–164. <https://doi.org/10.1016/j.procir.2019.04.184>

38. Javaid M, Haleem A (2019) 4D printing applications in medical field: a brief review. *Clin Epidemiol Glob Health* 7:317–321. <https://doi.org/10.1016/j.cegh.2018.09.007>
39. Rafiee M, Farahani RD, Therriault D (2020) Multi-material 3D and 4D printing: a survey. *Adv Sci* 7:1902307. <https://doi.org/10.1002/advs.201902307>
40. Chua CK, Yeong WY, An J (2017) 3D printing and bioprinting in MEMS technology. *Micromachines* 8:229. <https://doi.org/10.3390/mi8070229>

Chapter 2

Characterization Techniques for Shape-Memory Alloys



Praveen K. Jain, Neha Sharma, Rishi Vyas, and Shubhi Jain

2.1 Introduction

Shape-memory alloys are metallic alloys that exhibit the property of “remembering” their previously defined shape or dimension when subjected to either temperature change or mechanical pressure. The shape-memory effect (SME) was initially witnessed in Au–Cd alloy in 1932. SME has then been reported in several alloy systems, in particular Ni–Ti, Fe–Pt, Cu–Zn, Cu–Zn–X (X = Sn, Al, Si, Ga), etc. However, out of these, only Ni–Ti and Cu-substituted alloys have turned out to be commercially feasible with advantageous engineering properties. Ferromagnetic Shape-Memory Alloys (FSMAs) may be regarded as the next generation of SMAs. Including a lot of characteristics in common with SMAs, they also exhibit deformations in response to magnetic fields. A higher magnetic field-induced strain (MFIS) with a rapid response at low frequencies is displayed by FSMAs as compared to piezoelectric and magnetostrictive materials. Studies have reported that Ni–Mn–Ga alloys [1–3] show enormous magnetic field-induced strain (MFIS) and Ni–Mn–In [4] and Ni–Mn–Sn-based alloys [5] show metamagnetic shape-memory effect (MMSME).

The original version of this chapter was revised: Missing few lines are updated in Introduction section. The correction to this chapter can be available at https://doi.org/10.1007/978-3-030-94114-7_18

P. K. Jain (✉) · S. Jain

Department of Electronics and Communication Engineering, Swami Keshvanand Institute of Technology, Management & Gramothan, Jaipur 302017, India
e-mail: pkjain@skit.ac.in

N. Sharma

Department of Physics, Vishwavidyalaya Engineering College, Ambikapur, Surguja, Chhattisgarh 497001, India

R. Vyas

Department of Physics, Swami Keshvanand Institute of Technology, Management & Gramothan, Jaipur 302017, India

© The Author(s), under exclusive license to Springer Nature Switzerland AG 2022, corrected publication 2022

29

M. R. Maurya et al. (eds.), *Shape Memory Composites Based on Polymers and Metals for 4D Printing*, https://doi.org/10.1007/978-3-030-94114-7_2

These alloys additionally demonstrate other potential characteristics, namely huge magnetoresistance [6–9] and a giant magneto-caloric effect [8–12]. Additionally, as we increase the Ni composition, the transformation temperature of the martensitic phase significantly increases.

The two unique properties of superelasticity and SME are due to the occurrence of solid-state phase transformation in shape-memory alloys which implies molecular rearrangement leading to change in the crystal structure. Shape-memory alloys may be available in twin phases: martensite or austenite with three diverse crystal structures (twinned martensite, deformed martensite, and austenite).

The phase transformation between the two phases (martensite and austenite) allows SMAs to return to their previous shape through two diverse mechanisms.

- Superelasticity is the ability to return to its original shape as a result of a stress-induced phase transformation. When a load is applied to the shape-memory alloy in a stable austenite phase at a fixed temperature, it gets transformed to the martensite phase. Upon withdrawal of the applied load, the material gets transformed again to the austenite phase and hence returns to its preliminary shape.
- Shape-Memory Effect: This refers to the ability of a material to return to its original shape as a result of a temperature-induced phase transformation. The reversible transition from a phase at a higher temperature into a lower temperature phase takes place in this phenomenon. Austenite, the more symmetrical cubic phase, occurs at higher temperatures, whereas martensite, the less symmetric, relatively soft, and easily deformed phase, occurs at lower temperatures. Upon heating, the deformed martensite gets transformed to an austenite phase, which reverts to the original twinned martensite phase upon cooling. If a load is applied during cooling, the shape-memory alloy will attain a deformed martensite phase which will transform into an austenite phase upon heating. The temperature induced phase transformation in shape memory alloys has been displayed in Fig. 2.1.

Metallic alloys of Nickel and titanium, commonly known as Nitinol, exist in BCC crystal structure at higher temperatures and attain lower symmetric monoclinic phase at lower temperatures. Besides these two phases, the alloy also possesses an additional rhombohedral crystal structure at intermediate temperatures. The alloys existing in the austenite phase at higher temperature transform with decreasing temperature, initially to the intermediate rhombohedral phase and then to the martensite phase.

The properties of the SMAs, in which phase transformations occur at critical temperatures, are of immense significance. For different utilizations, it is very important to know the temperatures of commencement and ending of the austenite phase (A_s ; A_f). In addition to this, the martensite initial and final (M_s ; M_f) temperatures also play a major role in appropriate and adequate utilization of the material. Analysis of crystalline phase transition behavior includes a variety of techniques like differential scanning calorimetry, X-ray diffractometry, internal friction measurement, electrical resistivity, thermo-mechanical analyzer, and thermoelectric power.

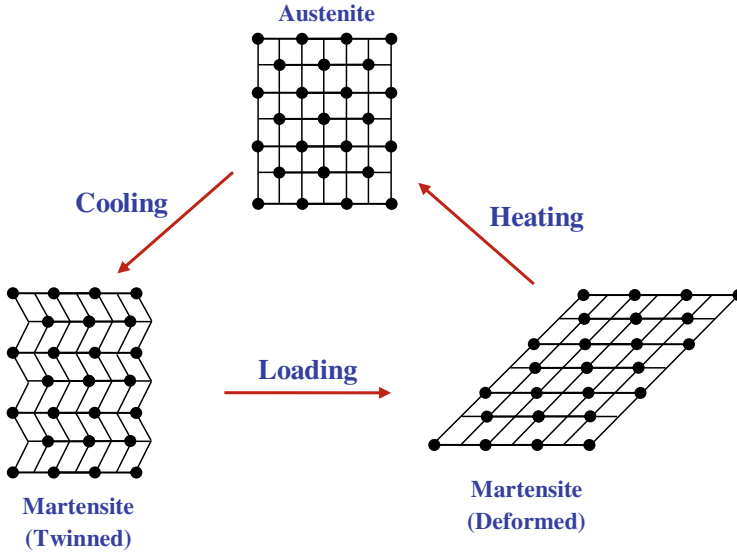


Fig. 2.1 Phase transformation of SMA material induced by temperature

2.2 DSC Characterization

DSC is the extensively deployed characterizing technique for assessing the temperatures and obtaining the energy of SMAs during phase transformations. From differential scanning calorimetry measurements, variations in transformation temperatures due to thermo-mechanical processing are calculated. SMAs most popular technique for evaluating phase transition temperatures (T_{trans}) is differential scanning calorimetry (DSC). As it tests thermal release and absorption from an existing sample with the test sample, DSC is known as a differential. This technique is generally used to thermally characterize SMAs under zero loading. DSC systems are defined as power compensated DSC and heat flow DSC according to the operating process [13]. As different stages in these alloys depend on heat-treatment temperatures, thermal treatment is highly significant in SMAs. In particular, the presence of the R-phase [14] is instrumental in deciding the properties of the shape-memory, such as recoverable strain and thermal cycling stability, which are some of the key engineering parameters.

Differential scanning calorimetry established the transfer temperatures between martensite and austenite, which are of decisive significance for practical materials. The reversibility of the thermoelastic martensitic transition is shown by peaks during the heating and cooling cycles, the hysteresis being indicative of the first-order level transformation. A standard Ni-Ti SMA DSC curve exhibits an exothermic peak at some stage in cooling, owing to the transformation of austenite to martensite, whereas the transformation of martensite to austenite is endothermic when heated. The values

of temperature referring to the commencement and termination of a phase transition can be calculated by adding the tangent approach to the transformation peaks. The initial (start) and final austenite formation temperatures (A_s and A_f), as well as the initial and final martensite formation temperatures (M_s and M_f), may therefore be defined if there is no intermediate R-phase formation in the material [15].

Differential Scanning Calorimetry is one of the thermo-analytical methods and used in quantitative analysis. When a sample material undertakes a physical transition (i.e., phase change), more or less heat must flow through it in addition to the reference sample to sustain them at the same temperature. If the process is exothermic or endothermic, the amount of heat flowing through the sample as compared to reference is determined. The temperature software was used to increase the temperature of the sample holder linearly with time. To run the study, just a few mg of material is needed. DSC, mainly because of its speed, simpleness to operate, and accessibility, has been used most commonly as a thermal analysis method [17].

In a shape-memory alloy, at a transition point followed by heat production and absorption, the crystal structure varies. The transition point of the shape-memory alloy can also be found by calculating and evaluating the peaks of heat production and absorption by DSC. Reverse transformation (martensite to austenite) refers to the endothermic reaction and forward transformation corresponds to the exothermic reaction (austenite to martensite).

The temperatures of transformation displayed by SMAs strongly depend on their structure. Minor improvements in their structure can result in major changes in the temperature of their transition. By selecting the composition of materials, the value of the transition temperature can be tailored for different applications.

Figure 2.2 illustrates the variation of heat flow as a function of the temperature of the DSC experiments conducted on the SMA. In comparison, the solid line is the

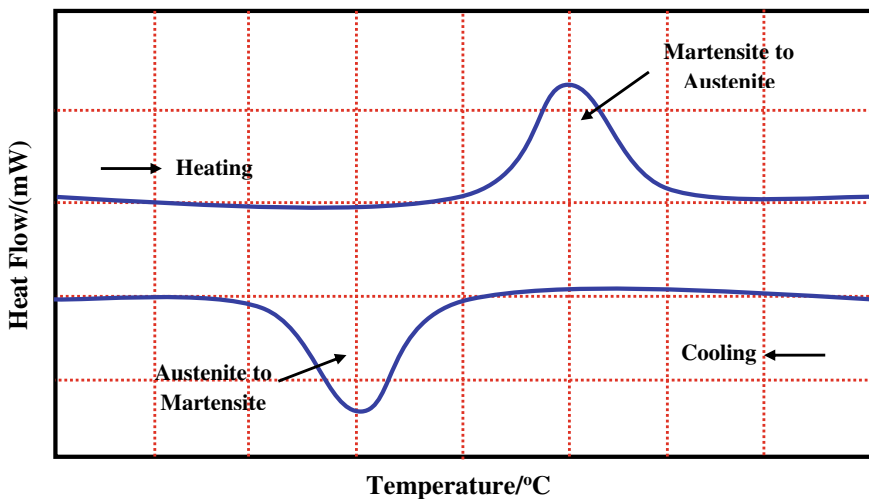


Fig. 2.2 Temperature variation of heat flow in DSC tests

result of a full thermal period (i.e., continuous heating without a break), which shows only one change from martensite (M) phase to austenite (A) when heated (the reverse martensitic transformation), whereas the austenite to martensite transition is through an indirect R-process phase when cooled; there are two different transformations from A to R and R to A. A tiny piece of martensitic Shape-Memory Alloy is heated to a temperature (T_s) lower than the end of the temperature of the reverse martensitic transition for a typical DSC. The previous heating stop temperature (T_s) can be discovered in the subsequent heating phase by contrasting the resultant heat flow versus temperature curve with that of a maximum thermal cycle in the final heating process (i.e., without the previous heating stop process).

The martensitic transition happens when the free energy of martensite falls below that of austenite at a temperature below T_0 , the critical temperature at which the two phases' free energies are equivalent. However, the transition does not begin at T_0 , but rather at a temperature M_s (martensite start) that is lower than T_0 in the absence of stress. As the temperature is reduced, the transformation proceeds until the M_f (martensite finish) temperature is achieved. Similarly, the reverse-phase transformation process, i.e., from martensite phase to austenite phase, starts at A_s (austenite start) and finishes at A_f (austenite finish). Because of the displacive nature of the martensitic transformation, applied tension is crucial. When a mechanical load is applied, martensitic variants reorient themselves into a single variant, which results in huge macroscopic inelastic strain. Nevertheless, when there are no applied stresses, the variants of the martensite phases organize themselves in a self-accommodating way by twinning, which results in no detectable macroscopic shapeshift. The low-symmetry martensitic phase recovers to its high-symmetry austenitic phase after being heated to a higher temperature, and the inelastic strain is, therefore, restored. Pure mechanical loading may cause martensitic phase transition when the SMAs are in the austenitic phase. In this case, stress-induced martensite phase, i.e., detwinned martensite phase is formed from the austenite phase at temperatures above M_s .

At T_0 equilibrium temperature, the difference of the Gibbs free energy (ΔG) between the austenite and martensite phases is negligible. For the assessment of the quantity of G , as described below, some calculations based on T_0 point can be performed for A-M conversion [18];

$$\Delta G_{A \rightarrow M}(T_0) = G_M(T_0) - G_A(T_0) = (H_M - T_0 S_M) - (H_A - T_0 S_A) = 0 \quad (2.1)$$

$$\Delta G_{A \rightarrow M}(T_0) = \Delta H_{A \rightarrow M} - T_0 \Delta S_{A \rightarrow M} = 0 \quad (2.2)$$

Consequently, the relation between entropy change (ΔS) and enthalpy change (ΔH) can be written as follows:

$$T_0 = \frac{\Delta H_{A \rightarrow M}}{\Delta S_{A \rightarrow M}} = \frac{\Delta H_{M \rightarrow A}}{\Delta S_{M \rightarrow A}} \quad (2.3)$$

For martensite nucleation, the free energy of Gibbs (ΔG) can be represented as follows [19]:

$$\Delta G_{A \rightarrow M}(M_S) = \Delta G_{M \rightarrow A}(T_0) - \Delta G_{M \rightarrow A}(M_S) = -(T_0 - M_S)\Delta S_{M \rightarrow A} \quad (2.4)$$

Using a theoretical method suggested by Kissinger [20] and Augis–Bennett [21], the activation energy of crystallization (E_c) was measured. The Kissinger model anticipated that, as provided by Eq. (2.5), peak crystallization temperature (T_p) could be represented in terms of heating rate (α). The activation energy was measured utilizing the slope between (α/T_p^2) and $1/T_p$ of the straight-line map.

$$(\alpha/T_p^2) = -E_c/RT_p + C \quad (2.5)$$

where C is a constant. In addition, the relation between on-set crystallization temperature (T_c) and heating rate (α), an approximation method proposed by Augis–Bennett, can be expressed as given by Eq. (2.6).

$$(\alpha/T_c) = -E_c/RT_c + \ln K_0 \quad (2.6)$$

The plot was used to measure the activation energy between (α/T_p^2) and $1/T_p$ and the slopes of this gradient. The intercept of this plot provides the frequency factor (K_0), defined as the number of attempts made to overcome the energy barrier by nuclei per second.

In general, Ni–Ti alloys are put to use as binary alloys. Over recent years, researchers have applied a third additive to the alloy and different properties such as mechanical and thermal hysteresis have been analyzed [22, 23]. In Ni–Ti binary alloys, these forms of Ni–Ti alloys are called equivalent atomic alloys if the Ni–Ti ratio is equal in alloys. If nickel concentrations are more, a sharp decrease has been found in the alloy’s processing temperature. The transition temperature for alloys that are Ti–rich is not much influenced by the structure. This is how the Ti_2Ni particles precipitate. These precipitations detach from the matrix and do not alter the temperature of transformation. An addition of a third element (replacement of titanium) reduces the transition temperature. In several cases, the addition of a third element raises the temperature value of the transformation of the Ni–Ti element. On the other hand, some additive elements minimize the temperature value of the transformation [24]. Ni–Ti alloys were developed at different rates in this research. Various elements were also added to Ni–Ti’s alloys and alloys developed that turn the martensitic process at the transition temperature. These alloys were studied according to their different crystal structures and microstructures, and related characteristics properties have been determined.

Ni–Ti-based SMAs have been studied and compared based on their varying thermal properties with the crystal structures and microstructures. Some of the Ni–Ti-based SMAs such as $Ni_{45}Ti_{55}Cr_{2.5}Cu_{2.5}$, $Ni_{48}Ti_{51}Mn$, and $Ni_{48}Ti_{51}Co$ show temperatures of transformation below body temperature (i.e., 37.5 °C), while some SMAs like

$\text{Ni}_{45}\text{Ti}_{55}$ and $\text{Ni}_{48}\text{Ti}_{51}\text{Sn}$ show temperatures of transformation above body temperature. The $\text{Ni}_{48}\text{Ti}_{51}\text{Mn}$ alloy is the perfect alloy that completes transformation at body temperature. $\text{Ni}_{48}\text{Ti}_{51}\text{Mn}$, which is distinct from other alloys, was found at the rhombohedral phase before the Austenite phase during warm-up. On the other hand, during cooling the following Martensite transformation, $\text{Ni}_{48}\text{Ti}_{51}\text{Co}$ was observed in the Rhombohedral phase. The rhombohedral formation depends on aging temperature, aging period, and Ni–Ti alloy chemical composition. When crystal structure and microstructure measurements were performed on Austenite alloys at room temperature, the phases B2 (Ni–Ti) and Ti_2Ni were observed; however, the phases B19 (Ni–Ti) and Ti_2Ni were discovered in Martensite alloys at room temperature. It is understood that the temperature of the transition is influenced less by the composition of alloys that are abundant in titanium. This is how the Ti_2Ni particles are precipitated [17, 25–27]. Table 2.1 shows the effect of additive materials on different parameters for martensite to austenite phase transformation.

2.3 Structural Characterization

X-ray diffraction (XRD) is primarily used to study the crystallographic structure and phase evolution in the SMAs. The XRD powder technique is used to evaluate the structures of the crystal at room temperature or in a temperature range (95 K–480 K). The average size of the SMAs is determined using the formulation Debye–Scherrer [38] mentioned as follows:

$$D = \frac{0.91\lambda}{\beta \cos \theta} \quad (2.7)$$

where λ represents the wavelength of incident X-ray, β is the full width at half maximum (FWHM) value of the highest peak in radians, and θ is the Bragg angle of diffraction in radians.

The structure of Heusler (L21) is an ordered structure of the BCC with a general X_2YZ composition. The ordering method is considered in a collection of A2, B2, and L21 of the ternary Heusler alloy [39]. Some of the Heusler alloys are transformative. In $\text{Pd}_{50}\text{Mn}_{25}\text{Ga}_{25}$, the XRD peaks were defined as standard structures of BCC with extra order peaks. The 100 reflection showing B2 was identified; 111, suggesting L21, was not seen in the XRD pattern. The XRD pattern was not shown as the L21.

During in situ thermal processes, synchrotron X-ray diffraction was used for the scale and morphology of the Ni–Ti–Hf-dependent nano-precipitates [40]. For calculating the precipitate size of the H-phase and observing precipitate development and coarsening, SR-XRD was used.

The most commonly studied SMA material system, Ni–Ti-based SMA, has been structural studied showing that the martensitic transition, as well as the corresponding memory impact of the shape and superelasticity properties of the grains at the

Table 2.1 A literature survey on different parameters for martensite \leftrightarrow austenite phase transformation (Binary and Ternary alloys, Effect of additives materials)

Alloys	A _s (°C)	A _f (°C)	M _s (°C)	M _f (°C)	A _s -M _f (°C)	ΔH_{M-A} (J/g)	ΔH_{A-M} (J/g)	ΔS_{M-A} (J/g °C)	ΔS_{A-M} (J/g °C)	References
Ni-Ti	54.8	69.6	24.9	4.7	50.1	-	-	-	-	Kök et al. [29]
Ni-Ti	58.0	70.0	37.8	21.0	37.0	27.6	-	0.53	-	Zhai et al. [30]
Cu-50% Sn	-	-	-	-	-	9.604	-	9.99	-	Dasgupta et al. [31]
Cu-Zn-Al	530	550	510	480	50	-	-	-	-	Espiritu and Amorsolo [32]
Cu-Zn-Sn (46.30%)	225.01	226.97	221.55	221.03	3.98	-	-	17.72	17.57	Kumar et al. [33]
Cu12.5Al5Mn	460	510	490	520	60	-	-	-	-	Raju and Sampath [34]
Cu10.21Al4.60Fe	416	478	308	243	173	-	-	-	-	Saud et al. [35]
Cu-Al-Ni	504.9	515.1	503.3	497.5	7.4	2.892	2.180	5.679	4.281	Adnan [36]
Cu-14%Al-4.5%Ni	129	165	133	100	29	1.9	-2.54	0.12	-0.17	Qader et al. [37]
Cu-14%Al-4.5%Ni-Te 0.3%	215	242	109	92	123	3.375	-2.9	0.022	-0.019	Qader et al. [37]
Cu-14%Al-4.5%Ni-Te 1.0%	181	199	129	76	105	8.025	-6.0	0.045	-0.036	Qader et al. [37]
Cu-14%Al-4.5%Ni-Te3.0%	150	186	165	127	23	32.5	-15.0	0.184	-0.085	Qader et al. [37]
Cu ₈₀ Al ₁₃ Ni ₃ Hf ₄	270.60	279.51	261.7	250.42	20.18	370	90	1.37	-0.33	Canbay et al. [22]
Cu-22.78%Al-2.59%Fe-2.44% Mn	114.03	139.78	119.67	77.57	36.46	4.36	-1.52	0.0336	0.011	Patterson [38]

nanoscale, is severely influenced. If grain size d is considerably finer than sample size D , it is stabilized, while when d is lower than the critical value in the range usually of many tens of nanometers, the austenite phase is stable. This removes the martensitic transformation [41].

2.4 Thermal Cycling Tests

To analyze the strain recovery in the form of memory alloys, thermal cyclic tests are used. Thermal cyclic experiments utilizing specimens in the temperature range from $M_f - 30^\circ\text{C}$ to $A_f + 30^\circ\text{C}$ are carried out to analyze the memory effects of the alloys under compressive stresses. In the thermal cyclic test [42], firstly the specimen was heated to $A_f + 30^\circ\text{C}$ and then cooled to $M_f - 30^\circ\text{C}$ and again heated to $A_f + 30^\circ\text{C}$.

2.5 ER Characterization

Electrical resistivity is often based on the crystal's composition. Typically, the DSC curve of SMAs indicates an exothermic and endothermic peak due to austenite \rightarrow martensite transformation and martensite \rightarrow austenite transition through cooling and heating of the specimen. SMAs comprise different crystal structures in different phases. For example, a Ni-Ti SMA exists in a monoclinic structure in low-temperature martensitic phase, BCC in high-temperature austenitic phase, and rhombohedral in the R-phase.

The electrical resistivity shows a rapid increase as we increase the temperature due to the change in martensitic phase to austenitic phase. The reverse nature is observed when the phase changes from austenitic phase to martensitic phase. The highest value of resistivity has been observed for the R-phase. The appearance of the R-phase may be observed using the peak value of resistivity in the Resistance-Temperature curve.

2.6 TMA Characterization

In the SMAs, solid-state phase transformations phenomena, the behavior of thermal expansion parameters plays a very major utility in engineering design. In the mixed phases of SMAs, DSC and ER techniques as discussed above have some limitations to determine the transformation temperatures.

2.7 Dynamic Mechanical Analyzer (DMA)

For characterization of material's mechanical properties such as viscosity (damping) and modulus (elasticity) defined as a function of stress, frequency, temperature, and time or combinations of these parameters, the technique of Dynamic Mechanical Analyzer is used. Presently, two methods are used. The first method is about the decay of free oscillations and the second method is about forced oscillation.

Free oscillation techniques include applying force on a sample and leaving it for oscillations after the removal of the force. Forced oscillations are sustained by continuous application of force on a sample. The common method used nowadays is to measure a sample material's final displacement after the sample is applied with an oscillating force.

If a simpler dynamic mechanical method is to be considered then, the forced non-resonance technique is the right option. A sample of force (stress) is given here with the help of an instrument and a motor. Through the drive shaft, the transmission of stress occurs on the sample (build up in a clamping mechanism). Now, the positional sensor of the linear variable differential transformer (LVDT) gives the displacement amount of sample deformation. The driven arm on which the LVDT is mounted measures frequency and strain (function of stress), and sample response, along with providing feedback to the motor. So, the calculation of strain is done by observing displacement. A defined frequency helps in applying a force/stress, sinusoidally.

Dynamic mechanical thermal analyzer (DMTA) is another name for DMA because, during the measurement, a variable sample temperature is defined. Inside the furnace, which is an environmental chamber, a sample is mounted. The specimen under test is attached between the stationary fixtures (with adjustable distance) and movable distance. Calculation of the stiffness of the material under stress is dependent on the magnitude of the applied stress and the resultant strain. Moreover, the damping factor ($\tan \delta$) is dependent on the phase lag between the two.

Dynamic mechanical analysis (DMA), by submitting to small swinging power, shows data concerning the mechanical characteristics of a specimen put in slight sinusoidal oscillation as a function of temperature and time (generally sinusoidal). Depending on the sample's characteristics, there are a number of ways to mount a sample in DMA. Six common arrangements are dual cantilever bending, single cantilever bending, three-point bending, compression, tension, and shear.

Stress, which is defined as a mechanical load, results in a corresponding deformation/strain whose amplitude and phase shift can be determined. A pre-selected force is subjected to a sample to measure the resultant deformation. An oscillatory stress (with a phase lag (δ)) is produced in response to an oscillatory strain wave, through which viscous contribution is measured. The phase/loss angle, (δ), is defined as the amount through which strain lags the resultant of the stress. Largely delayed response results in large viscosity of the material while less delayed response means the material is more elastic, e.g., steel which is a perfectly elastic material that has a phase angle to be zero ($\delta = 0^\circ$) and liquid which is a purely viscous material has $\delta = 90^\circ$. Intermediately, viscoelastic materials have δ to be: $0^\circ < \delta < 90^\circ$.

Abundant polymers reveal such a behavior and exhibit both elastic and viscous components.

After the application of sinusoidal stress on specimens, deformation takes place sinusoidal within the boundaries of linear viscoelastic regions. The stress (σ) applied to the material is formalized as

$$\sigma = \sigma_0 \sin \omega t \quad (2.8)$$

Stress variation rate is given by

$$\frac{d\sigma}{dt} = \omega \sigma_0 \cos \omega t \quad (2.9)$$

Now, the resultant strain wave of the material depends upon the depth of elastic and viscous behavior. Therefore, strain in terms of modulus (E) and stress (σ) is defined as follows:

$$\varepsilon(t) = \frac{\sigma}{E} = \frac{\sigma_0 \sin \omega t}{E} \quad (2.10)$$

Therefore, $\varepsilon(t) = \varepsilon_0 \sin \omega t$.

The phase lag between the applied stress and resultant strain is an angle $\delta = \pi/2$ for viscous material, i.e.,

$$\varepsilon(t) = \varepsilon_0 \sin(\omega t + \delta) \quad (2.11)$$

The ratio of real and imaginary modulus can be written as follows:

$$\frac{E''}{E'} = \tan \delta \quad (2.12)$$

where $\tan \delta$ is the damping factor showing the productivity of molecular configurations and internal tension with the substance losing energy.

A normal tension or pressure extends to a sample and the resultant stress or stress reaction is recorded. The stress which is in the applied tension is used as a measure of elastic activity to evaluate the elastic or storage module (E'), showing the capacity of the material to store elastic energy related to recoverable deformation. The tension, which is out of phase with the applied pressure, gives the measure of the viscous or loss modulation (E''). This module reflects the material's capacity to retain energies that are not emitted during the recoverable elastic transition. This energy is used to improve molecular segment vibrations or to translate the position of the chain. Loss tangent ($\tan \delta$) or mechanical damping is the phase angle in the oscillating experiment between dynamic tension and stress. The proportion of the viscous module to the elastic module [43–45] is dimensionless.

Transition temperature and mechanical properties of the glass were calculated by means of a temperature scan and stress–strain scans, such as tensile resilience, rigidity, resilience, Young elastic, and elongation at the split. DMA film samples were cut to scale 4–6 mm in width and 20 mm in length to reach tension-measuring limits. The temperature scan was performed between 30 °C and 180 °C at a heating/ramping rate of 2 °C/min, and a load 0.1 N/min load scan in tension mode was conducted. The oscillation frequency in the linear viscoelastic area was set at 1 Hz and the stress amplitude of 0.01 mm.

2.8 Electron Microscopy

The Scanning Electron Microscope is often deployed to investigate the microstructures of the formed shape-memory alloys. A wavelength dispersive X-ray (WDX) spectrometer is installed on an electron sample microanalyzer (ESMA) to detect SMAs.

An in situ optical microscope (OM) was used to observe the microstructure change in the $\text{Pd}_{50}\text{Mn}_{35}\text{Ga}_{15}$ sample during martensitic transformation. In this study, the heating and cooling rates were kept constant at 10 K/min, and micrographs were taken after holding samples at the desired temperatures for 90 s. Furthermore, transmission electron microscopy (TEM) was used to observe the microstructure and to determine the crystal structure [46]. Scanning electron microscopy (SEM) has also been used to analyze the microstructure of SMAs. SEM was employed to study the Cu–13.0Al–4.0Ni–xB HTSMA [46]. It has been observed that the microstructure of the Cu–13.0Al–4.0Ni–xB alloy has an 18R martensite structure with self-accommodating zig-zag groups [46]. When the B element content is increased to 0.25 wt%, the alloy exhibits a monophasic martensitic structure, and further addition of B results in the formation of the second phase. Moreover, the increment in B content, the volume, and the number of the second phase increased. The second phase of Cu–13.0Al–4.0Ni–xB mostly has boron and aluminum, and the content of nickel and copper is very slight, as observed by EDS results.

2.9 Magnetic Characterization

The Superconducting Quantum Interference Device (SQUID) magnetometer has been employed by various researchers for conducting thermal magnetization measurements to study magnetic transformation temperature in magnetic shape-memory alloys (MSMAs). Study and analysis of magnetic behavior are very essential for the Heusler-type alloys. Several researchers have documented the magnetic

behavior of $\text{Pd}_{50}\text{Mn}_{25}\text{In}_{25}$ with L_{21} and $\text{Pd}_{50}\text{Mn}_{25}\text{Al}_{25}$ with B_2 structure as antiferromagnetic, whereas most of the other Heusler alloys have been reported as ferromagnetic. In addition, the Heusler alloys with a B_2 structure and the Neel temperature of ~ 198 K were also reported to be antiferromagnetic [47].

2.10 Conclusion

SMA are metal alloys that show twin exclusive characteristics, such as pseudoelasticity and the shape-memory effect. In this chapter, the techniques used to characterize SMA have been discussed in order to further grasp the behavior of the alloys and use them for particular applications. Due to unique properties such as shape-memory effect, superelasticity, and damped vibrations, these materials can have a wide range of applications in almost all engineering fields. New technologies, implementations, and the number of goods manufactured in the industry using SMA are continually thriving, and different SMA will be created for usage in various application fields.

References

1. Ullakko K, Huang JK, Kantner C, O'handley RC, Kokorin VV (1996) Large magnetic-field-induced strains in Ni_2MnGa single crystals. *Appl Phys Lett* 69(13):1966–1968
2. Sozinov A, Lanska N, Soroka A, Zou W (2013) 12% magnetic field-induced strain in Ni-Mn-Ga-based non-modulated martensite. *Appl Phys Lett* 102(2):021902
3. Sozinov A, Soroka A, Lanska N, Rameš M, Straka L, Ullakko K (2017) Temperature dependence of twinning and magnetic stresses in $\text{Ni}_{46}\text{Mn}_{24}\text{Ga}_{22}\text{Co}_4\text{Cu}_4$ alloy with giant 12% magnetic field-induced strain. *ScriptaMaterialia*. 1(131):33–36
4. Kainuma R, Imano Y, Ito W, Sutou Y, Morito H, Okamoto S, Kitakami O, Oikawa K, Fujita A, Kanomata T, Ishida K (2006) Magnetic-field-induced shape recovery by reverse phase transformation. *Nature* 439(7079):957–960
5. Kainuma R, Imano Y, Ito W, Morito H, Sutou Y, Oikawa K, Fujita A, Ishida K, Okamoto S, Kitakami O, Kanomata T (2006) Metamagnetic shape-memory effect in a Heusler-type $\text{Ni}_{43}\text{Co}_7\text{Mn}_{39}\text{Sn}_{11}$ polycrystalline alloy. *Appl Phys Lett* 88(19):192513
6. Koyama K, Okada H, Watanabe K, Kanomata T, Kainuma R, Ito W, Oikawa K, Ishida K (2006) Observation of large magnetoresistance of magnetic Heusler alloy $\text{Ni}_{50}\text{Mn}_{36}\text{Sn}_{14}$ in high magnetic fields. *Appl Phys Lett* 89(18):182510
7. Zhang B, Zhang XX, Yu SY, Chen JL, Cao ZX, Wu GH (2007) Giant magnetothermal conductivity in the Ni–Mn–In ferromagnetic shape-memory alloys. *Appl Phys Lett* 91(1):012510
8. Han Z, Wang D, Qian B, Feng J, Jiang X, Du Y (2010) Phase transitions, magnetocaloric effect and magnetoresistance in Ni–Co–Mn–Sn ferromagnetic shape-memory alloy. *Jpn J Appl Phys* 49(1R):010211
9. Paramanik T, Das I (2016) Near room temperature giant magnetocaloric effect and giant negative magnetoresistance in Co, Ga substituted Ni–Mn–In Heusler alloy. *J Alloy Compd* 5(654):399–403
10. Krenke T, Duman E, Acet M, Wassermann EF, Moya X, Manosa L et al (2005) *Nat Mater* 4:450

11. Pathak AK, Dubenko I, Mabon JC, Stadler S, Ali N (2009) The effect of partial substitution of In by X = Si, Ge and Al on the crystal structure, magnetic properties and resistivity of Ni₅₀Mn₃₅In₁₅ Heusler alloys. *J Phys D Appl Phys* 42(4):045004
12. Sratong-on P, Chernenko V, Hosoda H. *Results in Materials*
13. Cunha MF, Sobrinho JM, Souto CR, dos Santos AJ, de Castro AC, Ries A, Sarmento NL (2019 Oct) Transformation temperatures of shape-memory alloy based on electromechanical impedance technique. *Measurement* 1(145):55–62
14. Ling HC, Roy K (1981) Stress-induced shape changes and shape-memory in the R and martensite transformations in EquiatomicNiTi. *Metall Trans A* 12(12):2101–2111
15. Zanaboni E (2008) One way and two way–shape-memory effect: Thermo–mechanical characterization of Ni–Ti wires. *UniversitadegliStudi di Pavia, Pavia, Italy*
16. Uchil J (2002) Shape-memory alloys—characterization techniques. *Pramana* 58(5):1131–1139
17. Kök M, Ateş G (2017) The effect of addition of various elements on properties of NiTi-based shape-memory alloys for biomedical application. *Eur Phys J Plus* 132(4):1–6
18. Canbay CA, Sampath V (2017) Microstructural and thermal investigations of Cu–Al–Mn–Ni shape-memory alloys. *Mater Today Proc* 4(10):10682–10689
19. Balo ŞN, Sel N (2012) Effects of thermal aging on transformation temperatures and some physical parameters of Cu–13.5 wt.% Al–4 wt.% Ni shape-memory alloy. *Thermochimicaacta* 536:1–5
20. Kissinger HE (1957) *Anal Chem* 29:1702
21. Augis JA, Bennett JE (1978) Calculation of the Avrami parameters for heterogeneous solid state reactions using a modification of the Kissinger method. *J Therm Anal* 13(2):283–292
22. Canbay CA, Karaduman O, Ünlü N, Baiz SA, Özkul İ (2019) Heat treatment and quenching media effects on the thermodynamical, thermoelastical and structural characteristics of a new Cu-based quaternary shape-memory alloy. *Compos Part B: Eng* 174:106940
23. Dasgupta R (2014) A look into Cu-based shape-memory alloys: Present scenario and future prospects. *J Mater Res* 29(16):1681
24. El-Bagoury N (2015) Precipitation of second phases in aged Ni rich NiTiRe shape-memory alloy. *Mater High Temp* 32(4):390–398
25. Marattukalam JJ, Singh AK, Datta S, Das M, Balla VK, Bontha S, Kalpathy SK (2015) Microstructure and corrosion behavior of laser processed NiTi alloy. *Mater Sci Eng, C* 1(57):309–313
26. Saedi S, Turabi AS, Andani MT, Moghaddam NS, Elahinia M, Karaca HE (2017) Texture, aging, and superelasticity of selective laser melting fabricated Ni-rich NiTi alloys. *Mater Sci Eng, A* 16(686):1
27. Chen G, Cao P, Edmonds N (2013) Porous NiTi alloys produced by press-and-sinter from Ni/Ti and Ni/TiH₂ mixtures. *Mater Sci Eng, A* 10(582):117–125
28. De Araújo CJ, Da Silva NJ, Da Silva MM, Gonzalez CH (2011) A comparative study of Ni–Ti and Ni–Ti–Cu shape-memory alloy processed by plasma melting and injection molding. *Mater Des* 32(10):4925–4930
29. Kök M, Dağdelen F, Aydoğdu A, Aydoğdu Y (2016) The change of transformation temperature on NiTi shape memory alloy by pressure and thermal ageing. *J Phys Conf Ser* 667(1):012011. IOP Publishing
30. Zhai W, Wang WL, Geng DL, Wei B (2012) A DSC analysis of thermodynamic properties and solidification characteristics for binary Cu–Sn alloys. *Acta Mater* 60(19):6518–6527
31. Dasgupta R, Jain AK, Kumar P, Hussein S, Pandey A (2014) Effect of alloying constituents on the martensitic phase formation in some Cu-based SMAs. *J Mater Res Technol* 3(3):264–273
32. Espiritu RD, Amorsolo AV Jr (2012) DSC analysis of Cu–Zn–Sn shape-memory alloy fabricated via electrodeposition route. *J Therm Anal Calorim* 107(2):483–487
33. Kumar P, Jain AK, Hussain S, Pandey A, Dasgupta R (2015) Changes in the properties of Cu–Al–Mn shape-memory alloy due to quaternary addition of different elements. *Matéria (Rio de Janeiro)* 20(1):284–292
34. Raju TN, Sampath V (2011) Influence of aluminium and iron contents on the transformation temperatures of Cu–Al–Fe shape-memory alloys. *Trans Indian Inst Met* 64(1–2):165

35. Saud SN, Hamzah E, Abubakar T, Ibrahim MK, Bahador A (2015) Effect of a fourth alloying element on the microstructure and mechanical properties of Cu–Al–Ni shape-memory alloys. *J Mater Res* 30(14):2258
36. Adnan RS (2019) Effect of Te addition on transformation temperature and thermal properties of Cu-14% Al-4.5% Ni Shape-Memory alloy. *Mater Today Proc* 18:2242–2249
37. Qader IN, Kök M, Dağdelen F (2019) Effect of heat treatment on thermodynamics parameters, crystal and microstructure of (Cu-Al-Ni-Hf) shape-memory alloy. *Phys B* 15(553):1–5
38. Patterson AL (1939) The Scherrer formula for X-ray particle size determination. *Phys Rev* 56(10):978
39. Zhang X, Zhang M, Cui T, Li J, Liu Q, Wang H (2019) The enhancement of the mechanical properties and the shape-memory effect for the Cu-13.0 Al-4.0 Ni alloy by boron addition. *J Alloys Compd* 776:326–333
40. Ley NA, Smith J, Wheeler RW, Young ML (2019) Effects of thermo-mechanical processing on precipitate evolution in Ni-rich high temperature shape-memory alloys. *Materialia* 8:100496
41. Waitz T, Tsuchiya K, Antretter T, Fischer FD (2009) Phase transformations of nanocrystalline martensitic materials. *MRS Bull* 34(11):814–821
42. Yamabe-Mitarai Y, Ohl B, Bogdanowicz K, Muszalska E (2020) Effects of Ni and Co on phase transformation and shape-memory effect of Ti–Pd–Zr Alloys. *Shape Mem Superelasticity* 6:170–180
43. Nahm S, Fibercast SM, Company V (2001) Use of dynamic mechanical analysis in thermoset resin development for composite applications. In: Composites convention and trade show
44. Tamareselvy K, Rueggeberg FA (1994) Dynamic mechanical analysis of two crosslinked copolymer systems. *Dent Mater* 10(5):290–297
45. Menard KP, Menard N (2006) Dynamic mechanical analysis. *Encycl Anal Chem Appl Theory Instrum* 15:1–25
46. Zhu H, Qin F, Chen H (2019) Retraction notice to Effect of ultrasonic temperature and output power on microstructure and mechanical properties of as-cast 6063 aluminum alloy:[*Journal of Alloys and Compounds* 777 (2019) 1025–1029]. *J Alloy Compd* 5(804):573
47. Ito T, Kimura Y, Xu X, Han K, Umetsu RY, Omori T, Kainuma R (2019) Martensitic transformation and shape-memory effect in Pd50Mn50– xGax alloys. *J Alloy Compd* 15(805):379–387

Chapter 3

Nitinol-Based Shape-Memory Alloys



Mukesh Kumar

3.1 General Background

In the recent past, nitinol-based thin-film alloys have played an important role in modern technology because of their functional properties. In order to use the nitinol in the fabrication of Micro-Electromechanical Systems (MEMSs), it is required to fabricate Ni–Ti alloy films of thickness below micron size. This condition can be easily achieved by using the magnetron sputter deposition technique [1]. Nitinol-based alloy films developed using the magnetron sputter technique are considered to be applied in the fabrication of micro-electromechanical devices. In addition, equiatomic Ni–Ti alloy is the most desirable for study to use in MEMS due to numerous reasons: its large resistance to deformations, large recovery strain, high recovery stress, biocompatibility, a high ratio of power to weight, decent mechanical property, excellent fatigue resistance, quite low driving voltage, and easy design. It has also been reported that Ni–Ti alloy film has the highest work density which is useful for the shape-memory effects [2]. However, the response time is not so fast in comparison to others, and this problem can be overcome by reducing the thickness below submicron size which allows small heat flow involved during cooling and heating. For these reasons, the demand for fabricating powerful micro-actuators which drive the MEMS device using the Ni–Ti thin films has been ever-increasing [2–6]. The Ni–Ti alloys can reversibly transform to its low-temperature crystallographic structure from its high-temperature crystallographic structure, that is to the monoclinic phase (B19, martensite) from the CsCl (B2, austenite), directly or through the intermediate rhombohedral phase (R-phase). And because of this austenite to martensitic transition, the Ni–Ti alloy films exhibit shape-memory behavior [7, 8]. To utilize the properties exhibited by shape-memory alloys, some factors need to be

M. Kumar (✉)

Department of Physics, Faculty of Science, Shree Guru Gobind Singh Tricentenary University
Gurgaon, Delhi-NCR 122505, Haryana, India

e-mail: mukesh.kumar@sgtuniversity.org

considered, for example, regulating Ni–Ti alloys composition and their heat treatment which helps in fabrication and processing. The most important feature of the martensitic transition is the start and finish temperatures which have been observed to be dependent on the processing techniques and composition of the Ni–Ti alloy films [9]. The working temperature of the micro-electromechanical devices is controlled by the composition of the Ni–Ti alloy films, since temperatures required for the phase transformation are sensitive to the ratio of Ti and Ni in the Ni–Ti alloy films. The variation in 1% of composition can result in a shift in transformation temperature of about 100 °C. In addition to governing the composition of Ni–Ti alloy films, other relevant parameters such as contamination of the Ni–Ti alloy films during processing due to the formation of oxides of titanium and compatibility with conventional designing processes of microdevices must be considered [10–12].

Additionally, the thin-film applications in the micro/nano-electromechanical systems (M/NEMS) have driven extensive research toward the processing-microstructure and characterization of Ni–Ti alloy thin films using different techniques. Though a number of techniques have been applied for the fabrication of Ni–Ti alloy films such as cathodic arc plasma ion plating, flash evaporation, sputtering, and laser ablation, in actual practice, the sputter deposition technique has got huge success in achieving the desired composition and microstructural properties [13, 14]. In sputtering, when the alloy target of Ni–Ti is used, then Ni-rich Ni–Ti alloy films have been formed in comparison to the sputtering of the individual targets due to the higher sputtering yield for Ni than Ti at the same power [14]. This problem can be avoided by placing pure Ti onto the target in the form of small pieces [15]. Otherwise, near-equiatomic Ni–Ti alloy films can be obtained using magnetron co-sputtering of a pure Ti target along with the Ti-enriched Ni–Ti alloy target or changing the sputter gas pressure inside the chamber [16, 17]. However, by varying the sputter gas pressure, it is difficult to regulate the composition of Ni–Ti alloy films because high gas pressures lead to poor microstructure and brittleness [18]. So, by regulating the individual target power ratio of Ti and Ni during magnetron co-sputtering, the Ni–Ti alloy film composition can be controlled. The most important advantage of the magnetron co-sputtering technique over other techniques is that its ability to produce alloy films with the desired composition using appropriate element target power [10, 19].

3.2 Ni–Ti Alloys' Phase Diagram

The Ni–Ti alloys' phase diagram had been provocative till the 1980s. The Ni–Ti alloys reveal numerous precipitates during their heat-treatment processes and there was no such phase diagram that helps to understand this process until the 1980s. Further, Massalski et al. [20] had proposed the phase diagram of Ni–Ti system which was able to explain this system quite well. The representative Ni–Ti alloy phase diagram is shown in Fig. 3.1.

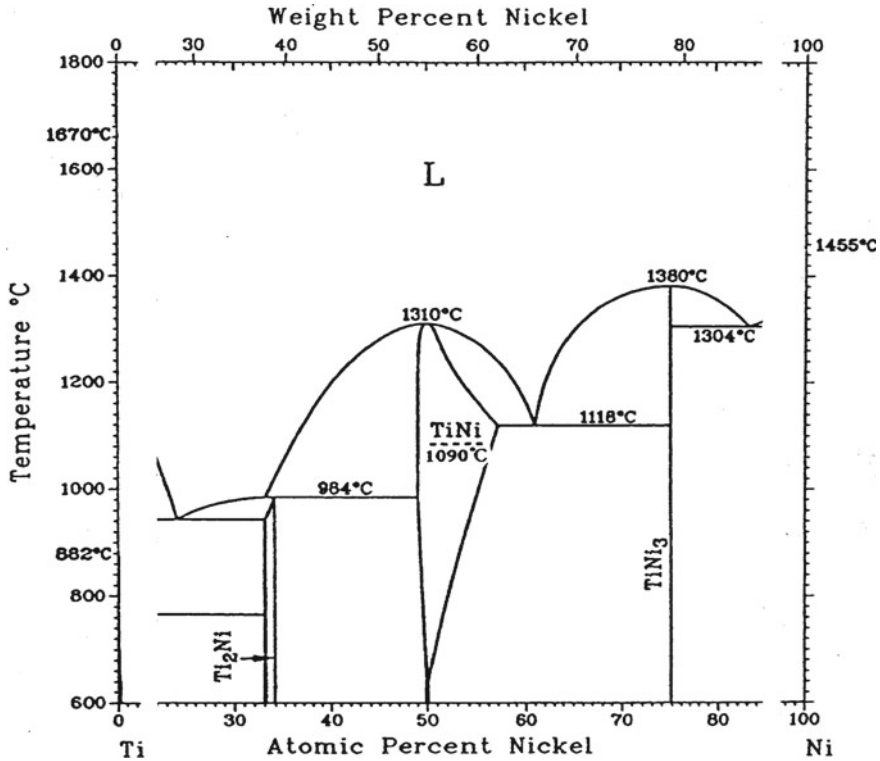


Fig. 3.1 Shows the Ni-Ti alloys' phase diagram. Reprinted from [7]. Copyright (1999) with permission from Elsevier Science S.A.

The importance of the Ni-Ti alloys phase diagram is because of their various heat-treatment processes and enhancement in their shape-memory properties. Laves and Wallbaum were the first to recognize the single-phase Ni-Ti alloy near the equiatomic composition at higher temperatures. The single-phase Ni-Ti has an ordered structure [B2 (CsCl) type] at room temperature which plays a crucial role in the martensitic phase transformation which is responsible for the shape-memory behavior in the Ni-Ti alloy system. On the Ti-rich side, Ti₂Ni phase is formed which is cubic. On the Ni-rich side, TiNi₃ phase is formed. On the nickel-rich side, the formation of Ti₃Ni₄, Ti₂Ni₃, and TiNi₃ has been reported, and over a period, there was confusion about whether a eutectoid reaction is occurring. The order-disorder transition temperature is at 1090 °C. The variation in atomic percentage should be kept close to the equiatomic composition for the excellent shape-memory properties since precipitates do not contribute to shape-memory behavior [21].

3.3 The Shape-Memory Effect in Nitinol (Ni–Ti Alloys)

Nitinol is one of the most significant shape-memory alloys [SMAs] having very good mechanical properties, excellent wear, and corrosion properties. The reasons for the shape-memory behavior in nitinol include not only martensitic phase transformation (which is diffusion less transformation) causes for shape-memory and pseudoelastic effects, but also diffusion transformations to improve shape-memory characteristics.

3.4 Ni–Ti Alloys Processed by Magnetron Sputtering

In many studies, it had been shown that the Ni–Ti film processed by magnetron co-sputter deposition was amorphous. The formation of amorphous film during the sputtering process might be due to the non-equilibrium conditions [22]. If there are more than three different kinds of elements with atomic size ratios above 12% and have the heat of mixing negative, then the glass will be formed by the constituent elements. This empirical rule for metals' ability to form glass was proposed by Inoue [23]. For the Ni–Ti alloy system, there are only two elements, Ni and Ti in place of three, but then again, the difference in atomic size is 19% (Ni atomic radius = 0.124 nm and Ti atomic radius = 0.147 nm), and the standard value of enthalpy of formation is -33.1 kJ/mol atom. Therefore, these reasons are proper to understand the amorphous nature of Ni–Ti alloy. Another explanation for the formation of amorphous Ni–Ti alloy film formed by sputter deposition technique given by Chu et al. [22] is that the higher temperature for the sputtered Ni–Ti atoms as compared to the substrate on which these atoms get deposited. Therefore, the substrate is at a lower temperature and behaves as a heat sink for the magnetron co-sputter-deposited Ni–Ti alloy atoms [24]. The lodging time required for the adatom to be in equilibrating with the depositing substrate has been predicted of the order of 10^{-12} s. The equivalent temperature for the adatom having energy 0.1 eV is equal to 1000 °C, and during deposition, the atoms are acquired at approximately 1015 °C/s of quenching rate [25]. The quenching rates for the sputter-deposited atoms are very much faster and have significantly high energy. Previous studies had shown the non-equilibrium atomic arrangements at high quenching rates which leads to amorphous microstructures in the developed films [26].

Ni–Ti alloys may be broadly categorized into equiatomic and near-equiatomic alloys (Ti–rich and Ni-rich alloys). For the bulk Ni–Ti alloy systems, on the Ni-rich side, the shape-memory properties can be improved by the Ti_3Ni_4 precipitates unless Ni content reaches nearly 50%. On the other hand, on the Ti–rich side, Ti_2Ni precipitates show poor shape-memory characteristics, because on the Ti–rich side, the solubility limit is almost vertical. However, for the crystallized Ni–Ti alloy films, this situation changes through a non-equilibrium amorphous state. At substrate temperature lower than 473 K, the as-deposited Ni–Ti films are amorphous in nature. Crystallization temperature depends upon the composition of the Ni–Ti films. For the

compositions Ti–51.1Ni and Ti–50.4Ni, crystallization temperature was observed at 756 K [21]. The heat-treatment temperature decides the grain size of crystallized Ni–Ti alloy films. The reported grain size ranges from 1 μm to 4 μm , which is significantly smaller than the grain size for bulk Ni–Ti alloys [21].

3.5 Ni-Rich Ni–Ti Thin Films

From the extensive researches in the past, it has already been established that magnetron co-sputter-deposited Ni–Ti alloy thin films exhibit very good mechanical properties due to their extremely fine grain size. The composition of Ni–Ti alloy films decides the phase transformation behavior is a function of temperature, as shown in Fig. 3.2. It shows very similar phase transformation behavior as the bulk Ni–Ti alloys. For the near-equiatomic Ni–Ti alloy films, the transformation behavior shown in Fig. 3.2a displays a single-stage $B2 \rightarrow B19'$ phase transformation, while for Ni-rich Ni–Ti alloy films, the phase transformation behavior shown in Fig. 3.2b displays two-stage $B2 \rightarrow R \rightarrow B19'$ phase transformation, because Ti_3Ni_4 precipitates suppress $B2 \rightarrow B19'$ transformation relative to $B2 \rightarrow R$ transformation alike bulk Ni–Ti alloys [27].

In more detail, the transformation behavior, which is a function of composition as well as the condition of heat treatment, is shown in Fig. 3.3. The phase transformation behavior, microstructures, and mechanical properties for Ni-rich Ti–Ni alloy thin films are the same as the bulk Ni–Ti alloys. In this alloy, the superelasticity, one-way shape-memory effect, and two-way shape-memory effect have been observed. All these properties of this alloy have been discussed in detail in the review paper by Otsuka et al. [21].

3.6 Ti-rich Ti–Ni Thin Films

For the Ti-rich side of the Ni–Ti alloy, Ti_2Ni precipitates appear only at grain boundaries because of the almost vertical solubility limit, as shown in Fig. 3.1. Therefore, in these alloy films, it is almost impossible to improve shape-memory properties by using precipitation. However, in such a case if alloys have been prepared through an amorphous state, then there is a possibility for uniform precipitation because amorphous Ni–Ti alloy film can supersaturate Ti atoms, and thereafter, excess Ti atoms may get precipitated upon crystallization. A detailed investigation on Ti-rich Ti–Ni alloy films is given below.

Nakata et al. [29], in 1995, observed a thin plate of Ti_2Ni precipitates surrounded by heavy strain contrast for the Ti-rich Ni–Ti alloys which is similar to GP-zones in Al–Cu alloy, obtained during heat treatment of the Ti51.5Ni48.5 alloy films for 600 s at 773 K. Similar results were observed by Zhang et al. [30] for the Ni–Ti

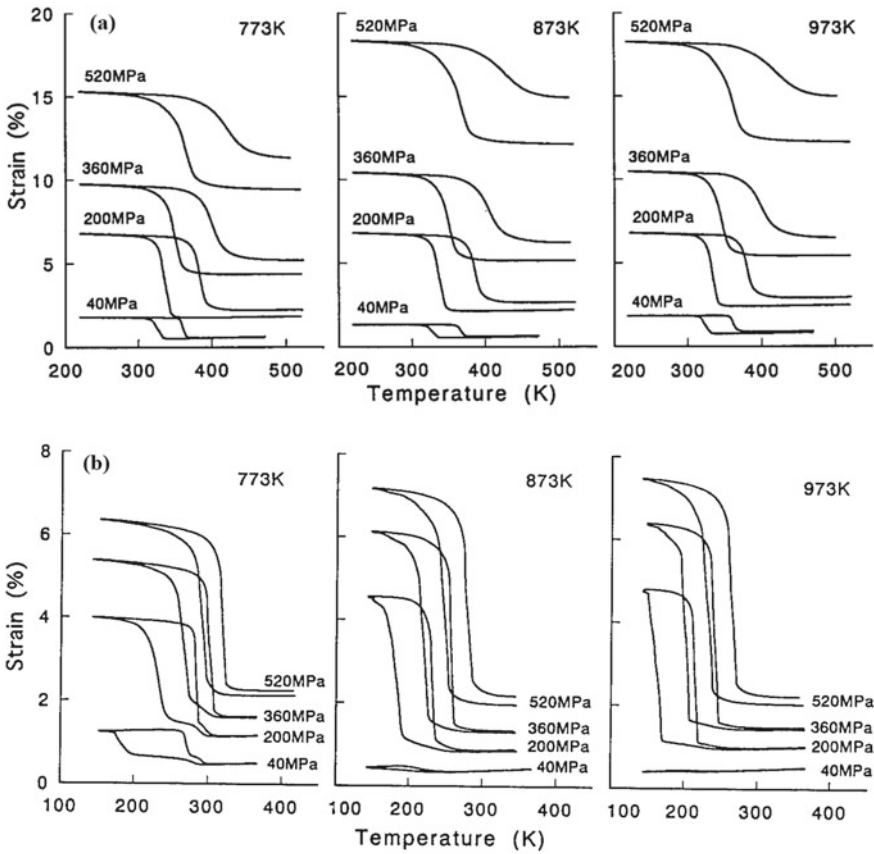


Fig. 3.2 Shows at constant stresses, the strain versus temperature curves of Ni–Ti alloy films: **a** Near-equiatomic Ni–Ti and **b** Ni-rich Ni–Ti alloys heat treated at 773, 873, and 973 K for 1 h. Further, Fig. 3.2a shows one-stage phase transformation for all the temperature, and (b) shows two-stage phase transformation at 773 K; on the other hand, it shows one-stage phase transformation for temperatures 873 and 973 K. Reprinted with permission from Springer Nature: The Materials Research Society Online Proceedings Library [28]. Copyright © 2021

alloy, as shown in Fig. 3.4. It was similar to GP-zones with a few atomic layers or monolayers in the B2 matrix.

In 1996, Kajiwara et al. [31] reported that for the heat-treated Ti_{51.8}Ni_{48.2} alloy film at 745 K, which is almost equal to crystallization temperature, similar thin plate precipitates appeared. The examination of these precipitates under high-resolution electron microscopy (HRTEM) revealed that the B2 matrix and Ti₂Ni precipitate lattice are continuous, which suggests the coherency of the precipitate. From the diffraction pattern, there has been also deduced body-centered tetragonal (BCT) structure of the precipitate due to the precipitation of excess Ti in Ni–Ti alloys on {100} B2 plane. Another work [30, 32] observed a similar structure for the

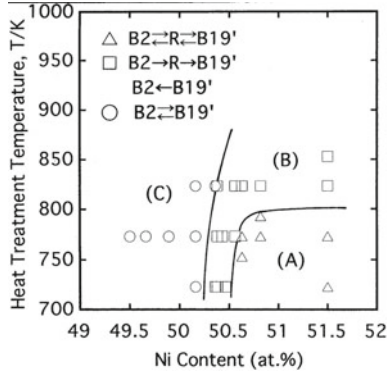


Fig. 3.3 Shows the variation in phase transformation behavior for Ni-rich and near-equiatomic Ni-Ti alloy thin films because of the variation in heat-treatment temperature. Reprinted from [8]. Copyright © (1999) with permission from Elsevier Science S.A.

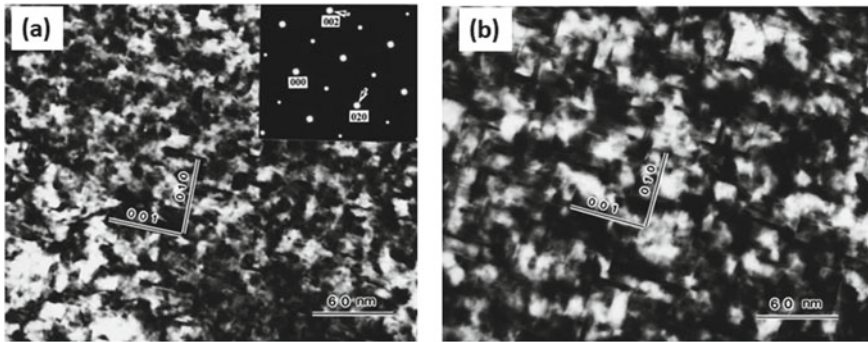
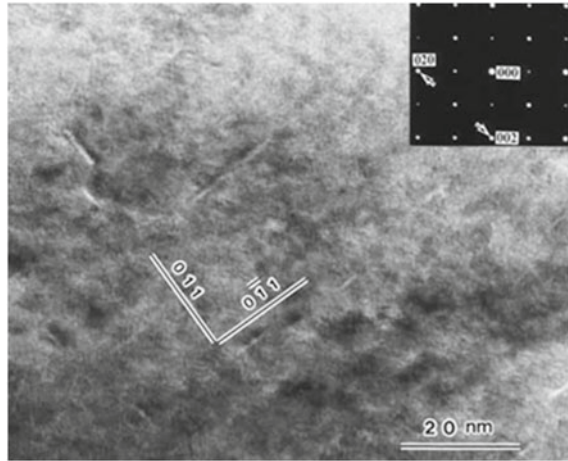


Fig. 3.4 High magnification images of GP-zones in the Ni-Ti alloy **a** annealed at 773 K for 30 min and **b** annealed at 823 K for 1 h. The inset represents corresponding diffraction pattern. Reprinted from [31]. Copyright © (2001) with permission from Acta Materialia Inc. Published by Elsevier Ltd.

precipitates by examining the bright contrast of the precipitate, as revealed in Fig. 3.5, because precipitates appear bright as compared to the matrix elements. There were also carried out simulations for the imaging of these thin precipitated plates built on the model of the the layers precipitates of excess Ti in Ni-Ti alloys on {100} B2 planes. Though, instead of bright contrast, only dark contrast was observed using this model. Only after the introduction of vacancies in addition to Ti atoms, bright contrast was obtained. Therefore, it was considered that about 20% Ti atoms in the thin plate of precipitates were substituted by vacancies. This is the vital difference between these two studies on the structure of precipitates. Since the distribution of precipitates is homogeneous, Kajiwara et al. [33] considered that Ti_2Ni precipitates appear only after the crystallization.

Fig. 3.5 Shows high-resolution TEM image of GP-zones for Ni–Ti alloy annealed at 773 K for 5 min (observed in martensite state). Reprinted from [30]. Copyright © (2001) with permission from Acta Materialia Inc. Published by Elsevier Ltd.



In this mechanism, it is presumed that the excess Ti atoms are somehow held within the matrix even after crystallization. Kajiwara et al. [33] also observed another morphology of the thin plate precipitate after the heat treatment of Ni–Ti alloy films at a lower temperature of about 50 K than the crystallization temperature. In this situation, most of the particles in the size range of 0.1–1 μm are associated with the crystallized films, and each particle consists of several nanocrystals of sizes varying from 20 to 40 nm. These nanocrystals are surrounded by the thin plate precipitates grown on $\{100\}$ B2 planes and have the same orientation in each particle. The following mechanism is considered for the formation of this microstructure. First, a nanocrystalline B2 structure is formed upon crystallization. Then excess Ti atoms present in the B2 matrix are pushed out in the amorphous region surrounding the nanocrystals and producing thin plates of precipitates on $\{100\}$ B2 planes. The above morphology is created on replication of this process. There has been also examined the mechanical properties of thin films of nitinol. It has been reported that the Ni–Ti alloy films with thin plate precipitates show great shape-memory behavior, as shown in Fig. 3.6. This also shows that without introducing plastic strain, there is a 5.5% recovery in the strain at 240 MPa stress. Likewise, Fig. 3.7a reveals that with decreasing heat-treatment temperature, the critical stress necessary for a slip in amorphous Ni–Ti alloy films increases rapidly, and it levels off at temperatures above 820 K. At this temperature (820 K), thin plate precipitates change to granular Ti₂Ni particles.

Figure 3.7b confirms that the recovery in strain is a function of heat-treatment temperature. This shows that at lower heat-treatment temperatures, the recovery in strain is larger. The increase of recovery in strain above 750 K is due to the high diffusion rate at a higher temperature. This means for the improvement in mechanical properties, the thin plate precipitates are more important.

In 1995, studies on the crystallization behavior of Ni–Ti shape-memory alloy started [29, 34], and in the B2 matrix, granular Ti₂Ni precipitates were observed

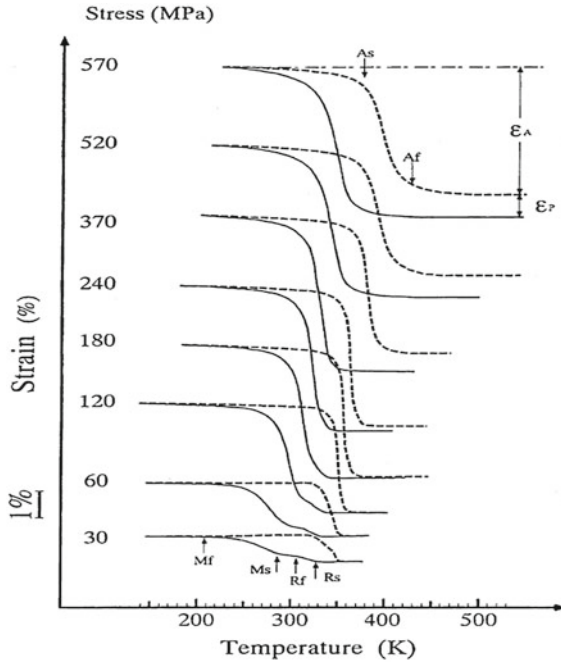


Fig. 3.6 Shows strain versus temperature plots for the heat-treated 51.8Ti-48.2Ni alloy film, at 745 K for one hour using constant stresses. Reprinted with permission from [31]. Copyright © 1996 Taylor & Francis Ltd.

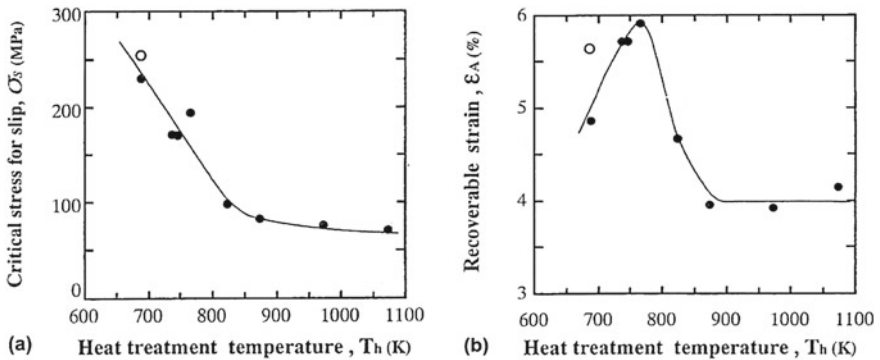


Fig. 3.7 **a** Shows the critical stress required for slip versus heat-treatment temperature plot, and **b** shows the recoverable strain versus heat-treatment temperature plot for the 51.8Ti-48.2Ni alloy thin films. Reprinted with permission from [31]. Copyright © 1996 Taylor & Francis Ltd.

above the critical temperature. In this condition, there were two classes of orientation relationships concerning the B2 matrix.

When excess Ti atoms percentage was lesser than about 53%, then granular Ti₂Ni precipitates had a definite orientation relationship with the B2 matrix. Ishida et al. [35] were the first to determine the orientation relationship as $004\text{Ti}_2\text{Ni} \parallel 001\text{B}_2; 040\text{Ti}_2\text{Ni} \parallel 010\text{B}_2$; that is, the crystal axes of Ti₂Ni precipitates and the B2 matrix are parallel to each other. However, when excess Ti atoms percentage was more than 53%, then granular Ti₂Ni precipitates were formed first, and then crystallization happened. Therefore, B2 matrix and granular Ti₂Ni precipitates had no specific orientation relationship. In detail, the relation between heat-treating condition, composition, and microstructures is shown in Figs. 3.8 and 3.9 which was first made by Kawamura et al. [36] and later modified by Ishida [9].

In Fig. 3.8, where Ti atoms percentage was lower than 53%, granular morphology of Ti₂Ni is developed in place of thin plate morphology along with the increase in heat-treatment temperature, but then again there is a region where granular morphology and thin plate morphology coexist (indicated by a symbol Δ) in between.

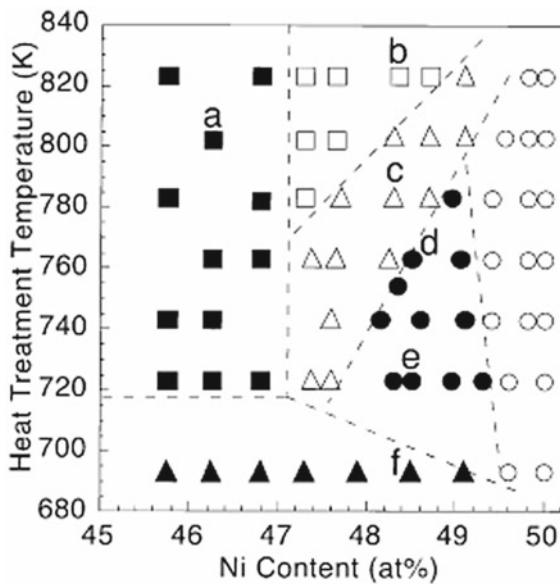


Fig. 3.8 **a** Solid squares (■) represent granular Ti₂Ni precipitates having a random orientation concerning B2 matrix; **b** open squares (□) represent granular Ti₂Ni precipitates having the same orientation concerning B2 matrix; **c** open triangles (Δ) represent thin plate precipitates and Ti₂Ni precipitates; **d** solid circles (●) represent thin plate precipitates grown at higher temperature and **e** thin plate precipitates grown at a lower temperature; **f** open circles (○) represent no precipitates; and solid triangles (▲) represent amorphous Ni–Ti film and, for Ti–rich Ni–Ti alloy, thin films heat treated at different temperatures for 1 h. The above-mentioned alphabets **a–f** also belong to the text figure of Fig. 3.9. Reprinted with permission from Springer Nature: The Materials Research Society: MRS Bulletin [9]. Copyright © 2002

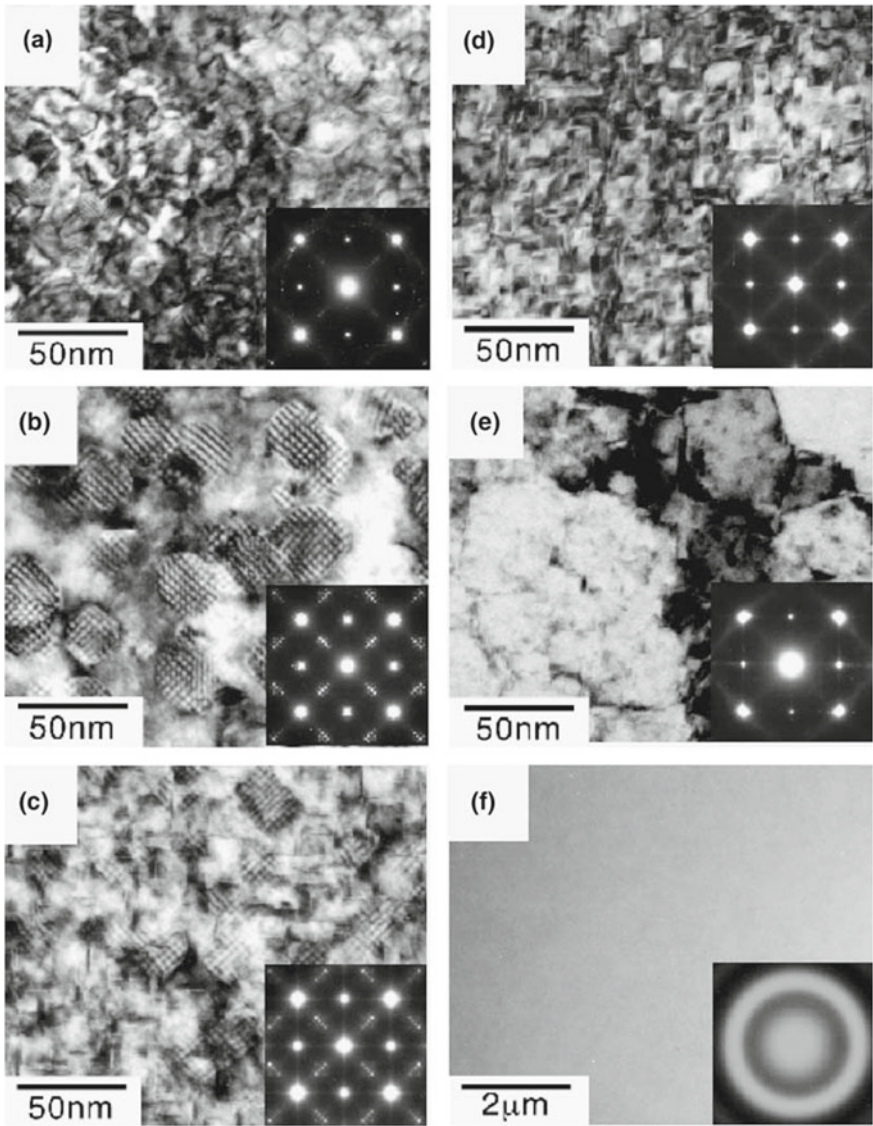


Fig. 3.9 Shows bright-field TEM micrographs of Ni-Ti alloys with various compositions and heat treatment and the corresponding electron diffraction patterns shown as insets. The alphabets **a-f** correspond to those in the previous Fig. 3.8. Reprinted with permission from Springer Nature: The Materials Research Society: MRS Bulletin [9]. Copyright © 2002

The network alike patterns along $\langle 110 \rangle$ directions were observed for the Ni–Ti alloys by Otsuka et al. [21], as shown in Fig. 3.9b, c. These images are of B2 matrix and granular Ti_2Ni . They also noticed that there were two different morphologies in the G.P. zone region, as shown in Fig. 3.9d, e. These images represent the morphologies that are related to thin plate precipitates heat treated at a temperature closer to crystallization temperature and lower than crystallization temperature, respectively. Near equiatomic Ni–Ti alloy films, there were no precipitates. Moreover, Ti-rich Ni–Ti alloy thin films show superelasticity [37], two-stage phase transformation via R-phase as well as two-way shape-memory effect [38], as shown in Fig. 3.6. In these alloy films, the phase transformation temperatures are greater than the Ni-rich Ni–Ti alloy films, because the martensitic transformation temperature of Ni–Ti alloy films has a propensity to decrease with increasing Ni content in Ni-rich Ni–Ti alloy, whereas it is almost constant for the Ti-rich Ni–Ti alloy [39].

Besides the Ni–Ti binary alloy, the examination of ternary shape-memory alloy is also interesting. Among these, Ni–Ti–Cu, Ni–Ti–Pd, and Ni–Ti–Hf ternary alloy are the most promising for the shape-memory behaviors [40]. The Ni–Ti–Cu ternary alloy thin films are quite fascinating for the design of actuators with small temperature hysteresis. However, Ni–Ti–Pd and Ni–Ti–Hf ternary alloy thin films are promising for the high-temperature shape-memory behavior.

3.7 Influence of Various Processing Parameters Related to Magnetron Sputtering on Film Quality

Relevant parameters which affect the microstructure and properties of the Ni–Ti alloy thin films are as follows:

- (1) Target power.
- (2) Substrate–target distance.
- (3) Substrate temperature.
- (4) Substrate rotation.
- (5) Substrate bias.
- (6) Ar gas pressure.
- (7) Deposition geometry.

- (1) **Target Power:** As the target power increases, a greater number of atoms will be ejected because Ar ions will strike the target with more energy thus increasing the deposition rate [41]. The sputtering rate is known to scale with the applied target power [42, 43]. It has been shown that the sputtering rate is related to the target power through the following relation [44]:

$$\left(\frac{dN}{dt}\right) = AYI/e \quad (3.1)$$

where N is the number of sputtered atoms, A is the area of the target, Y is the sputtering yield, I is the ion current, and e is the electronic charge. If the power is kept constant, then if there is an increase in the sputtering gas pressure, there is an increase in ion density. For low target power, the use of high pressure leads to lowering of the kinetic energy of the sputtered atoms because of the increased number of inelastic collisions with sputtering gas ions.

- (2) **Substrate–Target Distance:** Substrate–Target distance (STD) is a crucial parameter influencing the deposition rate, and this has been well investigated by Wuhler et al. [45]. If the value of STD is increased, the sputtered atoms have to travel more before reaching the substrate. During their travel, the atoms are easily scattered by collision with gas ions in the chamber, and therefore, the mean free path becomes shorter. As a result, only fewer atoms can reach the substrate. The deposition rate (R) is related to the prominent sputtering parameters by the following relation [46]:

$$R = k \cdot P / \rho \cdot (\text{STD}) \quad (3.2)$$

where P is the target power, ρ is gas pressure, and k is the proportionality constant which depends on the target materials and the type of the gas used for sputtering.

- (3) **Substrate Temperature:** From the phase diagram of the Ni–Ti alloys, it is clear that the Ni–Ti alloy is stable above the temperature $T_e \approx 630$ °C. Therefore, the Ni–Ti alloy thin films deposited at room temperature are unstructured but after the post-annealing above T_e , the films' nature becomes crystalline. The crystalline Ni–Ti alloy films can also be grown by using in situ heating of the substrates at a relatively higher temperature. It has been observed that the 300–450 °C substrate temperature is sufficient to get crystalline Ni–Ti alloy films with fantastic shape–memory properties [10, 47].
- (4) **Substrate Rotation:** Krulevitch et al. [11] observed that the magnetron sputtering technique for the deposition of Ni–Ti–Cu alloy films from Cu, Ti, and Ni targets with zero substrate rotation speed leads to a significant change in composition. In the absence of substrate rotation, the composition variation across the Ni–Ti-deposited substrate, where the target power of Ti was around three times more than the target power of Ni to maintain the same deposition rate of Ti and Ni, is shown in Fig. 3.10a. However, compositional uniformity was easily obtained for the Ni–Ti alloy films using substrate rotation. The variation in composition for the Ti–rich Ni–Ti films, near-equiatom Ni–Ti films, and Ni-rich Ni–Ti films is shown in Fig. 3.10b [12].
- (5) **Substrate Bias:** Substrate bias is the most effective parameter related to magnetron sputtering which was used for the formation of equiaxed grains in a microstructure whereas films formed without bias were mostly columnar as observed and nicely explained by R. Mitra et al. [48]. For the columnar microstructure, because of intercolumnar porosity, the density is expected to be lower, as shown in Fig. 3.11a, b, and hence in the transverse direction,

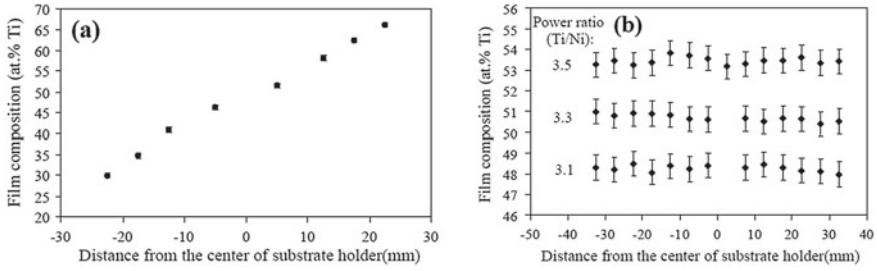


Fig. 3.10 Shows the variation in composition across the substrate **a** without substrate rotation and **b** with substrate rotation for the three different ratios of target power. Reprinted from [12] Copyright © (2005) with permission from Elsevier B.V.

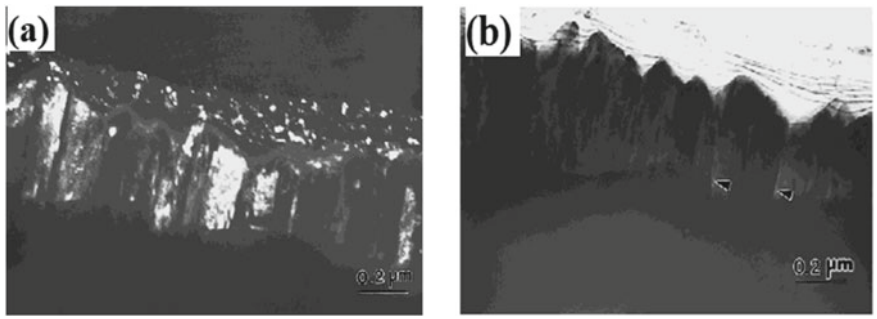


Fig. 3.11 Shows the TEM images of Ni film developed at room temperature in the absence of substrate bias: **a** dark-field image reveals equiaxed grains on the top and columnar grains below, and **b** bright-field image reveals the presence of columnar porosities as indicated by arrows. Reprinted with permission from Springer Nature: The Materials Research Society: Journal of Materials Research [48]. Copyright © 2001

the mechanical properties will be worse. Negative substrate bias increases the momentum of the sputter gas ions striking the growing films which break the columnar structure rising from the islands on the substrate by hitting the atoms into their nearest valleys. But at the same time, it leads to a higher rate of re-sputtering of atoms from the growing film which may cause a rough filmsurface.

- (6) **Ar Gas Pressure:** The Ar gas pressure generally controls the energies of the depositing atoms and therefore affects the microstructure, film density, and stress developed in the films. At low Ar gas pressures, the microstructure is denser with lesser defects, while at higher Ar gas pressures, the deposited films show microstructural defects and lower density. Sohrab et al. [12] observed that films having a range of compositions, grown at Ar gas pressures greater than one pascal (Pa), had cracks on the surface with brittle microstructure, as shown in Fig. 3.12a which reveals the wide delamination at the Ni–Ti/Si interface and cracks on the surface because of the tensile residual stress. Films prepared at

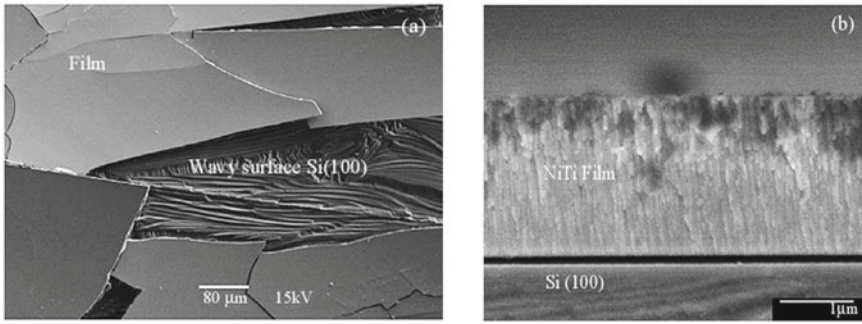


Fig. 3.12 **a** Shows SEM plan view micrograph of Ni–Ti/Si films deposited at 1.2 Pa Ar gas pressures, and **b** illustrates the FESEM cross-sectional micrograph of Ni–Ti/Si film developed at Ar gas pressure of 0.6 Pa. Reprinted from [12]. Copyright © (2005) with permission from Elsevier B.V.

low Ar gas pressures with the same composition showed a relatively smoother surface with featureless structure, as shown in Fig. 3.12b.

Chu et al. [22] also reported the effect of Ar gas pressure on the microstructure of the sputter-deposited film. The films grown at Ar gas pressures higher than 7mTorr showed a well-defined cluster of columnar microstructures, as shown in Fig. 3.13a, b. However, the film prepared below 0.5 mTorr argon gas pressures reveals a dense microstructure, as shown in Fig. 3.13c. The columnar microstructures are responsible for the relatively larger grain size because of the inadequate mobility of the depositing atoms. The main reason for the columnar microstructures is the high argon gas pressure which leads to a decrease in the energy of atoms released from the target by sputtering leads to a decrease in adatoms mobility which eventually develops the columnar microstructure [49]. Moreover, at high gas pressures, argon atoms that are absorbed on the growing film surface could restrict the motion of depositing atoms which results in a columnar microstructure in the grown films [50]. Sohrab et al. [12] investigated Ni–Ti thin films deposited at high gas pressure for the shape-memory applications; despite controlling the composition, the Ni–Ti films showed poor shape-memory properties. Whereas the Ni–Ti films processed at relatively lower Ar

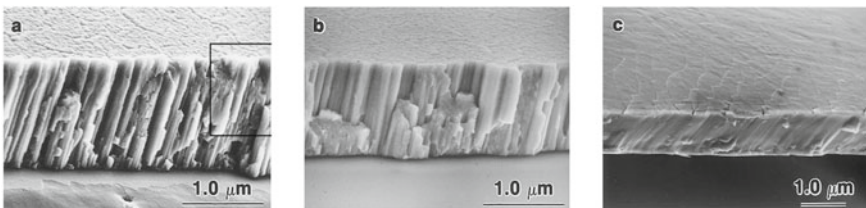


Fig. 3.13 Shows the cross-sectional SEM images of Ni–Ti alloy films processed at room temperature for constant time with Ar gas pressures of **a** 10 m Torr, **b** 7 m Torr, and **c** 0.5 Torr. Reprinted from [22]. Copyright © (2000) with permission from Elsevier Science S.A.

gas pressures preferably showed better shape-memory effects. In addition to that, the films deposited at high gas pressures showed poor film microstructure which affects phase transformation behaviors. The annealing temperature also affects the shape-memory behavior of the Ni–Ti films.

- (7) **Deposition Geometry:** The appropriate deposition geometry also controls the composition uniformity. The substrate–target distance, size, and shape of targets and inclining the axes of the targets are included in deposition geometry [50].

3.8 Surface Topography of Sputter-Deposited Films

Surface topography plays an important role to impart a good functional characteristic to thin films. Extensive work on the surface topography of Ni thin films grown at room temperature and liquid nitrogen temperature by applying various substrate biasing conditions was carried out by Mitra et al. [48], as shown in Fig. 3.14a, b, c. It shows 2.0- μm -thick Ni films developed at room temperature at a negative substrate bias voltage of 0 V, -150 V, and -200 V, respectively. From Fig. 3.14, it is clear that the Ni film deposited at zero substrate bias voltage is having extra surface porosity as compared to the Ni films deposited at relatively higher negative substrate bias. The Ni films deposited by applying 0 V and 200 V substrate bias voltages reveal a rough surface morphology. The roughness and porosities in the Ni film deposited at 0 V substrate bias voltage, as shown in Fig. 3.14a, are mainly because of the columnar and tapered grains. Figure 3.11b reveals the intercolumnar or grain boundary voids with larger surface porosities. These grain boundary voids are generated during the time of nucleation of islands that are also prevented by intergrain shadowing effects which cause tapered crystallites with the columnar grain morphology. Therefore, the intergrain boundaries are not true grain boundaries because of the presence of voids.

If the vacancies trapped in the grain boundaries have considerable mobility and coalesce, then the pores grow faster. The nanopores present at grain boundaries were also examined by TEM during the investigation of Ni films processed without a

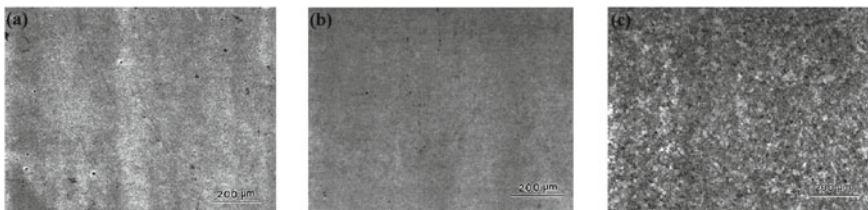


Fig. 3.14 Shows optical micrographs of Ni films deposited at room temperature and 200 W target power with a negative substrate bias voltage of **a** 0 V, **b** -150 V, and **c** -200 V. Reprinted with permission from Springer Nature: The Materials Research Society: Journal of Materials Research [48]. Copyright © 2001

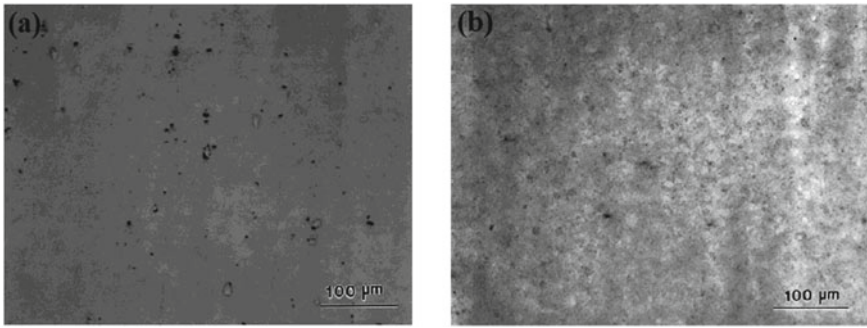


Fig. 3.15 Shows optical micrographs of the Ni films deposited at liquid nitrogen temperature using substrate bias voltage of **a** 0 V and **b** -150 V. Reprinted with permission from Springer Nature: The Materials Research Society: Journal of Materials Research [48]. Copyright © 2001

substrate bias voltage. By application of an intermediate substrate bias voltage, the entrapment of argon atoms is reduced because of the re-sputtering phenomenon that occurs due to argon ions bombardments. But at higher substrate bias argon entrapment is more, and a higher degree of re-sputtering causes a large concentration of points defects.

The surface morphology of Ni films grown at the temperature of liquid nitrogen has shown more surface porosity as compared to Ni films grown at room temperature. These things can be described by the inadequate mobility of the atoms on the growing film at a lower temperature. The sticking problem for the argon atoms reflected toward the growing film from the target materials would be more prominent while cooling the film growing substrate by liquid nitrogen as compared to room temperature. Whereas, during heating the substrate, the entrapped argon gas atom would escape from the surface and leave behind the pores.

The optical images of 2.0-mm-thick Ni films processed using negative substrate bias of 0 V and -150 V, at liquid nitrogen temperature, are shown in Fig. 3.15. From Fig. 3.15a, it is noticeable that Ni film surface deposited at 0 V substrate bias is very porous with larger pores size. On the other side, the Ni film surface deposited at -150 V substrate bias discloses fewer pores as compared to the Ni films deposited at 0 V substrate bias, as shown in Fig. 3.15b. It has been also examined that the Ni films grown at -150 V substrate bias (Fig. 3.15b) have a smoother surface relative to the Ni film deposited at 0 V substrate bias. Furthermore, the increase in negative substrate bias above -150 V leads to an increase in surface roughness of the deposited Ni film at room temperature as well as at liquid nitrogen temperature [48].

Moreover, it was reported that for the thick film deposited at -200 V substrate bias voltage, the surface roughness was quite high. The film surface roughness also increased with increasing film thickness due to the continued ion bombardment on the depositing surfaces [43].

3.9 Micro-Actuator

The micromachines such as micromanipulators and fluid microvalves with electronic behavior are pretty important and have important roles in different technologies and the design of various devices such as micromechanical devices, biotechnology, medicine industry, the semiconductor industry, precision optical devices, and automation technology. The nitinol (Ni–Ti alloys)-based Shape-Memory Alloy (SMA) films processed using sputter sputtering technique have potential applications in the making of micro/nano-electromechanical systems (M/NEMSs) and Bio-micro/nano-electromechanical systems-based microactuators (e.g., micro-positioners, microfluid pumps, microgrippers, and micro-wrapper), cantilevers, and stent for neurovascular blood vessels [18].

Nitinol-based shape-memory alloys are also considered as an essential material for generating actuation in M/NEMS-based devices, where periodic operation and large force/stroke have been required. This can be used in extreme environmental conditions, for example, biological, corrosive, and radioactive conditions. Therefore, the design of M/NEMS is a multi-disciplinary approach for their potential applications. Generally, the common microactuators, for example, microswitches and microsensors utilize shape-memory alloy (SMA) films for their inherent two-way shape-memory effect (TWSME) through a higher displacement, and homogenous composition among the film thickness. There may be variations in composition along with film thickness [51, 52]. The nitinol-based thin-film actuators can offer a quite large actuation force though foregoing their strain. With the help of suitable biasing force, the substrate of nitinol-based thin films can be activated and a mechanical TWSME with a relatively small actuation force is generated [53–55]. The two-way shape-memory effect (TWSME) can be realized in (1) entity of R-phase, (2) ability of aging and hot shaping, (3) their intrinsic residual stress, and (4) generation of the mechanical energy and displacement all through the phase transformation. The deformation in nitinol-based SMA actuators is generated because of the cooling and heating cycles which are the two most important parameters for the formation of SMA actuators [56, 57]. Nitinol-based SMA used in bimorph actuators provides a relatively much higher actuation force at a lower temperature which is essential to influence the fully actuated state that is austenitic phase as compared to other shape-memory alloy (SMA) materials [58]. The systematic design and development of nitinol-based micromanipulator developed using two bimorph micro-actuators together and its proposed application in handling small objects are shown in Figs. 3.16 and 3.17, respectively [59].

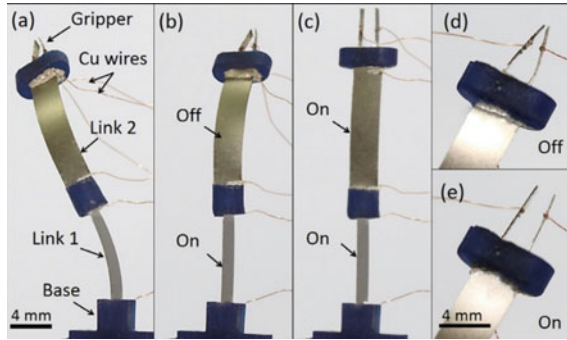


Fig. 3.16 Shows the advanced micromanipulator's state: **a** off-state, **b** first link in actuated state, **c** both links in actuated state, **d** the gripper without actuation, and **e** the gripper with actuation. Reprinted from [59] Copyright © (2016) with permission from Elsevier Ltd.

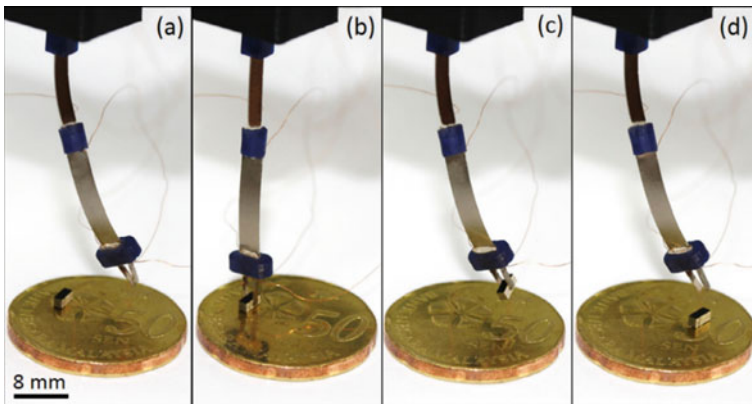


Fig. 3.17 Shows the advanced micromanipulator application in handling small objects. Reprinted from [59] Copyright © (2016) with permission from Elsevier Ltd.

3.10 Conclusions

This book chapter comprises a study of nitinol-based shape-memory alloys with emphasis on the processing of these alloys by the physical vapor deposition technique. Based on the focus of the present work, the topic of magnetron sputtering has been dealt with in detail. The studies deal with the effect of magnetron sputter-related parameters on the structure and properties of Ni-rich and Ti-rich Ni-Ti alloys. This chapter indicates that the effect of process parameters on growth rate as well as structure and properties of the Ni-Ti alloys needs further study. Furthermore, an overview of the nitinol (Ni-Ti alloys)-based shape-memory alloys (SMAs) processed using the sputtering technique in the making of micro/nano-electromechanical systems has been presented.

References

1. Cho H, Kim HY, Miyazaki S (2005) Fabrication and characterization of Ti–Ni shape-memory thin film using Ti/Ni multilayer technique. *Sci Technol Adv Mater* 6:678–683
2. Hae-Yong NOH, Kwang-Koo JEE, Kyu-Hwan LEE, Young-Kook LEE (2006) Electron beam deposition and characterization of thin film Ti–Ni for shape-memory applications. *Rare Metals* 25:237–242
3. Mahtabi MJ (2016) NimaShamsaei, Multiaxial fatigue modeling for Nitinol shape-memory alloys under in-phase loading. *J Mech Behav Biomed Mater* 55:236–249
4. Kannan TDB, Sathiyaa P, Ramesh T (2017) Experimental investigation and characterization of laser welded NiTiNol shape-memory alloys. *J Manuf Process* 25:253–261
5. Mani Prabhu SS, Madhu HC, Perugu CS, Akash K, Mithun R, Ajay Kumar P, Kailas SV, Anbarasu M, Palani IA (2019) Shape-memory effect, temperature distribution and mechanical properties of friction stir welded nitinol. *J Alloys Compd* 776:334–345
6. Bhardwaj A, Gupta AK, Padisala SK, Poluri K (2019) Characterization of mechanical and microstructural properties of constrained groove pressed nitinol shape-memory alloy for biomedical applications. *Mat Sci Eng A* 102:730–742
7. Otsuka K, Ren X (1999) Martensitic transformations in nonferrous shape-memory alloys. *Mat Sci Eng A* 273–275:89–105
8. Gyobu A, Kawamura Y, Horikawa H, Saburi T (1999) Martensitic transformation and two-way shape-memory effect of sputter-deposited Ni-rich Ti–Ni alloy films. *Mat Sci Eng A* 273–275:749–753
9. Ishida A, Martynov V (2002) Sputter-deposited shape-memory alloy thin films: properties and applications. *MRS Bull* 27:111–114
10. Arranz MA, Riveiro JM (2005) Shape-memory effect in sputtered Ti–Ni thin films. *J.M.M.M.* 290–291, 865–867
11. Krulevitch P, Ramsey PB, Makowiecki DM, Lee AP, Northrup MA, Johnson GC (1996) Mixed-sputter deposition of Ni–Ti–Cu shape-memory films. *Thin Solid Films* 274:101–105
12. Sanjabi S, Sadmezhaad SK, Yates KA, Barber ZH (2005) Growth and characterization of Ti_xNi_{1-x} shape-memory thin films using simultaneous sputter deposition from separate elemental targets. *Thin Solid Films* 491:190–196
13. Walker JA, Gabriel KJ, Mehregany M (1990) Thin-film Processing of TiNi Shape-Memory Alloy. *Sens Actuators A*. 23:243–246
14. Grummon DS, Hou L, Zhao Z, Pence TJ (1995) Progress on sputter-deposited thermoactive titanium-nickel films. *J de Phys* 5:665–670
15. Miyazaki S, Ishida A (1999) Martensitic transformation and shape-memory behavior in sputter-deposited TiNi-base thin films. *Mater Sci Eng A Struct Mater Prop Microstruct Process* 273–275, 106–133
16. Shih CL, Lai BK, Kahn H, Philips SM, Heuer AH (2001) A robust co-sputtering fabrication procedure for TiNi shape-memory alloys for MEMS. *J MEMS* 10:69–79
17. Quandt E, Halene C, Holleck H, Feit K, Kohl M, Schlomacher P, Skokan A (1996) Sputter deposition of TiNi, TiNiPd and TiPd films displaying the two-way shape-memory effect. *Sens Actuators A Phys* 53:434
18. Ishida A, Takei A, Miyazaki S (1993) Shape-memory thin film of Ti–Ni formed by sputtering. *Thin Solid Films* 228:210–214
19. Freund LB, Suresh S (2003) Thin film materials-stress, defect formation and surface evolution. Cambridge University Press, p 260
20. Massalski TB, Okamoto H, Subramanian PR, Kacprzak L (1990) Binary alloy phase diagrams, 2nd edn, vol 3. ASM International, Materials Park, OH, pp 2874
21. Otsuka K, Ren X (2005) Physical metallurgy of Ti–Ni-based shape-memory alloys. *Prog Mater Sci* 50:511–678
22. Chu JP, Lai YW, Lin TN, Wang SF (2000) Deposition and characterization of TiNi-base thin films by sputtering. *Mat Sci Eng A*. 277:11–17

23. Inoue A (2000) Stabilization of metallic supercooled liquid and bulk amorphous alloys. *Acta Mater* 48:279–306
24. Miyazaki S, Nomura K (1994) Development of perfect shape-memory effect in sputter-deposited Ti–Ni thin films. In: *Proceedings of IEEE micro electro mechanical systems (MEMS-94)*. Oiso, Japan, pp 176–181
25. Shin SM, Ray MA, Rigsbee JM, Greene JE (1983) Growth of metastable $\text{Cu}_{1-x}\text{Cr}_x$ solid solutions by ion mixing during bias-sputter deposition. *Appl Phys Lett* 43:249–251
26. Ho KK, Mohanchandra KP, Carman GP (2002) Examination of the sputtering profile of NiTi under target heating conditions. *Thin Solid Films* 413:1–7
27. Miyazaki S, Ishida A (1999) Microstructure and mechanical properties of sputter-deposited Ti–Ni alloy thin films. *Mater Sci Eng A* 273–275:106–133
28. Ishida A, Takei A, Sato M, Miyazaki S (1995) Shape-memory behavior of Ti–Ni thin films annealed at various temperatures. *MRS Symp* 360:381–386
29. Nakata Y, Tadaki T, Sakamoto H, Tanaka A, Shimizu K (1995) Effect of heat treatments on morphology and transformation temperatures of sputtered Ti–Ni thin films. *J Phys IV C8:671–677*
30. Zhang JX, Sato M, Ishida A (2001) Structure of martensite in sputter-deposited thin films containing GP-zones. *Acta Mater* 49:3001–3010
31. Kajiwara S, Kikuchi T, Ogawa K, Matsunaga T, Miyazaki S (1996) Strengthening of Ti–Ni shape-memory films by coherent subnanometric plate precipitates. *Philos Mag Lett* 74:137–144
32. Nakata Y, Tadaki T, Hirotsu Y, Sakamoto H, Tanaka A, Shimizu K (1999) High resolution observation of Guinier-Preston zones in sputter-deposited Ti-rich Ti–Ni thin films. In: *Proceedings of an international conference on solid phase transformations 99 (JIMIC-3)*. Japan Institute of Metals, pp 1088–1091
33. Kajiwara S, Ogawa K, Kikuchi T, Matsunaga T, Miyazaki S (1996) Formation of nanocrystals with an identical orientation in sputter-deposited Ti–Ni thin films. *Philos Mag Lett* 74:395–404
34. Kawamura Y, Gyobu A, Horikawa H, Saburi T (1995) Martensitic transformations and shape-memory effect in Ti–Ni sputter-deposited thin films. *J Phys IV C8:683–688*
35. Ishida A, Sato M, Takei A, Miyazaki S (1995) Effect of heat treatment on shape-memory behavior of Ti-rich Ti–Ni thin films. *Mater Trans JIM* 36:1349–1355
36. Kawamura Y, Gyobu A, Saburi T, Asai M (2000) Structure of sputter-deposited Ti-rich Ti–Ni alloy films. *Mater Sci Forum* 327–328:303–306
37. Ishida A, Takei A, Sato M, Miyazaki S (1996) Stress-strain curves of sputtered thin films of TiNi. *Thin Solid Films* 281–282:337–339
38. Gyobu A, Kawamura Y, Saburi T, Asai M (2000) Martensitic transformation and two-way shape-memory effect of sputter-deposited Ti-Rich Ti–Ni alloy films. *J Jpn Inst Met* 63:438–443
39. Gyobu A, Kawamura Y, Horikawa H, Saburi T (1996) Martensitic transformations in sputterdeposited shape-memory Ti–Ni films. *Mater Trans JIM* 37:697–702
40. Hashinaga T, Miyazaki S, Ueki T, Horikawa H (1995) Transformation and deformation behaviour in sputter-deposited Ti–Ni–Cu thin films. *J Phys IV C8:689–694*
41. Lehnert T, Grimer H, Boni P, Horisberger M, Gotthart R (2000) Characterization of shape-memory alloy thin films made up from sputter-deposited Ni/Ti multilayers. *Acta mater* 48:4069–4071
42. Chopra KL (1969) *Thin film phenomena*. McGraw Hill, New York
43. Ohring M (1991) *Materials science of thin films: deposition and structure*. Academic press, San Diego
44. Farooq M, Lee ZH (2002) Optimization of the sputtering process for depositing composite thin films. *J Korean Phys Soc* 40:511–515
45. Wuhrer R, Yeung WY (2003) Effect of target–substrate working distance on magnetron sputter deposition of nanostructured titanium aluminium nitride coatings. *Scr Mater* 49:199–205
46. Zendeenam A, Ghanati M, Mirzaei M (2007) Study and comparison of deposition rates, grain size of Ag and Cu thin films with respect to sputtering parameters, and annealing temperature. *J Phys: Conf Ser* 61:1322–1325

47. Li YH, Li LM, Meng FL, Zheng WT, Zhao J, Wang YM (2006) Effect of substrate temperature on the surface and interface oxidation of NiTi thin films. *J Electron Spectros Relat Phenomena* 151:146–148
48. Mitra R, Hoffman RA, Madan A, Weertman JR (2001) Effect of process variables on the structure, residual stress, and hardness of sputtered nanocrystalline nickel films. *J Mater Res* 16:1010–1027
49. Gadieu FJ, Chencinski N (1975) Selective thermalization in sputtering to produce high Tc films. *IEEE Trans Magn* 11:227–230
50. Wu SK, Chen YS, Chen JZ (2000) Composition control of r.f.-sputtered Ti₅₀Ni₄₀Cu₁₀ thin films using optical emission spectroscopy. *Thin Solid Films* 365:61–66
51. Psakhie S, Meisner S, Lotkov A, Meisner L, Tverdokhlebova A (2014) Effect of surface alloying by silicon on the corrosion resistance and biocompatibility of the binary NiTi. *J Mat Eng Perform* 23:2620–2629
52. Scoggin D, Wilson C (2008) Shape-memory alloys and their use in mems capable deployable sensors. In: 17th Biennial University/Government/Industry Micro/Nano Symposium
53. Gill JJ, Ho K, Carman GP (2002) Three-dimensional thin-film shape-memory alloy microactuator with two-way effect. *Microelectromechan. Sys.* 11:68–77
54. Gyobu A, Kawamura Y, Saburi T, Asai M (2001) Two-way shape-memory effect of sputter-deposited Ti-rich Ti-Ni alloy films. *Mat Sci Eng A* 312:227–231
55. Quandt E, Halene C, Holleck H, Feit K, Kohl M, Schlomacherl P, Skokan A, Skrobanck K (1996) Sputter deposition of TiNi, TiNiPd and TiPd films displaying the two-way shape-memory effect. *Sens Actuators A. Phys* 53:434–439
56. Elahinia E (2015) Shape-memory alloy actuators: design, fabrication and experimental evaluation. Wiley, New York
57. Wheeler RW, Hartl DJ, Chemisky Y, Lagoudas DC (2015) Modeling of thermo-mechanical fatigue and damage in shape-memory alloy axial actuators, SPIE smart structures and materials+ nondestructive evaluation and health monitoring. *Int Soc Opt Photonics* 94320K-94320K-10
58. Lott CD, McLain TW, Harb JN, Howell LL (2002) Modeling the thermal behavior of a surface-micromachined linear-displacement thermomechanical microactuator. *Sens Actuators A.* 101:239–250
59. Zaiter AA, Nafea M, Ali MSM (2016) Development of a shape-memory-alloy micromanipulator based on integrated bimorph microactuators. *Mechatronics* 38:16–28

Chapter 4

Molecular Dynamics Simulations for Nanoscale Insight into the Phase Transformation and Deformation Behavior of Shape-Memory Materials



Natraj Yedla, Sameer Aman Salman, and V. Karthik

4.1 Introduction

Molecular dynamics (MD) simulations find extensive application in the fields of materials science, physics, chemistry, and biomedical sciences. MD simulations are of atomic scale and are generally carried out to assess properties sensitive to the position, configuration, and movement of atoms [1]. Since many properties of interest in the study of shape-memory materials are dynamic, MD offers an obvious advantage. Mechanisms of deformation and phase transformation, phenomena related to superplasticity and mass transport, measurement of transport coefficients, and other time-dependent processes are well suited for MD [1, 2]. In general, simulations often tend to act as a bridge between theoretical models and empirical studies. In order to discover new systems exhibiting shape-memory effect (SME) and to upscale existing systems, simulations will play an important role.

MD simulations essentially consist of solving iteratively the classical equations of motion for a large number of particles (the more equations simultaneously solved, i.e., the larger n is, the more accurate and precise the results of the simulation). In order to solve these equations, we must first obtain the forces acting on the atoms. For this, we rely on potential energy functions (U), many of which have been formulated by first principles and are readily accessible on open sources. These potential energy functions are a function of the chemical nature of the interacting atomic species. The calculation of forces is expected to be complex in shape-memory systems since many shape-memory alloys (SMAs) have a large number of chemically distinct species [3].

N. Yedla

Department of Metallurgical and Materials Engineering, National Institute of Technology Rourkela, Rourkela 769001, Odisha, India

S. A. Salman · V. Karthik (✉)

Department of Metallurgical and Materials Engineering, National Institute of Technology Tiruchirappalli, Tiruchirappalli 620015, Tamil Nadu, India
e-mail: karthikv@nitt.edu

After having specified the potential energy function, the atomic forces (F_i) can be calculated by differentiating U .

$$F_i = \frac{\partial U}{\partial r_i} \quad (4.1)$$

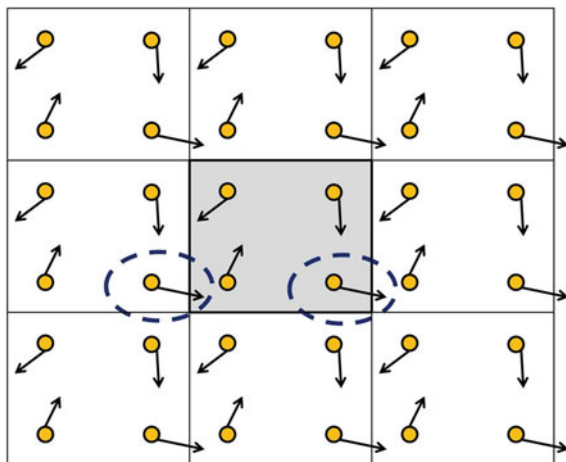
where r_i is the position vector of the i th atom. Numerical integration of the forces then yields the velocity and position of each atom.

We wish to ensure that the system of interest is rapidly sampled. For this, it is required to make the timestep as large as possible consistent with other requirements. Lower-order algorithms that do not involve higher-order derivatives of position and velocities are preferred for rapid sampling since they allow the timestep to be large [4]. The Verlet algorithm is favored by researchers since it fulfills the above requirements in addition to being time-reversible and easy to program [3, 4].

MD simulations, especially those with small sample sizes, tend to use periodic boundary conditions. For small samples, atoms on the surface faces make up a significant proportion of the total atoms and hence have a significant effect on the measured properties. For this, we essentially surround the simulation box with exact replicas of it which accounts for the disparity of properties in surface atoms. Each atom is considered to interact only with its nearest neighbors in a periodic lattice. One can visualize (Fig. 4.1) such a condition by imagining that once a particular atom leaves the simulation box by exiting to the right, it re-enters from the left.

The length and time scale of simulations is constrained by the availability of computational resources. Most simulations tend to occur for around 10^3 to 10^6 timesteps [5]. Since each MD timestep represents an infinitesimally small duration, this would translate to only a few nanoseconds in real life. Simulations running for more than a few microseconds are rarely encountered. One must be cautious to

Fig. 4.1 An illustration of periodic boundary condition



check if the system has attained equilibrium in this short amount of time, else, the simulation may be erroneous.

Shape-memory materials are alloys or polymers in which a macroscopic reversible shape change can respectively be induced either by martensitic/austenitic transition (SMAs) or by glass/melting transition from hard to soft phase (SMPs). They find application in a large variety of industries such as in biomedical engineering (to make cardiovascular stents), orthopedic and dental implants, aerospace and automotive industries, and also in bridge structures [6, 7].

The phase transformation which induces the shape change in SMAs is generally martensitic. It must be kept in mind that a detailed understanding of the microstructural mechanisms involved is necessary to model SMAs, and this may involve the nucleation of temporary phases, twinning, and the formation and shearing of precipitates [8–10]. The thermally induced shape-memory effect in polymeric materials is based on three working mechanisms namely dual-state mechanism, dual-component mechanism, and partial-transition mechanism [11]. All of them involve macroscopic shape changes caused by micro/nanoscale atomic movements.

Hence, an investigation is required across multiple length and time scales to understand the shape-memory behavior of shape-memory materials. Some phenomena occur over the microscale, spread out over the width of a few grains, while some occur at the atomic scale [12, 13]. While MD can offer significant insights and predictions about the deformation behavior of SMMs, it must be recognized that a variety of techniques will need to be adopted to obtain a holistic understanding, ranging from atomistic to continuum techniques [14].

Most experimental studies on SMMs are confined to the continuum scale, involving thermodynamic and mechanical studies, finite-element modeling (FEM) simulations, phase characterization using X-ray diffraction, and component quality control testing [15–17]. A significant, albeit narrower, focus has also been placed on the use of mesoscale experimental and simulation techniques such as digital image correlation and electron microscopy. The discussion on the mechanisms of the shape-memory effects is usually confined to the theoretical space, which has yet to be entirely validated by empirical observations [18]. The advent of MD simulations in the field of SMMs has garnered attention, due to the promise of MD simulations to describe atomic-scale and sub-microscale phenomena occurring in SMMs [19–22]. A better understanding of atomic movements within a single grain will help in the development of more robust and predictive models.

The reversible phase transformation between the austenitic and martensitic phase is generalizable to all SMAs and is the principal cause of the large recoverable strains associated with them. This phase transformation process is also accompanied by twinning processes such as nucleation and migration. The extent of recovered strain deteriorates with time in SMAs, due to plastic deformation via atomic slip. Whereas, in the case of thermally induced SMPs, the transformation from hard to soft phase during the glass transition or melting transition contributes to the shape-memory effect. The precise mechanism of the shape-memory behavior involves the coordinated movements of atoms, achieved by shear forces and occasionally shuffling, until a configuration that minimizes free energy is reached.

Most SMAs are principally composed of transition metals. For this class of metals, the filling of the d orbitals, along with electron spin and phonon spectra, account for the degree of twinning and the extent of phase transformation which can occur. It is essential to make use of computational techniques to study these phenomena since they occur at the electronic and atomic scale, and even the most advanced experimental techniques cannot resolve such minute spatial scales.

As suggested by different working mechanisms, the SMPs are composed of elastic part and transition part. The elastic component and transition component in the SMPs are simplified as matrix and inclusions [11]. The elastic component has good elasticity and stores the elastic energy during the programming stage for the subsequent recovery process. The transition part deforms plastically and becomes hard to retain the deformed shape after the removal of constraints. Once the stimulus (i.e., heat, light, chemical, or mechanical) is applied, the transition part becomes soft and utilizes the energy stored by the elastic component to regain the original shape [23]. The atomic-level movements in the inclusions determine the shape-memory capacity of the SMPs. Hence, molecular-level simulations are necessary to completely understand the shape-memory effect in the polymers as well as in the metallic alloys.

At the atomic scale, the properties of SMAs are governed by factors such as the extent of short- and long-range order, the presence of interstitial and substitutional solutes, the modulus of the solvent and solute atoms, and the stacking of atomic planes. At these length scales, the use of density functional theory (DFT) has resulted in the accurate prediction of elastic moduli for many systems [24]. However, DFT simulations remain computationally expensive, and most simulations have to be restricted to a scale of a few hundred atoms.

Hence, for the detailed analysis of molecular/atomic-level transition mechanisms, atomistic simulation techniques such as MD are essential. With the advancements in computing powers, the MD simulations can model the polymeric or metallic systems, which are composed of multiple million atoms. The detailed discussions on MD simulations of different shape-memory materials are presented in the ensuing section.

4.2 MD Simulations on SMMs

The shape-memory behavior of different metallic alloys and polymeric materials are modeled and simulated using the MD simulation technique. Among them, the Ni–Ti system is the most studied SMAs. The MD simulations on Ni₂MnGa, Co–Ni–Al, Cu–Zn–Al, Cu–Al–Ni, Fe–Pd, and polymeric materials are discussed in this section.

4.2.1 Binary Ni–Ti SMAs

The shape-memory effect in binary Ni–Ti shape-memory alloys is attributable to the reversible transformation from the austenite (B2) phase to the martensite (B19') phase. Of the two, the former is less stable, since it holds a large amount of entropy in its structure and is hence stable at higher temperatures. The martensitic phase has lower symmetry, energy, and entropy and is the dominant phase at room temperature [25]. The transformation of austenite to martensite can be induced by lowering the temperature or via the application of a mechanical load. It is to be noted that the most stable martensitic phase is the body-centered orthorhombic B33 phase [26]. It is theorized that an energy barrier exists in Ni–Ti, which prevents the B33 phase from being formed. Continuum-based models and DFT calculations have been extensively used in determining the elastic constants of Ni–Ti SMAs [27].

The first significant MD simulations on Ni–Ti were conducted over the 2000s. Farkas et al. [28] computed the two different embedded-atom-type interatomic potentials for the Ni–Ti system by empirically fitting to the observed properties of B2 Ni–Ti. The second potential was computed using experimental cohesive energy values at high temperatures (in the range of stability for B2 Ni–Ti). This potential was successfully used in the model for the prediction of the stability of the D024 Ni₃Ti phase. The authors were also able to predict the lattice parameters with precision. They calculated cohesive energy of 4.93 eV/atom and a lattice constant of 30 nm for B2 Ni–Ti.

However, their work was not able to reproduce the multi-phase B2/B19' stability observed in Ni–Ti SMAs. Lai and Liu [29] and Lai et al. [30] established interspecies bonding energies and functionals, which paved the way for the prediction of solid solubility of various Ni–Ti intermetallics in the alloys. Since the shape-memory effect is only observed in the vicinity of an equiatomic composition, the ability to predict non-stoichiometric behavior was helpful to further develop the theory of Ni–Ti SMAs. Their work applied a derived n-body Ni–Ti potential and simulated solid-state reactions in the Ni–Ti multi-layers to observe the growth of an amorphous interlayer. In the initial stages, the growth of the interlayer is proportional to t and then to $t^{1/2}$. The formation of the layer is accompanied by a sharp semi-coherent interface, which serves as a barrier to nucleation and prevents any interfacial reaction from occurring at temperatures below 873 K. They also observed that such an asymmetric rate of growth is attributable to the introduction of disorder in the alloy by addition of solute atoms beyond the solubility limit. Their simulation helped predict that in the composition range between 15 and 62 at.% Ni, the system is an intrinsic glass former.

It would be useful to briefly discuss the details of the simulation here. The simulation model of Lai and Liu [29] consisted of two interpenetrating crystalline lattices, composed of 2048 atoms of the FCC Ni lattice and 1440 atoms of the hexagonal close-packed (HCP) Ti lattice. The x- and z-axes were established parallel to the [100] and [001] crystalline directions. The y-axis was established along [010] for the FCC Ni lattice and along [120] for the HCP Ti lattice. Periodic boundary conditions

were established along all three dimensions. Ti and Ni atoms were randomly substituted into the opposite lattices to create the substitutional alloy. The authors avoided clustering by performing random substitution in each unit cell of Ni FCC (Ti HCP) lattice with the same probability. MD simulations were performed for the obtained random solid solutions, and the solute concentration was gradually increased to obtain the critical composition at which the crystalline lattices of the solid solutions become unstable and lose orders. The simulation was performed at 300 K for 20,000 timesteps.

The stability of the B2 Ni–Ti phase, against the disorder induced by ion irradiation, was also studied. The disordering was simulated by randomly exchanging Ni and Ti atoms and quantified by the long-range order (LRO) parameter. The parameter, obtained at ranges of temperatures, was able to isolate the range of stability for the B2 phase. The simulation verified that solutions with up to 10 at.% of Ti still retain the face-centered cubic (FCC) crystalline structure. For solid solutions with 30–60 at.% of Ti, a C-A transition takes place. For the Ti-rich HCP solid solutions, the C-A transition is observed when the Ni solute contents are greater than 15 at.%.

The variation of molar enthalpy and volume as a function of the LRO parameter in the B2 Ni–Ti crystal were obtained from another simulation performed for 20,000 timesteps at 1000 K. Decreasing the LRO parameter leads to a gradual increase in both enthalpy and volume. The increase plateaus off at approximately LRO parameter = 0.6. Hence, this value of LRO is where the C-A transition likely begins to occur. The simulation also produces a volume change of 5% after the C-A transition occurs, a value that is in good agreement with theoretical models.

Advancing on the work of Lai and Liu [29], Lai et al. [30] and Sato et al. [31] employed the pairwise potential computed by them and used it to predict the multiple microstructural transformation mechanism of the stress-induced martensitic transition between the B5 and B19' phases which occur at the equiatomic composition. Their simulation involved tensile loading of the Ni–Ti system at four different strain rates and discovered that the ratio of the martensitic phase does not seem to depend on the strain rate.

The MD simulation clearly showed the existence of multiple transformation pathways between the parent and martensitic phase, and the deciding factor between these multiple pathways was hypothesized to be the difference in the angular relationship between the tensile loading axis and the length of the unit cell of the parent phase. Depending on the transformation pathway followed, they showed that the ratio of the martensitic phase varies. The simulation also confirmed that the phase transformation between the B5 and B19' phases was, indeed, a stress-induced martensitic transformation. The simulation showed that the maximum stress and maximum ratio of the martensitic phase do not occur at the same value of strain. Instead, the stress first starts to decrease and then martensite starts to appear, and its ratio increases rapidly. Since the martensite ratio is very sensitive to the stress change, it suggests that the formation of the martensitic phase relaxes strain in the lattice. This process of martensite formation and subsequent stress relaxation continues to repeat locally. A particular type of transformation pathway identified by Sato et al. [31] shows a remarkable increase in the ratio of the martensite phase, particularly at high values

of strain rate. This could be attributed to the favorability of the tensile loading axis and the orientation of the parent crystal for the transformation.

The EAM potential derived by Lai et al. [30] made use of a cutoff radius of 0.42 nm. The more recent work in the MD simulation of Ni–Ti systems makes use instead of a cutoff function, as such an approach minimizes unwanted large displacements of atoms and hence such an approach is more successful at predicting the stability of phases and describing the B2 to B19' transformation.

Mutter and Nielaba [32, 33] made use of such an approach to study the aforementioned transformation, using a simulation of equiatomic Ni–Ti nanoparticles (diameters between 4 and 17 nm). They also made use of the LRO parameter, as earlier described, in order to locally distinguish between the monoclinic B19' at low temperatures and the cubic B2 structure at high temperatures. The simulation showed that the austenitic phase nucleated at the surface of the nanoparticles and subsequently propagates into the interior via a plane sliding mechanism. This provided a viable mechanism to explain the gap in austenite start and end temperatures. The work also obtained the absolute values of the start and end temperatures and also their dependence on the diameter of the nanoparticles as being inversely related.

Mirzaeifar et al. [34] showed that in a simulation of Ni–Ti nanowires, the tendency to reduce the surface energy leads to a new phase transformation mechanism (from the B2 to B19 phase). Their simulation further showed that the Ni–Ti nanowires exhibit pseudoelastic effects during thermo-mechanical cycling. The formation of $\{100\}_{B2} < 011 >_{B2}$ BCO compound twins was also observed, which are dominant at higher loads and propagate via the growth of wedge-like regions into the parent B19 phase. The formation of these twins was explained using the Poisson effect. The Poisson effect causes an increase in lateral contraction with increasing longitudinal (axial) strain. At a critical value of lateral contraction, the large negative value of lateral strain induces strain accommodation via the formation of these compound twins. At lower temperatures, the B19 phase reorients to a more favorable orientation under mechanical loading. This reorientation is associated with a pseudoelastic stress–strain response at temperatures below the martensite finish temperature, M_f .

The work of Zhong et al. [19, 35] presented two transformation pathways. The first occurs at around 400 K as $B2 \rightarrow B19 \rightarrow B19'$ and is associated with superelastic behavior, with complete reversal on unloading. At 350 K, superelastic behavior is also achieved via a different transformation route, $B2 \rightarrow B19 \rightarrow BCO \rightarrow$ Twinned BCO. The B19' phase is a precursor to the BCO phase at temperatures higher than 450 K. This transformation route is what contributes to the SME effect (high recoverable strains) of the nanowires due to macroscopic twin-like deformation of the entire nanowire. Stress–strain curves obtained by MD show a characteristic abrupt drop of stress in such models, due to the occurrence of a single highly localized nucleation event.

The simulations of Ko et al. [36] reported a decrease in transformation temperature with grain size in nanocrystalline Ni–Ti SMAs. The simulation confirmed empirical observations that the martensite phase nucleates in the interior of austenite grains and grows toward the grain boundaries during the characteristic transformation. A

small amount of irrecoverable plastic deformation is observed as a result of stress-induced transformation when the grain size is low. The simulation of Ko et al. [36] demonstrated that the origin of this strain is essentially due to plastic deformation at grain boundaries. The role of grain boundaries as a mechanical constraint during both thermal- and stress-induced phase transformation was demonstrated.

Nano-indentation simulations can also be performed using MD. The work of Chen et al. [37], for instance, shows that Ni–Ti SMAs show classical superelastic behavior on unloading, with the slope of the P-L curves increasing with temperature. While superplastic behavior was observed above the A_s temperature, the alloy behaves like a pseudoplastic at temperatures lower than A_s . This increase in slope can be attributed to an increase in critical stress. The region or zone around the tip of the indenter undergoes a stress-induced transformation. These regions can be divided into an elastic zone, along with a twinned and detwinned martensitic zone. The width of the region undergoing phase transformation was shown to decrease with an increase in temperature. The authors also noted a difference between the morphologies present when indenting at lower displacements with that at higher displacements. For the former case, the morphologies are similar before and after unloading, whereas for the latter case, evidence of indentation can be found even after unloading, along with a “pile-up” appearance on the surface, a sign of plastic deformation.

4.2.2 *Ni₂MnGa SMAs*

Since Ni₂MnGa SMAs are the most well-researched and documented magnetic SMAs, a brief discussion of MD simulations on this system follows. Most computer simulations are performed using electronic scale simulation techniques such as density functional theory (DFT) since the magnetic properties of interest often originate from electronic interactions. In these SMAs, a large elastic recovery can be induced by magnetic stimuli, in addition to the general temperature and mechanical stimuli of regular SMAs.

Breczko et al. [38] used VASP to perform MD simulations on the Ni₂MnGa alloy system, in order to study the physical properties of the alloy and the phase transformations taking place in the alloy. The lattice constant of the alloy was calculated as 5.826 Å, along with the total magnetic moment of a unit cell being equal to 16.53 BM. The authors concluded that the Mn atoms make the maximum contribution to the overall magnetic moment.

4.2.3 *Co–Ni–Al SMAs*

This class of SMAs has also been studied using MD simulations. Properties of interest are their high ferromagnetic nature and their narrow thermal hysteresis characteristics. Pun et al. [39] constructed an embedded-atom method (EAM) ternary Ni–Al–Co potential by crossing the binary Ni–Al potential with the pure Co potential. The application of this potential yielded results closely matching existing experimental results and was able to capture some commonly documented features, such as the formation of a twinned martensitic structure upon deformation. The correlation of transformation temperature and chemical composition was also reliably reproduced.

In addition, the simulation demonstrated the possibility of the formation of a regular array of Co-rich nanowires embedded in the matrix. This structure was stable at temperatures below 1600 K, above which it is transformed into a more familiar uniform martensitic structure. However, this structure was shown to only exist for certain combinations of structure and temperature, although it could have a significant impact on the mechanical properties of the bulk alloy.

4.2.4 *Cu-Based SMAs*

Zhang et al. [40] have investigated at the atomic level the several factors responsible for the two-way shape-memory effect in Cu-based SMA using MD simulations. The study reports that the effect arises from the oriented stress fields of the precipitates, pair dislocation bands, and reoriented martensite. Gui et al. [41] have used the embedded-atom method (EAM) to calculate the energies and lattice parameters of the parent and 18R1 martensite phases for several Cu–Zn–Al and Cu–Al–Ni SMAs. In their investigations, it is reported that the bond angles increase in the B2-type order for both the Cu–Zn–Al and Cu–Al–Ni SMAs. For an increase in the L2-type order, an increase in the bond angle is observed in the Cu–Zn–Al alloy while it decreases in Cu–Al–Ni SMAs. The grain formation studies on Cu–19.9 at.% Al shape-memory alloy have been studied by Ozgen et al. [42] using MD simulations. The solidification of the Cu–Al system is investigated by heating it to 2500 K and double-stage cooling resulted in the formation of grain boundaries in the Cu–Al SMAs.

4.2.5 *Fe-Based SMAs*

Entel et al. [43] have investigated the structural phase transformations in ferromagnetic Fe and Fe–Ni alloys using MD simulations. Ferrous alloys are characterized by a very broad hysteresis which is linked to the magnetic disorder. They have observed austenitic transformations during heating and martensitic transformation upon cooling. Also, for such transformations, a large number of defects are

necessary. A many-body potential is used by Mayr and Hasemi [44] for investigating the energetics behind the martensite \leftrightarrow austenite transformations in Fe–Pd alloys. They employed massively parallel MD simulations to investigate the effects of order/disorder, defects, and severe plastic deformation on the above transformations. The studies reveal that disorder favors martensitic transformation, while ordering results in austenitic structure. Further, they report that defects raise the martensitic formation temperature, and severe plastic deformation of austenite results in martensitic structure. A martensitic transformation in the ferromagnetic Fe₇₀Pd₃₀ SMAs is induced by shockwaves created using laser shock peening [7]. The austenite to martensite transformation occurs with the preferred orientation of the martensitic c-axis along the shockwave direction.

4.2.6 Shape-Memory Polymers

Shape-memory effect is an intrinsic character of many polymeric materials; it is not a special feature in most polymers. The shape-memory behavior in SMPs is induced by light, heat, electricity, or chemical reaction. The deformed polymer returns to its original shape in the presence of a suitable stimulus. It is suggested that during the deformation process, net points are introduced in the polymer chain which helps to retain the temporarily deformed shape in the polymer. On the application of the right stimulus such as heat or light, the net points are removed which helps in recoiling of the polymer chain to return to its original shape before the deformation process.

Zhang et al. [45] used fully atomistic MD simulations to attain molecular-level mechanisms for experimental observations of shape-memory polyurethane with 60% hard phase (SMPU60). The experiments show that the tensile modulus of the material drastically decreases with increasing temperature. The MD simulation revealed that the hydrogen bonding of type C = O...H is predominant and attributes to the higher moduli of the materials. The temperature rise decreases C = O...H-type hydrogen bonds in the system, which leads to a drastic decrease in moduli. The calculation of radial distribution function is exploited for analyzing the different types of molecular-level hydrogen bonds in the SMPU60, which is well utilized to understand the underlying mechanism of the experimental observations.

A coarse-grain molecular dynamics (CGMD) approach is adapted by Abberton et al. [21] to study the shape-memory effect in a generic copolymer system with hard phase and soft phase. The deformation temperature, hard phase fraction, and recovery temperature are major influencing parameters of the shape-memory effect in the copolymer model. The hard phase undergoes partial disintegration during the deformation process which attributes the unrecoverable strain observed in the simulations and experiments. If the hard phase fraction is increased, the mechanical strain applied during the deformation process will be stored as elastic energy in the hard phase which in turn reduces the recovery temperature. The stored elastic energy in the hard phase is utilized for the release of mechanical strain in the soft phase during the recovery process [21].

The shape-memory effect and deformation behaviors of commercial thermoset epoxy system E-51 with curing agent 4,4'-methylenedianiline are studied using MD simulations [46]. The recovery temperature, i.e., the glass transition temperature is strongly influenced by the amount of curing agent added to the epoxy system. A higher glass transition temperature is obtained for the epoxy system with more curing agent content. The calculation of radius gyration is used to analyze the molecular structure in the polymer. The radius of gyration value is more in the glassy state compared to the rubbery state, which correlates well with the higher yield stress at the glassy state compared to low yield stress in the rubbery state. The MD simulation results were able to explain the experimental behavior of the epoxy system.

The radial distribution function and radius of gyration obtained from MD simulations are exploited by Amini et al. [22] to provide an underlying molecular-level mechanism of shape-memory behavior in graphene sheets-reinforced poly(D, L-lactic acid) nanocomposites. It is suggested the entropy changes and the potential energy contribute to the shape fixing and the conformational entropy helps to the shape recovery in these nanocomposites. It is evident that the MD simulations can be successfully employed to attain an atomic-scale insight into the experimental observations in SMPs.

4.3 Conclusion

It is observed that the atomic- or molecular-level transformations attribute to the shape-memory effect present in metallic alloys and polymeric materials. It warrants atomic- or molecular-scale modeling and simulation techniques to mimic the shape-memory effect in these materials and to know the underlying transformation mechanisms. The MD simulations are well suited for studying the transformation and deformation behavior of SMMs, which is evident from the number of research articles published in this area. The Ni-Ti SMAs are the most widely investigated system using MD simulations. The experimental observations obtained on the Ni-Ti SMAs are well explained by MD simulations. Apart from Ni-Ti systems, other materials like Ni₂MnGa, Co-Ni-Al, Cu-Al, Cu-Al-Ni, Cu-Zn-Al, Fe-Pd, and some polymer materials are also investigated by MD simulations to realize the underlying transformation mechanisms. It can be summarized that the MD simulations can be successfully employed for availing nanoscale insight into the phase transformation and deformation behavior of SMMs. But the limitation lies in the availability of interaction potentials/forcefields for a wide variety of experimentally investigated SMMs.

References

1. Steinhauser MO, Hiermaier S (2009) A review of computational methods in materials science: examples from shock-wave and polymer physics. *Int J Mol Sci* 10:5135–5216. <https://doi.org/10.3390/ijms10125135>
2. Landman U (1988) Molecular dynamics simulations in material science and condensed matter physics BT—computer simulation studies in condensed matter physics. In: Landau DP, Mon KK, Schüttler H-B (eds) Springer. Berlin Heidelberg, Berlin, Heidelberg, pp 108–123
3. Kastner O (2012) First principles modelling of shape-memory alloys: molecular dynamics simulations, 1st edn. Springer, Berlin Heidelberg
4. Nakano A, Kalia RK, Vashishta P, Campbell TJ, Ogata S, Shimojo F, Saini S (2001) Scalable atomistic simulation algorithms for materials research. In: SC '01: proceedings of the 2001 ACM/IEEE conference on supercomputing, p 10
5. LeSar R (2013) Introduction to computational materials science: fundamentals to applications. Cambridge University Press, Cambridge
6. Mohd Jani J, Leary M, Subic A, Gibson MA (2014) A review of shape-memory alloy research, applications and opportunities. *Mater Des* 56:1078–1113. <https://doi.org/10.1016/j.matdes.2013.11.084>
7. Lendlein A, Gould OEC (2019) Reprogrammable recovery and actuation behaviour of shape-memory polymers. *Nat Rev Mater* 4:116–133. <https://doi.org/10.1038/s41578-018-0078-8>
8. Allafi JK, Ren X, Eggeler G (2002) The mechanism of multistage martensitic transformations in aged Ni-rich NiTi shape-memory alloys. *Acta Mater* 50:793–803. [https://doi.org/10.1016/S1359-6454\(01\)00385-8](https://doi.org/10.1016/S1359-6454(01)00385-8)
9. Nishida M, Ohgi H, Itai I, Chiba A, Yamauchi K (1995) Electron microscopy studies of twin morphologies in B19' martensite in the Ti–Ni shape-memory alloy. *Acta Metall Mater* 43:1219–1227. [https://doi.org/10.1016/0956-7151\(94\)00332-C](https://doi.org/10.1016/0956-7151(94)00332-C)
10. Shaw JA, Kyriakides S (1995) Thermomechanical aspects of NiTi. *J Mech Phys Solids* 43:1243–1281. [https://doi.org/10.1016/0022-5096\(95\)00024-D](https://doi.org/10.1016/0022-5096(95)00024-D)
11. Huang WM, Zhao Y, Wang CC, Ding Z, Purnawali H, Tang C, Zhang JL (2012) Thermo/chemo-responsive shape-memory effect in polymers: a sketch of working mechanisms, fundamentals and optimization. *J Polym Res* 19:9952. <https://doi.org/10.1007/s10965-012-9952-z>
12. Hatcher N, Yu OK, Freeman JA (2009) Structural stabilities, elastic constants, generalized stacking fault energetics, and the martensitic transformation mechanisms for the Ni₅₀–xTiPt_x (x = 0–30) ternary system: ab initio investigation. *Eur Symp Martensitic Transform*
13. Zarkevich NA, Johnson DD (2014) Shape-memory transformations of niti: minimum-energy pathways between austenite, martensites, and kinetically limited intermediate states. *Phys Rev Lett* 113:265701. <https://doi.org/10.1103/PhysRevLett.113.265701>
14. Kastner O (2003) Molecular-dynamics of a 2D model of the shape-memory effect. *Contin Mech Thermodyn* 15:487–502. <https://doi.org/10.1007/s00161-003-0128-2>
15. Kudoh Y, Tokonami M, Miyazaki S, Otsuka K (1985) Crystal structure of the martensite in Ti-49.2 at.%Ni alloy analyzed by the single crystal X-ray diffraction method. *Acta Metall* 33:2049–2056. [https://doi.org/10.1016/0001-6160\(85\)90128-2](https://doi.org/10.1016/0001-6160(85)90128-2)
16. Pons J, Chernenko VA, Santamarta R, Cesari E (2000) Crystal structure of martensitic phases in Ni–Mn–Ga shape-memory alloys. *Acta Mater* 48:3027–3038. [https://doi.org/10.1016/S1359-6454\(00\)00130-0](https://doi.org/10.1016/S1359-6454(00)00130-0)
17. Sedmák P, Pilch J, Heller L, Kopeček J, Wright J, Sedlák P, Frost M, Šittner P (2016) Grain-resolved analysis of localized deformation in nickel-titanium wire under tensile load. *Science* (80-) 353:559 LP–562. <https://doi.org/10.1126/science.aad6700>
18. Bhattacharya K, Conti S, Zanzotto G, Zimmer J (2004) Crystal symmetry and the reversibility of martensitic transformations. *Nature* 428:55–59. <https://doi.org/10.1038/nature02378>
19. Zhong Y, Gall K, Zhu T (2012) Atomistic characterization of pseudoelasticity and shape-memory in NiTi nanopillars. *Acta Mater* 60:6301–6311. <https://doi.org/10.1016/j.actamat.2012.08.004>

20. Mutter D, Nielaba P (2013) Simulation of the shape-memory effect in a NiTi nano model system. *J Alloys Compd* 577:S83–S87. <https://doi.org/10.1016/j.jallcom.2012.01.095>
21. Abberton BC, Liu WK, Keten S (2013) Coarse-grained simulation of molecular mechanisms of recovery in thermally activated shape-memory polymers. *J Mech Phys Solids* 61:2625–2637. <https://doi.org/10.1016/j.jmps.2013.08.003>
22. Amini M, Hasheminejad K, Montazeri A (2020) Experimentally guided MD simulation to enhance the shape-memory behavior of polymer-based nanocomposites: towards elaborating the underlying mechanism. *Compos Part A Appl Sci Manuf* 138:106055. <https://doi.org/10.1016/j.compositesa.2020.106055>
23. Sun L, Wang TX, Chen HM, Salvekar AV, Naveen BS, Xu Q, Weng Y, Guo X, Chen Y, Huang WM (2019) A brief review of the shape-memory phenomena in polymers and their typical sensor applications. *Polymers (Basel)* 11:1049. <https://doi.org/10.3390/polym11061049>
24. James RD, Zhang Z, James RD, Zhang Z (2005) A way to search for multiferroic materials with “Unlikely” combinations of physical properties BT—magnetism and structure in functional materials. In: Planes A, Mañosa L, Saxena A (eds) Springer. Berlin Heidelberg, Berlin, Heidelberg, pp 159–175
25. Huang X, Ackland GJ, Rabe KM (2003) Crystal structures and shape-memory behaviour of NiTi. *Nat Mater* 2:307–311. <https://doi.org/10.1038/nmat884>
26. François A, Veyssi re P (1994) A TEM investigation of the deformation microstructure of CoZr and Co40Ni10Zr50 ordered alloys. *Intermetallics* 2:9–22. [https://doi.org/10.1016/0966-9795\(94\)90046-9](https://doi.org/10.1016/0966-9795(94)90046-9)
27. Wang J, Sehitoglu H (2012) Resolving quandaries surrounding NiTi. *Appl Phys Lett* 101:81907. <https://doi.org/10.1063/1.4747488>
28. Farkas D, Roqueta D, Vilette A, Ternes K (1996) Atomistic simulations in ternary Ni–Ti–Al alloys. *Model Simul Mater Sci Eng* 4:359
29. Lai WS, Liu BX (2000) Lattice stability of some Ni–Ti alloy phases versus their chemical composition and disordering. *J Phys Condens Matter* 12:L53
30. Lai WS, Zhang Q, Liu BX, Ma E (2000) Structural stability and amorphization transition in the Ni–Ti system studied by molecular dynamics simulation with an n-body potential. *J Phys Soc Jpn* 69:2923–2937. <https://doi.org/10.1143/JPSJ.69.2923>
31. Sato T, Saitoh K, Shinke N (2006) Molecular dynamics study on microscopic mechanism for phase transformation of Ni–Ti alloy. *Model Simul Mater Sci Eng* 14:S39
32. Mutter D, Nielaba P (2011) Simulation of the thermally induced austenitic phase transition in NiTi nanoparticles. *Eur Phys J B* 84:109–113. <https://doi.org/10.1140/epjb/e2011-20661-4>
33. Mutter D, Nielaba P (2010) Simulation of structural phase transitions in NiTi. *Phys Rev B* 82:224201. <https://doi.org/10.1103/PhysRevB.82.224201>
34. Mirzaeifar R, Gall K, Zhu T, Yavari A, DesRoches R (2014) Structural transformations in NiTi shape-memory alloy nanowires. *J Appl Phys* 115:194307. <https://doi.org/10.1063/1.4876715>
35. Zhong Y, Gall K, Zhu T (2011) Atomistic study of nanotwins in NiTi shape-memory alloys. *J Appl Phys* 110:33532. <https://doi.org/10.1063/1.3621429>
36. Ko W-S, Grabowski B, Neugebauer J (2015) Development and application of a Ni–Ti interatomic potential with high predictive accuracy of the martensitic phase transition. *Phys Rev B* 92:134107. <https://doi.org/10.1103/PhysRevB.92.134107>
37. Chen Y, Moln rov  O, Tyc O, Kadeř vek L, Heller L, Šittner P (2019) Recoverability of large strains and deformation twinning in martensite during tensile deformation of NiTi shape-memory alloy polycrystals. *Acta Mater* 180:243–259. <https://doi.org/10.1016/j.actamat.2019.09.012>
38. Brezcko TM, Nelayev V, Dovzhik K, Najbuk M (2009) Computer simulations of the Ni2MnGa alloys. In: *Proceedings of SPIE*
39. Pun GPP, Yamakov V, Mishin Y (2015) Interatomic potential for the ternary Ni–Al–Co system and application to atomistic modeling of the B2–L10 martensitic transformation. *Model Simul Mater Sci Eng* 23:65006
40. Zhang XM, Fernandez J, Guilemany JM (2003) Origin of two way shape-memory effect in Cu-based shape-memory alloys. *J de Physique IV (Proceedings)*. EDP sciences 487–493

41. Gui J, Cui Y, Xu S, Wang Q, Ye Y, Xiang M, Wang R (1994) Embedded-atom method study of the effect of the order degree on the lattice parameters of Cu-based shape-memory alloys. *J Phys Condens Matter* 6:4601
42. Ozgen S, Orhan O, Canbay CA, Brazolin GF, Silva RAG (2018) Investigation of grain formation mechanism in CuAl shape-memory alloy by molecular dynamic simulation. *AIP Conf Proc* 2042:20039. <https://doi.org/10.1063/1.5078911>
43. Entel P, Meyer R, Kadau K (2000) Molecular dynamics simulations of martensitic transitions. *Philos Mag B* 80:183–194. <https://doi.org/10.1080/13642810008208607>
44. Mayr SG, Arabi-Hashemi A (2012) Structural defects in Fe–Pd-based ferromagnetic shape-memory alloys: tuning transformation properties by ion irradiation and severe plastic deformation. *New J Phys* 14:103006
45. Zhang C, Hu J, Ji F, Fan Y, Liu Y (2012) A combined experimental and computational study on the material properties of shape-memory polyurethane. *J Mol Model* 18:1263–1271
46. Yang H, Wang Z, Guo Y, Shi X (2016) A molecular dynamics investigation of the deformation mechanism and shape-memory effect of epoxy shape memory polymers. *Sci China Physics, Mech Astron* 59:634601. <https://doi.org/10.1007/s11433-015-5758-4>

Chapter 5

Influences of Powder Size (SMAs) Distribution Fe–Mn/625 Alloy Systematic Studies of 4D-Printing Conceivable Applications



S. Shanmugan

Nomenclature

$\varepsilon_{\varepsilon \rightarrow \gamma}^T$	The recovered strain of $\varepsilon \rightarrow \gamma$ of the materials.
σ_{rs}	The recovered stress of the materials.
$(T_i - T_f)$	Metals are made of hard, shiny, rugged, and very significant Shape-memory alloy (SMA) resource construction.
E_M	The elasticity Modulus of the materials.
α	The coefficient of thermal expansion of the tested wire of the materials.
T_m	The higher temperature of the materials in the heating process.
$\varepsilon_p^{T,\sigma r}$	The recovery stress occupied of the plastic strain by a samples.
ε	martensite transformation is induced by a stress–strain.

5.1 Introduction

Metals are made of the properties with hard, shiny, rugged, and very significant Shape-memory alloy (SMA) resource construction. SMA samples are extracted from the earth with human progress. The measure of functional materials has been grown like giant static constructions (bridges, skyscrapers); society is an attraction for spawning tools, jewelry, engines, and machines. The high-temperature production of the SMA samples of Cu–Al–Ni has been grown different considerations—and various processing with the applications' effect. It is various processing of the routes for processing Cu–Al–Ni like casting path, powder metallurgy route, rapid solidification, and spray forming properties. SMAs of a pro, cons with different

S. Shanmugan (✉)

Research Center for Solar Energy, Department of Physics, Koneru Lakshmaiah Education Foundation, Green Fields, Guntur District, Vaddeswaram 522502, Andhra Pradesh, India

ways are additive industrial, an emerging process, and prepared Cu–Al–Ni shape-memory for high-temperature applications. The 4D-printable innovative materials have improved recent research of materials science. An included stimuli-responsive capability was the conversation of shape-memory materials, metamaterials, self-healing materials, etc., which are responses from the thermal, pH, moisture, light, magnetic, and electrical exposures. Many researchers have developed such systems' potential applications and included progress in health monitoring, electrical devices, deployable structures, soft robotics, and tunable metamaterials. The advance materials of Fe–Mn/625, alloys were significant consideration as a historical period in probable applicants to supplementary very highly affluent Ti–Ni constructed shape-memory alloys (SMAs). The materials are developed to be as follows: of low cost, good workability, machinability, and weldability, and no original submissions were SMAs. The alloys' shape-memory effects' main drawback has something to small sound as in Ti–Ni alloys. They are accepted in exceptional cases, as followed in thin foil or single crystal specimens [1, 2]. Many researchers have been interested in involving that of communities, and industry was used in three-dimensional (3D)-printed soft robots by [3–5]. We have operated in dynamic environments in which the scope of dements by autonomy increases 4D applications and have closed by the 4D-printed soft robot and closed-loop integrates for 3D-printing sensor. Recovery stress of Fe–Mn–Si with SMAs was very low during stress reduction. The shape-memory effect of factors to moving in Fe–Mn–Si alloys were enhanced these alloy materials by [6, 7], the quantity of a strain [8, 9], distortion temperature as by [10], the annealing behavior to develop of a thermal exercise by [11] were produced. Many researchers have been instantaneously documented the design of resistivity recovery with stress alloy to force heating and cooling. The shape-memory effect of a thermal process used in Fe–Mn alloys is not good. We have enhanced good resistance to decomposition by associating with Fe–Mn/625 alloys.

The material resistivity has penetrated the microstructure with a physical quantity. Assessed conversion performance was on the resistivity transformation with temperature. It is created as a rational consequence with a stress equation for forced heating and cooling increases. Fe–Mn/625 alloys as composition samples have better shape-memory effects of higher recovery stress. Finally, it is concluded that decreasing the plastic deformation's quantity, then ϵ -martensite transformation increases recovery stress.

5.2 Materials and Methodology

The study of Fe–Mn/625 alloy SMAs have been organized by using an orientation melting underneath the argon sky with high purity for the iron, manganese materials. Fe–Mn/625 alloy is analyzed in the chemical composite materials and is obtainable in Table 5.1.

The non-vacuum homogenization is used at about 1200 K at 12hours, as shown in Table 5.2, which sets at a hot forged to circular bars of 15 mm diameter ingots. It

Table 5.1 Fe–Mn/625 alloy has been tested in mass (%) chemical compositions alloys

S. No	Alloy	Alloying elements		
1	1	Mn	Cr	Fe
2	1	14.70	7.94	Poise
2	2	14.90	7.88	Poise

Table 5.2 Fe–Mn/625 alloys are quenched wire with elastic modulus and thermal expansion coefficient as transformation temperatures

Alloy	The samples with transformation temperature (K)			The samples of elastic modulus (MPa)	The samples in coefficient of thermal expansion (K^{-1})
	M_s	A_s	A_f		
Class- 1	298	386	573	169×10^3	14.9×10^{-6}
Class-2	< 181	395	554	/	/

has swayed to wires of 3.5 mm diameters after the cold haggard to wires of 1.5 mm. The measure of the samples drawn that were cut from cold wires is 1.5 mm in diameter. The cold drawn is eliminated that the effect of ϵ -martensite induced at that during the process. We implemented that a specimen's memory the shape in a straight line has straightened with the force of a stainless-steel tube. It is strengthening of 1200 K at 40 min as tracking in water quenching. The variations of electrical resistivity measuring temperature for the phase transformation have been quenched in alloys. Dupont TA2000 calorimeter needs to be measured in a coefficient of thermal expansion of the alloys. The elasticity modulus is analyzed in physical parameter measuring with resonance vibration apparatus CJS-42, as shown in Table 5.2. The different temperatures of the Fe–Mn/625 alloy arrangement of a stress–strain curve have been calculated by Shimadzu AG-10TA tensile testing machine at the cross speed of 2.5 mm/min.

The stress curves of the different temperatures are examined as proof of 0.3%. Fe–Mn/625 alloys have measured that heating and cooling are used in WD-10A tensile testing machine for the recovery stress and the electrical resistivity. The quenched specimens were strained at 305 K at the sample of zero levels (unloaded). The clamping head of unloading is static with a model heated 700 K shape recovery as shown in Fig. 5.1. It records instantaneous recovery stress to the resistivity of the occupation with temperature.

5.3 Results and Discussion

The stress analysis of recovery resistivity temperature the Fe–Mn/625 alloys (Class-1) function in 0.020% for C after 0.3% deformation, as shown in Figs. 5.1 and 5.2 changes stress cure temperature, and the point (A) of 370 K is activated to grow the

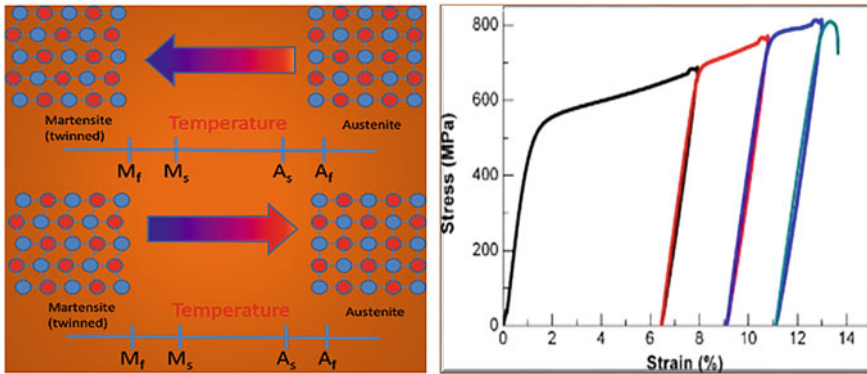
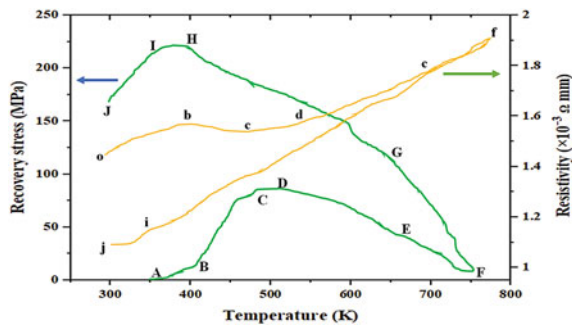


Fig. 5.1 A variation of strain and stress temperature analysis of Fe-Mn/625 alloy

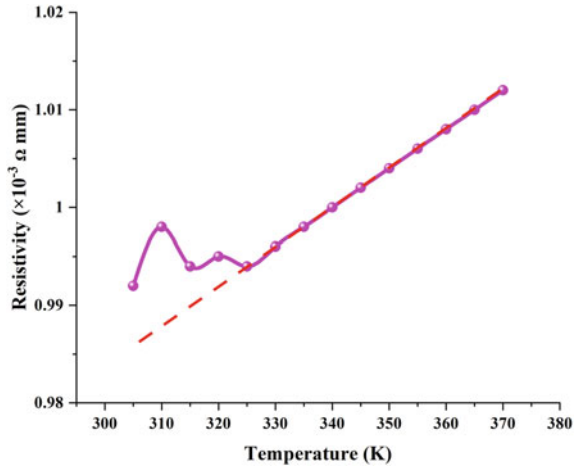
Fig. 5.2 The temperature function of Fe-14.60 Mn-4.22/625 alloys, 3% deformation



recovery stress temperature. The stress temperature quickly improved at a Point (B) of 425 K. The point (C) continually increases temperature for the pressure (stress) value of 490 K for 520 K. The point (D) is activated the stress and reduced at 530 K. Fe-Mn/625 materials were increased of the pressure then linearly cooling process and decreases the temperature from (F) to (G) that the values about 745 to 640 K. To develop the materials are increased, the range values of 400 K and below at 400 K stress activates to decrease below values of 365 K. Figure 5.2 is used the resistivity that temperature curve functions in parallel through the below no constraints. The new materials are existing apparent inflections of the under constraint.

The resistivity temperature is determined as the below temperature constraints start martensite to austenite transformation and achieved at 350 K temperature, a lower temperature is below no constraint about 405 K. The A_f temperature is finished martensite to austenite transformation of 620 K higher than below no constraints of 590 K. Fe-Mn/625 materials used in constraints have been increased in that area of martensite to austenite transformation. The temperature of 315 K is shown in Fig. 5.3, with a decrease in the resistivity temperature diverged from a straight-line region. Fe-Mn/625 alloy materials have been accredited to the rate of austenite to martensite transformation. Fe-Mn/625 materials have the recovery stress, as followed

Fig. 5.3 An increase of resistivity–temperature curve i–j portion as a sample



in Fig. 5.4. The materials are verified that of 0.3% with the stress of Fe–Mn/625 alloy (Class-1) by the function of temperature. The materials achieve 525 K for clearly the temperature for recovery stress is greater than the 0.2% proof stress. Hence plastic slip cannot be circumvented of the Fe–Mn/625 materials.

Fe–Mn/625 alloy (Class-2) with 0.20% is the recovery stress by the temperature’s function after a 3% deformation, as shown in Fig. 5.5. It is changed to the recovery stress with the materials (1) of 0.015%. Though the recovery stress was different for alloy (Class-1 and Class-2) in cooling, it still increases the materials. It does not decrease with the decrease of the temperature by the materials. Fe–Mn/625 alloy is have been highlighted recovery strain for the alloy (Class-2) was lesser than values of the alloy (Class-1) by [12], and the recovery stress in an alloy (Class-2) at 305 K is 372 MPa, 129 MPa higher than that of an alloy (Class-1).

Fig. 5.4 Shows the 0.3% proof stress as a function of Fe–14.60Mn–4.22/625 alloys

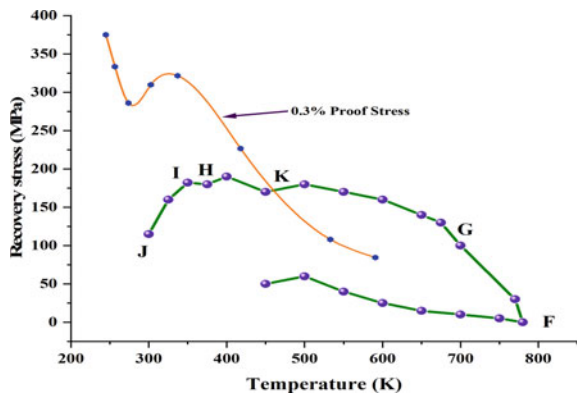
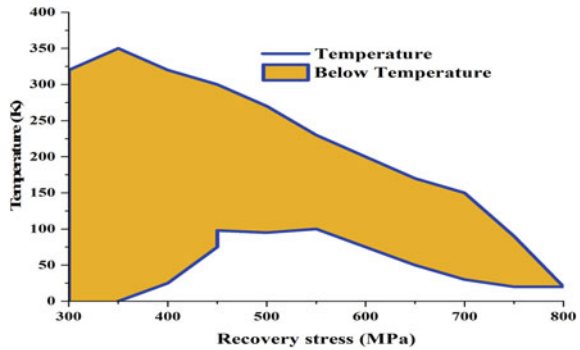


Fig. 5.5 Shows 3% deformation temperature of Fe–14.8Mn–4.78/625 alloys



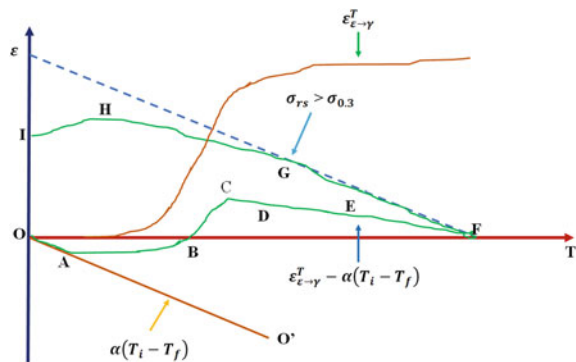
5.3.1 Heat in Recovery Stress

Fe–Mn/625 alloy has been loaded at the total strain of the SMAs. It is separated into a phase transformation for the strain ($\epsilon_{\gamma \rightarrow \epsilon}$). From austenite (γ) to martensite (ϵ), the transformation has been influenced by the stress for an elastic strain (ϵ_e). The plastic strain (ϵ_p) is rising from the slip of the materials. The elastic strain (ϵ_e) is unloaded in materials for the recovers wholly to the phase transformation strain ($\epsilon_{\gamma \rightarrow \epsilon}$) from the remain values of the plastic strain (ϵ_p). The process of the materials is constrained such that heating of the strain is reserved constant. Therefore, the recovery stress is dependent on two opposite phenomena. They are two ways as (i) the sample is increased for the recovery to arising of the deformation; (ii) the model is decreased with arising from the thermal expansion. These are given in Eq. (5.1):

$$\sigma_{rs} = E_M [\epsilon_{\epsilon \rightarrow \gamma}^T - \alpha(T_i - T_f)] \tag{5.1}$$

The recovery stress equation during heating for the materials' temperature is as has been followed in Eq. (5.1). The material of the temperature is changed for $[\epsilon_{\epsilon \rightarrow \gamma}^T - \alpha(T_i - T_f)]$ schematic establishes as exposed in Fig. 5.6. Which the

Fig. 5.6 Show thermal expansion strain in heating and cooling for Fe–Mn/625 SMAs



temperature of A_s is cannot take place for the shape recovery origin by the materials. $\varepsilon_{\varepsilon \rightarrow \gamma}^T$ of the recovered strain is zero, then the stress of the thermal expansion is negative levels for the line of OA in Fig. 5.6. The temperature is occupied with the A_s levels of recovery points. Though line AB shows that stress is negative, the recovered strain $\varepsilon_{\varepsilon \rightarrow \gamma}^T$ is lower than $\alpha(T_i - T_f)$ thermal expansion strain. The temperature of Fe-Mn/25 is lower at point A of 350 K and the stress is zero. The materials' main reason is minimal close to the results with stress always less than the minimum value.

The materials increase the temperature in a large portion of martensite transforms from austenite. The materials of $\varepsilon_{\varepsilon \rightarrow \gamma}^T$ are quickly increased from the $\alpha(T_i - T_f)$ is greater than values. The line of BC results for the stress is greater than zero then quickly increases by the temperature. Figure 5.2 shows a recovery stress and resistivity curves. Recovery stress temperature with a point of B to Crapid is increased recovery stress corresponded to the temperature from b to c. The materials have decreased the resistivity that a huge share of martensite transforms into austenite.

5.3.2 Cool During Recovery Stress

The FG line is displayed in Fig. 5.6; the recovered strain $\varepsilon_{\varepsilon \rightarrow \gamma}^T$ is constant from the materials as cooling to the recovery stops. The recovery stress is increased linearly by the decreases in temperature due to thermal contraction. The recovery stress is greater than that of point G product strength when the temperature decreases the plasticity, resulting in reduced recovery stress. A ε -martensite transformation-occupied region induces the stress after the recovery stress equals the grave stress for stress-induced martensite and phase transformation. The results are also show a fundamental reduction in recovery stress. Figure 5.1 is given by a part of the drastic relaxation in the recovery stress with temperature from i to j the quantity for the martensite transformation. The recovery stress follows Eq. (5.2) which satisfies as a cooling process.

$$\sigma_r = E_M [\varepsilon_{\varepsilon \rightarrow \gamma}^T - \alpha(T_i - T_f) - \varepsilon_p^{T \cdot \sigma r} - \varepsilon_{\gamma \rightarrow \varepsilon}^{T \cdot \sigma r}] \quad (5.2)$$

The temperature reduces to T_f yet again from Eq. (5.2) have been abridged of the materials.

$$\sigma_r = E_M [\varepsilon_{\varepsilon \rightarrow \gamma}^{T_m} - \varepsilon_p^{T \cdot \sigma r} - \varepsilon_{\gamma \rightarrow \varepsilon}^{T \cdot \sigma r}] \quad (5.3)$$

The room temperature was occupied for the materials to form the recovery stress in the process of Eq. (5.3) with T_f .

The material strength is sufficient to the plastic deformation cannot yield that point. The stress tempted for the martensite transformation has occupied that region of the temperature from the low sufficient a martensite from cannot be presented to ways of $\varepsilon_p^{T \cdot \sigma r}$ and $\varepsilon_{\gamma \rightarrow \varepsilon}^{T \cdot \sigma r}$ those values were zero from Eq. (5.3) concentrated as

$$\sigma_r = E_M \varepsilon_{\varepsilon \rightarrow \gamma}^{T_m} \quad (5.4)$$

The 0.3% occupied for materials was deformed at 700 K with the recovery stress being 9 Mpa, which is following those values approximately in Eq. (5.1) as

$$\varepsilon_{\varepsilon \rightarrow \gamma}^{700\text{K}} \approx \alpha (T_i - T_f) \quad (5.5)$$

The material mixture is $\alpha = 17.6 \times 10^{-6} \text{ K}^{-1}$ than $T_f = 305 \text{ K}$ as given that values, we can write as

$$\varepsilon_{\varepsilon \rightarrow \gamma}^{700\text{K}} \approx \sim 0.79\% \quad (5.6)$$

The mixture of the materials from Eqs. (5.4)–(5.6) is $E_M = 183 \times 10^3 \text{ MPa}$ given value of $\sigma_r = 1445.7 \text{ MPa}$. The material data is visibly showing at six times increases of 172 MPa and submit the reduction rising for the plastic deformation than the α -martensite transformation has distinguished. So, which is projected to reduce plastic deformation, the α -martensite transformation has strangely higher recovery stress.

The plastic deformation has been used to decrease and increase, producing very high performance at a higher temperature. Fe–Mn/625 alloy is attained by the precipitation inurement, the α -martensite transformation that values are reduced and reached to decrease for the temperature of M_s . Another script was comparted that Fe–Mn/625 alloys good result of shape-memory effect. M_s and M_s^σ the temperature is deformed to a higher temperature after martensite transformation has changed in stress-induced that region. The sensible of Fe–Mn/625 alloys have improved that quantity for the α -martensite transformation during decreases from a lower temperature of M_s performance for alloys (Class-2) design.

The alloys (Class-1) of 0.016% C, 0.21% C were, and compared that produce strength at a higher temperature, and M_s values are lower temperature. The alloys (Class-2) of recovery stress are 0.21% C at room temperature, which is 360 MPa, 135 MPa advanced materials higher than that of alloy (1) about 0.016% C. The based-on carbon, the best effective materials produce strength of increased, and M_s values deserted the temperature. The materials' influence has been explained by the results of [13–15]. The SMAs way of recovery stress has been used at room temperature in Fe -18.4, Mn - 5.10/625 alloys. We are occupied in this thermal–mechanical exercise of 700 MPa. The major purpose of austenite was significantly bound through an excellently isolated nitride. It is a martensite transformation that cannot yield at that point to get room temperature.

Fe–Mn/625 alloys have been analyzed for results of SAMs better shape effect. They is composited perfectly, with very high recovery stress at room temperature performance. They gratify the subsequent circumstances as follows:

- (a) These materials have been used for the temperature of paramagnetic near anti-ferromagnetic transformation was good lower the M_s for the Neel temperature

(T_N). Fe–Mn/625 alloys are meted the stress-induced martensite origin with possessing of SME.

- (b) M_s the temperature is lower than the room temperature with gaining the greatest shape-memory effect below no constraint.
- (c) The Fe–Mn/625 alloys have been elevated to higher produce strength of the temperature. They are obtained that different from the principles occupied the greatest shape-memory effect below no constraint. The SME of the alloys has been considered by the higher produce strength of room temperature.

Fe–Mn/625 alloys are measured have been designed for composition values in SMAs by the better shape-memory effect. They have higher recovery stress at room temperature.

5.3.3 *Smart 4D-Printing Materials*

To transform the emerging materials are completely an external stimuli proposal the stimulating creative chance of 3D-printing technologies. Fe–Mn/625 composite alloys power has been led to the novel field recognized as 4D printing, the fourth dimension mentioning time. Skylar Tibbit has first introduced that technology with the association by Stratasys TM as printed material. It is automatic to transform done time in reply to an external stimulus. Many researchers have reported in 4D printing and absorbed from publishing utilizes innovative, intelligent material. The gifted in 4D printing was with the general materials science occupation by [16, 17]. Fe–Mn/625 composite alloys have been transformed result time outstanding recovery stress shaped during the printing process produced by the chemical responses and resin diffusion between the printed layers by [18, 18]. Fe–Mn/625 bright alloy powders have been required environmental alterations such as moisture, heat for transformations. This environment is a detrimental consequence of near requests such as electronics. A well-disciplined portable by plotted stresses at multiple positions is a proposal to attain changes without using innovative materials [19, 21]. The 4D print measured the constituent required to familiarize and modified the time using Fe–Mn/625 innovative alloy materials. Fe–Mn/625 bright alloy powder has been separated into subgroups with shape-memory alloys. The thermodynamic changes are self-healing materials supramolecular vicissitudes, and metamaterials engineered vicissitudes, as followed in Table 5.3.

Fe–Mn/625 alloy powders are required conditions for the being of shape-memory effect the incidence of reversible martensitic transformation. It is under the martensitic transformation during cooling from a high temperature well-ordered L_{21} cubic structure to countless lower temperatures, lower symmetry martensitic structures. The martensitic transformation was reversible during heating the samples of diffusion less than absenteeism of a biasing field to lower symmetry martensitic phase found the housed microstructure by the formation of martensitic areas or crystallographic alternatives. Due to the higher produce strength of the temperature and low

Table 5.3 4D-printing smart materials are used in transformative properties and applications

S. No	Smart materials	Technology for printing	Stimulus	4D-printing applications	Reference
1	The alloy powder and thermoplastic binder of Ti–50.5%Ni	J-jet Ink	Process of thermal	alloys of NiTi	[20]
2	The magnetic SMA of Ni–Mn–Ga	3D-binder jet	Process of thermal	Applications in Energy process in weightless materials	[21]
3	SMA for Cu–Al–Ni	Process of SLM	Process of thermal	SMA-medical devices	[22]
4	SMA of Ni–Ti	Process of SLM	Process of thermal	Medicine-aerospace	[23]
5	hydroxyapatite (HA) and (PLA)/15 wt%	Process of FFF	Process of thermal	Bone-fitting implants	[24]
6	PDMS and ZrO ₂ NPs	Process of DIW	Process of thermal	Aerospace and hybrid materials	[25]
7	Polycrystalline zirconia doped with ceria and yttria	Ion-beam miller	Process of thermal	Mechanical plan and energy applications	[26]
8	Fe–Mn/625 alloys	Process of SLM	Process of thermal	Applications in Energy process in weightless materials	Present work

symmetry martensite crystal, the variants energy density difference is the driving force. The reversible transformation martensitic behavior is the typical martensitic as shown in Fig. 5.1. The development of Fe–Mn/625 smart alloy powders has been recognized as an enhancement of 4D printing as a basis for a quicker stride in progress.

5.4 Conclusion

Fe–Mn/625 shape-memory alloys have been measured for electrical resistivity. The recovery stress instantaneously with heating and cooling is performed to force the sample's transformation. It is calculated that for the forced heating and the recovery, stress was increased with decreases for the temperature. As the ref [27, 28] following that, the temperature to recovery stress has produced that strength to a better result with took the plastic deformation region. The ε -martensite transformation was occurred by reducing the temperature. The recovery stress was equal to the critical pressure for the stress-induced ε -martensite. The recovery stress is quickly

reduced at lower temperature with plastic deformation. The ε -martensitic transformation made in the recovery stress reduces the recovery stress considerably. The experimental results analyzed on transformation performance based on the above region to the recovery stress equations in heating and cooling were recognized. The SMAs of Fe–Mn/625 are improved the measurement of the shape-memory effect of powder samples are advanced recovery stress test at room temperature. We are followed that the recovery stress at room temperature formed that sample as a way of 360 MPa, 135 MPa increases the selection with the greatest occupied to shape-memory effect below no restriction. The plastic deformation is decreased to values of ε -martensite transformation has increased the recovery stress. The present improvement of 4D printing has been adapted in stabilizer industrial of time approachable for Fe–Mn/625 alloy powder. The improver work appears to be a feasible method is solved to the plan matters of portion functional complete that parts made of Fe–Mn/625 temperature depend on shape-memory alloys powder.

Acknowledgements I would say thanks a lot to the Department of Science and Technology (DST, Delhi), Government of India, for the award of the DST-FIRST Level-1 (SR/FST/PS-1/2018/35) scheme to the Department of Physics. A grateful let me express thanks to the KLEF offering infrastructure, facilities, basically found (Perform basic instruments), and support to the current investigation.

References

1. Sato A, Yamaji Y, Mori T (1985) *Acta Metall* 34:287–294
2. Sato A, Chishima E, Soma K, Mori T (1982) *Acta Metall* 30:1177–1183
3. Gul JZ et al (2018) 3D printing for soft robotics—a review. *J Sci Technol Adv Mater* 19(1):243–262
4. Miriyev A, Stack K, Lipson H (2017) Soft material for soft actuators. *J Nat Commun* 8(1):596
5. Zolfagharian A et al (2016) Evolution of 3D printed soft actuators. *J Sens Actuators A: Phys* 250:258–272
6. Yan M (1995) *Scr Metall Mater* 32:1313–1317
7. Baruj A, Kikuchi T, Kajiwara S, Shinya N (2002) *Mater Trans JIM* 43:585–588
8. Wang XX, Zhao LC (1992) *Scr Metall Mater* 26:303–307
9. Inagaki H (1992) *Z Metall* 83:90–104
10. Yang JH, Chen H, Wayman CM (1992) *Metall Trans* 23A:1431–1437
11. Bergeon N, Kajiwara S, Kikuchi T (2000) *Acta Mater* 48:4053–4064
12. Li N, Wen YH, Chen MS, Tu MJ (1998) *J Funct Mater* 29:501–502
13. Ullakko K, Jakovenko PT, Gavriljuk VG (1996) *Scripta Mater* 35:473–478
14. Fadiran OO, Girouard N, Meredith JC (2018) Pollen fillers for reinforcing and strengthening of epoxy composites. *Emergent Mater* 1:95–103
15. Bhadra J, Al-Thani N (2019) Advances in blends preparation based on electrically conducting polymer. *Emergent Mater* 2:67–77
16. Tibbitts S (2014) 4D printing: multi-material shape change. *Archit Des* 84:116–121
17. Skylar Tibbitts: The emergence of “4D printing” | TED Talk (n.d.) https://www.ted.com/talks/skylar_tibbitts_the_emergence_of_4d_printing?language=en. Accessed 24 Oct 2019
18. Sundaram S, Kim DS, Baldo MA, Hayward RC, Matusik W (2017) 3D-Printed SelfFolding Electronics. *ACS Appl Mater Interfaces* 9:32290–32298

19. Studart AR, Erb RM (2014) Bioinspired materials that self-shape through programmed microstructures. *Soft Matter* 10 :1284–1294
20. Sibeko MA, Saladino ML, Armetta F et al (2019) Effect of preparation method on the properties of poly(methyl methacrylate)/mesoporous silica composites. *Emergent Mater* 2:363–370
21. Mohamed AMA, Afify R, Omar WAE et al (2020) Influence of deposition temperature and time on the optical behavior of sprayed Cu_2SnS_3 thin films. *Emergent Mater* 3:15–24
22. Carreno-Morelli E, Martinerie S, Bidaux JE (2007) Three-dimensional printing of shape-memory alloys. *Mater Sci Forum Trans Tech Publ* 477–480
23. Mostafaei A, Rodriguez De Vecchis P, Stevens EL, Chmielus M (2018) Sintering regimes and resulting microstructure and properties of binder jet 3D printed Ni–Mn–Ga magnetic shape-memory alloys. *Acta Mater* 154:355–364
24. Donoso GR, Walczak M, Moore ER, Ramos-Grez JA (2017) Towards direct metal laser fabrication of Cu-based shape-memory alloys. *Rapid Prototyp J* 23:329–336
25. Ma J, Franco B, Tapia G, Karayagiz K, Johnson L, Liu J, Arroyave R, Karaman I, Elwany A (2017) Spatial control of functional response in 4D-printed active metallic structures. *Sci Rep* 7:1–8
26. Senatov FS, Niaza KV, Zadorozhnyy MY, Maksimkin AV, Kaloshkin SD, Estrin YZ (2016) Mechanical properties and shape-memory effect of 3D-printed PLA-based porous scaffolds. *J Mech Behav Biomed Mater* 57:139–148
27. Liu G, Zhao Y, Wu G, Lu J (2018) Origami and 4D printing of elastomer-derived ceramic structures. *Sci Adv* 4
28. Lai A, Du Z, Gan CL, Schuh CA (2013) Shape-memory and superelastic ceramics at small scales. *Science* (80)341:1505–1508

Chapter 6

Copper-Based Shape-Memory Alloy



Gopal Krushnaji Kulkarni and Girish Sambhaji Gund

6.1 Introduction

Shape-memory alloys (SMAs) are composed of a distinctive combination of two or more metal alloys. SMAs can regain their original shape or dimension under the circumstance of a certain temperature or magnetic field. This shape recovery phenomenon is named as shape-memory effect (SME), which is a result of the rearrangement of metal atoms and phase of material [1]. The shape-memory alloys possess two stable phases, i.e., martensite (at very low temperature) and austenite (at high temperature) [2]. SMAs contain four inherent and characteristic temperatures corresponding to the beginning and termination of austenite and martensite phase transitions. Generally, these transition temperatures are denoted by A_s (austenite start), A_f (austenite finish), M_s (martensite start), and M_f (martensite finish) [1]. Martensite phase materials are soft and easily deformable. After phase transition of the same material to the austenite phase, it becomes very hard and gains much higher Young's modulus. Therefore, the properties of SMAs can be tuned by the phase transition (with heating and cooling) process [3] and SMAs hold potential applications in various areas such as aerospace, automotive, sensors, actuators, robotics, and biomedical [2].

The phase transition characteristics of SMAs with the variation of temperature and mechanical loading are illustrated in Fig. 6.1. Initially, materials like NiTiNOL at room temperature exhibit a twinned martensite state. This state changes to deformed martensite under the subjection of load, which is generally considered as forward transformation. Further, material heating modifies the deformed martensite state to austenite state (parent state) at high temperature, which is recognized as a reverse

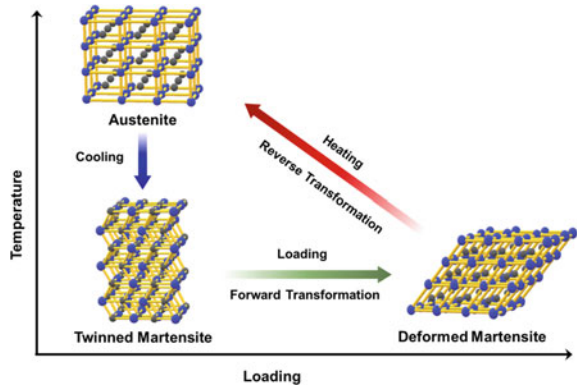
G. K. Kulkarni

Thick and Thin Film Device Laboratory, Department of Physics, Shivaji University, Kolhapur 416004, India

G. S. Gund (✉)

Department of Physics, M.P.A.S.C. College, Panvel 410206, India

Fig. 6.1 Graphical illustration of the different stages of the SMAs



transformation. Further cooling of the material, austenite state converted back into martensite state, which is the basic principle of shape-memory effect [3].

SMAs are of two types: one-way shape-memory alloys (OWSMAs) and two-way shape-memory alloys (TWSMAs). OWSMAs recover their original shape on heating alone, whereas TWSMAs regain their original dimensions (shape or size) on both the heating and cooling processes. Two-way temperature variation features of TWSMAs played a key role in a variety of applications such as aircraft and spacecraft, actuators, automotive, robotics, civil structures, piping, telecommunication, optometry, and medical field. But strain recovery of TWSMAs is mostly half of the recovery strain produced by OWSMAs for the same material. Therefore, strain recovery of TWSMAs needs to develop to explore the variety of applications [2]. Hysteresis is another criterion of SMAs to measure the transformation temperature difference between heating and cooling (i.e., $DT = A_f - M_s$). At these temperatures, material transformed 50% to austenite phase during heating and 50% to martensite phase during cooling [4]. These are the key properties to consider cautiously while choosing SMA material for targeted technical applications; e.g., small hysteresis is essential for fast actuation applications (such as robotics and micro-electromechanical systems (MEMSs)) and large hysteresis to regain the predefined shape within a high-temperature range.

Pseudoelasticity (Superelasticity) is the key property of SMAs, which helps to regain their shape under subsection or removing the load. For example, initially, SMAs are heated till critical temperature, where they transform to an austenite state. Further, the subsection of the load to the same material and at the same temperature drives the phase transition to the martensite phase. Interestingly, elimination of load without varying the temperature is transformed back to austenite phase of same SMA material. Therefore, Pseudoelasticity is a special property of SMAs to easily change the phase of material by applying or removing the load without varying the temperature [3].

6.2 Copper-Based Shape-Memory Alloys

Most of the copper (Cu)-related SMAs contain abundant, cost-effective, easily processable, and exceptional heat and electrical conductivity than the commercially available Ni–Ti SMAs. Therefore, Cu-related SMAs have drawn considerable attention from the research community. Their distinctive properties and capability to regain their original dimensions or shape after heating or cooling even at low transition temperature helped to cover a broad range of commercial applications. Cu-based SMAs like Cu–zinc (Cu–Zn), Cu–aluminum (Cu–Al), and Cu–tin (Cu–Sn) alloys [5] have shown great potential for good shape recovery with and without ternary additions. However, the brittleness, low thermal stability, and low mechanical strength of Cu-related SMAs restricted their commercialization and wide application range. These weaknesses of Cu-related SMAs are accompanying their microstructural characteristics such as elastic anisotropies, coarse grain sizes, and the aggregation of secondary phases or impurities on the grain boundaries [6]. The large grain size of these alloys is the key origin of brittleness. The addition of grain additives keeps grain size down and helps to defeat the brittleness issue. Generally, boron, cobalt, iron, cerium, vanadium, titanium, and zirconium are used as the growth control additives less than 1% to control the grain size of Cu-based SMAs. Also, additives should be added carefully, since they can upset the stability of the structure and lead to affect the shape-memory properties of alloys [7]. Currently, to overcome these issues, efforts are being made like effective alternate processing methods, optimizing the heat treatment, and selective ternary additives (such as Ni, Al, Mn, Zn, and Sn). Altering the internal elemental composition tunes dynamically results of the phase transitions and modifies the mechanical characteristics of the Cu-based SMAs.

Two important binary Cu-based SMAs are Cu–Al and Cu–Zn alloys, which accomplished their shape-memory effect property in the β -phase domain. Further addition of the third constituent in the binary or fourth element in the ternary Cu-based SMAs are modified to adjust and control the phase transformation temperatures ($T \approx 100\text{--}370\text{ }^\circ\text{C}$) in a comprehensive range to fulfill the necessity of commercial applications. It is crucial to mention that the role of transformation temperatures is strongly dependent on the elemental composition of alloys. Copper-based SMAs usually exhibit considerably less hysteresis in comparison with NiTi. Cu–Zn–Al ternary alloy is very easy to fabricate and relatively cheap. Whenever overheated, it decomposes into a stable martensitic phase. The characteristics and shape-memory performance matrix of Cu–Al–Ni and Cu–Zn–Al SMAs are summarized in Table 6.1.

Additives like B, Co, Ti, and Zr play a key role to control grain size from 50 to 100 nm. Usually, boron is utilized to increase the material's ductility. Cu–Al–Ni alloy is considerably less sensitive to stability and aging phenomena. This ternary alloy show slows hysteresis than NiTi alloy and downgrades mechanical features as the concentration of Ni enhances beyond 4 wt% [8]. The martensite phase stabilizes with the increase of Al content within the alloy. Also, Al addition decreases the transformation temperatures. Cu-related SMAs are capable to display a pseudoelastic

Table 6.1 Shape-memory performance matrix of Cu-based SMAs

S. No	Composition of Alloy	Transition temperature (°C)	Hysteresis (°C)	Strain (Tensile) (%)	Strain Recovery (%)	Comments
1	Cu–Al–Ni	100.0–400.0	21.50	3.0–5.0	60.0–90.0	<ul style="list-style-type: none"> • Cost-effective • Good shape-memory • Worth pseudoelastic performance • Brittle mechanical features • Steady phase precipitation about 200° C • Atomic reordering in a quenched sample produces a change in transition temperature
2	Cu–Zn–Al	120.0	15.0–25.0	4.0	70.0–85.0	<ul style="list-style-type: none"> • Good thermal conductivity • Good recovery of SM strain • Low cost • Very delicate
3	Cu–Al–Be	150.0–200.0	20.0–25.0	3.0–5.0	80.0–90.0	<ul style="list-style-type: none"> • Good recovery of SM strain • Good transition temperatures • Anticorrosive in nature
4	Cu–Al–Ni–Mn	230.0–280.0	15.0–20.0	3.0–4.0	90.0–100.0	<ul style="list-style-type: none"> • Good SM performance • Low cost • High transition temperatures • Anticorrosive in nature
5	Cu–Al–Ni–Ti	120.0–260.0	12.0–20.0	2.50–4.0	90.0–100.0	<ul style="list-style-type: none"> • Good SM performance • Low cost • High transition temperatures • Anticorrosive in nature

(continued)

Table 6.1 (continued)

S. No	Composition of Alloy	Transition temperature (°C)	Hysteresis (°C)	Strain (Tensile) (%)	Strain Recovery (%)	Comments
6	Cu–Al–Ni–Fe	210.0–250.0	12.0–15.0	9.0	40.0	<ul style="list-style-type: none"> • Low SM performance • High elasticity • Low cost • High transition temperatures • Anticorrosive in nature

strain ~ 4.0–6.0%. High pseudoelastic strain levels were gained with the martensite-to-martensite transition. Nearly 18% of the pseudoelastic strain can be illustrated by the single crystal of $\text{Cu}_{81.8}\text{Al}_{14}\text{Ni}_{4.2}$ SMA accompanying 100% of the shape recovery [9]. The addition of the third component specifically Sn with a weight level of 34.7% in the Cu–Zn binary alloy has displayed fewer transformation temperatures, $M_f \sim 208 \text{ }^\circ\text{C}$ and $A_f \sim 235 \text{ }^\circ\text{C}$ [10]. Recently, beryllium (Be) added (~0.6 wt. %) Cu–Al alloy revealed a reduction of transition temperatures from $200 \text{ }^\circ\text{C}$ to $150 \text{ }^\circ\text{C}$ of Cu–Al SMAs with superior thermal stability.

Cu-based SMAs can comprise various alloy combinations. Still, Cu–Al–Ni and Cu–Zn–Al are mostly favored alloys because of their low cost and stable functional features. The Cu-based SMAs are much attentive to the research community than NiTi due to their low production cost and high transformation temperature range. The operating temperature range of SME of various alloys for automobile applications is summarized in Fig. 6.2. The Cu-based SMAs cover a wide temperature region of operation than the commercially available NiTi-based binary and ternary alloys.

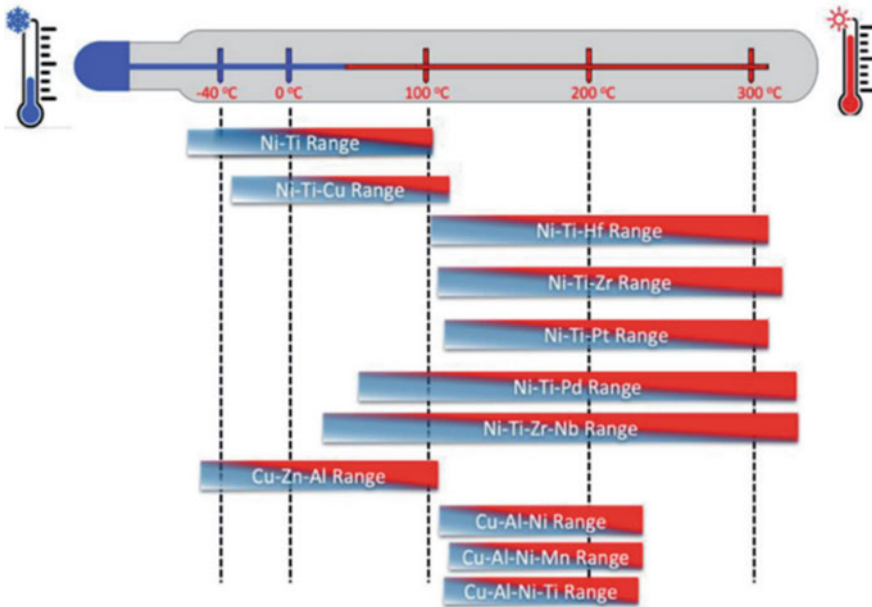


Fig. 6.2 Operating temperature range of various SMAs for automobile applications. Reproduced from [11], originally published under a CC BY 4.0 license, <http://dx.doi.org/10.5772/intechopen.86193>

6.2.1 *Brief Applicability of Cu-Based SMAs Over NiTiNOL*

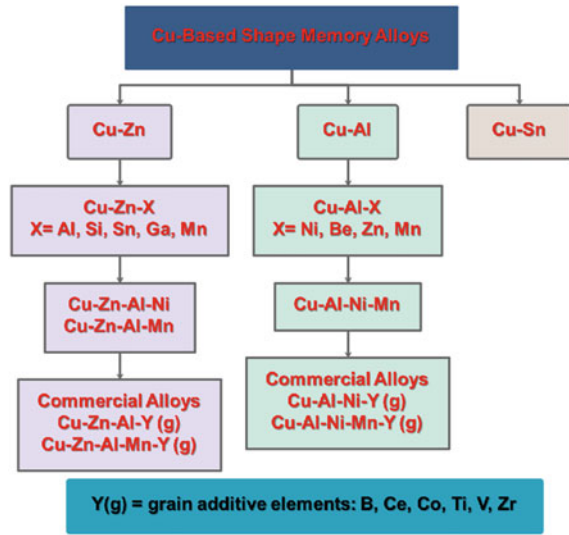
Principally, the SMA applications are classified into four classes depending on the fundamental limit of their shape-memory component [12, 13]. SME can be used to move the load and store the twisting vitality. The SMAs clamped potential applications in the automobile, machine, aviation, robotics, ventilation and warming, safety and security, and MEMS devices. Among these, most of the applications are covered by commercially available NiTiNOL SMAs, whose operational temperature range lies from $-40\text{ }^{\circ}\text{C}$ to $+125\text{ }^{\circ}\text{C}$ [14, 15]. The binary alloy system of NiTi SMA works well for different cycles inside vehicle zones with the temperature variation from $-50\text{ }^{\circ}\text{C}$ to $+110\text{ }^{\circ}\text{C}$ [15, 16, 17], but not in higher temperature zones like under the engine hood. The SMAs must have a high M_f temperature over the extreme working temperatures for proper working. The widely recognized and cost-effective Cu–Al–Ni SMAs can change the temperatures up to $200\text{ }^{\circ}\text{C}$, but these SMAs are delicate, unstable, of low fatigue quality, and unsuitable for cyclic activities [16, 18–20]. A wide temperature range of SMAs can be achieved, but those materials are generally expensive and used in vehicle applications [15].

Another huge usage of SMAs is as an absorber in bridges, which was successfully utilized by European Association. They studied the effect on the earthquake harm and the catastrophe harm using seismic vibration. This investigation developed a four-story construction, which proposed tendons methods to limit the earthquake conceivable harm. This investigation discovered that the structure without SMA was demolished, whereas SMA got less harm. The executed tendons as an absorber depend on the SME features like elastic behavior, which decreased the shocking waves of the seismic earthquake. The different alloy compositions of Cu-based SMAs are being investigated across the globe, which is summarized below in Fig. 6.3 with the base alloys.

6.2.2 *Cu–Zn System*

It is observed that the Cu–Zn binary alloy system has shown better shape-memory characteristics, better ductility, and is less disposed to grain boundary fracture than Cu–Al alloys. However, the Cu–Zn alloy system possesses the issue of low M_s phase at room temperature. Therefore, unstable thermal behavior at fewer temperatures (below $100\text{ }^{\circ}\text{C}$) restricted its applications. This problem motivated the researcher community to focus on developing ternary alloys using different kinds of additives. Some of them are Al, Ga, Si, and Sn, which play the main role to achieve low M_s as well as parent austenite phase in Cu–Zn binary alloys. The adaptability of Al as a ternary alloying element can reduce grain boundary fracture, so easy to melt and enhances deformability at lower temperatures [21].

Fig. 6.3 Taxonomy of Cu-based SMAs



6.2.2.1 Cu–Zn–Al System

The Cu–Zn–Al ternary alloy was comprehensively investigated to utilize its shape-memory characteristics for the applications such as actuators and fasteners [22]. The Cu–Zn–Al alloy is mostly studied than other Cu-based SMAs due to its high strain recovery percentage. Ahlers recognized the effect of composition change in Cu–Zn–Al alloy on M_s temperature, which revealed the lower shift of M_s temperature with an increase in Zn content. Such SMAs lead to the ordered phase transformation from the austenitic phase to the martensitic phase. The Cu–Zn–Al ternary alloy is facile in synthesis, but issues of brittleness, low fracture, and fatigue strength will exist from the coarse grain structure. The fatigue properties of different alloy combinations can be modified by grain size refining and texture of alloy. Also, Cu–Zn–Al alloys are susceptible to aging, which affects the transformation temperatures and constrains their broad range of applications.

Additives like Ce, Ti, Zr, Co, Fe, B, V, and Be are continuously playing an important role to improve the grain structure along with their mechanical and shape-memory characteristics of SMAs [23]. Therefore, the adoption of the additive approach is crucial to overcome the problems possessed by the Cu–Zn–Al system, as it is the future commercial system.

6.2.2.2 Cu–Zn–Ni System

These SMAs are engineered by controlling Ni and Zn concentrations. The concentrations of Ni and Zn tune the transformation temperatures, the morphology of the martensite phase, and strain recovery contained by Cu–Zn–Ni SMAs [5]. Tables 6.2

Table 6.2 Transition temperatures of the alloys with increasing Zn concentrations

Chemical composition wt%				Transition Temperatures (°C)			
Alloy	Cu	Zn	Ni	M _f	M _s	A _s	A _f
1	49.3	45.25	5.5	74.0	90.0	95.0	138.0
2	48.5	45.6	5.8	82.0	106.0	105.0	145.0
3	48.2	45.65	6.1	88.0	112.0	116.0	152.0
4	47.7	46.1	6.2	108.0	115.0	118.0	143.0

Table 6.3 Transition temperatures of the alloys with increasing Ni concentrations

Chemical composition wt%				Transition Temperatures (°C)			
Alloy	Cu	Zn	Ni	M _f	M _s	A _s	A _f
5	48.9	48.0	2.9	86.0	111.0	101.0	126.0
6	49.2	46.9	3.7	72.0	121.0	116.0	143.0
7	49.3	45.9	4.5	66.0	132.0	126.0	156.0
8	48.5	45.6	5.8	41.0	143.0	143.0	176.0

and 6.3 summarize the variation of transformation temperatures with the chemical composition of alloys. From both tables, it is seen that Cu/Zn ratio is kept nearly the same, whereas Ni content is kept comparatively much less and varies. From the tables, it is observed that the transformation temperatures change with a change in Ni or Zn contents. Specifically, increasing Zn concentrations lowers down the transformation temperature, whereas Ni concentrations shift up the transformation temperature.

From Tables 6.2 and 6.3, it is found that the alloy is martensitic below the M_s temperature, and austenitic above the A_f temperature. Therefore, such kinds of alloys can be preferably intended to use in various temperatures and for low-temperature applications [16]. Figure 6.4 shows the morphology of Cu–Zn–Ni SMAs gained by step quenching [24]. Cu–Zn–Ni SMAs exhibited good anticorrosive behavior with increasing wt % from 2 to 9 of Ni content in freshwater, Hank's solution, and seawater.

6.2.3 Cu–Al System

Cu–Al alloy has also attracted immense attention from researchers due to its superior properties. This system is also based on Cu-based SMAs. These alloys are cost-effective and facile in synthesis. The properties of Cu–Al alloys can be effectively tuned by adding ternary elements like Be, Mn, and Ni [25]. The addition of the third element in Cu–Al alloy expands the single phase at higher temperatures and improves the thermal stability of the alloys. This ternary addition empowers the applicability

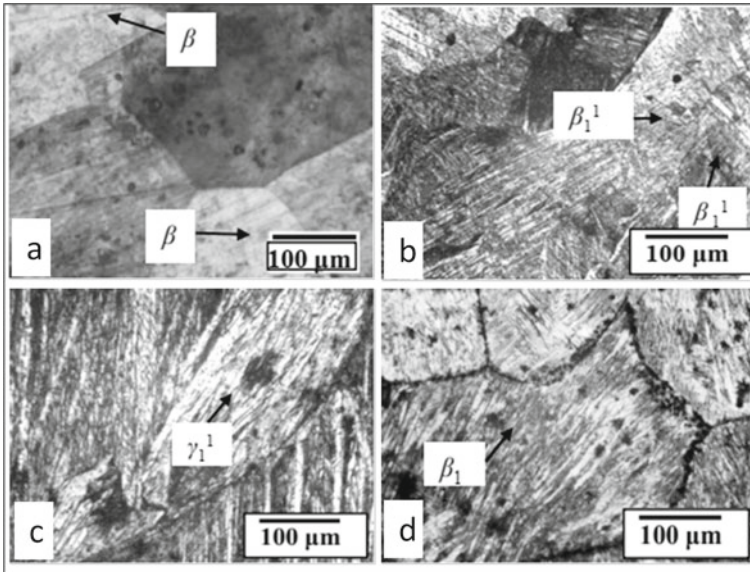


Fig. 6.4 SEM images of Cu–Zn–Ni SMAs prepared by step quenching. **a** Alloy 2; **b** Alloy 4; **c** Alloy 5; **d** Alloy 7. Reproduced from [5], originally published under a CC BY 4.0 license, <https://doi.org/10.4236/jmmce.2014.22011>

of Cu–Al–based ternary alloy in the broader temperature range than commercially available NiTi alloy.

6.2.3.1 Cu–Al–Fe System

The Cu–Al SMAs have been investigated with the additions of Ni, Fe, and Mn in the previous study for their shape-memory effect [1]. Figures 6.5 and 6.6 show the SEM micrographs of Cu–Al–Fe alloys during the aged and quenched states [26]. Cu–Al–Fe alloys are a good choice to work above 200 °C with a great shape-memory effect and mechanical properties. The microstructural advancement of the martensite structure has been observed during the different cooling rates. However, a more in-depth analysis needs to be carried out on the ductility, martensitic transformation, microstructure, and SME characteristics under the aged and quenched states.

6.2.3.2 Cu–Al–Ni System

This system is the most noticed class of the Cu–Al–based ternary SMAs owing to its good thermal and electrical conductivity whereas, other features like high transformation temperatures, large recoverable strain, and thermal stability of Cu–Al–Ni SMAs have confirmed its importance for commercial applications [27]. In

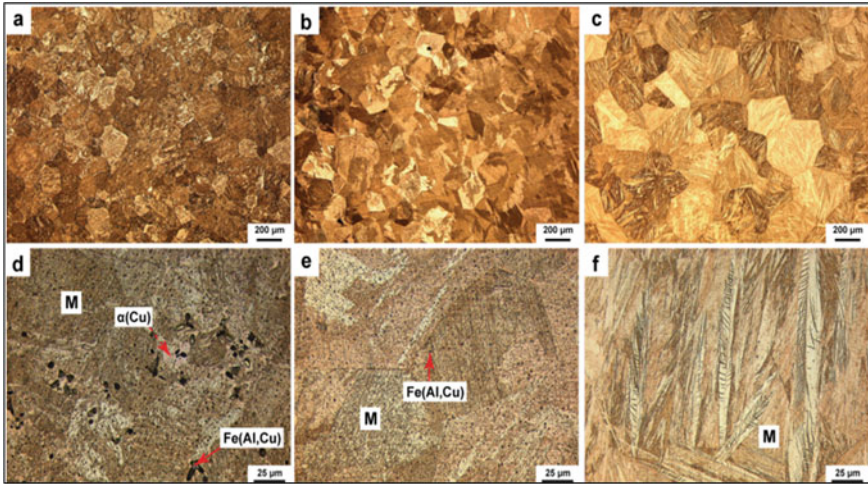


Fig. 6.5 The SEM images of $\text{Cu}_{84-x}\text{Al}_{11+x}\text{Fe}_5$ ($x = 0, 1, 2$) alloys (**a–c**) low and (**d–f**) high magnification under quenched state. **a** and **d** $x = 0$, **b** and **e** $x = 1$, and **c** and **f** $x = 2$. Reprinted from [26] Copyright © 2014 with permission from Elsevier B.V

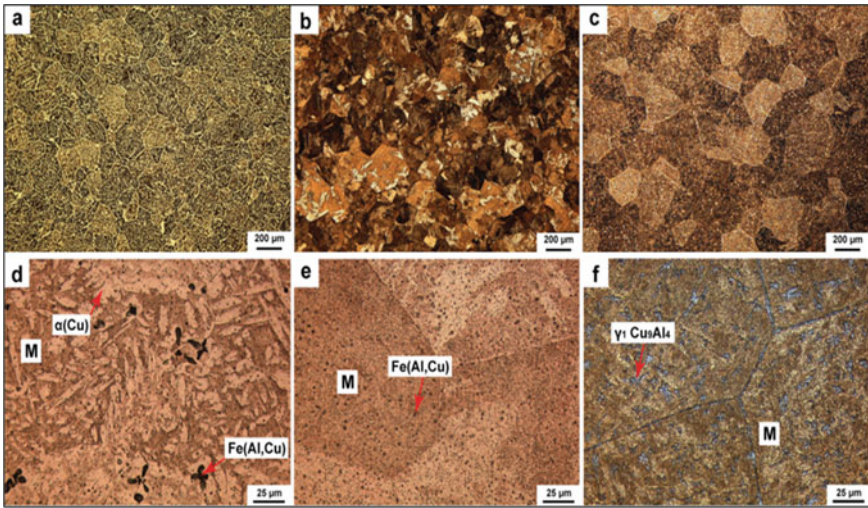


Fig. 6.6 The SEM images of $\text{Cu}_{84-x}\text{Al}_{11+x}\text{Fe}_5$ ($x = 0, 1, 2$) alloys (**a–c**) low and (**d–f**) high magnification under aged state. **a** and **d** $x = 0$, **b** and **e** $x = 1$, and **c** and **f** $x = 2$. Reprinted from [26] Copyright © 2014 with permission from Elsevier B.V

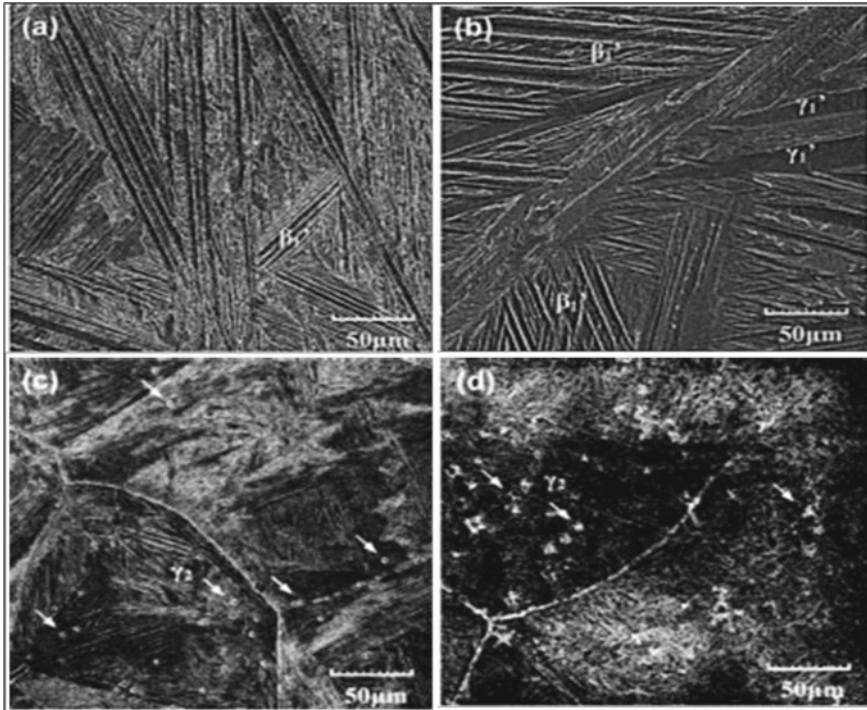


Fig. 6.7 SEM images of Cu–13.0Al–4Ni **a**, Cu–13.5Al–4Ni **b**, Cu–13.7Al–4Ni **c**, and Cu–14.0Al–4Ni **d** SMAs. Reprinted from [20] Copyright © 2010 with permission from Elsevier B.V

the Cu-based SMA group, this ternary alloy only contains high-temperature SMA, which may be used for load-bearing high-temperature applications.

These ternary alloys are less inclined to aging than Cu–Zn–Al but have restricted formability because of their brittle nature. Usually, the Cu–Al–Ni system comprises 4 wt. % Ni; after that, the alloy becomes more brittle and lowers down the transformation temperature. The grain refining additives and processing methods strongly influence the SME properties of these alloys. Figure 6.7 displays the SEM images of Cu–Al–Ni alloys [11]. Micro-alloying with the rapid solidification method, elements like B, V, Zr, and Ti, and powder metallurgy significantly modified the ductility and mechanical properties of these alloys [28].

6.2.3.3 Cu–Al–Mn System

Usually, the Cu–Al–Mn system is advantageous for high ductility. This ternary alloy revealed excellent cold workability and very good shape-memory properties for Al content of 18% and below it. At low Al concentrations, the austenitic (parent) phase possesses a low degree of order which favors the martensitic transformation and

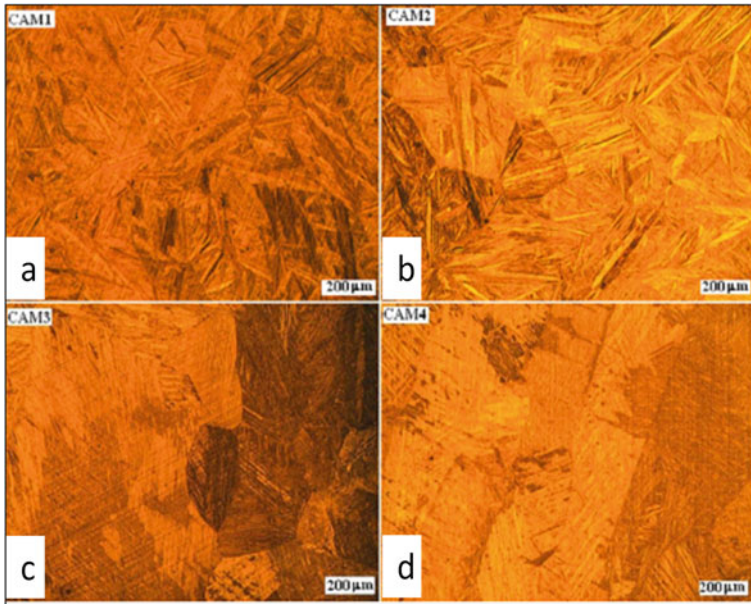


Fig. 6.8 SEM micrographs of **a** CuAlMn1, **b** CuAlMn2, **c** CuAlMn3, and **d** CuAlMn4 samples. Reproduced with permission from [32]. Copyright ©2014 Acta Physica Polonica A

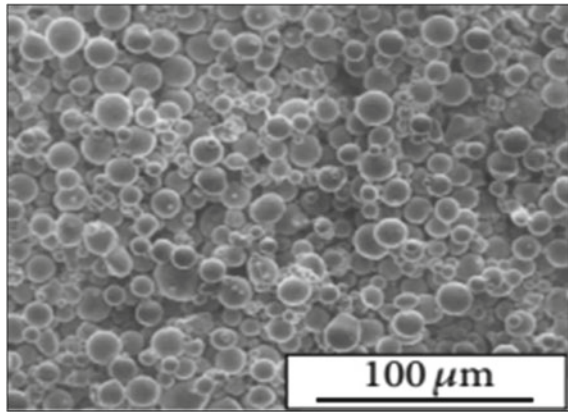
leads to good shape recovery. It is also observed that the tensile strength and the ductility of these ternary alloys can be enhanced by adding the cerium (Ce) [29]. In comparison with commercially available NiTi alloys, this ternary alloy displays large superelastic strain and other functional characteristics like TWSMA behavior and high damping feature [30, 31]. Figure 6.8 displays the SEM images of Cu–Al–Mn alloys [32].

The addition of Ni to these ternary alloys was found to be an effective approach to attain the fine-grain morphology and superelasticity within the specific temperature domain [33]. Even small additions of a new quaternary element to this ternary alloy system led to improving the shape-memory features but lowered the transition temperatures [34].

6.2.3.4 Cu–Al–Be System

The incorporation of constituent Be in the Cu–Al system plays a crucial role to reduce the transformation temperature of these alloys [35]. Moreover, Cu–Al–Be possesses superior heat resistance like Cu–Al–Ni alloys. Additionally, thermal treatment is employed to control martensite phase stability and enhance its utilization in a broad range of high-temperature applications [36].

Fig. 6.9 SEM image of Cu–Sn alloy. Reproduced from [37], originally published under a CC BY 4.0 license. Copyright © 2016 Ahmed Nassef and Medhat El-Hadek, <https://doi.org/10.1155/2016/9796169>



6.2.3.5 Cu–Sn System

The majority of the Cu–Sn combination-based SMAs show their transformation temperatures (M_s , M_f , A_s , and A_f) below room temperature. In this way, these composites are not advantageous for the devices, which work at a temperature near or above room temperature. The transformation temperature tunes with the chemical compositions of the alloys. Additionally, Cu–Sn alloy shows shape-memory effect in a narrow range of compositions [13], very low strain recovery, and large thermal hysteresis. Figure 6.9 displays the spherical type morphology of prepared Cu–Sn alloy [37].

Usually, the Cu–Sn alloys go through martensitic transitions, which have inferior thermoelastic features and deteriorate SME properties during aging at low temperatures. The drawbacks of narrow parent phase and aging restricted studies and potential applications of the Cu–Sn alloy system. To achieve thermal stability, parent phase and higher ductility addition of Mn are found to be more effective in the Cu–Sn alloy system [37].

6.3 Transition Temperature-Controlling Component

The martensitic phase transition and shape-memory properties are key properties of SMAs, which are displayed during heating and cooling cycles within the temperature range. The thermo-mechanical features are controlled by the irrational habit planes, austenite–martensite interphases, and complex orientation relationships. These features are examined by calorimetric and resistivity studies. Additionally, the transition temperature is sensitive to the content of elements, alloy composition, and impurities within SMAs, and can considerably affect the SME properties. Consequently, precise control of composition has extreme significance to obtain the ideal transformation temperature for the SMAs in the strip or wire structure to display

SME at a specific temperature. Loss of volatile and low melting components (Zn, Al, etc.) can't be prevented in air melting furnaces; therefore, the induction melting method is preferred.

Studies have been involved to anticipate the impact of composition and thermal conductivity on transformation temperatures, which are targeted to enhance the temperature range or increase achievable temperature. Such optimizations are important for making important engineering parts of actuators and pinpointing the temperature scope of their function [38–49]. Table 6.4 depicts the comparison of transformation temperature for the various compositions of alloys. Such comparative study gives an understanding of the impact of additives, composition, and thermal cycle on the transition temperatures.

Finally, the outcomes are summarized as follows:

- (i) The transformation temperature range revealed for the three fundamental Cu-based SMAs without any other elemental additives are in the range of.
 - (1) –200–150 °C by Cu–Al–Mn;
 - (2) –200–120 °C by Cu–Zn–Al;
 - (3) –200–170 °C by Cu–Al–Ni.
- (ii) However, a wide variation has been accounted for additives, composition, fundamental elements, and processing/aging factors [12, 15, 50–53].
- (iii) Small differences in the composition of the fundamental alloy combinations like Cu–Al–Mn combinations bring remarkable progress in transformation temperature variation ~50 K [54].
- (iv) The increase of Al content in Cu–Al–Mn alloy caused a decrease in transformation temperature [55].
- (v) Small addition of additives like Zn or Ni in the Cu–Al–Mn alloy brings down the transition temperature [Ms] drastically. The amount of Zn or **ration** of Mn: Zn play key role to control the transition temperature. A higher proportion brings down the temperature [56].
- (vi) The temperature range of MT of Cu–Al–Ni alloy can be “balanced” within –200 to 200 °C [4, 7]. However, a few cases of Cu–Al–Ni alloys recorded exceptionally high transformation temperatures due to aging conditions involved during processing [57].
- (vii) Zn content of 62.0% within the Cu–Al–Zn alloy brings down transformation temperature up to 30 °C through an intermediate process [58].
- (viii) It is also observed that the application of pressure influenced the transition temperature of Cu–Al–Mn–Ni alloy [59]. The increase of pressure from 0.1 to 0.4 GPa reported around 20 K enhancement of transformation temperature.
- (ix) A difference of 30 K has been accounted for assuming small variations in the aging conditions in a similar alloy [Cu–Al–Mn–Ni] treated indistinguishably till quenching [60].
- (x) Melt spinning of Cu–Al–Mn composites to ribbons reduces the transition temperatures [61].

Table 6.4 Tuning of transition temperatures with treatment and composition of alloys

Composition Wt %		Transformation temperatures (K)							Remarks	Ref. No
Cu	Al	Mn	Ni	Zn	M _f	M _s	A _s	A _f		
81.9	9.5	8.6	-	-	342	364	373	396		
83.3	10.2	6.5	-	-	379	400	408	425		
80.9	10.5	8.5	-	-	310	326	327	342		
81.10	10.80	8.10	-	-	332	355	342	367	[38]	
87.82	11.27	0.91	-	-	381	404	413	428		
83.52	11.36	5.12	-	-	373	395	393	419		
82.08	12.45	5.47	-	-	391	412	417	435		
69.02	27.6	-	3.2	-	-	265	-	-		
69.6	20.1	5.5	-	4.8	-	-	-	-	[39]	
70.1	20.4	4.2	-	5.3	-	260	-	-		
82	14	-	4	-	699	801	830	883	[40]	
62.86	6	-	-	10.28	-	-	303	-	With an intermediate process of rebetaizing	
81.5-83	14	-	3-4.5	-	300	-	-	-	[42]	
82	14	-	4	-	273	-	-	-	[43]	
83	13	-	4	-	420	-	-	-		
69.8	3.8	-	-	26.4	316	297	310	323	Different thermal cycles adopted	
-	-	-	-	-	345	336	347	360		
-	-	-	-	-	443.5	396.6	427.7	477.6		
-	-	-	-	-	457.3	417.4	429.7	471.1		

(continued)

Table 6.4 (continued)

Composition Wt %		Transformation temperatures (K)					Remarks	Ref. No	
Cu	Al	Mn	Ni	Zn	M _f	M _s			A _s
-	-	-	-	-	448.6	419.8	439.9	473.1	
85.18	11	3.82	-	-	444.4	417.6	438.9	496	Different heat cycles implemented
					469.40	440.40	452.10	484.80	[45]
					466.7	438.8	456.5	478.9	
					475.4	444.8	456.6	480	
									Pressure GPa
					327.9	355.1	327.9	355.1	0
					334	365.4	334	365.4	0.1
80.3	12.7	2	5	-	338.1	369.2	338.1	369.2	0.2
					340.9	370.4	340.9	370.4	0.3
					343	371.8	343	371.8	0.4
Bal	3.30	-	-	25.40	546				
Bal	5.8	-	-	20.80	341				
Bal	5.34	-	-	18.10	532				
					215	-	-	240	Different heat cycles implemented
71.5	17	11.5	-	-	221	-	-	239	
					231	-	-	242	
73	17	9.5	2	-	227	-	-	243	Different heat cycles implemented
					223	-	-	239	

(continued)

Table 6.4 (continued)

Composition Wt %		Transformation temperatures (K)							Remarks	Ref. No
		Cu	Al	Mn	Ni	Zn	M _f	M _s		
73.50	17.0	9.50	3.0	-	235	249	-	-	-	
					239	-	-	254		Different heat cycles implemented
					240	-	-	253		
82	14	-	4	-	801	699	830	883		[48]
71.54	16.6	9.80	2.0	-	211	-	-	240		
72.13	16.9	10.4	0.5 Co	-	209	-	-	238		-
71.28	16.9	11.5	0.1 Si; 0.2 B	-	254	-	-	275		

- (xi) Excessive transformation temperatures greater than 500 °C have been reported for the Cu–Al–Ni alloy system. Although this isn't conventional, yet presumably the preparing parameters or use of high purity metals can be the reason [62].
- (xii) Aging temperatures compared to aging time are imperative to give the large enthalpy in various Cu–Al–Mn composites.

6.4 Challenges and Perspectives

Cu-based ternary SMAs (specifically basic Cu–Al–Mn, Cu–Zn–Al, and Cu–Al–Ni alloys) have been a key focus of numerous theoretical and experimental investigations predominantly centered on the thermoelastic martensitic transformation (MT) for a couple of decades. Along with the SME, pseudoelastic, and superelastic properties, these alloys reveal a temperature memory effect (TME) after an inadequate reverse MT. Engineering the SME, TME, and high damping applications feasible with the SMAs can discover commercial use in diverse applications, like biomechanics, vibration control, medication, industry, and aeronautics. Presently, a couple of Cu-based SMAs are commercially available, but their uses are limited owing to its poor properties mentioned as follows:

- (i) High brittleness, low thermal stability, and low mechanical strength correspond to microstructure, for example, high flexible anisotropies, coarse grain sizes, and the accumulation of secondary phases or contaminations along the grain boundaries.
- (ii) SME (Pseudoelasticity) of the different alloys is sensitive to microstructural topography and chemical composition. Besides, basic impurities like carbon, nitrogen, and oxygen can cause a massive change in the phase transformation temperature while losing the mechanical characteristics of these combinations.

Efforts should be conducted to defeat the above-mentioned limitations through ternary additions, which can modify the SME, thermal stability, and optimize the thermal cycles. Likewise, alternative preparing procedures such as rapid solidification, powder metallurgy procedures, and proper mixing of grain refiners could address those issues. Nevertheless, the powder metallurgy technique is hard to apply efficiently due to its unpredictability, while the rapid solidification method is not suitable to prepare the bulk of fine-grained alloys. Still, commercial applications need engineering of material, which transform at very high temperature (over 150 °C), contain stable martensite phase even exposed for an extremely long time at elevated temperatures, and consist of high regain of stresses. Still, significant advancement is not accounted for issues like the stability of the martensite phase, decomposition of the austenite or martensite phase, fragility, and huge cost. The research activities in the area of SMAs to be discovered worldwide are illustrated in Fig. 6.10 and mentioned as follows:

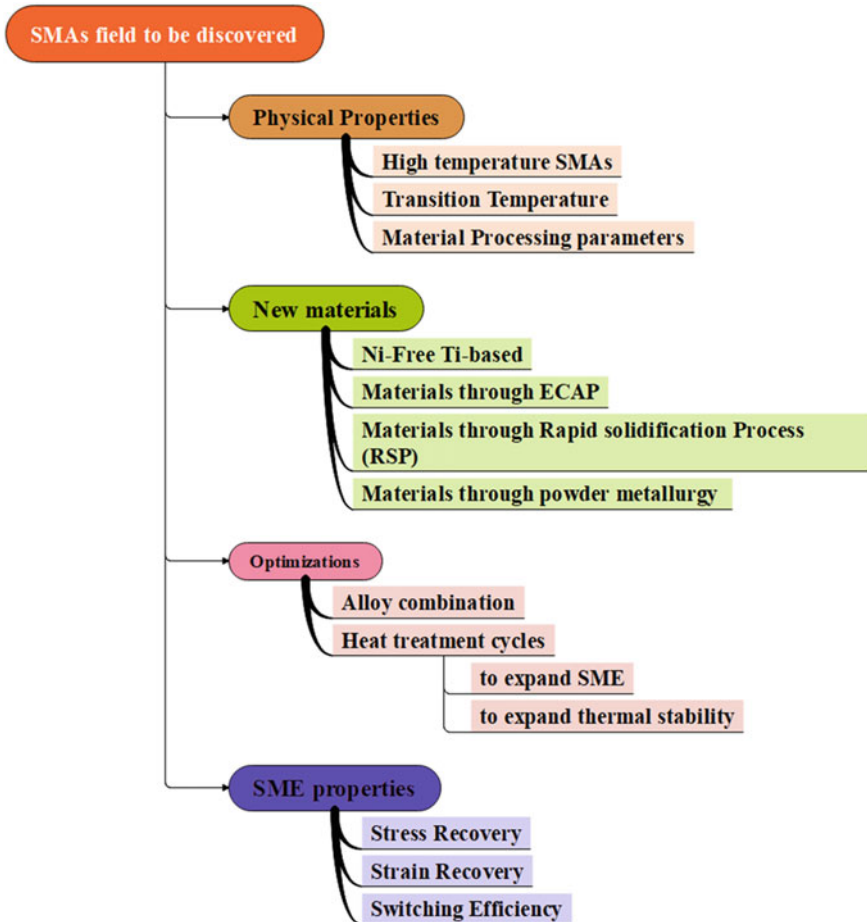


Fig. 6.10 Illustration of research field to be focused for the development of SMAs and SME

- (i) Enhanced characteristics in present SMAs, like high-temperature SMAs, enhancing transition temperature, diminishing M_f temperature, advancement of preparation parameters, etc.
- (ii) Creation of new SMAs, such as SMA thin films, Ni-less and Ti-related SMAs, porous, nanocrystalline, and amorphous SMAs, by using techniques like ECAP, rapid solidification processing (RSP), Powder Metallurgy (PM), etc.
- (iii) Enhancement of strain and stress recovery and switching efficiency.
- (iv) Optimization of alloy combinations and thermal treatment cycles to increase the thermal stability and SME in the strip and wire structure. Specifically, the Cu–Al–Ni system for enhanced mechanical characteristics, Cu–Al–Mn alloy combinations for a variety of compositions for better ductility, and Cu–Zn–Al for high transformation temperatures (375–475 K).

References

1. Sampath V, Gayathri SV, Srinithi R (2019) *Bull Mater Sci* 42:229
2. Jani JM, Leary M, Subic A, Gibson MA (2014) *Mater Des* 56:1078–1113
3. Alaneme KK, Okotete EA (2016) *Eng Sci Technol Int J* 19:1582–1592
4. Buehler WJ, Wang FE (1968) *Ocean Eng* 1:105–108
5. Sathish S, Mallik US, Raju TN (2014) *J Miner Mater Charact Eng* 2:71–77
6. Sutou Y, Omori T, Kainuma R, Ono N, Ishida K (2002) *Metall Mater Trans A* 33:2817–2824
7. Guerioune M, Amiour Y, Bounour W, Guellati O, Benaldjia A, Amara A, Chakri N E, Ali-Rachedi M, Vrel D (2008) *Int J Self Propag High Temp Synth* 17(1):41–48
8. Tadaki T (1998) Cu-based shape-memory alloys. In: Otsuka K, Wayman CM (eds) *Shape-memory materials*. Cambridge University Press, Cambridge, pp 97–116
9. Otsuka K, Sakamoto H, Shimizu K (1979) *Acta Metall* 27(4):585–601
10. Eisenwasser J, Brown L (1972) *Metall Trans* 3(6):1359–1363
11. Al-Humairi SNS (2019) Cu-based shape-memory alloys: modified structures and their related properties. *Recent Adv Eng Mater Metall Intech Open*. <http://dx.doi.org/https://doi.org/10.5772/intechopen.86193>
12. Baghani M, Ganjiani M, Rezaei M (2018) *Int J Appl Mech* 10(07):1850070
13. Velmurugan C, Senthilkumar V, Dinesh S, Arulkirubakaran D (2018) *Mach Sci Technol* 22(3):355–401
14. Leo DJ et al (1998) Vehicular applications of smart material systems. In: *Smart structures and materials 1998: industrial and commercial applications of smart structures technologies*. 5th annual international symposium on smart structures and materials. San Diego, CA, United States. <https://doi.org/10.1117/12.310625>
15. Stoeckel D (1990) *Mater Des* 11(6):302–307
16. Hodgson D, Wu MH, Biermann RJ (1990) Properties and selection: nonferrous alloys and special-purpose materials, metals handbook, vol 2. ASM International, USA, p 897
17. Rao A, Srinivasa A (2018) *Mech Adv Mater Struct* 1–13
18. Wilkes KE, Liaw PK (2000) *JOM* 52(10):45–51
19. Kaya E, Kaya I (2019) *Int J Adv Manuf Tech* 100(5–8):2045–2087
20. Chang SH (2011) *Mater Chem Phys* 125(3):358–363
21. Asanovic V, Delijic K (2007) *J Metall* 13(5):59–64
22. Bujoreanu LG, Lohan NM, Pricop B, Cimpoesu N (2011) *J Mater Eng Perform* 20(3):468–475
23. Mallik US, Sampath V (2008) *Mater Sci Eng A* 478:48–55
24. Sathish S, Mallik US, Raju TN (2013) *J Miner Mater Charact Eng* 1:49–54
25. Alaneme KK (2014) *Acta Metall Slov* 20(4):366–374
26. Yang S, Wang YSC, Liu X (2014) *Mater Sci Eng B* 185:67–73
27. Todorovic A, Rudolf R, Romecivic N, Dordevic I, Milosevic N, Trifkovic B, Veselinovic V, Colic M (2014) *Contemp Mater* 2:228–238
28. Fugazza D (2003) Shape-memory alloy devices in earthquake engineering: mechanical properties, constitutive modelling and numerical simulations (Master thesis). University of Pavia, Italy
29. Motoyasu G, Kaneko M, Soda H, Mclean A (2001) *Metall Mater Trans A* 32A(3):585–592
30. Dasgupta R (2014) *J Mater Res* 29:1681–1698
31. Sutou Y, Omori T, Wang JJ, Kainuma R, Ishida K (2004) *Mater Sci Eng A* 378:278–282
32. Canbaya CA, Karagozb Z, Yakuphanoglua F (2014) *Acta Phys Pol A* 125:1163–1166
33. Omori T, Koeda N, Sutou Y, Kainuma R, Ishida K (2007) *Mater Trans* 48(11):2914–2918
34. Kumar P, Jaina K, Hussain S, Pandey A, Dasgupta R (2015) *Rev Mater* 20(1):284–292
35. Chentouf SM, Bouabdallah M, Cheniti H, Eberhardt A, Patoor E, Sari A (2010) *Mater Charact* 61:1187–1193
36. Lopez-ferreno I, Breczewski T, Ruiz-larrea I, Lopez-echarri A, No ML, Sanjuan J (2013) *J Alloys Compd* 577:S463–S467
37. Nassef A, El-Hadek M (2016) *Adv Mater Sci Eng* 9796169:1–10. <https://doi.org/10.1155/2016/9796169>

38. Yi HC, Moore JJ (1990) *J Mater Sci* 25:1159–1168
39. Asanovic V, Delijicm K, Jaukovic N (2008) *Scr Mater* 58:599–601
40. Ma J, Karaman I, Noebe RD (2010) *Int Mater Rev* 55(5):257–315
41. Saule F, Ahlers M, Kropf F, Rivero EB (1992) *Acta Metall* 40(12):3229–3238
42. Ling-Fei C, Ming-Pu W, Zhou L, Ben X, Yu-Chang S (2002) *Trans Nonferrous Soc China* 12(4):716–719
43. Wang Q, Han F, Cui C, Bu S, Bai L (2007) *Mater Lett* 61:5185–5187
44. Chen J, Lia Z, Zhao YY (2009) *J Alloys Compd* 480:481–484
45. Dagdelen F, Gokhan T, Aydogdu A, Aydogdu Y, Adiguzel O (2003) *Mater Lett* 57:1079–1085
46. Miki M, Maeshiro N, Ogino Y (1989) *Mater Trans JIM* 30(12):999–1008
47. Shajil N, Das D, Chandrasekaran L (2009) *Int J Struct Changes Solids—Mech Appl* 1(1):171
48. Sutou Y, Koeda N, Omori T, Kainuma R, Ishida K (2009) *Acta Mater* 57:5759–5770
49. Vajpai SK, Dube RK, Sangal S (2011) *Metall Mater Trans A* 42:3178–3189
50. Prashantha S, Ranganatha Swamy MK, Shivasiddaramaiah AG, Mallikarjun US (2012) *Int J Metall Mater Sci Eng* 2:13–20
51. Tatar C, Zengin R (2005) *Thermochim Acta* 433:55–58
52. Asanovic V, Delujc K (2007) *Metalurgija* 13(1):59–64
53. Sauda SN, Hamzaha E, Abubakara T, Hosseinian R (2013) *J Teknologi* 64(1):51–56
54. Sutou Y, Omori T, Kainuma R, Ishida K (2008) *Mater Sci Technol* 24(8):896–901
55. Mallik US, Sampath V (2008) *Mater Sci Eng A* 481–482:680–683
56. Mallik US, Sampath V (2009) *J Alloys Compd* 469:156–163
57. Segui C, Cesari E, Humbeek VJ (1990) *Mater Trans JIM* 31(5):375–380
58. Sharma M, Vajpai SK, Dube RK (2010) *Metall Mater Trans A* 41:2905–2913
59. Harchekar VR, Singla M (2007) Cu-Zn-Al (6%) shape-memory alloy with low martensitic temperature and a process for its manufacture. Patent US7195681B2, USA
60. Zengin R, Ceylan M (2004) *Thermochim Acta* 414(2):155–158
61. Kneissl AC, Unterweger E, Lojen G (2006) *Adv Eng Mater* 8(11):1113–1118
62. Yang S, Su Y, Wang C, Liu X (2014) *Mater Sci Eng B* 185:67–73

Chapter 7

Synthesis Techniques of Shape-Memory Polymer Composites



Gautam M. Patel, Vraj Shah, and Miral Vora

7.1 Introduction

The most important stimuli-responsive materials are shape polymer composites (SMPCs), which are smart materials with the ability to return from a tarnished structure to their original structure when activated by a backyard set-off, such as microwave, water, alternate temperature, electric, electromagnetic enchantment, and chemical compounds, to name a few [1]. Polymeric compounds have been used in aerospace and civil applications several times; the properties of these composites are an excessive particular strength, tunability and stiffness, proper corrosion resistance, and low cost [2]. Moreover, shape-memory polymer composites (SMPCs) are fascinating cumulative global lookup interest due to the fact of their successful purposes such as autonomy, actuators, sensors, faraway detectoi, far-flungedness, and biomedical value [3].

Ununiversally, shape-memory polymer composites (SMPCs) are considered to include molecular changes and net points. In cross-linked structures, the net points can be either chemical or physical. Polymer chains contain robust interactions because of the heavier mechanical properties; this can be concluded [4]. In the last few years, significant efforts have concentrated on the resulting main areas of SMPCs like an improvement of effects of two-way shape-memory, mechanical properties, and also multi-shape-memory effects. Among mechanical properties,

G. M. Patel (✉)

Department of Industrial Chemistry, Institute of Science and Technology for Advanced Studies and Research (ISTAR), CVM University, V.V. Nagar 388120, Gujarat, India

V. Shah

Department of Chemistry, School of Sciences, ITM SLS Baroda University, Vadodara 391510, Gujarat, India

M. Vora

Industrial Chemistry Department, Faculty of Life, Health and Allied Sciences, ITM Vocational University, Vadodara 391760, Gujarat, India

SMPCs contain many inorganic nanofillers and organic fibers such as polyhedral oligomeric silsesquioxane (POSS), SiO₂, ZnO, carbon fillers, and cellulose. The Ni metal was also described by an SMP based on polyurethane protected by carbon nanotubes. Furthermore, by retaining one form and other shapes, a different conservative such as dual SMPs and multi-shape-memory polymers may be produced [4]. Two types of polymer material are as follows: one is a naturally occurring polymer and the other one is a synthetic polymer material. Natural polymer materials have cellulose, silk, hemp, wool, shellac, etc. Synthetic polymer materials are thermoplastic, polystyrene, polyvinyl chloride, polyethylene, and so on [1].

The capable polymer groups have the capability of dynamically moving their form: SMPs and shape-changing polymers (SCPs). These kinds of polymers act as a modification through established specific functional groups in the polymer configuration. Upon generating the shape change starts, these alterations can be induced by exposing them to a suitable external stimulation. The primary distinctions between SMPs and SCPs increase when various degrees of freedom effect the shape of geometry; the shape varies with reversibility, and the stimulus outcome [5]. The factors of SMPs and SCPs essential like a structure of polymer network that keeps elasticity to allow bend of the polymeric material and shape transformation, polymer network structure has been applied to the net points, that expresses the shape of permanent material like chemically or physically nature. In a temporary shape, the stimuli-responsive structure switches that afford reversibly fix the network with additional temporary cross-links, and a designer shape-change encoding procedure for the distortion of the material, by the mixture of proper stimuli [5].

The key advantages of SMPs and SCPs are including low-density high deformation capacity mechanical properties, biocompatibility, potential recyclability at relatively low costs, transparency, easy processing, chemical stability, modification, and biological degradability. They have a large number of applications such as at certain temperatures they could be easy to process, and stiffness would be tunable and also tailored. Metal alloys as well as some polymers have separate uses due to the inherent changes in their mechanical strengths, optical and also viscoelasticity. To add to that, shape-memory polymer composites are less difficult to develop, not heavy, and are also cheaper in contrast to their steel counterparts, alloys which are made by shape-memory. Therefore, SMPCs and SCPs have been specifically capable of applications in the biomedical field due to these attractive capabilities, outcomes of their procedure in surgical fields tissue manufacturing, orthodontic, cardiovascular, and drug delivery [6].

The information related to the semi-crystalline polymers for the crystalline molecular chain, segments reveal thermal changes into the the “one-way” shape-memory structures. As the polymers which are semi-crystalline are described in the literature, the “two-way” shape-memory structures can be obtained conversely. The effect of reversible shape-memory has been controlled thermally because of the thermo-mechanical conditions like the reversible change within a continuous tensile load of the crystalline areas [7]. Here in the molecular form of polymer, the crystalline chain sections form and extend beside the track of the load. After crystalline chain

reduction, the rewarmed crystal melts, resulting in crystalline chain reduction. Shape-memory polymers used to operate in response to environmental stimuli such as light, magnetic, water, thermal, and electric stimulation. Furthermore, the shape-memory polymers' transitional one-shape-memory and single stimulus applications are restricted (SMPs). As a result, new SMP nanocomposites may be made using a variety of external stimuli and can complete multi-shape transitions, which are becoming increasingly popular among scientists [7].

Applying crystalline and amorphous segments in the soft segment in Polyurethane can show the shape-memory effect [8, 9]. It has numerous merits like low density, high deformation, flexibility, and easy dealing out relation to shape-memory alloys; apart from that, it has demerits like shape recovery rate as well as shape recovery force. Now, to eliminate these circumstances, nanomaterial which includes graphene, nanoclay, and metal particles can be used to prepare polyurethane [10, 11]. Several reports are there till now for the enlargement of the actuating properties of SMPs with graphene nanocarbon and carbon nanotubes (CNT) [12]. It detailed infrared-setoff activation of composites of polymer with decreased in addition graphene which is sulfonated. The fuse graphene which is sulfonated demonstrated great mechanical strengths plus fantastic light-setoff incitation because of good solvency and a generally reestablished aromatic organization [13].

The polymeric materials should be mechanically strengthened like SMPCs by incorporating fibers [14, 15]. Carbon and glass are commonly found in reinforced fibres, as well as other types of fibres such as woven fabric, cover cloth, and unidirectional fibres [16]. SMPC loaded with split strands achieves a usually limited improvement in mechanics while still exhibiting massive reversible deformation. A shape-memory polymer (like polystyrene-butadiene-b-styrene) triblock and direct lesser density polyethylene composed through hacked glass filaments which have the higher flexibility modulus, and the related strain limit diminishes from 5.5 to 3%. Consistent fiber-fortified SMPC sets up the great mechanical show and holds high recuperation stress in any case less reversible strain, that includes woven overlays, angle-ply, and unidirectional fiber [15, 17]. The SMPC cover of the unidirectional fiber-fortified, the properties of shape-memory are the elementary boundaries used for planning point handle overlaid plates, woven overlaid plates, as well as additional covered SMPC structures with huge mutilation size. However, templates related to this theme are uncommon because of regular readiness processes like filament winding, resin transfer molding process of resin, compression molding, also tape laying, in recent years, it is tough to understand when new composite of SMP resin setup [18]. At this point, while woven filaments have been used, SMPC could be set up over physical material laying, which doesn't need SMP handling boundaries, for example, dynamic consistency and its flow. For woven fiber fortified (reinforced) SMPC, SMP which is dependent on epoxy with the proportion of 38 vol % woven glass fiber shows improved pressure recuperation by two significant degrees contrasted and unadulterated epoxy-based SMP under flexural deformation [15].

The shape-memory impact of the TiNi combination was regularly used to enhance the mechanical strengths of the composites. By making compressive pressure into

the lattice, the product quality and the exhaustion life of the composite are enhanced essentially [19–21]. Through Varying the TiNi fiber's recovery power would change the compressive pressure into the reinforced material [22]. Furthermore, because of the interface rubbing plus twin limit development in the martensite, the TiNi compound has a greater damping limit [23]. Porous TiNi amalgams have been utilized as a lattice to create TiNi-based composites coupling great mechanical properties and high damping limits [24, 25]. Lately, a few investigations about aluminum-based composites fortified with SiC molecule and TiNi fiber have been accounted for. Both the wear characteristics and mechanical properties of the composite had been definitely studied [26, 27].

Some research articles consider that SMPCs have more stiffness and strength; fillers are added to determine their special characteristics, and it could provide more rewards over shape-memory polymer composites [28]. Shape-memory composite polymers have been produced by mixing with shape-memory foams and composite shells. Mixing shape-memory composite polymers with shape-memory foams and composite shells has resulted in shape-memory composite polymers. The form of polymeric materials with qualities that have been recovered, mechanically tested, and dynamically tested. The amount of the components might easily change their form without affecting the mechanical hardness of the recovered polymeric materials [29]. SMPCs can provide less stiffness and recovery forces, but they can also cause greater strain. Shape-memory composites, on the other hand, may have more recovery capabilities, but the recovered strain is reduced and the material is less unbending. The SMPCs have been acknowledged for a long time; in the last 20 years, it has attracted a certain amount of attention in the field of research, much like modern societies. As a result, several development applications are expected.

For micro-mechanisms, several models are offered for these kinds of laminates [30]. It had been found through studies that “fiber micro-buckling” is the mode of deformation principle, while in the case of hard resin composites this is a “failure mode”. Here, the structural uses needed the structure to withstand stiffness plus load; particles reinforced with SMPCs do not serve for that. Henceforth, fiber-strengthened SMPC is utilized generally for these kinds of applications. The recuperation stresses have been larger when SMPs have been fortified with manufactured strands like Carbon, Glass, as well as Kevlar textures. The shear modulus of carbon textures, woven Glass, and Kevlar textures with Epoxy, Styrene based SMPs is higher than that of pure SMPs, according to analytical results from dynamic mechanical analysis tests [31, 32].

Kim et al. observed that in SMP composites, silica particles are present in ambiguous polyurethanes, which improve mechanical characteristics significantly [33]. Fu examined different inorganic compounds like clay, alumina, in addition to silica, reinforced polystyrene (PS) copolymer used for cross-linked with that. Those shape-memory polymer composites revealed advanced shape-memory and mechanical properties. Also, the clay which was in the rod shape revealed greater reinforcement compare with the spherical particles, because of its strength to improve in numerous ways as well as great phase relation [34].

The determination of this chapter is to evaluate the different methods that are established for the production of SMPCs by different materials such as reinforcement fillers such as SiC fiber, TiNi fiber, chopped fiberglass, woven fiberglass, Kevlar fiber, carbon fiber, carbon nanotubes, polyurethane nanocomposites, and nanoclays.

7.2 Methodology and Experimental Results of Shape-Memory Polymer Composites (SMPCs)

7.2.1 SMPC-Based Reinforcement Fillers

7.2.1.1 SMPCs from SiC Fiber

In the SMP epoxy system, fiber compounds were synthesized by a profitable thermoset, DP7AR, provided through Composite Technology Development (CTD) and integrated. For SMP, the glass transition temperature is nearly 90 °C. Then, at 60 °C temperature, the 25-inch mercury vacuum furnace was used to mix three-part epoxy which consists of hardener, resin, and accelerator. Then Teflon molds were utilized to cast a liquid mixture of epoxy. Three paths are used for the curing process: (i) 40 °C temperature for 4 h had been held which is a low temperature, (ii) 80 °C for 8 h had been held which is a high temperature, and (iii) a 4 h clamp at 150 °C. At that point restoring, as-projected shape-memory polymer blocks had been delivered to get yield three-point flexure specimens with measurements of almost $20 \times 3 \times 1$ mm, from the molds and machined.

Experimental Results of SiC Fiber:

As per the literature, silicon carbide (SiC) nanopowder-reinforced SMP composites' elastic modulus and hardness surge with a surge in the weight fraction of SiC [35]. However, 30 wt. % of particle mass was found in SMP nanocomposite which is higher in comparison with SiC weight fraction. In the study, the 20 wt. % of SMP nanocomposite has fabricated the SiC nanopowder. At room temperature, the SiC nanopowder was injected into the hardener, which is significantly less viscous than the resin. The common diameter of SiC nanoparticles is 700 nm. The ultrasonic mixing had been active when combined with the hardener and filler. Afterwards, the accelerator and resin had been stirred by hand into the mixture. Furthermore, the degassed process was established for the composite predecessor and cured with the equal technique as the SMP resin. Indeed, Fig. 7.1a elicits the dispersion of the particles of the personal SMP matrix as represented in the SEM image. Moreover, nanocomposite beams with equal measurements as the pure SMP without reinforced SiC nanopowder specimens had been previously machined [36].

For the thermo-mechanical study, a DMA had been utilized for the compartment. Compression, tension, and flexure had been utilized to characterize the SMP material properties. The deformation modes (three-point flexure) used to be the most beneficial

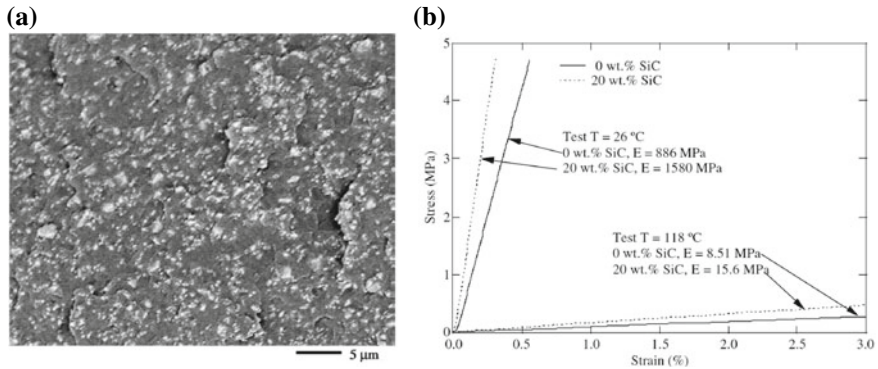


Fig. 7.1 **a** SEM image of SiC nanopowder. **b** SMP and SMPCs for elastic moduli at 26 and 118 °C temperature [36]. Reprinted from Liu Y, Gall K, Dunn ML, McCluskey P (2004) Thermomechanics of shape-memory polymer nanocomposites. *Mechanics of Materials* 36 (10):929–940, Copyright © (2004), with permission from Elsevier Ltd.

mode for recuperation tests. The DMA gadget could function in position and load control. Following the application of the load, the influence of shear strain could be neglected due to deflection, which is mostly caused by pure bending, based on the size of the specimens load-point displacement had been measured. The rudimentary essential beam hypothesis was utilised to compute the equivalent greatest axial strain and axial stress that occur beneath the heap point at the outside of the beam. Three-point flexure (5 and 10 mm) loading allows functional maximum stress/strain ranges in SMP specimens for temperature variations covering the glassy to rubbery states of the SMPs. A 15 mm span bigger than the specimen geometry moderately meets the elementary beam theory. However, when the gap was short, the higher pressure degrees resulted in smoother stress recovery responses. The samples had been carried to the most axial stress close to 30%. The fundamental bending concept is used to calculate the corresponding most axial stress and strain at this deformation level. Furthermore, the most axial stress and axial strain are advised when we refer to “stress” and “strain”.

Thermal Transition and Stress—Strain Behavior of SiC Fiber

A phase angle δ with Dynamic force is based on loading frequency and also temperature. The corresponding strain and dynamic stress relationship exhibited the complex modulus with E_r (real part) which stands for storage modulus in addition to E_i (imaginary part) which stands for loss modulus. Equation (7.1) below represents the relation of loss modulus (E_i) to the storage modulus (E_r).

$$\tan \delta = \frac{E_i}{E_r} \quad (7.1)$$

The T_g could be measured in some paths as per the various standards. To describe the glass transition temperature (T_g) here, the peak of the $\tan \delta$ versus temperature has been illustrated as a curve.

From temperature range 0 to 140 °C at a rate of heating 5 °C/min. Then, at 26°C and 118 °C, dynamic thermal scans had been accomplished. Isothermal quasi-static stress–strain tests had been performed under flexure for the SMP as well as SMP nanocomposite. The modulus of SMP nanocomposite which consists of weight in the percentage of twenty of silicon carbide at temperatures 26°C and 118 °C is around twice times in comparison with unadulterated SMP. At the comparable temperature, modulus detected through dynamic tests is higher in the proportion of 18–28% as compared to modulus detected by static test (Fig. 7.1b). Here, these distinctions are ascribed to the viscoelastic reaction of the SMP materials. At a frequency of 1 Hz, the dynamic force of 40 mN had been applied in the dynamic test whereas, 10mN/s force was applied in the static test.

The unreinforced SMP has a lesser modulus as compared to reinforced SMP (illustrated in Fig. 7.1b). In comparison with the SMP matrix, the stiffness has been surged because of the better elastic modulus of the silicon carbide (SiC) reinforcement. The stiffness could also be influenced by the addition of chemical changes in the polymer close to the particle/polymer interface, and the T_g of the nanocomposites. In SMP nanocomposites, the stiffness is growing crucial for the expanded recoverable stress ranges in inhibited restoration distribution [37]. Figure 7.2 represents that at 15% of the pre-deformation state, the stress recovery behavior would be under full strain

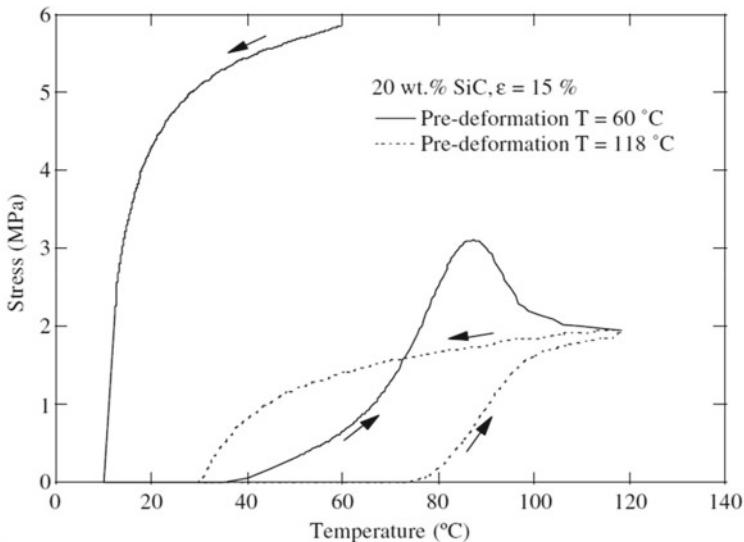


Fig. 7.2 The SMP Composite with pre-deformation for stress recovery at temperatures 60 and 118 °C [36]. Reprinted from Liu Y, Gall K, Dunn ML, McCluskey P (2004) Thermomechanics of shape-memory polymer nanocomposites. *Mechanics of Materials*, 36 (10):929–940, Copyright © (2004), with permission from Elsevier Ltd.

restriction. Intermediate temperatures had been studied however no longer shown and pre-deformation had proficient at 60 and 118. Noted that the equal pre-deformation stress level, greater stress levels, and reap result from the rest for two hours in a bend the SMP nanocomposite versus the unreinforced SMP at the low temperature versus the over-the-top temperature. The entirety of the bends delineates that after cooling underneath stress limitation, the burdens routinely drop to zero.

In the polymeric substances pre-deformed at above T_g , the pre-deformed stress level and restoration are speedy at the commencement monotonically to the saturates' recovery stress. At 118°C, the pre-deformation stress has been decreasing with surges quickly to a peak and stress recovery initials from a lesser temperature (material which has T_g below the pre-deformed). Although it is desirable for the pre-deformation stress to be zero and structural fixity to occur at a lower temperature in the glassy state, pre-deformation at a lower temperature is possible (T). In addition, it is significant for applications such as medicinal research (in vivo/vitro) carried out by medical equipment, as well as higher strain outcomes achieved in the defeat of recoverability, particularly in composites. It is necessary to conduct a specific assessment of the recoverability loss of SMP composites as a component of the reinforcing and strain levels.

7.2.1.2 SMPCs from TiNi Fiber

The TiNi fiber (50 at % Ni–50 at % Ti) wires were used as reinforcements, which were taken in diameters 0.5 mm and 0.3 mm and obtained from GRIKIN Advanced Materials, China. The wire had been reinforced at the temperature of 973 K with a 1.2 Ks vacuum value. Differential scanning calorimeter (DSC) instrument was used to determine the transformation temperature. The starting temperature of martensitic transformation (M_s), finishing temperature (M_f), and starting temperature of reverse transformation (A_s), finishing temperature (A_f) of wire–0.5 and wire–0.3 were 44, 56, 65, 78, 46, 57, 67, and 82 °C, in that order. The matrix with epoxy had been primed with the aid of mixing an epoxy monomer (E51) such as neopentyl glycol di glycidyl ether (NGDE) and 4,4'-diamino diphenylmethane with the mass quantity of 40:7:8. T_g s SMP matrix was previously obtained at 42°C. Through testing with a tensile test, the values of structure recovery and structure fixity were nearly a hundred percent. To top it off, epoxy's structural reminiscence property was validated. The matrix was thought to improve first in the composites recovery process since the healing rates of TiNi wires were much faster than the matrix. As a result, the epoxy matrix for glass transition temperature was set below the TiNi wires' reverse transformation starting temperature (A_s). As the composites for the monitors were being made. After removing an epoxy mixture, bubbles were cast using a preheated poly fluortetraethylene (PTFE) mould, with TiNi–SMA wire placed in each groove. Furthermore, the composite was created and cured at temperatures of 80°C for 2.5 hours and 150°C for 2.5 hours. With the composites that contained a single wire-0.5 and 0.3, respectively, the TiNi wire volume fraction of 1% and 0.4% was evaluated.

Here, to analyze the mechanical behavior of the composites as well as the matrix, the samples had been prepared with a tensile test and an environmental chamber by a machine called an electronic universal mechanical testing machine with the temperature at 25°C and 70 °C. The matrix shows maximum elongation at 70 °C (T_g+30 °C). This outcome illustrated that 70 °C is the best temperature for composite and deforming matrix. It Predictable to direct machine-driven actions at an important heat of 70 °C had been developed in the deformation process. At 25°C, the constant displacement rate was 1 mm/min, according to testing. While the sample was heated to 70°C for 2 minutes, it was stretched and tested at a high temperature at a continuous displacement rate of 2 mm/min [37]. Tobushi et al. was given the procedure as follows: (1) at the strain of 8% at T_g+30 °C, the samples had been stretched. (2) The specimens had been cooled at T_g+30 °C with the aid of retaining the force. After the unloading of the deflections had been estimated, also the charges of R_f (shape fixity) were found (3) up to T_g+30 °C below no load, the samples had been heated and then measurement was done for the deflections which were generated by heating [39]. Afterwards, calculation of shape recovery (Rf) would be done. By the accordance Eqs. (7.2) and (7.3) below, the Rf and Rr can be calculated.

$$R_f = \frac{l_{\text{fixed}}}{l_{\text{pre}}} \times 100\% \quad (7.2)$$

$$R_r = \frac{l_{\text{pre}} - l_r}{l_{\text{pre}}} \times 100\% \quad (7.3)$$

where R_f denoted the shape fixity rate, R_r denoted a shape recovery rate, l_{pre} denoted pre-stretched length, l_{fixed} denoted the length after unloading at T_g+30 °C, and l_r denoted the temperature T_g+30 °C which says that the size heating could be up to this value. The restoration stresses had been organized with the stress taken off at 4, 6, 8, and 10%. The methods (1) and (2) were comparable to those used in restoration and fixity testing. The samples were heated in technique (3) while maintaining a constant deflection constant. The heat was monitored for the duration of the force and the recovery stresses were noted. Experimental results of TiNi fiber:

In the martensite state and glass state, the TiNi wires and the epoxy matrix are carried out at room temperature. The TiNi wires and epoxy matrix are carried out at room temperature in the martensite and glass states. The matrix is then relatively rigid, and the composite's elongation is based on it. Figure 7.3a [38] shows many TiNi wire volume fractions of the matrix, as well as composites for stress–strain curves.

Figure 7.3b represents the stress–strain curves of composites and matrix had been carried out with different wire of TiNi extent fraction at excessive temperature. With the surging volume of wire fraction at room temperature with the samples also rises the breaking strength plus the Young modulus. However, the elongation of composites at excessive temperatures is a great deal decrease than the matrix. The morphology of the fractured specimen, while the matrix is torn, the wire is entire and is drawn

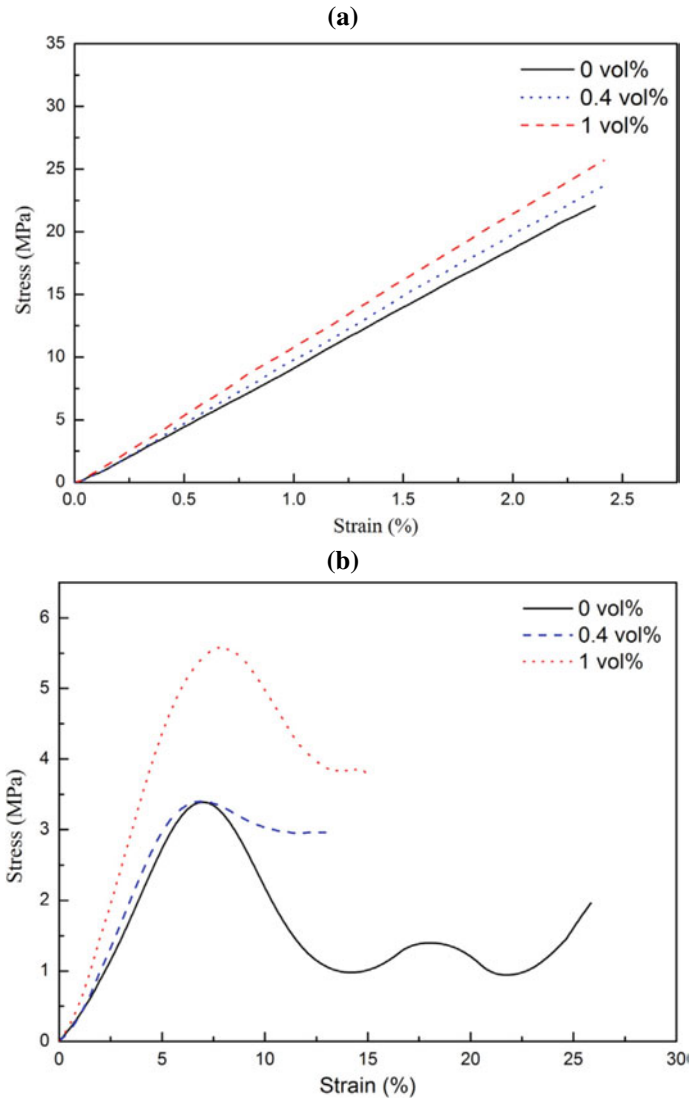


Fig. 7.3 **a** The composites and matrix with different TiNi wire volume fractions in stress–strain curves at room temperature. **b** The composites and matrix with different TiNi wire volume fractions in stress–strain curves at high temperatures [38]. Reprinted from Feng X, Zhao L, Mi X, Li Y, Xie H, Xiangqian Y, Gao B (2013) Improved shape-memory composites combined with TiNi wire and shape-memory epoxy. *Materials & Design* 50:724–727. doi:10.1016/j.matdes.2013.03.060, Copyright © (2013), with permission from Elsevier Ltd.

out from the matrix. The matrix turns to a rubbery state when growing temperature to above T_g main to an apparent limit in dramatic expand and the Young modulus in elongation [39].

The recovery matrix stress, as well as the characteristic of pre-strains temperature, were measured at different proportions such as 4, 6, 8, and 10%. When the temperature reaches T_g , the restorative stress begins to expand and reaches its peak around T_g+30 °C. The composite recovery stress curves, which are in the proportion of 1 vol percent for the function of temperature in the percentages of four, six, eight, and ten pre-strains, are also shown. In the case of T_g , according to the comparison matrix, the recovery stress begins to increase, but the maximum restoration stress is acquired from temperature, and the postponed with high temperature and strain growth. Stress-triggered TiNi wire martensitic inverse section transformation hysteresis might be connected to this theory. Figure 7.4 represents the comparison of the highest recovery stress of composites and matrix. Through pre-strain it could be claimed that the highest recovery stress for matrix upsurge linearly. At 8% pre-strain, the peak is acquired where first amplify and then minimize style is acquired from the composites of the curve.

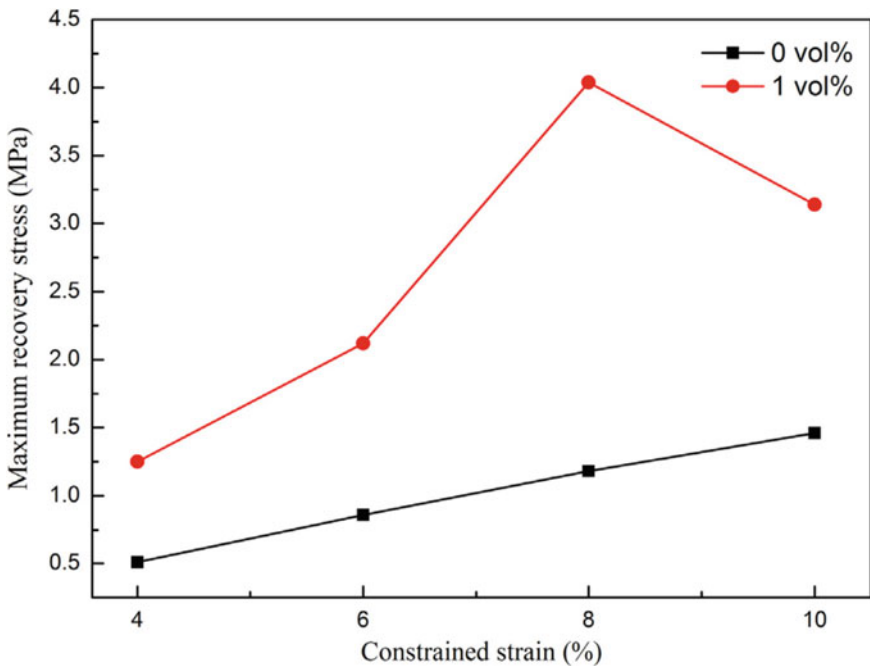


Fig. 7.4 Graph representing highest recovery stress of composites plus matrix with different pre-strains [38]. Reprinted from Feng X, Zhao L, Mi X, Li Y, Xie H, Xiangqian Y, Gao B (2013) Improved shape-memory composites combined with TiNi wire and shape-memory epoxy. *Materials & Design* 50:724–727. doi:10.1016/j.matdes.2013.03.060, Copyright © (2013), with permission from Elsevier Ltd.

7.2.1.3 SMPs from Chopped Fiberglass

In the hand lay-up method, SMP polyurethane and chopped strand mat glass fibers had been synthesized as composite materials. In this study, glass fibers have utilized various extent fractions such as 0, 5, 10, 15, and 13% and are mentioned as pure SMP, 5SMPC, 10SMPC, 15SMPC, and 30SMPC, correspondingly. As per Eq. (7.4) below, the quantity fraction (V_f) of fibers had been calculated [40].

$$V_f = \frac{W_f \times \rho_f}{(W_f \times \rho_f) + (W_m \times \rho_m)} \quad (7.4)$$

Here, volume is denoted by V , W stands for weight, and ρ elicits density; polymer matrix, and fiber are represented with the subscripted f and m , respectively. When 2 elements A and B have been carefully mixed manually for the half-minute within the fraction of 40:60 by quantity, this is done for the hand lay-up method. To keep away from any extra air bubbles in the resin, the mixing was done entirely slowly. Pot life of isolated reactive mixture is about 5, mold with chopped fiberglass was used for the pouring of the solution which needs to be done immediately. Through the hand-rolling tool, all the air bubbles were removed with extremely good care. Furthermore, to gain the favored thickness of the poured mixture, a roller had been utilized to roll as well as spread the mixture over the surface of the mold. For 4 h at 70 °C, it was post-cured and cured for 10 min at room temperature, to grant void-free specimens with a clean surface and it should be reproducible. The specimens had been reduced to 35 mm × 6 mm × 2 mm and stored at room temperature before testing in a dynamic mechanical test.

To study viscoelastics well as morphology performance behavior of the composite materials dynamic mechanical analysis had been utilized. Furthermore, under 3 °C/min heating rate and 1 Hz fixed frequency, with a constant deformation of 0.1%. With a dimension of 35 mm × 6 mm × 2 mm, the fibers (pure SMP, 5SMPC, 10SMPC, 15SMPC, and 30SMPC) had been tested, sample with various volume fractions. DMA test was done at normal temperature, from 298.15 K to 423.15 K using three-point bending mode.

Experimental Result of Glass Fiber:

Dynamic mechanical analysis (DMA) was mostly used for the reinforcement of fillers and fibers in thermoplastic and thermosetting-dependent composites. Elastic region of the material is elicited through storage modulus (E') which is the quantity of saved energy. With rising temperature, it is obvious that the storage modulus (E') declines [41]. It might be linked to matrix softening as a result of the chain's operations expanding at a higher temperature [42]. The E'_g , E' , and E'_r values were taken at extreme temperatures of 303.15 K, 328.15 K, and 393.15 K, respectively. At low temperatures, fibres no longer contribute much to the stiffness of the fabric; the reason for this is that the E'_g values for pure SMP and SMPC have been closely next to one other, resulting in lower temperatures [43].

Here, larger stress transmission from resin to fibre occurs from the matrix fibre of the composite owing to the increased density of cross-linking and significant quantity of hydrogen bonding between the composite [44]. The efficacy of fibres for composites as a Coefficient is explained in Eq. (7.5) below: [43].

$$C = \left(\frac{E'g}{E'r} \right)_{\text{composite}} / \left(\frac{E'g}{E'r} \right)_{\text{resin}} \quad (7.5)$$

Larger effectiveness of the filler or fiber received when the value of constant C is lower in composite material [16]. In this research, 5SMPC and 15SMPC elicit the decreased value of constant C which endorses adequacy of the interactions of fiber-matrix.

An assurance of E'' is crucial than that of E' . The viscous reaction of the material caused losses of both modulus, whether E' or E'' , and this might be related to the material's characteristics or the disseminate energy delivered [45, 46]. It can also be related to the "internal friction", plus it is delicate to several kinds of motion, like the process of relaxation, transitions, molecular chains, and the structure of morphology.

It was noticed that upon the increment of temperature, E'' decreased. The E peak value decreased with high fractions of glass fibres volume below the glass transition temperature, whereas the value of E'' increased with increasing volume fractions of fibres above the glass transition temperature. Previous investigations [43] have shown that E'' values have the similar trend. From the above and below glass transition region, sample (15SMPC) revealed a larger quantity of E'' . Among all composites, the lowest $\tan \Delta$ was observed in 15SMPC which authorizes the effectiveness of glass fiber [47]. Shifting of the temperature occurs due to the combination of fibers. When the shifting of T_g occurs toward the higher temperature, the mobility of chains declined due to the addition of glass fiber.

7.2.1.4 SMPCs from Woven Fiberglass

For the cross-linker liquid form of tert-butyl prop-2-enoate, α -(methacryloyloxy)- ω -methacryloylpoly(oxyethylene) and 2-[2-(2-methylprop-2-enoyloxy)ethoxy]ethyl 2-methylprop-2-enoate had been utilized in as-gotten condition in the proportion of weight in percentage of 30 2-[2-(2-methylprop-2-enoyloxy)ethoxy]ethyl 2-methylprop-2-enoate with weight in proportion to 70 α -(methacryloyloxy)- ω -methacryloylpoly(oxyethylene). Through a proportion of 60 tert-butyl prop-2-enoate with weight in percentage 40 cross-linker had been used to prepare SMP solution in the past. 0.1 wt% concentration of the 2, 2-dimethoxy-2-phenylacetophenone was blended to the shape-memory polymer mixture like an initiator for photopolymerization. The magnetic stirrer was used to stir the solution for 10 min to isolate a soluble solution. T300 carbon which is stable plain-woven fiber had been assigned as the support for the SMPC.

As per Fig. 7.5, a particular curing mold had been arranged to get samples with uniform fiber spreading and thickness. The described steps below state how SMPC

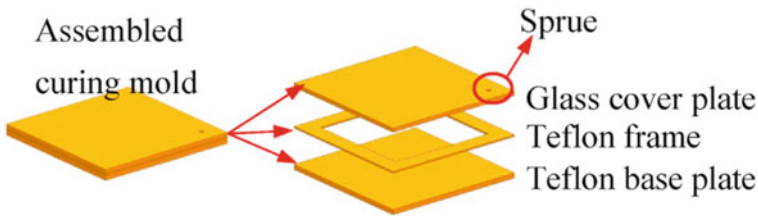


Fig. 7.5 Diagram representation of the forming system of SMPC [48]. Reprinted from Su X, Wang Y, Peng X (2020) An anisotropic visco-hyperelastic model for thermally-actuated shape-memory polymer-based woven fabric-reinforced composites. *International Journal of Plasticity*:102,697, Copyright © (2020), with permission from Elsevier Ltd.

specimens had been equipped: (i) on the base plate preform of the carbon fiber fabric had been employ; (ii) In order to avoid the leak of the SMP resin, silicon grease and mold with clips had been used to aggregate-seal the cavity; (iii) Inject the SMP resin into the mould from the sprue on the glass spread plate; (iv) The box which consists of ultraviolet curing had been used to place the mold and then for 15 min the solution is polymerized; (v) dismantle the mold, upset the sample, to assemble the mold one more time add a frame; (vi) repetition of the procedures (iii) and (iv) the proper dispersal of the SMP matrix on equally faces of the fabric it should complete a two-step ultraviolet curing; (vii) Through additional thermal curing, total polymerization occurs for 1 h at 90 °C by moving the mold to the oven. Then, the sheets of the composite had been demolded. 87% and 13% are the volume fractions of SMP and fabric of carbon, respectively. SMP samples had been prepared like a cycle. Furthermore, for the DMA test, 30 mm × 10.5 mm × 2 mm rectangular specimens had been used. 30 mm × 4 mm × 2 mm dimensions for dog-bone-shaped specimens were utilized for isothermal uniaxial tractable assessments. For memory test dimensions of 130 mm × 25 mm × 2 mm, rectangular specimens had been utilized. For shape-memory tests and isothermal tension of SMPC, rectangular samples through measurements of 130 mm × 25 mm × 2 mm had been utilized. For each case, three specimens had been set up.

Experimental Results of Woven Fibers:

The fabric of woven in inclination strain had been simulated debilitating ABAQUS with the anisotropic hyper elastic portion of that pattern incorporated in the UANISO-HYPER_INV. A four-sided plate with similar measurements like samples of fabric had been lodged in with shell components S4R for the determinate element simulations. One side of the square had been protected along with another side filled during the loaded step. In Fig. 7.6a, b illustrate the comparison for simulations graph and experimental graph. Furthermore, Fig. 7.7a, b shows the acceptable consistency. In light of the designing strain–stress bends of the SMPC between the uniaxial tension to bias expansion tests. At various temperatures, the underlying flexible moduli can be thought of. As per the factors of the matrix SMP as well as fabric of woven decided, a

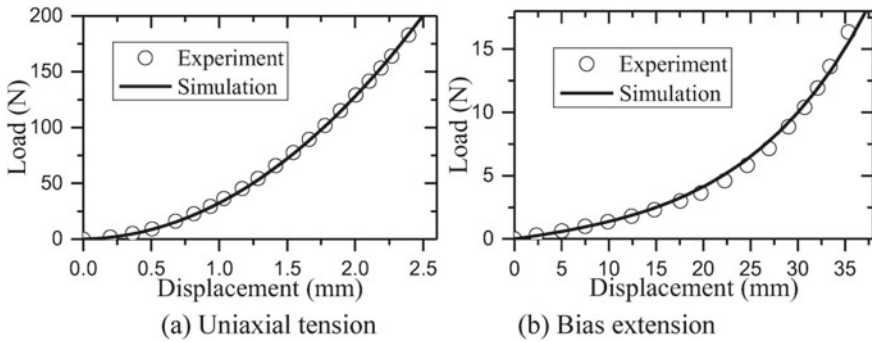


Fig. 7.6 Engineering stress–strain bends of the woven fabric [48]. Reprinted from Su X, Wang Y, Peng X (2020) An anisotropic visco-hyperelastic model for thermally actuated shape-memory polymer-based woven fabric-reinforced composites. *International Journal of Plasticity*:102,697, Copyright © (2020), with permission from Elsevier Ltd.

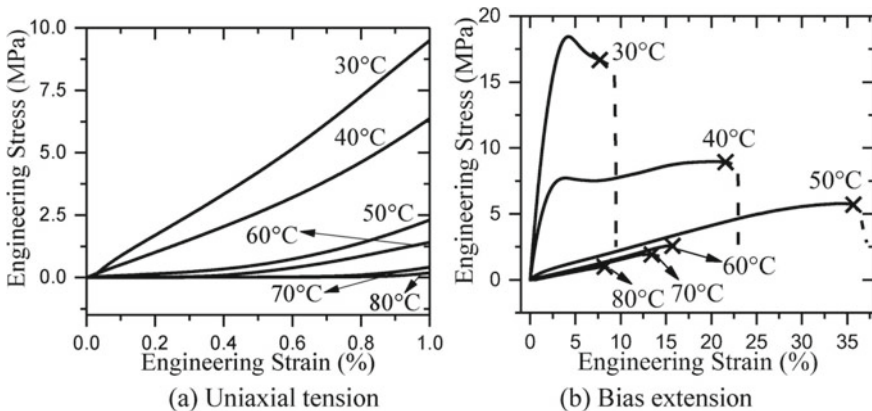


Fig. 7.7 Engineering stress–strain curves of the SMPC [48]. Reprinted from Su X, Wang Y, Peng X (2020) An anisotropic visco-hyperelastic model for thermally actuated shape-memory polymer-based woven fabric-reinforced composites. *International Journal of Plasticity*:102,697, Copyright © (2020), with permission from Elsevier Ltd.

temperature rectification coefficient has been acquired utilizing the underlying versatile moduli of the SMPC in the isothermal uniaxial strain at various temperatures depending on the boundary.

7.2.1.5 SMPCs from Kevlar Fiber

SMP by epoxy was integrated by assessing the synthetics like appeared in methodology by utilizing chemical like DGEBA (Di-glycidyl ether of bisphenol an epoxy monomer) was warmed at temperature 343.15 K in an oven and it was added in

poly(polypropylene glycol)bis(2-aminopropyl) ether and neopentyl Glycol diglycidyl ether (NGDE), the combination was hand shacked then mixed well with the rod of glass for 300 s. Close by lay-up strategy, the creation technique is acknowledged. The examples 150 mm × 50 mm had been made. On the smooth card board, the Kevlar texture as per the above size had been laid where epoxy SMP has been pragmatic then the following layers were manufactured. At (0/90)₃, (±45)₃, ((0/90)/(±45/(0/90))) value the textures had been set. Points to discover the impact on shape-memory show and the proportion of fiber to tar is 35:65. To dodge voids or air holes, a roller is utilized. Finally, weight is put to pound out over abundance tar. At that point, it is post relieved at temperature 373.15 K for 180 min into the hot air oven. In the wake of restoring it had been cut in a 150 mm X 10 mm by a hack saw along with a crushing machine (Kevlar) for bend test then slice to measure of 60 mm × 10 mm [49].

Bend test

The epoxy-based SMPC had been synthesised for a water complex SMP, at various curing cycles; an attempt had been made to test through the bend test with a jig. In order to find out bend recovery time and recoverability ratio calculations, the bend test with jig type had been used. At 100 °C temperature for 15 min, the SMPC sample had been heated in a hot air oven; the SMPC has a dimension of 10 × 150 × 1 mm³. Except for a few samples, all the specimens sprung to return to the initial or real shape.

Bend test results

According to the strengthened fabric, polymeric materials have been particularly orthotropic in addition to the direction of SMPC. Specimens have been stable, with no coupling effect, and symmetric. The flexural modulus can be determined when bending stiffness [D] and coupling stiffness matrix [B] = 0 so that the stiffness of bending could be measured. The estimated value of bending stiffness for carbon cloth. Kevlar fibre memory presentation is better in the positioning compounds (0/90/±45/0/90). Due to the cause for the recovery, the time needed to recover the Kevlar sample as well as the glass that took the location of (±45) was long and the bending recovery ratio was low. The bending stiffness was lower with these types of laminate repel shear load, but no bending loads were applied, therefore for (0/90)₃ no explanation for its poor bending recovery ratio was developed [50].

The three-point twist after-effects of the Kevlar cover composites converged with polyether ether ketone (PEEK-1), and PEEK-0.5 was used to fuse with Kevlar laminate composite after-effects of the three-point bend results. The Tedlar obstruction films with the presence as well as the absence of deionized water. The yields of Tedlar films were 34.58, 32.02, 33.70, 33.43, and 32.73 in unit MPa SBS strength values with the coupons of the Kevlar laminate complexes at controls like dry and wet, PEEK-1, PEEK-0.5, respectively, as it was observed. Water-molded coupons with no obstruction film displayed around 7.4% lesser shear quality contrasted with the undefined resistor ones in the Kevlar composite panels. The barrier films had been helpful for the panels of composite; a decrease in SBS quality had just 2.6 rates (%).

As Kevlar can be a polymeric as well as a malleable material, the disappointment mode is distinguished as twisting into the SBS experimentations [51].

A nearby survey that the composites of Kevlar have the biggest zone within the line of the plot as found through the FEA model [52]. This information demonstrates that for a similar burden, alteration is more prominent with the coupons of Kevlar, contrasted with the other coupons like glass and carbon. Through the bending and bucking process, this demonstrates that coupons of Kevlar disseminated energy as compared to other laminate complexes, and might be the significant explanation behind Kevlar coupons would not exhibit any shear stress, but rather buckling and bending behaviours.

7.2.1.6 SMPCs from Carbon Fiber

Here, in the preparation, the fiber of carbon had been used for obtaining the Trans-1,4-polyisoprene shape-memory polymer composites (TPI SMPCs). At room temperature, a vacuum drying oven was used to put TPI first for 1440 min at a normal temperature [53]. Acetone was used as a solvent in which addition of chopped carbon fiber was done with various proportions like 0, 4, 6, 8, 10, 12, and 14% and for 10 min it prompted ultrasonic treatment, then distilled water was used for rinsing followed by drying and was set aside. Furthermore, the reflux process was started in which a three-neck round bottom flask was used in which the concentrated nitric acid (HNO_3) was added; then at 300 K temperature, it was heated followed by condensation process with water; this process was carried out on a magnetic stirrer; after 3 h, successfully carbon fiber was eliminated. To reach a pH of more than 6, carbon fibre was washed using anhydrous ethanol and distilled water, and it was then dried and set away. Now, into the TPI with communal monomer charge order, fiber of carbon which treated in the previous step had been added, down orientation had been utilized for mixed and acquired. Afterwards, under vulcanization temperature, the optimum time for the cure of rubber employing specimen was estimated which is t_c90 . Before the hot pressing was used, raw material had been vacuumed and then an Electric Flat vulcanizing machine was used for vulcanization molding. Saving conditions: The curing temperature was 423 K and the curing pressure was 10 Mpa. Then, at room temperature reinforced composition had been cooled. A lesser cutting machine had been exploited to make dumbbell specimens. 3 mm, 33 mm, in addition to 6 mm are the viable thickness, length, and width of TPI specimens, respectively, and ASTM D412 standard had been used as a base for the synthesis process of the specimen. Figure 7.8a represents the dumbbell-shaped specimens [54].

Property Test of Shape-Memory Polymer-based Carbon Fiber Composite.

The thermal conductivity of TPI complexes is determined at various temperatures like 319, 299, and 339 k. Experiment method: when graphite was regularly sprayed upon specimens on both the top and bottom sides in similar amounts, the above side got a particular laser beat wave; simultaneously, the temperature reaction of the lower side had been estimated as well as noted. As per the numerical model of the

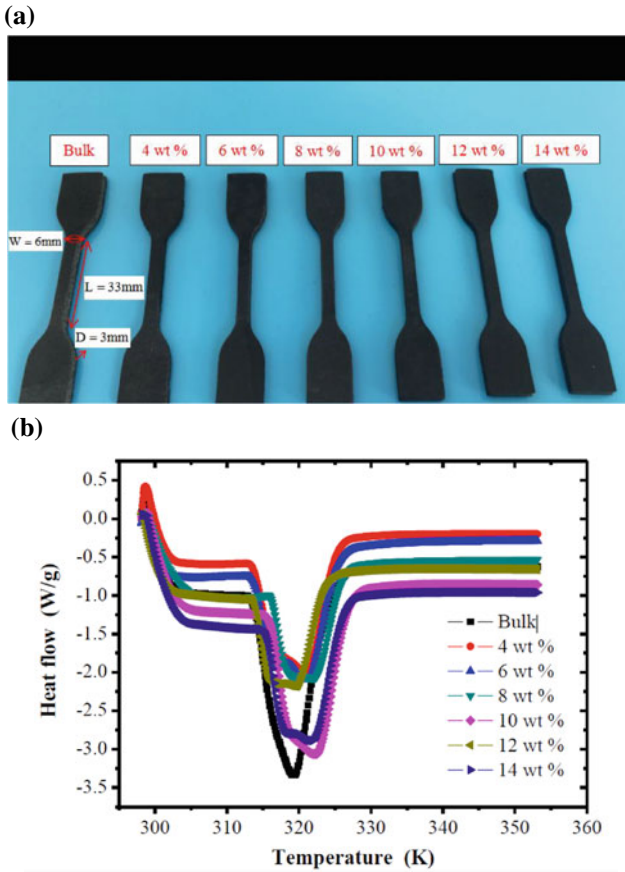


Fig. 7.8 a Diagram of TPI SMPC samples. b DSC thermogram of sliced carbon fiber-fortified TPISMPc with various weight fractions. Reproduced from [54] originally published under a CC BY 4.0 license, <https://doi.org/10.3390/polym9110594>

consistent conduction of heat measure, it was determined the thermal conductivity $\lambda(T)$ and $\alpha(T)$ of the samples at various temperatures as displayed in conditions (7.6) and (7.7), individually [54].

$$\alpha(T) = 0.1388 \times d^2 / t_{50} \tag{7.6}$$

$$\lambda(T) = \alpha(T) \times C_p(T) \times C_\rho(T) \tag{7.7}$$

In the explanation of the equations, d stands for the thickness of the specimen; time required for the temperature at the upper surface of the specimen is denoted by t_{50} which ascends to half of the most extreme incentive after receiving light

pulse radiation; at temperature T, the specific heat is represented as $C_p(T)$ and at temperature T the density of the sample is shown by $\lambda(T)$.

Static Mechanical Property Test

At various temperatures, for example, 299 K ($T_t - 20$ K), 319 K (T_t), and 339 K ($T_t + 20$ K), the static tensile test had been done at the speed of 30 mm/min which is a crosshead speed. Consistent speed had been provided for the complete stretching of dumbbell specimens of TPI SMPC until complete disappointment (failure). By engineering strain and stress, the static mechanical strengths of TPI SMPCs were definite.

Mechanical Cycle Property Test

At room temperature with a consistent rate of 30 mm/min, the cyclic tension test was done by the implemented mode of loading for equivalent displacement. Standing to test clarifications, as far as possible strain esteem had been arranged to be hundred percent plus the number of cycles was five. Then, engineering stress as well as strain were characterized.

Shape-Memory Property Test

Here, the compression test had been used to conduct the cutting-edge shape-memory test. By utilizing compressive or tensile stress–strain curves, the shape-memory strengths of SMPs/fiber of carbon composites were determined. However, because of their twist and overlap attributes of the SMP/fiber of carbon complexes, they have been utilized for outer layer of the creative airplane and space-deployable structures of the shuttle. Henceforth, a new method is used in this paper called “folding-deploy shape-memory test”. TPI SMPC shape-memory properties were used for the characterization. The cycle of the “folding-deploy shape-memory test” includes three stages. In the initial step, the sample had been warmed more than the T_g which was up to 349 K; the greatest bending angle and θ_{max} were obtained when U shape around the focal shaft was provided by folded and twisted process; the diameter of the shape was 4 nm. Before the shape of the sample had been sustained for some time, the external forces had been eliminated and the specimen was quickly cooled in the second step. With the fixed θ , the specimen’s fixed angle was acquired, and the elastic recovery of the specimen, which would appear to be marginal, was obtained. To achieve the original form of the specimen, it was heated to T_i again in the following phase. The temperature was stored for 300 seconds for every 5 K rise between 25.85 °C and 75.85 °C, as well as the corresponding twisting point and test duration for each round of cycle at each temperature. Equations (7.7), (7.8), and (7.9) below show how to calculate shape recovery ratio (Rr), shape retention ratio (Rf), and shape recuperation proportion/shape recovery rate (Vr).

$$Rf = \frac{\theta_{fixed}}{\theta_{max}} \times 100\% \quad (7.8)$$

$$Rr = \frac{\theta_{\max} - \theta_i}{\theta_{\max}} \times 100\% \quad (7.9)$$

$$Vr = \pi \frac{(\theta_{\text{fixed}} - \theta_i)}{180t} \quad (7.10)$$

Experimental Results of carbon fiber:

Differential scanning calorimetry (DSC)

In the heating process, transformation occurs; the crystallization melting temperature of TPI SMPs shows a peak at 319 K. DSC thermogram of chopped carbon fiber-fortified TPI SMP composites with varied weight fractions (Fig. 7.8b). The temperature of liquefying crystallization of tough cables of carbon fiber-strengthened TPI SMP complexes has expanded along with an expansion of cleaved fiber of carbon weight fraction; it had been connected with a TPI SMP grid. It implies the polymer composites for heat obstruction are more upgraded than that of the mass example. Furthermore, the increase in the crystallisation process liquefying temperature of difficult chains demonstrates that the polymer composites for tiny (micro-phase) stage detachment degree is formed. Because the mechanical possessions were identical to the smallest stage degree of separation. The degree of micro-stage separation is greater than the mechanical properties of polymer composites.

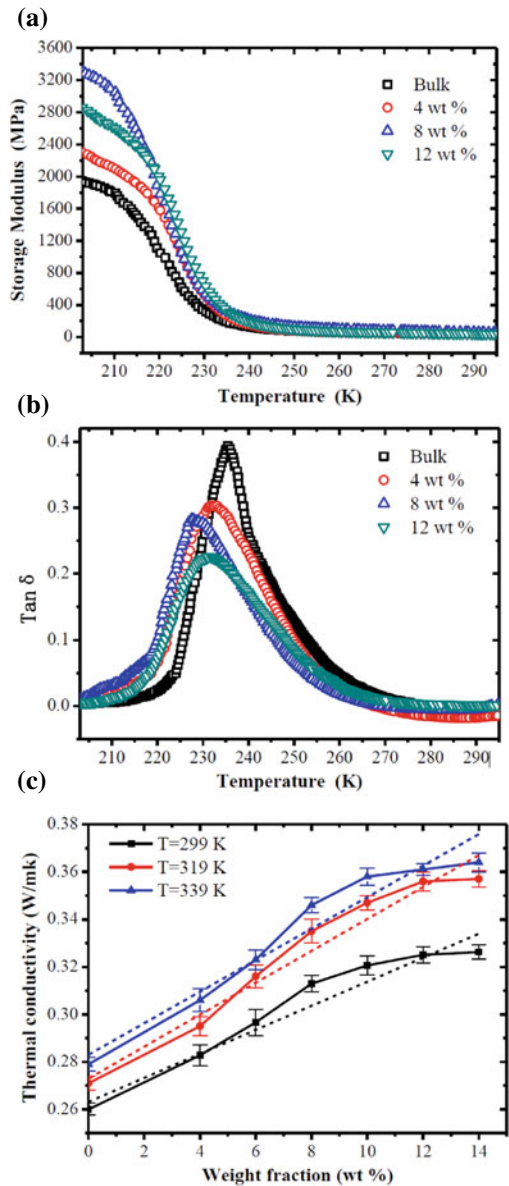
Dynamic Mechanical Analysis (DMA)

At various temperatures, E' as well as TPI SMPCs are increased by rich chopped carbon fiber. With a surge in fiber content, the storage modulus (E') of reinforced TPI SMPCs increase. Furthermore, the fiber of carbon mass portion is in the proportion of four and eight. Furthermore, the carbon fibre contained in the reinforced composition contributes to the inflexibility and interfacial stress transmission of TPI SMPCs. Figure 7.9a represents the DMA of the loss tangent ($\tan \delta$) and the E' in the opposition of the temperature diagram. It is notable that the mass bulk has the glass transition (t_g) of 235 K, T_g fluctuates at lower temperatures, the mass fraction of the carbon fibre has increased, indicating that the motion of the chain between filler and polymer is more evident. Furthermore, the loss variables of TPI SMPCs decrease with an increase in sliced fibre mass portion, and are smaller than the mass loss factor, as illustrated in Fig. 7.9b.

Thermal Conductivity

Thermal conductivity of the composite at various temperatures and mass percentages of carbon fibre is varies due to the obvious difference in thermal conductivity of polymer composites at various temperatures (25.85 °C, 45.85 °C), the thermal conductivity of polymer composites at various temperatures was calculated. The thermal conductivity of complexes normally exhibits a linear development with an

Fig. 7.9 The curves of SMPC samples along with sliced carbon fiber **a** storage modulus (E') versus temperature (K), **b** loss tangent (δ) versus temperature (K), **c** Curve representative of thermal conductivity of composite systems with various carbon fibers at different temperatures. Reproduced from [54] originally published under a CC BY 4.0 license, <https://doi.org/10.3390/polym9110594>



elevation of the fibre carbon content, as seen in Fig. 7.9c. When the thermal conductivity of complexes increases with the weight percentage of carbon content, which ranges from 0% to 14% at high temperatures such as 25.85, 45.85, and 65.85 °C.

Remarkable thermal conduction showed from the TPI polymer which consists of chopped carbon fibers that the amount of filled carbon fiber in TPI influences a critical

value. After that in the TPI polymer, filler starts to steadily form a constant thermal conduction network chain. When the number of fillers surged, the filler would be stacked extra densely, due to which the path of heat flow would strengthen. Likewise, fibers of carbon which have excessive thermal conductivity are used as a leading position in the thermal conductivity of complexes, then there's the rapid variation in thermal conductivity. The linkage between carbon fiber and the TPI polymer would not be good due to the smooth surface of carbon fiber. While the quantity of carbon fibre is substantial, the distortion of fibre carbon into the inferior TPI polymer results in a larger degree of agglomeration. A magnified variation of thermal conductivity of the complexes has been lowered as a result of fibre of carbon amount material's increasing minor involvement in the conduction of heat community chain.

Static mechanical property

At three various temperatures such as (i) 25.85 °C, (ii) 45.85 °C, and (iii) 65.85 °C: The various chopped quantities of carbon with its tensile stress–strain curves of SMPC specimens. The strains of samples along with fiber of carbon weight fractions of the proportion 0%, 4%, 6%, and 8% had been all more than 300% at a temperature of 25.85 °C. Figure 7.10a represents that the strain value of the specimen declined significantly while the sliced fiber of carbon total mass fraction had been greater than 8 percent.

Mechanical cycle properties

Figure 7.10b illustrates the alternative for the most extreme cyclic burdens of SMPCs along with the number of cycles at normal temperature. At the beginning period of the cycle, the most extreme cyclic stress immediately expanded, and at the end it slanted to be steady as the number of cycles continually expanded. Also, the most extreme cyclic stress demonstrated a propensity right off the bat expanding and afterwards diminishing as the fiber of carbon weight fraction expanded. The maximum cyclic pressure estimation of the example with a fibre of carbon weight division of the proportion of eight had the most notable, which would be 76% greater than the mass specimen. Composite structures seen in SMP complexes are likewise a marvel of carbon fibre accumulation.

Shape-Memory Properties

The shape recovery proportion of SMP composite with varied carbon fibre content at various heat ranges is depicted in Fig. 7.10c. The shape recuperation proportion expanded gradually with an expansion of the temperature at an underlying period of temperature rising. Similarly, when the temperature was set to 319 K, the shape recuperation proportion of instances with fibre of carbon mass portions, for fractions, 0, 4, 6, 8, 10, 12 and 14% was 11.5, 9.5, 7.6, 6.8, 5.9, 5.2 and 4.6%, respectively. Following with the temperature repeatedly rising, while the temperature was higher in comparison to the progress temperature and form recovery proportion of all specimens plan rapidly. A higher temperature is required for the macromolecule to acquire enough energy enticing for the section of the chain. At that point, the solidified pressure in the chain portion can be delivered proficiently, subsequently

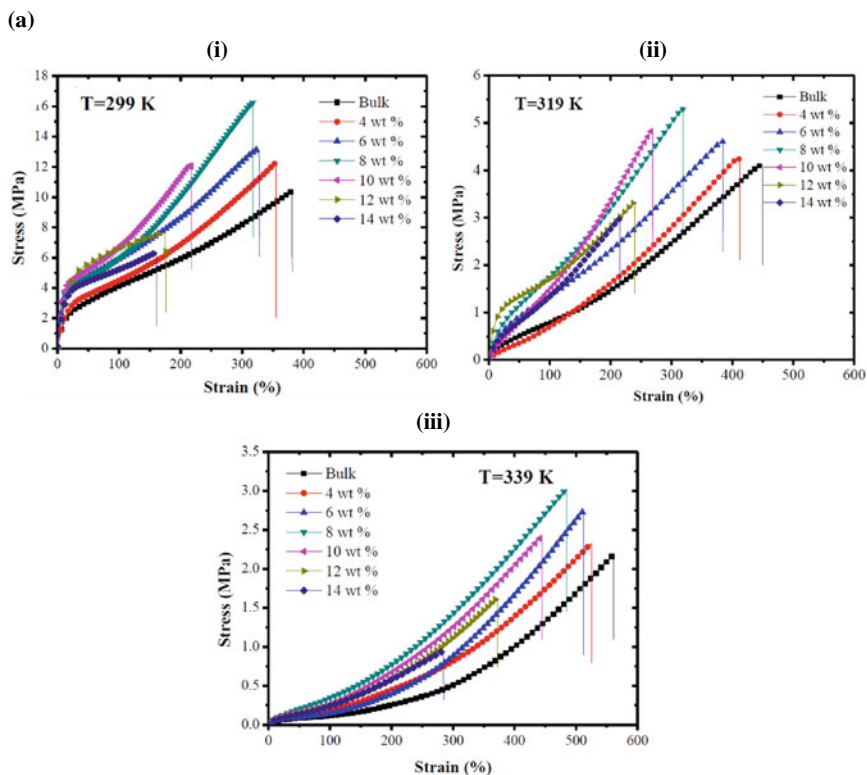


Fig. 7.10 a The static tensile stress–strain curves of SMPC samples with various chopped carbon fiber contents at three test temperatures: (i) 299 K, (ii) 319 K, and (iii) 339 K. **b** Graph representation of maximum cyclic stresses versus SMP composites with various chopped carbon fiber contents. **c** The shape recovery ratio of SMP composites with various chopped carbon fiber contents at different temperatures. **d** The shape recovery rate of shape-memory polymer composites with various chopped carbon fiber content at different temperatures. Reproduced from [54] originally published under a CC BY 4.0 license, <https://doi.org/10.3390/polym9110594>

acknowledging shape recuperation. However, the shape recuperation proportion of the mass example was higher than that of different examples; the shape recuperation proportions of examples were improved by over 90 percent. Here, this representation that the shape recuperation shows of TPI SMPCs is acceptable.

Apart from this, Fig. 7.10d displays the shape recuperation pace of SMP complexes with the modified fiber of carbon substance at various heat ranges. The shape recuperation paces of the samples expanded along with expanding hotness. The carbon fiber content is expanding at a similar temperature, and the shape recuperation pace of the specimen diminished. In a polymer complex, the recuperation power of the complex structure is higher as compared to the SMP matrix. Along with the more complicated structures that require more energy to achieve form recovery

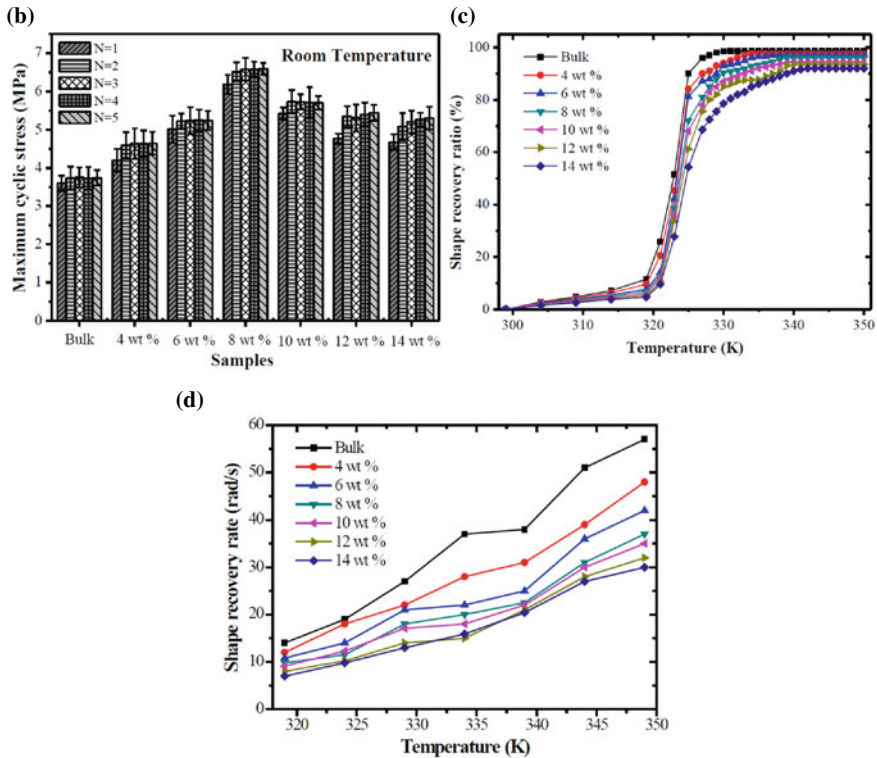


Fig. 7.10 (continued)

in a specimen. The temperature should remain constant in order to achieve shape-memory recovery. It unquestionably needs additional time, in this manner influencing lessening of the shape recuperation rate.

7.3 SMPC-Based Carbon Nanotubes

Carbon nanotubes (CNTs) with strong elastic modulus and electrical conductivity have astonishing mechanical properties. In order to strengthen the significant characteristics of SMPs, CNTs have emerged as potential reinforcements [55, 56]. It is important to keep in mind that the establishment of property–structure relations for CNT/SMP nanocomplexes is a vital step in the effective and efficient plan of certain novel applications, and that is why various operational research takes place to decide the physical behavior of CNT/SMPs. Raja et al. studied the dynamic, electroactive, and mechanical shape-memory capabilities of MWCNTs, thermoplastic PU/poly lactide (PLA) nanocomposites. By the melt processing method, PU/PLA

blend composites with varying CNT portions were prepared in which the mixture of PU/PLA and MWCNTs was blended with rotation at 190 °C for 15 min. They reported based on the experimental results that the elasticity of the PU/PLA nanocomposites increments as the weight portion of MWCNTs increments [57]. CNT/SMP nanocomposites with typical vapor growth carbon fiber (VGCF) CNTs have been developed by Ni et al. First, VGCFs are dispersed at 45 °C by sonication in solvent and then SMP solution is progressively poured into this dispersed mixture, and then the whole solution had been stirred up to 180 min. Finally, this mixture was dried at 70 °C to prepare CNT/SMP composites. From the experimental results, it was found that by increasing the CNT weight fraction, the storage elastic modulus improves and shows a better shape-memory effect [58]. Hui et al. fabricated the SMP epoxy resin matrix with CNT to enlarge shape-memory effects and mechanical properties. CNT and viscous SMPs are combined at 5000 rpm at normal temperature for 1800s using the curing process. Then hardener was applied while the mixture was stirred, then poured into the mold. Then the mixture was heated for several hours to obtain CNT/SMP composite [59]. Instead of thermal heating, PU/MWCNT composites were produced by utilising a voltage to provide an electroactive shape-memory efficiency. As electroactive actuators, this type of composite is valuable, which is significant in several useful applications, like smart actuators for micro-aerial vehicle control. Surface-modified MWCNTs was mixed with PU in HNO₃ and H₂SO₄ (3:1) for 600 s, then after sonication process done in Ethyl alcohol up to 2 h. finishing complex film was prepared by casting in THF: DMF solvents [60]. By using the Mori–Tanaka micromechanical process, several research groups have researched CNT/SMP nanocomposites to investigate the impacts of CNT waviness and its conveyance on the versatile modulus and properties [56, 61].

7.4 SMPC-Based Polyurethane Nanocomposites

To increase the dispersibility of micro-crystalline cellulose (MCC) in the reaction system, a solution of 1-allyl-3-methylimidazolium chloride was initially created for MCC homogenous derivatization using green reaction medium. A solution of AmimCl (19 g) was combined with 15 mL of a solvent system (deionized H₂O/absolute ethanol: 2:1) solvent system. The solution had been sonicated for half an hour in a water bath for comprehensive suspension. Following that, 2 mL 3-glycidyloxypropyl trimethoxy silane was added to the produced mixed solution with steady stirring, and the pH of the acetic acid adjusting solution is 5. Subsequently, the compound had been added, the prepared reaction combination was vigorously stirred at a temperature of 80 °C for 1 h. Then the MCC (1 g) which was dried in the oven had been mixed into the mixture of the reaction. At 80 °C temperature for 180 min, the reflux setup was done for the continuation stirring of the reaction mixture. After the accomplishment of the reaction, the mixed solution had been filtered out and cleaned with an appropriate quantity of ultrapure H₂O 2–3 times for filtrate elimination in the

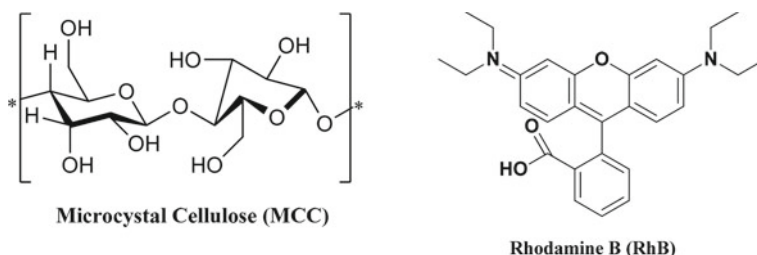
reaction system. Finally, the f-MCC was oven-dried for 48 hours, and compounds can be produced desirably.

The multi-stimuli-responsive polyurethane (PU) syntheses through dual networked structures could be found by a facile as well as a simple technique of solution mix and forming in N-Methyl pyrrolidone (NMP) by the subsequent process. First, PU-combined films were arranged, followed by neat PU pellets and oven dried f-MMC at 35 °C temperature for 3 hours prior to processing. PU (2 g) pellets were soluble in NMP (20 mL) solvent under dynamic stirring at room temperature for 360 minutes. Following that, f-MCC (0.1-g weight of 5%) and a small volume of rhodamine B (RhB) (0.25 wt percent) were added to the NMP solution under dynamic stirring at room temperature for 240 minutes. Before transferring the obtained solution to a petri plate, it should be sonicated for half an hour to remove air bubbles. In the Petri dish, at a temperature of 25 °C, the mixed solution was dried in the oven; then after 3 days, the solvent can be evaporated. MCC/PU and RhB/MCC/PU of the other mixed solution syntheses had produced in the same existing method using the same processing parameters for combined films. The corresponding chemical arrangements of PU, GPS, MCC, and RhB are represented in Scheme 7.1 [62].

Experimental Results of Polyurethane Nanocomposites:

Here, 735, 840, 1083, and 1130 cm^{-1} are the strongest point which was adapted by f-MCC in the FT-IR spectrum, that is similar to the distortion as well as vibration of the stretching of the metal-carbon and metal-oxygen bonds Si-C, Si-O-C, Si-O-Si, and Si-O-C bonds, individually. So, Fourier transform infrared spectroscopy range of f-MCC exhibited related vibration things of the structural skeleton to natural cellulose by bands carbon and hydrogen vibration of bending at 1450 cm^{-1} , hydrogen, oxygen and hydrogen vibration of bending at 1648 cm^{-1} , and -OH stretching vibration at 3350 cm^{-1} , signifying the complete elemental structure of cellulose another than enhanced reactivity of the surface from consistent functionalization [63].

The measured characteristic frequencies at 3300 and 2960 cm^{-1} in SMPU composites have been derived to N-H and C-H extending from the hard division of PU. Other



Scheme 7.1 The chemical arrangements of MCC and RhB [62]. Reprinted with permission from Cai C, Wei Z, Wang X, Mei C, Fu Y, Zhong W (2018) Novel double-networked polyurethane composites with multi-stimuli-responsive functionalities. *J. Mater. Chem. A* 6 (36):17,457–17,472, Copyright © 2018, The Royal Society of Chemistry

absorption bands, Si–O–C at around 1130 cm^{-1} and Si–O–Si at 1083 cm^{-1} in the f-MRPUs, representative the probable newfangled elemental bonds among f-MCC and PU. It has been shown that responsive groups on both end sides of PU could relate with -OH on the superficial of f-MCC to form the inflexible cross-linked linkages for potency enhancement of the subsequent f-MRPUs, like reinforced through the subsequent tensile tests. The band of f-MRPUs exhibited the unique amine and carbonyl stretching band concentrations associated with the different wavelengths. Especially, the obvious changes allocated to free and hydrogen-bonded stretching bands in the 2 different peaks of the carbonyl band at 1728 plus 1698 cm^{-1} [64]. Stretching vibration with the free N–H bond at 3450 cm^{-1} and nonappearance of free amine stretching bond and the frequency at 3328 cm^{-1} of a strong banding the FT-IR spectra, it was directed that the amine groups of completely H bonded in the subsequent PU composites. A comprehensive analysis in the FT-IR could approach valued data to know the PU H bonding characteristics as well as phase-separated structures of PU and it is dependent on the peaks from 1720 to 1600 cm^{-1} [65].

The silicon (Si) metal was clearly present in the f-MRPUs and is covalently coupled with PU segments, indicating the possibility of silicon bonding, as seen in the XPS spectra in Fig. 7.11. Because of the destruction of conjugated C–C on the PU skeleton made from the combination of f-MCC plus RhB, the C–C which has hybridization sp^2 band from the aromatic ring skeleton of PU rigid segments extinct into the greater resolution C 1 s of the RhB/MCC/PU and f-MRPUs. The decline in conjugated C–C lastly managed to the atrical upsurge in the sp^3 hybridized C–C bond.

The ^{29}Si solid state may be discovered in the NMR spectrum using a material that is similar to the probable chemical structure of f-MRPUs, and it was utilised to describe the consistent reaction process of network building for comprehending the heterogeneity. The obtained peak at -66.4 ppm in the f-MRPUs shows the existence

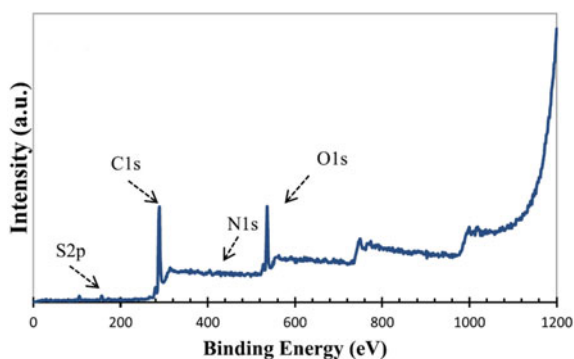


Fig. 7.11 Curve representation of XPS spectra of PU composites [66]. Reprinted from Miraftab R, Ramezanzadeh B, Bahlakeh G, Mahdavian M (2017) An advanced approach for fabricating a reduced graphene oxide–AZO dye/polyurethane composite with enhanced ultraviolet (UV) shielding properties: Experimental and first-principles QM modeling. *Chemical Engineering Journal* 321:159–174, Copyright © 2017, with permission from Elsevier Ltd.

of T_4 structures rising from the cross-linking responses of stiff sections of PU with the dynamic epoxide groups.

In X-Ray diffraction analysis, the results obtained of the structures of crystal of PU complexes had been assessed in Fig. 7.12c. The dominant considerations at $2\theta = 21.7^\circ$ – 22.4° , in addition to that at 24.2° in neat PU would be allocated to the crystalline PBA stage. Comparable patterns were also seen in PU composites, and when f-MCC or RhB were added, the crystalline structures of the PBA phase remained unaffected [67].

The f-MRPU simply reverted to their unusual shapes even to a difficult geometry within 30 s after being heated at 333.15 K temperature. The crucial shape-memory

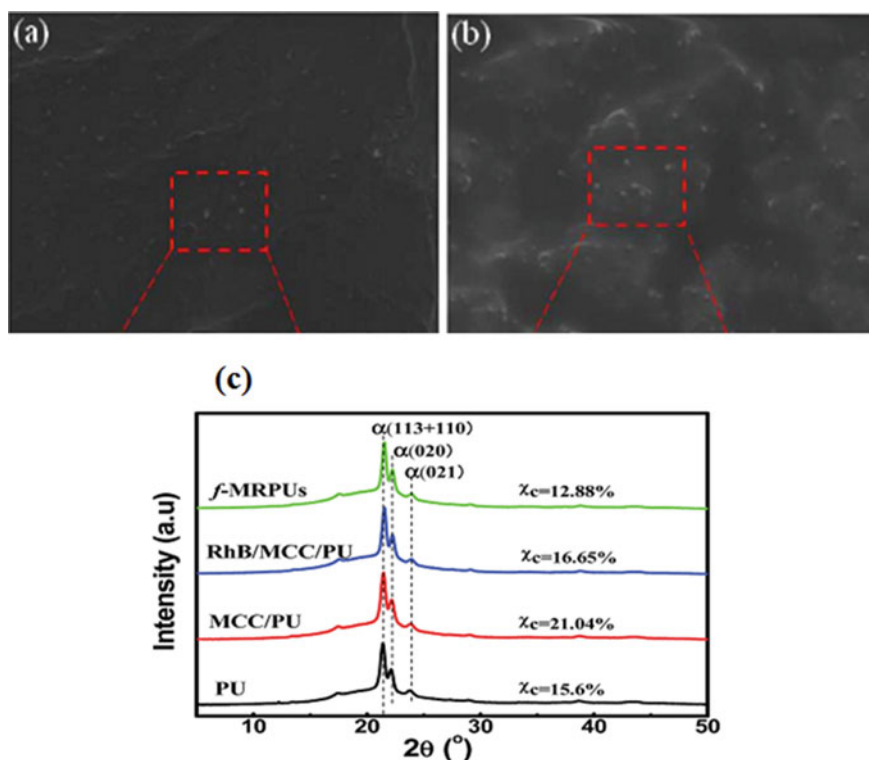


Fig. 7.12 SEM pictures representing the fracture surface of the PECU/CNCs nanocomposites: **a** PECU/CNC-C₆H₄NO₂ (weight of ten percent) and **b** PECU/CNC-C₆H₄NO₂ (weight of twenty percent) [68]. Reprinted with permission from Li Y, Chen H, Liu D, Wang W, Liu Y, Zhou S (2015) pH-responsive shape-memory poly (ethylene glycol)-poly (ϵ -caprolactone)-based polyurethane/cellulose nanocrystals nanocomposite. *ACS Appl. Mater. Interfaces* 7 (23):12,988–12,999, Copyright © 2015, American Chemical Society. **c** Representation of XRD curves of PU and PU composites [62]. Reprinted with permission from Cai C, Wei Z, Wang X, Mei C, Fu Y, Zhong W (2018) Novel double-networked polyurethane composites with multi-stimuli-responsive functionalities. *J. Mater. Chem. A* 6 (36):17,457–17,472, Copyright © 2018, The Royal Society of Chemistry

components could be revealed by collected network heterogeneity from RhB and f-MCC, which helped like flexibly as well as elementally cross-linked links. The representation of the shape-memory conduct of the complexes of PU, cyclic thermo-mechanical compression tests are usually approved. Symbolizing the adaptability of some genuine variations in reaction to an outside stimulus as offered by cooling and heating processes, as well as the adjustable form changes in compression mean of all PU combinations. The PU and f-MRPU of shape-memory recoverability were found to be less sensitive and more sensitive, respectively. This improves the shape-memory recoverability of f-MRPU. Following that, the higher dimensional versions. Secondary flexible cross-linked networks may typically regulate the dimensional modification rising to the opposite PU segment mobility synthesis.

The materials' flexible actions had regarded investigating the elements of fillers as a fortifying stage upon the matrix of PU. Results of the impacts of MCC and RhB on the mechanical things of the PU complexes, a remarkable upsurge in the elastic modulus and tensile strength were detected Compared with neat PU when MCC had mix along with the PU matrix. The tensile strength and elastic modulus have surged between 25.9 ± 2.6 to 31.6 ± 2.1 MPa and 3.0 ± 0.2 to 3.4 ± 0.1 MPa for PU and MCC/PU, correspondingly [69, 70]. It is identified like the overview of stiff fillers in the polymers mostly progresses the elastic modulus and tensile strength at the rate of an expense into the elongation at interruption from a repressed elasticity of deformation [71, 72].

7.4.1 Poly (Ethylene Glycol)–poly(ϵ -Caprolactone)-Based Polyurethane (PECU) and Its Nanocomposites

In the ring-opening polymerization method, a 3-necked round bottom flask was used for the addition of PCL–PEG–PCL with the amount 0.36 mmol and further parched at the vacuum within the compressed pressure at 353.15 K temperature up to 120 min. To make this prepolymer, originally known as 4,4-diphenylmethane diisocyanate (MDI), 0.92 mmol of MDI was placed in a flask under a moving and argon (Ar) gas environment at 80 °C for 2 hours. After that, for 2 hMDI at 80 °C, Stannous octoate (Sn(Oct)) and chain extender 2,2-Bis(hydroxymethyl) propionic acid (DMPA, 2.1 mmol) were added to the reaction mixture. To get the required films, the reaction mixture was transported out and evaporated at 353.15 K for 480 minutes. These films have been dried out at normal temperature for 48 hours at room temperature. The PECU is designated as (PCL–PEG–PCL) 70% -MDI-DMPA, and the numerical figures under the PCL–PEG–PCL identify the weight percentages of PCL–PEG–PCL in the PECU. In the DMF (50 mg/mL), the PECU had been dissolved by stirring for 240 min. Furthermore, ultrasonic treatment had been used to prepare cellulose nanocrystals (CNC–CNC–C₆H₄NO₂ or CNC–COOH suspension in DMF and consequently added into PECU solutions concurring with the different proportions of 5, 10, 20, and 30 wt %). The statistical values under the CNCs show

the weight percentage of CNCs in the nanocomposites. Later, these solutions had been shaken for 360 min, Teflon dishes had been used to cast them, then at 60 °C temperature for 8 h it was evaporated to attain films. Then, under vacuum, the film was additionally dried out at normal temperature for 48 h, and after that at 80 °C temperature for 12 h it was dried out under vacuum to eliminate filtrate [73].

The fracture outward of samples containing PECU nanocomposites was observed using a SEM imaging. The CNC-C₆H₄NO₂ in the perpendicular plane of the nanocomposites from the white dots would be perceptibly known in the matrix of the nanocomposites [74] as exposed in Fig. 12a. The nanocomposite may be detected as a superior expansion of the cracked surface, in addition to the presence of the CNC-C₆H₄NO₂ filler in the PECU matrix as shown in Fig. 12b [75]. Furthermore, because of the H-bonding between the CNC-C₆H₄NO₂ and the molecular chains of the PECU, the solvent exchange sol-gel method isolated these CNC-C₆H₄NO₂ fillers in the PECU matrix, indicating that a high level of compatibility between the polymer matrix and nanofillers has been achieved. Because of the inter connections between CNC-C₆H₄NO₂ as , the CNC-C₆H₄NO₂ saturating network architecture was constructed in nanocomplexes [76].

Mechanical and Thermal Properties of the Nanocomposites

The stress-strain bend nanocomposites expanded, from 9.6 ± 0.3 to 54.2 ± 0.6 MPa Young's modulus increased; however, the stretching to break decreased 91 %, which was attributed to a higher crystallinity and maximum viewpoint fraction of the nanocrystals. The improvement in quality and modulus in this type of material is straightforwardly inferable from the reinforced supplied via cellulose nanofibrils disseminated by the nanoscale [76]. Moreover, CNCs contented expanding, the resoluteness of the resources builds, and that is destructive by the shape-memory recuperation of polymer.

The nanocomposites of the PECU as a result of DSC Every nanocomposites' thermal ranges changed by roughly 316.15 K. The nanocomposite through modified CNCs of 20% wt percent was assigned for the test. The nanocomposite for the progress temperature is lower than the unadulterated PECU (367.65 K), conceivably because of an expansion of the series difficulty grade after the PECU blended in through nanocrystals. Additionally, at temperature 37 °C, the nanocomposite is caught up in the water for half an hour. The argument in this nanocomposite framework is that the series of polymer bonds within changed CNCs through H bonds, thus H₂O atoms has a next with no influence on the growth of polymer chains. This is not quite the same as usual, in that H₂O or additional dissolvable dispersed in the significant matrix is commonly interpreted as a plasticizer that lowers the T of shape-memory polymers [77].

In FT-IR spectra of PECU nanocomposites, because of the O-H stretching the range was received for the range of 3000–500 cm⁻¹, apart from this for the N-H, C = O and pyridine ring the range had obtained the 1500–1750 cm⁻¹. Due to the hydrogen bond, it causes wavelengths in numbers to shift lesser to broader in the material, main peaks are found at the wavelength from 1500–1750 cm⁻¹ to 3000–3500 cm⁻¹ sections. Figure 7.13a, b illustrates the Fourier Transform-Infrared Radiation ranges

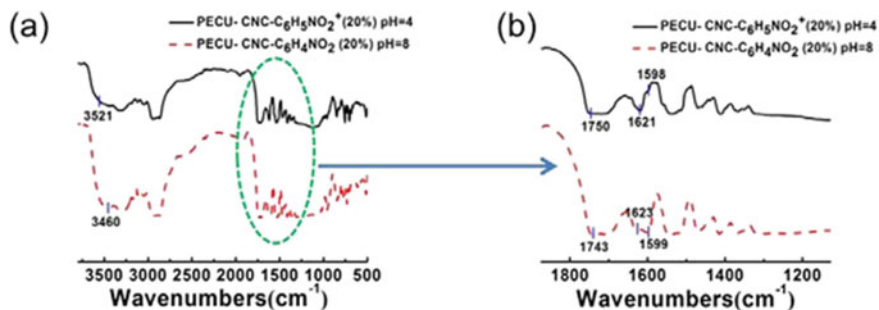


Fig. 7.13 FT-IR ranges of **a, b** PECU/CNC-C₆H₄NO₂ (20 weight %) film after involvement in acidic media (pH = 4) or basic media (pH = 8) for 30 min [68]. Reprinted with permission from Li Y, Chen H, Liu D, Wang W, Liu Y, Zhou S (2015) pH-responsive shape-memory poly (ethylene glycol)-poly (ϵ -caprolactone)-based polyurethane/cellulose nanocrystals nanocomposite. ACS applied materials & interfaces 7 (23):12,988–12,999, Copyright © 2015, American Chemical Society

of PECU/CNC-C₆H₄NO₂ (20 weight percentage) film subsequent submersion in acidic media (pH = 4) or fundamental media (pH = 8) intended for 30. Furthermore, Fig. 7.14a, as well as Fig. 7.14b, shows The FT-IR spectra of PECU/CNC-COOH (20 wt %) film after ingestion in acidic media (pH = 1) and essential media (pH = 0) for half an hour. The pyridine ring on the outside of CNC-C₆H₄NO₂ has protonated, prompting the harm of Hydrogen-holding connections of isocyanate gatherings of PECU and pyridine of CNC-C₆H₄NO₂; this is in acidic condition. At 1598 cm⁻¹, the vibration highest of the pyridine ring was received; that peak vanished in acidic media, demonstrating the H connection among N-H. Furthermore, the pyridine ring had wrecked in the pyridine by protonation in acidic media [78]. In the base, the pyridine on the outside of CNC-C₆H₄NO₂ was deprotonated, initiating the arrangement of

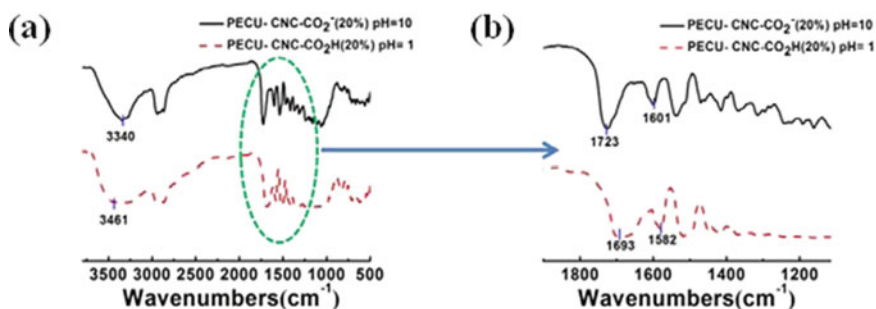


Fig. 7.14 PECU/CNC-COOH (20 weight %) film after immersion in acidic media (pH = 1) as well as basic media (pH = 10) for 30 min [68]. Reprinted with permission from Li Y, Chen H, Liu D, Wang W, Liu Y, Zhou S (2015) pH-responsive shape-memory poly (ethylene glycol)-poly (ϵ -caprolactone)-based polyurethane/cellulose nanocrystals nanocomposite. ACS applied materials & interfaces 7 (23):12,988–12,999, Copyright © 2015, American Chemical Society

Hydrogen holding communications among nanocrystals and materials. H-holding associations among the carboxyl gatherings on the outside of CNC-COOH as well as isocyanate gatherings of PECU were set up through the Fourier Transform-Infrared Radiation spectroscopy.

7.5 SMPC-Based Nanoclay

Organic-exfoliated nanoclays are a good material for the manufacture of functional chemicals as well as progressive belongings under particular conditions. Organic-exfoliated nanoclay is a promising choice for improving the shape recovery stress and mechanical characteristics of SMP. Among a display of Na-MMT (sodium montmorillonite) from Intercalated macro azo-initiator (MAI) [79], is a piece of hydrophilic poly (ethylene-glycol) (PEG). For the Na-MMT implanted using MAI, in situ radical polymerization was employed to design polymer nanocomposites (ethyl methacrylate). The PEG/Na-MMT component, which is linked to poly(ethyl methacrylate), takes its role additionally as per the complex step, adding shape-memory qualities as well as a component to boost mechanical properties. Jana and Cao [80]. SMPU/organoclay compositions combined into a Brabender Plastic order [82]. Molar proportion of alcoholic (-OH) and isocyanine (-NCO) bunches was kept up at 1:1 through -CH₂ CH₂ OH gatherings and particles of quaternary ammonium in organoclay providing an aspect of aggregate -OH usefulness. For hard segments, the secured responsive clay used on polyurethane series provides a new system that enhances more restraints to the chain signal of SMPU. As compared to pure SMPU, the nanocomposite at the proportion 1%wt. organoclay provides around 20% larger recovery strain.

For many polymers, clay has been a typical filler. Different nanofillers, including clay, powder, silica, ceramic, etc., have been used to resolve the low stiffness problem of SMP in the reinforced SMP matrix. Nanoclay based on attapulgite is a naturally hydrated silicate of magnesium-aluminum that can broaden upon wetting. Pan et al. have synthesized PU/Attapulgite composites in dry and wet conditions, in which they have melted SMP pellets first at 200 °C and then dry (heated at 850 °C for 2 h) and wet clay was mixed in different proportions. The actuation stress and stiffness of SMPs were enhanced by synthesized composite [77]. Another experiment was investigated to improve mechanical properties; mechanical mixing of attapulgite clay with smart memory PU was prepared. Firstly, clay had been heated at 850 °C for 2 h and then mechanically mixed with PU at 200 °C followed by hot press made composites. These composite mechanical properties depend extensively on the pretreatment nanopowder that has been tested using a micro-indentation tester [78]. The same group improved the interactions between nanoclay and polymer by extending the portion of clay and analyzing nano-indentation and microhardness tests. They have used PU-MM5520 pellets and preheated attapulgite clay to prepare composite. Both were mixed and held in the oven for 12 h at 100 °C. In tensile testing, this composite demonstrated a great shape-memory effect [79]. Rezanejad

et al. examined the variance of the mass fractions of nanoclay in cross-linking with low-density polyethylene (LDPE). Originally updated cloisite clay and LDPE melt were blended at 170 °C, followed by rotating the mixture slowly for 30 min that gave an excellently mixed system. After that, the mixture was mixed with dicumyl peroxide and anti-oxidant by rotation at 130 °C, the LDPE/Cloisite composite was then cured in a hot press under pressure at 180 °C. The resultant smart nanocomposite has higher modulus and strength, allowing it to operate as an actuator with increased recovery force [80].

7.6 Applications of SMPCs

Transforming structures and an increasing variety of deployable were considered and investigated, including deployable optical frameworks, supports, pivots, deployable mirrors, blasts, adaptable reflectors, receiving apparatuses, solar-powered clusters, and transforming skins [81]. Specifically, SMP-based organization gadgets can doubtful, therefore most of the downsides of conventional deployable structures, especially the mind-boggling get together systems and huge degrees. Additionally, elite fiber-strengthened SMP composites will slowly expanding substitute customary aviation materials. Various notable foreordained component models were set up to dissect the twist and strain of the flexural. It very well may be likely that SMPs and their composites will stay to convey novel advancements that meet the difficult needs of the aviation area. In addition to aviation, current advancement in shrewd polymer innovations is rapidly stretching out to arrive at additional fields. Like SMPs, similar to a strand, yarns and textures can be utilized to make savvy materials, dress, and related yields [82]. SMP filaments with tunable shape and progress temperature can be utilized to make responsive attire with predominant flexibility and fit that normally acclimates to the environment. Biocompatible polymers, particularly polyurethane-based SMPs, have demonstrated exceptional results in the biomedical area and have been used in drug delivery frameworks, micro-actuators for blood clot clearance, smart surgical sutures, and other applications [83, 84]. The yield recovery strength was developed in shape-memory consequence that SMPC with electrically begun, it has also been applied activating ability, and is established to activate the indication of a ball on the table, as shown in Fig. 7.15.

BMW is reconsidering the project of automobile body shells, presenting non-metal materials to illustrate an associated connection between aesthetics, materials, and functions in the automotive field. The SMPs suggest a great contract likely for such projects. Specified the movement of advancement, SMPs will surely remain to assume a critical function in the improvement of new advances intended for biomedical designing. Notwithstanding the substance arrangement and full-scale structure, the exhibition of the material surface relies generally upon the nano/miniatuure structure of the surface. The structure of polymer surface miniatuure nanostructures has significant application prospects, in wettability guidelines, meager surface optical

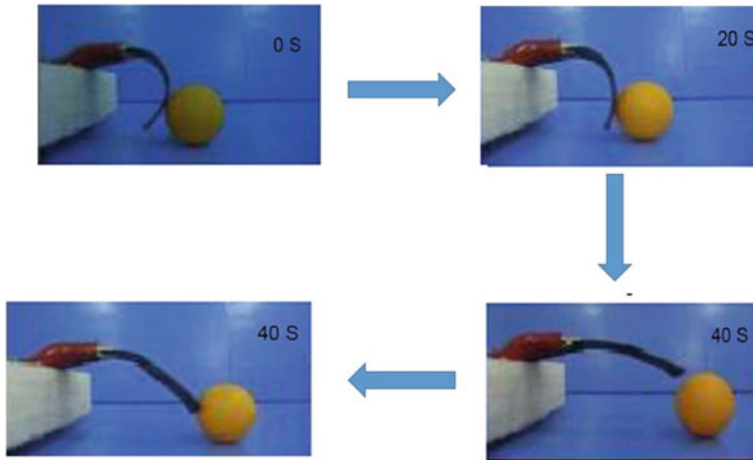


Fig. 7.15 Sequence of photographs exhibiting SMP composite plus the activating motion of ball (table-tennis ball). The temporary figure is distorted as the right-angle figure permanent figure is a plane stripe of complex material [85]. Reprinted with permission from Essabir H, Nekhlaoui S, Bensalah M-o, Bouhfid R (2020) Shape-memory based on composites and nanocomposites materials: from synthesis to application. In: *Polymer Nanocomposite-Based Smart Materials*. Elsevier, pp 103–120, Copyright © 2020, with permission from Elsevier Ltd.

execution upgrade, microfluidic transport and control, drug-controlled delivery, planning of tissue designing materials and microelectronic gadgets, and so on. Expected applications for shrewd polymers will comparatively keep on growing in another region. SMPs were proposed for applications, for example, optical gadgets, assorted as wind stream control, and self-mending gadgets [86, 87].

7.7 Conclusion

All in all, it can be concluded that the possible recovery force as well as the modulus of the material escalate in the reinforced silicon carbide (SiC) nano-particulate in the resin of shape-memory polymer composite. As compared to the higher glass transition temperature, a comparison of reinforced or unreinforced SMPs is to be done based on glass transition temperature. It has been observed that the evolution of recapture stress may be assessed as a utilisation of temperature, and it soaks by stress equivalent toward stress pre-distortion. The results in TiNi fibre shown that increasing the volume fraction of wire enhanced breaking strength and Young modulus no at high heat or else at normal (room) temperature. SMPs' fragility decreases at high temperatures to compensate for TiNi wire. The strength of the interface, as well as the potency of the interface matrix, has proved critical to additional gains in higher temperatures in mechanical characteristics. The recovered stress of a composite can be altered by

changing the pre-strain. TiNi wires shape-memory properties were played a foremost part in the composites. The composite laminates related through a diversity of Teflon, PEEK-0.5, PEEK-1, as well as Tedlar is examples of the hydrophobic barrier films that were invented using Kevlar fiber prepares, DI water for saturation period can be submerged in the composite panels. Without moisture-barrier films, the equilibrium time of coupons is based on the duration of water exposure. Paint tape and SBS tests were subjected to the coupons. The needful things of the paint tape tests could be different rather than film of Teflon and additional barrier films passed. Through the SBS test, it was confirmed that significantly mechanical improvement of properties that complex panels possible as a result of the utilization of barrier films and also decreased water ingress in the laminate composite structure. Likewise, results of SBS strength, demonstrating that PEEK-1 films would change the commercially used Tedlar films can be provided by Tedlar films and The PEEK-1. The volume fraction of glass fibers containing dynamic mechanical properties of SMP. The incorporation of glass fibers was enormously improved with the storage modulus. As the paper shows that 15SMPC has maximum accommodate modulus related to the added SMPC also shows the minimum worth of constant C. Moreover, the value of loss modulus is 15SMPC that can describe the largest rate for two provinces of temperature (over T_g and under T_g) they show 15SMPC has do not disintegrate more energy associated with others and shows good interface bonding. Further, it also has confirmed that the supporting efficiency about fraction volume of glass fibers and it also shows a minimum 0.429 tan delta value. Thermally encouraged with woven fabric-reinforced material an anisotropic visco-hyperplastic constitutive model was developed. Heterogeneity developed in this work with the multi-stimuli-responsive PU networks the advanced large strain sensors and designing multiple functionalities and micro-actuators in latent fields designing multiple functionalities open new avenues to the development of high-performance SMPs.

From this study, shape-memory properties and the thermo-mechanical properties of TPI SMP syntheses, DMA test, static tensile test, DSC test, thermal conductivity test, thermodynamic cycling test, mechanical cycle test as well as shape-memory test can be studied with various carbon fiber contents. 8% was the present experimental results of the sliced carbon weight fraction fiber. The composite of reinforced TPI SMP has the finest properties through mechanical and better shape-memory resources. The ideal value for an SMP is shown as a proportion of 8% of the carbon fibre mass settled using the intended manufacturing technique.

References

1. Verma D, Purohit R, Rana RS, Purohit S, Patel KK (2020) Enhancement of the properties of shape-memory polymers using different nano size reinforcement—a review. *Mater Today: Proc* 26. <https://doi.org/10.1016/j.matpr.2020.02.631>
2. Li F, Leng J, Liu Y, Remillat C, Scarpa F (2020) Temperature dependence of elastic constants in unidirectional carbon fiber reinforced shape-memory polymer composites. *Mech Mater* 148:103518

3. Lu W, Le X, Zhang J, Huang Y, Chen T (2017) Supramolecular shape-memory hydrogels: a new bridge between stimuli-responsive polymers and supramolecular chemistry. *Chem Soc Rev* 46(5):1284–1294
4. Bai Y, Zhang X, Wang Q, Wang T (2014) A tough shape-memory polymer with triple-shape-memory and two-way shape-memory properties. *J Mater Chem A* 2(13):4771–4778
5. Kirillova A, Ionov L (2019) Shape-changing polymers for biomedical applications. *J Mater Chem B* 7(10):1597–1624. <https://doi.org/10.1039/C8TB02579G>
6. Peterson GI, Dobrynin AV, Becker ML (2017) Biodegradable shape-memory polymers in medicine. *Adv Healthcare Mater* 6(21):1700694
7. Li W, Liu Y, Leng J (2014) Shape-memory polymer nanocomposite with multi-stimuli response and two-way reversible shape-memory behavior. *RSC Adv* 4(106):61847–61854
8. Liang C, Rogers C, Malafeev E (1997) Investigation of shape-memory polymers and their hybrid composites. *J Intell Mater Syst Struct* 8(4):380–386
9. Lee BS, Chun BC, Chung Y-C, Sul KI, Cho JW (2001) Structure and thermomechanical properties of polyurethane block copolymers with shape-memory effect. *Macromolecules* 34(18):6431–6437
10. Koerner H, Price G, Pearce NA, Alexander M, Vaia RA (2004) Remotely actuated polymer nanocomposites—stress-recovery of carbon-nanotube-filled thermoplastic elastomers. *Nat Mater* 3(2):115–120
11. Yang B, Huang WM, Li C, Chor JH (2005) Effects of moisture on the glass transition temperature of polyurethane shape-memory polymer filled with nano-carbon powder. *Eur Polymer J* 41(5):1123–1128
12. Jung YC, Kim JH, Hayashi T, Kim YA, Endo M, Terrones M, Dresselhaus MS (2012) Fabrication of transparent, tough, and conductive shape-memory polyurethane films by incorporating a small amount of high-quality graphene. *Macromol Rapid Commun* 33(8):628–634
13. Liang J, Xu Y, Huang Y, Zhang L, Wang Y, Ma Y, Li F, Guo T, Chen Y (2009) Infrared-triggered actuators from graphene-based nanocomposites. *J Phys Chem C* 113(22):9921–9927
14. Liu Y, Du H, Liu L, Leng J (2014) Shape-memory polymers and their composites in aerospace applications: a review. *Smart Mater Struct* 23(2):023001
15. Lan X, Liu L, Liu Y, Leng J (2020) Thermomechanical properties and deformation behavior of a unidirectional carbon-fiber-reinforced shape-memory polymer composite laminate. *J Appl Polym Sci* 137(14):48532
16. Leng J, Lan X, Liu Y, Du S (2011) Shape-memory polymers and their composites: stimulus methods and applications. *Prog Mater Sci* 56(7):1077–1135
17. Wei H, Liu L, Zhang Z, Du H, Liu Y, Leng J (2015) Design and analysis of smart release devices based on shape-memory polymer composites. *Compos Struct* 133:642–651
18. Fej's M, Romhány G, Karger-Kocsis J (2012) Shape-memory characteristics of woven glass fibre fabric reinforced epoxy composite in flexure. *J Reinf Plast Compos* 31(22):1532–1537
19. Park YC, Lee GC, Furuya Y (2004) A study on the fabrication of TiNi/Al6061 shape-memory composite material by hot-press method and its mechanical property. *Mater Trans* 45(2):264–271
20. Park YC, Kang JH, Lee JK, Lee GC, Furuya Y (2007) Effect of cold rolling on fatigue crack propagation of TiNi/Al6061 shape-memory composite. *Smart Mater Struct* 16(4):982
21. Park Y-C, Jo Y-J, Baek S-H, Furuya Y (2009) Fatigue design curve of a TiNi/Al shape-memory alloy composite for aircraft stringer design. *Smart Mater Struct* 18(5):055009
22. Yamashita K, Shimamoto A (2005) Control of shape recovery force in SMA fiber reinforced composite materials. In: *Smart structures and materials 2005: active materials: behavior and mechanics*. International Society for Optics and Photonics, pp 429–439
23. Otsuka K, Ren X (2005) Physical metallurgy of Ti–Ni-based shape-memory alloys. *Prog Mater Sci* 50(5):511–678
24. Li D, Zhang X, Xiong Z, Mai Y-W (2010) Lightweight NiTi shape-memory alloy based composites with high damping capacity and high strength. *J Alloy Compd* 490(1–2):L15–L19
25. Ahn I-S, Bae S-Y, Kim Y-Y (2004) Properties of Al/TiNi composite using porous TiNi fabricated by a self-propagating high temperature synthesis method. *Met Mater Int* 10(1):39

26. Chaudhury Z, Hailat M, Liu Y, Newaz G (2011) Aluminum-based composites reinforced with SiC particles and NiTi fibers: influence of fiber dimensions and aging time on mechanical properties. *J Mater Sci* 46(6):1945–1955
27. Akalin O, Ezirmik KV, Urgan M, Newaz GM (2010) Wear characteristics of NiTi/Al6061 short fiber metal matrix composite reinforced with SiC particulates. *J Tribol* 132(4)
28. Ohki T, Ni Q-Q, Ohsako N, Iwamoto M (2004) Mechanical and shape-memory behavior of composites with shape-memory polymer. *Compos A Appl Sci Manuf* 35(9):1065–1073
29. Wei Z, Sandström R, Miyazaki S (1998) Shape-memory materials and hybrid composites for smart systems: Part I Shape-memory materials. *J Mater Sci* 33(15):3743–3762
30. Xiong Z, Wang Z, Li Z, Chang R (2008) Micromechanism of deformation in EMC laminates. *Mater Sci Eng, A* 496(1–2):323–328
31. Gall K, Mikulas M, Munshi NA, Beavers F, Tupper M (2000) Carbon fiber reinforced shape-memory polymer composites. *J Intell Mater Syst Struct* 11(11):877–886
32. Yarborough CN, Childress EM, Kunz RK (2008) Shape recovery and mechanical properties of shape-memory composites. In: ASME International mechanical engineering congress and exposition, pp 111–119
33. Bae C, Park J, Kim E, Kang Y, Kim B (2011) Organic–inorganic nanocomposite bilayers with triple shape-memory effect. *J Mater Chem* 21(30):11288–11295
34. Xu B, Fu YQ, Ahmad M, Luo J, Huang WM, Kraft A, Reuben R, Pei YT, Chen ZG, De Hosson JTM (2010) Thermo-mechanical properties of polystyrene-based shape-memory nanocomposites. *J Mater Chem* 20(17):3442–3448
35. Gall K, Dunn ML, Liu Y, Finch D, Lake M, Munshi NA (2002) Shape-memory polymer nanocomposites. *Acta Mater* 50(20):5115–5126
36. Liu Y, Gall K, Dunn ML, McCluskey P (2004) Thermomechanics of shape-memory polymer nanocomposites. *Mech Mater* 36(10):929–940
37. Plastics-determination of tensile properties: Part 1: General principles. The International Organization for Standardization. (2012). 2(12). ISO527–1:2012
38. Feng X, Zhao L, Mi X, Li Y, Xie H, Xiangqian Y, Gao B (2013) Improved shape-memory composites combined with TiNi wire and shape-memory epoxy. *Mater Des* 50:724–727. <https://doi.org/10.1016/j.matdes.2013.03.060>
39. Payandeh Y, Meraghni F, Patore E, Eberhardt A (2012) Study of the martensitic transformation in NiTi-epoxy smart composite and its effect on the overall behavior. *Mater Des* 39:104. <https://doi.org/10.1016/j.matdes.2012.02.041>
40. Gibson RF (2011) Principle of composite material mechanics. CRC Press
41. Nor Hanim K, Azerai Ali R, Mohd Fadzil A, Mohd Khairul K, Sajith Totthatil AR (2019) Dynamic mechanical properties of Polyurethane Shape-Memory Polymer Composites (SMPC) with different volume fractions of chopped strand mat glass fiber. *Int J Integr Eng* 10(9)
42. Joseph P, Joseph K, Thomas S, Pillai C, Prasad V, Groeninckx G, Sarkissova M (2003) The thermal and crystallisation studies of short sisal fibre reinforced polypropylene composites. *Compos A Appl Sci Manuf* 34(3):253–266
43. Pothan LA, Oommen Z, Thomas S (2003) Dynamic mechanical analysis of banana fiber reinforced polyester composites. *Compos Sci Technol* 63(2):283–293
44. Chua PS (1987) Dynamic mechanical analysis studies of the interphase. *Polym Compos* 8(5):308–313. <https://doi.org/10.1002/pc.750080505>
45. Jawaid M, Khalil HA, Hassan A, Dungani R, Hadiyane A (2013) Effect of jute fibre loading on tensile and dynamic mechanical properties of oil palm epoxy composites. *Compos B Eng* 45(1):619–624
46. Khiyon NH, Rahman AA, Arshad MF, Kamarudin MK, Rahman STA (2018) Dynamic mechanical properties of Polyurethane Shape-Memory Polymer Composites (SMPC) with different volume fractions of chopped strand mat glass fiber. *Int J Integr Eng* 10(9)
47. Essabir H, Elkhaoulani A, Benmoussa K, Bouhfid R, Arrakhiz F, Qaiss A (2013) Dynamic mechanical thermal behavior analysis of doum fibers reinforced polypropylene composites. *Mater Des* 51:780–788

48. Su X, Wang Y, Peng X (2020) An anisotropic visco-hyperelastic model for thermally-actuated shape-memory polymer-based woven fabric-reinforced composites. *Int J Plasticity* 102697
49. Mohanakrishnan D, Sureshkumar M (2015) A comparative analysis of orientation on the shape-memory effect of fabric reinforced shape-memory polymer composites. *Mater Sci Forum* 830–831:529–532. <https://doi.org/10.4028/www.scientific.net/MSF.830-831.529>
50. Mohanakrishnan D, Sureshkumar MA (2015) Comparative analysis of orientation on the shape-memory effect of fabric reinforced shape-memory polymer composites. *Materials Science Forum*. *Trans Tech Publ*, pp 529–532
51. Kececi E, Asmatulu R (2014) Effects of moisture ingress on polymeric laminate composites and its prevention via highly robust barrier films. *Int J Adv Manuf Technol* 73(9):1657–1664. <https://doi.org/10.1007/s00170-014-5974-5>
52. Kececi E (2012) Highly durable hydrophobic thin films for moisture prevention of composite structures for aerospace applications. *Wichita State University*
53. An Y, Zhang X, Wang X, Chen Z, Wu X (2018) Nano@lignocellulose intercalated montmorillonite as adsorbent for effective Mn(II) removal from aqueous solution. *Sci Rep* 8(1):10863. <https://doi.org/10.1038/s41598-018-29210-2>
54. Wang Z, Liu J, Guo J, Sun X, Xu L (2017) The study of thermal, mechanical and shape-memory properties of chopped carbon fiber-reinforced tpi shape-memory polymer composites. *Polymers* 9(11):594
55. Pieczyska EA, Nowacki WK, Tobushi H, Hayashi S (2009) Thermomechanical properties of shape-memory polymer subjected to tension in various conditions. *Quant InfraRed Thermogr J* 6(2):189–205
56. Dastgerdi JN, Marquis G, Salimi M (2013) The effect of nanotubes waviness on mechanical properties of CNT/SMP composites. *Compos Sci Technol* 86:164–169
57. Raja M, Ryu SH, Shanmugaraj A (2013) Thermal, mechanical and electroactive shape-memory properties of polyurethane (PU)/poly (lactic acid)(PLA)/CNT nanocomposites. *Eur Polymer J* 49(11):3492–3500
58. Ni Q-Q, Zhang C-s, Fu Y, Dai G, Kimura T (2007) Shape-memory effect and mechanical properties of carbon nanotube/shape-memory polymer nanocomposites. *Compos Struct* 81(2):176–184
59. Li H, Zhong J, Meng J, Xian G (2013) The reinforcement efficiency of carbon nanotubes/shape-memory polymer nanocomposites. *Compos B Eng* 44(1):508–516
60. Cho JW, Kim JW, Jung YC, Goo NS (2005) Electroactive shape-memory polyurethane composites incorporating carbon nanotubes. *Macromol Rapid Commun* 26(5):412–416
61. Yang Q-s, He X-q, Liu X, Leng F-f, Mai Y-W (2012) The effective properties and local aggregation effect of CNT/SMP composites. *Compos B Eng* 43(1):33–38
62. Cai C, Wei Z, Wang X, Mei C, Fu Y, Zhong W (2018) Novel double-networked polyurethane composites with multi-stimuli responsive functionalities. *J Mater Chem A* 6(36):17457–17472
63. Baidya A, Ganayee MA, Jakka Ravindran S, Tam KC, Das SK, Ras RH, Pradeep T (2017) Organic solvent-free fabrication of durable and multifunctional superhydrophobic paper from waterborne fluorinated cellulose nanofiber building blocks. *ACS Nano* 11(11):11091–11099
64. Yilgor I, Yilgor E, Guler IG, Ward TC, Wilkes GL (2006) FTIR investigation of the influence of diisocyanate symmetry on the morphology development in model segmented polyurethanes. *Polymer* 47(11):4105–4114
65. Chen K, Tian Q, Tian C, Yan G, Cao F, Liang S, Wang X (2017) Mechanical reinforcement in thermoplastic polyurethane nanocomposite incorporated with polydopamine functionalized graphene nanoplatelet. *Ind Eng Chem Res* 56(41):11827–11838
66. Miraftab R, Ramezanzadeh B, Bahlakeh G, Mahdavian M (2017) An advanced approach for fabricating a reduced graphene oxide-AZO dye/polyurethane composite with enhanced ultraviolet (UV) shielding properties: experimental and first-principles QM modeling. *Chem Eng J* 321:159–174
67. Fritzsche N, Pretsch T (2014) Programming of temperature-memory onsets in a semicrystalline polyurethane elastomer. *Macromolecules* 47(17):5952–5959

68. Li Y, Chen H, Liu D, Wang W, Liu Y, Zhou S (2015) pH-responsive shape-memory poly (ethylene glycol)–poly (ϵ -caprolactone)-based polyurethane/cellulose nanocrystals nanocomposite. *ACS Appl Mater Interfaces* 7(23):12988–12999
69. Auad ML, Contos VS, Nutt S, Aranguren MI, Marcovich NE (2008) Characterization of nanocellulose-reinforced shape-memory polyurethanes. *Polym Int* 57(4):651–659
70. Hadjadj A, Jbara O, Tara A, Gilliot M, Malek F, Maafi EM, Tighzert L (2016) Effects of cellulose fiber content on physical properties of polyurethane based composites. *Compos Struct* 135:217–223
71. Li Z, Young RJ, Kinloch IA (2013) Interfacial stress transfer in graphene oxide nanocomposites. *ACS Appl Mater Interfaces* 5(2):456–463
72. McNally T, Pötschke P, Halley P, Murphy M, Martin D, Bell SE, Brennan GP, Bein D, Lemoine P, Quinn JP (2005) Polyethylene multiwalled carbon nanotube composites. *Polymer* 46(19):8222–8232
73. Li Y, Chen H, Liu D, Wang W, Liu Y, Zhou S (2015) pH-responsive shape-memory poly(ethylene glycol)–Poly(ϵ -caprolactone)-based polyurethane/cellulose nanocrystals nanocomposite. *ACS Appl Mater Interfaces* 7(23):12988–12999. <https://doi.org/10.1021/acsami.5b02940>
74. Zhao Q, Sun G, Yan K, Zhou A, Chen Y (2013) Novel bio-antifouling agent based on waterborne polyurethane and cellulose nanocrystals. *Carbohydr Polym* 91(1):169–174
75. NCCLS, National Committee for Clinical Laboratory Standards, Performance Standards for Antimicrobial Disk Susceptibility Test (1997). 6th ed, Approved Standard, Wayne, PA, M2-A6
76. Annamalai PK, Dagnon KL, Monemian S, Foster EJ, Rowan SJ, Weder C (2014) Water-responsive mechanically adaptive nanocomposites based on styrene-butadiene rubber and cellulose nanocrystals processing matters. *ACS Appl Mater Interfaces* 6(2):967–976
77. Pan G, Huang W, Ng Z, Liu N, Phee S (2008) The glass transition temperature of polyurethane shape-memory polymer reinforced with treated/non-treated attapulgite (playgorskite) clay in dry and wet conditions. *Smart Mater Struct* 17(4):045007
78. Xu B, Huang WM, Pei YT, Chen ZG, Kraft A, Reuben R, De Hosson JTM, Fu YQ (2009) Mechanical properties of attapulgite clay reinforced polyurethane shape-memory nanocomposites. *Eur Polymer J* 45(7):1904–1911
79. Xu B, Fu YQ, Huang WM, Pei YT, Chen ZG, De Hosson J, Kraft A, Reuben RL (2010) Thermal-mechanical properties of polyurethane-clay shape-memory polymer nanocomposites. *Polymers* 2(2):31–39
80. Rezanejad S, Kokabi M (2007) Shape-memory and mechanical properties of cross-linked polyethylene/clay nanocomposites. *Eur Polymer J* 43(7):2856–2865
81. Luo X, Mather PT (2013) Shape-memory assisted self-healing coating. *ACS Macro Lett* 2(2):152–156
82. Xu H, Yu C, Wang S, Malyarchuk V, Xie T, Rogers JA (2013) Deformable, programmable, and shape-memorizing micro-optics. *Adv Func Mater* 23(26):3299–3306
83. Gladman AS, Matsumoto EA, Nuzzo RG, Mahadevan L, Lewis JA (2016) Biomimetic 4D printing. *Nat Mater* 15(4):413–418
84. Chung T, Romo-Uribe A, Mather PT (2008) Two-way reversible shape-memory in a semicrystalline network. *Macromolecules* 41(1):184–192
85. Essabir H, Nekhlaoui S, Bensalah M-o, Bouhfid R (2020) Shape-memory based on composites and nanocomposites materials: from synthesis to application. In: *Polymer nanocomposite-based smart materials*. Elsevier, pp 103–120
86. Tibbitts S (2014) 4D printing: multi-material shape change. *Arch Des* 84(1):116–121
87. Zhang Y, Shi L, Hu D, Chen S, Xie S, Lu Y, Cao Y, Zhu Z, Jin L, Guan B-O (2019) Full-visible multifunctional aluminium metasurfaces by in situ anisotropic thermoplasmonic laser printing. *Nanoscale Horizons* 4(3):601–609

Chapter 8

Wet Synthesis Methods of Shape-Memory Polymer Composites



Ashok Bhogi and T. Rajani

8.1 Introduction

Among the various active smart materials, shape memory polymer composites (SMPCs) are emerged as a promising materials. These materials are having the ability to recuperate to their original state from the programmed impermanent shapes (high shape deformability and shape recoverability) when they are exposed to suitable environmental stimuli like light, electric field, pH manipulation, temperature, magnetic field, and specific ions etc. [1, 2]. This property is assigned to the molecular architecture and is also termed as shape-memory effect (SME) [3]. Shape-memory polymer composites are having molecular switches and net points. The molecular switches in crystalline or amorphous polymer composite chains are used to control the shape stability/fixity and retrieval upon revealing to prearranged external stimuli. The net points are used to find out the permanent/lasting shape, which may be made up of either physical or chemical cross-linking points [4]. The innumerable advantages of the shape-memory polymer composites make them more attractive than the shape-memory alloys. These materials also have a high capacity for elastic deformation (up to 200% in most cases), much lower cost, lower density, easy processing, potential biocompatibility, biodegradability, and they can exhibit superior mechanical properties than shape-memory alloys.

The synthesis of these craved materials is the beginning point of materials science research. The synthesis of shape-memory polymer composites is significant due to the intensification in the requirements of SMPC materials for various industrial applications such as aerospace, smart textiles, 4D printing of active origami structures, fabrics, self-healing composite systems, etc. [5, 6]. The synthesis of these materials is having a sequence of operations that scientifically changes the physical and chemical aspects of the structure which eventually influence the physical properties of the materials. The core objective of the science behind the ceramics processing of

A. Bhogi (✉) · T. Rajani

Department of Humanities and Sciences (Physics), VNR Vignana Jyothi Institute of Engineering and Technology, Hyderabad, Telangana 500090, India

© The Author(s), under exclusive license to Springer Nature Switzerland AG 2022

155

M. R. Maurya et al. (eds.), *Shape Memory Composites Based on Polymers and Metals for 4D Printing*, https://doi.org/10.1007/978-3-030-94114-7_8

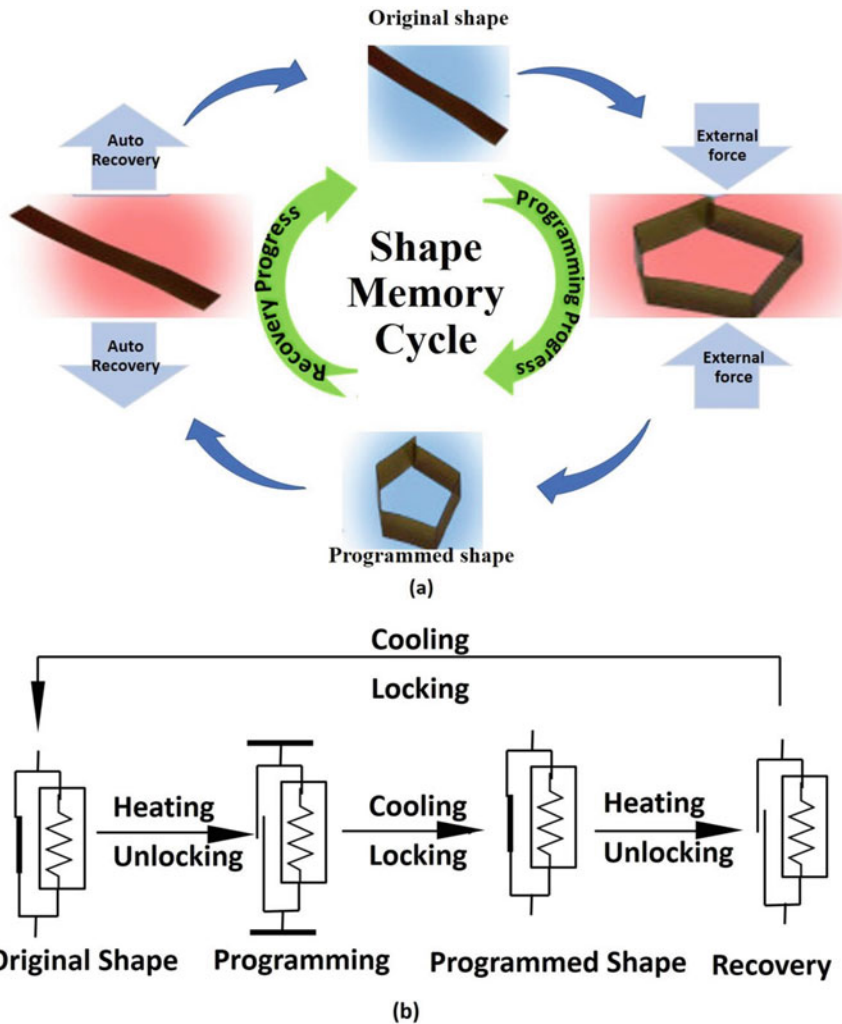


Fig. 8.1 a Shape-memory cycle. b Analogy to understand the shape-memory effect

SMPCs is to identify the imperative properties and to comprehend the influence of processing parameters on the physical and structural properties of the materials [7]. The wet synthesis techniques are having more advantages than other methods and they are, it is possible to accomplish selective surface structures, phases, shapes, and sizes of shape-memory polymer composites, leading to a set of desired properties. These methods also allow fine-tuning of the reaction conditions (temperature, concentration of substrate, additives or surfactants, pH, etc.) to provide the desired shape-memory polymer composites [7]. Figure 8.1 represents the shape-memory cycle and its analogy.

A comprehensive description of the wet synthesis techniques used in the preparation of shape-memory polymer composites (SMPCs) are introduced in this chapter. The following are the wet approaches to prepare the shape-memory polymer composites:

1. In situ polymerization
2. Solution mixing
3. Melt mixing
4. Co-precipitation
5. Sol-gel process
6. Electrospinning

8.2 In Situ Polymerization

The in situ polymerization technique is the simple, effective, and traditional route to prepare the shape-memory polymer composites with augmented functional properties. The general principle involved in this technique is the mixing of the nanofiller with the monomers in a solvent, followed by in situ polymerization. The polymerization of the mixture can be done using various techniques like radiation, heat treatment, organic initiator or initiator diffusion [8, 9]. Then the monomer is polymerized by sandwiched between interlayers thereby producing either intercalated or exfoliated polymer composites [10]. After completing the polymerization mechanism, the shape-memory polymer composites are produced. These SMPCs contains of polymer molecules and which are bound to nanoparticles. In order to accomplish this method (In situ polymerization), to form shape-memory polymer composites, the low viscosity prepolymers (typically < 1 Pa) have to be used. In Situ, template synthesis is analogous to this technique. In this technique, the clay layers have been manufactured in the existence of polymer chains. Both the polymer matrix and clay layers are liquified in an aqueous solution and the gel flows backward through a vessel (i.e., refluxed) at a very elevated temperature. These polymer chains are imprisoned in the interior of the clay layers. On these polymer chains the nucleation and rise of the clay layers occurs at very elevated temperature [11]. The drawback of this practice is that the decomposition of the polymer occurs at a very high temperature, i.e., the high-temperature synthesis leads to the decomposition of the polymer. Figure 8.2 illustrates the strides which are involved in this in situ polymerization to prepare SMPCs.

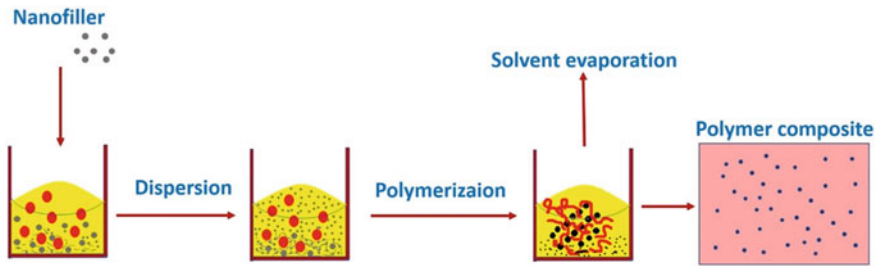


Fig. 8.2 The strides presented in the in situ polymerization technique

8.2.1 Advantages

The following are several advantages of this method:

1. The use of cost-effective materials.
2. Easy to automate
3. It has the ability to integrate with many other heating and curing methods
4. It endorses great spreading and nanoparticle dissemination in the polymer matrix.

8.2.2 Disadvantages

The detriment of this approach is that the synthesis of polymer composites at high temperatures causes the decomposition of the polymer composites.

8.3 Solution Mixing

Solution mixing is the most repeatedly used method to synthesize the shape-memory polymer composites (SMPCs), sometimes which is also called as solution blending method [12, 13]. This approach is completely dependent on the solvent system where the prepolymers or polymers are easily soluble, i.e., this method is applicable only to prepolymers or polymers where they can be easily soluble in one or more solvents. The solution mixing of polymer composites involves the dispersion of nanoparticles or nanofillers into the suitable polymer solution through various methods like mechanical stirring or magnetic stirring (Agitation), reflux, high shear mixing (homogenization) or probe sonification [14]. This technique offers a relatively modest approach for preparing shape-memory polymer composites in contrast to the various techniques. The following are the three main steps that are involved in the fabrication of shape-memory polymer composites in the solution mixing technique:

Step 1: The nanoparticles or nanofillers are sprinkled into a suitable solvent followed by fusing or blending with the appropriate polymer matrix or polymer solution.

Step 2: This mixture is thoroughly homogenized (thoroughly ground) through an appropriate method.

Step 3: The mixture is sculpted to develop a shape-memory polymer nanocomposite film. The solid shape-memory polymer nanocomposite film has been established after the vaporization of the solution or by the precipitation.

The dispersal of nanofillers into the suitable polymer solution is the biggest challenging step of this method and can be done through ultrasonication, which helps the accumulation of the nanoparticles, consequently, accomplishing a well-disseminated polymer composite [15]. In the majority of cases, the nanofillers or nanoparticles are scattered in various solvents and should have admirable miscibility with the polymer to accomplish the uniform mixing. It is a lot simpler to simply merge the nanofillers or nanoparticles into the appropriate polymer solution after which ultrasonication follows. A lot of attention has to be taken throughout the sonication method as the usage of very high power may harm the morphology of the nanofillers or nanoparticles and subsequently the properties of the shape-memory polymer composites [16]. The various properties of the solvent and mostly the boiling point has been demonstrated to have a significant impression on the shape-memory polymer composite material characteristics [17, 18]. Since shape-memory polymer nanocomposite film will be developed after the vaporization of the solution, low boiling point solvents are required as it wishes to ensure that fast evaporation and drying. On the other hand, the high boiling point solvents may produce complications through removal and thereby getting trapped in the shape-memory polymer nanocomposite which influences their properties such as electrical conductivity negatively. Figure 8.3 shows the steps involved in the solution mixing method.

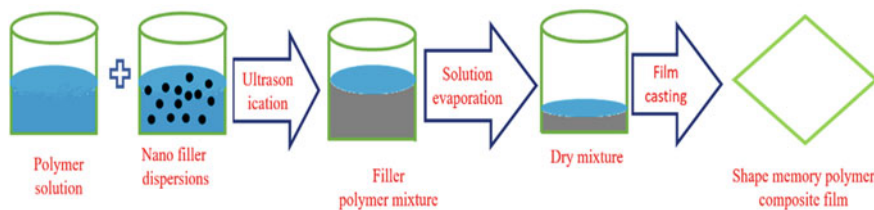


Fig. 8.3 The steps involved in the solution mixing approach

8.3.1 Advantages

- The main advantage of this method is that it can be employed to produce solid-state shape-memory polymer composites even at room temperature.
- The solution mixing is the low viscosity of the solution that easily allows dispersion of nanoparticles.

8.3.2 Disadvantages

- The main drawback of this method is that it is only suitable for polymers that are dissolved in a solvent.
- This method is not preferred to prepare the shape-memory polymer composites at large scales or commercial scales.

8.4 Melt Mixing

One of the widely used melt mixing methods is employed to prepare shape-memory polymer composites. Apart from melt mixing method, melt processing or melt blending method can also be employed for fabricating shape-memory polymer composites (SMPCs) from the polymers which are insoluble in the solvent [19]. This method includes the dispersion of nanofillers into the liquefied polymer. The conversion of these nanofillers into the liquefied polymer (polymer matrix) by scattering process is found to be more complicated compared to other methods [20, 21]. During this process, the liquefied polymer applies some strain on the particles and the amount of strain that is applied by the liquefied polymer depends on weight distribution and molecular weight. It is observed that with an increase in shear stress, the size of the agglomerates decreases [20]. The impact of shear stress during the process of scattering of the nanofiller into the liquefied polymer (polymer matrix) is shown in Fig. 8.4.

In this method, initially, the small agglomerates are formed by breaking the large agglomerates and these small agglomerates are dispersed into the liquefied polymer (polymer matrix). During this dispersion process, some amount of strain is transferred from the polymer matrix into small agglomerates which will tend to rise in shearing. An increase in shearing breaks the small agglomerates into individual particles, thereby increasing the chemical affinity between the polymer matrix and surface of the nanoparticles [22, 23]. The single paired screw extruders are frequently employed for melt blending [24]. At certain conditions, the high temperatures can be inflicted with disapproving effects on the revised nanofiller surface [25]. Knitting and co-rotating twin-screw extruders are very much admired for this purpose. In this method, different types of polymer matrix have been used to prepare shape-memory polymer

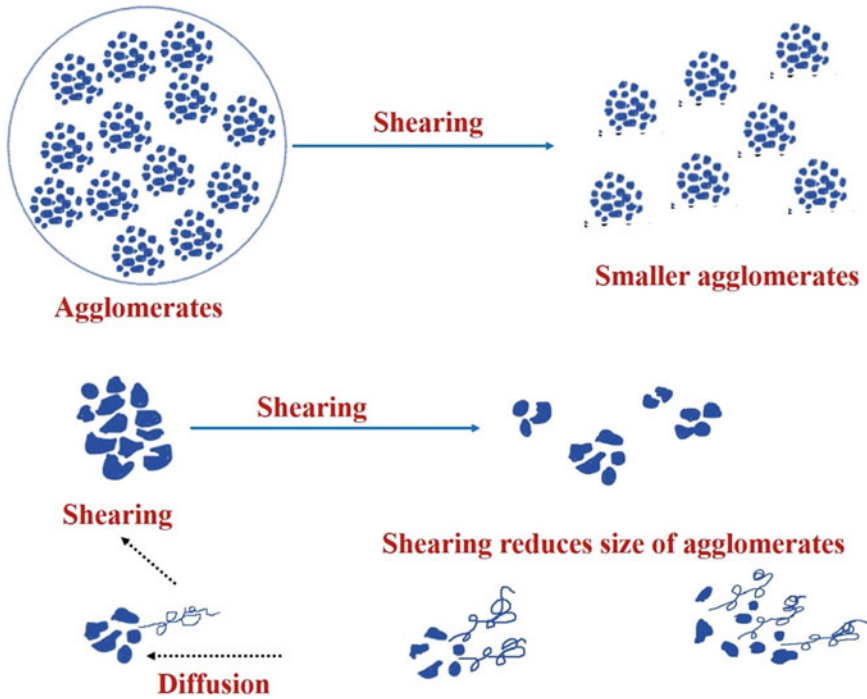


Fig. 8.4 Impact of shearing on the diffusion on of the polymer nanoparticles in melt mixing process

composites, like polypropylene, poly (methyl methacrylate), poly (lactic acid), poly (vinyl chloride), polycarbonate, polyamide 6, etc.

8.4.1 Advantages

The following are several advantages of this method:

- Excellent diffusion of nanofillers in the polymer matrix.
- Low-cost ecofriendly method.
- Augmentation of the heat stability

8.4.2 Disadvantages

The following are several disadvantages of this method:

- Controlling processing conditions like temperature and residence time is very difficult.
- Difficult to acquire well-dispersed nanoparticles (In some cases).

8.5 Co-Precipitation Method

Reactants are allowed to combine or mix in the normal synthesis techniques, either manually or mechanically. In the manual process, the reactants are allowed to mix by grinding process and in the mechanical process, the reactants are mixed by ball milling process. In both the processes, the consequent rate of reaction depends mainly on the reactants particle size, degree of homogenization attained, and temperature [26, 27]. The Co-Precipitation method is useful to accomplish a high degree of homogenization even with tiny particle size and a quicker rate of reactions. [28].

In this method, the formation or separation of a solid substance from the solution has been occurred by changing the substance (material) into an insoluble form. The extent to which the solid substance is separated from the solution has been found from the solubility-product constant attained by calculating the amount of soluble substance present in a known quantity of saturated solution. Solubility will be drastically modified by the accumulation of ions in the solution that produces the precipitate. Though the solubility of the solution can be modified broadly, the solubility product will remain constant within range. This process is intended, to accomplish desired stoichiometry. The methods which are based on the solution are commonly used to enhance homogeneity, purity, and decrease the particle size. The Soluble metallic nitrates or salts are made to dissolve in the aqueous solvent and subsequently made to precipitate out from the liquid state. The anionic solution is also utilized simultaneously to precipitate out the cationic substance in the form of carbonates or hydroxides. Very low handling temperatures are being used in the technique to give the result in an amorphous state with small particles of nano-size [29, 30]. The reaction rates are enhanced by homogeneously mixed precursors during the calcination process. Figure 8.5 gives the schematic presentation of the sample solutions prepared by the co-precipitation method.

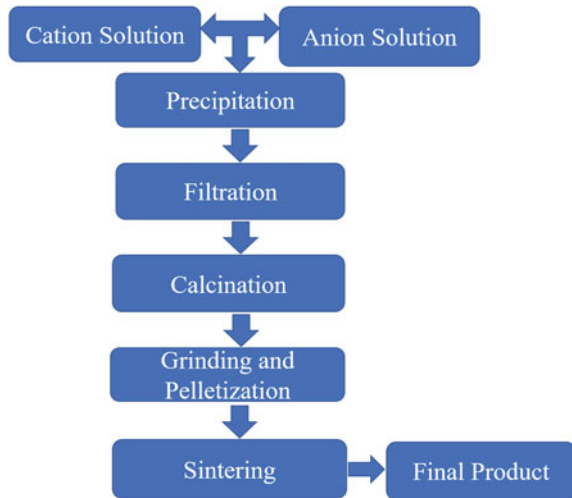
The following are the strides that are involved to prepare the shape-memory polymer composites:

Step 1: Using stoichiometric amounts of starting materials.

Step 2: Using calculated amounts of basic solution with high pH.

Step 3: Attaining the diminishing state or acidic state of starting materials mixture by centrifugation.

Fig. 8.5 Schematic presentation of a sample prepared by co-precipitation method



Step 4: Maintaining a very high pH which is around 14 among the precipitated solutions.

Step 5: Removal of excess water and other impurities and decantation has to be performed.

This Co-precipitation technique for shape-memory polymer composites gives nano-sized homogeneous particles and is evenly dispersed with a single structure phase. It requires very low heating treatment and sometimes does not require to sinter the product, so the only calcination of the substance is appropriate. This method is desirable only when huge quantities of a product are needed. It recommends a variety of precursor materials as beginning materials ranging from simple salts to complex organic–inorganic materials. In this technique, the pH is a highly sensitive parameter and is carefully controlled to get a better product [31].

8.5.1 Advantages

- This method produces a huge quantity of products simultaneously
- It recommends different types of precursor materials to prefer as starting materials starting from simple salts to complex organic–inorganic materials.

8.5.2 Disadvantages

This method cannot work under the following cases:

- When the two reactants in the solution have various solubilities in water
- When the rate of reaction of reactants is not the same
- When supersaturated solutions occur.

8.6 Sol–Gel Method

The sol–gel approach is one of the wet synthesis (chemical solution deposition) and cost-competitive techniques, which is used in the materials science field for the fabrication of various active smart materials like shape-memory polymer composites (SMPCs). It can also be viewed as the making of the sol, gelation of the sol, and elimination of the solvent. The main advantage of this method is that it can be brought out or employed at very low temperatures, i.e., low-temperature processing, either starting from the chemical solution or colloidal particles (i.e., sol) to create an integrated network (i.e., gel). With the help of this method, one can prepare the high purity and high homogeneity shape-memory polymer composites with improved or desired properties. The following chain represents the order of transformations of the sol–gel method [32].

→ Precursor → Sol Gel → Product

Precursors: These are the beginning materials and are having indispensable essential entities in the correct stoichiometry for the development of gel/network (in both liquid and solid phase). The Metal alkoxides and the metal chlorides are the commonly used precursors in the sol–gel method, and they endure hydrolysis and polycondensation reactions to nurture a colloid.

Sol: A solution (sol) is a colloidal or molecular suspension of tiny solid particles in a liquid or the monomer solution and constantly exhibits Brownian movement. The diameter of these colloidal or solid particles are ranging from 1 to 100 nm and is stable owing to the Van der Waals attractive forces (short-range forces) and surface charges.

Gel: A gel is a semi-solid or solid phase of a colloidal solution or it may also be well-defined as a substance that includes a continuous solid skeleton, and which is enclosed by a liquid phase of colloidal dimensions (i.e., 3D interconnecting network). Thus, sol-gels are the suspensions of colloids in a liquid, which keeps their shape.

In this technique, the solution of a given precursor was furnished, which consists of dissolution of metal ions either metal–organic compounds/metal alkoxides or metal chlorides/inorganic salts which endure hydrolysis, shadowed by condensation and

polymerization reactions to develop the 3D interconnecting network, the gel. This 3D interconnecting network (gel) is based on the functionality of the metal alkoxides or metal chlorides [33]. In this process, the two types of gels are commonly formed and are termed colloidal and polymeric. The colloidal gels are prepared from metal chloride solutions and polymeric gels are prepared from metal alkoxide solutions. A sudden rise in the viscosity has been observed at a particular point in this technique and is a common feature of the sol–gel process which indicates the formation of gel [34]. Hence, the conversion of sol to gel takes place through hydrolysis, condensation, and polymerization reactions of the precursors. The polymer acts as a nucleating agent and endorses the progression of layered crystals. As the crystals grow up, the polymer is percolated between layers and thus shape- memory polymer composite (SMPC) is formed.

The following are the series of sequential steps in the sol–gel process.

Step 1: Hydrolysis.

In this step, the metal alkoxide or metal chloride precursor (raw material) is hydrolyzed through blending with water, then the metal hydroxide is established.

Step 2: Polycondensation (Formation of a Gel).

An oxide (M–OH–M) 3D interconnecting network (gel) forms by polycondensation reaction which leads to a rise in the viscosity of the solution. The hydrolysis and polycondensation rates play a vital role to ascertain the characteristics of final products. Slower is the hydrolysis process and smaller is the particle size along with distinctive properties.

Step 3: Aging (Syneresis).

This process improves the strength of the gel. In this step, the polycondensation reactions have been continued till the gel becomes a solid mass with the reduction of the interconnecting gel network.

Step 4: Drying.

This drying process is used to remove the water and other unpredictable liquids from the 3D interconnecting network (gel) and it is complicated owing to the vital changes in the gel structure. If those unpredictable liquids are extracted from the gel under supercritical conditions, the product is named aerogel and this product is also abridged as xerogel if it is isolated by thermal evaporation.

Step 5: Dehydration.

In order to obtain the stabilized gel, the surface-bound M-OH groups are removed by a drying process. This is generally achieved through calcinating the material (xerogel) at high temperatures.

Step 6: Densification.

Heating the porous/permeable gel at elevated temperatures, take the lead to densification, i.e., the densified polycrystalline can be obtained [35]. The solidification

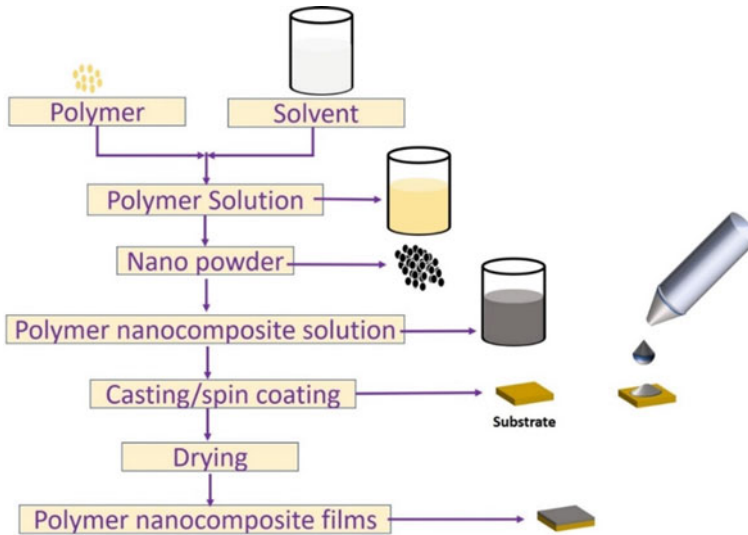


Fig. 8.6 The Successive steps involved in the sol-gel process

temperature depends significantly on the dimensions of the pore network, surface area, and the connectivity of the pores. The successive strides engaged in the sol-gel procedure are shown in Fig. 8.6.

8.6.1 Advantages

The following are the advantages of this method:

- Employed at low temperatures.
- Increase the homogeneity of the shape-memory polymer composites.
- High purity products are obtained by this method.
- An economically effective method to synthesize high-quality SMPCs [36–38].

8.6.2 Disadvantages

The following are the disadvantages of this method:

- Huge shrinkage through processing.
- Health risks of organic solvents.
- Controlling the growth of the polymer composites is also very difficult in this method [39, 40].

8.7 Electrospinning Method

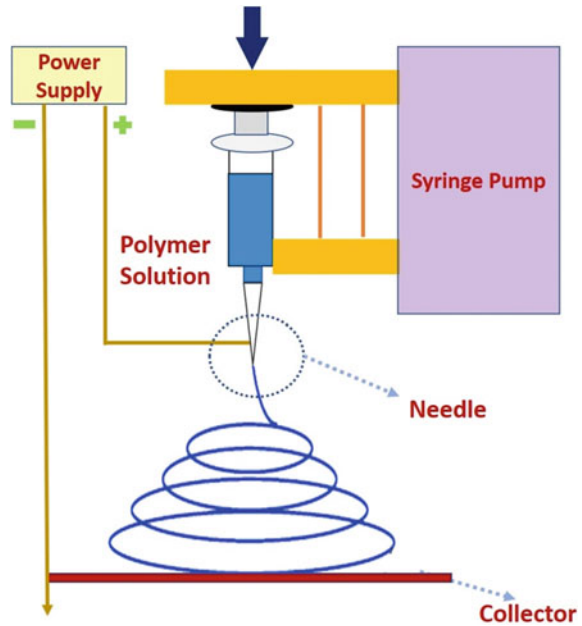
The Electrospinning technique was invented by Anton in the year 1934 [41]. This approach is employed to produce the shape-memory polymer composites by imposing an external electric field or electrostatic force on polymer composite solutions or melts [42]. This method has several advantages against the other methods, and it has been acknowledged as the highly efficient method to electrospin various polymers into shape-memory polymer composites. The enhancement of electrospinning equipment led to the advancement of shape-memory polymer composites with desired structures. There are three ways of electrospinning process, they are downward, upward, and horizontal electrospinning process. Among the above three ways, the downward electrospinning process is the extremely appropriate method for a minor scale owing to the uncomplicated optimization and operational scrutinizing. The upward electrospinning process is favorable for the industrial fabrication scale for the reason that the bulk fabrication of the SMPCs by using the traditional single-needle which is tricky and interesting [43]. The traditional electrospinning equipment mainly consists of three primary parts, a syringe needle, grounded collector (either solid substrate or liquid media), and high voltage power supply (mostly kV range) has been used to prepare shape-memory polymer composites extensively.

In the standard electrospinning method, the syringe pump containing various polymer composite solutions or melts attached to the spinneret (i.e., stainless steel capillary tube) is fixed. The spinneret is attached to the high voltage power supply. The liquefied polymer composite solution suspended from the spinneret is maintained through its surface tension. The high voltage power supply is switched on, then the electric field is generated. This electric field, which is imperiled to the capillary tube (spinneret) provokes a charge on the liquid surface. Hence, the mutual repulsion among charges on the droplet at the tip of the needle leads to electrostatic force and is opposite to the surface tension. While the intensity of the electric field increases, the shape of the droplet at the tip of the needle will be changed to a conical droplet and is also called a Taylor cone. While increasing the electric field intensity, at the stage, the electrostatic repulsive force surpasses the surface tension, a charged polymeric jet of the solution will be expelled from the tip of the conical droplet (Taylor cone). Then it (polymeric jet of the solution) undergoes a stirring process as soon as the solvent is evaporated, turning itself into shape-memory polymer composites. Finally, the SMPCs were deposited onto the grounded collector enclosed by the aluminum foil and left randomly on the foil. [44, 45]. The downward electrospinning setup in the diagrammatical view is shown in Fig. 8.7.

8.7.1 Advantages

A distinctive lead of the electrospinning method is that one can obtain the complex hierarchical structures through controlled calcination [46]. These complex structures

Fig. 8.7 Schematic view of the downward electrospinning setup



are very complicated to manufacture utilizing traditional methods such as Chemical Vapor Deposition (CVD), self-assembly, and other solution-based techniques.

8.7.2 Disadvantages

The variety of polymer composite solutions or melts used in this technique are limited.

8.8 Applications

A huge variety of demonstrated as well as proposed shape-memory polymer composites applications in different industries including aerospace, biomedical equipment, smart textiles, self-healing systems, and the latest active origami structures in 4D printing methodology are presented.

8.8.1 *Aerospace*

The strength and other requirements of shape-memory polymer composites (SMPCs) in the arena of aerospace applications may not be high but due to their less weight and capability of retaining the shape-memory is highly appreciated and hence are being used more in aerospace technology mostly parts like hinges morphing, etc. [47–49].

8.8.2 *Biomedical Equipment*

Due to their novel properties, shape-memory composites occupied a good place even in the biomedical industry in making various biomedical devices. The important properties which can stimulate these shape-memory polymers by their effect are light, electric, and magnetic fields. Another important feature about these biodegradable shape-memory polymer composites is they decompose within the body avoiding the risk of removal of these devices after use [50, 51].

8.8.3 *Smart Textiles*

The distinctive and attractive functionalities of the shape-memory polymer composites have gained a remarkable place in the field of smart textiles also. SMPCs are first converted into fibers by several wet synthesis techniques which can then be used to develop fabrics [52, 53].

8.8.4 *4D Printing*

4D printing is the latest advancement, which is originating from 3D printing. 3D printed structures are targeted for transformation in terms of shape, property, and functionality by 4D printing technology. 3D printing and 4D printing is differentiated fundamentally like the printed object. In 3D printing, the characteristic feature of the final printed object is in static structure, whereas in the 4D printing method, the nature of the final printed object is in a dynamic structure. The time needed in reacting to the stimulus (light, electric field, etc.) and consequent transformation in terms of shape is believed as the 4th dimension. The dynamic 4D printed part can self-heal compared to static 3D. The 4D printing increases efficiency and saves time by decreasing the number of steps involved in making the programmed part.

8.9 Conclusions

Undoubtedly a great achievement has been accomplished in shape-memory polymer composites research. To encourage the transition of knowledge of shape-memory polymer composites from the invention to the latest research, our work is precisely accessible. Concentrating mainly on the key research points about SMPCs, their classification, various stimuli, method of fabrication demonstrated, and proposed applications in the fields of aerospace and biomedical, Smart textiles, 4D printing, etc.

SMPCs are expected to have a prominent part in producing smart materials with novel and high-end applications. SMPCs are attracting the materials scientists and we are expecting many more wonders in this area in the future.

References

1. Cheng H, Liu J, Zhao Y, Hu C, Zhang Z, Chen N (2013) Graphene fibers with predetermined deformation as moisture-triggered actuators and robots. *Angewandte Chemie International Edition* 52:10482–10486
2. Chan BQY, Low ZWK, Heng SJW, Chan SY, Owh C, Loh XJ (2016) Recent advances in shape-memory soft materials for biomedical applications. *ACS Appl Mater Int* 8(16):10070–10087
3. Leng J, Lan X, Liu Y, Du S (2011) Shape-memory polymers and their composites: stimulus methods and applications. *Progr Mater Sci* 56(7):1077–1135
4. Hu J, Zhu Y, Huang H, Lu J (2012) Recent advances in shape-memory polymers: structure, mechanism, functionality, modeling and applications. *Prog Polymer Sci* 37(12):1720–1763
5. Meng QH, Hu JL, Zhu Y, Lu J, Liu Y (2007) Morphology, phase separation, thermal and mechanical property differences of shape-memory fibres prepared by different spinning methods. *Smart Mater Struct* 16:1192–1197
6. Meng QH, Hu JL, Yeung LY (2007) An electro-active shape-memory fibre by incorporating multi-walled carbon nanotubes. *Smart Mater Struct* 16:830–836
7. Lendlein A, Jiang H, Jünger O, Langer R (2005) Light-induced shape-memory polymers 434(7035):879–882
8. Lan T, Kaviratna PD, Pinnavaia TJ (1995) Mechanism of clay tactoid exfoliation in epoxy-clay nanocomposites. *Chem Mater* 7:2144–2150
9. Wang Z, Pinnavaia TJ (1998) Nanolayer reinforcement of elastomeric polyurethane. *Chem Mater* 10:3769–3771
10. Zilg C, Thomann R, Mulhaupt R, Finter J (1999) Polyurethane nanocomposites containing laminated anisotropic nanoparticles derived from organophilic layered silicates. *Adv Mater* 11:49–51
11. Ke Y, Long C, Qi Z (1999) Crystallization, properties and crystal and nanoscale morphology of PET clay nanocomposites. *J Appl Polymer* 71:1139–1146
12. Iijima S (1991) Helical microtubules of graphitic carbon. *Nature* 354:56–58
13. Moses JC, Gangrade A, Mandal BB (2019) Carbon nanotubes and their polymer nanocomposites. In: Karak N (ed) *Nanomaterials and polymer nanocomposites*, pp 145–175
14. Khan W, Sharma R, Saini P (2016) Carbon nanotube-based polymer composites: synthesis, properties and applications. In: Berber M, Hafez IH (eds) *Carbon nanotubes-current progress of their polymer composites*. IntechOpen, London, pp 1–45
15. Sahoo NG, Rana S, Cho JW, Li L, Cha SH (2010) Polymer nanocomposites based on functionalized carbon nanotubes. *Prog Polymer Sci* 35:837–867

16. Saini P, Choudhary V (2013) Enhanced electromagnetic interference shielding effectiveness of polyaniline functionalized carbon nanotubes filled polystyrene composites. *J Nanopart Res* 15:1415–1422
17. Saini P (2013) Electrical properties and electromagnetic interference shielding response of electrically conducting thermosetting nanocomposites. In: Mittal V (ed) *Thermoset nanocomposites*. Wiley-VCH Verlag, Hoboken, pp 211–237
18. Ari GA, Aydin I (2008) Nanocomposites prepared by solution blending: microstructure and mechanical properties. *J Macromol Sci Part B Phys* 47:260–267
19. Barrett R, Taylor R, Keller P, Codell D, Adams L (2007) Deployable reflectors for small satellites. *AIAA* 1–6
20. Mallakpour S, Naghdi M (2018) Polymer/SiO₂ nanocomposites: Production and applications. *Prog Mater Sci* 34:118–124
21. Passador FR, Ruvolo-Filho A, Pessan LA (2017) Nanocomposites of polymer matrices and lamellar clays. In: *Nanostructures*. 1st edn. Elsevier, pp 187–207
22. Mistretta MC, Morreale M, La Mantia FP (2014) Thermomechanical degradation of polyethylene/polyamide 6 blend-clay nanocomposites. *Polym Degrad Stab* 99:61–67
23. Fornes TD, Yoon PJ, Keskkula H, Paul DR (2001) Nylon 6 nanocomposites: the effect of matrix molecular weight. *Polymer* 42:9929–9940
24. Isobe H, Kaneko K (1999) Porous silica particles prepared from silicon tetrachloride using ultrasonic spray method. *J Colloid Interface Sci* 212:234–241
25. Fawaz J, Mittal V (2014) Synthesis of polymer nanocomposites: review of various techniques. In: *Synthesis techniques for polymer nanocomposites*, vol 245. WileyVCH Verlag GmbH & Co. KGaA, Weinheim, Germany, pp 1–30
26. Lu AH, Salabas EL, Schüth F (2007) *Angew Chem Int Ed*. 46:1222–1244
27. Rodriguez Carvajal J (1995) fullproof version 3.0 Laboratorie Leon Brillouin. CEACNRS, 24:256–263
28. Schroder DK (1990) *Semiconductor material and device characterization*. Wiley, New York, pp 361–368
29. Valdes LB (1954) *Proc IRE* 42:420–429
30. Jones B (1993) *Phys Teach* 31:48–56
31. Hummel RE (1993) *Electronic properties of materials*, vol 43. Springer, New York, pp 182–188.
32. Hiavacek V, Puszynski J (1996) Chemical engineering aspects of advanced ceramic materials. *Ind Eng Chem Res* 35:349–377
33. Brinker CJ, Scherer GW (1990) *Sol-gel science: the physics and chemistry of sol-gel processing*. Academic Press, Boston
34. Iler RK (1979) *The chemistry of silica: solubility, polymerization, colloid and surface properties and biochemistry*. Wiley, New York
35. Hench LL, West JK (1990) *Chem Rev* 90:33
36. Deng Z, Wang J, Wei J, Shen J, Zhou B, Chen L (2000) *J Sol Gel Sci Technol* 19:677–680
37. Venkateswara Rao A, Bhagat SD, Hirashima H, Pajonk GM (2006) *J Colloid Interface Sci* 300:279–285
38. El Rassy H, Buisson P, Bouali B, Perrard A, Pierre AC (2003) *Langmuir* 19:358–363
39. Harrels JH, Ebina T, Tsubo N, Stucky G (2002) *J Non-Cryst Solids* 298:241–251
40. Allie C, Pirard R, Lechloux AJ, Pirard JP (1999) *J Non-Cryst Solids* 246:216–228
41. Anton F (1934) Process and apparatus for preparing artificial threads, US 1975504, United States
42. Ko F, Wan Y (2014) *Introduction to nanofiber materials*. Cambridge University Press, p 39
43. Abdel-Hady F, Alzahrany A, Hamed M (2011) Experimental validation of upward electrospinning process. *ISRN Nanotechnol* 85:1317–1324
44. Frenot A, Chronakis IS (2003) Polymer nanofibers assembled by electrospinning. *Curr Opin Colloid Interface Sci* 8:64–75
45. Baumgarten PK (1971) Electrostatic spinning of acrylic microfibers. *J Colloid Interface Sci* 36:71–79

46. Ramakrishna S, Jose R, Archana PS (2010) Science and engineering of electrospun nanofibers for advances in clean energy, water filtration, and regenerative medicine. *J Mater Sci* 45:6283–6312
47. Dao TD, Ha NS, Goo NS, Yu W-R (2018) Design, fabrication, and bending test of shape-memory polymer composite hinges for space deployable structures. *J Intell Mater Syst Struct* 29(8):1560–1574
48. Liu T (2018) Integrative hinge based on shape-memory polymer composites: material, design, properties, and application. *Compos Struct* 206:164–176
49. Li F (2016) Modal analyses of deployable truss structures based on shape-memory polymer composites. *Int J Appl Mech* 8(7):1640009
50. Zhao W, Liu L, Zhang F, Leng J, Liu Y (2019) Shape-memory polymers and their composites in biomedical applications. *Mater Sci Eng C* 97:864–883
51. Xie H (2018) Biodegradable near-infrared-photo-responsive shape-memory implants based on black phosphorus nanofillers. *Biomaterials* 164:11–21
52. Chakraborty JN, Dhaka PK, Sethi AV, Arif M (2017) Technology and application of shape-memory polymers in textiles. *Res J Text Appar* 21(2):86–100
53. Ji F (2006) Smart polymer fibers with shape-memory effect. *Smart Mater Struct* 15:1547–1554
54. Hu J, Mondal S (2006) Study of shape-memory polymer films for breathable textiles. In: Mattila HR (ed) *Intelligent textiles and clothing*. Woodhead Publishing, Sawston, pp 143–164

Chapter 9

Recent Progress in Synthesis Methods of Shape-Memory Polymer Nanocomposites



Kalpna Madgula and Venkata Sreenivas Puli

9.1 Introduction

Polymer nanocomposites (PNCs) are an important class of functional materials [1, 2]. Classically, PNCs contain one or more nanoparticles (NPs) within a polymer matrix. Polymeric materials are multicomponent systems, which are not chemically stable or molecularly homogeneous for most of the applications. An infinite variety of PNCs materials can be made with unique physical properties at low cost, by adding fillers, such as minerals, ceramics, metals, and even air [1, 2]. Polymers are easy to process and possess robust mechanical properties, whereas NPs can provide mechanical reinforcement, as well as their unique optical properties, enhanced electrical conductivities, high electrical breakdown strength, decreased gas permeability and ease of processing in large areas/volumes, and self-healing ability [3–5]. In particular, polymer, dielectrics have the above-mentioned advantages over traditional electroactive ceramics. The combination of the desired physical properties in PNCs will impart that these materials are useful for multifunctional applications. Multicomponent PNCs have been studied from the 1940s and were reinvigorated in the 1990s [3], which consist of a majority of a polymer or a polymer blend and the minor component with a particle size of less than 100 nm.

The polymers are composed of giant macromolecules [many- “poly” repeated units- “mers” or long-chain molecules of identical structure], and their properties are heavily dependent on the configuration or structure of the individual macromolecules themselves and as well as on the ordering of the molecules [2]. Nano-sized fillers in these PNC materials will certainly show performance enhancements, and there is a

K. Madgula (✉)

SAS Nanotechnologies LLC, 550 S College Avenue, Newark, DE 19716, USA

V. S. Puli

Smart Nanomaterials Solutions LLC, Casselberry, Orlando, FL 32707, USA

Materials and Manufacturing Directorate, Air Force Research Laboratory, 3005, Hobson Way, Wright Patterson Air Force Base, Fairborn, OH 45433, USA

lot of ongoing research work [6] around the globe in this direction. Size reduction and concomitant increase in surface area of nano-fillers in these PNCs are more advantageous. In particular, improvements in optical and electrical properties of these materials are attributed to a new physical phenomenon called the quantum confinement effect, which is in turn induced by Nanoparticles or nanoscale dimensions of the materials. It is also to be noted here that the reduction in filler dimension from micrometer-sized fillers to NP-sized fillers in PNCs leads to an increase in the surface area ($\sim 10^6$), i.e., that the surface-to-volume ratio increases considerably, and magnifies the importance of interfaces [3, 6]. However, there is a difficulty in the PNCs (polymer—NP coupling) system, which is that there is no uniformity in the physical properties. And the impacted physical properties include viscoelastic and thermo-mechanical response in a fundamentally different way above and below glass transition temperature (T_g), and the composition and structural importance of the interface PNCs also varies widely; and its interface also impacts their conductivity, dielectric breakdown strength, permeability, optical transparency, etc.

Hence, developing a common concept for interface engineering of PNCs is a challenging task [3]. The PNCs are attractive materials in compacted electronics and geometrically precise electrical devices with unique features of mechanical flexibility as well as the ability to mold into intricate configurations [4, 5].

Currently, PNCs are a billion-dollar industry around the globe, and their products range from reinforcing components for transportation to the plastics commodity industry with superior electrical properties for electromagnetic interference (EMI) shielding and electronics. PNCs are utilized in a wide range of potential device functions, e.g., in packaging, structural, electronic, electrical, automotive, actuators, high-energy storage capacitors, static-charge dissipation devices, aerospace, EMI shields, and photovoltaic (PV) devices [4]. There are numerous numbers of synthesis techniques available for PNCs that can be used in different branches of polymer applications. Furthermore, PNCs propose abundant advantages while processing such as mechanical resilience and ease with which they can be molded into customizable shapes; these are the features that appeal to them for electrical and electronic devices that demand low-cost, compact applications [6]. PNCs for different applications are shown in Fig. 9.1.

Hence, most of the polymeric materials research has been impacted by the reinforcement of nanoparticles, and various synthesis methods were discussed in the literature. Shape-memory polymers (SMPs) and shape-memory polymer nanocomposites (SMPNCs) are no exception in this direction. Herein further, we discuss synthesis techniques of shape-memory polymer nanocomposites.

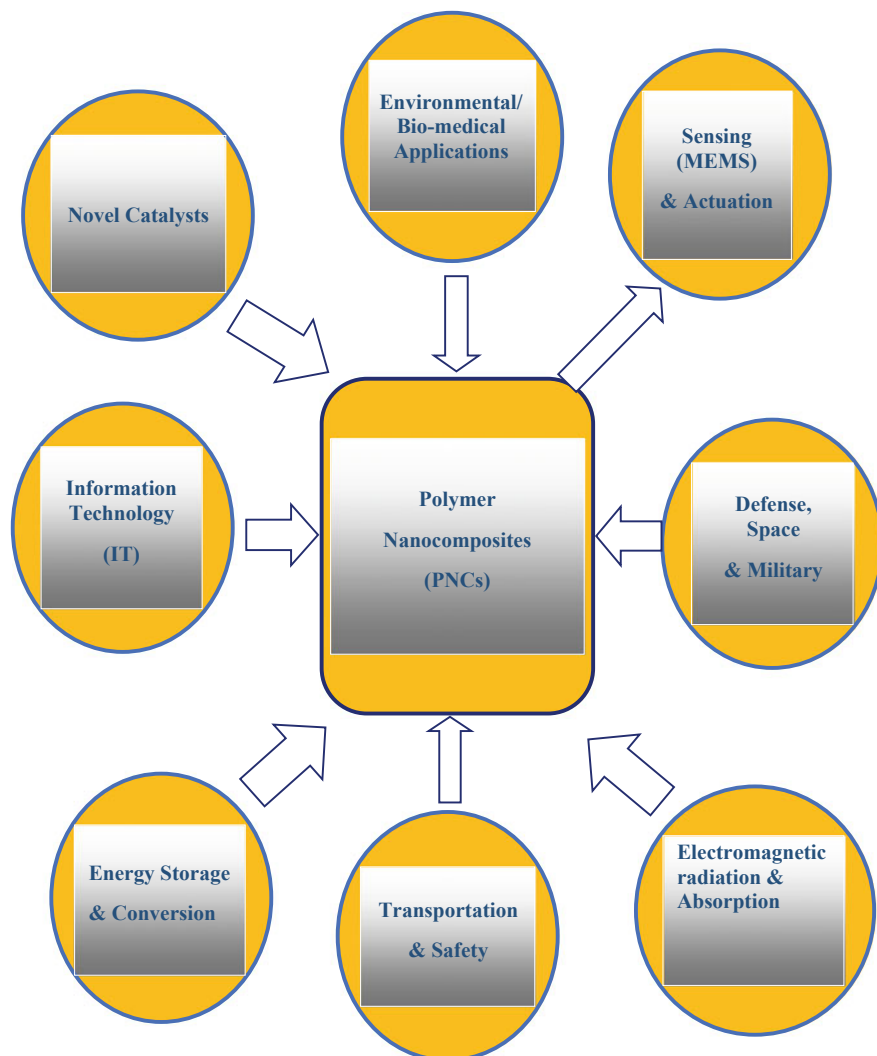


Fig. 9.1 Polymer nanocomposites (PNCs) for different applications

9.2 Basics of Shape-Memory Polymers (SMPs) and Shape-Memory Polymer Nanocomposites (SMPNCs)

In 1941, a US patent reported by Vernon et al. [7] has explained the shape-memory effect [8]. However, until the 1960s, the significance of SMPs is not realized, till the tubes and films of cross-linked polyethylene (PE) were utilized for heat-shrinking

applications [9]. Since then, more rigorous research was begun and continued with notable progress in the last decade. In general, shape-memory materials (SMMs) are those materials that remember their original shape even after changing such as mechanical deformation (a one-way effect), or a change by heating and cooling (a two-way effect). This phenomenon is based on a structural phase transformation. SMMs are also termed dual-shape capability materials. Various materials such as shape-memory polymers, shape-memory ceramics, shape-memory metal alloys, and shape-memory gels can be classified as SMMs. Among these materials, shape-memory alloys (SMAs) and shape-memory polymers are widely studied materials for the shape-memory effect. The shape-memory effect in metal alloys was reported after a decade later in 1951, and these are more prominent and widely studied than SMPs [9–11]. Both SM polymers and SM alloys vary in every aspect of their basic mechanism to their material properties such as modulus and transition temperature.

Initially, TiNi (Nitinol), CuZnAl, and FeNiAl metal alloys have shown a change of their shape with an external stimulus such as in response to heat. Upon cooling, SMAs transform from austenite phase to martensite phase. The martensite phase is comparably soft and easily deformable, whereas the austenite phase develops at higher temperatures and is stronger. Structural phase transformation of SMA materials is known as martensitic transformation, and they have been used for various applications such as vascular stents, medical guide wires, orthodontic wires, vibration dampers, pipe couplings, electrical connectors, thermostats, actuators, eyeglass frames, and brassiere under wires. However, one drawback of these materials is they are relatively expensive; due to this reason, they are not widely in use. When compared to SMAs, SMPs are lightweight (or low dense) and high in shape recoverability (recoverability strain ~400%) [9–11]. As well, they have many advantages to that of SMAs and shape-memory ceramics: ease of processing and modifying the physical properties, such as transition temperature, stiffness, and biodegradability, and ease of functional grading, programmability and controllable recoverability, and low cost [11, 12]. Table 9.1 summarizes the merits and demerits of SM alloys and SM polymers.

Certain block copolymers are soluble in water at a temperature lower than body temperature and become hydrogels at the high temperature of the body. When such block copolymer are incorporated as blocks into the SMPs, then these materials could generate the capability to respond to temperature changes, which is completely contrary to those of typical SMPs. And these materials when cooled below the shape-recoverable temperature will recover to their original shape somewhat being heated above the temperature of shape recovery. This outcome is referred to as the inverse thermal shape-memory effect [9, 10]. However, SMPs are limited not only to the heating effect but also by stimuli based on electricity, light, moisture, magnetism as well as chosen chemical stimuli (such as pH changes) [11–13].

These materials are suitable potential alternatives for shape-memory metallic alloys (SMMAs) due to their flexibility, lightweight, biocompatibility, biodegradability, and high strain capacities in advanced applications comprising ergonomic products and biomedical devices. Pure SMPs display lower modulus and forces of recovery as compared to SMAs and/or SM ceramics. For efficient increase in strength

Table 9.1 Advantages and disadvantages of shape-memory alloys and shape-memory polymers

Advantages of shape-memory alloys	Disadvantages of shape-memory alloys	Advantages of shape-memory polymers	Disadvantages of shape-memory polymers
High mechanical strength and High recoverability stress	Expensive	Cheap	Low mechanical strength, stiffness, and Low shape recovery stress
Good elasticity	Sensitivity of material properties in fabrication	Viscoelasticity	
Fatigue resistance	Residual stress developed in thin films	High shape deformability	
Wear resistance/High corrosion resistance	Nonlinearity of actuation force		
Easy fabrication	Lower maximum frequency compared to other micro-actuator devices		
Easy to sterilize	Poor fatigue Property		
Highly dense—High Power/weight ratio	Low energy efficiency	Less dense—offer a weight advantage per unit volume of material	
Lightweight	Complex thermo-mechanical behavior		
Shape-memory	Low operational speed	Constrained force is fraction	
Electrically Controlled	Temperature-dependent effect		
	Shaping difficulty	Shaping ease	
Constrained force is higher	Very low recoverable strain less than 8%	High shape recoverability strain, nearly 200%	
Constrained strains are lower		Constrained strains are magnitude higher	
	Difficult to process (formability and workability)	Ease of processibility (formability and workability)	

(continued)

Table 9.1 (continued)

Advantages of shape-memory alloys	Disadvantages of shape-memory alloys	Advantages of shape-memory polymers	Disadvantages of shape-memory polymers
Low thermal conductivity (Higher than SMPs)		Low thermal conductivity (lower than SMAs) (low thermal conductivity is desirable if the thermal insulation is required)	Low thermal (heat) conductivity is a disadvantage if an SMP is used in an application where heat flow into or out of the polymer in a short period is desirable
Low thermal conductivity is desirable if thermal insulation is required			

and high recovery force-related applications, these unreinforced pure SMPs are not suitable, and hence to overcome these issues, materials with specific performance are essential to diversify their utilization in the above-mentioned applications. This can be achieved by using the incorporation of various reinforcing fillers within SMPs, where its pristine mechanical properties (high strength and high Young's modulus) can be improved. The knowledge of the relationship among the composition and structure of SMPs along with their properties of shape-memory (SM) in addition to limitations enables one to better define high-performance SMPs for developmental areas.

The fundamentals of SMPs with the portrayal of their fabrication, characterization, and basic model are discussed. In addition, the SMP composites as functional materials or structural materials that perform to advance a certain task or physical/mechanical properties are briefly presented. The present chapter mainly focuses on evolution, highlights, and, overall, the recent progress in synthesis techniques of shape-memory polymer composites and their proposed applications.

9.2.1 Basics of Shape-Memory Polymers (SMPs) and Working Principle

SMP materials are stimuli-responsive polymer processes that have the capability of changing their shape upon application of a stimulus (such as thermal, humidity, light, magnetic energy, electric field, pH, and so on) externally. SMPs possess two phases, which include net hard phase or frozen phase and switching soft phase or reversible phase [10]. Further, the SM effect is not confined to a single polymer; however, it is a combined effect of the structure of the polymer and its morphology with simultaneously applied processing and programming steps [11].

Figure 9.2 displays the shape-memory polymer programming cycle. SMPs undergo two unique stages, which include "programming" and "recovery". SMPs demonstrate the ability to regain or remember material's original shape, either

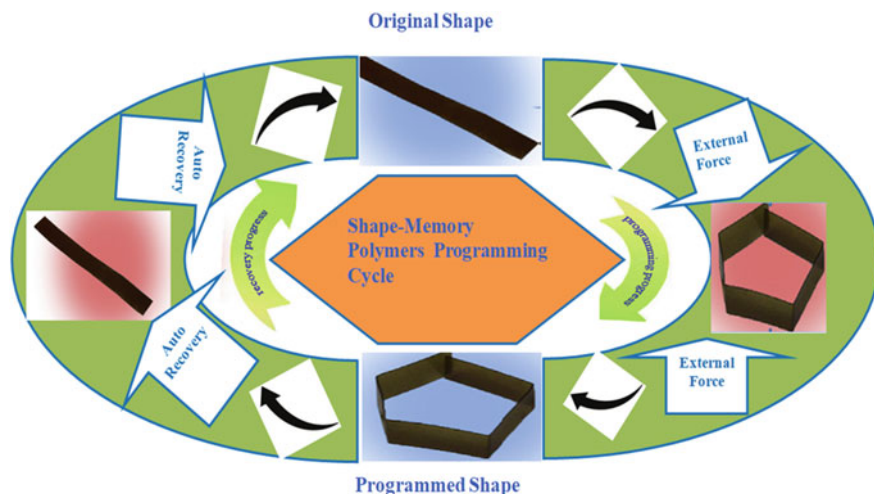


Fig. 9.2 Programming cycle and shape-memory effects in SMPs

employing a mechanical deformation, a one-way effect, or by cooling and heating, called a two-way effect, and this whole phenomenon is believed to be due to a structural phase transformation of these particular types of polymers [10]. From the literature, it is found that SMPs are exemplified as phase segregated linear block copolymers having a crystalline hard segment with a defined melting point and amorphous, soft segments with a defined glass transition temperature. In general, SMP phenomena arise from the coupled segment system: (a) permanent shape determined by cross-links and (b) switching segment which fixes the temporary shape with a transition temperature (T_{trans}) [9–13].

Nevertheless, in some representations, the hard segment is amorphous; with glass transition temperature (T_g), instead of melting point, and the soft segment is crystalline with a melting point instead of T_g and is substantially less than the glass transition temperature of the hard segment. SMPs also change their shape with the temperature; this effect is called the thermally induced shape-memory effect. SMP effect is not confined to a particular property of a single polymer; however, it is a combination of the structure of the polymer and the morphology of the polymer with applied processing and programming technology. The same effect seems to exist also in heat-shrinkable polymer films; however, it results from its morphology and structure that is not specific to the polymer's bulk property, and further the effect is important in numerous polymers and is chemical composition-dependent.

Programming technology is the one in which the polymer is first processed conventionally to obtain its permanent shape. Once it attains a permanent shape, the polymer is deformed, and a temporary shape is fixed and then it regains its original permanent shape [7–13]. Hence, SMP programming cycle is combined to be the whole process of programming and recovery from its temporary shape. In this, cycles of shape deformation, shape fixation, and shape recovery process occur when the permanent shape

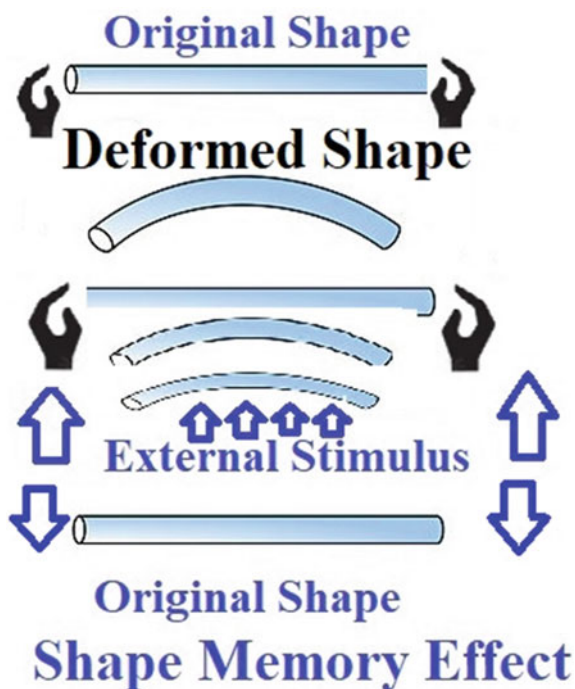
is set aside, and then it is recovered repeatedly from the temporary shape (shown in Fig. 9.2). During this process, the various steps that the polymer undergoes are heating, deformation, and cooling or cold drawing (which is the polymer at low temperature). SMPs are stiff below T_{trans} , and they are relatively soft upon heating above this temperature and subsequently deform into the desired temporary shape when an external force is applied with freezing Brownian motion and stress [13]. However, when an external force is removed and then cooled subsequently, its temporary shape can be maintained for a longer time and upon reheating, the temporary shape is automatically recovered into the original permanent shape [7–10].

SMPs have both the forms, like a noticeable, current temporary form and a permanent form that is stored whereas, the permanent form is produced using conventional manufacturing methods and this changes into temporary form by processing through the steps, heating, deformation, (temporary form), and lastly cooling. The temporary form is retained by the polymers until it is activated by the external programmed stimulus to change it into a permanent form.

The molecular network structure that exists in two different phases influences the mechanism of shape conversion between the phases. The T_{perm} or the phase that will show transition at the highest temperature should be exceeded to create physical cross-links leading to the permanent shape. Alternatively, the switching or soft segments can soften themselves after a certain temperature, called T_{trans} (that can be, for example, either T_g or T_m , melting temperature) [9–12] and can contribute to temporary form. Experimentally, if the material is activated above T_{trans} while remaining below T_{perm} , this can activate switching between the segments by softening, and hence the material is allowed to come back to its permanent or original form. However, the flexibility of these segments would be partially limited below T_{trans} . For example, if T_m is the step selected for SMP programming, the initiation of crystallization is induced by strain, when it is stretched above T_m and afterwards cooled below T_m . The covalent net points that are originated by these crystallites prevent the polymer from getting into the original coiled structure to be formed, and ideally the ratio of hard to soft segment lies between 20/80 and 80/20. During the stage of temporary shaping, the first stage permanent shape (recovery of the original shape) is stored, and heating the polymer above the T_{trans} induces the SM effect or the thermal SM effect [9–13]. As depicted in Fig. 9.3, the SM effect displayed in SM polymers is viscoelastic, as displayed in many models or by analysis methods. The stress is introduced during the deformation of the temporary form and the strain absorbed by the soft segment, and this strain is ultimately relieved by the soft segment when it is heated above its T_g or T_m (of the soft segment) and below that of the hard segment.

SMPs contain both net points and molecular switches. Net points can be achieved either by intermolecular interactions or by covalent bonds. Hence, SMPs can be classified into two categories, physically cross-linked SMPs and chemically cross-linked SMPs [11]. As stated in the earlier section, SMP actuation methods can be divided into various categories such as heat, electricity, light, and magnetism moisture, and the SM effect is triggered by Joule heating from either a hot source or hot gas. However, due to their difficulty in applications, both hot gas and hot water source

Fig. 9.3 Different stages of shape-memory effect



have received less attention. Alternatively, various functional fillers were incorporated into SMPs, to induce the shape-memory effect through the above categories of sources, intrinsically by Joule heating, and here indirect methods [10] produce heat. Solvent molecules that are easily diffused into the polymeric material can act as plasticizers when immersed in water, and hence water or solvent-driven SMPs can easily reduce the transition temperature, which can ultimately lead to shape recovery and is known as indirectly the thermally induced polymer actuation method [11–13].

In addition to the above, the stress–strain–temperature behavior of the material is important in evaluating the shape-fixing and shape-memory effects. The features that determine the properties of the SMP element can be evaluated as it is frequently submitted to cyclic deformation. For example, in an actuator, one could evaluate the durability of the SMP element [14] by this method. The two important quantities, rate of strain recovery (R_r), i.e., material's ability to remember its permanent shape, and rate of strain fixity (R_f), i.e., switching segment's ability to fix the temporary shape, can also define the SM effects.

The mathematical models proposed by Kim et al. [15] detail the shape-memory effects in polyurethane (PU) materials. Further, the authors have also tested shape memory effects of over 15 different types of segmented PUs that were formulated from polycaprolactone diol (e.g., a soft segment), 4, 4'-diphenylmethane diisocyanate, and 1,6-butanediol, (a hard segment and extender), with regards to their tensile cyclic properties, dynamic mechanical and mechanical properties as shown

in Fig. 9.4 for the thermo-mechanical cyclic tensile test performed with loading at high temperature (T).

When the second cyclic test or process of shaping has to be performed at a temperature higher than the shape recovery temperature, the fixed points remain hard, whereas reversible phase or soft points are subjected to softening–hardening upon heating above T and cooling below T_S , respectively. Here, T_S is the crystalline melting temperature (T_m) or shape recovery temperature of the reversible phase or soft segment. Figure 9.4 demonstrates a thermo-mechanical and cyclic tensile test with loading at high temperatures ($T > T_S$). In the first step, T_1 to T_u , the sample is elongated at a constant elongation rate ($\dot{\epsilon}$) maintaining a constant strain (ϵ_m), and in

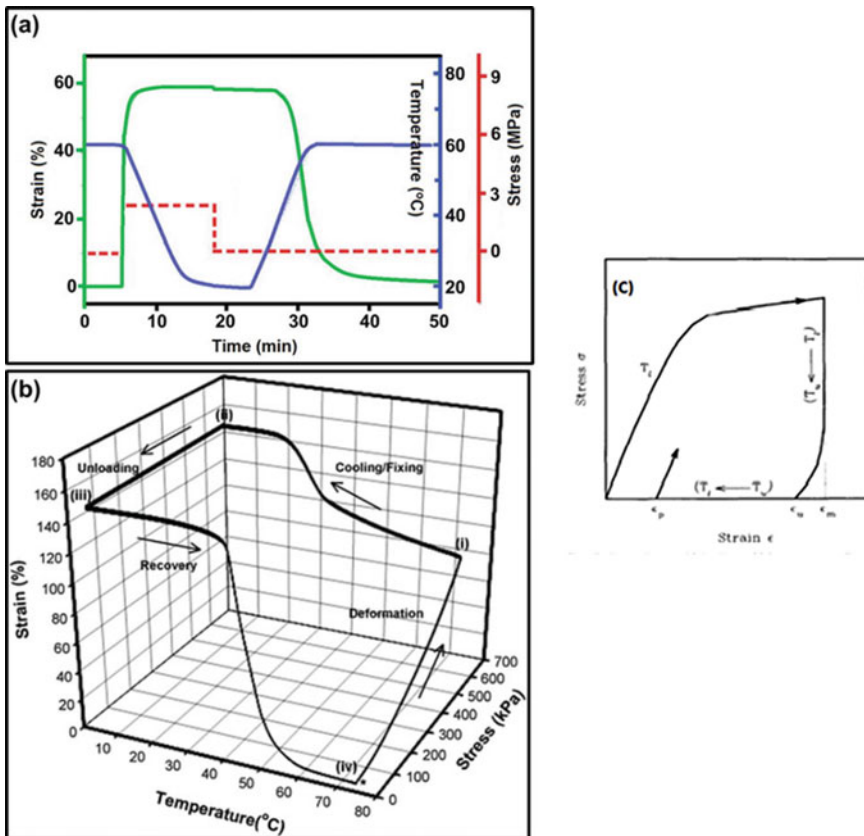


Fig. 9.4 Representation of stress and strain (%) curves to study shape-memory effect and cycles **a** 2D diagram. Reprinted with permission from Springer Nature: Macmillan Publishers Limited: Nature [17], Copyright © 2010. <https://doi.org/10.1038/nature08863>. **b** 3D diagram (I–IV). Reproduced with permission from [8], Copyright © 2008 The Royal Society of Chemistry. **c** Thermo-mechanical and cyclic tensile test with loading at high temperature ($T > T_s$). Reprinted from [15], Copyright © 1996 with permission from Elsevier Ltd.

the second step, it is cooled to low temperature (T_u) with unloading. When the limitation of T_u is removed, the noticeable strain of recovery ϵ_u has occurred. (ϵ_p —residual strain; T_S —Crystalline melting temperature of the soft segment or reversible phase of Polyurethane; T_l —loading and T_u —unloading temperatures). During the primary processing, the material is heated above T_h (T_h —softening—hardening temperature of fixed phase) to erase any previous memories of the material and while cooling ideally below T_h , the emerged fixed phases are completed at the T_s . The second shaping process is normally performed to fix the defects.

The figure exemplifies the SM parameters (shape fixity ratio of (ϵ_u/ϵ_m) and shape recovery (ϵ_r/ϵ_m) where $(\epsilon_r = \epsilon_m - \epsilon_p)$ where $(\epsilon_m$ —constant strain, ϵ_u —strain of recovery, and ϵ_p —residual strain). The comparison of various areas in which the area under the loading curve corresponds to the total strain energy per unit volume and the one below the unloading curve to that of recovery strain energy. It was also observed that the dynamic mechanical properties, which depend on temperature, are in close relation with the shape-memory characteristics of the segmented PUs with crystallizable soft segments (e.g., PCL4000 and PCL8000). Increments in the length of soft segment and content have increased glassy state due to soft segment crystallization but decreased rubbery state modulus (or decreased hard segment content). In general, it is desired to have large shape fixity that allows precise shaping and sizable shape recovery that leaves minimum hysteresis.

Representative 2D and 3D quantitative shape-memory polymer cycle diagrams [16–18] derived from a thermo-mechanical analyzer (or dynamic mechanical analysis) can yield the information on SM performance of a material, for example, in a dual shape-memory cycle (Fig. 9.4a) where strain induced at 60 °C (onset of T_g) is recovered completely at the same temperature with $\approx 97\%$ shape fixity and recovery whereas, in Fig. 9.4b, a one-way shape-memory cycle is illustrated for a cross-linked SM polymer with added sensing dye. The stages (I–IV) demonstrate the increasing of the stress to yield the fixed temporary strain and recovering the original strain upon heating in the last stage. As described in the figure (or stress curve), first, the sample is normally heated to a temperature (deformation or T_d) above T_{trans} and then force is applied. The strain is achieved when the sample cooled subsequently to T_f under the load (ϵ_{load}) normally below T_{trans} . The fixing cycle or a programming step is completed when the stress is removed along with the sample strain responding proportionately to a fixed strain, ϵ . Furthermore, a stress-free condition involving a strain of recovery can be achieved by simple heating of the sample to a recovery temperature, T_r . Shape fixity, R_f , and the shape recovery, R_r , can be expressed [18] in the following empirical Eqs. (9.1) and (9.2):

$$R_f = \frac{\epsilon}{\epsilon_{load}} \times 100 \quad (9.1)$$

$$R_r = \frac{\epsilon - \epsilon_{rec}}{\epsilon} \times 100 \quad (9.2)$$

SMPs intended in device fabrications and functions, evaluation by single cycle as well as multiple cycle procedures would help to test the robustness of the shape-memory performance. It was demonstrated for the cyclic experiments performed for two cross-linked ethylene–vinyl acetate copolymer (EVA) samples [19] in which low gel fraction has a noticeable strain shift from cycle to cycle and the same shift was absent in high gel fraction sample.

Dynamic mechanical analysis (DMA) is a technique useful in studying and characterizing, i.e., the viscoelastic behavior of the materials and polymers [18]. In DMA, the ratio of stress to strain is determined by applying sinusoidal stress and measuring resultant strain that allows one to determine the modulus under vibratory conditions. Further, the variations in the modulus are determined by varying the sample temperature or frequency of the stress, which further helps to find the glass transition temperature of the material and identify transitions corresponding to molecular chain movements. DMA has been utilized to quantitatively evaluate shape-memory effects and shape-memory cycle curves (e.g., controlled force mode) of polymers and polymer composites.

Under a constant load, the sample would be deformed by heating and then the deformation energy is stored after the temperature goes down, but the strain could be sustained after the load was released. In the final step, the deformed sample will begin to recover once the temperature is increased under thermal stimulus ($T < T_{\text{trans}}$). R_f and R_r can be readily calculated using the following Eqs. (9.3 and 9.4) [16]:

$$\text{Shape fixing ratio } (R_f, \%) = \frac{\varepsilon_2}{\varepsilon_1} \times 100\% \quad (9.3)$$

$$\text{Shape recovery ratio } (R_r, \%) = \frac{\varepsilon_2 - \varepsilon_3}{\varepsilon_2} \times 100\% \quad (9.4)$$

where ε_1 (%) is the maximum strain under the constant force, ε_2 (%) is the fixed strain after cooling and unloading the force, and ε_3 (%) represents the strain after reheating. In addition, the analysis of stress–strain curves (Young’s modulus) can be tested on the universal testing machine (UTM) with varied crosshead speeds and standard dimensions of the samples.

The thermal properties like crystalline and melting behaviors of thermoplastic in a blend can be studied by Differential Scanning Calorimetry (DSC) which is performed in the nitrogen atmosphere. In this technique, a weighed (approx. 3–5 mg) sample is first heated at a constant rate above its transition temperature which eliminates any prior thermal history and cooled again at a constant rate to obtain the cooling curves. Finally, repeated heating at the same scanning rate could provide the heating curves. The crystallinity of glassy polymer (thermoplastic, e.g., PCL) is calculated using Eq. (9.5):

$$\chi_c = \frac{\Delta H_m}{\omega \Delta H_m^o} \quad (9.5)$$

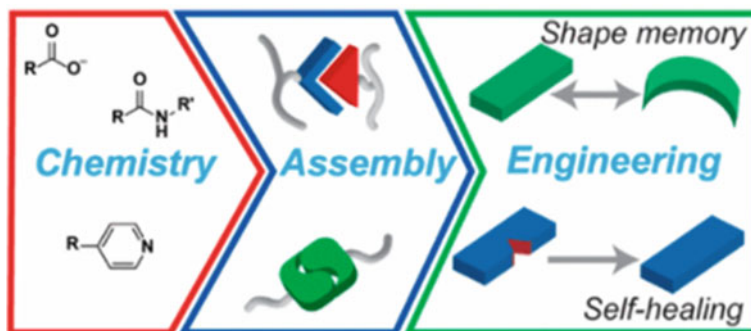


Fig. 9.5 Schematic illustration of supramolecular polymer systems—Chemistry of self-assembly, strategies to control the self-assembly, and engineering them for next generation of shape-memory polymer applications. Adapted with permission from [21], Copyright © 2020 American Chemical Society

where ΔH_m = heat of fusion for 100% crystalline thermoplastic or PCL, and ω is the mass fraction of the crystalline polymer (e.g., PCL) in the blends [20].

Recent advances in supramolecular systems can provide design methodology to produce tough, functional dynamic materials by taking the advantage of various self-assembly approaches and non-covalent interactions in tuning the material properties for stimuli response applications. In this direction, a discussion by Korley et al. [21] is significant on the current methodologies for the advancement of glassy and elastomeric supramolecular polymeric systems. These are considered to be the dynamic materials produced by the ability to control the self-assembly process and are accounted for the intricate secondary interactions among the elements such as supramolecular structure and the polymer backbone. In addition to this, a detailed mechanism on the type of interactions responsible for engineering their stimuli-responsive behavior and control to utilize the materials for the design of functional polymeric devices is illustrated in Fig. 9.5.

There are reports [22] in which the supramolecular self-assembly approaches have been adopted in designing hydrogels, polymer nanoparticles of single chain, and polymer arrays that are based on solutions.

9.3 Fabrication Strategies of Shape-Memory Polymer Nanocomposites (SMPNCs)

SMPs have remarkable properties: considerable rate of shape recovery with ease in processing, less cost, and lightweight when compared to shape-memory alloys (SMAs). Hence, SMPs have received great significance in technology and have been promoted to commercialization [23]. However, to address the still existing drawbacks of pure SMPs such as low recovery stress and size limitation, the synthetic approaches

in making polymer nanocomposites are believed to play a crucial part in improving their physical properties to be utilized in technological applications [24, 25].

To overcome the aforementioned drawbacks of pure SMPs, the reinforcement of the SMPs with functional filler materials such as nanoparticles (e.g., carbon black (CB), carbon nanotubes (CNT), carbon nanofibers, graphene oxide (GO), SiC, Ni, Fe₃O₄, and clay) and short or continuous thermoplastic fibers, etc., is widely in common practice. Polymer matrix added with functional fillers could result in multi-phase composites called polymer nanocomposites (PNCs) [26]. Significant improvement in the material properties of the PNCs is evidenced by many factors which include processing techniques, functional filler distribution, filler size, interfacial effect, aspect ratio, and matrix nature [11, 24].

In this direction, the emerging class of SMPs is the SMP (micro/nano) composites (SMPCs), which includes shape-memory polymers, alloys, hybrids, ceramics, and gels. Even though SMPs have adopted a great range of desirable shapes, they still, deal with limitations like low tensile strength, and the actuation that is mostly confined to systems that are heat-linked and treatment without appropriate action. In addition, crucial drawbacks are slow response, low thermal conductivity, and less efficient ability to display time of low recovery for actuation along with inertia toward the electrical-, photo-, and electromagnetic stimuli. Accordingly, their potential applications are adopted where high performance is expected. The design of a new generation of shape-memory composites is aimed to meet these challenges [27, 28].

The gain in the functions and properties of nanocomposites are controlled by micro- or nanostructural parameters such as size, dimension, distribution, volume fraction, along with the way the fillers are aligned and packed in the matrix. For example, most of the fiber-reinforced composites exhibit anisotropic properties excluding very short or randomly distributed fibers, whereas randomly distributed particles or fillers in polymers give rise to isotropic properties. On the other hand, macro-sized fillers offer increased tensile strength but a higher concentration of macro-sized fillers with the increased weight and decreased gloss, with low optical clarity and no enhancement in the barrier properties. Thus 'critical filler volume concentration', defined as the optimum concentration of the filler which is required to show substantial enhancement in overall properties of the material and it would be the significant factor for the final functional performance of polymer nanocomposite [29].

Further, the fillers can be categorized based on geometry or size. The morphological characteristics like surface area or volume ratio of fillers would help in understanding the structure–property relationships in the polymer nanocomposites. Similarly, the filler materials can be further classified as particulates (e.g., silica, metal, polyhedral oligomeric silsesquioxane (POSS), and other organic and inorganic particles), layered materials (e.g., graphite and layered silicates, and clay), fibrous materials (e.g., nanofibers), and single-walled and multi-walled carbon nanotubes (SWCNT) [30]. According to reported literature [31–33], the change from micro to nanometer, either in size of the particle or thickness of the layer or in diameter,

dramatically changes the surface area to volume ratio by three orders of magnitude and leads to distinct size dependence material properties.

The fundamental understanding and challenge in designing the polymer nanocomposites [34] is their complex structure, dispersibility of filler into polymer matrix leading to optimal properties without the agglomeration, and uniform dispersibility of fillers. The major step in the processing of nanocomposites require homogeneous dispersion of nano-sized particles or tubes avoiding agglomeration due to the Van der Waals [35, 36] bonding. Several successful approaches [37] to disperse (or exfoliation) layered materials like clays and graphitic layers include solvent casting (combined with surface functionalization and/or pretreated sonication), melt processing, and in situ polymerization. Among these, better dispersion is mostly achieved by blending polymer and filler components in solvent or by in situ polymerization, as compared to melt processing.

Similarly, another method where modification of filler surface is achieved is where macromolecules are grafted onto the filler surface, to achieve high compatibility of filler to the polymer matrix. This will allow better possible ways of adhesion and transfer of stress from the matrix to the fiber. The stiff fillers or fibers incorporated into the SMPs [38–42] can increase the stiffness and recovery stress. For example, 50% increase in constrained bending recovery is achieved in the case of epoxy SMPs with the addition of 20wt% silicon carbide (SiC) nanofillers [43], whereas a decrease in recovery strain and recovery rate (from 98 to 65%) occurred in shape-memory polyurethane on the addition of 30wt% carbon black [44]. On the contrary, CNT showed improved strain and stress recovery [45, 46]. Apart from stress recovery, the incorporated fillers (though in small amounts) into the polymer matrix (or SMPs) can introduce additional features, such as mechanical and electrical properties or bio-functionality (for example, SMPs containing hydroxyapatite (HA)) [47].

Moreover, conductive fillers that are actuated by electric field include carbon fillers, viz., carbon black (CB), or CNTs significantly reduce the electric resistance to form conductive SMPC, and these SMPCs are actuated via Joule heat. Likewise, a class of magnetic particles (iron oxide and nickel–zinc ferrite) on exposure to an alternating magnetic field could be inductively actuated to utilize in wireless/remote applications. The notable examples for flexible blends of characteristics included lightweight satellite supports made from trusses and torus-shaped structures, or antenna reflectors, and unmanned aerial vehicles having deployable wings. Again, such SMPC can be put into use for a subsequent application for orbit or in the atmosphere and facilitated to pack firmly large, lightweight assemblies into small volumes [48] by the users.

9.3.1 *Conventional Methods*

In general, conventional SMPs respond to one temperature trigger (or T_g of that material) and are unable to respond to a broad range of temperatures. Recently, functionally graded materials (FGMs) belonging to thermoset polymer are reported [49–53] where the control of T_g is done by spatially localized ambient temperature during photo-cross-linking. It has been applied on synthetic materials that have dimensionally controlled compositions, microstructures, and correlated properties. A variety of FGMs have been used in the field of aerospace and tissue engineering applications and are being processed and fabricated with photo-filters or photodegradation based on the UV polymerization technique.

Diorio et al. [54] demonstrated a functionally graded SMP material formulation from thiolene-based glassy thermoset that is photo-cross-linkable and encompasses a range of T_g distributed in a linear temperature gradient by post-curing the material, allowing vitrification to occur at different temperatures along the gradient. It resulted in a material that showed glass transition temperature (T_g) on 1D gradient from T_{min} to T_{max} and thus can respond to a range of temperatures ($T_{min} < T < T_{max}$) leading into elastic modulus at a given temperature along with shape recovery response when under external heating, in which case both elastic modulus and shape recovery were spatially dependent. The effect was further utilized to demonstrate the gradient recovery properties of the material over the broad range of temperatures by indentation-based surface shape-memory. The FGMs can be utilized for material-based temperature sensors or in applications requiring controlled evolution of shape during the recovery.

For example, proper utilization of processing methods can facilitate the change in local network geometry, wherein within the polymeric material, the spatial arrangement of cross-links is potentially controlled. For example, in the case of multi-material systems, when polymers are combined with gels to form structured hybrid materials and could enable the design of a multifunction device, which is a biomimetic and actuation-based shape-memory polymer [55–59].

9.3.2 *Electrospinning to Produce Nano- and Microfiber SMP Composites*

The electrospinning method is recognized [60–64] as an effective technique to prepare polymeric nanofibers. Successful electrospun ultra-fine nanofibers or microfibers of poly(ϵ -caprolactone) (PCL), polyurethane (PU), Nafion membranes (based on perfluorosulfonic acid (PFSA) or polytetrafluoroethylene (PTFE) copolymer) as well other compound polymers were prepared using this method. Electrospinning methods offer benefits such as simple processing at low cost with resulting nanofibers having desirable characteristics like small diameter, varied structures with multifunctionalities leading to the electrospun nanofibers for promising

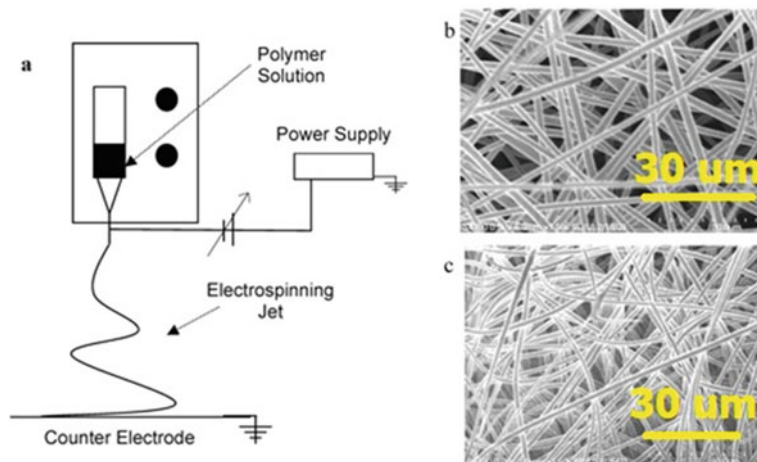


Fig. 9.6 Schematic representation of electrospinning setup **a** and SEM micrographs of nylon-6 **b** and nylon-12 **c** electrospun fibers with an average fiber diameter of 1.25 μm and 750 nm, respectively. The scale bar on both the micrographs is 30 μm . Adapted with permission from [67], Copyright 2004 American Chemical Society

biomedical/material applications, e.g., in drug release and hemostatic gauze, for tissue engineering (e.g., artificial vessels and scaffolds) as well as in textiles, nanosensors, filters, and so on [64, 65].

The process of electrospinning involves [66] applying enough strong electric field, while a polymer jet can be formed whenever polymer solution (or drop) overcomes the surface tension. The polymer jet flow is stretched and divided to form ultrathin fibers to obtain them onto the collector after the solvent evaporates. Figure 9.6 [67] displays the electrospinning setup and the corresponding scanning electron micrographs (SEM) of electrospun nylon-6 (b) and nylon-12 (c) that have average fiber diameter 1.25 μm and 750 nm, respectively.

Electrospinning has the advantage of fabricating varying structures and morphologies of fibers by varying processing parameters, as extended to SMPs and SMPCs. Jinlian Hu and co-workers reported a change in morphology of shape-memory PU nanofibers is dependent on the change in voltage applied, the concentration of the solution, and rate of feeding the polymer. In general, a rise in the concentration increased the diameter [68] of fibers.

Electrospinning methods have been extended to non-woven fibrous structures to form excellent pore networks and are employed in applications such as filters and catalysts. One such example is DuPont's Nafion[®] PFSA polymer with a polytetrafluoroethylene backbone and perfluoroether sulphonic acid side chains that possess excellent properties to be super-selective, with superior performance in chemical and thermal stabilities, electrical conductivity, and mechanical properties with acidity as

well [68, 69]. Nafion nanofibers are employed in a variety of applications for functional composite materials ranging from membranes for fuel cells, sensors to ionic conducting nanofibers [70–75].

Zhang et al. [76] reported the successful fabrication of electrospun nanoscaled non-woven fibers having (170–410 nm) average diameter (Fig. 9.7) with excellent shape-memory effects (Fig. 9.8) in Nafion solutions having few amounts of poly(ethylene oxide) (PEO). On stimulating deformed Nafion nanofibers by heating, the response of temporary shape is rapid and its recovery to permanent shape is in less than one minute. The SEM images of Nafion fibers with different weight ratios of PEO in Nafion membranes were found to be smooth, having no beads with good quality and a porous structure. During the annealing process at 130 °C for 120 min, most fiber voids are closed forming a complete and fused nanostructure.

Chen et al. obtained a stable, reversible micro/nanofibrous SMP film from cross-linked and electrospun gamma-aminopropyl triethoxysilane (APS) end-capped polyurethane oligomer (ASPU) [77]. In contrast to thermoplastic SMP or same-size

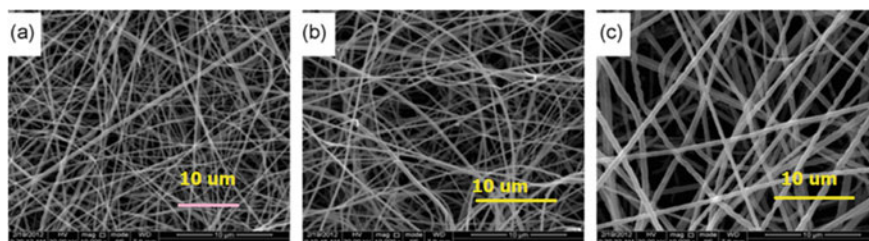


Fig. 9.7 SEM of Nafion nanofibers with PEO concentrations: **a** 0.3 wt%, **b** 0.5 wt%, and **c** 0.7 wt% at a magnification of 10,000X. Reprinted with permission from Springer Nature: The Korean Fiber Society and Springer Science Business Media Dordrecht: *Fibers and Polymers* [76], Copyright © 2014

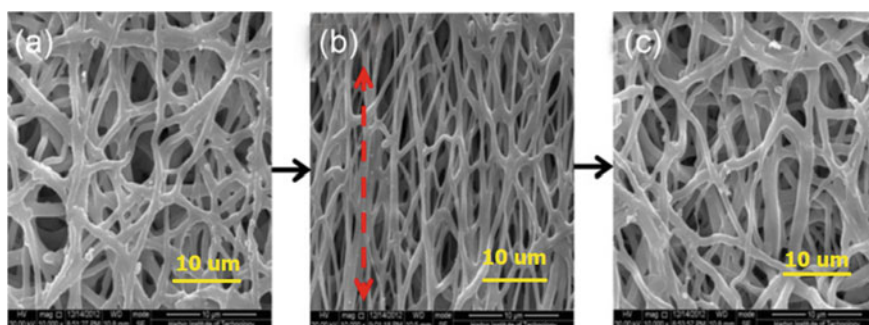


Fig. 9.8 SEM images of Nafion nanofibers demonstrating shape-memory and recovery **a** original fibers, **b** fibers that are stretched, and **c** fibers that are recovered. Reprinted with permission from Springer Nature: The Korean Fiber Society and Springer Science Business Media Dordrecht: *Fibers and Polymers* [76], Copyright © 2014

bulk SMP films, as-prepared micro/nanofibrous film exhibits early and sharp recovery in all the three test cycles, viz., change in contact angles and surface morphology. SMP nanocomposites are prepared from the class of multifunctional nanomaterials and composites, hierarchical structured porous/mesoporous materials, not limited to the membrane, particulate nanostructures, nanotubes, and nanowires. Research studies [77, 78] are supplemented with experimental data interpretations and rational designs and descriptions.

Dan Kai et al. [79] have prepared electrospun, nanofiber and hybrid inorganic–organic composites by blending varying amounts of polydimethylsiloxane (PDMS) urethane, carbon black (CB) in polycaprolactone as shown (93%PCL and 7% PDMS) in Fig. 9.9. The resultant nanocomposite scaffolds had optimum electrical conductivity (due to CB) with SM properties along with considerable biocompatible features to support the interaction and communication between the nerve cells. These nanofibrous 4D scaffolds further promoted nerve cell regeneration and also expected to facilitate minimally invasive, injectable (by needle) nerve guidance channels on the scaffolds. Also, in Fig. 9.10, the nerve (PC12) cells interacted with the shape-memory (SM) nanofibers by intimately attaching to the fibers after 9 days of culture. The cells on (pristine form) nanofibers were more elongated and oriented along the nanofibers with elliptical or spindle morphologies. Improved interaction among the cells for CB with 0.5% and 1% composition (or conductive scaffolds) is observed due to the extension of neurites to neighboring cells to improve communication and interface. NF200 protein expression was carried out to differentiate PC12 cells on

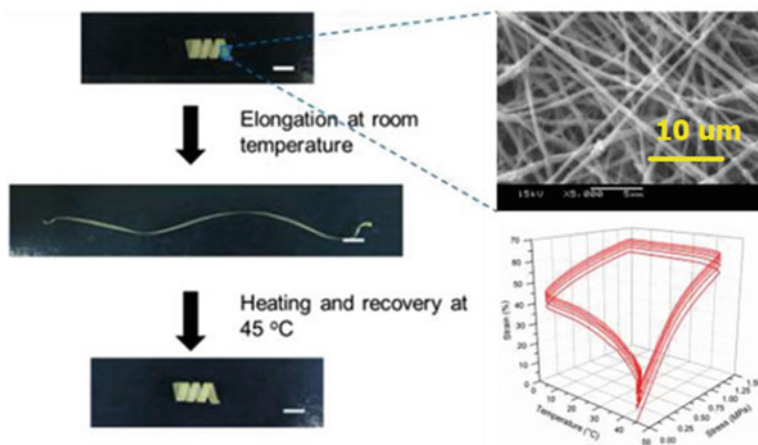


Fig. 9.9 The characteristic shape-memory and electrically conductive, 4D scaffolds made from poly (PCL/PDMS urethane) and nanofibers of carbon black for nerve tissue regeneration. Five cycles of dynamic mechanical analysis and thermo-mechanical analysis tests were performed on (A) P5 and (B) P5C2 nanofibers and their corresponding SEM micrographs. The shape recovery of the SMP fibers when heated at ~ 45 °C is shown in the photo-series. Scale bar = 1 cm. Reprinted from [79], Copyright © 2016 with permission from Elsevier B.V

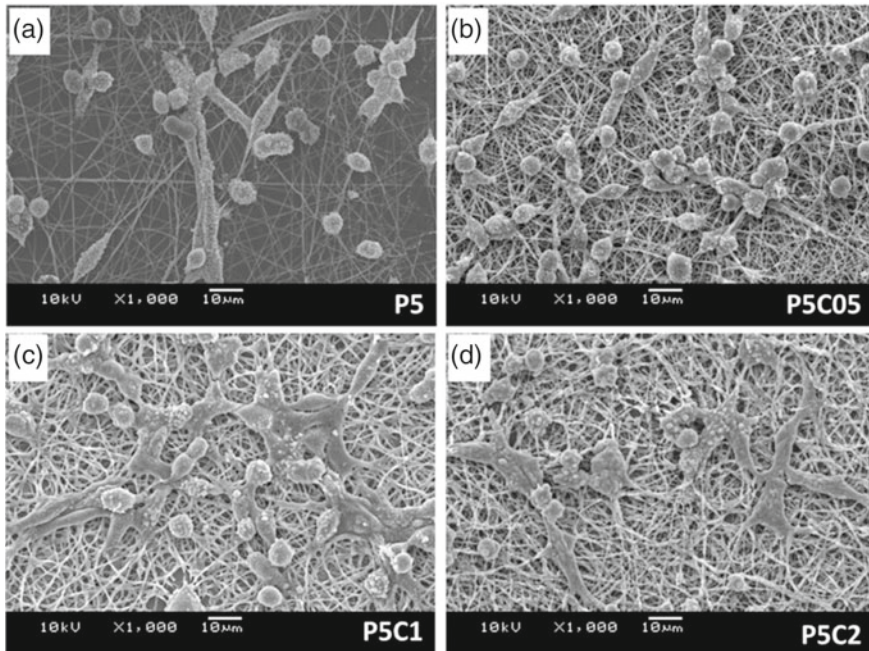


Fig. 9.10 Interaction of nerve cells (PC12) with electrospun nanofibers showing varying morphology. PC12 cells on electrospun **a** P5 pristine form or no carbon black, **b** P5C05 (0.5% carbon black), **c** P5C1 and P5C2 nanofibers with 1% and 2% carbon black, respectively. The scale bar is 10 μm . Reprinted from [79], Copyright © 2016 with permission from Elsevier B.V

SM nanofibers, and Fig. 9.11 shows the SEM results of various sets of cells (on pristine polymer, with 0.5% and 1% CB, respectively) that were found to interact with each other (elongate, orient, extend their neurites to touch, and interact with other cells) in contrast to the cells on nanofibers of 2% CB that showed round morphology or undifferentiated and, believed to be due to the toxicity of excess carbon black.

The pure or pristine SMPs have lower modulus and recovery forces as compared to SMAs and shape-memory ceramics, and thus unreinforced SMPs are not suitable for advanced applications which require higher modulus, strength, and high recovery force [80, 81]. The SMP property is not intrinsic material property, so final properties would depend on the combination of polymer architecture along with polymer morphology, tailored processing, and adopted programming technology to attain a temporary shape.

SMP composites were explored with simple methods of polymer blending or by complex chemical synthetic methods. For example, Sessini et al. [82] used melt blending to make a biodegradable PLA/PCL shape-memory nanocomposite and Behl et al. [83] reported a multi-step method from poly(ω -pentadecalactone) (PPD)

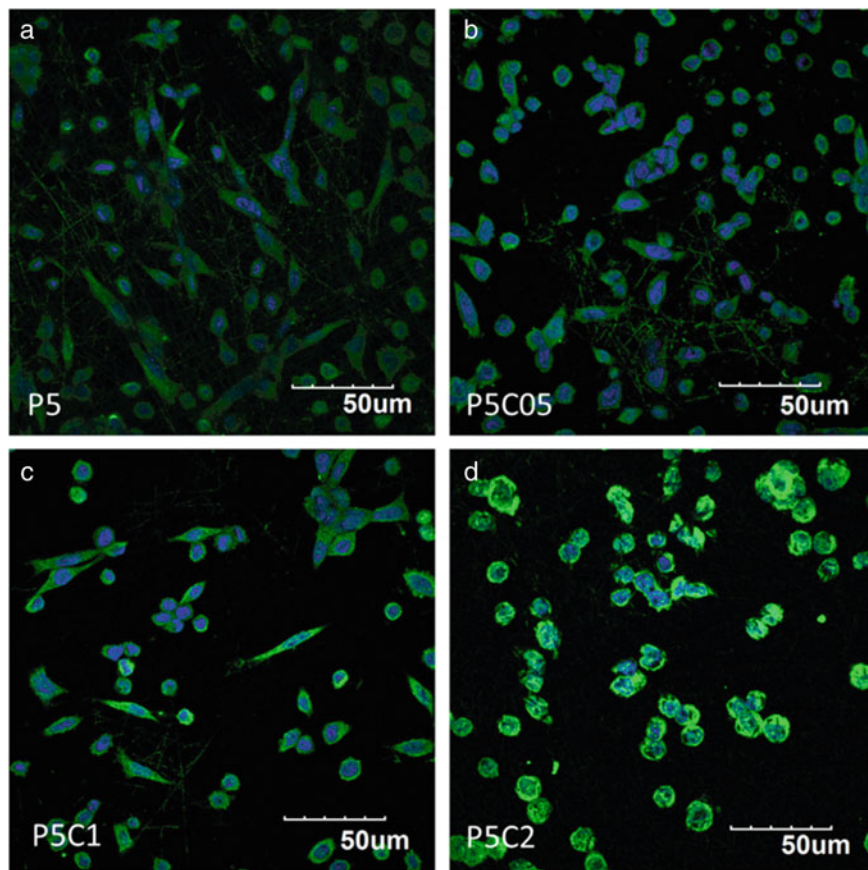


Fig. 9.11 NF200 protein expression was carried out to differentiate PC12 cells on SM nanofibers **a** P5—pristine nanofibers, **b** P5C05—nanofibers with 0.5% carbon black, **c** P5C1—1% carbon black, and **(D)** P5C2—2% carbon black on day 9. The scale bar is 50 μm . The interactions among nerve cells have increased when cultured on conductive scaffolds of poly(PCL/PDMS urethane)/carbon-black nanofibers as compared to pristine nanofibers. Reprinted from [79], Copyright © 2016 with permission from Elsevier B.V

and poly(ϵ -caprolactone) (PCL) to derive a reversible SMP from bidirectional PPD-PCL. Similarly, self-knotting sutures and actuators [84–86] are made from PCL/TPU (thermoplastic polyurethane) blends that are biodegradable.

Chen et al. [87] have reported an SMP composite where TPU is considered to be the net point and PCL to be a reversible switch segment and here T_{trans} of the SMP system is T_m of PCL. PCL/TPU are solution blended polymer matrices, in which polydopamine (PDA) nanospheres are incorporated to bestow light-responsive and self-healing dual functionalities to the microporous PCL/TPU blend as shown in Fig. 9.12. Here, the PDA nanospheres with a photothermal property are incorporated as fillers into PCL/TPU blends to enable a light-responsive SM effect with shape

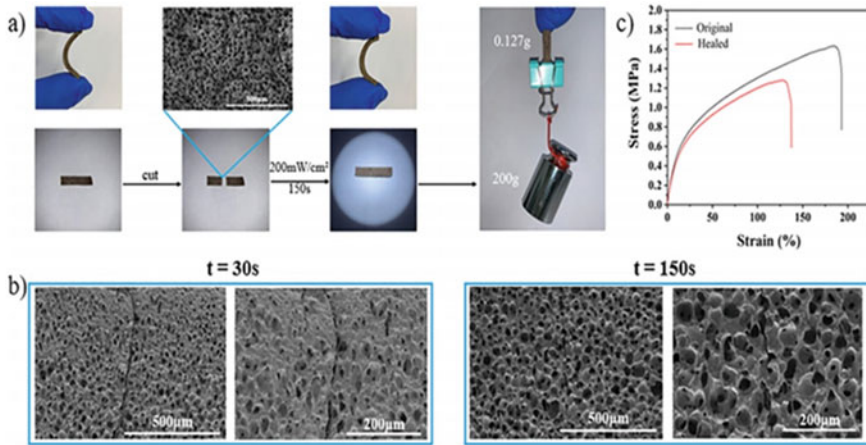


Fig. 9.12 P/T/D-3 composite (PDA content 3 wt% in the blended matrix of PCL and TPU in varying ratios) showing self-healing performance: **a** Photographs and SEM images of the sample; **b** SEM image of the sample when exposed to varying times of illumination by light; **c** Corresponding stress–strain curves. Reprinted from [87], Copyright © 2020 with permission from Elsevier Ltd

recovery of 100%. The crack on the surface is found to be healed with the light of efficiency, 78.53%, and in 150 s.

9.3.3 Additive Manufacturing or 3D Printing or Rapid Prototyping

Additive manufacturing (AM) or three-dimensional (3D) printing is the layer-by-layer addition of material to print the desired shapes. The AM is enhancing the ability to print a variety of intricate, complex structures utilizing basic fused deposition modeling to more complex energy beam methods. The reality is equipping the ability to print simple or complex structures that are intricate and prototypes on demand with accuracy and precision; though not cost-effective for mass production, it could save time and capital. The reception of these techniques is due to their capability in offering the choice to design and improvise with a variety of materials to produce unique shapes and configurations [88]. Especially, 3D printing is gaining popularity among current consumer applications to advanced applications in printed electronics and biomedical fields, i.e., tissue engineering and pharmaceuticals, where mammoth growth has been witnessed in the last decade for creating human tissues and organs [89].

The modernization in the bioprinters has advantages, such as the integrated tissue-organ printer (ITOP) to fabricate human-scale tissue construction utilizing the unique blends (of biodegradable polymers and hydrogels) or advancement in the printing

techniques comprising (e.g., inkjet and extrusion-based printers or variable property rapid prototyping, VPRP) to overcome the limitation of bulk material handling (of AM) and to produce multi-material and highly customizable prototypes having a choice of ratios and fusion grades. Each of these techniques [90] provides its unique printing procedures, materials potentialities, prospects, and challenges.

The AM field has grown extensively with potential applications. The AM field has grown extensively with potential applications especially in the development of biomedical components, whereby using a 3D scanner one can recreate custom-made prostheses and allied devices to supplement the small-scale biomedical components. Leigh et al. [91] formulated a simple thermoplastic conductive composite material “carbomorph” to print electronic sensors in a conventional low-cost 3D printer to sense mechanical flexing and change in capacitance.

The introduction of integrated circuits or sensors within conventional structures has provided a range of possibilities for smart structures. For example, functional electronic sensors or piezoresistive sensors that can sense mechanical leaning either placed in an existing object or embedded inside the printed object and capacitive sensors, as custom interface devices, sense the quantity and availability of the liquid inside the “smart” vessel. On the contrary, limitations to print the composites still exist, as it is difficult to produce and maintain [92] both the shape and function, especially as the complexity of composites surges, cheaper and less-effective alternatives are employed.

A variety of 3D-printing methods for SMPs have been demonstrated [93, 94] over the years for comprising techniques based on extrusion, i.e., fused deposition modeling or fabrication (FDM) [95–98], direct ink writing [99–101], and stereolithography (SL) techniques, including laser sintering [102], polyjet technology [103, 104], and digital light processing (DLP, also known as vat polymerization printing) [105–108]. SL offers the advantage of producing virtually any design of highly resolved prototypes and with speed in 3D printing yet with the limitation of being expensive.

Conventionally, SMPs have produced either mixing materials with varying compositions [109] as suitable to polyjet printing [104] or mixing two different inks in optimum compositions at the same voxel, to control the SMP cross-linking degree [110–112] or agents [106] or employing an approach similar to vat polymerization to appropriately enable the use of non-commercial inks without depending on ink properties. In addition, cutting-edge research is aiming toward the all-printed smart structures [113] that have the existential benefits of manufacturing materials with extreme accuracy and the ability to combine all AM techniques and control all the material or mechanical properties in one single process, by which the devices and processes are allowed to scale up with increased overall accuracy and precision especially for photovoltaic–thermal systems and as remote sensors for advanced robotic systems.

A 3D-printable SMP [114] with optimized temperature transitions is fabricated from monomers of methacrylated polycaprolactone (PCLMA) and reactive diluent, N-Vinylcaprolactam (NVCL). The report described locally activated, DLP multi-material printing of a 3D structure at two different temperatures (and tuning the

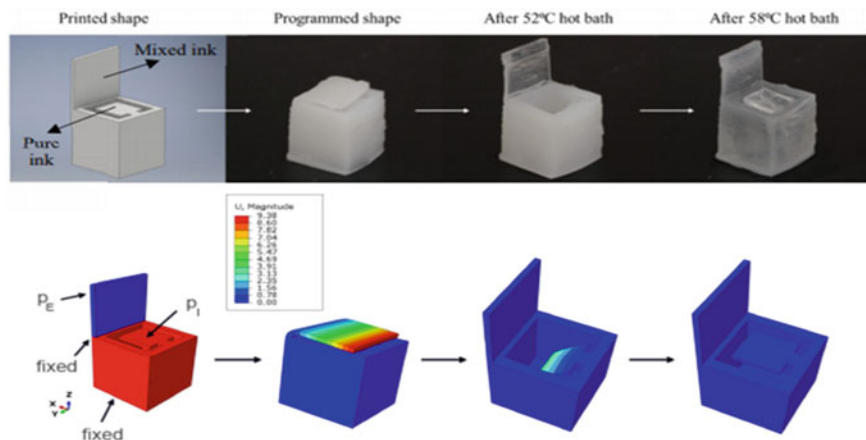


Fig. 9.13 Top images—The two-lid 3D-printed box is programmed to open at 52 °C and close at 58 °C. Bottom images—Results of the simulation by finite element methods. Red and blue colors (in the first figure on the left) denote pure and mixed ink, respectively. The pressures applied are P_E - 0.0645 MPa and P_I - 0.00002 MPa, respectively. In the inset, contour plots of the displacement magnitude [mm] are shown. Reproduced from [114], originally published under a CC BY 4.0 license, <https://doi.org/10.3390/polym12030710>

ratio of monomers and diluents), under the stimuli influence of heating directly and irradiating with light. Carbon nanotubes are coated and get absorbed onto the printed object to enable remote light activation. As shown in Fig. 9.13 a dual activation process involving temperatures (a 3D-printed box that opens at 52 °C and closes at 58 °C), two stimuli have enabled the activation by local, precise, and isolated functions. Heat transfer ability through the material is defined by the lid thickness, as well as movement efficiency and time of recovery.

9.4 4D Printing and Other Advanced Methods

The concept of 4D printing is believed to be an extension of 3D printing or additive manufacturing, where the fourth dimension, i.e., the constraint of time or shape-changing mechanism on exposure to external stimuli has been considered and taken advantage of, to derive “smart” polymers [115].

3D printing takes the advantage of printing layer-by-layer addition of polymer materials to arrive at desired shapes that can be complicated to print in other ways and provide freedom to tune configurations and functionalities during manufacturing. Considerable progress has been achieved in the 3D printing of tissues and organs for biomedical applications [116]. The concept of 4D printing was very well presented in multiple research reviews [117–120].

Sequential movement of 4D-printed photopolymers having broad glass transition was proposed by various reviewers [122]. Nicoletta et al. [121] worked on multifaceted shape-shifting motions that get transformed over a period sequentially. Here, the response of a commercial photopolymer having characteristic wide glass transition temperature also called temperature memory effect (TME) is studied by the SL technique. A correlation between deformation and recovery temperature has been presented by systematically varying the deformation temperature during the shape-memory cycles or the TME, that is, a response controlled by deformation temperature, and the SM effect occurs within this temperature region. Hoehner et al. [123] have considered the fabrication of triple-shaped SMP blends of polyethylene (PE) blends in varying compositions of high- and low-density PEs and ethylene olefin copolymer (EOC) to derive their potential for strain storage. Due to their extensive cross-linking, recycling would be an issue.

Lai et al. [124] reported olefin block copolymer (OBC)-based triple-shape-memory polymer (TSMP) composites that are similar to both TPU and polycaprolactone (PCL) bio-based polymers that use simple melt-blending or cross-linking processes. In this study, PCL and OBC due to their low and medium crystalline temperatures act as switching phases, whereas TPU with high crystalline temperature considered fixed phase and resulted in an alternative three-layered shape-memory polymer (TSMP). Various SMP parameters like shape recovery, shape fixity, effect of the ratio of compositions of each polymer, and the effect of compatibilizers in the blend have been evaluated. Further, refined modification in the distinction of temperatures in the range of deformation temperatures could facilitate the ready tailoring of multi-shape-memory polymers to meet varied applications.

Chen et al. [125] used the technique of multi-material 4D printing to fabricate soft untethered robots that exhibit sequential propulsion arising due to the presence of several bistable actuators made from SMPs which respond to different temperatures, utilizing commercially available 3D printers and materials. As illustrated in Fig. 9.14, the printed SMP muscles are heated above their glass transition temperature (T_g) and deformed mechanically to the programmed shape just before deploying the robot. In state I and when the robot is deployed in water and when the temperature is equal to or larger than T_g , the muscle relaxes while it transformed back to its original/printed shape (state II). Here, muscle relaxation is under controlled conditions; the activation force of the bistable element should be exceeded by the muscle at all points between states I and III. After propulsion, the system changes back into state III. The application of material strain while printing could potentially eliminate the prior programming requirement to allow instant robot functioning. These types of long stroke length bistable actuator designs can further allow the fabrication of load-bearing, large shape-changing, and multi-state reconfigurable 3D-printed structures. The untethered robots fabricated by Chen et al. utilize SMPs named bistable muscles, and they are designed to actuate and respond to changes in temperature around their environment [124].

- (A) The energy potential representation of bistable elements I and III as stable states. As indicated by the asymmetry in the curve, the backward movement

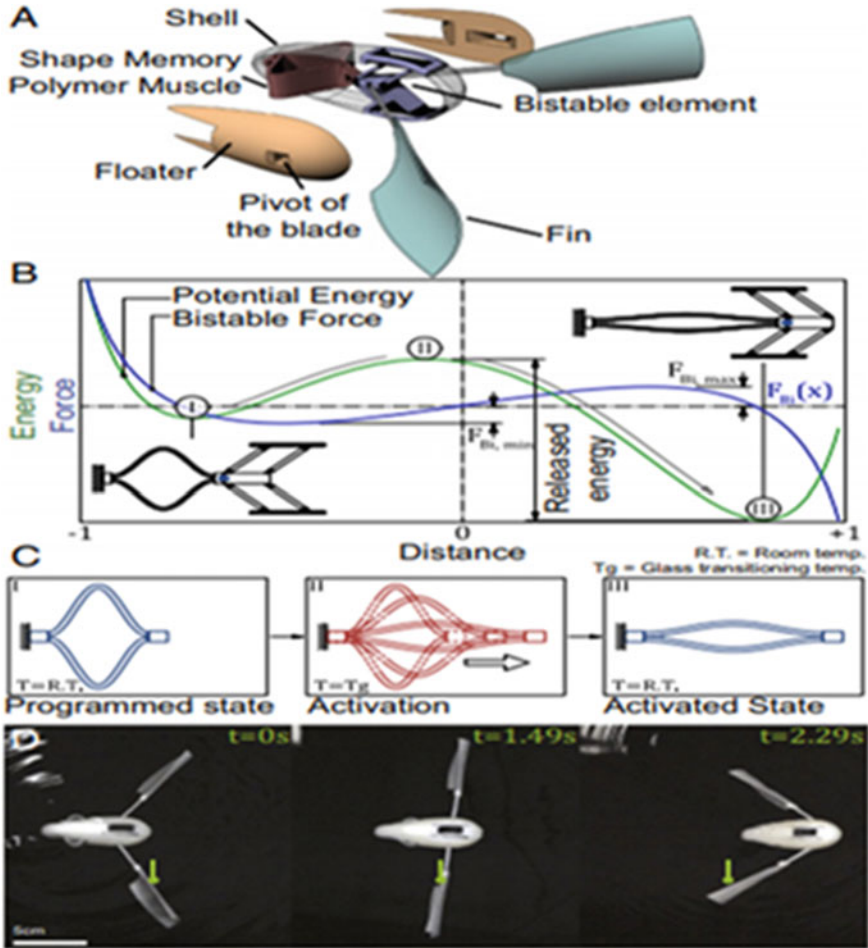


Fig. 9.14 Graphical representation of multi-material 4D-printed soft untethered robots that exhibit sequential propulsion arising due to the presence of several bistable actuators made from SMPs which respond to different temperatures (parts are false-colored for visualization)

required more energy than the forward movement. For better visualization, the 90° rotation of SMP muscle corresponding to the bistable element has been shown in the inset.

- (B) The asymmetry in the curve indicates the need for a larger amount of energy to move backward than forward. The SMP muscle shown in Insets is rotated 90° with respect to the bistable element for visualization.
- (C) Various stages of SMP muscle showing programmed deployment (I), into transition (II), and phases activated (III), and captured screen images for the robots deployed at various temperatures ($T \geq T_g$) along with their travel times

activated at different phases. Reproduced from [125], originally published under a CC BY 4.0 license <https://doi.org/10.1073/pnas.1800386115>.

The novel, direct 4D fabrication process for SMPs is proposed [125] to be contrary to the traditional 4D method, generating temporary printed shape, and the permanent shape is evolved under the influence of environmental stimuli over time and marks into relatively stiff 4D-printed shapes at room temperature. Similarly, the effective control of the photopolymerization process while printing the complex geometric forms at high resolved dimensions and directly taken out from the build tray exceed and could lead to features with high fidelity, but with controlled built-in strains.

Direct 4D-printing approaches adopted by Ding et al. [126] can print controlled multi-material systems that integrate multiple stages into a single one. This new approach integrated multiple programming and printing steps, e.g., five into a single one. In this process, a highly resolved temporarily configured component is polyjet-printed (the process jets ink droplets of multi-material materials into layers that are smooth and later cure the layers by ultraviolet light) and a second permanent configuration is achieved by simple heating. The compressive strain is built in the composite due to the strong bonding between the elastomer and the SMP (laminated strip printed from two materials) and owing to critical printing/processing criteria such as temperature, intensity, and curing time of light and layer printing time. In addition, the composite maintains stability at room temperature along with retaining high-fidelity features.

9.5 SMP Composite Response to Stimuli

SMP composites have unique properties dedicated to the type and nature of functional fillers that not only respond to stimuli but provide unique structural variations to the final material.

SMP composites that respond to light (LASMPs) use photo-cross-linking and photocleaving to change the T_g , and the light affects only the cross-linking density within the material and does not affect the temperature. Photo-cross-linking can be done at one type of wavelength, and the second one is used to reversibly cleave the photo-cross-linked bonds, where the material is switched reversibly between an elastomer and rigid polymer section as shown in Fig. 9.15.

Based on the molecular structure, the photo-cross-links can be net points or molecular switches with inherent reversibility or under a given situation of SMP. For example, irreversible photo-cross-links can be only net points, whereas reversible photo-cross-links can be both net points and molecular switches. LSMPs can display the properties based on either efficient photo-cross-linking reactions or due to the existence of photoactive groups, (e.g. acrylate-acrylate, thiol-ene, thiol-yne, thiol-epoxy, and azide-alkyne(copper(I)-catalyzed), covalently bound benzophenone group, cinnamic group, coumarin, and anthracene)that can contribute to both irreversible and reversible cross-linking. Similarly, illumination with one type of UV

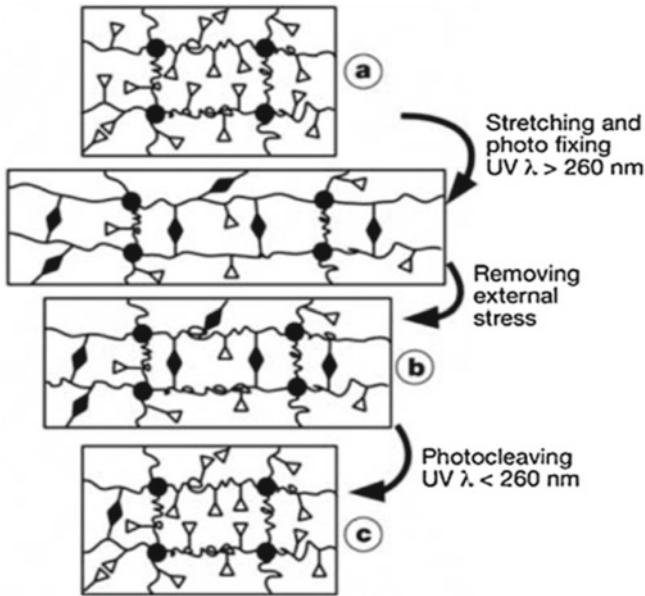


Fig. 9.15 Graphical illustration of the LSMP molecular mechanism. **a** Because of its flexible polymer backbone, LSMP is deformable at room temperature and here a deformed shape can be obtained by simply applying a force. **b** maintain the applied force and irradiate the LSMP by > 260 nm UV light and during the process, the photo-cross-linking of free cinnamic groups is expected to determine shape fixing, and then a temporary shape can be achieved after releasing force. **c** after being irradiated by < 260 nm UV light, the cleavage of photo-cross-links in LSMP activates shape recovery direct. Reproduced with permission from [127], Copyright © 2005 Nature Group

wavelength can fix the predetermined shapes, and exposure to another wavelength can recover the original shape of SMP [127].

Electricity has been utilized to activate the SMP effects in polymers, where heat cannot be employed. In practice, as in electroactive SMPs and composites, SMP effects are activated by adding either CNT [128] or short carbon fibers (CNFs) [129] carbon black, metallic Nickel powder [130] are in practice. The chemically or surface-modified conducting fillers such as multi-walled carbon nanotubes (MWNTs) are expected to better the interfacial bonding when mixed with polymers to form conducting SMPs. Moreover, the properties of these conducting SMPs depend on the filler content and extent to which the modification of MWNT surfaces is done, which in turn can result in efficient energy conversion and better mechanical properties. Surface-modified superparamagnetic nanoparticles or magnetite nanoparticles (2 to 12%) in combination with oligo (*ε*-caprolactone) dimethacrylate/butyl acrylate composite have been reported [131] for remote actuation of shape transitions.

SMPs that respond to moisture or solvents (e.g., toluene) [132, 133] usually belong to the class of polyurethanes where the water-driven actuation and recovery can be

programmable and the formation of hydrogen bonding (reduced T_g value) can be a reason for a response to moisture. Huang et al. [132] have proposed the water-driven polyurethane SMP mechanism with programmable sequential recovery with evidence of hydrogen bonding. In addition, the effect of absorbed water is either free or bound to that of T_g of polyurethane SMP.

SMP composites, with the combination of photopolymer resin and SiO_2 particles, are employed for surface coating in the polymer industry. Choong et al. successfully developed 4D-printable SMP composite [134, 135] reinforced with nanosilica (SiO_2) particles into tert-butyl acrylate-di (ethylene glycol) diacrylate polymer with Phenyl bis (2,4,6-trimethylbenzoyl) phosphine oxide as a UV photoinitiator (tBAco-DEGDA) using DLP printing. Further, the printing speed based on the photopolymerization process has been enhanced by the improvement in the resin curability with the addition of NanoSiO_2 fillers (optimum concentration). In a way, as sketched in Fig. 9.16, nanoSiO_2 are considered to modify the light scattering features of resin, by forming nucleating sites, and increase the rate of polymerization and reduce the curing time for each layer of printing.

9.6 Current Efforts and Future Directions

The modern-day industry uses shape remembrance (or SM) foams to carry grip on pre-tension in the initial stages, as used in Robotics [136] or in buildings where foam expands when warm, to seal the window frames, and as sportswear for helmets (judo or karate suits) with thermochromic additives to facilitate the observation of thermal profile [137]. The dynamic areas of photonics where rigid components are replaced by SMPs were used to create reversible shape-memory-tunable, multifunctional optical elements, e.g., photonic gratings [138], and advanced soft lithography techniques enable the idea of replica molding where periodic nanostructures are imprinted onto the SMP block surface tuned to the sizes and the order of scale of visible light.

The potential applications extend to self-repairing structural components used in automobile buffers in which the dents (or caused by undesired deformation) are repaired with the application of temperature (or a simple heat source like a hair dryer) with inherent or induced SM properties of the material. The aircraft that morphs during flight has also been in the production as an example of self-repairing plastic SMP [139].

The promising value of SMPs for the medical field continues to unfold as new devices are entering the market with expanded applications [140–144] in the areas like surgical orthopedics and ophthalmic devices (e.g., punctual plugs, glaucoma shunts, and intraocular lenses) along with intravenous cannula, self-adjusting orthodontic wires, and selectively bendable tools for small-scale surgical procedures to replace SMAs (e.g., Nitinol) being generally used.

Medical implants make entry into SMPs as materials that have potential applications in minimally invasive, miniature temporary shaped implant devices that use small incisions or natural orifices, in applications like cardiovascular stents (facilitate

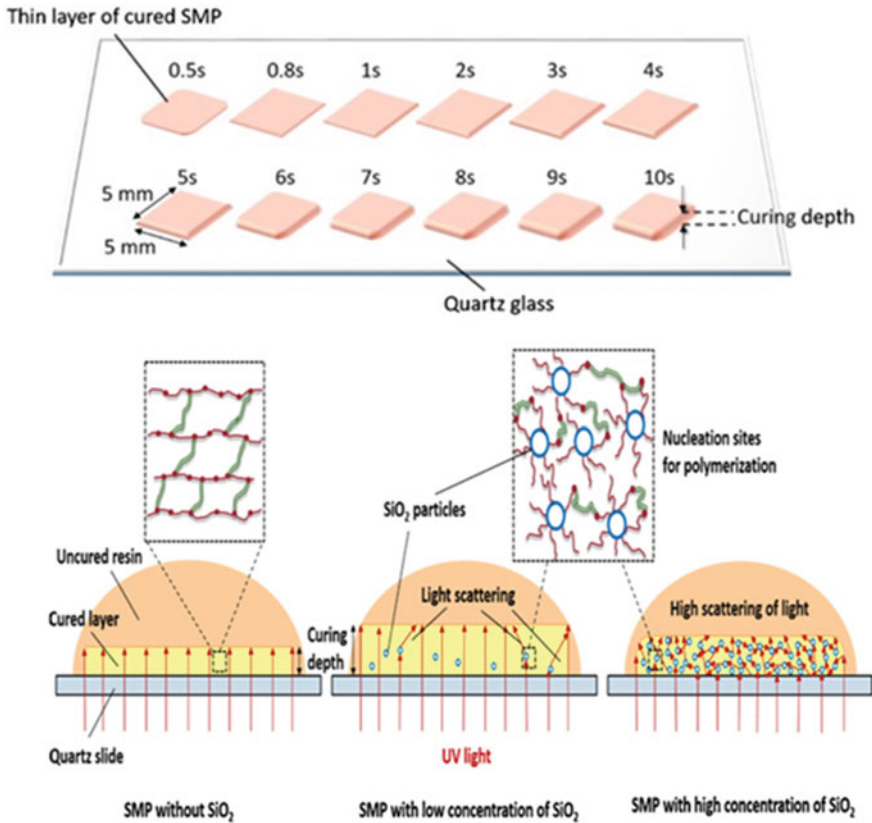


Fig. 9.16 Formation and mechanism of SiO₂-SMP composite. **a** Illustration of curing depth test for a thin layer of cured resin for 0.5–10 s. **b** A schematic diagram representing the nucleation sites formed by nanosilica particles for polymerization in the initial stages. Reprinted from [136], Copyright © 2019 with permission from Elsevier Ltd.

insertion of small stents along a vein or artery and then expanded to prop it open) assume permanent shape under the activation of shape-memory temperature modification or mechanical stress. The additional characteristic for temporary implants, biodegradability (or biodegradable polymers), is achieved once intended use is met, e.g., after healing or tissue regeneration, the implant material can be degraded and eliminated safely by the body without the need for (another surgery) removal of the implant. Likewise, the shape-memory feature of surgical sutures (SMPs) is employed to support healing and regeneration enabled by wound closure with self-adjusting optimal tension.

The researchers at Georgia [145] developed a novel, high-throughput thermo-plastic manufacturing process Mnemosynthesis, for mass-producing thermosetting plastics of low strain endurance, flexible T_g, to arrive at restorable and tunable force in

cross-linked SMP devices that are cost-restrictive by traditional thermosetting polymerization methods. The process utilizes the technique of covalent cross-linking induced by the radiation that imparts controlled memory in amorphous thermoplastic material similar to vulcanization using sulfur cross-link results in recoverable elastomeric behavior of rubbers.

SMPs may serve as a technology platform in brand protection and anti-counterfeiting labels for a benign way of storing and release of information [146]. A face stock (or a top layer of a thermal label) for use in anti-counterfeiting, brand protection, tamper-evident seals, anti-pilferage seals, etc., is in huge need [147, 148]. Early research in the SMPs for biomedical applications focused on the thermo-responsive materials and later extended to multi-stimuli-responsive materials. The properties of biodegradability and biocompatibility are major parameters in fabricating SMP materials for biomedical applications. Materials or matrices such as cross-linked poly(ϵ -caprolactone) [149], polyurethane [150], ethylene vinyl acetate copolymer [151], polymer blends and/or composites, and a networked supramolecular system [28, 152, 153] have been reported.

Langer group in 2002 [154] pioneered the groundbreaking work in biomedical areas in developing, for example, temperature-sensitive, biodegradable sutures at 41 °C, which can be tightened and sealed, and this research further led to the SMP role in other key areas of biomedical research. A porous, nanofibrous SMP scaffold is desirable (in preference to solid and impermeable SMP) in tissue engineering [155–157] applications, which necessitates the diffusion of nutrients, exchange of oxygen, and cell penetration. Significant research efforts [158–166] are also directed to develop extracellular (ECM) mimicked and/or embedded bioactive constituent SMP structures that favor cell adhesion/growth, proliferation, migration, and even differentiation.

The combination of shape-memory capabilities and electrical conductivity has been utilized [79] in designing tissue engineering scaffolds or as nerve tissue scaffolds or neural implants, for minimally invasive deployment (e.g., keyhole surgery) and also for the conductive nerve cell adhesive and proliferative activation. SMP capability has been potentially applied, whereas temporary form is attained by stretching and fitting the bulkier device for the deployment in the body through the narrow passages (or brain surgeries) and can be tuned for on-demand (within 2 s) exposures (at temperature 45 °C, slightly higher than body temperature).

9.7 Conclusions and Summary

SMP materials and composites undergo significant macroscopic deformation upon the application of an external stimulus, in the form of heat, electricity, light, magnetism, moisture, and even a change in pH value. In particular, SMP materials that respond to heat by changing their shape, i.e., the thermally induced shape-memory effect has witnessed its importance in industry and research has been actively

conducted for more than 30 years. These materials are suitable potential alternatives for shape-memory metallic alloys (SMAs) due to their flexibility, lightweight, biocompatibility, and high strain capacities for a variety of advanced applications in ergonomic products and biomedical devices. On the other hand, pure SMPs exhibit lower modulus and recovery forces, when compared to shape-memory alloys and/or shape-memory ceramics. For efficient high strength and high recovery force-related applications, these unreinforced pure SMPs are not suitable. Recently to overcome these issues, materials with specific performance have been used to diversify their utilization in aforementioned applications by the combination of numerous reinforcing fillers into SMPs, where its pristine mechanical properties (such as strength and Young's modulus) are improved. The design of stimuli-responsive materials, inspired by nature such as shape-memory hydrogels, are another class of attractive materials for the biomedical application that favor the designed SMP biomaterials for their exceptional properties in achieving self-healable, biocompatible materials with a triggered response by various stimuli but suffer from weak mechanical properties.

The enthusiasm in controlling the material properties and functions for achieving rapid response times plays a crucial role in the real-time application of SMPs, such as detection of toxins or signaling a mechanical defect. It is strongly believed that innumerable opportunities to develop advanced SMPs are possible when controllable and predictable mechanisms are achieved by slow and gradual tuning in the material properties. Recent and continued advancements in 3D-, 4D-printing manufacturing technology, flexible electronics, unconventional or advanced composites, and cutting-edge technologies in medical and tissue engineering will follow through in the development of SMPs to improve day-to-day life.

Acknowledgements One of the authors, VSP, acknowledges the support of National Research Council Senior Research Associate Fellowship (National Academy of Science, Washington, DC, USA, Energy Directorate, Air Force Research Laboratory, Kirtland Air Force Base, NM, and Materials and Manufacturing Directorate, Air Force Research Laboratory, Wright Patterson Air Force Base, OH, USA). KM acknowledges the support of her supervisor, Sumedh P Surwade, CEO and Founder, SAS Nanotechnologies LLC, for working toward polymer nanocomposite self-healing materials.

References

1. Winey KI, Vaia RA (2007) Polymer nanocomposites. *MRS Bull* 32:314
2. Carter GF, Paul DE (1991) *Materials science and engineering*. ASM International, ©
3. Kumar SK, Benicewicz BC, Vaia RA, Winey KI (2017) 50th anniversary perspective: are polymer nanocomposites practical for applications? *Macromolecules* 50:714–731
4. Adireddy S, Puli VS, Lou TJ, Elupula R, Sklare SC, Riggs BC, Chrisey DB (2015) Polymer-ceramic nanocomposites for high energy density applications. *JSol-Gel Sci Technol* 73:641–646
5. Puli VS, Ejaz M, Elupula R, Kothakonda M, Adireddy S, Katiyar RS, Grayson SM, Chrisey DB (2016) Core-shell like structured barium zirconium titanate-barium calcium

- titanatepoly(methyl methacrylate) nanocomposites for dielectric energy storage capacitors. *Polymer* 105:35–42
6. Kakkar R, Sherly ED, Madgula K, Devi DK, Sreedhar B (2012) Synergetic effect of sodium citrate and starch in the synthesis of silver nanoparticles. *J Appl Polym Sci* 126(S1):E154–E161. <https://doi.org/10.1002/app.36727>
 7. Lester B, Vernon B, Vernon HM (1941) Process of manufacturing articles of thermoplastic synthetic resins. US Patent No. 2234993
 8. Kunzelman J, Chung T, Mather PT, Weder C (2008) Shape-memory polymers with built-in threshold temperature sensors. *J Mater Chem* 18:1082–1086
 9. Andreas, KS (2005) Shape-memory polymers. *Angew Chem Int Ed* 41:2034–2057
 10. Langer RS, Lendlein A, Schmidt A, Grablowitz H (2000) Biodegradable shape-memory polymers, USA Patent No. 6,160,084
 11. Leng J, Lan X, Liu Y, Shanyi Du (2011) Shape-memory polymers and their composites: stimulus methods and application. *Prog Mater Sci* 56:1077–1135
 12. Tong Mu, Liu L, Lan X, Liu Y, Leng J (2018) Shape-memory polymers for composites. *Compos Sci Technol* 160:169–198
 13. Wang W, Liu Y, Leng J (2016) Recent developments in shape-memory polymer nanocomposites: actuation methods and mechanisms. *Coord Chem Rev* 320–321:38–52
 14. Tobushi H, Hayashi S, Kojima S (1992) *Jpn Sot Mech Engrs Int J* 35:296
 15. Kim BK, Lee SY, Xu M (1996) Polyurethanes having shape-memory effects. *Polymer* 37(26):5781–5793. [https://doi.org/10.1016/s0032-3861\(96\)00442-9](https://doi.org/10.1016/s0032-3861(96)00442-9)
 16. Ponnamma D, Sadasivuni KK, Strankowski M, Moldenaers P, Thomas S, Grohens Y (2013) Interrelated shape-memory and Payne effect in polyurethane/graphene oxide nanocomposites. *RSC Adv* 3:16068–16079
 17. Xie T (2010) Tunable polymer multi-shape-memory effect. *Nature* 464:267–270. <https://doi.org/10.1038/nature08863>
 18. Thakur S, Jinlian Hu (2017) Polyurethane: a Shape-Memory Polymer (SMP), aspects of polyurethanes, Faris Yilmaz. *Intech Open*. <https://doi.org/10.5772/intechopen.69992>
 19. Li JJ, Rodgers WR, Xie T (2011) Semi-crystalline two-way shape-memory elastomer. *Polymer* 52:5320–5325
 20. Guo Q, Groeninckx G (2001) Crystallization kinetics of poly(ϵ -caprolactone) in miscible thermosetting polymer blends of epoxy resin and poly(ϵ -caprolactone). *Polymer* 42(21):8647–8655
 21. Thompson CB, Korley LTJ (2020) 100th anniversary of macromolecular science view point: engineering supramolecular materials for responsive applications- design and functionality. *ACS Macro Lett* 9:1198–1216. <https://doi.org/10.1021/acsmacrolett.0c00418>
 22. Huurne GMT, Palmans ARA, Meijer EW (2019) Supramolecular single-chain polymeric nanoparticles. *CCS Chem* 1:64–82
 23. Qin B, Yin Z, Tang X, Zhang S, Wu Y, Xu JF, Zhang X (2020) Supramolecular polymer chemistry: from structural control to functional assembly. *Prog Polym Sci* 100:101167
 24. Chan BQY, Low ZWK, Heng SJW, Chan SY, Owh C, Loh XJ (2016) Recent advances in shape-memory soft materials for biomedical applications. *ACS Appl Mater Interfaces* 8, 16:10070–10087
 25. Bocsan IA, Conradi M, Zorko M, Jerman I, Hancu L, Borzan M, Fabre M, Ivens J (2012) Shape-memory polymers filled with SiO₂ nanoparticles. *Mater Technol* 46, 3:243–246
 26. Meng Q, Hu J (2009) A review of shape-memory polymer composites and blends. *Compos: Part A* 40:1661–1672
 27. Herbert KM, Schrett S, Rowan SJ, Weder C (2017) 50th anniversary perspective: solid-state multi stimuli, multi responsive polymeric materials. *Macromolecules* 50, 22:8845–8870 <https://doi.org/10.1021/acs.macromol.7b01607>
 28. Liu Y, Lv H, Lan X, Leng J, Du S (2009) Review of electroactive shape-memory polymer composite. *Compos Sci Technol* 69(13):2064–2068
 29. Wang WX, Liu D, Lu L, Chen H, Gong T, Lu J, Zhou S (2016) The improvement of shape-memory function of Poly(ϵ -caprolactone)/nanocrystalline cellulose nanocomposite via the recrystallization under a high-pressure environment. *J Mater Chem A* 4(16):5984–5992

30. Hussain F, Hoojati M, Okamoto M, Gorga RE (2006) Review article: Polymer-matrix nanocomposites, processing, manufacturing, and application: an overview. *J Compos Mater* 40:1511
31. Madgula K, Shubha LN (2020) Conducting polymer nanocomposite-based gas sensors, functional nanomaterials. Springer, Singapore, pp 399–431
32. Sun H, Zhang H, Zhang J, Ning Y, Yao Y, Bao X, Wang C, Li M, Yang B (2008) *J Phys Chem C* 112:2317
33. Koval'chuk AA, Shevchenko VG, Shchegolikhin AN, Nedorezova PM, Klyamkina AN, Aladyshev AM (2008) *Macromolecules* 41:7536
34. Iyer S, Schiraldi DA (2007) Role of Specific interactions and solubility in the reinforcement of Bisphenol A polymers with polyhedral oligomeric Silsesquioxanes. *Macromolecules* 40:4942
35. Kakkar R, Madgula K, Saritha Nehru YV, Shailaja RM, Sreedhar B (2014) Polyvinyl alcohol-melamine formaldehyde resin composite and nanocomposites with Ag, TiO₂, ZnO nanoparticles as antimicrobial films. *Coat Sprays* 3, 10–12:1088–1097. <http://dx.doi.org/https://doi.org/10.17628/ecb.2014.3.1088-1097>
36. Atif R, Inam F (2016) Reasons and remedies for the agglomeration of multilayered graphene and carbon nanotubes in polymers. *Beilstein J Nanotechnol* 7:1174–1196. <https://doi.org/10.3762/bjnano.7.109>
37. Lu H, Yao Y, Huang WM, Hui D (2014) Noncovalently functionalized carbon fiber by grafted self-assembled graphene oxide and the synergistic effect on polymeric shape-memory nanocomposites. *Compos Part B- Eng* 67:290–295
38. Samy A (2010) Madbouly and Andreas Lendlein. Shape-Memory Polym Compos Adv Polym Sci 226:41–95. https://doi.org/10.1007/12_2009_28
39. George J, Sreekala MS, Thomas S (2001) A review on interface modification and characterization of natural fiber reinforced plastic composites. *Polym Eng Sci* 41, 9:1471–1485. <https://doi.org/10.1002/pen.10846>
40. Müller K, Bugnicourt E, Latorre M, Jorda M, Echegoyen Sanz Y, Lagaron JM, Miesbauer O, Bianchin A, Hankin S, Bölz U, Pérez G, Jesdinszki M, Lindner M, Scheuerer Z, Castelló S, Schmid M (2017) Review on the processing and properties of polymer nanocomposites and nano-coatings and their applications in the packaging, automotive and solar energy fields. *Nanomaterials (Basel, Switzerland)* 7(4):74. <https://doi.org/10.3390/nano7040074>
41. Liu Y, Lv H, Lan X, Leng J, Du S (2009) Review of electro-active shape-memory polymer composite. *Compos Sci Technol* 69:2064
42. Ratna D, Karger-Kocsis J (2008) Recent advances in shape-memory polymers and composites: a review. *J Mater Sci* 43:254
43. Gunes IS, Jana SC (2008) Evaluation of nanoparticulate fillers for development of shape-memory polyurethane nanocomposites. *J Nanosci Nanotechnol* 8:1616
44. Wei ZG, Sandstrom R, Miyazaki S, Shape-memory materials and hybrid composites for smart system—Part I Shape-memory materials *J Mater Sci* 33, 3743(1998)
45. Gall K (2002) Shape-memory polymer nanocomposites. *Acta Mater* 50:5115
46. Li H, Zhong J, Meng J, Xian G (2013) The reinforcement efficiency of carbon nanotubes/shape-memory polymer nanocomposites. *Compos B Eng* 44(1):508–516
47. Zheng X, Zhou S, Li X, Weng J (2006) Shape-memory properties of poly(D, L-lactide)/hydroxyapatite composites. *Biomaterials* 27:4288–4295
48. Scarborough SE, Cadogan DP (2006) Applications of inflatable rigidizable structures. In: The society for the advancement of material and process engineering conference sampe. Long Beach, CA
49. Wong JY, Velasco A, Rajagopalan P, Pham Q (2003) Directed movement of vascular smooth muscle cells on gradient-compliant hydrogels. *Langmuir* 19:1908–1913
50. Yao XF, Liu DL, Yeh HY (2007) Mechanical properties and gradient variations of polymers under ultraviolet radiation. *J Appl Polym Sci* 106:3253–3258
51. Zhao PZ, Hua XY, Wang YS, Zhu JH, Wen QZ (2007) *Mater Sci Eng A* 457:231–235
52. Hexig B, Alata H, Asakawa N, Inoue Y (2005) Novel biodegradable poly(butylene succinate)/poly(ethylene oxide) blend film with compositional and spherulite-size gradients. *J Polym Sci Part B: Polym Phys* 43:368–377

53. Zhu YB, Ning NY, Sun Y, Zhang Q, Fu Q (2006) A new technique for preparing a filled type of polymeric gradient material. *Macromol Mater Eng* 291:1388–1396
54. DiOrto AM, Luo X, Lee KM, Mather PT (2011) A functionally graded shape-memory polymer. *Soft Matter* 7,1:68–74
55. Larson C et al (2016) Highly stretchable electroluminescent skin for optical signaling and tactile sensing. *Science* 351:1071–1074
56. Laschi C, Mazzolai B, Cianchetti M (2016) Soft robotics: technologies and systems pushing the boundaries of robot abilities. *Sci Robot* 1, eaah3690
57. Mazzolai B, Mattoli V (2016) Robotics: generation soft. *Nature* 536:400
58. Sadeghi A, Mondini A, Mazzolai B (2017) Toward self-growing soft robots inspired by plant roots and based on additive manufacturing technologies. *Soft Robot* 4:211–223
59. Sadeghi A, Tonazzini A, Popova L, Mazzolai B (2014) A novel growing device inspired by plant root soil penetration behaviors. *PLOS ONE* 9(2):e90139
60. Kotek R (2008) Recent advances in polymer fibers. *Polym Rev* 48:221–229
61. Gong T, Li WB, Chen HM, Wang L, Shao SJ et al (2012) Remotely actuated shape-memory effect of electrospun composite nanofibers. *Acta Biomater* 8:1248–1259
62. Andreas G, Joachim HW (2007) Electrospinning: a fascinating method for the preparation of ultrathin fibers. *Ange Chem Int Ed Engl* 46:5670–5703
63. Zhang FH, Zhang ZC, Liu YJ, Lu HB, Leng JS (2013) The quintuple-shape-memory effect in electrospun nanofiber membranes. *Smart Mater Struct* 22:085020
64. Banikazemi S, Rezaei M, Rezaei P, Babaie A, Eyvazzadeh-Kalajahi A (2020) Preparation of electrospun shape-memory polyurethane fibers in optimized electrospinning conditions via response surface methodology. *Polym Adv Technol*. <https://doi.org/10.1002/pat.4940>
65. Xia R, Zhou H, Wu R, Wu WP (2016) Nanoindentation investigation of temperature effects on the mechanical properties of nafion[®] 117. *Polymers (Basel)* 8(9):344. Published 2016 Sep 20. <https://doi.org/10.3390/polym8090344>
66. Garg, Bowl GL (2011) Electrospinning jets and nanofibrous structures. *Biomicrofluidics Am Inst Phys (AIP)* 5:013403
67. Stephens JS, Chase DB, Rabolt JF (2004) Effect of the electrospinning process on polymer crystallization chain conformation in Nylon-6 and Nylon-12. *Macromolecules* 37(3):877–888
68. Meng QH, Hu JL, Zhu Y, Lu J, Liu Y (2007) Morphology, phase separation, thermal and mechanical property differences of shape-memory fibres prepared by different spinning methods. *Smart Mater Struct* 16:1192–1197
69. Deitzel JM, Kleinmeyer J, Harris D, Beck Tan NC (2001) The effect of processing variables on the morphology of electrospun nanofibers and textiles. *Polymer* 42:261–272
70. Matsumoto H, Ishiguro T, Konosu Y, Minagawa M, Tanioka A et al (2012) Shape-memory properties of electrospun non-woven fabrics prepared from degradable polyester urethanes containing poly(x-pentadecalactone) hard segments. *Eur Poly J* 48(18):66–74
71. Mostafa G, Samaneh S, Manal I, Zahira Y, Wan R, Wan D (2012) New generation of carbon nanocomposite proton exchange membranes in microbial fuel cell systems. *Chem Eng* 184:82
72. Jang WL, Yoo YT (2011) Preparation and performance of IPMC actuators with electrospun Nafion[®]-MWNT composite electrodes. *Sens Actuat B-Chem* 159:103
73. Lei S, Chen DJ, Chen YQ (2011) surface acoustic wave/humidity sensor with high sensitivity based on electrospun MWCNT/Nafion nanofiber films. *Nanotechnology* 22:265504
74. Laforgue A, Robitaille L, Mokrini A, Ajji A (2007) *Macromol Mater Eng* 292:1229
75. Dong B, Gwee L, Cruz DS, Winey KI, Elabd YA (2010) Super proton conductive high-purity nafion nanofibers. *Nano Lett* 10:3785
76. Zhang FH, Zhang ZC, Liu YJ, Leng JS (2014) Shape-memory properties of electrospun nafion nanofibers. *Fibers Polym* 15:534–539
77. Chen HL, Cao XY, Zhang JN, Zhang JJ, Ma YM et al (2012) Electrospun shape-memory film with reversible fibrous structure. *J Mater Chem* 22:22387–22391
78. Haase MF, Jeon H, Hough N, Kim JH, Stebe KJ, Lee D (2017) Multifunctional nanocomposite hollow fiber membranes by solvent transfer induced phase separation. *Nat Commun* 8:1234. <https://doi.org/10.1038/s41467-017-01409-3>

79. Kai D, Tan MJ, Prabhakaran MP, Chan BQY, Liow SS, Ramakrishna S, Loh XJ (2016) Biocompatible electrically conductive nanofibers from inorganic-organic shape-memory polymers. *Colloids Surf B: Biointerfaces* 148:557–565. <http://dx.doi.org/https://doi.org/10.1016/j.colsurfb.2016.09.035>
80. Carey J, Goldstein E, Cadogan D, Pacini L, Lou M (2000) Inflatable sunshield in space (ISIS) versus next generation space telescope (NGST) sunshield—a mass properties comparison. In: *AIAA structures, structural dynamics and materials conference*. Atlanta, GA
81. Dornheim M (1999) Inflatables structures taking to flight. *Aviat Week Space Technol* 150(4):60–62
82. Navarro-Baena I, Sessini V, Dominici F, Torre L, Kenny JM, Peponi L (2016) Design of biodegradable blends based on PLA and PCL: From morphological, thermal and mechanical studies to shape-memory behavior. *Polym Degrad Stab* 132:97–108
83. Behl M, Lendlein A (2007) Shape-memory polymers. *Mater Today* 10(4):20–28
84. Jing X, Mi HY, Huang HX, Turng LS (2016) Shape-memory thermoplastic polyurethane (TPU)/poly(epsilon-caprolactone) (PCL) blends as self-knotting sutures. *J Mech Behav Biomed Mater* 64:94–103
85. Thakur S, Karak N (2015) A tough, smart elastomeric bio-based hyperbranched polyurethane nanocomposite. *New J Chem* 39(3):2146–2154
86. Zheng Y, Dong R, Shen J, Guo S (2016) Tunable shape-memory performances via multilayer assembly of thermoplastic polyurethane and polycaprolactone. *ACS Appl Mater Interfaces* 8(2):1371–1380
87. Chen Y, Zhao X, Luo C, Shao Y, Yang M-B, Yin B (2020) A facile fabrication of shape-memory polymer nanocomposites with fast light-response and self-healing performance. *Composites Part A* 135:105931
88. Gao W, Zhang Y, Ramanujan D, Ramani K, Chen Y, Williams CB, Wang CCL, Shin YC, Zhang S, Zavattieri PD (2015) Computer-aided design the status, challenges, and future of additive manufacturing. *Comput Des*. <https://doi.org/10.1016/j.cad.2015.04.001>
89. Zhao Q et al (2015) Recent progress in shape-memory polymer: new behavior, enabling materials, and mechanistic understanding. *Prog Polym Sci* 49–50:79–120
90. Khoo ZX, Ee Mei Teoh J, Liu Y, Chua CK, Yang S, An J, Leong KF, Yeong WY (2015) 3D printing of smart materials: a review on recent progresses in 4D printing. *Virtual Phys Prototyp* 10, 3:103–122. <https://doi.org/10.1080/17452759.2015.1097054>
91. Leigh SJ, Bradley RJ, Purssell CP, Billson DR, Hutchins DA (2012) A simple, low-cost conductive composite material for 3d printing of electronic sensors. *PLOS ONE* 7(11):e49365. <https://doi.org/10.1371/journal.pone.0049365>
92. Gibson RF (2010) A review of recent research on mechanics of multifunctional composite materials and structures. *Compos Struct* 92(12):2793–2810
93. Hassan RU, Jo S, Seok J (2018) Fabrication of a functionally graded and magnetically responsive shape-memory polymer using a 3 D printing technique and its characterization. *J Appl Polym Sci* 135:45997
94. Hua D, Zhang X, Ji Z, Yan C, Yu B, Li Y, Wang X, Zhou F (2018) 3D printing of shape changing composites for constructing flexible paper-based photothermal bilayer actuators. *J. Mater. Chem. C* 6:2123–2131
95. Liu W, Wu N, Pochiraju K (2018) Shape recovery characteristics of SiC/C/PLA composite filaments and 3D printed parts. *Compos A Appl Sci Manuf* 108:1–11
96. Zhang Q, Yan D, Zhang K, Hu G (2015) Pattern transformation of heat-shrinkable polymer by three-dimensional (3D) printing technique. *Sci Rep* 5:8936
97. Zhao W, Zhang F, Leng J, Liu Y (2019) Personalized 4D printing of bioinspired tracheal scaffold concept based on magnetic stimulated shape-memory composites. *Compos Sci Technol* 184:107866
98. Yang H, Leow WR, Wang T, Wang J, Yu J, He K, Qi D, Wan C, Chen X (2017) 3D printed photoresponsive devices based on shape-memory composites. *Adv Mater* 29:1701627
99. Su J-W, Gao W, Trinh K, Kenderes SM, Pulatsu ET, Zhang C, Whittington A, Lin M, Lin J (2019) 4D printing of polyurethane paint-based composites. *Int J Smart Nano Mater* 10:237–248

100. Wan X, Zhang F, Liu Y, Leng J (2019) CNT-based electro-responsive shape-memory functionalized 3D printed nanocomposites for liquid sensors. *Carbon* 155:77–87
101. Wei H, Cauchy X, Navas IO, Abderrafai Y, Chizari K, Sundararaj U, Liu Y, Leng J, Theriault D (2019) Direct 3D printing of hybrid nanofiber-based nanocomposites for highly conductive and shape-memory applications. *ACS Appl Mater Interfaces* 11:24523–24532
102. Choong YYC, Maleksaedi S, Eng H, Su P-C, Wei J (2017) Curing characteristics of shape-memory polymers in 3D projection and laser stereolithography. *Virtual Phys Prototyp* 12:77–84
103. Zhang YF, Zhang N, Hingorani H, Ding N, Wang D, Yuan C, Zhang B, Gu G, Ge Q (2019) Fast-response, stiffness-tunable soft actuator by hybrid multimaterial 3D Printing. *Adv Funct Mater* 29:1806698
104. Ding Z, Yuan C, Peng X, Wang T, Qi HJ, Dunn ML (2017) Direct 4D printing via active composite materials. *Sci Adv* 3:e1602890
105. Zarek M, Layani M, Eliazar S, Mansour N, Cooperstein I, Shukrun E, Szlar A, Cohn D, Magdassi S (2016) 4D printing shape-memory polymers for dynamic jewellery and fashionwear. *Virtual Phys Prototyp* 11:263–270
106. Wu H, Chen P, Yan C, Cai C, Shi Y (2019) Four-dimensional printing of a novel acrylate-based shape-memory polymer using digital light processing. *Mater Des* 171:107704
107. Yang C, Boorugu M, Dopp A, Ren J, Martin R, Han D, Choi W, Lee H (2019) 4D printing reconfigurable, deployable and mechanically tunable metamaterials. *Mater Horiz* 6:1244–1250
108. Zarek M, Layani M, Cooperstein I, Sachyani E, Cohn D, Magdassi S (2016) 3D printing of shape-memory polymers for flexible electronic devices. *Adv Mater* 28:4449–4454
109. Yu K, Ritchie A, Mao Y, Dunn ML, Qi HJ (2015) Controlled sequential shape changing components by 3D printing of shape-memory polymer multimaterials. *Procedia Iutam* 12:193–203
110. Zhang Y, Huang L, Song H, Ni C, Wu J, Zhao Q, Xie T (2019) 4D printing of a digital shape-memory polymer with tunable high performance. *ACS Appl Mater Interfaces* 11:32408–32413
111. Inverardi N, Pandini S, Bignotti F, Scalet G, Marconi S, Auricchio F (2019) Sequential motion of 4D printed photopolymers with broad glass transition. *Macromol Mater Eng* 305:1900370
112. Ge Q, Sakhaei AH, Lee H, Dunn CK, Fang NX, Dunn ML (2016) Multimaterial 4D printing with tailorable shape-memory polymers. *Sci Rep* 6:3110
113. O'Donnell J, Ahmadvkhanlou F, Yoon H-S, Washington G (2014) All-printed smart structures: a viable option? Active and passive smart structures and integrated systems. In: Liao W-H (ed) *Proceedings of SPIE*, vol 9057, p 905729
114. Keneth ES, Lieberman R, Rednor M, Scalet G (2020) Ferdinando auricchio and shlomo-magdassi, multi-material 3D Printed shape- memory polymer with tunable melting and glass transition temperature activated by heat or light. *Polymers* 12:710. <https://doi.org/10.3390/polym12030710>
115. Joshi S, Rawat K, Karunakaran C et al (2019) 4D printing of materials for the future: Opportunities and challenges. *Appl Mater Today*. <https://doi.org/10.1016/j.apmt.2019.100490>
116. Ravnic DJ, Leberfinger AN, Koduru SV, Hospodiuk M, Moncal KK, Datta P, Dey M, Rizk E, Ozbolat IT (2017) Transplantation of bioprinted tissues and organs. *Ann Surg* 266:48–58. <https://doi.org/10.1097/SLA.000000000000214>
117. Khoo ZX, Teoh JEM, Liu Y, Chua CK, An J, Leong KF, Yeong WY (2015) 3D printing of smart materials: a review on recent progresses in 4D printing. *Virtual Phys Prototyp* 10. <http://dx.doi.org/https://doi.org/10.1080/17452759.2015.1097054>
118. Ramesh S, Usha C, Naulakha NK, Adithyakumar CR, Reddy MLK (2018) Advancements in the research of 4D printing—a review. In: *IOP conference series material science engineering*, p 376. <http://dx.doi.org/https://doi.org/10.1088/1757-899X/376/1/012123>
119. Yu K, Ritchie A, Mao Y, Dunn ML, Qi HJ (2015) Controlled sequential shape changing components by 3D printing of shape- memory polymer multimaterials. *Procedia IUTAM* 12:193–203. <http://dx.doi.org/10.1016/j.piutam.2014.12.021>

120. An J, Chua CK, Mironov V (2016) A perspective on 4D bioprinting. *Int J Bioprinting* 2:3–5
121. Inverardi N, Pandini S, Bignotti F, Scalet G, Marconi S, Auricchio F (2020) Sequential motion of 4D printed photopolymers with broad glass transition. *Macromol Mater Eng* 305:p1-11
122. Meng H, Mohamadian H, Stubblefield M, Jerro D, Ibekwe S, Pang S-S, Li G (2013) *Smart Mater Struct* 22:093001
123. Hoehner R, Raidt T, Krumm C, Meuris M, Katzenberg F, Tiller JC (2013) Tunable multiple-shape-memory polyethylene blends. *Macromol Chem Phys* 214(23):2725–2732
124. Lai S-M, You P-Y, Chiu YT, Kuo C (2017) W, Triple-shape-memory properties of thermoplastic polyurethane/olefin block copolymer/polycaprolactone blends. *J Polym Res* 24:10
125. Chen T, Bilal OR, Shea K, Daraio C (2018) Harnessing bistability for directional propulsion of soft, untethered robots. *Proc Natl Acad Sci USA* 115:5698–5702
126. Ding Z, Yuan C, Peng X, Wang T, Qi HJ, Dunn ML (2017) Direct 4D printing via active composite materials. *Sci Adv* 3(4):e1602890
127. Lendlein A, Jiang H, Jünger O et al (2005) Light-induced shape-memory polymers. *Nature* 434:879–882. <https://doi.org/10.1038/nature03496>
128. Liu Y, Lv H, Lan X, Leng J, Du S (2009) Review of electro-active shape-memory polymer-composite. *Compos Sci Technol* 69, 13:2064–2068. <https://doi.org/10.1016/j.compscitech.2008.08.016>
129. Leng J, Lv H, Liu Y, Du S (2007) Electroactive shape-memory polymer filled with nanocarbon particles and short carbon fibers. *Appl Phys Lett* 91,14:144105. <https://doi.org/10.1063/1.2790497>
130. Leng J, Lv H, Liu Y, Du S (2008) Synergic effect of carbon black and short carbon fiber on shape-memory polymer actuation by electricity. *J Appl Phys* 104, 10:104917. <https://doi.org/10.1063/1.3026724>
131. Schmidt AM (2006) Electromagnetic activation of shape-memory polymer networks containing magnetic nanoparticles. *Macromol Rapid Commun* 27, 14:1168–1172. <https://doi.org/10.1002/marc.200600225>
132. Huang WM, Yang B, An L, Li C, Chan YS (2005) Water-driven programmable polyurethane shape-memory polymer: demonstration and mechanism. *Appl Phys Lett* 86:114105. <https://doi.org/10.1063/1.1880448>
133. Leng J, Lv H, Liu Y, Du S (2008) Comment on, water-driven programmable polyurethane shape-memory polymer: demonstration and mechanism. *Appl Phys Lett* 92, 20:206105. <https://doi.org/10.1063/1.2936288>
134. Choong YYC, Maleksaeedi S, Eng H, Yu S, Wei J, Su P-C (2017) 4D printing of high-performance shape-memory polymer using stereolithography. *Mater Des* 126:219–225
135. Choong YYC, Maleksaeedi S, Eng H, Yu S, Su P-C, Wei J (2016) Curing characteristics of shape-memory polymers in 3D projection and laser stereo lithography. *Virtual Phys Prototyp* 1–8
136. Choong YYC, Maleksaeedi S, Eng H, Yu S, Wei J, Su PC (2020) High speed 4D printing of shape-memory polymers with nanosilica. *Appl Mater Today* 18:100515. [10.1016/j.apmt.2019.100515](https://doi.org/10.1016/j.apmt.2019.100515)
137. Brennan M (2001) Suite of shape-memory polymers. *Chem Eng News* 79:6, 5. <https://doi.org/10.1021/cen-v079n006.p005>
138. Monkman GJ, Taylor PM, Memory foams for robot grippers robots in unstructured environments. In: Proceedings of 5th international conference on advanced robotics. Pisa, pp 339–342
139. Tippets CA, Li Q, Fu Y, Donev EU, Zhou J, Turner SA, Jackson AMS, Ashby VS, Sheiko SS, Lopez R (2015) Dynamic optical gratings accessed by reversible shape-memory. *ACS Appl Mater Interfaces* 7, 26:14288–14293 (2015). <https://doi.org/10.1021/acsami.5b02688>
140. Toensmeier PA (2009) Shape-memory polymers reshape product design. *Plast Eng*
141. Yakacki CM, Shandas R, Lanning C, Rech B, Eckstein A, Gall K (2007) Unconstrained recovery characterization of shape-memory polymer networks for cardiovascular applications. *Biomaterials* 28(14):2255–2263. <https://doi.org/10.1016/j.biomaterials.2007.01.030>

142. Chan BQY, Low ZWK, Heng SJW, Chan SY, Owh C, Loh XJ (2016) Recent advances in shape-memory soft materials for biomedical applications. *ACS Appl Mater Interfaces* 8(16):10070–10087. <https://doi.org/10.1021/acsami.6b01295>
143. Lendlein A, Langer R (2002) Biodegradable, elastic shape-memory polymers for potential biomedical application. *Science* 296(5573):1673–1675. <https://doi.org/10.1126/science.1066102>. PMID 11976407
144. Monkman GJ (2000) Advances in shape-memory polymer actuation. *Mechatronics* 10(4/5):489–498. [https://doi.org/10.1016/S0957-4158\(99\)00068-9](https://doi.org/10.1016/S0957-4158(99)00068-9)
145. Fritzsche N, Pretsch T (2014) Programming of temperature-memory onsets in a semicrystalline polyurethane elastomer. *Macromolecules* 47(17):5952–5959. <https://doi.org/10.1021/ma501171p>
146. Voit W, Ware T, Gall K (2010) Radiation crosslinked shape-memory polymers. *Polymer* 51(15):3551. <https://doi.org/10.1016/j.polymer.2010.05.049>
147. Leverant C, Leo S-Y, Cordoba MA, Zhang Y, Charpota N, Taylor C, Jiang P (2019) Reconfigurable anti-counterfeiting coatings enabled by macroporous shape-memory polymers. *ACS Appl Polym Mater* 1:36–46. <https://doi.org/10.1021/acsapm.8b00021>
148. Ecker M, Pretsch T (2014) Multifunctional poly(ester urethane) laminates with encoded information. *RSC Adv* 4(1):286–292. <https://doi.org/10.1039/C3RA45651J>
149. Ecker M, Pretsch T (2014) Novel design approaches for multifunctional information carriers. *RSC Adv* 4(87):46680–46688. <https://doi.org/10.1039/C4RA08977D>
150. Ping P, Wang W, Chen X, Jing X (2005) Poly (ϵ -caprolactone) polyurethane and its shape-memory property. *Biomacromolecules* 6(2):587–592
151. Zhang ZX, Liao F, He ZZ, Yang JH, Huang T, Zhang N, Wang Y, Gao XL (2015) Tunable shape-memory behaviors of poly(ethylene vinyl acetate) achieved by adding poly(L-lactide). *Smart Mater Struct* 24, 12:125002
152. Xie T, Xiao X, Cheng YT (2009) Revealing triple-shape-memory effect by polymer bilayers. *Macromol Rapid Commun* 30(21):1823–1827
153. Wang WX, Liu D, Lu L, Chen H, Gong T, Lu J, Zhou S (2016) The improvement of shape-memory function of poly(ϵ -caprolactone)/nano-crystalline cellulose nanocomposite via the recrystallization under a high-pressure environment. *J Mater Chem A* 4(16):5984–5992
154. Zhang S, Yu Z, Govender T, Luo H, Li B (2008) A novel supramolecular shape-memory material based on partial α -CDPEG inclusion complex. *Polymer* 49(15):3205–3210
155. Small W, Singhal P, Wilson TS, Maitland DJ (2008) Biomedical applications of thermally activated shape-memory polymers. *J Mater Chem* 20:3356–3366
156. Lendlein A, Langer R (2002) Biodegradable, elastic shape-memory polymers for potential biomedical applications. *Science* 296(5573):1673–1676
157. Goh YF, Shakir I, Hussain R (2013) Electrospun fibers for tissue engineering, drug delivery, and wound dressing. *J Mater Sci* 48:3027–3054
158. Prabhakaran MP, Venugopal J, Ghasemi-Mobarakeh L, Kai D, Jin G, Ramakrishna S (2012) Stem cells and nanostructures for advanced tissue regeneration. In: Jayakumar R, Nair SV (eds) *Biomedical applications of polymeric nanofibers*. Springer, Berlin, pp 21–62
159. Kubinova S, Sykova E (2010) Nanotechnologies in regenerative medicine. *Minim Invasive Ther Allied Technol* 19:144–156
160. Jin GR, Prabhakaran MP, Kai D, Annamalai SK, Arunachalam KD, Ramakrishna S (2013) Tissue engineered plant extracts as nanofibrous wound dressing. *Biomaterials* 34:724–734
161. Kai D, Prabhakaran MP, Stahl B, Eblenkamp M, Wintermantel E, Ramakrishna S (2012) Mechanical properties and in vitro behavior of nanofiber-hydrogel composites for tissue engineering applications. *Nanotechnology* 23:10
162. Xie J, Willerth SM, Li X, Macewan MR, Rader A, Sakiyama-Elbert SE et al (2012) The differentiation of embryonic stem cells seeded on electrospun nanofibers into neural lineages. *Biomaterials* 30:354–362
163. Yang F, Murugan R, Ramakrishna S, Wang X, Ma Y, Wang S (2004) Fabrication of nanostructured porous PLLA scaffold intended for nerve tissue engineering. *Biomaterials* 25:1891–1900

164. Woo KM, Jun JH, Chen VJ, Seo JY, Baek JH, Ryoo HM et al (2007) Nano-fibrous scaffolding promotes osteoblast differentiation and biomineralization. *Biomaterials* 28:335–343
165. Tseng LF, Mather PT, Henderson JH (2013) Shape-memory-actuated change in scaffold fiber alignment directs stem cell morphology. *Acta Biomater* 9:8790–8801
166. Stimuli-Responsive Micro-Reservoirs for release of Encapsulants, S Surwade, K Madgula - US Patent App.16/513, 220 (2020)

Chapter 10

Effect of Nano and Hybrid Fillers on Shape-Memory Polymers Properties



G. V. S. Subbaroy Sarma, Murthy Chavali, Maria P. Nikolova,
and Gagan Kant Tripathi

10.1 Introduction

Shape-memory materials (SMM), which can twist into an impermanent shape once a warm procedure over a specific heat. Shape-memory ceramic then again can be either a reversible stage change looking like the shape-memory alloy (SMA) or a multiphase framework, which takes after the shape-memory polymer (SMP). The SMM can turn into a fragile state after this temperature change and can efficiently distort by adding a heap. The SMM can embrace its unique form when a specific upgrade is added to the twisted arrangement because of flexible vitality put away during programming [1–6]. The form and coming back to introductory shape forms called programming and the recuperation procedure individually. The method of encoding and recouping the state of a polymer is demonstrated schematically in Fig. 10.1.

The categories of shape-memory materials are shape-memory alloys and shape-memory ceramics [7, 8]. Shape-memory impact in shape-memory alloys is activated by warm acceptance. The compound arrangement chilled off from the austenitic stage to the martensitic stage where the firmness is diminished and the assembly can be effectively distorted. SMA can hold the transitory shape, and possibly re-visitation of the first shape occurs when warmed over the austenite temperature in the austenite

G. V. S. Subbaroy Sarma
Department of Basic Sciences & Humanities, Vignan's Lara Institute of Technology and Science,
Guntur 522213, Andhra Pradesh, India

M. Chavali (✉) · G. K. Tripathi
Office of the Dean (Research) & Division of Chemistry, Department of Science, Faculty of
Science & Technology, Alliance University, Bengaluru 526106, Karnataka, India

M. P. Nikolova
Department of Material Science and Technology, University of Ruse "A. Kanchev", 8 Studentska
Str, 7000 Ruse, Bulgaria
e-mail: mpnikolova@uni-ruse.bg

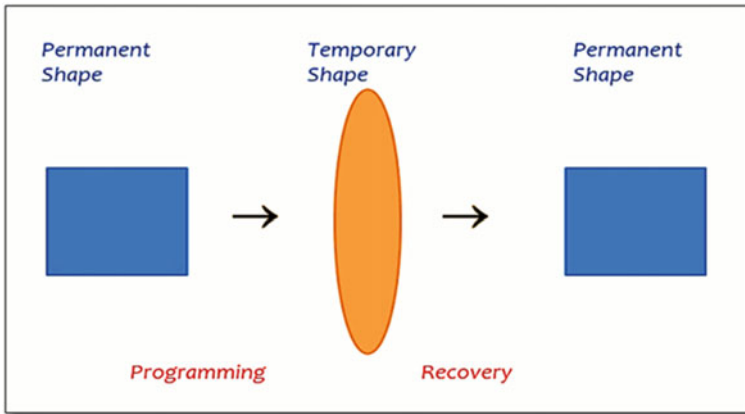


Fig. 10.1 Process of a shape-memory polymer

stage. Then again, the changing temperature for SMP is generally the glass temperature; at this point, the polymer structure gets rubbery with low firmness, allowing huge distortions. At the point when it is cooled beneath the glass temperature, the SMPs firmness increments radically [9]. The commonly known improvements on a shape-memory material are temperature and light. A warm reactive shape-memory polymer is foremost to be identified [10].

Electro responsive shape-memory polymers, which have highly charged fillers, are integrated into the shape-memory polymer grids to provide assemblies as touchy toward power [11–13]. On the other hand, light-reactive ingredients were arranged into two groups. The first is SMP which only responds to a particular frequency of light and is not influenced by the warm light effect, and the subsequent classification is SMP which ingest slight heat that incites warm warming that executes form retention reaction [14, 15]. The shape-memory process portrayed before is delegated in a single direction shape-memory impact fit as fiddle changing impact is irreversible. A case of a two-way shape-memory impact is observed in shape-memory alloys and fluid glass [16–18]. Bellin et al. found an unmistakable warm change in heats, which are utilized to get the triple-shape memory impact [19].

10.1.1 Shape-Changing Polymers

10.1.1.1 Molecular Mechanism of Shape-Changing Polymers

Polymers alter their form when often they were subjected to an acceptable stimulation. The unique shape recuperated when the incitement ended. Its original 3D shape, how such a work piece is moving, determines the geometry. Although it is not possible to vary the shape shift for SCP/SCG, the cycle of invigorated misshaping

with resulting recuperation was rehashed a few times. For SCP/SCG, heat, light, and electromagnetic fields are identified as stimuli.

Completely SCP/SCG needs an elastically deformable polymer network, wherein the net points regulate the eternal form. Such polymer systems should be sufficiently flexible to allow flexible distortion of the sequence sectors. Covalent connections and physical connections are being progressed as net points. Whereas covalent cross-linking was found, oligomers having other sensitive sets, physical cross-linking is obtained by physical connections initiating from ionic clusters. While totally, SCP/SCG accomplished shape changes such as twisting or large contraction. SCG is a smart gel that forms polymer networks enflamed by a massive level of fluid solutions. In which tolerance to stimulation is included whether to regulate the volume of cross-links or to provoke mechanisms of remixing. The allocation of symmetrical variations from the molecular to the macroscopic stages confirmed photo isomerization that permitted a reactive SCC, recognized extra methodology for SCC.

Stimulus sensitivity to energy, pH, electromagnetic vibration, or electric flux can be achieved unless stimulation-sensitive circuits capable of regulating the molecular network is scaling or dwelling upon activation adjust the molecular systems. It was possible to distinguish the two techniques. While the swelling capacity reflects on chain length, the first method is designed to persuade the number of extra covalent bonds. While ion-exchange categories are still in the major or lateral block, pH tolerance identified, throughout the molecular chains, those that were perturbed with ionic bonds are included. Its scale for bonding could have been managed through pH change. The stimulation-induced adjustment mostly in mixtures of link chains and fluid is also a process of receiving stimulation sensitivity in SCG. The melting point heating rate of N-isopropylacrylamide (NIPAM) or polyethylene oxide (PEO) in water is a common representation for stimulus-induced assessment. Components are still highly hydrophilic just below transition temperature correlations, a rearrangement of function method sections arises underneath transition temperature, leading to a sharp modification throughout the hydrodynamic radius and NIPAM component deposition.

To produce gels that have light compassion, a linear relationship is included. Leuco equivalents or multi phenyl methane structures are included in the polymer links. Such groups are likely to produce ions once subjected via UV light that contributed toward electrostatic repulsion for link sections such as a gels' growing may have managed with radioactivity.

10.1.1.2 Intelligent Gels as Shape-Changing Materials

The majority of polymers depicted are thermoset; but variations throughout the capacity of polymers could also affect by a combination of pH values, ionic content or the behaviour of the growing user. Besides, the use of electric field, heat, or physiologically relevant materials, may activate some SCG [20]. In such a synthesis setting, copolymers of solvents, NIPAM, and N-acryloxysuccinimide contributed to

polymers having actual long chains beyond LCST. The NIPAM sections vanished and declined until the rate was raised beyond LCST, emptying its liquid mostly as a different process. The solution maintained the compositions of one's earlier processed structure at that deformation, creating a large scaled-up model of one's new form. The regions supplying the functional gross positions were water-soluble if the heat lowered under LCST, leading there in hydrogel's incomplete breakdown. To construct a modern stable form, such a pattern must be used. The polymer was initially reswollen, switched to a new form container of that new regular form, and once the regular formed by cooled under LCST but instead boiling beyond LCST. Polymers fabricated by acrylic acid and acryloyl compounds provided with aliphatic ω -amino acids and SCC, induced by some transition metal ions [21].

Dependent on a molecule such as Cu^{2+} , Pb^{2+} , Cd^{2+} , Zn^{2+} or Fe^{3+} , a conical liquid specimen can be preferentially reshaped into a polymeric or inverted cone structure. Such polymers developed based on the concentrations of existing organic compounds had a crucial balancing of organic and aqueous categories, resulting in lower hydrophilicity and self-organization including its element facilitating locations. The relative importance is based on the ionic strength and was transmitted to the middle of the liquid from its surface, resulting in a void internal. As the mechanism is dispersion-controlled, the time needed is only for the deformation compared to the initial width of its gel. It was cleaned out with the concentration of HCl, while the original shape of liquid is now recovered to stimulate the SCC by the composition of organic compounds. Moreover, it is possible to change the shape second shape to a limited degree, it is completely dependent on the initial gel style and therefore not easily switchable.

10.1.1.3 Indirect Actuation of Thermally Triggered Shape-Changing Effect

The structure variance is fixed out with electric fields in LCE by ferroelectric mesogens, Due to the extremely versatile modules, interestingly, stable regions in the MVm^{-1} zone have been allowed. In contrast to temperatures given apart from LCE, for which time delay is regulated by the movement of heat, this can be noticed out within ferroelectric LC component response times with close with ~ 10 ms. Unfortunately, the strain has been relatively small, which is accomplished with some ferroelectric LC polymers. For example, the inclusion of major nanomaterials, carbon dark or carbon nanotubes might enhance the accessible discharges. For instance, the inclusion of prominent nanoparticles, carbon dark or carbon nanotubes may enhance the available extracts [22]. The stack of LCEs with carbon nanotubes of its stimulation by Infrared light might achieve some appreciated now [23].

Improvement of versatile hydrogen bonding in liquid crystallines LCE allowed morphological variations to leave with heat and humidity [24]. A benzoate altered acrylate was cross-linked with a mesogenic diacrylate crossed ligand-binding via compression ratio until structure to update the principle through an LCE. Although mechanical quality and compound opposition were provided by the mesogenic

diacrylate cross-linker, cleavage of the flexible chemical bonds ultimately resulted in some kind of a bowing reconfiguration of mesogens. Since the cleavage of the chemical bonds is affected by the moisture or pH and perhaps even the deformity of the material concerned, an in-stream check valve is used for such mechanisms [25].

10.1.1.4 Contrast Among Shape-Memory Alloys Besides Shape-Memory Polymers

By heating across a specific concentration associated with features of amalgam, shape-memory composites will deform at such a room temperature and then return to their original structure. Upon freezing, SMA switches through austenite toward the marten location. At room temperature, the marten location process occurs which is the slightly fragile or actively twisted cycle of SMAs. Austenite is a phase of even more based SMAs, which occurs at extreme temperatures. The shape-memory effect occurs either at a stage where the SMA temperature is dropped to below the change in temperature (T_s) and indeed the mixture was exclusively composed of marten-site. This warped design would recover with its effective alignment through cross warming over its progressive temperature. The distorted martensite shifts further into the process of cube austenite [26].

SMAs expose the influence including both particular direction and two-way size-memory. The form transforms toward its specific for the one-way shape-memory influenced by melting SMA only at strained martensite point. For any circumstance, this should remain within heated form if the mixture cools further. Melting through extreme temperatures does not produce a noticeable shaping shift with such a fixed-direction effect. If an SMA lowered at such a high austenite phase for a two-way shape-memory effect, would thus humiliate without external bending. In other cases, mostly in the heating-cooling process, the cold distorted form and heat ability to discover will normally shift. SMPs shape-memory effect depends on the existence of separate complementary insights with either the form of the compressed material or cross-joints. The macromolecular links of SMPs are connected by either a chemical or a physical cross-interface mostly in the warped version below T_g . Such macromolecular links may revert to random crawled form whenever heated yet again. The shift in shape-memory depends mostly on the portion whereby polymer particles make across changes that are coerced and abnormally trapped. SMPs only illustrate the shape-memory effect of a specific path. To be specific, the benefit of SMPs against SMAs lies in its typical features, such as reduced costs, lower width, easier preparation as well as greater possible variants. Table 10.1 records the principle properties analyzed between NiTi SMA and polystyrene SMP.

Table 10.1 Properties related between characteristic SMA and SMP

Parameter	NiTi SMA	Polystyrene SMP
T_s , °C	40–100	62
Conversion strain, %	8	50–100
Actuation stress, MPa	100	2–10
Young's Modulus $> T_s$, GPa	83	1.24
Young's Modulus $< T_s$, MPa	28–41	2–10
Poisson's Ratio	0.33	0.3
Density, gms/cc	6.45	0.92

10.2 Shape-Memory Effect (SME)

10.2.1 One-Way SMPs

The deformity approach becomes self-acting but focuses upon its inherent characteristics of SMP, the latter approach involves external forces in any situation. The normal ability to conduct this one-way shape adjustment lies mostly in the polymer's atomic structure. The fundamental component of certain SMPs shows that an atomic chain provides two distinctly separate categories in a manner that delivers a variable exchange tool as well as a device structure. For instance, these situations are provided throughout square polyesters when the different squares collect phase isolated along these lines, building two kinds of parts. The distinction in the concoction structure brings about an alternate reaction to outside upgrades.

For example, those two sections show inconsistent cooperation powers in high-temperature enacted polymer SMPs. The fragments with the more grounded parts display greater advancement or softening conditions of a crystal than a more fragile cooperation portion. Subsequently, one form of the base pairing is strong through one temperature, but the other is sensitive. Twisting the polymer component within that phase can produce delicate parts throughout extended or compacted sections, yet the hard portions will remain almost unaltered because of their higher mechanical opposition. The hard portions work there by a grid of net focuses, which is the necessity for the controlled shape recuperation. On the off chance that the polymer piece is twisted at a temperature, where both of the portions are delicate, one can characterize another changeless form. Cooling the polymer in this shape brings about a framework of net focuses connected by totally loosened up delicate sections.

If the polymer is distorted at such a level that increases or dissolves the temperature of the fragile fragments under the material, the fragile parts are extended but compacted. Diminishing the temperature solidifies the delicate sections by expanding the intermolecular association powers and prompts an incidentally fixed shape. After warming the chain portability increments, the entropic vitality is delivered. The point of all-polymer bind store turns around to their casual compliance. They unwind and recoup the special adaptation as the chains can shift at an increased rate. When all links strive to regain their compliance with the original, individuals step away from

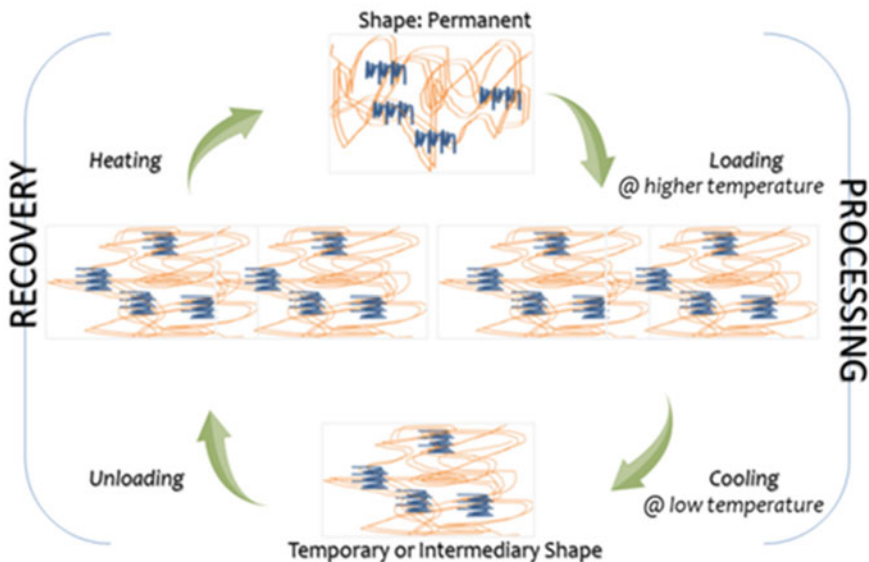


Fig. 10.2 Thermally-induced shape-memory

the net lattice to its underlying arrangement. Figure 10.2 demonstrates the procedure at the sub-atomic stage of the processing and recovery period by delineating the variations in adapted link.

10.2.2 Multi-shape SMPs

A few examinations teams concentrated on the turn of events and plan of SMPs highlighting more than one brief shape coming about fit as a fiddle SMPs. Each unmistakable outline is modular and retrievable at each of the picked-up progress levels in program transfer requests. At a fundamental level, any blend of trigger-related exchange systems, such as heat, light, solvents, etc., is used to upgrade a triple-shape-memory capacity with an SMP.

10.2.3 Two-Way SMPs

The main downside of SMPs depicted is the inability to play out the form shift again at the brief to that same lasting form for just a single time. There will be, however, a few polymers designed for a temporary change of form. Shape-evolving polymers (SCPs) are recognized here and there, which could only alter a size measurement

between two connecting harmony systems regularly, and two-way SMPs, which can perform a programmable reversible shape change. The important component is the difference in conformity with the polymer matrix and crystallization structure that varies the persuasive sizes.

As an example modified fluid glass-like areas with fluid transparent elastomers drop the arrangement once the temperature is elevated above a certain basic value that visibly affects the compression of its duration of the example. While the temperature decreases again, the spaces are reshaped and the example regains the unique size. Therefore, a form shift of fully reverse two-way structure shift action is conceivable upon warm stage development. Comparative conduct can be watched for semi-glasslike systems. The crystallization of chain spaces under a consistent pliable burden causes a stretching of the example through the example contracts after liquefying of the glass-like areas. Thus, the polymer moves between two equilibrium points by warming or freezing the instances beyond or under a basic level. In guaranteeing the elastic load, the usually reversible shift in size could be balanced. The essential impediments of semi-translucent systems, however, were critical and the restriction of small changes is in just one direction. Joining a two-route SMP with such a subsequent material itself is a chance to solve those constraints. The bilayer twists the infinite supply of the two-route SMP because it is viewed at a raised temperature by maintaining a pre-extended semi-translucent framework polymer layer to an elastomeric layer. The furnishing of two distinctive translucent stages with two diverse softening temperatures, within a lattice of net focuses, integrated a three-way shape SMP that includes additionally a two-way SME. The temperature subordinate compression/extension because of liquefying/crystallization of glass-like spaces of the humble dissolving stage went about as exchanging component; though the translucent areas of the exceptionally softening stage remained solidified at this exchanging temperature and decided the shape-moving math. In customary single direction SMPs, the exchanging fragments empower the entropy-driven shape recuperation just as the obsession of the impermanent shape. The key innovation of this two-way SME concept is the parathion of these two tasks to two different molecular domains. The switching process, therefore, depends once more entirely upon its crystallization and cooling of its low heat regions, because this deformation or compressions are also the basis for the ultimate shape transition.

10.2.4 SMP Composites

The advancement of inner warming for shape recuperation would enormously extend the field of potential applications. Fillers such as carbon nanotubes (CNTs), carbon particles, conductive fibers, and metal elements have thus joined through temperature-initiated SMPs to allow the polymer test to change illumination, current or attractive factors toward energy. SMP polymers are designed for a shift of current through electro-dynamic heating in which the SMP obstruction is reduced by supplements to allow Joule heating. In comparison to metal conveyors, permeable polymeric

materials provide essential focal points, such as easy preparation, low thickness, and minimal effort.

Conductivity creates new areas of use for a part of a multi-utilitarian SMP. Incorporate dark carbon and nickel particles modified in bands to minimize the polymer matrix's objections by more than many times as opposed to haphazardly circulated Ni particles to warm the test to 80 °C with just 30 V to initiate the recovery of the form [27]. Using these nanoparticles or multi-walled carbon nanoparticles for SMP polymers, similar results have been obtained [28–30]. Polymers with a small concentration of nanoparticles and SMPs exhibit improved structural and warmer properties other than the modified physical properties. It suggested that nanocomposites target less to 5 wt percent can have the potential to increase not just the stringy module from a scale factor around low temperatures, but to upgrade their cover concern in a synthetic polymer by about half [31]. SMP polymers including interesting grains, such as iron oxide or nickel-zinc ferrite, are designed to allow analytic warming through an attractive exchange area, which can even remotely regulate shape recovery with this methodology. In considering the privilege of magnetic nanoparticles, due to the shift of the molecule to Para attraction over their Curie temperature, they will fill in from an under-warming assurance device. Along these lines, a matrix of polymer SMP stacked with 10 vol. % nickel-zinc ferrite particles at a distance of 43.6 μm is covered from harm produced by the covering tissue [32]. They could expand a temperature to 64 °C via uncovering tests of such a polymer to such an enticing exchange area of 12.2 MHz as well as approximately 400Am^{-1} in the ambient atmosphere, which was adequate for implementing a complete notation through SMP in less than 25 s. The generation of heating by engrossing lighting in exceptionally retaining composites or materials using the photograph warm effect is a third procedure that acquires recovery through external warming [33–35].

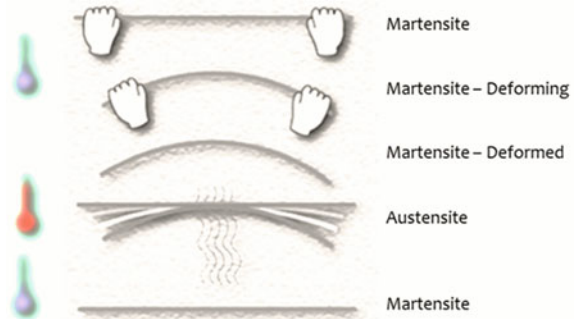
10.3 Synthesis

10.3.1 SMPs

Hu and Chen showed a blossom form made with an SMP [36]. The accessible bloom has been the first form. For example, by expanding its temperature toward an over exchange value of 80 °C, the bloom blossoms were looped on crafting a shut blossom, which is shown in (Fig. 10.3). Each shut bloom was set again after the bloom was chilled out onto low temperatures (T_{room}). If the shut bloom is put in a stove at 80 °C at that point, the blossom exposes the petals within 5 s.

By cooling off to a temperature below the T_{trans} , an SMP is warped to a temperature above an exchange progress temperature (T_{trans}). Warming the SMP over its T_{trans} brings recuperating its lasting shape. Either synthetic or mechanical cross-joins in polymer systems with SME assume the role as system particples that balance the system mostly during progression in thermo-mechanical activities. The machine links

Fig. 10.3 The illustrative procedure for shape-memory



including its SMPs can be either glasslike or shapeless which, in this way, whether it is a softening shift or crystal progress is the warm progress of setting the SME off. SMPs also may have indeed a dissolving temperature (T_m) or a temperature rise in a crystal (T_g) like T_{trans} . Where $T_{trans} = T_m$, it is possible to obtain a strain-actuated crystal structure of the exchange parts through chilling twisted products down through the temperature below T_m . The crystals prevent the recovery of the form once the material is heated beyond T_m [37, 38]. Where $T_{trans} = T_g$, the particle's small-scale Brown movements get solidified and the exchanging parts were also put in the lustrous condition once each substance is cooled down to below T_g [39, 40].

In this way, the material cannot recoup its unique structure and stays with a non-balance condition once warmed well beyond T_{trans} when Brown's miniaturized scale movements were enacted. It has been generally accepted that SMPs programming invention affects the properties of shape-memory. Otherwise, the programming procedure is called a thermostatic loop. Thermo-mechanical processes, for example, twisting, form fixation or structure restoration, are commonly made up of 3 stages:

- a. *The polymers of the shape-memory are skewed to some value that may be above or below its exchanging value.*
- b. *After lowering its material to a level below the exchange value, the SMP was placed into a short form.*
- c. *The SMP has restored the unique form.*

Many thermo-mechanical limits will affect an exhibition of SMPs within that thermo-mechanical phase change period. Displacement temperatures, curvature duration, heat-reducing velocity, temperature raising velocity, and magnitude of elongation were its typical variables, respectively.

10.3.1.1 Physically Cross-Linked

Throughout its initial specific group, mechanical crossed connections are associated with indistinct polymers, which always typically have poor notation relative to mass

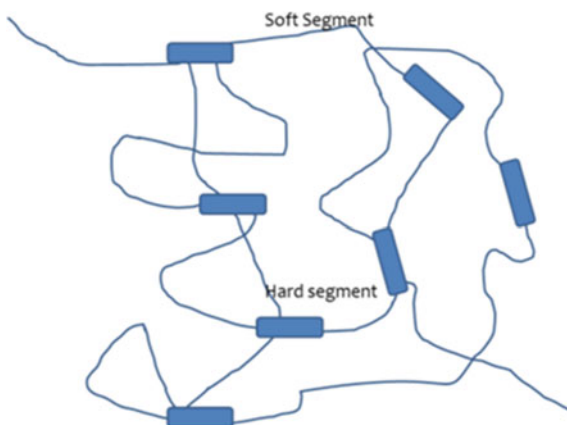
composites. The undefined and glasslike districts fill in along with actual cross-joins in mixable polymer blends. The shape-memory activity in these composites is attributed with their T_g of the fragile, namely a formless section, or the perpetual form is attributed toward a mechanical cross-connection of that same tough or translucent portion realized between adjoining particles by intuitive forces. For the most part, these shape-memory polymers display reduced shape-memory impacts in both the previously described synthetic arrangement courses. Soluble polyurethane blends, as well as phenoxy pitches, were examples of SMPs of this kind [41].

Same with the amorphous polymers, mechanically cross-linked microcrystalline layer copolymers have shapes identical with that for amorphous thermoplastics; nevertheless, such composites exhibit material storage activity around the melting point of the soft segment and retaining with its permanent shape are induced through cross-links among certain strong portions throughout crystallinity across molecular forces. Such characteristics are being changed by manipulating natural and artificial regions. These tough blocks shape structural complexes through hydroxyl groups or crystallizations which, once applied with elongation or cumulative stresses, avoid nearby chains from sliding beyond everyone else. While its structure healing process, such locations often serve like significant metal plates. Therefore, with any form, that influences phase change activity, physical characteristics, or thermal expansion, its position including its cross-links is much more essential. Such composites were simple to produce which display excellent stability toward organic compounds and organic solvent. These often exhibit long-term stability toward direct sunlight, provide outstanding, stable physical modulus but are bioactive. They, therefore, have quite a strong probable for application, especially for operation and practical diagnostics [42].

Another very widely utilized form of certain polyesters consists of polyurethane diol as an amorphous phase or Methylene diisocyanates as the tough component was polyurethane-based structures. In this regard, it is quite surprising, as shape-memory polyurethanes (SMPUs) grown into experts through this rapidly developing field of speculation that even become pioneered such a result. In Fig. 10.4, the complicated yet fragile outlines of SMPUs were presented.

Smaller-scale stage isolation in polyurethane directed by the concoction idea of the polymer was used in techniques for amalgamation. Contingent upon the hard/delicate ratios and sort of cross-linker utilized, extreme properties will vary. SMPs provide much with a quite prevalent shape-memory recovery of high cross-joins upon its rough sections as those with high cross-joins on the rough delicate interfaces [43]. Besides, with the polymer molecular weight and the number of hydroxyl bunches in the molecules, a range of available functional cross-interface targets are defined, and those specifically the polymers used in instigating SMPUs [41, 44].

Fig. 10.4 Hard and soft segments in SMPUs



10.3.1.2 Covalently Cross-Linked Major Arrangement

Monomers charge transfer polymeric materials have a 3D structure, which defines the critical large-scale scope shape of the substance, artificially, whereas the shape-memory transition uses a warm change of the material portions. The cross-linked shiny material having any smooth T_g at plotting temperature and suggesting polymer stability over concentrations beyond T_g obtained from covalent cross-links is among the least difficult forms of SMPs. Then again, through any softening improvement accounting only to a shape-memory effect, its sections could be partially crystal-like in design.

Polymers arrange related SMPs that could only be combined after polymer chains either by using any multifunctional cross-linker and through any straight as well as extended polymer cross-link. A wide variety of polymer spines, such as polyolefins, polyurethanes (PUs), polyacrylates, and polystyrene, are being based on the systems. The material-based frameworks display virtually zero wet blankets concerning genuinely cross-connected SMPs, so any irreversible disfigurement throughout design and delivery development is tremendously reduced. As a result, SMPs polymer-based organization exhibit attractive properties, particularly fantastic proportions of shape recovery and a tuneable working edge during phase transformation, defined by such a rubbery module that could be balanced by the thickness of the cross-connect.

10.3.1.3 SMP Networks Based on Polyurethanes

Since PUs are anything but difficult to configure throughout the broad boundary storage of parts including added substances to suit a vast variety of necessities including materials, the PU typically becomes a significant class of the SMP. Among such products, the effects of cross-joints are mainly as seen in polyolefines: the warm

strength is increased, and the wet blankets are being reduced impressively. Therefore, the cross-interfaces may not only go around with its inducer of the proportion of shape recovery, but can also fully assume control throughout a difficult step task as the critical cross-joints throughout its PU structure. If crystallizable exchange fragments occur, the proximity of cross-joints decreases the crystallization of the exchange portion. If there should be an occurrence of crystallizable exchanging fragments, the nearness of cross-joints decreases the crystallization of the exchanging section.

Such top-quality characteristics allow its usage in the medical field since unwavering quality with precise control remains essential, and the structures were cared for to display outstanding structural properties as well as a design progress temperature [45]. A vast scope in available sections through an integration with their PU or a charge transfer PU empowers the layout of polyethylene glycol (PEG) fragments to form liquid-swell capable PU systems. The water absorption of these substances due to the proximity of hydrophilic PEG parts is assumed to have a beneficial effect on the biocompatibility of the materials. The miniaturized scale stage isolated half-breed system of this sort was acknowledged by utilizing the technique of interpenetrating systems (IPN). Poly (tetrahydrofuran)-based PUs were glycerol-cross-connected [46] and PEG-cross-connected [47] but mostly their findings were compared against specific SM-PUs of a comparable structure for gain and awareness of its impact with polymer engineering on the physical characteristics (Fig. 10.5).

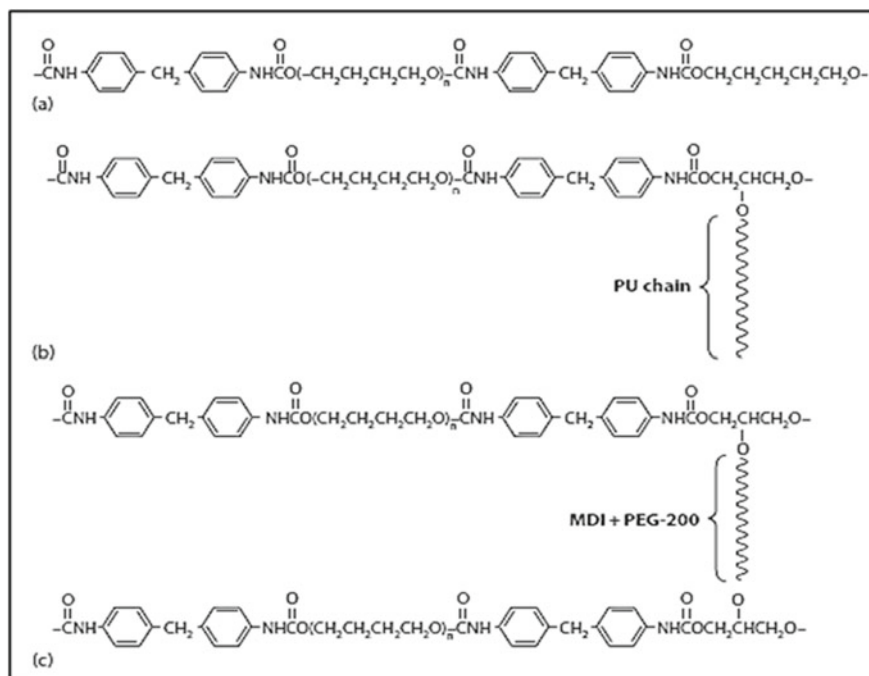


Fig. 10.5 PU-SMPs Structures by **a** direct, **b** stitched, and **c** cross-linking frameworks

To add in its robust characteristics among its devices, the adaptable PEG sections are accounted for. Poly-dependent SMPs of chemically secure inserts have been accounted into is suggested. Poly (ester urethanes) with large-scale polylactide-based diolandtriols and poly (ϵ -caprolactone) (PCL) of structural features tuneable through cross-connecting thicknesses are considered a choice dependent on biodegradable polyester portions [48–50].

10.3.1.4 Thermoplastic Shape-Memory Polymers

In thermoplastic elastomers and shape-memory materials, a charge transfer design of the SMPs previously introduced consists of direct polymer chains linked with mechanical cross-links which could have been delivered through heat or through using some dissolvable which take liquefy or arrangement handling into account. Subsequently, throughout this design phase, the entomb chain cross-joints determine that the 3D structure of a given gadget should remain steady through each programming method, implying if they prefer a high climate of improvement and are far above the rate of shape change.

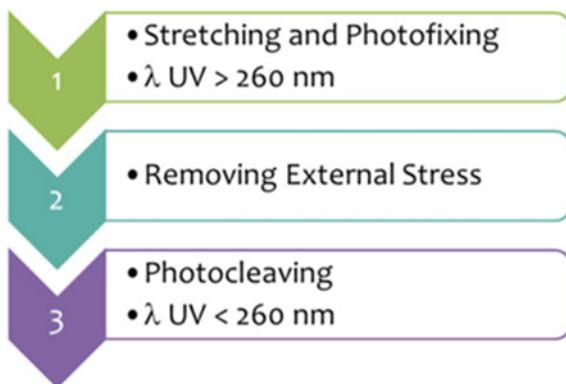
Thermo actuated shape-memory effect depends on the growth of stage-isolated morphology, with one step going on as an atomic shift or a phase giving the actual cross-joints. Although the phase for its most noteworthy point, the mechanical quality of a substance gives the entire temperature range throughout its processing method by the creation of the structural traverse. Due to its versatile design including structural features, Push as obtained articulated consideration among thermoplastic SMPs.

10.3.1.5 Light-Induced SMP

The programming cycle consisted of disfiguring the examples to ϵ_m accompanied by UV light illumination of $\lambda > 260$ nm. Fresh covalent bonds were thus described among CA entities and the short structure (ϵ_m) can become set. All newly framed covalent bonds were broken around the point, of illumination with the UV light around $\lambda < 260$ nm, as well as its unchanging form, is recovered (Fig. 10.6).

The research examined two distinct sub-atomic systems: a joint polymer and an interpenetrating polymer association (IPN). The copolymers of n-butyl acrylate (BA), hydroxyethyl methacrylate (HEMA), and ethylene glycol-1-acrylate-2-CA (HEA-CA) were recognized through a compound associated with both the combined heat-delicate set. Also, as a cross-linker, poly (propylene glycol) dimethacrylate ($M_n = 560 \text{ g mol}^{-1}$) was utilized. For each case, everything can be calculated by R_f approximately 52% as well as R_r approximately 95%. Through copolymerizing BA using 3.0 wt % poly (propylene glycol) dimethacrylate ($M_n = 1,000 \text{ g.mol}^{-1}$) both as polymer, the IPN matrix were gained through mixing in with about 20 wt % star-poly(ethylene glycol) including CAA marginal collections. The heat-prompted SMEs were tracked by R_f up at 33% and R_r at 98% [51].

Fig. 10.6 SME of nanostructured composites transplanted polymeric membrane process



The glow-initiated SMP may have been selected depending on alpha, alpha-hydroxyl polyesters (PLA, PCL, PEG) whereby the heat-touchy CA clumps are integrated throughout the fundamental sequence. Then, its flexible crystallization of polymers was achieved through lighting from ultraviolet light [52], based upon its [2 + 2] cycloaddition response. With the two-advance poly addition method using N, N-bis (2-hydroxyethyl) cinnamon (BHECA), alpha, al-hydroxyl PLLA, and PCL, Multi-block compostable polymer (ester-urethane) s (PEUs) comprising bracelet cinnamate substituent are merged. For any linking expert, Hexamethylene diisocyanate (HDI) has been used. An R_f reached half of a 20% BHECA material, while the R_r reached >95% of a 50% PLLA substance [53]. Comparable PEUs including receptive substituents of its necklace photograph (diethyl 2, 20-[cinnamoylazediy1] diacetate and diethyl 3-[cinnamoyloxy] pentanedioate) as stated should display 70–85% R_f and 40–70% R_r [54]. Also, moiety bunches were fit to undergo their reversible [2 + 2] cycloaddition, so these may be used in photographic actuated SMP [55–57]. PCL through its swinging moiety bunch was set up via arranging poly build-up of carbonyl methoxy coumarin dichloride and alpha, ω -dihydroxy-terminated PCL ($M_n = 1250, 3000, \text{ and } 10,000 \text{ gmol}^{-1}$) 7-(3, 5-dicarboxyphenyl).

Once exposed by light with exchange frequencies (280/254 nm) without an additional photograph initiator, such light-sensitive polymeric materials experienced a fast, flexible photograph cross-link. The shape-memory characteristics were provided by Gotten systems within particular R_f and R_r estimates are somewhere in the 88% range and 100% for 100–500% pliable strains. The shape-memory ability was strongly dependent on the degree of PCL section crystal growth and the polymers cross-linking thickness. Photoisomerization processes, usually using azobenzene substituents, would often trigger their light-sensitive shape change [58, 59].

Through access with sunlight insufficient different wavelengths, Azobenzenes are being moved reversibly through cis to Tran's functional groups (Fig. 10.7a). Mesoscopic variations throughout its polymer content are being caused by the formation of complexes between two photo-isomers connected with the polymer matrix. Such influence, indeed, has been further analyzed in the sense of flexible shape changes in polymer systems but never because SMEs have historically interpreted [60–64].

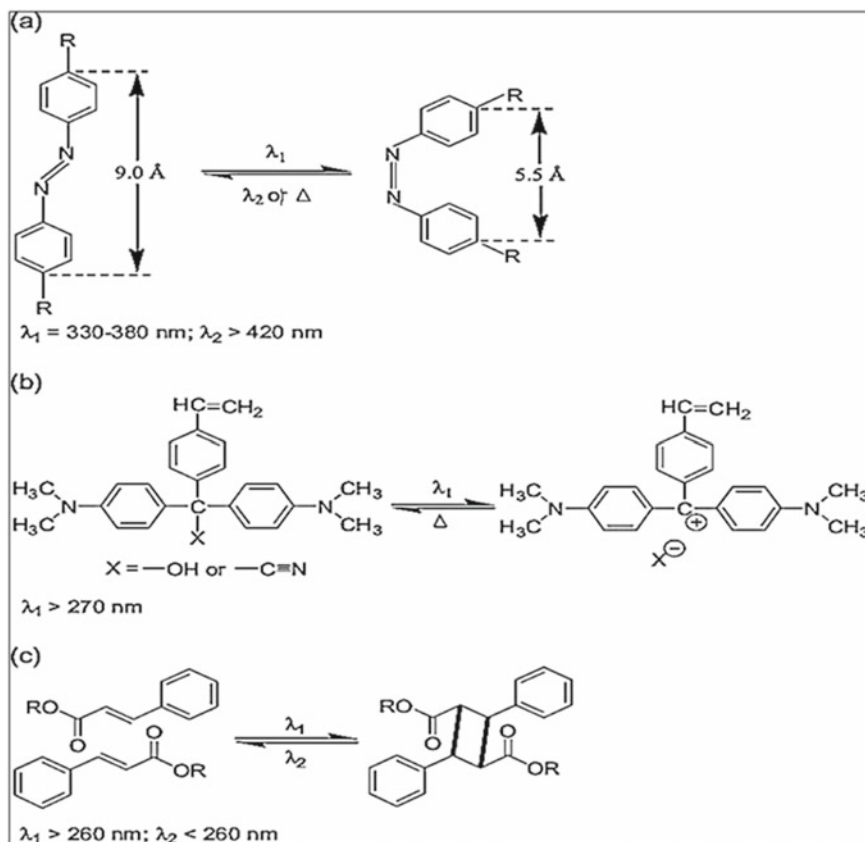


Fig. 10.7 Light-induced isomerization and photochemical reactions **a** Azobenzene groups, trans-cis photoisomerization. **b** Triphenylmethaneleuco compounds photo-induced aqueous disorientation. **c** Cinnamic acid (CA) response characteristics

Likewise, variations throughout the polymer shape have been reported through triphenylmethaneleuco-containing systems (Fig. 10.7b) that detach as ion couple's replication phase happens at a high temperature throughout the dark. An explanation with a light source made an impact SMP was affected by an image polymerization of cinnamic corrosive (CA) or cinnamyliden acid corrosive (CAA). Such nanostructured devices (Fig. 10.7c) are experiencing a spontaneous [2 + 2] cycloaddition reaction activated by the intensity with the different frequencies.

10.4 Electro-Active SMPs

10.4.1 SMP Packed by CNT

Goo et al. present that shape recovery through an electronic flow of controlling SMP alloys using carbon nanotubes, just through implementing mild warming [67–69]. These achievements can prompt the use of SMPs as techno-initiate sensors, which are critical throughout varied uses down-to-earth, such as shrewd actuators for small-scale ethereal vehicle control. Throughout its surface altered in a mixed solvent with nitric acid and sulfuric acid, multi-walled carbon nanotubes (MWNTs) are used toward its production with interfacial keeping between polymeric materials and permeable additives that obtain guiding SMPs.

In the request for 10^{-3} S cm for tests, the electrical conductivity throughout its compound estimated with its four-point testing phase is 5wt per cent-modified MWNT material. While that measurement for altered MWNT material increased, electrical conductivity also increased. The electrical conductivity in its substrate-adjusted MWNT compound to a comparable filling material is less than those among composites filled for uncontrolled MWN. That is also ascertainable from extended abnormalities due to corrosive process throughout the layout of carbon-carbon bonds formed mostly on nanoparticle's layer. This drastic improvement within nanomaterials took its electrical conductivity down completely. Subsequently, its mechanical and electrical properties were also dependent upon the substrate modification degree of its MWNTs, as well as the destructive process around 90°C gives their form memory impressive features.

10.4.2 SMP Filled Through the Electromagnetic Filler

By integrating superparamagnetic surface-changed nanomaterials through shape-memory material networks, complex shape developments are far from activated via electromagnetic fields. Perhaps between this ranges from 2 to 12 wt percent magnetite nanomaterials forming just as small accepting lines with electromagnetic field heating seem to be the polymeric matrix developed utilizing oligo (ϵ -caprolactone) dimethacrylate/butyl acrylate. Then materials' unique failure effect is determined to be 30Wg^{-1} about 300 kHz as well as 5.0 W. Neither any additional thermal gradient is detected mostly during structure shift around 43 °C.

The electromagnetically actuated shape-memory impact of the test shown in Fig. 10.8a, mostly for rectangle frame, that one used illustration extracted with a composite film, referred with at its permanent form. Upon heating around 70 °C, it is distorted to a helix and cooled by the formation of an oligo(ϵ -caprolactone) crystal structure to stabilize its simple form. That illustration retains the helical shape despite any external forces since that implementation phase, as shown in Fig. 10.8b. That structure shift in the 300 kHz AC field was captured using a specialized webcam.

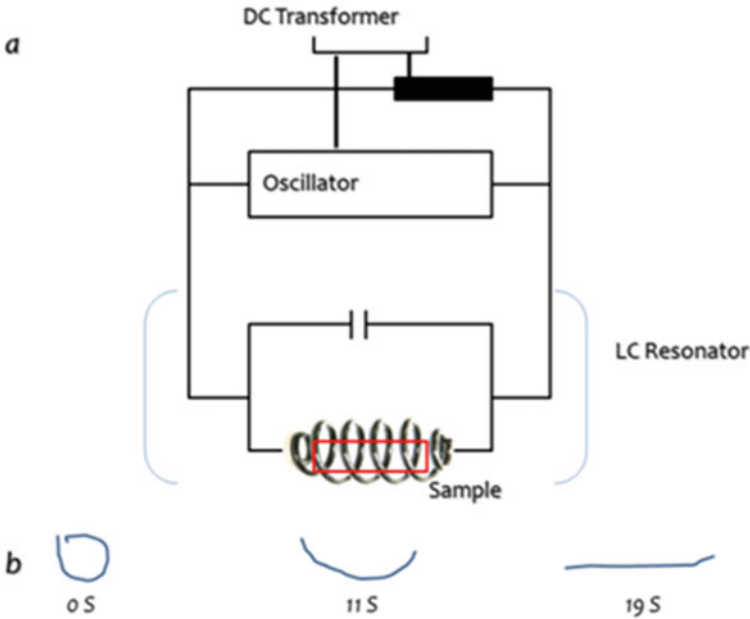


Fig. 10.8 **a** LC resonant circuit-based HF generation schematic diagram **b** shape-memory transition picture sequence caused by its influence of even an electromagnetic HF field

Upon 10 s, the helix's initial transformation was observed, consuming around 10 s until complete. Including a certain residual range of motion, the last form is close to the first bar due to corrosion between the fragile material and its crystal surface. Throughout its way, a temperature control warming indicated—their heat including its state during its sample [70], its observed time window was inappropriate to correspond to its heating rate.

10.4.3 SMP Packed Through Ni Chain

Leng and Huang include attractive substances under SMP; in the restored procedure, such specimens framed blocks by adding a desirable region. SEM photos show that solitary chains are getting with a position around 1% for Ni through volume. Formed cross-chains through each growth to Ni material, however, toward its result, unfaltering Ni link interpreted (Fig. 10.9, left section). During several prolonged shape recovery phases, Ni links remain (Fig. 10.9, right section), that shows their possibility that use anchored polymeric materials to copolymer incitation [71].

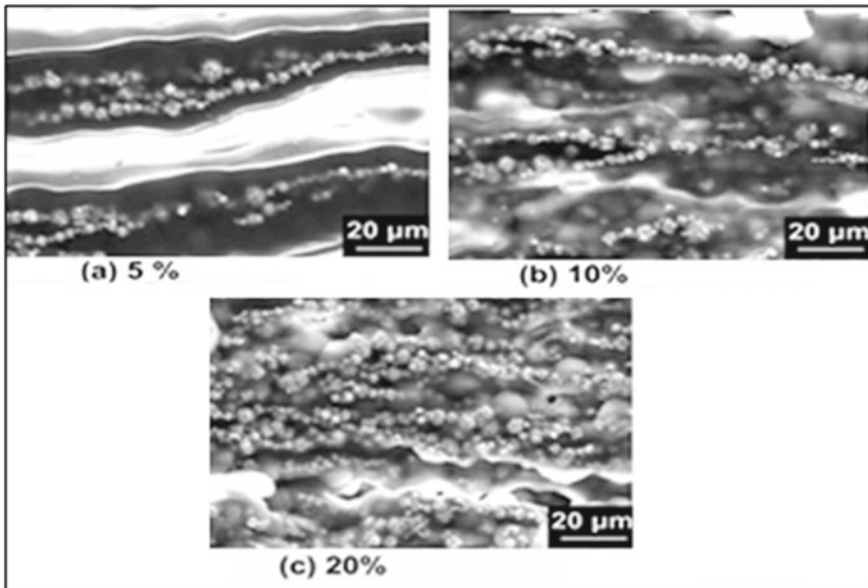


Fig. 10.9 SEM Images **a** 5%; **b** 10%; **c** 20%. Reprinted from [71]. Copyright © 2008 with permission of AIP Publishing

10.5 SMP Composites

Compared to composition-memory metals and pottery, the lightweight, minimal effort, easy handling, and strong reclaimable stretch allow polymeric materials great possibilities for some planned applications. The inconvenience of SMPs in their lower pressure recovery than SMAs, under imperative circumstances, limits their use in particular applications. SMPC progression offers the response to this dilemma, which makes them more grounded enough to generate greater stresses of recovery. In this way, several examination efforts also concentrated on extending that weak overall firmness but low recovery concern of SMPs across its enhancement with polymers that join the structure storage component for its structural component.

In any structure, its fuse through fortification provides structural solidity, quality, and incitement throughout their structural system. The fortification may be nanoparticles, carbon strands slashed, glass. The polymer material can be attached to certain fillers such as carbon dark, carbon filaments or cylinders, which enables its material to activate via the effect of Joule when providing the structure current flowing. SMPCs including attractive substances, such as iron oxide can thus become inductively stimulated through a presentation with the attractive rotating sector.

10.5.1 Carbon Black (CB)/SMP

In the electrical and gadget sector, polymer composites loaded by guiding CB include wide implementations such as chemical conduits, sub-transmitters, and energy moving devices mostly within the area including electricity and gadgets. CBs do seem to be not very effective in enhancing the structural quality and size recovery concerns of SMPs, in contrast to nanoparticles and nanostructure. In addition, CBs seriously damage its recovery with SMPs by structure. Li et al. arranged composites of polymers against its confidence because SME composite materials possess good thermal and electrical conductivity [72]. Such polymers developed through bonding procedure as well as accumulation arrangement. Thus, CBs decreased the proportion of shape recovery and the velocity of SMPU shape recovery, particularly for a higher material, that was due to its decreased crystallization with its CBs SMPUs. Through softening blending, Gunes et al. arranged CB/SMPU composite materials thus observed which only its sensitive portion particle size decreased through some supporting role for CBs over brittle segment compatibility throughout representation [73].

10.5.2 Carbon Nanofiber (CNF)/SMP

CNTs and CNFs were also viable for enhancing their structural efficiency including structure recovery problems under SMPs due to the remarkable make matters including large elastic tensile strength to elevated perspective proportions. Making use for smaller scale the dual-screw extruders, polymers, accumulation including composite cross-linking of the CNT/CNF substrate and in site polymerization [74–78] in efforts to increase the CNT/CNF dispersion in crystal lattices.

Through dissolving mixing during its link enhancements for any Tm form SMPU, Gunes et al. developed CNF/SMPU materials, which use in CNF, which were 60–200 nm throughout the thickness and 30–100 mm long. Each CNF has decreased its SMPUs, structure memory ability, which was due to the interruption including its crystallization from a sensitive section by the CNFs. In quite another previous investigation, Jimenez and Jana organized CNF/SMPU nanocomposites by in situ synthesis inside a disturbed mixer through unruly 2D blending [79] may boost that dispersion from CNFs throughout the polymer network. Those CNFs shown are oxidized mostly to substrate. Polymers equipped with oxidized composites on the substrate displayed greater dispersion, particle size, manageable characteristics, including stronger recovery strength compared to their uncontrolled CNF partners.

Through arrangement blending, Koerner et al. produced CNF/SMPU polymers throughout both permanent dissolvable with mild disappearance to each dissolvable [80]. A standard measurement with those CNFs was 100 nm while indeed its duration exceeded Ten meters. Inhomogeneous nanocomposites, that extended their elastic modulus over some rate between 2 and 5. Leading to the enhanced condition of crystal

growth, design atomicity enhanced. Shape-memory polymers have a homogenous distribution between 1 and 5 vol. Once tested using unmitigated SMPs. Up to half the percentage of CNFs created more recovery stress. Ni et al. thereby combined CNF/SMPU polymers into high-frequency distribution through a response-blended process [81].

Either width or even distance for its CNFs is about 150 nm as well as 10–20 nm. Each recovery problem of polymers extended double by unadulterated SMPUs around 3.3 wt. percent CNF layering. MWNTs synthesized by aniline under high temperatures with its scale of about 15 nm and a distance of about 50 nm. Its tough part, alongside MWNTs, found to restore their warped version. MWNTs/SMPU materials structured through in situ synthesis following MWNTs concoction functionalization [82]. Furthermore, these found how CNTs have the potential to boost SMPUs' recovery issues. CNTs have also been used to reinforce phase change polyvinyl liquor (PVA) despite its SMPU structure.

Miaudet et al. assembled storage spans of CNT/polyvinyl liquor (PVA) with its special crystallization turning method [83]. Throughout its co-streaming system with that crystallizing PVA process, polymer stable CNTs were injected. This overall pressure produced for these polymer membranes pronounced over those generated with normal SMPs about 1 or 2 major degrees. Its intensity during regeneration was far above SMAs. The analysis shows how CNTs/CNFs were convincing SMPs to boost their solidity and recovery issues. Similar dimensions to CNTs and CNFs will provide significant consequences to their crystallization for sensitive sections with SMPUs [84]. Each result regarding its effects for heterostructures supplements influence between different SMPs in composite materials was not accurate. Such contradictory findings may be attributed to such difficulty with polymer composites preparation. Several parameters, such as preparation processes, filler acquisition, design, filler scale, including perspective ratio and structure existence, were profoundly affected by their characteristics among its past structural objects.

10.5.3 Nano SiC/SMPs

SiC will strengthen flexible modulus with SMPs using a filling substance, incorporating silica through tetra ethoxy silane (TEOS) towards SMPU framework [85]. With TEOS 10 wt.% material, it intensifies shattering stress, as well as a module, is collected. Liu et al. reinforced storage polymer thermoplastic form to SiC particles [86]. That SiC nanoparticles were applied throughout the group process with their hardener. Each SiC extended its form information latex elastic tensile strength. For this SiC material at 20 wt.%, its advancement capacity increased by nearly 50%. Their fraction of form regeneration, as well as regeneration velocity, decreased, but throughout the comparison, Gunes et al. noted its detrimental effect from SiC onto its SME for SMPUs that they attributed to SiC's dramatically reduced sensitive sample crystallite size.

10.5.4 Self-Healing Composites

The self-mending substances are grouped into three classes, to be specific: case-based, vascular, and inherent, which were illustrated in Fig. 10.10a, b, c [87]. This area presents an outline of the methodologies utilized to set self-up mending materials and the striking highlights for each approach.

10.5.4.1 Container-Based Self-Mending Materials

At the point when a split bursts the containers or harm, oneself mending system is set off which delivers the recuperating specialist in the area of harm (Fig. 10.10a). After delivery, the nearby recuperating operator responds with the impetus to yield a hardened polymerized organize.

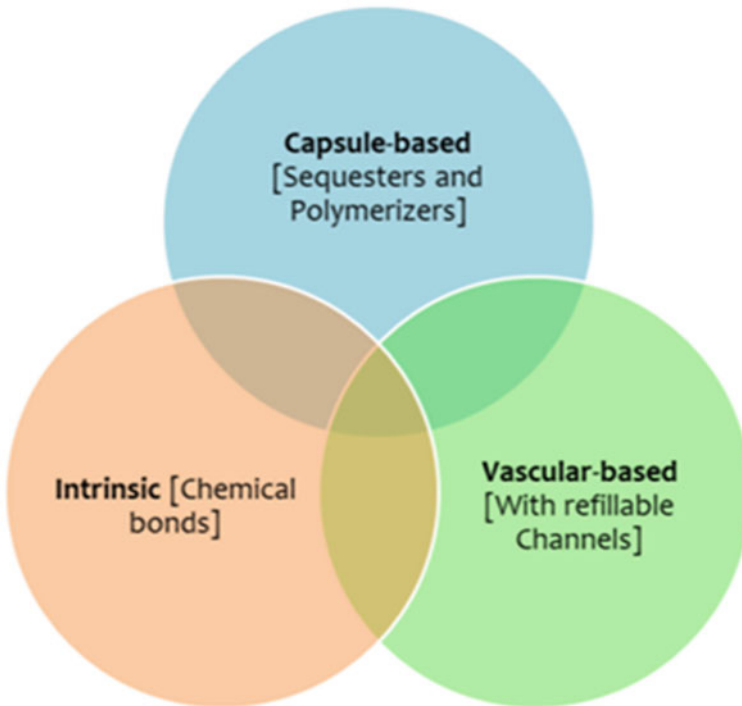


Fig. 10.10 Types of self-mending materials

10.5.4.2 Vascular Self-Mending Materials

Sequester the recuperating specialist in a system as vessels that may be interconnected, until harm triggers self-recuperating (Fig. 10.10b). After the vasculature is harmed and the principal conveyance of a mending operator happens, the system might be topped off by an outer source or from a flawless yet associated area of the vasculature. This topping off activity takes into consideration various nearby recuperating occasions.

10.5.4.3 Characteristic Self-Mending Materials

Self-mending materials do not have a different recuperating specialist yet have a self-mending instrument that is set off by harm or by an outside upgrade (Fig. 10.10c). These materials depend on connection portability as well as trap, flexible polymerizations, thermoset phase loosening, hydrogen holding, or ionic collaborations to begin with oneself mending process. Since every one of these responses is reversible, numerous mending occasions are conceivable.

10.6 Hybrid Composites

Haphazardly appropriated nano-sized fillers strengthen the hybrid composites, additionally named nanocomposites. For SMPCs, two sets of fillers were used for micro polymers. Silica, mercury, nitrides, minerals, also transition metals are part of its main category. Such coatings have a much stronger compressive strength over any polymer network. These may gradually enhance their mechanical characteristics throughout each SMP system, which could even often have been designed to include the new enhancement approaches via its strength processor. Polymer coatings, including celluloses, transparent composites, including thermoplastic, are its corresponding array.

10.6.1 Cellulose

Cellulose is another essential material that normally occurs through its storage within environmentally friendly plants, cells that are used to produce papers and polymers. Cellulose possesses outstanding biocompatibility. Its raw products with polymers could easily be restructured through soaking into liquid hydrogen bonds stocks that must be easily generated as well as extracted from its hydroxy array within cellulose. For reinforcing polymeric materials, for enhancing their mechanical properties or their structure sensitivity with liquid, celluloses were selected earlier. Through contrast, Auad et al. discovered that cellulose alternative improves its boiling rate

but PU fragile segments, crystallization heat that produces its crystallinity [88]. Zhu et al. found whether each polymers structural ability module displays some flexible variation throughout their moisture cycles [89–91]. This ability module steadily decreases when wetted, and then structure recovery was switched apart. That wet state with cellulose is chosen for stabilizing its structure throughout polymers composites, as well as certain entropy mobility within a PU system was utilized for allowing its recovery for its structure.

10.6.2 Crystalline Polymers

Each shape-memory method for ambiguous SMPs depends on an extraordinary variation across its T_g during the accumulating period. This weakening advancement for polymers provides every aspect, which achieves phase change effects despite crystal changes. Each compound exhibited two autonomous changes separately, the glass progress of the epoxy lattice and the liquefying change of PCL filaments. Correspondingly, the capacity modulus bends show two uncommon drops, individually, throughout T_g with adhesive and smoothing temperature (T_m) of PCL.

The semi glass-like stage can be utilized to achieve a temporary phase change effect through weakening and recrystallization yet should be cross-connected with the atom organization. Along these lines, reversible SMPs cannot be named composites. Another utilization of glasslike polymers is to bring oneself recuperating features into SMPCs. Later splits starting in the SMPCs, glasslike parts are being melted during breaks beginning throughout each SMPCs via raising their heat toward recovering any fracture.

10.6.3 Elastomers

Elastomer seems to be another indistinguishable material of T_g well below room temperature, also despite weak Young's modulus but mostly strong dissatisfaction pressure, which displays good flexibility near low temperatures. This elastomer will accelerate this process of phase transformation or change its heating rate. Those electrospinning PVA molecules are introduced within its polyether squared amide elastomer (PEBA) [92]. PVA prompts products to over shape-memory characteristics; however, SMPCs to its stronger PVA product demonstrate greater structure constancy toward recovery. To generate recyclable SMPCs, that be agreed to provide wide usage across biomedical regions, this qualitative procedure was used. Zhang et al. mounted polylactic corrosive (PLA) strings through polymers of poly trimethylene carbonate, which can achieve 3D structures of compostable structure processing [93].

10.6.4 Multi-Fillers

Leng et al. studied different polymer mechanisms for enhancing its electronic & thermal tensile strength in SMPCs. After designing, certain interaction depends on CB, their extension for CNTs moves around as a large range charge carrier, but their interruption through SMPCs reduced through each substantial extent. Ag nano-materials as Lu et al. used as composite filaments established a three-scale bridge structure whereby electrical conductivity becomes continually enhanced [94]. 3D graphite structure creates porous polymer foamed as well as Ag NWs move around with constant conductance. Guo et al. used Al nanomaterials with shattered graphene polymers that reinforce SMPs which noticed that SMPCs for its strongest structural characteristics with 7 wt. % graphene molecules of 1 wt. % Al nanoparticles [95].

A warm conductivity and crystal structure flexural strength were typically never the same to polymers, such as CNTs, CNFs, and CB. The feeble design between matrix and additives regulates its representation for SMPCs due to their extreme range with structures. Raja et al. used metal nanoparticles to light up CNFs to strengthen their surface characteristics, creating CNT/metal/PU SMPCs around this phase [96].

This improved design among CNTs and PU was associated with its excellent dispersion for CNTs throughout each PU. CNTs enhance their thermal and mechanical tensile strength within SMPCs through optimizing nanomaterials. In softening oxide, Gong et al. self-assembled Fe_3O_4 across their β -cyclodextrin (β -CD) substance that has been attached for its CNTs to obtain nanostructures CNTs, but then compostable SMPC fibers developed via electro-turning process, similar approaches were achieved [97]. Lu et al. assembled aluminum nanomaterials through carbon molecules via wavering to strengthen its design, altered their Al layer with silicon oxide assemblies, and then inserted carbon fibers within epoxy SMPs [98]. That modified Al interfaces for siloxane can enhance their interfacial properties among carbon molecules and the epoxy system, thereby demonstrating fast structure recovery by its SMPCs.

Multi-capacities may also be introduced through SMPCs by using multiple fillers, however, for their coordination among various polymers, structural activities, as well as implementation with phase transformation, were extended by Liu et al. Moreover, polymeric SMPCs have been developed via chemically cross-connecting nanomaterials of cholesteric celluloses (CCs), PCL, and PEG [99]. For sensitive components, such SMPC interacts through PCL and PEG, and CC nanofillers to display their excellent effect towards thermally and liquid smart material applications.

10.6.5 Patterned Composites

To bring more structure capacity into SMPCs, the specialist additionally attempted to design the fillers. Within its external field, the starter effort is to change strands, and the modified nanoparticles must increase their compressive strength as well as

conductivity or even fracture strength across each path of its material. Meng and Hu used adjusted nanoparticle additives that reinforce SMPCs then reported whether their adjusted CNTs can assist which putting away and delivering flexible vitality and quicken shape recuperation [100]. Yu et al. adjusted the nanoparticles within its external electrical field, which observed whether its electromechanical porosity among SMPCs changed CNTs are decreased over then many occasions while ones containing outside electrical field were compared [101].

10.6.5.1 Nano Papers or Bucky Papers

CNF nano paper-enhanced SMPCs [102, 103], a constant and smaller mechanism used in the nanopaper through that its in-plane conductivity was enhanced. Through its rise in nanopaper size, thermal conduction for SMPCs increases, but their proportion of recuperation decreases. By implementing voltage, the Joule heat produced by the inner sections of the nanopaper, as well as its adjusted nickel nano strands promote the transfer of heating from the nanopaper to the SMP lattice. The recovery proportion routinely extended to about 100% by this strategy. A comparative approach was likewise utilized by Lu et al. [104] to narrowly change nanoparticles in an attractive sector.

Lu. et al. combined hexagonal BNs with CNF nanosheets, that improved their structural relationship among CNF nanopaper and polymer networks [105]. Its electrical conductivity for SMPCs as well as the thermal conductivity including its layer-filling device was enhanced with hexagonal BN molecules. The above technique, therefore, speeds the electro-initiated structure recovery. Wang et al. used this to reinforce polymer SMPs [106]. During their main process, its composites show marvelous reliability; however, fast recovery is achieved when implementing some minimum of around Six Volts.

10.6.5.2 Surface Patterns

Each illustration of the substrate was an option that performs with its multiplier of strength. This substrate illustration could also capably design processed, as well as implemented boosters with contrasting and overlapping polymer. Especially early polymers equipped to alter their 2D form sheet into their 3D forms used for their enhancement by four-dimensional manufacturing. Liu et al. designed this modern and simple method for dealing mostly with collapse between sensitive polymer sheets using light [107]. Each sheet made of optically simple but well before PS would shrink while heated throughout its plane. Along such PS layer, deep color patterns were drawn that serve with light persistence that generates heat mostly in the surrounding. That pre-strain can recover only on points where PS gets heated it T_g , and thus allow each linear layer to overlap through just any 3D shape.

Davis et al. make understood that the heating communicates bit by bit from the dye part toward their reverse part across any layer, whereas the heating angle constantly

relaxes the pressure throughout each layer thickness [108]. Lu et al. objected to this throughout their open recovery phase, increasing temperature, as well as quitting fragments; this was another demanding aspect for conflict adjustments. On the SMP network, Zarek et al. reprinted its Ag unit but used sufficient Joule temperature for push influences onto shape-memory [109]. Similarly, Wang et al. reported CNT surfaces against SMPs [110].

10.6.5.3 Oriented Fibers and Laminas

Ge et al. raise its probability to flexible polymers through expertise using either changed lamina through using mechanical and thermal preparation initially [111]. That flexible polymer, consisting of coated SMP fibers and elastic membrane, is created through 3D modeling. Two laminas are included within certain polymers. One comprises SMP fibers, but the other is never. Those flexible polymers, supposedly 4D manufacturing, will crease into their 3D design.

To configure some polymers, their temperatures must initially increase beyond T_g through coated fibers, polymers could have expanded throughout this stage then finally, with keeping stacked, their expansion within filament will be balanced while lowering temperatures below T_g . fibers grow larger than its elastic matrix throughout that process during processing. Those polymers will bend through ejecting its layer, produced through its tension jumble between two layers. Through order that achieves freezing anisotropic shape-memory effects, Robertson et al. even used PVA with structure fixation including PDMS with its sensitive network [112, 113]. A crystalline lattice will illustrate identifiable distorted forms of different fiber hyperlinks. Complex 3D designs constructed with any polymer layer due to its strain interaction between elastomers and SMP particles. Yuan et al. used another indirect concentric circle triggered through warmer extension [114]. By contrast, Ding et al. used its strain mishmash created throughout 3D printing through the polymerization process, which transmitted its strain through heating. While processing, its paint expansion of the essential relief surfaces throughout its low related elastomer lamina generates this residual strain throughout each elastomer [115].

10.7 Multi-Blocks

A few fields were composed of multi-square polymers, but that section had its outstanding asset. He et al. originally put forward such an approach [116]. They developed tri-square composites, polymers loaded with CNT, gross SMPs, including composites loaded with Fe_3O_4 individually. To ensure strong configurations, their three elements utilize identical epoxy SMPs. For its chronicity around 13.56 MHz, CNT-packed polymers will sustain their radiofrequency, or for 296 kHz, Fe_3O_4 packed polymers absorb its radiofrequency (RF). In such a manner, those SMPCs will have implemented progressively implementing RF at different frequencies.

A quantitative technique has been achieved by Li et al. [117]. They accidentally used that enticing 30 kHz region that activates this region loaded with Fe_3O_4 particles. Notwithstanding specific vital transformations, various areas with various T_g can likewise be utilized to accomplished successively collapsing. Yu et al. planned the interlocking structure with a few pivots [118]. Each pivot with an alternate T_g . While submerging in high-temperature water, that pivots within this smaller T_g will recuperate quicker. Subsequently, the shape recuperations along the interlocking structure are progressively set off.

10.8 Controlled Behavior of Composite Material (CBCM)

Using substances including piezoelectric, electrostrictive, magnetostrictive properties including storage alloys of form, several structured polymer composites were developed. Such designs have discovered possible uses, however, display issues identified with weight and interfacial bond. CBCM is a fiber-strengthened polymer composite plate; the guideline is to utilize warm anisotropy properties of the overlays to acquire the ideal shape in a warmed plate [119, 120]. Additionally, the CBCM plate is warmed inside by utilizing electrically conductive carbon filaments.

10.9 Applications

10.9.1 4D Printing

4D printing would be another late-generated invention that relies on upon around 3D printing, however, has its embedded ability that alters structure through response toward normal as well as necessary external rises [121]. This final indicator is used for 4D printing to sensitive components because this stimulates models, which modify their form over a certain duration through any acceptable raise. Furthermore, 4D printing combines, sensitive substances through technologies by processing added substances that give some smoothed out a path by thinking via practise and utility guided by implementation changed directly onto each material [122].

Frameworks manufactured utilizing unpretentious surface micropatterns and showed dynamic remotely invigorated 4D shape changes. 4D printed shape-memory polymers with thermally prompted recuperating capacities were introduced by Suriano et al. besides, accomplished through advanced light forecast innovation [123]. Sensitive LCE-based designs rendered using 4D manufacturing improvements. Throughout its printing process, control across its position with its LC heading deposited substances. That allowed their scale and dimensionality of the strain could be effectively programmed, thus thereby their system's 3D pattern behavior. Through this different approach, thermally sensitive LCEs immediately

written through their regulated elemental demand are deposited onto 3D shapes. After manipulating its printing system utilized for creates their 3D element employed that monitor their improvement response, this sub-atomic query has been individually tailored. Upon heating, the modified LCE fiber encountered some 40% flexible contractions across that its printing header. Enhanced structure adjustments were recognized by printed images of managed measurement as well as reactivity improvements.

4D biological printed technology relies upon through its mixture with adaptive biomaterials improvements throughout each advancement with 3D biomanufacturing which produce inherently flexible developments which always could change its designs and achieve optimal utility through desired incitement, such as inundation in water. This methodology allowed empty self-collapsing tubes manufactured with exceptional authority across its sizes as well as layouts against higher targets. Two diverse biomaterials were used in designing polymers to demonstrate their flexibility within this technique.

10.9.2 Stents

After inflatable angiography, stents become extensible platforms designed to anticipate vasospasms including restenosis within its vessel. In cardiac stent discussions, making use of that structure effect suggested that reduce maximum catheter width through transport and negotiate heavily regulated as well as a personalized structure under room temperature [124]. Using photopolymerization with tertbutyl acrylate and PEG dimethacrylate, size molecular structures were optimized for giving exact control throughout its platform's mechanical and thermal reactions. While each portion with T_g , cross-linking size, numerical diameter, including disfigurement temperature, its enhancement mechanism for its polymer stents only near the heating energy stage has been focused, that would everything been regulated independently. It is illustrated that normal temperatures processing with its stents were unusually sensitive with T_g as well as cross-links thickness. Furthermore, this forced response for stents is found to depend on cross-linking size. A wide range with a structure including microstructural processes was shown in the proposed polymer system, which fit that, satisfies its basic requirements for negligibly obstructive cardiac equipment.

Wang et al. as of late showed a compostable structure sedate solubilized catheter by double medication discharge patterns [125]. The stent indicated a shape-memory impact, transforming from a transitory direct structure to a perpetual winding shape with the changing temperature near the internal heat level. The stent could reasonably deliver the anticoagulant tranquillize for more than 14 days and the counter multiplication sedate for more than 70 days. Within those initial stages, such combination among distribution patterns reduced red blood cell control but doused extreme abundance for lengthy shape-memory ceramics, thus moderately influencing their validity of HUVECs.

10.9.3 Vascular Repair Devices

Through their use with any cardiovascular repair tube, their combination with structure but also self-recovering characteristics within each structure matrix may remain beneficial [126]. The vessel might be broken because of a medical procedure or under harm, while the regular vascular fix may include tedious embroidery. Thus, utilization of form recovery capacities of SMPs could prompt the least obtrusive techniques using shape recuperation systems. The implanted semi-glasslike thermoplastic served a double job in the exchanging stage for shape-memory capacity and the recuperating for oneself mending conduct. The composite could be used like a fixed cardiovascular tube. Moreover, the thermoplastic pipe has a length of ~10 mm including distinctive inward/external widths were designed throughout such purpose. The cylinder was extended and compacted through 1/2 width around 70 °C for this short shape, trailed after sealing the size within its wake of chilling off. It fully recovered the underlying form after warming.

10.9.4 Aerospace Applications

SMPs have one unambiguous bit of leeway, especially when thinking about aviation's uses: its load. With its improvement toward modern SMPs for aviation uses, gigantic efforts are welcomed. SMPs are of extraordinary enthusiasm for minimal effort self-deployable structures, e.g., sunlight-based clusters, sun-oriented sails, sun shields, or radar receiving wires [127].

Physical assembly techniques as well as animatronic devices, separately, probably become wayward due to its extreme density, considerable costs, overall tremendous volume needed. Constructions based upon its invention of pleasant sleep versatile memories investigated within these environments. Through their T_g , its initial arrangement gets heated then folds across its short form. These returned as efficiency following freezing. That framework becomes heated further following its automobile toward vacuum, inflaming the recovery of its form. These frameworks would diminish the mass of the absolute framework impressively. First trials under smaller scale gravity uncovered that the SMPs show comparative SME contrasted with probes the ground [128].

In terms of sophistication among such personality uses, its consumption with SMPs toward aircraft transformation remains sensitive even its a further level. Through their flight, each transformation with its aircraft will alter their structure within each wing, which corresponds toward its existing necessities [129]. Such requirement was synopsis: their feathers among winged insects were away but rigid. That unusual skill was some notable demonstration for any Golden Eagle moving through a drop plane. SMP may probably be implemented independently that change their arrangement around either exterior throughout that wing including their basic condition within each wing inside.

10.9.5 Industrial Applications

Early improvements in SMPs incorporate polynorbornenes and styrene-butadiene copolymers. Polynorbornenes and styrene-butadiene copolymers were used in early improvements in SMPs. The revelation of acrylic thermoset shape-memory eliminated its problematic preparation among its previous composites. As a result, certain products have encountered several broad varieties with applications, as protective tags and self-conveying benches, among examples. These materials are intriguing for transforming frameworks. Furthermore, SNPs are considered a quick fix and assurance arrangement.

10.9.6 Electronics

Using SMP for its surface with implementation sheet, several phase change composite flexible electronic devices, namely shape-memory polymer light-radiating diodes (SMPLDs) and shape-memory polymer dainty film semiconductors (SMPTFTs), were developed. Simple Polymers such as thiolene/acrylate SMP, cross-connected polyacrylates with shape-memory including poly (tert-butyl acrylate) besides shape-memory were used as polymers within several LED devices [130, 131]. Similar illustrations might retain consistent fluorescent characteristics during enormous misforming even over several phases to bowing; recovery would provide sufficient capacity to provide fit bit displays.

Another regularly utilized substrate for SMPTFTs is thiolene/acrylate SMP with a T_r of 70 °C when placed into the physiological condition, the dissolvable incited plasticization would significantly decrease its T_r to 37 °C, which is near the internal heat level. Such a particular system enables certain substances perfect for medicinal injectable devices. For any relatively rigid system, their devices based upon such substance would remain embedded, whereas then that processing would allow those devices to comfort each tissue then boost their layout.

10.9.7 Civil and Architectural Engineering

SMP-based foams with self-mending characteristics are traditionally used. Using polymeric materials for coatings has, therefore, been a particularly important feature for architectural engineering. Especially, polymeric materials of adjustable temperature-detection potentials will have the ability to identify revolutionary uses to auxiliary fellow humans [132]. The use of embedded sensor and actuator technologies in structural elements allowed by SMP composites that could detect the burdens, loads, and various components placed on them, giving basic well-being observation and control during administration conditions. Despite its large structure recovery

temperature changes, moderately low recovery stress, slow recovery rate, including single-direction structure storage by several current SMPs, there are important as well as energizing challenges to including SMPs under built situations [133].

10.10 Recent Progress and Prospects

The benefits of SMPs incorporate lower thickness, lower cost, simpler preparation, bigger recoverable strains, and so on. This generally small module which results in its lower recovery stress, its lengthy response duration, even lower cycle life, including its impotent tensile stress is some fraction among this retract with SMPs. Polymeric materials are enthusiastic about creating medical devices. Central shape-memory research focuses on introducing enhancements rather like heating for the trigger as well as remotely inciting shape-memory polymers. These initial methods include its glow stimulation with shape-memory composites with its use for attractive field substitution. With the vast variety of possible uses explored as well as within the initial mechanical uses, just some commercially usable polymers are being identified. Such fact would become another crucial catalyst again toward its development with SMPs including that usage. Finally, among its greatest interesting polymer groups within this area for functional composites are shape-memory polymers. These were beyond fabricated materials demonstrating parts of the exceptional properties of natural materials. In light of the aggregation of the ongoing works here, endeavors to create 4D printing innovation as a reasonable device in cutting-edge assembling and prototyping are required to extend quickly sooner rather than later.

10.11 Conclusion

SMPs phase change effect, as well as adjustable flexural strength, might spend extra capacity on flexible electronic devices, causing further SMP-based efficient technology area to be explored. Depending on types of SMP polymers, glow diodes, delicate picture electronic components including optics accessories rely on. Any from its SMPs extraordinary properties would prove profitable with unique uses. Besides, its reduction experienced by a considerable difference in temperatures and thiolen/acrylate SMP compressive strength following inundation during biomedical conditions makes this material suitable for biological uses to SMPFEDs. Throughout its development with SMPFEDs, their manufacturing technology is currently being used flexible devices, comparable toward moving printer development. This latest update of 4D manufacturing promises that combine SMPFEDs even further muddled abilities.

Similarly, its incitation with SMPFEDs might refer to its usual triggering strategies with SMPs that fulfill identifiable basic requirements besides implementation. However, with SMP-based flexible technology to realistic uses including business creation, there were still numerous problems. All usage by SMPFEDs will be extended by its association among SMP materials systems, through large advancement temperature ranges, huge device varies including two-way or separate shape-memory effects, enhancement with novel manufacturing strategies toward electronic gadgets.

Acknowledgements We thank our lab members for their valuable suggestions.

Author Contributions GVSSS contributed conception and design of the study; writing the first draft of the Manuscript. Authors MPN and ZA helped us with the literature, MC wrote sections of the manuscript and formatted the manuscript, including editing and refining. All authors read and equally contributed to this manuscript.

Conflict of Interest The authors declare that this is independent with no commercial or financials involved and have no potential conflict of interest.

References

1. Xie T (2011) Recent advances in polymer shape-memory. *Polymer* 52:4985–5000
2. Behl M, Lendlein A (2007) Shape-memory polymers. *Mater Today* 10:20–28
3. D Ratna J Karger-Kocsis (2008) Recent advances in shape-memory polymers and composites: a review. *J Mater Sci* 43:254–269
4. PT Mather X Luo IA Rousseau (2009) Shape-memory polymer research. *Annu Rev Mater Res* 39:445–471
5. Xie T (2010) Tunable polymer multi-shape-memory effect. *Nature* 464:267–270
6. Gall K, Dunn ML, Liu Y, Finch D, Lake M, Munshi NA (2002) Shape-memory polymer nanocomposites. *Acta Mater* 50:5115–5126
7. Chen S, Hu J, Zhuo H (2010) Properties and mechanism of two-way shape-memory polyurethane composites. *Comp Sci Technol* 70:1437–1443
8. Wang Y, Tian W, Xie J, Liu Y (2016) Thermoelectric responsive shape-memory graphene/hydro-epoxy composites for actuators. *Micromachines* 7:145
9. Leng J, Lan X, Liu Y, Du S (2011) Shape-memory polymers and their composites: stimulus methods and applications. *Prog Mat Sci* 56:1077–1135
10. Lendlein A, Kelch S (2002) Shape-memory polymers. *Angew Chem Int Ed* 41:2034–2057
11. Liu Y, Du H, Liu L, Leng J (2014) Shape-memory polymers and their composites in aerospace applications: a review. *Smart Mater Struct* 23:023001
12. Liu Y, Lv H, Lan X, Leng J, Du S, (2009) Review of the electro-active shape-memory polymer composite. *Comp Sci Technol* 69:2064–20688
13. Yu K, Liu Y, Peng H-X, Leng J (2013) Mechanical and shape recovery properties of shape-memory polymer composite embedded with cup-stacked carbon nanotubes. *J Intel Mat Syst Struct* 25:1264–1275
14. Behl M, Razzaq MY, Lendlein A (2010) Multifunctional shape-memory polymers. *Adv Mat* 22:3388–3410
15. Jiang H, Lendlein A, Langer R, Junger O (2005) Light-induced shape-memory polymers. *Nature* 434:879–882
16. Himuro Y, Tanaka Y, Sutou Y, Kainuma R, Ishida K, Omori T (2010) Ferrous polycrystalline shape-memory alloy showing huge superelasticity. *Science* 327:1488–1490

17. Hogan PM, Tajbakhsh AR, Terentjev EM (2002) UV manipulation of order and macroscopic shape in nematic elastomers. *Phys Rev E Soft Matter Phys* 65:041720(1–10)
18. Keller P, Thomsen DL, Pink R, Naciri J, Shenoy D, Jeon H (2001) Liquid crystalline elastomers with mechanical properties of a muscle. *Macromolecules* 34:5868–5875
19. Kelch S, Bellini LA, Langer R (2006) Polymeric triple-shape materials. *Proc Natl Acad Sci USA* 103:18043–18047
20. Gil ES, Hudson SA (2004) Stimuli-responsive polymers and their bioconjugates. *Prog Polym Sci* 29:1173–1222
21. Varghese S, Lele AK, Srinivas D, Sastry M, Mashelkar RA (2001) Novel macroscopic self-organization in polymer gels. *Adv Mater* 13:1544–1548
22. Chambers M, Zalar B, Remskar M, Zumer S, Finkelmann H (2006) Actuation of liquid crystal elastomers reprocessed with carbon nanoparticles. *Appl Phys Lett* 89:243116(1–3)
23. Yang LQ, Setyowati K, Li A, Gong SQ, Chen J (2008) Reversible infrared actuation of carbon nanotube–liquid crystalline elastomer nanocomposites. *J Adv Mat* 20:2271–2275
24. Bastiaansen CWM, Harris KD, Broer DJ, Lub J (2005) Self-assembled polymer films for controlled agent-driven motion. *Nano Lett* 5:1857–1860
25. Bastiaansen CWM, Harris KD, Broer DJ (2006) A glassy bending-mode polymeric actuator which deforms in response to solvent polarity. *Macromol Rapid Commun* 27:1323–1329
26. Hu JL (eds) (2007) *Shape-memory polymers and textiles*. Introduction, Woodhead Publishing, Elsevier, The Netherlands, p 360. Hardcover ISBN: 9781845690472
27. Leng JS, Huang WM, Lan X et al (2008) Significantly reducing electrical resistivity by forming conductive Ni chains in a polyurethane shape-memory polymer/carbon-black composite. *Appl Phys Lett* 92:204101(1–3)
28. Cho JW, Kim JW, Jung YC et al (2005) Electroactive shape-memory polyurethane composites incorporating carbon nanotubes. *Macromol Rapid Commun* 26:412–416
29. Ni QQ, Zhang C-S, Fu Y, Dai G, Kimura T (2007) Shape-memory effect and mechanical properties of carbon nanotube/shape-memory polymer nanocomposites. *Comp Struct* 81:176–184
30. Sahoo NG, Jung YC, Cho JW (2007) Electroactive shape-memory effect of polyurethane composites filled with carbon nanotubes and conducting polymer. *J Mater Manuf Process* 22:419–423
31. Koerner H, Price G, Pearce NA et al (2004) Remotely actuated polymer nanocomposites: stress-recovery of carbon-nanotube-filled thermoplastic elastomers. *Nat Mat* 3:115–120
32. Buckley PR, McKinley GH, Wilson TS et al (2006) Inductively heated shape-memory polymer for the magnetic actuation of medical devices. *IEEE Trans Biomed Eng* 53:2075–2083
33. Boyles JK, Liu Y, Dickey MD, Genzer J (2012) Self-folding of polymer sheets using local light absorption. *Soft Matter* 8:1764–1769
34. Xiao Z, Wu Q, Luo S et al (2013) Shape matters: a gold nanoparticle enabled shape-memory polymer triggered by laser irradiation. *Part Syst Cha* 30:338–345
35. Zhang H, Xia H, Zhao Y (2012) Optically triggered and spatially controllable shape-memory polymer-gold nanoparticle composite materials. *J Mater Chem* 22:845–849
36. Hu JL, Chen S (2010) A review of actively moving polymers in textile applications. *J Mater Chem* 20:3346–3355
37. Kim BK, Lee SY, Xu M (1996) Polyurethane having shape-memory effect. *Polymer* 37:5781–5793
38. Li FK, Zhang X, Hou JA, Xu M, Luo XL et al (1996) Studies on thermally stimulated shape-memory effect of segmented polyurethanes. *J Appl Polym Sci* 64:1511–1516
39. Takahashi T, Hayashi N, Hayashi S (1996) Structures and properties of shape-memory polyurethane block copolymers. *J Appl Polym Sci* 60:1061–1069
40. Tobushi H, Hara H, Yamada E, Hayashi S (1996) Thermomechanical properties in a thin film of shape-memory polymer of polyurethane series. *Smart Mater Struct* 5:483–491
41. Liu C, Qin H, Mather PT (2007) Review of progress in shape-memory polymers. *J Mater Chem* 17:1543–1558

42. Langer R, Lendlein A (2002) Biodegradable elastic shape-memory polymers for potential biomedical applications. *Science* 296(5573):1673–1676
43. Xu J, Song J (eds) (2011) Thermal responsive shape-memory polymers for biomedical applications. *Biomed Eng Front Chall Reza Fazel-Rezai IntechOpen* 125–141 <https://doi.org/10.5772/19256>
44. Mather PT, Liu C (2011) Blends of amorphous and semicrystalline polymers having shape-memory properties. US Patent PCT number PCT/US2003/032329
45. Lendlein A, Kratz K, Kelch S (2005) Smart implant materials. *Med Device Technol* 16(3):12–14
46. Yang B, Huang WM, Li C, Chor JH (2005) Effects of moisture on the glass transition temperature of polyurethane shape-memory polymer filled with nano carbon powder. *Eur Poly J* 41:1123–1128
47. Lan X, Huang WM, Leng JS, Liu N, Phee SJ, Yuan Q (eds) (2007) Electrically conductive shape-memory polymer with anisotropic electrothermal-mechanical properties. In: *Polymers in defence and aerospace applications* (polymers in defence and aerospace applications, smithers rapra technology; ISBN:9781847350190)
48. Sokolowski WM, Chmielewski AB, Hayashi S, Yamada T (1998) Cold hibernated elastic memory (CHEM) self-deployable structures. *Proc SPIE* 3669:179–185
49. Metcalfe A, Desfaits AC, Salazkin I, Yahia L, Sokolowski WM, Raymond J (2003) Cold hibernated elastic memory foams for endovascular interventions. *Biomaterials* 24:491–497
50. Sokolowski W, Metcalfe A, Hayashi S, Yahia L, Raymond J (2007) Medical applications of shape-memory polymers. *Biomed Mater* 2:S23–S27
51. Lendlein A, Jiang HY, Junger Langer R (2005) Light-induced shape-memory polymers. *Nature* 434:879–882
52. Nagata M, Sato Y (2005) Synthesis and properties of photocurable biodegradable Multiblock copolymers based on poly (ϵ -caprolactone) and poly(L-lactide) segments. *J Polym Sci Part A: Polym Chem* 43:2426–2439
53. Wu L, Jin C, Sun X (2011) Synthesis properties and light-induced shape-memory effect of multiblock polyester urethanes containing biodegradable segments and pendant cinnamide groups. *Biomacromolecules* 12:235–241
54. Ashby VS, Rochette JM (2013) Photoresponsive polyesters for tailorable shape-memory biomaterials. *Macromolecules* 46:2134–2140
55. Nagata M, Yamamoto Y (2009) Synthesis and characterization of photo cross-linked poly(ϵ -caprolactone)s showing shape-memory properties. *J Polym Sci Part A: Polym Chem* 47:2422–2433
56. Nagata M, Yamamoto Y (2010) Photocurable shape-memory copolymers of ϵ -caprolactone and L-Lactide. *Macromol Chem Phys* 211:1826–1835
57. He J, Zhao Y, Zhao Y (2009) Photoinduced bending of a coumarin-containing supramolecular polymer. *Soft Matter* 5:308–310
58. Jiang H, Kelch S, Lendlein A (2006) Polymers move in response to light. *Adv Mater* 18:1471–1475
59. Li Y, Rios O, Keum JK, Chen J, Kessler MR (2016) Photoresponsive liquid crystalline epoxy networks with shape-memory behaviour and dynamic ester bonds. *ACS Appl Mater Interfaces* 8:15750–15757
60. Lee KM, Koerner H, Vaia RA, Bunning TJ, White TJ (2011) Light-activated shape-memory of glassy azobenzene liquid crystalline polymer networks. *Soft Matter* 7:4318–4324
61. Kondo M, Yoshino T, Kinoshita M, Mamiya JI, Ikeda T, Yu Y (2010) Three-dimensional photomobility of cross-linked azobenzene liquid-crystalline polymer fibres. *Adv Mater* 22:1361–1363
62. Yamada M, Kondo M, Mamiya JI, Yu Y, Kinoshita M, Barrett CJ, Ikeda T (2008) Photo mobile polymer materials: towards light-driven plastic motors. *Angew Chem Int Ed* 47:4986–4988
63. Naka Y, Mamiya J, Ishishido A, Washio M, Ikeda AT (2011) Direct fabrication of photo mobile polymer materials with an adhesive-free bilayer structure by electron-beam irradiation. *J Mater Chem* 21:1681–1683

64. Tanchak OM, Barrett CJ (2005) Light-induced reversible volume changes in thin films of azo polymers: the photomechanical effect. *Macromolecules* 38:10566–10570
65. Zhou Q, Zhang X, Liu H, Liu H (2014) UV light-induced plasticization and light-activated shape-memory of spiro-pyran doped ethylene-vinyl acetate copolymers. *Soft Matter* 10:3748–3754
66. Zhu M-Q, Zhu L, Han JJ, Wu W, Hurst JK, Li ADQ (2006) Spiropyran-based photochromic polymer nanoparticles with optically switchable luminescence. *J Am Chem Soc* 128:4303–4309
67. Goo NS, Paik IH, Yoon KJ, Jung YC, Cho JW (2014) Actuation of MAV control surface using conducting shape-memory polymer actuator. *Proc SPIE* 5390:194–201
68. Cho JW, Kim JW, Jung YC, Goo NS (2005) Electroactive shape-memory polyurethane composites incorporating carbon nanotubes. *Macromol Rapid Commun* 26:412–416
69. Paik IH, Goo NS, Jung YC, Cho JW (2006) Development and application of conducting shape-memory polyurethane actuators. *Smart Mat Str* 15:1476–1482
70. Schmidt AM (2006) Electromagnetic activation of shape-memory polymer networks containing magnetic nanoparticles. *Macromol Rapid Commun* 27:1168–1172
71. Leng JS et al (2008) Electrical conductivity of thermoresponsive shape-memory polymer with embedded micron-sized Ni powder chains. *Appl Phys Lett* 92:014104(1–3)
72. Li F, Qi L, Yang J, Xu M, Luo X, Ma D (2000) Polyurethane/conducting carbon black composites: structure/electric conductivity/strain recovery behaviour and their relationships. *J Appl Poly Sci* 75:68–77
73. Gunes I, Cao F, Jana S (2008) Evaluation of nanoparticulate fillers for development of shape-memory polyurethane nanocomposites. *Polymer* 49:2223–2234
74. Thostenson ET, Chou TW (2002) Aligned multi-walled carbon nanotube-reinforced composites: processing and mechanical characterization. *J Phys D: Appl Phys* 35:L77–80
75. Hou H, Ge JJ, Zeng J, Li Q, Reneker DH, Greiner A et al (2005) Electrospun polyacrylonitrile nanofibers containing a high concentration of well-aligned multiwall carbon nanotubes. *Chem Mater* 17:967–73
76. Kwon J, Kim H (2005) Comparison of the properties of waterborne polyurethane/multi-walled carbon nanotube and acid-treated multi-walled carbon nanotube composites prepared by in situ polymerization. *J Poly Sci Part A: Poly Chem* 43:3973–3985
77. Chen W, Tao XM (2005) Self-organizing alignment of carbon nanotubes in thermoplastic polyurethane. *Macromol Rapid Commun* 26:1763–1767
78. Hu JL, Monda IS (2006) Shape-memory studies of functionalized MWNT-reinforced polyurethane copolymers. *IranPoly J* 15:135–142
79. Jimenez GA, Jana SC (2007) Polyurethane-carbon nanofibre composites for shape-memory effects. *SPEANTEC Conf Proc* 65(1):18–22
80. Koerner H, Price G, Pearce NA, Alexander M, Vaia RA (2004) Remotely actuated polymer nanocomposites-stress-recovery of carbon-nanotube-filled thermal plastic elastomers. *Nat Mater* 3:115–120
81. Ni QQ, Zhang CS, Fu YQ, Dai GZ, Kimura T (2007) Shape-memory effect and mechanical properties of carbon nanotube/shape memory polymer nanocomposites. *Compos Struct* 81:176–84
82. Meng Q, Hu J, Mondal S (2008) Thermal sensitive shape recovery and mass transfer properties of polyurethane/modified MWNT composite membranes synthesized via in situ solution pre-polymerization. *J Membrane Sci* 319:102–110
83. MIAUDET P, DERRE A, MAUGEY M, ZAKRI C, PICCIONE PM et al (2007) Shape and temperature memory of nanocomposites with broadened glass transition. *Science* 318:1294–1296
84. Jung YC, Sahoo NG, Cho JW, Yoo HJ (2007) Influence of carbon nanotubes and polypyrrole on the thermal/mechanical and electroactive shape-memory properties of polyurethane nanocomposites. *Compos Sci Technol* 67:1920–1929
85. Cho JW, Lee SH (2004) Influence of silica on shape-memory effect and mechanical properties of polyurethane-silica hybrids. *Eur Poly J* 40:1343–1348

86. Liu Y, Gall K, Dunn M, Mc Cluskey P (2004) Thermomechanics of shape-memory polymer nanocomposites. *Mech Mater* 36:929–940
87. Kramer SLB, Blaiszik BJ, Moore JS, Olugebefola SC, White SR, Sottos NRR (2010) Self-healing polymers and composites. *Ann Rev Mat Res* 40:179–211
88. Auad ML, Richardson T, Hicks M, Mosiewicki MA, Aranguren MI, Marcovich NE (2012) Shape-memory segmented polyurethanes: dependence of behaviour on nanocellulose addition and testing conditions. *Poly Int* 61:321–327
89. Zhu Y, Hu J, Luo H, Young RJ, Deng L, Zhang S et al (2012) Rapidly switchable water-sensitive shape-memory cellulose/elastomer nano-composites. *Soft Matter* 8:2509–2517
90. Luo H, Hu J, Zhu Y, Zhang S, Fan Y, Ye G (2012) Achieving shape-memory: reversible behaviours of cellulose–PU blends in wet-dry cycles. *J Appl Poly Sci* 125:657–665
91. Mather PT, Luo X (2010) Triple-shape polymeric composites (TSPCs). *Adv Fun Mater* 20:2649–2656
92. Shirole A, Sapkota J, Foster EJ, Weder C (2016) Shape-memory composites based on electrospun poly (vinyl alcohol) fibers and a thermoplastic polyether block amide elastomer. *ACS Appl Mater Inter* 8:6701–6708
93. Zhang X, Geven MA, Grijpma DW, Peijs T, Gautrot JE (2017) Tunable and processable shape-memory composites based on degradable polymers. *Polymer* 122:323–331
94. Lu H, Liang F, Gou J, Leng J, Du S (2014) Synergistic effect of Ag nanoparticle-decorated graphene oxide and carbon fiber on electrical actuation of polymeric shape-memory nanocomposites. *Smart Mat Struct* 23:085034(1–7)
95. Guo J, Wang Z, Tong L, Liang W (2016) Effects of short carbon fibres and nanoparticles on mechanical thermal and shape-memory properties of SMP hybrid nanocomposites. *Compos Part B- Eng* 90:152–159
96. Raja M, Shanmugaraj A, Ryu SH, Subha J (2011) Influence of metal nanoparticle decorated CNTs on polyurethane-based electroactive shape-memory nanocomposite actuators. *Mater Chem Phys* 129:925–931
97. Li W, Gong T, Wang L, Chen H, Zhou S, Shao S (2012) Remotely actuated shape-memory effect of electrospun composite nanofibers. *Acta Biomaterialia* 8:1248–1259
98. Lu H, Wang X, Yao Y, Gou J, Hui D, Xu B et al (2015) Synergistic effect of siloxane modified aluminium nanopowders and carbon fiber on electrothermal efficiency of polymeric shape-memory nanocomposite. *Compos Part B- Eng* 80:1–6
99. Liu Y, Li Y, Yang G, Zheng X, Zhou S (2015) Multi-stimulus-responsive shape-memory polymer nanocomposite network cross-linked by cellulose nanocrystals. *ACS Appl Mater Inter* 7:4118–4126
100. Meng Q, Hu J (2008) Self-organizing alignment of carbon nanotube in shape-memory segmented fibre prepared by in situ polymerization and melt spinning. *Compos Part A- Appl Sci* 39:314–321
101. Yu K, Zhang Z, Liu Y, Leng J (2011) Carbon nanotube chains in a shape-memory polymer/carbon black composite: to significantly reduce the electrical resistivity. *Appl Phys Lett* 98:074102(1–3)
102. Lu H, Liu Y, Gou J, Leng J, Du S (2010) Electrical properties and shape-memory behaviour of self-assembled carbon nanofiber nanopaper incorporated with shape-memory polymer. *Smart Mater Struct* 19:075021(1–7)
103. Lu H, Liu Y, Gou J, Leng J, Du S (2010) Synergistic effect of carbon nanofiber and carbon nanopaper on shape-memory polymer composite. *Appl Phys Lett* 96:084102(1–4)
104. Lu H, Gou J, Leng J, Du S (2011) Magnetically aligned carbon nanotube in nanopaper enabled shape-memory nanocomposite for high-speed electrical actuation. *Appl Phys Lett* 98:174105(1–3)
105. Lu H, Lei M, Leng J (2014) Significantly improving electro-activated shape recovery performance of shape-memory nanocomposite by self-assembled carbon nanofiber and hexagonal boron nitride. *J Appl Polym Sci* 131:40506(1–7)
106. Wang W, Liu D, Liu Y, Leng J, Bhattacharyya D (2015) Electrical actuation properties of reduced graphene oxide paper/epoxy-based shape-memory composites. *Compos Sci Technol* 106:20–24

107. Liu Y, Boyles JK, Genzer J, Dickey MD (2012) Self-folding of polymer sheets using local light absorption. *Soft Matter* 8:1764–1769
108. Davis D, Chen B, Dickey MD, Genzer J (2016) Self-folding of thick polymer sheets using gradients of heat. *J Mech Robot* 8:031014(1–8)
109. Zarek M, Layani M, Cooperstein I, Sachyani E, Cohn D, Magdassi S (2016) 3D printing of shape-memory polymers for flexible electronic devices. *Adv Mater* 28:4449–4454
110. Wang X, Sparkman J, Gou J (2017) Electrical actuation and shape-memory behaviour of polyurethane composites incorporated with printed carbon nanotube layers. *Compos Sci Technol* 141:8–15
111. Ge Q, Qi HJ, Dunn ML (2013) Active materials by four-dimension printing. *Appl Phys Lett* 103:131901(1–5)
112. Robertson JM, Torbati AH, Rodriguez ED, Mao Y, Baker RM, Qi HJ et al (2015) Mechanically programmed shape change in laminated elastomeric composites. *Soft Matter* 11:5754–5764
113. Mao Y, Robertson JM, Mu X, Mather PT, Qi HJ (2015) Thermoviscoplastic behaviours of anisotropic shape-memory elastomeric composites for cold programmed non-affine shape change. *J Mech Phys Solids* 85:219–244
114. Yuan C, Ding Z, Wang TJ, Dunn ML, Qi HJ, S (2017) Shape forming by thermal expansion mismatch and shape-memory locking in polymer/elastomer laminates. *Smart Mater Struct* 26:105027(1–23)
115. Sundaram S, Kim DS, Baldo MA, Hayward RC, Matusik W (2017) 3D-printed self-folding electronics. *ACS Appl Mater Inter* 9:32290–32298
116. He Z, Satarkar N, Xie T, Cheng YT, Hilt JZ (2011) Remote controlled multi-shape polymer nanocomposites with selective radiofrequency actuations. *Adv Mater* 23:3192–3196
117. Li W, Liu Y, Leng J (2015) Selectively actuated multi-shape-memory effect of a polymer multi-composite. *J Mater Chem A* 3:24532–24539
118. Yu K, Ritchie A, Mao Y, Dunn ML, Qi HJ (2015) Controlled sequential shape changing components by 3D printing of shape-memory polymer multi-materials. *Procedia IUTAM* 12:193–203
119. Wetherhold RC, Wang J (1996) Controlling thermal deformation by using laminated plates. *Compos B* 27:51–57
120. Asanuma H, Haga O, Ohira JI, Hakoda G, Kimura K (2002) Proposal of an active composite with embedded sensor. *Sci Technol Adv Mater* 3:209–216
121. Kirillova A, Maxson R, Stoychev G, Gomillion CT, Ionov L (2017) 4D Biofabrication using shape-morphing hydrogels. *Adv Mater* 29:1703443(1–8)
122. Hu GF, Damanpack AR, Bodaghi M, Liao WH (2017) Increasing dimension of structures by 4D printing shape-memory polymers via fused deposition modelling. *Smart Mater Struct* 26:1250239(1–38)
123. Invernizzi M, Turri S, Levi M, Suriano R (2018) 4D printed thermally activated self-healing and shape-memory polycaprolactone-based polymers. *Eur Polym J* 101:169–176
124. Yakacki CM, Shandas R, Lanning C, Rech B, Eckstein A, Gall K (2007) Unconstrained recovery characterization of shape-memory polymer networks for cardiovascular applications. *Biomaterials* 28:2255–2263
125. Yang CS, Wu HC, Sun JS, Hsiao HM, Wang TW (2013) Thermo-induced shape-memory PEG-PCL copolymer as a dual-drug-eluting biodegradable stent. *ACS Appl Mater Interfaces* 5:10985–10994
126. Kuang X, Chen K, Dunn CK, Wu J, Li VCF, Qi HJ (2018) 3D printing of highly stretchable, shape-memory, and self-healing elastomer toward novel 4D printing. *ACS Appl Mater Interfaces* 10:7381–7388
127. Liu Y, Du H, Liu L, Leng J (2014) Shape-memory polymers and their composites in aerospace applications. *Smart Mater Struct* 23:023001(1–22)
128. Santo L, Quadri F, Squeo EA, Dolce F, Mascetti G, Bertolotto D, Villadei W, Ganga PL, Zolesi V (2012) Behavior of shape-memory epoxy foams in microgravity: experimental results of the STS-134 mission. *Microgravity Sci Tech* 24:287–296

129. Barbarino S, Bilgen O, Ajaj RM, Firswell MI, Inman DJ (2011) A review of morphing aircraft. *J Intell Mater Syst Struct* 22:823–855
130. Gaj MP, Wei A, Fuentes-Hernande C, Zhan Y, Rei R, Voit W, Marder SR, Kippelen B (2015) Organic light-emitting diodes on shape-memory polymer substrates for wearable electronics. *Org Electr* 25:151–155
131. Yu Z, Niu X, Liu Z, Pei Q (2011) Intrinsically stretchable polymer light-emitting devices using carbon nanotube-polymer composite electrodes. *Adv Mater* 23:3989–3994
132. Kunzelman J, Chung T, Mather PT, Weder C, (2008) Shape-memory polymers with built-in threshold temperature sensors. *J Mat Chem* 18:1082–1086
133. Zhang XY (2015) Biomedical engineering for health research and development. *Eur Rev Med Pharmacol Sci* 19(2):220–224

Chapter 11

Meso, Micro, and Nano Particulate Filled Shape-Memory Polymers



T. Rajani and Ashok Bhogi

11.1 Introduction

Shape-memory polymers are introduced in 1980 and they continue to grow as smart polymers today. The Shape-Memory Polymers (SMP) have been under intensive research investigation due to their great potential and exhibit novel properties. They come underclass of stimuli-responsive smart materials. They are grown rapidly due to their versatile structure, ease in processing and can obtain elastic deformation at low cost and temperature, biocompatibility, and biodegradability [1]. The Shape-memory polymers arise from phase structural movements which depend on energy barriers. They exhibit a shape-memory effect [2]. Shape-memory polymers can be turned temporarily into a new shape. They can be retrieved to original by applying external stimulus effect. This new shape obtained will be at a higher one. They can be recovered by applying several external stimulants such as heat, electrical energy, magnetic energy, optical energy, etc. [3–9]. They can be differentiated depending on the various stimulus factors such as electric-actuated SMP, thermo-actuated SMP, light-actuated SMP, etc. These are named as stimuli-responsive polymers. The SMP can be programmed into any shape on demand. Stable polymer networks, reversible switching transition are the criteria for the SME [10]. The shape-memory polymers consist of net points which act as reversible switching segments. Net points are responsible to regain the original shape. The switching segments render the secondary shape which allows change to occur in shape [11–16]. It has been observed from the recent literature that shape-memory functionality can be affected with the addition of various fillers /particulates of different sizes. Thereby a continuing interest in the behavior of polymer networks due to the altered role of particulate fillers of various sizes and shapes was developed. Microscopically, polymeric materials can respond to external forces in a broad frequency range. Fillers are reinforced into polymers

T. Rajani (✉) · A. Bhogi

Department of Humanities and Sciences (Physics), VNR Vignana Jyothi Institute of Engineering and Technology, Hyderabad, Telangana 500090, India

to create various new functional properties. The fillers increase stiffness, lower the shrinkage, and enhance the quality of composites. Also, when they are added in thermoplastic processing specific heat can be decreased. Thereby increasing heat conductivity and productivity [17–20]. In addition, this shape is dependent on the kind of polymer matrix and the type of fillers such as mesoparticles, microparticles, and nanoparticles. This chapter focuses mainly on types and characteristics of fillers, the functionality of shape-memory polymers due to the addition of various sizes of particulates such as meso, micro, and nanoparticles to the polymer network.

11.2 Shape-Memory Effect in Shape-Memory Polymers

The shape-memory effect is a unique ability exhibited by shape-memory polymers. It can be linked to a cross-linked polymer structure or combination of suitable molecular architecture. The SMPs are deformed to a temperature below the glass temperature (T_g). This deformation depends on factors such as molecular structure, chemical composition, and physical cross-linked structure of SMP's. When external energy in the form of temperature is given, these molecular chains can return to the original coiled-shape structure. During this transformation, the polymer molecules transpose [21, 22] (Fig. 11.1).

The development of SMP shows repeated actuation and various functionalities that implies (i) shape-changing soft materials that are intrinsically reversible [23] (ii) shape-memory soft materials, in which programming can be done for complex shape variations [24, 25]. Depending on the type of recovery, shape-memory polymers are classified into (i) one-way SME; polymers which have one permanent and one temporary shape. This phase transformation is defined as soft. (ii) multiple-way SME possess one permanent and multi temporary shapes (iii) two-way SME; these polymers show the reversible transition between temporary shapes. These are shown in Figs. 11.2 and 11.3 below.

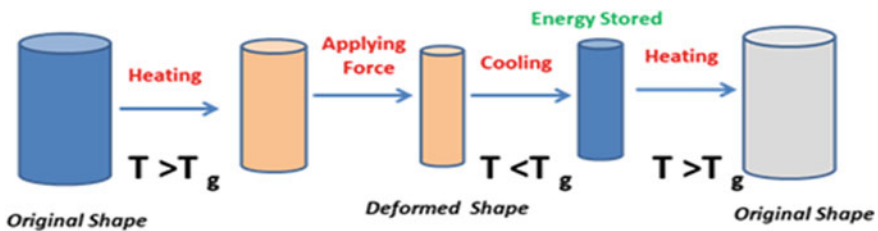


Fig. 11.1 Outline of shape-memory polymer

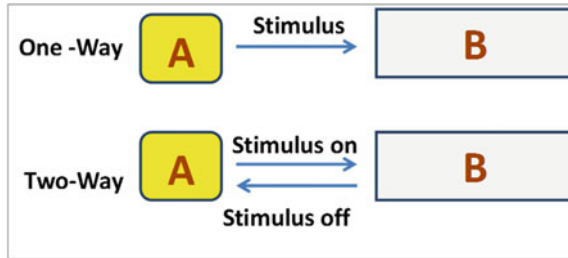


Fig. 11.2 One-way and two-way shape-memory effect

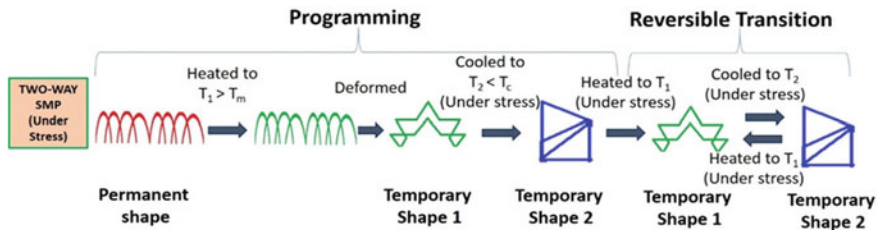


Fig. 11.3 Multiple-way shape-memory effect

11.3 Reinforcement of SMP

The two methods that are frequently used to reinforce the SMP's are (i) Thermo-mechanical cycle (ii) Particle/fiber reinforcement.

11.3.1 Thermo-Mechanical Cycle

In this method, initially, SMP was heated to a temperature above T_g without applying any stress and strain. Then the SMP was allowed to deform to a new shape by inducing stress and strain on it. This temporary shape is fixed by maintaining the stress and strain. After that, the SMP's are allowed to cool below T_g and upon removal of stress, the material reaches to temporary shape. This procedure is known as programming [26–28].

To complete the cycle, the material is again heated above T_g because of which regains its original shape as shown in Fig. 11.4. These steps are repeated for the next cycles.

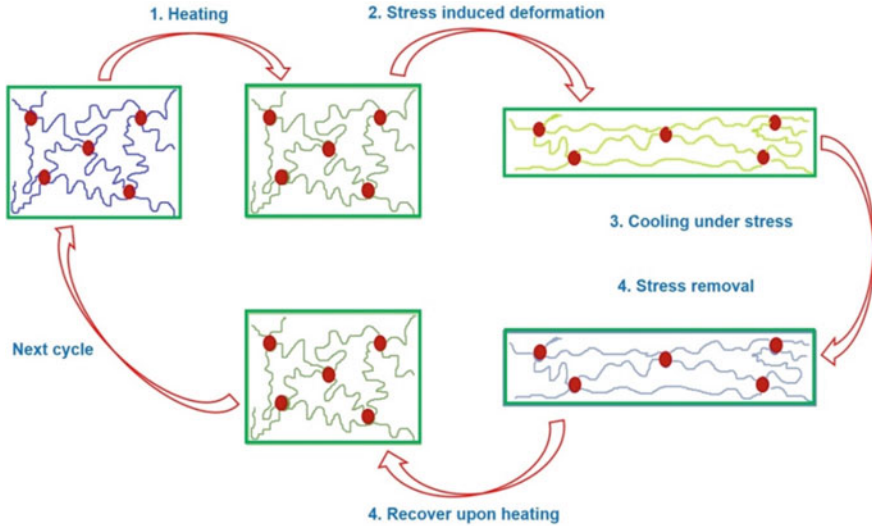


Fig. 11.4 Steps of shape-memory polymer

11.3.2 Particle/Fiber Reinforcement

In composites, matrix is a primary and continuous phase. Matrix is less hard and ductile. Filler or fiber is a discontinuous phase and embedded with matrix in heterogeneous form. The matrix binds and shares the load with the dispersed phase. This dispersed phase called as reinforcing phase is stronger than the matrix.

The design of SMPs and their behavior can be altered by modifying the molecular structure of the matrix and the addition of functional fillers. They can form multi-phase composite SMPs. The reinforcement of SMP composite under a particle/filler can be modified [29]. Different fillers can be incorporated with SMP such as organic, metallic, inorganic, magnetic [30–32], etc., depending on the required application [33, 34]. Thus, the addition of fillers in the polymer matrix will trigger the functional properties. This method has been extensively studied and gained importance.

11.4 Fillers

The particulates that are added to improve the properties of the polymer matrix are called fillers. They can be in the form of solid, liquid or gas. The filler characteristics are influenced by (1) Particle size, (2) Surface area and surface energy, and (3) Particle shape.

11.4.1 Particle Size

Particle size or filler size affects the composite properties such as modulus, deformability, and impact resistance [35–38]. Apart from the size of filler, the distribution of filler in the polymer matrix or any matrix is equally important. After a certain period, particles of larger size degenerate the deformation and failure characteristics of composites. The weak bonding between particles and matrix causes failure. Also, further loading leads to failure. But it is observed from reports that the stress decreases with increment in particle size and defects are formed in the composite [39, 40]. On the other, the particle size distribution of small particles is evenly important. Smaller particles agglomerate if they are not coated. The agglomeration can be prevented through coating which improves interaction with the matrix. Aggregation between matrix and fillers improves with decreasing particle size [41–43]. But if the aggregation is extended to a sufficient value, homogeneity, rigidity, and low impact strength will be affected. This gives rise to crack initiation sites due to aggregated filler particles [44–47]. Any polymer composite properties can be analyzed by particle characteristics.

11.4.2 Surface Area and Surface Energy

The filler's surface area has an impact on composite properties. It depends on particle size and its dispersion in the matrix. In many composites, on the surface, small molecular additives can be observed. This affects the interface of matrix/filler. The additives influence stability, whereas matrix/filler interaction determines the properties of polymer composites [48, 49]. If the fillers are uniformly distributed, then the surface will be more interactive. The interactions between matrix/filler and particle/particle can be understood with the help of the surface free energy of fillers. It was reported that matrix/filler interaction affecting the mechanical properties of the composite and particle/particle interaction determines aggregation [35, 50, 51]. They can be altered by surface treatment.

Surface modifications can be carried out either by physical or chemical methods. Chemical methods lead to strong filler interaction between filler and modifier. The physical method can be implemented by adsorbing surfactants onto the surface of the filler.

11.4.3 Particle Shape

In a composite, the particle shape of filler plays a vital role in the properties. As the shape of filler changes, reactions on the surface can be observed [52]. Filler particles of asymmetric shapes effectively are used in enhancing the magnetic and

electrical properties of synthesized polymer composite samples. The aggregation and sedimentation behavior can be emphasized in the composites for both regular and irregular shapes of fillers. Adding Hybrid fillers [53, 54] selected from three or four irregular filler shapes of various sizes, strength can be increased. Also, these fillers are differentiated based on the aspect ratio. The modulus increases with the aspect ratio [55]. Also, as the impact resistance increases, there is a decrease in particle size. Large particles show defects and with a high aspect ratio increases stress [56–58].

11.5 Types of Fillers

Fillers' significant differences can be remarked based on molecular weight, compounding technique, presence of other additives in the preparation [59, 60]. They can be classified broadly based on the type of constituent as (1) Particulate fillers, (2) Rubbery fillers, and (3) Fibrous fillers.

11.5.1 Particulate Fillers

This is one type of reinforcement added in composites. They can be broadly parted into two types, namely: inert fillers and reinforcing fillers. With the incorporation of inert filler, many properties are affected. If the size of the particle is fine, variation in the properties of SMP can be observed and the phenomenon is called reinforcement [61]. The reinforcement of filler depends on filler–polymer interaction or bonding, the total amount of surface area occupied by filler per unit volume with polymer, porosity, the structure of particles, fillers or fibers.

11.5.2 Rubbery Fillers

These kinds of fillers are used in thermoplastics which develop fracture resistance in the materials by increasing toughness [62].

11.5.3 Fibrous Fillers

These fillers are used in plastic materials. They are used in laminar form. Fibrous fillers show high modulus than the resins. Thus, the fibrous layer holds bulk strain and stress. Because of this, the strength, the modulus is altered when compared to the unfilled resin [63, 64]

11.6 Addition of Fillers

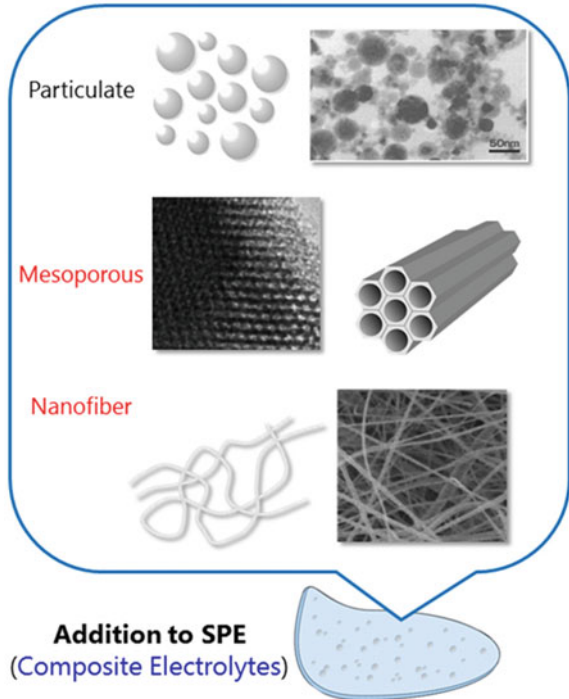
In the theory of polymerization, combining particles into multi-component systems shows a significant impact on phase separation. Phase separation is a physical phenomenon that controls the morphology of the material that affects electrical, mechanical, and transport properties. It was reported that dispersion of fillers will affect the affinity of particles [65]. Fillers that chemically bond with SMP chains show more efficient performance. Such kinds of fillers exhibit the function of cross-linking agents after reinforcing into SMP. The fillers can be three-dimensional, two-dimensional, one-dimensional, and also zero-dimensional in a network. Shape-memory polymers are advantageous for high strain and low-cost applications. They maintain lower stiffness when compared with other smart materials. During the shape-memory recovery, thermally induced triggering conditions practically develop uncertainties in most applications upon increasing heat energy /temperature. These shortcomings can be overcome by introducing fillers of respective dimensions. Moreover, conventional filler particles will be less optimum in terms of shape recovery effect. Thereby changes in recoverable strain due to size and stiffness with respect to polymer matrix are observed [66, 67].

Also, the bending properties change with filler content. Thus, incorporating particulates has been studied to improve the properties and the practical triggering conditions help to broaden the applications of SMPs [68–72]. From broader perspective, fillers can be divided into two categories. In the first, silica, carbons, nitrides, metals, and metallic oxides at micro and nano-level can be used to design SMP. The modulus of these fillers is much higher than the polymer matrix. Nanoparticles such as nanoclay, carbon nanotube (CNT), nano silicon carbides are also in use. The second group is polymer fillers such as celluloses, crystalline polymers, elastomers, etc. They enable the multi-functionalities. In order to extend multifunctional ability and applications in various fields, the shape-memory polymers are needed to be designed by using various types of fillers of dimensions such as meso, micro, and nanoscale which are shown in Fig. 11.5.

11.6.1 Meso Particles in SMP

The meso fillers are larger compared to polymer chains. This causes changes in the stress coupling and the morphology of a non-miscible polymer blend with dynamic asymmetry. The dynamic asymmetry between the constituents excites differences in size or transition temperature. Here, the minority phase transiently can show a continuous phase. The different phase structures can be obtained by varying different properties in the polymers like composition, molecular weight, temperature, etc. When high molecular weight particles are introduced in polymers, then an increase in elasticity and viscoelastic moduli of composite material are observed [73–76]. Fillers distributed in a parent matrix make confinement of polymer chains and slow

Fig. 11.5 Examples of particulate, mesoporous, nanofiber structures that can be added to SMP



down chain dynamics. Entanglements are trapped in a confined space. Both dynamic asymmetry and chain entanglement provide an environment for the distribution of meso fillers in slow dynamic phases. This is closely related to the shape of the filler [77–79].

Meso fillers affect the structure and properties of material substantially [80]. Phase structure and phase separation process is affected by the viscoelastic effect caused due to dynamic asymmetry. This enhancement in the viscoelastic parameter is due to the meso fillers which are inorganic. Xiaolin Tang [81] reported the process of phase separation, morphology that is impacted by the addition of meso fillers from their surface affinity to the epoxy rich matrix phase at a higher temperature.

11.6.2 Microparticles in SMP

Microstructure is an important phenomenon to understand the properties of a material. A single microparticle has a larger surface area. The micro-filled composites have lower size particles when compared to traditional composites. In the initial stage, micro-filler particles are finely dispersed which are created by using various synthesis methods, e.g., hydrolysis and precipitation. In terms of intermediate composites, the weight is 85% and the loading is generally 50–65% for micro-filled composites.

These micro-fillers can be blended in both homogeneous and heterogeneous ways [82]. In the homogeneous method, both matrix and micro-filler will be distributed in the composite. By this method, superior wear properties can be enhanced. In the heterogeneous method, there will be matrix directly admixed with micro filled particles and complexes. Maximum loading is observed with micro filler particles [83]. Also, microfibers which are made up of carbon fibers, glass fibers, etc., show high elastic modulus, strength which significantly increase the mechanical strength of SMP's and can bear a high mechanical load. It was reported that this kind of reinforcement lowers SME in SMP. These microfibers' role is superior to microparticles while reinforcing SMP [84, 85]. Iskender Ozsoy et al. [86] reported that the tensile strength decreases as the filler content ratio increases in micro-filled composites. This is caused due to the weak adhesive forces between matrix and fillers which causes the decrement in the strength of the epoxy composite. It was reported that the mechanical properties of micro-filled composite resins depend on the type of inorganic filler and the properties of the polymer matrix.

When compared with conventional composites, micro-filled composites maintain a smooth surface [87]. Also, in [88], wear resistance was increased due to micro filler content in large volumes. The properties of composites depend on the microstructure and [89] are used for the making of high-performance composites. The distribution of fillers reflects the performance. This can be achieved by changing micro-fillers alignment which is applicable for the multilayer network [90–92]. Jinsong Leng, et al. reviewed and reported that SMP with carbon black is filled with micro-Ni particles, i.e., SMP/CB/micro-NI and SMP/CB/nano Ni. It was observed that the conductivity of SMP/CB/nano Ni has higher conductivity than the micro dimension conductive fillers [93].

11.6.3 Nanoparticles in SMP

A single nanoparticle has a far greater specific surface area when compared with a single microparticle. The nanofillers come in a variety of shapes which can be classified by their aspect ratio. Different novel properties can be studied by introducing various shapes of nanofillers in SMP. The aspect ratio influences the number of filler particles that are required. Depending on application requirement different nanoparticles under filler can be reinforced with the matrix. Besides the shape recovery effect, a high modulus of elasticity and mechanical strength needs to be required for a good SMP. It was observed that when silica nanofillers [94, 95] were used as a reinforcing agent, no change in shape recovery is observed. Mechanical properties were also enhanced.

Rod shape nanofillers like fibers, CNT showed improvement in stiffness and actuation stress [96]. Layered clay nanofillers used by Cao and Jana [97] reported that there is a decrease in the crystallinity of the soft segment phase, and the phase mixing between the hard and soft segment phases is elevated. Bin Xu et al. [98] developed a SMP matrix in which nano-size clay powder was used as filler. Thereby storage

modulus was increased at ambient temperatures and as the clay powder content is increased SME was decreased. In some nanofillers, as the additive concentration increases in the polymer matrix, the electrical conductivity increases sharply and after that modest increase can be observed as the additive is increased [99]. Because of high surface area, nano noble metals can absorb high plasmonic resonance of specific wavelength. The absorbed energy is converted into heat energy with high shape actuation and wavelength actuation [100–102]. The nanofillers can provide a conductive network, thereby changes in conductivity and resistivity are observed in the case of nano-Ag [103]. One of the external stimuli is magnetic energy. For this, the polymer is reinforced with magnetite nanoparticles that transform electromagnetic energy into heat.

In [104], shape-memory polyurethane-POSS nanocomposites, POSS nanoparticles have bonded to the matrix and the addition of nanoparticles caused improvement in the shape recovery of synthesized nanocomposites. Sithara Gopinath et al. [105] reported that thermal, mechanical, and shape responsive effect was enhanced in SMPC/Fe₂O₃, and shape fixing property has increased in the order of SMPC–CuO > SMPC–Fe₂O₃ > SMP > SMPC/CuFe₂O₄.

11.7 Conclusion

Shape-memory effect is the phenomenon of shape-memory polymer. The shape-memory effect can be understood from polymer structure. Fillers play important role in SMP. These fillers exhibit various characteristics like particle size, particle shape, surface area, etc. Out of several types of fillers, particulate fillers are having more importance and interest. These particulate fillers can be of different sizes and shapes. Particularly, meso, micro, and nanofillers. The mesoscopic fillers show the effect on properties and phase separation due to the viscoelastic effect. The distribution of microscopic fillers affects the various properties of SMP. When compared with micro, nanofillers of different sizes and shapes are used in SMP to enhance modulus, toughness, stress, strain, magnetic and electric properties, and show a greater effect on SME in SMP.

Acknowledgements The author is grateful to the management of the VNR Vignana Jyothi Institute of engineering and technology for their continuous support and encouragement.

References

1. Liu C, Qin H, Mather P (2007) Review of progress in shape-memory polymers. *J Mater Chem* 17:1543–1558
2. Mather PT, Luo X, Rousseau IA (2009) Shape-memory polymer research. *Annu Rev Mater Res* 39:445–471

3. Jiang HY, Kelch S, Lendlein A (2006) *Adv Mater* 18:1471e5
4. Yang, B., Huang, WM., Li, C., Li, L.: *Polymer* 47,1348e56 (2006).
5. Hu JL, Meng QH, Zhu Y, Lu J, Zhuo HT (2007) Shape-memory fibers prepared by wet, reaction, dry, melt, and electro spinning. US Patent 11907012
6. Tobushi H, Hayashi S, Hoshio K, Miwa N (2006) *Smart Mater Struct* 15:1033e8
7. Lendlein A, Langer RS (2004) Self-expanding device for the gastrointestinal or urogenital area, WO/2004/073690, PCT/US2004/004776. USA
8. Marco D, Eckhouse S (2006) Biodegradable self-inflating intragastric implants for curbing appetite. US Patent Office, Pat. No.0156248
9. Leng J, Lu H, Liu Y, Huang WM, Du S (2009) *MRS Bull* 34:848e55
10. Hu JL, Mondal S (2005) *Polym Int* 54:764e71
11. Hu JL, Yang Z, Ji FL, Liu YQ (2005) *Polym Int* 54:854e9
12. Liu C, Qin H, Mather PT (2007) *J Mater Chem* 17:1543e58
13. Beloshenko VA, Varyukhin VN, Voznyak YV (2005) *Russian Chem Rev* 74:265e83
14. Voit W, Ware T, Dasari RR, Smith P, Danz L, Simon D (2010) *Adv Funct Mater* 20:162e71
15. Zhang S, Yu Z, Govender T, Luo H, Li B (2008) *Polymer* 49:3205e10
16. Yu Z, Liu Y, Fan M, Meng X, Li B, Zhang S (2010) *J Polym Sci Part B: Polym Phys* 48:951e7
17. Bertelli G, Camino G, Marchetti E, Costa L, Casorati E, Locatelli R (1989) *Polym Degrad Stabil* 25:277
18. Acosta JL, Rodriguez M, Linares A, Jurado JR (1990) *Polym Bull* 24:87
19. Almeras X, Le Bras M, Poutch F, Bourbigot S, Marosi G, Anna P (2003) *Macromol Symp* 198:435
20. Almeras X, Le Bras M, Hornsby P, Bourbigot S, Marosi G, Keszei S, Poutch F (2003) *Polym Degrad Stabil* 82:325
21. Hu J (2007) Shape-memory polymers and textiles. Taylor & Francis
22. Rousseau IA (2008) Challenges of shape-memory polymers: a review of the progress toward overcoming SMPs limitations. *Polym Eng Sci* 48:2075–2089
23. Han J, Jiang W, Niu D, Li Y, Zhang Y, Lei B, Liu H, Shi Y, Chen B, Yin L (2019) Untethered soft actuators by liquid-vapor phase transition: remote and programmable actuation. *Adv Intell Syst* 1:1900109
24. Kang D, An S, Yarin A, Anand S (2019) Programmable soft robotics based on nanotextured thermo-responsive actuators. *Nanoscale* 11:2065–2070
25. Carrico J, Tyler T, Leang K (2018) A comprehensive review of select smart polymeric and gel actuators for soft mechatronics and robotics applications: fundamentals, freeform fabrication, and motion control. *Int J Smart Nano Mater* 8:144–213
26. Lendlein A, Kelch S (2002) *Angewandte Chemie* 41:2034
27. Gall K, Dunn ML, Liu Y, Finch D, Lake M, Munshi NA (2002) *Acta Mater* 50:5115
28. Liu Y, Gall K, Dunn ML, McCluskey P (2004) *Mech Mater* 36:929
29. Yakacki CM, Satarkar NS, Gall K, Likos R, Hilt JZ (2009) Shape-memory polymer networks with Fe₃O₄ nanoparticles for remote activation. *J Appl Polym Sci* 112:3166–3176
30. Zheng X, Zhou S, Xiao Y, Yu X, Li X, Wu P (2009) Shape-memory effect of poly (d, l-lactide)/Fe₃O₄ nanocomposites by inductive heating of magnetite particles. *Colloids Surfaces B, Biointerfaces* 71:67–72
31. Meng H, Li G (2013) A review of stimuli responsive shape-memory polymer composites. *Polymer* 54:2199–2221
32. Meng Q, Hu J (2009) A review of shape-memory polymer composites and blends. *Compos A Appl Sci Manuf* 40:1661–1672
33. Lan X, Liu Y, Lv H, Wang X, Leng J, Du S (2009) Fiber reinforced shape-memory polymer composite and its application in a deployable hinge. *Smart Mater Struct* 18:024002
34. Cogswell FN (2013) Thermoplastic aromatic polymer composites: a study of the structure, processing and properties of carbon fibre reinforced polyetherether ketone and related materials. Elsevier
35. Pukánszky B (1995) Polypropylene. Structure, blends and composites. J. Karger-Kocsis Ed., pp 1–70

36. Nielsen LE (1974) Mechanical properties of polymers and composites. Marcel Dekker
37. Mitsuishi K, Kodama S, Kawasaki H (1985) *Polym Eng Sci* 25:1069
38. Nielsen LE, Landel RF (1993) Mechanical properties of polymers and composites. Marcel Dekker
39. Vollenberg PHT, Heikens D (1986) Composite interfaces. In: Ishida H, Koenig JL (ed). Elsevier, pp 41, 171–175
40. Bezar D (1986) *Oesterr Kunstst Z.* 17:174
41. Pukánszky B (2004) *J Móczó Macromol Symp* 214:115
42. Suetsugu Y, Kikutani T, Kyu T, White JL (1990) *Colloid Polym Sci* 268:118
43. Suetsugu Y, White JL (1987) *Adv Polym Technol* 7:427
44. Riley AM, Paynter CD, McGenity PM, Adams JM (1990) *Plast Rubber Process Appl* 14:85
45. Xu T, Lei H, Xie CS (2002) *Polym Test* 21:319
46. Svehlova V, Poloucek E (1987) *Angew Makromol Chem* 153:197
47. Fekete E, Molnár SZ, Kim GM, Michler GH, Pukánszky B (1999) *J Macromol Sci Phys* B38:885
48. Pukánszky B, Turcsányi B, Tüdös F (1988) Interfaces in polymer, ceramic, and metal matrix composites. In: Ishida H (ed). Elsevier, pp 467–475
49. Pukánszky B (1990) *Composites* 21:255
50. Pukánszky B, Fekete E, Tüdös F (1989) *Makromol Chem Macromol Symp* 28:165
51. Busigin C, Lahtinen R, Martinez GM, Thomas G, Woodhams RT (1984) *Polym Eng Sci* 24:169
52. Kubát J, Szalánczi A (1974) *Polym Eng Sci* 14:873
53. Gupta VB, Mittal RK, Sharma PK (1989) *Polym Compos* 10:8
54. Tausz SE, Chaffey CE (1982) *J Appl Polym Sci* 27:4493
55. Haggemueller R, Du F, Fischer JE, Winey KI (2006) Interfacial in situ polymerization of single wall carbon nanotube/nylon 6, 6 nanocomposites. *Polymer* 47:2381–2388
56. Guo J, Liu Y, Prada-Silvy R, Tan Y, Azad S, Krause B, Poetschke P, Grady BP (2014) Aspect ratio effects of multi-walled carbon nanotubes on electrical, mechanical, and thermal properties of polycarbonate/MWCNT composites. *J Polym Sci Part B Polym Phys* 52:73–83
57. Castillo FY, Socher R, Krause B, Headrick R, Grady BP, Prada-Silvy R, Poetschke P (2011) Electrical, mechanical, and glass transition behavior of polycarbonate-based nanocomposites with different multi-walled carbon nanotubes. *Polymer* 52:3835–3845
58. Caamano C, Grady B, Resasco DE (2012) Influence of nanotube characteristics on electrical and thermal properties of MWCNT/polyamide 6, 6 composites prepared by melt mixing. *Carbon* 50:3694–3707
59. Crawford RJ (1998) *Plastics engineering*, elsevier, butterworth heinemann, 3rd edn, pp 4, 14, 59
60. Li J (2010) Friction and wear properties of PA6—reinforced PTFE composites. *J Reinf Plast Compos* 29:490–496
61. Deniz V, Karakaya N, Ersoy OG (2009) Effects of fillers on the properties of thermoplastic elastomers. *Soc Plast Eng.* 01–04
62. Zhou W, Liu X, Zhang Y (2006) Simple approach to SiC nanowires: synthesis, optical and electrical properties. *Appl Phys Lett* 89
63. Monroy E, Ommes F, Calle F (2006) Wide-bandgap semiconductor ultraviolet photo detectors. *Semicond Sci Technol* 18:33–51
64. Katz HS, Milewski JV (1987) *Handbook of fillers for plastics*, Van Nostrand Reinhold, New York, p 10003
65. Zhong X (2011) Enhanced viscoelastic effect of mesoscopic fillers in phase separation. *Soft Matter* 7:3642
66. Kim KH, Ong JL, Okuno O (2002) The effect of filler loading and morphology on the mechanical properties of contemporary composites. *J Prosthet Dent* 87:642–649
67. Leng JS, Zhang DW, Liu Y, Yu K, Lan X (2010) Study on the activation of styrene-based shape-memory polymer by medium-infrared laser light. *Appl Phys Lett* 96

68. Leng JS, Wu XL, Liu YJ (2009) Infrared light-active shape-memory polymer filled with nanocarbon particles. *J Appl Polym Sci* 114:2455–2460
69. Small W, Gjersing E, Herberg JL, Wilson TS, Maitland DJ (2009) Magnetic resonance flow velocity and temperature mapping of a shape-memory polymer foam device. *Biomed Eng Online* 8:42–50
70. Zhang CS, Ni QQ, Fu SY, Kurashiki K (2007) Electromagnetic interference shielding effect of nanocomposites with carbon nanotube and shape-memory polymer. *Compos Sci Technol* 67:2973–2980
71. Razzaq MY, Anhalt M, Frommann L, Weiden Feller B (2007) Thermal, electrical and magnetic studies of magnetite filled polyurethane shape-memory polymers. *Mater Sci Eng Struct Mater Prop Microstruct Process* 444:227–235
72. Vialle G, Di Prima M, Hocking E, Gall K, Garmestani H, Sanderson T, Arzberger SC (2009) Remote activation of nano magnetite reinforced shape-memory polymer foam. *Smart Mater Struct* 18:115014
73. He Z, Shi W, Chen F, Liu W, Liang Y, Han CC (2014) *Macromolecules* 47(5):1741–1748
74. Tanaka T (1992) *Macromolecules* 25(23):6377–6380
75. Tanaka H, Miura T (1993) *Phys Rev Lett* 71(14):2244
76. Tanaka H (1994) *J Chem Phys* 100:5323
77. Tanaka H, Lovinger AJ, Davis DD (1994) *Phys Rev Lett* 72(16):2581
78. Tanaka H (2000) *J Phys Condens Matter* 12(15):R207–R264
79. Tanaka H (2012) *Faraday Discuss* 158:40–371
80. Zhong BXH, Liu Y, Su HH, Zhan GZ, Yu YF, Gan WJ (2011) Enhanced viscoelastic effect of mesoscopic fillers in phase separation. *Soft Matter* 7:3642–3650
81. Kumar PK, Lagoudas DC (2008) Introduction to shape-memory alloys. *Shape-memory alloys*. Springer, Berlin, pp 1–51
82. Liu C, HQ (2007) Review of progress in shape-memory polymers. *J Mater Chem* 17:1543–1558
83. Lang BR (1992) Filler particle size and composite resin classification systems, *onrnat of Oval RchayiiiUilioii* 19:569–584
84. Ohki T, Ni QQ, Ohsako N (2004) *M Composites Part A* 35:1065e73
85. Zhang CS, Ni QQ (2007) *Compos Struct* 78:153–161
86. Ozsoy I (2015) The influence of micro- and nano-filler content on the mechanical properties of epoxy composites. *J Mech Eng* 61:601–609
87. Tanimoto Y, Nishiwaki T, Nemoto K, Ben G (2004) Effect of filler content on bending properties of dental composites: numerical simulation with the use of the finite element method. *J Biomed Mater Res B Appl Biomater* 15,71(1):188–195
88. Xu HH, Moreau JL, Sun L, Chow LC (2008) Strength and fluoride release characteristics of a calcium fluoride based dental nanocomposite. *Biomaterials* 29(32):4261–4267
89. Lang BR, Jaarda M, Wang RF (1992) Filler particle size and composite resin classification systems. *J Oral Rehabil* 19(6):569–584
90. Sekiya K, Okamoto A, Fukushima M, Iwaku M (1994) In vivo wear pattern of experimental composite resins containing different filler components. *Dent Mater J* 13:36–46
91. Lim BS, Ferracane JL, Condon JR, Adey JD (2002) Effect of filler fraction and filler surface treatment on wear of micro filled composites. *Dent Mater* 18:1–11
92. Yuasa S (1990) Influences of composition on brush wear of composite resins and Influences of particle size and content of filler 9(4):659–678
93. Jinsong L, Lan X, Liu Y, Shanyi D (2011) Shape-memory polymers and their composites: stimulus methods and applications. *Progress Mater Sci* 56:1077–1135
94. Suprapakorn N, Dhamrongvaraporn S, Ishida H (1998) Effect of CaCO₃ on the mechanical and rheological properties of a ring-opening phenolic resin: polybenzoxazine. *Polym Compos* 19:126–132
95. Mihaylova B, Briggs A, Hlatky M, Armitage J, Parish S, Gray A, Collins R (2009) Statin cost-effectiveness in the United States for people at different vascular risk levels. *Circ Cardiovasc Qual Outcomes* 2:65–72

96. Pan GH, Huang WM, Ng ZC, Liu N, Phee SJ (2008) The glass transition temperature of polyurethane shape-memory polymer reinforced with treated/non-treated attapulgite (playgorskite) clay in dry and wet conditions. *Smart Mater Struct* 17:045007
97. Cao F, Jana SC (2007) Nano clay-tethered shape-memory polyurethane Nanocomposites. *Polymer* 48:3790–3800
98. Liu C, Chun SB, Mather PT, Zheng L, Haley EH, Coughlin EB (2005) Chemically cross-linked polycyclooctene: synthesis, characterization, and shape-memory behaviour. *Macromolecules* 35:9868–9874
99. Diani J, Gilormini P, Frédy C, Rousseau I (2012) Predicting thermal shape-memory of crosslinked polymer networks from linear viscoelasticity. *Int J Solids Struct* 49:793–799
100. Leng J, Lan X, Liu Y, Du S (2011) Shape-memory polymers and their composites: stimulus methods and applications. *Prog Mater Sci* 56:1077–1135
101. Zhang H, Zhao Y (2013) Polymers with dual light-triggered functions of shape-memory and healing using gold nanoparticles. *ACS Appl Mater Interfaces* 5:13069–13075
102. Pilate F, Toncheva A, Dubois P, Raquez JM (2016) Shape-memory polymers for multiple applications in the materials world. *Eur Polym J* 80:268–294
103. Gojny FH, Wichmann MH, Fiedler B, Kinloch IA, Bauhofer W, Windle AH (2006) Evaluation and identification of electrical and thermal conduction mechanisms in carbon nanotube/epoxy composites. *Polymer* 47:2036–2045
104. Forouzan K, Kazemi HR (2019) Synthesis and evaluation of the effect of structural parameters on recovery rate of shape-memory polyurethane-POSS nanocomposites. *Eur Polym J* 114:446–451
105. Sithara G, Nayarassery N, Adarsh P, Radhakrishnan N, Suresh M (2021) Shape-memory polymer nanocomposites of poly(ϵ -caprolactone) with the polystyrene-block-polybutadiene-block-polystyrene-triblock copolymer encapsulated with metal oxides. *ACS Omega* 6:6261–6273

Chapter 12

Fiber- and Fabric-Reinforced Shape-Memory Polymers



Murugesan Gowri, Nachimuthu Latha, and Mariappan Rajan

12.1 Introduction

Fiber has been defined as a slight and greatly elongated solid substance and can be used for many industrial applications such as textiles, aerospace, medicine, etc. [1]. The physical appearances of fibers are long, light in weight, fine forms of matter, and the diameters are varying from tens of nanometers to tens of micrometers. Fibers possess remarkable properties with flexible nature. The flexible characteristic is of great importance and allows the fiber into the desired structures. Nowadays, there is a wide range of fibers, fabricated with different types of materials used in many advanced engineering structures. Fiber contains high strength, stiffness, and mechanical properties, which reinforce composite materials such as natural as well as the synthetic type of polymers, for example, cellulose, lignin among others [2]. Shape-memory polymers (SMPs) exhibit thermal, optical, chemical properties, and are used in many industries including footwear products, electrical appliances, the medical field, and shape-memory fiber-based polymers are utilized in the field of textile and garments. The extensive use of SMPs in the field of textile and garments can be implemented to develop smart textiles that respond to thermal stimuli [3].

M. Gowri
Department of Chemistry, V.S.B Engineering College, Tamil Nadu, Karur 639111, India

N. Latha
Department of Chemistry, Kandaswami Kandar's College, Tamil Nadu, Velur 638182, India

M. Rajan (✉)
Department of Natural Products Chemistry, School of Chemistry, Madurai Kamaraj University,
Tamil Nadu, Madurai 625021, India

12.2 Fiber Classification

Fibers are classified into two types such as natural fiber and synthetic fiber. The natural and synthetic fibers are further classified as given below in the flow diagram (Fig. 12.1).

12.2.1 Natural Fiber

Natural fibers of cotton, jute, wool, and silk are used by humans in different forms several years ago and exhibit excellent properties. Biocompatibility and good mechanical properties of silk fibers might be used in daily life. Natural fibers showed a significant role in reinforcing composites. The natural fibers are obtained from various sources and it was from minerals as mineral fibers; animals as animal fibers; and plants as plant fibers. Plant fiber fabrication of composites has significant economic benefits due to simple extraction, being environmentally friendly, low cost, natural degradability, and superior properties. The presence of lignin and cellulose in the plant fiber enriches the fiber’s mechanical property. The plant fibers contain a hydroxyl group on its surface, so the structural modifications are easy with some functional group’s introduction, so it is mostly used [4].

After plant fiber, the most important in reinforcement for composites are animal fibers. The sources of animal fibers are wool extracted from bison, sheep, goat, rabbits, etc.

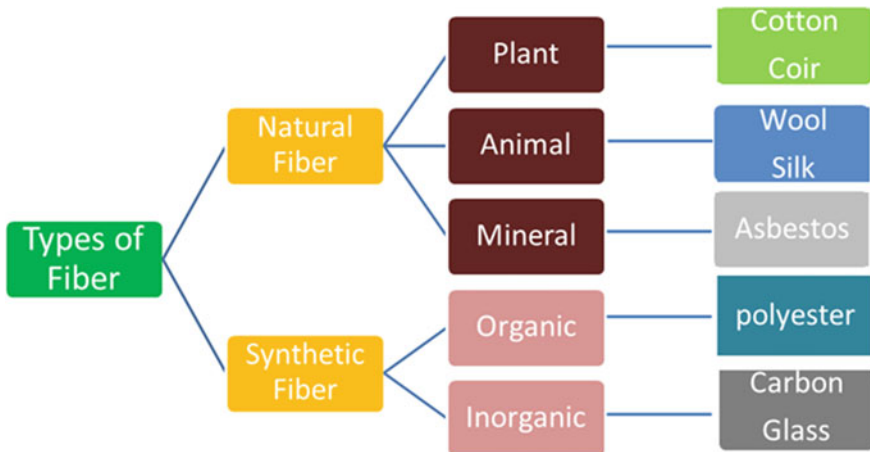


Fig. 12.1 Flow diagram for fiber classification

12.2.2 Synthetic Fiber

Synthetic fibers are manmade fibers that were derived from chemical resources which have been developed at the end of the nineteenth century. Synthetic fibers such as carbon fiber, glass fiber, polyester fiber, nylon, acrylic fiber are mostly used. Synthetic fiber reinforced the composite materials owing to attain better stiffness and strength. Synthetic fibers are widely used in automotive industries and aerospace components.

Some of the polymers possess good shape-memory properties, for example, polyurethane and polyethylene. Fiber-coated polymeric materials exist in the car manufacturing industry, sports equipment, etc. Different types of fiber surface modification methods are reported by many authors such as coating [5], thermal treatment [6], plasma treatment [7], which increase the surface roughness of carbon fibers so that better physical and chemical interactions occur with polymer materials and fiber.

12.2.2.1 Carbon Fiber

The precursors desired the shape of the fiber. Carbon-based fibers are named carbon nanotube fibers, graphene fibers, etc., Carbon fibers are flexible and comprise high mechanical strength, electrical conductivity, and electrochemical properties. High specific stiffness, strength, high carbon yield, low cost, chemical and thermal stability of carbon fiber has been selected as the reinforcement materials. The limitation of this process is multifaceted. It is well-known that the way of loading transfer from matrix to fibers disturbs the carbon fiber-based composite properties. It has significant applications in automobiles, aerospace, brake materials in racing cars, deodorants, decolorizing agents, solvent recovery agents, and catalyst supports in various fields including chemical and pharmaceutical industries [8]. In the medicine field, this fibers act as scaffolds for recreating medicine such as plates, artificial connections for fractures, middle ear implantations [9].

To improve the interfacial adhesion properties of materials, surface modification is necessary. The surface modification can be achieved using the process of coating, oxidation, and grafting among others. Coupling agents perform molecular bridges among matrix and fiber. Xie et al. [10] synthesized carbon fiber-based polymeric composites. The composite possesses excellent melting, crystallization capability, mechanical properties, and is also used for space engineering applications.

12.3 Method of Synthesis

To enrich the productivity and quality, to enhance the monodispersed and homogeneous, to increase the number of layers of nanofibers different types of methods are available to synthesize the fibers through electrospinning, microfluidic method, rotary spinning, and wet spinning [11, 12]. All the above methods have particular

benefits, making them fit for particular applications. In this review, we have discussed the electrospinning and microfluidic approach.

12.3.1 Electrospinning Method

Electrospinning is an adaptable and attractive method to produce the fiber in the nanometer range with diverse morphology and dimensions which is suitable in drug delivery applications, particularly tissue engineering. Materials such as composites, metals, polymers, carbon nanotubes can be incorporated into nanofibers using electrospinning techniques. The nanofibers prepared by electrospinning methods possess optical transparency, size effect, mechanical and thermal properties, so it exhibits better reinforcements [13]. Cellular interactions and matrix deposition of fiber within the scaffold can be controlled in the electrospinning technique. A simple and versatile method of electrospinning is influenced by more than a few factors, including temperature, voltage, pressure, and also flow rate. Using this approach, sometimes the high voltage may prevent the loading of biological materials into the solution, but extra care must be taken to align the fiber with biological materials. Inorganic fibers can be synthesized using an electrospinning approach with polymers incorporated in the precursor solution. The functionalization of polymers may change the surface tension, viscosity, conductivity, and other properties of electrospinning solution [14]. Chao et al. [15] developed the fiber-based drug-coated polymeric composite for wound dressing application. The result showed the developed fibers exhibit smooth uniform morphology with 356 ± 5.98 nm diameter. They found 84.25% of drug encapsulation efficiency and 75% of drug release from the carrier. A zone of inhibition was noticed for 30.13 and 40.51 mm against *Escherichia coli* and *Bacillus subtilis* pathogen. Tao et al. [16] reported the cell line activity for the developed composites and the result implies that there is no significant cytotoxicity and the developed composites exhibit better mechanical properties.

12.3.2 Microfluidic Method

Microfluidic methods are used to synthesize biocompatible and biodegradable polymeric fibers. This method improves biological compatibility and does not need high temperature, pressure, and also high electric currents for fiber fabrication. To get the desired shape and size of the fiber materials, these parameters are to be slightly tuned. In addition this method uses the materials in lesser quantity and used for energy devices, and biomedical areas applications especially tissue engineering [17]. By using the microfluidic approach, the formation of fiber, as well as the particles, are exhibiting the nanometer scale to a few hundred-micron structures without utilizing other facilities. The synthesis method may be completed under ambient circumstances and also the fluid is not exposed to high voltages and high temperatures. For

the incorporation of biological materials into the fiber the microfluidic technologies are mostly used without any loss of biological materials function and simple, with continuity of this process is mostly used in drug delivery applications. This technique need not require higher voltage, higher temperature, and higher pressure, and also it is a cost-efficient approach [18]. Ahn et al. [19] reported the ampicillin-loaded system for wound healing applications using the micro-fluidic spinning approach. The in-vivo studies results showed the developed fiber carrier is suitable for testing wound healing for rat. Zhang et al. [20] developed the alginate microfibers via a simple microfluidic spinning approach. Solution of alginate concentration raises, fiber diameter also increased. They changed the concentration of the solutions from 1 to 2%, the grooved structure depth also increased. They reported that alginate fibers maybe a suitable applicant for tissue scaffolds.

12.4 Fiber in Biomedicine

Fiber plays an important role in medicinal applications, especially drug delivery and tissue repair and regenerations. Fiber-based drug delivery carriers possess significant potential in clinical medicine [20]. In drug delivery, therapeutic molecules target the specific tissue or organs, hence the efficiency of the drug is maximized. Advanced properties and easy preparation methods of nanofibers are attractive carriers in drug delivery [21].

Harmless is important in human tissue so the biocompatible nature of gelatin and alginate-based fibers are the effective carriers of therapeutic molecules. Artificial fiber-shaped muscles possess excellent movement like twisting, bending, and tensile, and nowadays, it is required in biological systems [22].

The interaction of drug molecules with fibers is attained through spinning. The drug release activity depends on the factors of fibers component, pH variation, surface area, magnetic fields, and light [23]. However, fiber strengthening enriches the material mechanical properties and similarly reduces the deformability. The reinforcement process is cost-effective.

12.5 Shape-Memory Polymers

Global challenges in environment and healthcare, the energetic smart materials are forefront so-called shape-memory to improve the quality of human health. Shape-memory structures include polymers, composites, hybrids, ceramics, and fibers among others. Shape-memory polymers (SMPs) exhibit the high recoverable strain, transparency, biocompatibility, and biodegradability nature as discussed [24].

Structural deformations of SMPs are due to a variety of stimuli responses such as light, heat, electricity, etc. The stimulation of electromagnetic fields is responsible to heat the material incidentally. Moreover, SMPs are lightweight, easier to process,

and less expensive compared to others [25]. In recent years, SMPs combined with polymer materials and used in many industries including biomedicine, aerospace, etc.,

Based on the selection of monomer type, the polymers are classified as linear, branched, and network. Polymer chains are cross-linked and make the polymer networks and prevent chain displacement. Furthermore, SMPs comprise molecular switches and net points. Chemical cross-links can be occurring in polymers, containing more than one reactive group. Meanwhile, the physical cross-links occur via hydrogen bonds and ionic clusters [26]. However, the rate and time of shape recovery strongly depend on the source power which was tuned upon microwave irradiation.

12.6 Reinforcements

SMPs can often be reinforced with fiber materials to improve their mechanical properties and significant improvements have been occurred to balance the material temperature similar to human body temperature. To attain a high recovery force, high strength, and good electrical conductivity, SMPs are combined with particles such as carbon black, carbon nanofiber, carbon nanotubes, organoclay, Ni, Fe₃O₄, silicon carbides to enrich the strength, stiffness, and also magnetic properties [27]. Carbohydrate biopolymers such as chitosan, starch, and cellulose acetate were used in shape-memory materials [28–30] (Fig. 12.2).

12.6.1 Carbon Nanotube

Carbon nanotube is one of the promising materials in the field of nanoscience and nanotechnology, for its greater structural, electrical, and mechanical properties but also influence the recoverable strain of shape-memory polymers. In carbon nanotube, the hexagonal arrangement of carbon atoms varied from angstroms to nanometers in size [32, 33]. However, carbon nanotubes have a strong tendency to aggregate together due to their high surface area and strong Vander Waals interaction and are used to develop multifunctional polymer composites [34]. The carbon nanotube-loaded SMPs improve the tensile strength, electrical and thermal conductivity [35]. Raja et al. [36] reported the surface-modified carbon nanotubes and noticed the development in the mechanical properties. Ni et al. [37] studied the carbon nanotube-based SMPs nanocomposites with mechanical properties. Results indicate the strong shape recoverable property and temperature dependence property. Hassanzadeh-Aghdam et al. [38] reported the SMPs nanocomposites thermoelastic properties. They reported the elastic behavior of synthesized composites improved by the reduction of carbon nanotube diameter.

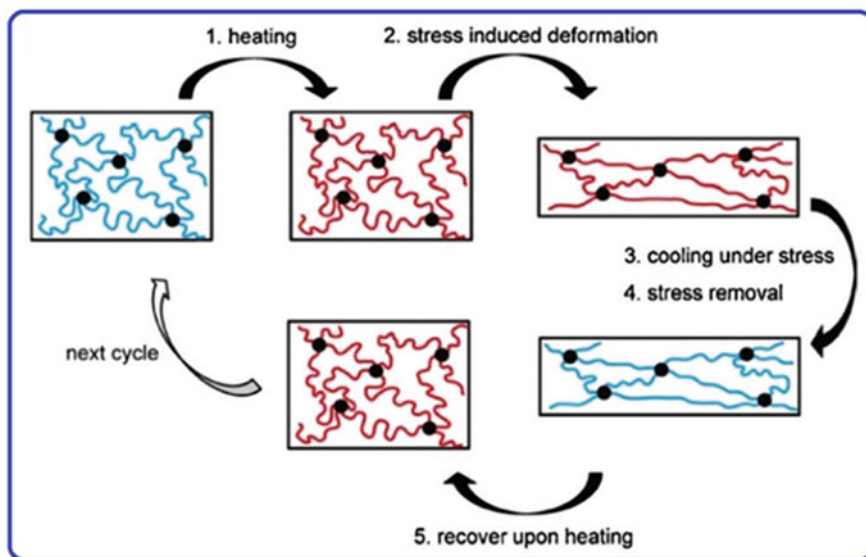


Fig. 12.2 Mechanism of shape-memory polymers throughout the thermal cycle. Reprinted from [31] Copyright © (2015) with permission from Elsevier Ltd.

12.6.2 Hydrogel

Soft, flexible, enough to enable deformations nature of hydrogels are water-swollen three-dimensional polymeric networks with a highly open structure and the large inner surface which are required for the application of tissue engineering, drug delivery etc. In addition, the outstanding quality and excellent fabrication of biomaterials play a significant role in the development of novel topical hydrogel scaffolds for skin tissue engineering applications. The external stimuli, such as heat, light, or electricity are responsible for the shape deformations nature of hydrogel. The capability of the hydrophilic chain in polymeric networks is to strongly intermingle with water and allow the expansion of materials and the formation of hydrogel [39–41]. 3D polymer networks of hydrogels are powerfully absorbed by water, upon stimulation, the quantity of water in the polymer network changes [42]. The shape-memory hydrogels may change their shapes in particular conditions and upon stimulation, they reproduce their original shapes. Nan and co-authors [43] designed imidazole-zinc ion-based hydrogels. They reported that the concentration of zinc ions is important in toxicity analysis such as retaining the viability of the cells. Dalton et al. [44] reported the biomedical application of developed materials. Results showed the SMP foam hydrogel composites enhanced the fluid uptake abilities. Xue et al. [45] prepared the composite hydrogels through physical interactions. The results showed that the interaction of hydrogen bond and metal coordinates is responsible for the enhancement of toughness, stiffness, extension, and self-healing efficiency.

12.7 Synthetic Procedure of SMPs

SMPs are not pure polymeric systems. Initially, SMPs are formed using the conventional method and then the sample is deformed again to retain their specific shape. After that, the functional groups are attached to SMPs through chemical crosslinking and the functional groups may form rescindable covalent bonds through reaction with others. It may be controlled by using external stimulations [46].

12.7.1 *Thermally Stimulated SMPs*

Thermally stimulated SMPs have been attained for cross-linked and thermoplastic polymers. The polymeric network has been synthesized using copolymerization of monomers with functional cross-linkers [47]. Baker et al. [48] designed the poly(3-caprolactone)-copoly(ethylene glycol) (PCL-co-PEG) shape-memory foams for the application of scaffold for tissue engineering. They aimed to develop the SMPs scaffolds capable of changing the size and shape under body temperature triggering. Yu et al. [49] reported the thermal stimulated SMPs with carbon nanotubes using microwave radiation. The synthesized specimens were induced at the microwave radiation of 40 W, 2.45 GHz.

12.7.2 *Light Stimulated SMPs*

Light stimulated SMPs are independent of temperature effects and the permanent shapes of these polymers are determined by net points. Coumarin-based poly(ϵ -caprolactone) and azobenzene-based crystalline elastomer is the example of light active polymers [50, 51]. Zhang et al. [52] reported cross-linked polymer with gold nanoparticles. The developed cross-linked nanoparticles exhibit optical therapeutic abilities.

12.8 Properties of SMPs

SMPs exhibit the physical as well as the mechanical properties in the biomedical environment and allow the materials to human tissue. So, the design of materials is an important one. The rigidity and flexibility properties of SMPs are to diminish the destruction produced by the neighboring tissue. Biodegradable property of SMPs used in the biomedical field. Strength and stiffness are the compulsory factors for the materials to produce the scaffolds, due to this nature, SMPs are used in the bone tissue engineering field [54].

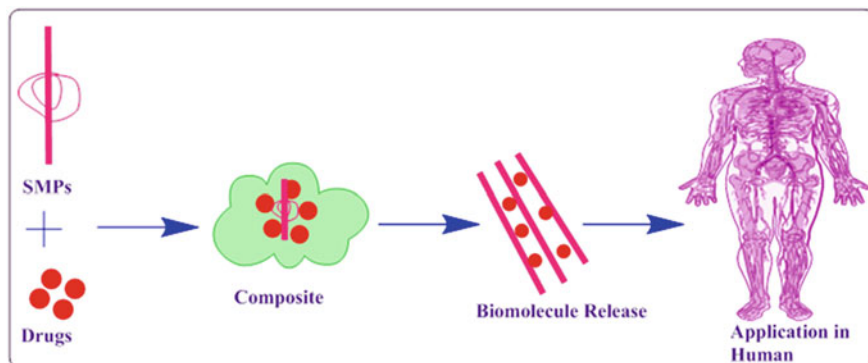


Fig. 12.3 Nanotechnology with SMPs

12.9 The Importance of Nanotechnology in SMPs

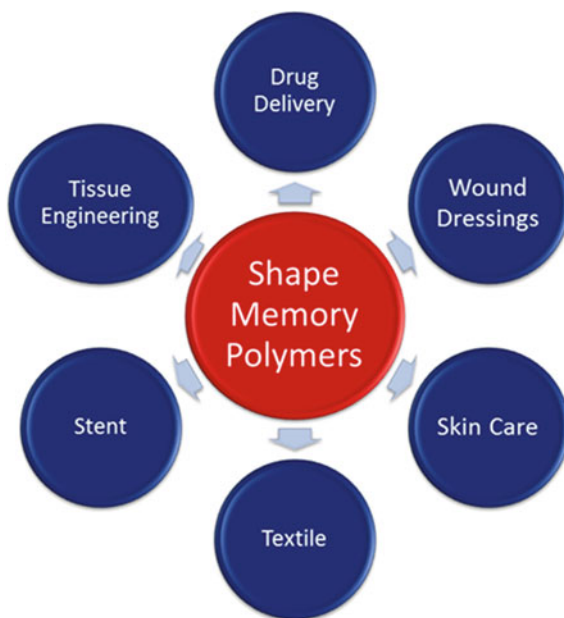
The designed polymeric materials may encode the physical data into their assembly and as a result, use that data to react and familiarize themselves to environmental changes. Hence, high surface area, high stiffness, and water responsive properties of nanorods, nanofillers, nanotubes, nanocomposites, and nanofibers are incorporated into the SMPs matrix to further enhance the functionality, mechanical behavior, processability of material [55]. The increased hydrophilic nature and roughness of the surface in nanohybrid materials help the tissue/cells to observe well and create the developed materials as enhanced biomaterials.

Poly(lactide) and poly(ϵ -caprolactone) based nanoparticles, and their copolymer-based SMPs are frequently used in biomedical applications because of flexibility, and also tuning the properties of materials such as mechanical, thermal, and degradation [56, 57]. Beauty et al. [58] reported that Fe_3O_4 in SMPs could act as nano-reinforced agents and showed better antimicrobial properties, thus preventing the formation of biofilm against two pathogens with better cytocompatibility for various cells lines (Fig. 12.3).

12.10 Application of SMPs

SMPs enlarge their implementation in many fields including medical and electronic devices [59, 60], textiles [61], aerospace applications [62], and many others. The dual character of SMPs particularly beneficial for medical devices. For biomedical applications, basic requirements of biocompatibility and nontoxic nature are most important to design the materials (Fig. 12.4).

Fig. 12.4 Different applications of SMPs



12.10.1 Textile

Superior processability, mechanical properties, and high recoverability of SMPs are used in textile. In textile, SMPs can change the structures from macro to micro-level to realize the function for heat adjustment and moistness among fabric besides skin [63]. For example, SMPs perform as a dual character, while the wearer feels hot, if the holes in the fabric are automatically exposed and permit the heat outside then make it comfortable and in cool conditions, it make as warm. Thermo-responsive SMPUs of polyurethane were reported by Saenz-Perez et al. [64]. Shape-memory polyurethanes displayed admirable retrieval higher than 99.9%. Results imply that the synthesized shape-memory polyurethane acts as the potential application of breathable fabrics in moisture control in textiles. Wang et al. [65] prepared the chitosan-graft-poly (N-isopropylacrylamide) using the sonication method. Further, the addition of crosslinkers onto the cotton fabric was achieved in the easy pad-dry-cure method. At 40 °C, the finished fabric water vapor permeation was measured as 90% relative humidity. Polyvinylidene fluoride nanofibers then polytetrafluoroethylene nanoparticles on the surface of polyethylene terephthalate fabric using electrospinning and electro spray technique for textile applications reported by Qiu et al. [66]. They developed the power generation fabric which is comfortable to wear, easy to breathe, tailorable, and also easily washable. These fabrics are effortlessly deformable in all direction and are cleverly combined with personal clothes, it exhibits excellent performance for energy scavenging from human running or walking.

12.10.2 Garments

In the textile industry, the garment can be used to fabricate the SMPs to maintain the molecular free volume and control the glass transition temperature which regulates the heat to the wearer's body. Garment made by using SMPs fiber is flexible to the wearer's body size and not at all noteworthy pressure is applied and breathing is normal. Hence, fabric-reinforced SMPs are an upright choice to preserve the constant body temperature. Without shrinkage, no wrinkle, crease maintenance outcome, and energetic artistic cloths are synthesized by treating SMPs on fabrics using garments. While cotton type of fabrics are treating with SMPs it accomplishes the wrinkle-free effect moreover the wool fiber with SMPs reduces the frictional effect before the packing process. SMPs treated woolen garments are not affected in size, but SMPs untreated woolen garments shrink in size after the laundering process. Fiber surface is covered by SMPs, it demonstrates the various shrinkage effects consequently heating and cooling and achieving the water repellent effect as well as controlling water spreading effect [67]. Hence, weaving, knitting, coating, and lamination are relating SMPs into textiles. Lu et al. [68] reported wool knitted fabric and garments treated with SMPs. The shape-memory finishing is an easy approach and saves water and the results showed that the finished fabrics exhibit better resistance, stability, crease retention effect along with recovery.

12.10.3 Biomedical Application

Several conditions must be considered to encounter clinical use. Safety is important in using biomedical devices. Biodegradability would be advantageous for many medical applications. The viability of cells, biocompatibilities are the significant factor for some materials designed for biomedical uses. Biodegradability with shape-memory ability is the combination to meet the multi functionalities for the material. For such materials supports for tissue engineering application, self-retractable and changeable stents, self-tightening stitches, and drug delivery application. Diverse medical devices contacts are implanted in humans. SMPs are playing an important role in medical devices. SMPs exhibit the stimulating mixtures of tunable properties and functionalities, so the design necessities of SMPs with respect to their potential application by way of biomedical devices.

The medicinal device is implanted with the aid of marginally offensive surgical laser treatment into the blood vessel, SMPs material coils to its stable shape, supporting the eradication of blood coagulation. Surgery followed by removal of the implant is not needed if the implant degrades within the time. In cardiovascular surgery, the SMPs of nickel–titanium are used as suture clips [69]. Some of the shape-memory polymer material's medicinal uses are mentioned in the tabular column (Table 12.1).

(I) Tissue engineering

Table 12.1 Shape-memory polymers with medicinal application

S. No	Shape-memory polymer materials	Medicinal applications	Results	Reference
1	Polytetrafluoroethylene (PTFE), Ultra High Molecular Weight Polyethylene (UHMWPE), PolyEtherEtherKetone (PEEK)	Knee and hip joint replacement	Materials possessed good mechanical properties, high stability, and high wear resistance. Different types of fractures and prevention measures are discussed	[70]
2	Polyesterurethane networks	Control release of dexamethasone and aspirin drug	They demonstrated the developed networks could control the release of DEX and ASP for the long term. They have the high application of drug-loaded shape-memory cardiovascular stents, smart implants or medical devices	[71]
3	Polyurethane	Orthodontics	polyurethane wire samples showed an average shape recovery of 80–85% at 30–50 hard segments wt.%	[72]
4	Polyurethane	Use the stent as the drug delivery system	An elongated stent is introduced in the catheter using pliers. Polymer stent as the drug delivery system will lead to a significant reduction of restenosis and thrombosis	[73]
5	Ag-coordinated isonicotinate functionalized polyester (PIE) (Ag-PIE),	Wound dressings	The films exhibited antibacterial properties against Escherichia coli and good cytocompatibility with osteoblast cells favoring their biomedical application as smart medical devices	[74]

In bone tissue engineering, the formation of the extracellular matrix is most important which involves the subsequent step, migration, proliferation, and differentiation of osteoprogenitors. Scaffolds-based SMPs are used in bone tissue engineering and surgery applications. Gorgeous benefits with shape modifying ability of SMPs scaffold may be embedded in affected area efficiently. Biodegrading properties of

materials would help the implanted structure to dissolve completely and allow the tissue to grow [75]. Sa et al. [76] prepared the biphasic calcium phosphate with zirconia scaffold for tissue engineering applications. They reported the synthesized scaffold is highly biocompatible and has higher compressive strength. An et al. [77] reported the ZrO_2 /hydroxyapatite scaffold to improve mechanical properties and bone regeneration. Feng et al. [78] prepared zinc oxide doped scaffolds which enhance the biological as well as the mechanical properties, especially the bone repair and replacement. Bao et al. [79] reported the nanofibrous SMPs scaffold using the electrospinning method to bone defects in bone repair and regeneration applications.

(II) Drug delivery

The release of drugs from developed materials is mainly based on the surface area to volume ratio. Hydrogels and SMPs are playing a crucial role to attain the beneficial effect of drug delivery. Yang et al. [80] reported the thermal-induced drug-eluting stent with dual drug delivery. Melocchi et al. [81] developed SMPs-based drug release profile in the application of gastric retention. They used glycerol, Eudragit RS /RL, SMPs, with allopurinol drugs. The developed formulation attains prolonged release over 6 h. Chen et al. [82] developed the pH-sensitive polymer system and reported the significance of pH in shape-memory along with the drug delivery effect. Wischke et al. [83] reported multidrug such as enoxacin, nitrofurantoin, and ethacridine lactate-loaded star shape polymer and investigated their pharmaceutical applications. They found the synthesized polymer showed better biodegradable, shape-memory, and controlled release properties (Fig. 12.5).

(III) Orthodontics

In orthodontic, SMPs have great potential because of the capability of thermally stimulated shape alterations to create force and their enhanced biocompatible properties. Liu et al. [84] prepared the glass fiber-based SMPs carrier for orthodontic applications. Glass fibers addition improves the properties of synthesized SMPs carrier. SMPs carriers enhance the dentation aligning in the initial step. Shape-memory alloy of nickel–titanium is used for the development of orthodontic wire reported by Fercec et al. [85]. They confirmed the developed wire's electrical resistivity and stresses.

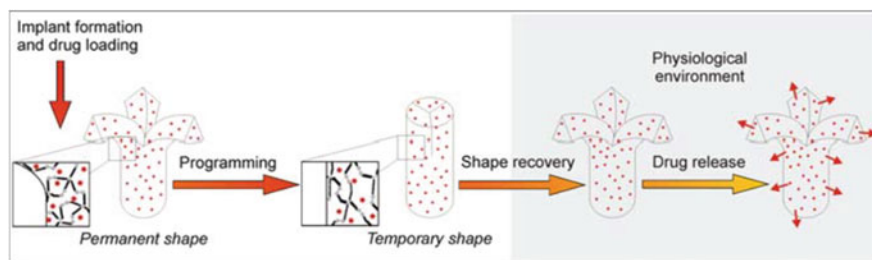


Fig. 12.5 SMP device for drug delivery application. Reprinted from [83] Copyright © (2009) with permission from Elsevier B.V.

(IV) Stents

The flexibility of stents is intended to avoid vasospasms besides restenosis of a vessel after the treatment of balloon angioplasty. SMPs were planned for cardiovascular stent involvements and diminish the size of the catheter for delivery also maintains the body temperature. Established room temperature storage of stents is greatly dependent on crosslinking density and glass transition temperature. Yakacki et al. concluded the period for complete shape recovery is extremely reliant on crosslinking density, T_g and deformation temperature [86]. Baer et al. [87] developed the laser-activated thermoplastic polyurethane SMPs stent and fiber-based delivery. They reported that the stent did not completely enlarge more than 60% with power 8.6 W. Photothermal actuation of the stent was done in water occupied mock artery. Jia and co-others [88] studied 3D printed SMPs polylactide. They confirmed the developed stent consumed outstanding fixity of shape also its preserve temporary shape even at room temperature. They suggested that the 3D printed PLA stents may be useful for cardiovascular diseases. Gu et al. [89] developed stent-based biodegradable SMPs composites. The composite possessed biocompatibility, biodegradability, and mechanical properties, which was confirmed by cytotoxicity evaluation.

(V) Skincare

Hydrogel treated SMPs in the textiles industry possess whitening, moisture-free, brightening, and also anti-aging properties on human skins as well as it controls the release of perfumes, other drugs, nutritious ingredients to human skin without harm. Gong et al. [90] reported the SMPs composite for potential morphing skin applications. They reported human skin delivers an exterior smooth aerodynamic surface due to one side filled with SMP. SMPs support the skin to adjust its stiffness in various atmospheres.

(VI) Wound dressing

In wound healing, the SMPs can act as a wound dressings material. In wound closures, the biodegradable SMPs act as a smart suture that could allow optimized tightening of the knot. Wounds can quickly heal while using the smooth dressing materials because it releases the drug in response to deviations of pH and temperature. Better antibacterial properties of chitosan-based products are used to synthesize the wound dressing materials owing to better wound-healing effects [91]. Hydrogel requires excellent tissue adhesiveness and cell affinity to incorporate with infected tissue in practical applications. Li et al. [92] developed zwitterionic SMPs to study the application of wound dressings. They also used cross-linking agent. The circular shape of the developed dressing sample can accurately fit and then bind compactly to the wound site. Chen et al. [93] developed the hydrogel for wound dressing application. They found the hydrogel having self-healing ability (in 6 h, 80% mechanical recovery), tensile strength (0.109 MPa), also ultra-stretchability (2550%). Kokabi et al. [94] reported the polyvinyl alcohol hydrogel-based Na-montmorillonite clay and studied their wound dressing properties. Results showed the developed nanocomposites and

their function act as the barriers against microbe penetration and to protect the spread of infection further.

(VII) Sterilizability

Before clinical applications, sterilization is essential for all medical devices. Sterilization of SMPs must be accompanied without compromising their quality. Yakacki et al. [95] investigated the sterilization function of synthesized SMPs networks. They used different types of sterilization methods such as steam sterilization, ethylene oxide, irradiation low-temperature plasma, and noxilizer. Among these, noxilizer technique was done at 25.1 °C for sterilization. Peniston et al. [96] studied the effect of sterilization of orthopedic implants produced from PLA (polylactic acid). They reported ethylene oxide method produces better results compared to the hydrogen peroxide gas plasma (HPGP) sterilization method.

12.11 Conclusion

In this chapter, we have endeavored to outline the synthesis, properties, and application of fibers reinforced stimulus-responsive SMPs. Nanofibers are gifted aspirants in materials for drug delivery carriers due to surface to volume ratio, as well as the properties of nanomaterials. The electrospinning, microfluidic methods are usually used for the synthesis of fibers applied for drug delivery applications. Synthesis of a new carrier that reacts to outside surroundings needs an innovative molecular proposal in a single molecule.

The trials of systematic determinations in the area of SMPs carrier would focus on the proposal of novel methods. Polymeric materials possess shape-memory function and respond to one or more exterior inducements including light and thermal-induced SMPs. Proposal of stimulus approachable carrier has directed to stimulating advances for shape-memory materials as shape-memory hydrogels, shape-memory composites, and shape-memory polymers (SMPs). Among these, SMPs have advantages including low cost, simple synthesis approach, desirable properties, lesser density, and easier shape programming procedures. SMPs are applied in the biomedical field such as biodegradability, biocompatibility, sterilizability, ability to exhibit shape-memory effect, and nonimmunogenic effect to the human body. Present applications of SMPs in the biomedical region involve stent, tissue engineering, artificial skin, textile then drug delivery systems are revealed in this chapter.

References

1. Chen S, Qiu L, Cheng H-M (2020) Carbon-based fibers for advanced electrochemical energy storage devices. *Chem Rev* 120(5):2811–2878

2. Schreiber M, Vivekanandhan S, Mohanty AK, Misra M (2014) Iodine treatment of lignin-cellulose acetate electrospun fibers: enhancement of green fiber carbonization. *ACS Sustain Chem Eng* 3(1):33–41
3. Gök MO, Bilir MZ, Gürçüm BH (2015) Shape-memory applications in textile design. *Procedia Soc Behav Sci* 195:2160–2169
4. Sun Z (2019) Hyperbranched polymers in modifying natural plant fibers and their applications in polymer matrix composites—a review. *J Agric Food Chem* 67:8715–8724
5. Jinxiang P, Selvakani P, Mariappan R (2019) In-vivo assessment of minerals substituted hydroxyapatite/poly sorbitol sebacate glutamate (PSSG) composite coating on titanium metal implant for orthopedic implantation. *Biomed Pharmacotherapy* 119:109404
6. Xin L, Kandasamy V, Thiagarajan R, Mariappan R, Andy R (2020) Combined photodynamic-chemotherapy investigation of cancer cells using carbon quantum dot-based drug carrier system. *Drug Deliv* 27:791–804
7. Montes-Morán MA, Young RJ (2002) Raman spectroscopy study of HM carbon fibres: effect of plasma treatment on the interfacial properties of single fibre/epoxy composites. Part I: fibre characterisation. *Carbon* 40:845–855
8. Gao B, Zhang R, Gao F, He M, Wang C, Liu L, Zhao L, Cui H (2016) Interfacial microstructure and enhanced mechanical properties of carbon fiber composites caused by growing generation 1–4 dendritic poly(amidoamine) on a fiber surface. *Langmuir* 32(33):8339–8349
9. Murugan S, Mariappan R, Rajendran P, Marraiki N, Abdallah ME (2020) In vivo assessment of a hydroxyapatite/ κ -Carrageenan-maleic anhydride-casein/doxorubicin composite-coated titanium bone implant. *ACS Biomater Sci Eng* 6:1650–1662
10. Xie H, Li L, Deng XY, Cheng CY, Yang KK, Wang YZ (2018) Reinforcement of shape-memory poly (ethylene-co-vinyl acetate) by carbon fibre to access robust recovery capability under resistant condition. *Compos Sci Technol* 157:202–208
11. Kenry LCT (2017) Nanofiber technology: current status and emerging developments. *Prog Polym Sci* 70:1–17
12. Zhang L, Chen Q, Ma Y, Sun J (2020) Microfluidic methods for fabrication and engineering of nanoparticle drug delivery systems. *ACS Appl Bio Mater* 3:107–120
13. Jiang S, Chen Y, Duan G, Mei C, Greiner A, Agarwal S (2018) Electrospun nanofiber reinforced composites: a review. *Polym Chem* 9(20):2685–2720
14. Tan AR, Ifkovits JL, Baker BM, Brey DM, Mauck RL, Burdick JA (2008) Electrospinning of photocrosslinked and degradable fibrous scaffolds. *J Biomed Mater Res* 87A:1034–1043
15. Chao S, Li Y, Zhao R, Zhang L, Li Y, Wang C, Li X (2018) Synthesis and characterization of tigeicycline-loaded sericin/poly (vinyl alcohol) composite fibers via electrospinning as antibacterial wound dressings. *J Drug Deliv Sci Tec* 44:440–447
16. Tao F, Cheng Y, Tao H, Jin L, Wan Z, Dai F, Xiang W, Deng H (2020) Carboxymethyl chitosan/sodium alginate-based micron-fibers fabricated by emulsion electrospinning for periosteal tissue engineering. *Mater Des* 194:108849
17. Changwei L, Guolin M (2020) Lanthanides-substituted hydroxyapatite/aloe vera composite coated titanium plate for bone tissue regeneration. *Int J Nanomed* 15:8261–8279
18. Jun Y, Kang E, Chae S, Lee SH (2014) Microfluidic spinning of micro- and nano-scale fibers for tissue engineering. *Lab Chip* 14:2145–2160
19. Ahn SY, Mun CH, Lee SH (2015) Microfluidic spinning of fibrous alginate carrier having highly enhanced drug loading capability and delayed release profile. *RSC Adv* 5:15172–15181
20. Zhang X, Weng L, Liu Q, Li D, Deng B (2019) Facile fabrication and characterization on alginate microfibrils with grooved structure via microfluidic spinning. *R Soc Open Sci* 6(5):181928
21. Sun Y, Cheng S, Lu W, Wang Y, Zhang P, Yao Q (2019) Electrospun fibers and their application in drug-controlled release, biological dressings, tissue repair, and enzyme immobilization. *RSC Adv* 9:25712–25729
22. Periyakaruppan P, Naresh Kumar R, Abdullah AA, Murugan AM, Mariappan R (2018) Deep eutectic solvent-mediated FA-g- β -Alanine-co-PCL drug carrier for sustainable and site-specific drug delivery. *ACS Appl Bio Mater* 1:2094–2109

23. Sim HJ, Jang Y, Kim H, Choi JG, Park JW, Lee DY, Kim SJ (2020) Self-helical fiber for glucose-responsive artificial muscle. *ACS Appl Mater Inter* 12(18):20228–20233
24. Shang L, Yu Y, Liu Y, Chen Z, Kong T, Zhao Y (2019) Spinning and applications of bioinspired fiber systems. *ACS Nano* 13(3):2749–2772
25. Pilate F, Toncheva A, Dubois P, Raquez J-M (2016) Shape-memory polymers for multiple applications in the materials world. *Eur Polym J* 80:268–294
26. Singhal P, Wilson TS, Maitland DJ (2010) Controlling the physical properties of random network based shape-memory polymer foams. *Mater Res Soc Symp Proc* 1274:43–49
27. Kirillova A, Lonov L (2019) Shape-changing polymers for biomedical applications. *J Mater Chem B* 7:1597–1624
28. Lan X, Liu Y, Lv H, Wang X, Leng J, Du S (2009) Fiber reinforced shape-memory polymer composite and its application in a deployable hinge. *Smart Mater Struct* 18(2):024002
29. Zhang Y, Zhang M, Jiang H, Shi J, Li F, Xia Y, Zhang G, Li H (2017) Bio-inspired layered chitosan/graphene oxide nanocomposite hydrogels with high strength and pH-driven shape-memory effect. *Carbohydr Polym* 177:116–125
30. Coativy G, Gautier N, Pontoire B, Buléon A, Lourdin D, Leroy E (2015) Shape-memory starch-clay bionanocomposites. *Carbohydr Polym* 116:307–313
31. Bai Y, Liu Y, Wang Q (2016) Cellulose acetate for shape-memory polymer: Natural, simple, high performance, and recyclable. *Adv Polym Technol* 37(3):869–877
32. Zhao Q, Qi HJ, Xie T (2015) Recent progress in shape-memory polymer: New behavior, enabling materials, and mechanistic understanding. *Prog Polym Sci* 49–50:79–120. <https://doi.org/10.1016/j.progpolymsci.2015.04.001>
33. Lu H, Liu Y, Gou JJ, Leng J, Du S (2011) Surface coating of multi-walled carbon nanotube nanopaper on shape-memory polymer for multifunctionalization. *Compos Sci Technol* 71:1427–1434
34. Wang Z, Liang ZY, Wang B, Zhang C, Kramer L (2004) Processing and property investigation of single-walled carbon nanotube (SWNT) buckypaper/epoxy resin matrix nanocomposites. *Compos Part A—Appl Sci Manuf* 35(10):1225–1232
35. Wernik JM, Meguid SA (2010) Recent developments in multifunctional nanocomposites using carbon nanotubes. *Appl Mech Rev* 63(5):050801
36. Wan T (2010) Shape-memory polymer yarns. *Tech Textile Yarns* 429–451. <https://doi.org/10.1533/9781845699475.2.429>
37. Raja M, Ryu SH, Shanmugaraj AM (2013) Thermal, mechanical and electroactive shape-memory properties of polyurethane (PU)/poly (lactic acid) nanocomposites. *Eur Polym J* 49(11):3492–3500
38. Ni QQ, Zhang CS, Fu Y, Dai G, Kimura T (2007) Shape-memory effect and mechanical properties of carbon nanotube/shape-memory polymer nanocomposites. *Compos Struct* 81:176–184
39. Hassanzadeh-Aghdam MK, Ansari R, Mahmoodi MJ (2019) Effective thermo-mechanical properties of shape-memory polymer nanocomposites reinforced by carbon nanotubes. *Mech Mater* 129:80–98
40. Shang J, Le X, Zhang J, Chen T, Theato P (2019) Trends in polymeric shape-memory hydrogels and hydrogel actuators. *Polym Chem* 10:1036–1055
41. Periyakaruppan P, Anbalagan S, Mariappan R (2019) Synthesis of bio-degradable poly (2-hydroxyethyl methacrylate) using natural deep eutectic solvents for sustainable cancer drug delivery. *SN Appl Sci* 1:568
42. Kalai Selvan N, Shanmugarajan TS, Uppuluri VNVA (2019) Hydrogel based scaffolding polymeric biomaterials: approaches towards skin tissue regeneration. *J Drug Deliv Sci Technol* 101456. <https://doi.org/10.1016/j.jddst.2019.101456>
43. Jeon SJ, Hauser AW, Hayward RC (2017) Shape-morphing materials from stimuli-responsive hydrogel hybrids. *Acc Chem Res* 50(2):161–169
44. Nan W, Wang W, Gao H, Liu W (2013) Fabrication of a shape-memory hydrogel based on imidazole-zinc ion coordination for potential cell encapsulating tubular scaffold application. *Soft Matter* 9:132–137

45. Dalton E, Chai Q, Shaw MW, McKenzie TJ, Mullins ES, Ayres N (2019) Hydrogel-coated polyurethane/urea shape-memory polymer foams. *J Polym Sci Pol Chem* 57:1389–1395
46. Xue S, Wu Y, Guo M, Liu D, Zhang T, Lei W (2018) Fabrication of Poly(acrylic acid)/boron nitride composite hydrogels with excellent mechanical properties and rapid selfhealing through hierarchically physical interactions. *Nanoscale Res Lett* 13(1):393
47. Behl M, Lendlein A (2007) Actively moving polymers. *Soft Matter* 3(1):58–67
48. Barot G, Rao IJ (2006) Constitutive modeling of the mechanics associated with crystallizable shape-memory polymers. *Z angew Math Phys* 57:652–681
49. Baker RM, Henderson JH, Mather PT (2013) Shape-memory poly(ϵ - caprolactone)-co-poly (ethylene glycol) foams with body temperature triggering and two-way actuation. *J Mater Chem B* 1:4916–4920
50. Yu K, Liu Y, Leng J (2014) Shape-memory polymer/CNT composites and their microwave induced shape-memory behaviors. *RSC Adv* 4:2961–2968
51. Defize T, Thomassin JM, Ottevaere H, Malherbe C, Eppe G, Jellali R, Alexandre M, Jérôme C, Riva R (2018) Photo-cross-linkable coumarin-based poly(ϵ -caprolactone) for light-controlled design and reconfiguration of shape-memory polymer networks. *Macromolecules* 52(2):444–456
52. Lee KM, Koerner H, Vaia RA, Bunning TJ, White TJ (2011) Light-activated shape-memory of glassy, azobenzene liquid crystalline polymer networks. *Soft Matter* 7:4318–4324
53. Zhang H, Zhao Y (2013) Polymers with dual light-triggered functions of shape-memory and healing using gold nanoparticles. *ACS Appl Mater Inter* 5:13069–13075
54. Biswas A, Pratap Singh A, Rana D, Aswal VK, Maiti P (2018) Biodegradable toughened nanohybrid shape-memory polymer for smart biomedical applications. *Nanoscale* 10:9917–9934
55. Lu H, Lei M, Yao Y, Yu K, Fu Y (2014) Shape-memory polymer nanocomposites: nano-reinforcement and multifunctionalization. *Nanosci Nanotechnol Lett* 6(9):772–786
56. Xu J, Song J (2015) Polylactic acid (PLA)-based shape-memory materials for biomedical applications. *Shape-Memory Polym Biomed Appl* 197–217
57. Periyakaruppan P, Abdallah Mohamed E, Ali Hassan B, Mariappan R (2018) Natural solvent-assisted synthesis of amphiphilic co-polymeric nanomicelle for prolonged release of camptothecin delivery. *New J Chem* 42:10366–10375
58. Beauty D, Manabendra M, Aadesh U, Pronobesh C, Niranjana K (2013) Bio-based hyper branched polyurethane/Fe₃O₄ nanocomposites: smart antibacterial biomaterials for biomedical devices and implants. *Biomed Mater* 8(3):035003
59. Sokolowski W, Metcalfe A, Hayashi S, Yahia L, Raymond J (2007) Medical applications of shape-memory polymers. *Biomed Mater* 2(1):S23–S27
60. Ware T, Simon D, Hearon K, Liu C, Shah S, Reeder J, Khodaparast N, Kilgard MP, Maitland DJ, Rennaker RL, Voit WE (2012) Three-dimensional flexible electronics enabled by shape-memory polymer substrates for responsive neural interfaces. *Macromol Mater Eng* 297(12):1193–1202
61. Naito Y, Nishikawa M, Hojo M (2015) Effect of reinforcing layer on shape fixity and time-dependent deployment in shape-memory polymer textile composites. *Compos Part A Appl Sci Manuf* 76:316–325
62. Liu Y, Du H, Liu L, Leng J (2014) Shape-memory polymers and their composites in aerospace applications: a review. *Smart Mater Struct* 23(2):023001
63. Hu J (2013). Future developments in shape-memory polymers. *Adv Shape-Memory Polym* 320–334
64. Saenz-Perez M, Bashir T, Laza JM, Garcia-Barrasa J, Vilas JL, Skrifvars M, Leon LM (2018) Novel shape-memory polyurethane fibers for textile applications. *Text Res J* 0(00)1–11
65. Wang W, Yu W (2015) Preparation and characterization of CS-g-PNIPAAm microgels and application in a water vapour-permeable fabric. *Carbohydr Polym* 127:11–18
66. Qiu Q, Zhu M, Li Z, Qiu K, Liu X, Yu J, Ding B (2019) Highly flexible, breathable, tailorable and washable power generation fabrics for wearable electronics. *Nano Energy* 58:750–758

67. Thakur S (2017) Shape-memory polymers for smart textile applications. *Textiles Adv Appl* 323–337.
68. Lu J, Hu JL, Zhu Y, Liu YJ (2012) Shape-memory finishing of wool fabrics and garments. *Adv Mater Res* 441:235–238
69. Lirici M, Salerno F, Califano A (2008) The use of superelastic suture clips in laparoscopic gastric banding. *Minim Invasiv Ther Allied Technol* 17:176–180
70. Abitha H, Kavitha V, Gomathi B, Ramachandran B (2020) A recent investigation on shape-memory alloys and polymers-based materials on bio artificial implants-hip and knee joint. *Mater Today: Proc* <https://doi.org/10.1016/j.matpr.2020.07.711>
71. Feng Y, Zhang S, Wang H, Zhao H, Lu J, Guo J, Behl M, Lendlein A (2011) Biodegradable polyesterurethanes with shape-memory properties for dexamethasone and aspirin controlled release. *J Control Release* 152(1):21–23. <https://doi.org/10.1016/j.jconrel.2011.08.098>
72. Jung YC, Cho JW (2010) Application of shape-memory polyurethane in orthodontic. *J Mater Sci Mater Med* 21:2881–2886
73. Wache HM, Tartakowska DJ, Hentrich A, Wagner MH (2003) Development of a polymer stent with shape-memory effect as a drug delivery system. *J Mater Sci Mater Med* 14:109–112
74. Wang L, Wang W, Di S, Yang X, Chen H, Gong T, Zhou S (2014) Silver-coordination polymer network combining antibacterial action and shape-memory capabilities. *RSC Adv* 4:32276–32282
75. Murugan S, Dharman G, Murugaraj J, Abdulla Al A, Murugan AM, Selvaraj MR (2017) Sustainable pectin fascinating hydroxyapatite nanocomposite scaffolds to enhance tissue regeneration. *Sustain Chem Pharm* 5:46–53
76. Sa MW, Nguyen BNB, Moriarty RA, Kamalidinov T, Fisher JP, Kim JY (2018) Fabrication and evaluation of 3D printed BCP Scaffolds reinforced with ZrO₂ for bone tissue applications. *Biotechnol Bioeng* 115(4):989–999
77. An SH, Matsumoto T, Miyajima H, Nakahira A, Kim KH, Imazato S (2012) Porous Zirconia/Hydroxyapatite scaffolds for bone reconstruction. *Dent Mater* 28(12):1221–1231
78. Feng P, Wei P, Shuai C, Peng S (2014) Characterization of mechanical and biological properties of 3-D scaffolds reinforced with zinc oxide for bone tissue engineering. *Plos One* 9(1):e87755
79. Bao M, Lou X, Zhou Q, Dong W, Yuan H, Zhang Y (2014) Electrospun biomimetic fibrous scaffold from shape-memory polymer of PDLLA-co-TMC for bone tissue engineering. *ACS Appl Mater Inter* 6(4):2611–2621
80. Yang CS, Wu HC, Sun JS, Hsiao HM, Wang TW (2013) Thermo-induced shape-memory PEG-PCL copolymer as a dual-drug-eluting biodegradable stent. *ACS Appl Mater Inter* 5:10985–10994
81. Melocchi A, Uboldi M, Inverardi N, Vangosa FB, Baldi F, Pandini S, Scalet G, Auricchio F, Cerea M, Foppoli A, Maroni A, Zema L, Gazzaniga A (2019) Expandable drug delivery system for gastric retention based on shape-memory polymers: development via 4D printing and extrusion. *Int J Pharm* 571:18700
82. Chen H, Li Y, Liu Y, Gong T, Wang L, Zhou S (2014) Highly pH-sensitive polyurethane exhibiting shape-memory and drug release. *Polym Chem* 5:5168–5174
83. Wischke C, Neffe AT, Steuer S, Lendlein A (2009) Evaluation of a degradable shape-memory polymer network as matrix for controlled drug release. *J Control Release* 138:243–250
84. Liu YF, Wu JL, Song SL, Xu LX, Chen J, Peng W (2018) Thermo-mechanical properties of glass fiber reinforced shape-memory polyurethane for orthodontic application. *J Mater Sci Mater Med* 29:148
85. Fercec J, Anzel I, Rudolf R (2014) Stress dependent electrical resistivity of orthodontic wire from the shape-memory alloy NiTi. *Mater Des* 55:699–706
86. Yakacki CM, Shandas R, Lanning C, Rech B, Eckstein A, Gall K (2007) Unconstrained recovery characterization of shape-memory polymer networks for cardiovascular applications. *Biomaterials* 28(14):2255–2263
87. Baer GM, Small W, Wilson TS, Benett WJ, Matthews DL, Hartman J, Maitland DJ (2007) Fabrication and in vitro deployment of a laser-activated shape-memory polymer vascular stent. *Biomed Eng Online* 6:43

88. Jia H, Gu S-Y, Chang K (2018) 3D printed self-expandable vascular stents from biodegradable shape-memory polymer. *Adv Polym Technol* 37:3222–3228
89. Gu SY, Chang K, Jin SP (2017) Dual-induced self-expandable stent based on biodegradable shape-memory polyurethane nanocomposites (PCLAU/Fe₃O₄) triggered around body temperature. *J Appl Polym Sci* 135(3):45686
90. Gong X, Liu L, Scarpa F, Leng J, Liu Y (2017) Variable stiffness corrugated composite structure with shape-memory polymer for morphing skin applications. *Smart Mater Struct* 26(3):035052.
91. Ribeiro MP, Espiga A, Silva D, Baptista P, Henriques J, Ferreira C, Silva JC, Borges JP, Pires E, Chaves P, Correia IJ (2009) Development of a new chitosan hydrogel for wound dressing. *Wound Repair Regen* 17:817–824
92. Li G, Wang Y, Wang S, Liu Z, Liu Z, Jiang J (2018) A Thermo- and moisture-responsive zwitterionic shape-memory polymer for novel self-healable wound dressing applications *Macromol Mater Eng* 304:1800603
93. Chen T, Chen Y, Ur Rehman H, Chen Z, Yang Z, Wang M, Li H, Liu H (2018) Ultra-tough, self-healing, and tissue-adhesive hydrogel for wound dressing. *ACS Appl Mater Inter* 10(39):33523–33531
94. Kokabi M, Sirousazar M, Hassan ZM (2007) PVA-clay nanocomposite hydrogels for wound dressing. *Eur Polym J* 43(2007):773–781
95. Yakacki CM, Lyons MB, Rech B, Gall K, Shandas R (2008) Cytotoxicity and thermomechanical behavior of biomedical shape-memory polymer networks post-sterilization. *Biomed Mater* 3:015010.
96. Peniston SJ, Choi SJ (2007) Effect of sterilization on the physicochemical properties of molded poly(L-lactic Acid). *J Biomed Mater Res B Appl Biomater* 80(1):67–77

Chapter 13

Organic Shape-Memory Polymers and their Foams and Composites in Space



Loredana Santo, Daniele Santoro, and Fabrizio Quadrini

13.1 Application of Organic Shape Memory Foams

Organic shape-memory foams (OSMFs) may be used in different sectors, ranging from Space to the biomedical sector. The lightweight property and the ability to exhibit suitable forces during shape recovery allow OSMFs to be very attractive for aerospace applications. Most of the studies are focused on the use of shape-memory materials for self-deployable structures such as solar sails or space debris grabbing systems. All these examples shall not need high-force levels for the actuation, whereas a high level of compaction and low weight is required to be compliant with the requirements imposed by space-launch vectors.

For designing an actuator made of shape-memory epoxy foam produced by solid-state foaming [1] for space applications, Quadrini et al. [2] have carried out multiple recovery tests and measured the actuation load as a function of the temperature. The activation temperature has been set in the range 90–130 °C, depending on the configuration: torsion, compression, and bending. For all configurations, the maximum actuation force has been measured as a function of the recovery percentage. The recovery percentage has been defined as the ratio between the recovered deformation during each shape-memory test and the initial deformation of the frozen OSMF. The actuation load exerted by OSMF have been almost a linear function of the recovery percentage in the compression and the flexure configuration with a maximum force of 6.31 N and 5.31 N, respectively, at a recovery percentage of about 10%; in the case of torsion, the trend has been almost linear with a load of 0.32 N.

Building light actuators and expandable/deployable structures based on OSMFs requires feasibility studies in the absence of gravity (or in microgravity conditions). Shape-memory foams by solid-state foaming have been tested in two space missions onboard the International Space Station (ISS) and BION-M1 capsule through the

L. Santo (✉) · D. Santoro · F. Quadrini
Department of Industrial Engineering, University of Rome Tor Vergata, Rome, Italy
e-mail: loredana.santo@uniroma2.it

Soyuz-2 launch vehicle. The first experiment, named I-FOAM [3, 4], has been performed in 2011. An autonomous apparatus made up of a control and heating system, battery pack, and data acquisition system is used. Three different configurations (torsion, compression, and bending) have been chosen during the memorizing step of the foams to obtain their recovery in microgravity. It has been observed that microgravity does not affect the shape-memory effect. The final recovery has been 72% for the sample in bending configuration, 71% for the sample in torsion; only a 10% recovery has been reached for the sample in compression due to problems during heating [4]. Experiments on the ground showed that 100% recovery is reached just by increasing the maximum temperature to 120 °C. This lack of shape recovery has been due to the maximum nominal temperature of 100 °C on ISS for safety reasons.

Thanks to the results obtained in [3, 4], in 2013, Santo et al. [5] developed a new experiment called Ribes_Foam2 in the BION-M1 mission. Such an on-orbit experiment comprised the heating of three samples in different configurations: a prototype of the actuator and a parallelepiped based on OSMFs and a sheet of composite laminate with shape-memory interlayer [6]. The device has been packed on the ground, to evaluate the shape recovery behavior in microgravity. The actuation force in this condition has been acquired by using a compression configuration. The recovery has been obtained with a maximum of up to 90% only by increasing the heating time (55 min instead of 25 min) and maintaining the maximum temperature practically unchanged. The prototype actuator showed a low actuation rate (about 0.2 mm/min) and a loading speed of about 0.1 N/mm for a shape-memory foam with the size of $14 \times 8 \times 8 \text{ mm}^3$. These results have shown the possibility to apply OSMFs actuators for self-deployable structures, where a low actuation rate or fine regulation is needed (e.g., shields, mirrors, other satellite subsystems).

Experimentations in microgravity on OSMFs have been also performed by Babaevskii et al. [7] on polyurethane foam composites, varying the quantity of the main and secondary components of the polyurethane foam composite. The authors have investigated the glass transition temperature (T_g) and porosity of the highly porous polyurethane foams and the shape-memory behavior in microgravity conditions aboard the ISS.

In [8], the authors proposed medium size actuators based on OSMFs. The maximum load exerted was 50 N in dependence on the recovery temperature and a maximum stroke up to 30 mm. The active element in epoxy resin has been produced by solid-state foaming [1], shaping it in the same metallic frame of the actuator. The work has shown that OSMF-based small and medium-size actuators can be easily designed and manufactured. Moreover, the discussed actuators are characterized by simplicity of the structure and low displacement rate, but the maximum load is reached only for a small time during the initial heating phase of the foam. These aspects shall be considered during the design process of such actuators.

Other medium-size actuators and structures with great potential for space applications based on solid-state foamed OSMF [1], or shape-memory interlayer [6] have been also developed for satellite antennas [9] and solar sails [10]. Quadrini [6] has manufactured and tested a shape-memory composite frame based on solid-state

foamed OSMF hinges. In particular, the frame has been composed of two carbon fiber-reinforced (CFR) prepregs for each side and one angular OSMF for each edge. The angular hinges have been machined after molding in cylindrical molds. Heat-shrink X-linked polyethylene tube has been used to consolidate the composite structure. After post-curing, a rigid square frame with a height of 25 mm and a length of 50 mm has been obtained. In the memory step, only the foam hinges were subjected to deformation resulting in the complete closure of the structure. The recovery of the deployed shape has been obtained in about 60 s through a hot air gun.

Interesting results came also from Sokolowski et al. [11], who developed a polyurethane shape-memory polymer. The authors referred to this material as “cold hibernated elastic memory” (CHEM). A structure is reduced to a very small volume in a rubbery state above the transition temperature and subsequently cooled below this temperature to a glassy state. The compacted part can be heated above the transition temperature and the original shape can be recovered thanks to foam elastic recovery and the shape-memory properties. The structure has been fixed in the deployed shape after a cooling phase under the glass transition temperature. After, the OSMF-based structure has been heated and re-stored to the compacted initial configuration. Theoretically, several shape-memory recovery cycles can be applied, although some contributions on OSMFs have shown an impact on cyclic deformation on thermo-mechanical properties [12, 13].

Self-healing is the capability of a structure to fix the damage that occurred after the impact. Self-healing composite structures find a wide range of technical applications both in the aeronautical sector and in the marine field. Unmanned Aerial Vehicles (UAV) structures have a great potential to ensure a self-healing capability [14] although the major promising usages are in the marine field. Self-healing structures usually combine healable resin, structural health monitoring (SHM), and integrated autonomous repair for increased survivability in composite structures.

In [15], the authors inserted self-healing capabilities in composite sandwich panels with OSMFs core and epoxy-based CFR skins. Two different foams have been used as core: poly(ethylene terephthalate) (PET, thermoplastic) and epoxy (thermosetting). In the case of PET foam core, the composite skins have been attached to the core foam by gluing with an epoxy adhesive (Pattex Power Epoxy). The epoxy sandwich core foam has been obtained by solid-state foaming [1]. Both exhibit shape-memory properties that have been utilized for self-healing together with local applications of liquid-state epoxy resin on the skins and core cracks. A commercial epoxy resin (Duraloid AL-30 by Prochima) was used, and the resin polymerization has been achieved by using a hot-air gun simultaneously with shape recovery of composite sandwiches (in particular, the foam core). All sandwich samples have been tested in bending configuration up to failure. Later, they have recovered the initial geometry by using a hot air gun. After self-healing, other mechanical tests in bending configuration have been performed to establish the residual mechanical properties. Interesting results come from this feasibility study, where the combined effects of the shape-memory recovery of cores and the epoxy resin on cracks have determined residual stiffness after self-healing of about 90% for the epoxy foam sandwich and 80% for the PET one.

A similar investigation has been performed in [16], where a shape-memory polymer has been used to demonstrate multiple impact self-repair capability by requiring heating of the damaged area as only external intervention. The self-healing is obtained by implementing limited confinement of the damaged foam: this has been achieved by surrounding materials in the in-plane direction and by the skin in the transverse direction during the shape recovery process. Since the foam has been programmed by compression (volume reduction), thanks to the shape-memory effect, this tried to grow in volume after heating up to the activation temperature. Because of the confinement, however, this volume growth has been not fully allowed. As a result, the cracked foam has been forced into the internal open space such as a crack, narrowing or fully closing the damage.

Zhang et al. [17] studied the healing of conventional syntactic foam without shape-memory properties embedded with shape-memory polyurethane fibers. Particulate thermoplastic particles have been used as a solid healing agent. The damaged beam samples have been subjected to different tensile stress levels (22.5, 24.5, and 26.5 kPa) during the healing process, thus showing their in-service self-repairability. The authors have also discussed the influence of tensile stress levels and healing agents on healing property. Results have shown that self-repair efficiency is 90%, where the stress of 22.5 kPa is applied (as peak condition). The work has also shown the dependency of healing efficiency on thermoplastic (TP) particulate content. In fact, with the increase of TP particulate content, the mechanical properties decrease while the self-healing capability improves.

OSMFs gained significant interest in the bio-medical field for their great potential use in medical devices allowing minimally invasive surgical procedures. Since their capability to significantly reduce their volume, OSMFs-based medical devices can be easily packed and thermally stimulated for shape recovery and used as stents or wires. Within the OSMFs, polyurethane foams exhibit great interest because of their compatibility with biological organisms. In this context in [18], the authors studied the application of shape-memory polyurethane (SMPU) as an embolic agent for blood vessels or to prevent the flow of blood into the diseased part of a blood human vessel. The interventional radiology technique (IRT) has been chosen as the implantation method for SMPU: this technique is based on medical imaging guidance, such as x-ray fluoroscopy, computed tomography, magnetic resonance imaging, or ultrasound. For this aim, the authors developed a laboratory-scale process to increase SMPU radio-capacity and bio-inertness without reducing shape-memory property to perform IRT with SMPU as the embolic agent. The aim has been achieved with good results by adding barium sulphate (BaSO_4) and hydroxyapatite (HaP) as fillers into SMPU foams. These nanoparticles have been inserted into the SMPU matrix by using a twin-screw extruder. The radiopacity of the composites is observed to be increased with filler content, whereas BaSO_4 played a fundamental role in comparison to that of hydroxyapatite nanoparticles.

Landsman et al. [19] aimed at investigating the mechanical properties, the safety, and the efficiency of a peripheral embolization device based on shape-memory polymer in “in-vitro” configuration. The OSMFs biocompatibility and ability for endovascular catheter-based delivery to a variety of vascular beds make these foams

ideal candidates for use in various embolic applications. The device has been manufactured with a biocompatible polymer hydroxypropylethylenediamine (HPED) and it has been verified by performing blood flow studies. The affinity for thrombus formation and blood penetration throughout the foam has been investigated. The results have shown very promising performances: HPED has performed a complete vessel occlusion with ease of visualization using ultrasound.

Interesting results came also from [20], where the authors have studied and tested both “in vitro” and “in vivo” endovascular coils for vascular aneurysm treatments based on OSMFs. Since the current metal coils used in aneurysm treatment have limited efficacy, the authors proposed the introduction of OSMFs synthesized using the monomer diethanolamine (DEA) in place of triethanolamine (TEA) to provide improved mechanical properties for medical device applications. In vivo porcine aneurysms were successfully occluded with theoretical volume occlusion values greater than 72% with rapid and stable thrombus formation.

Advances in OSMFs-based biomedical devices are also discussed by Wang et al. [21], that developed a polyurethane-based shape-memory foam (SMPU) material with optimal shape recovery function and properties for potential applications in the endovascular embolization of intracranial aneurysms (ICAs). In [22], the same authors developed highly porous carbon nanotube (CNT)/shape-memory polymer nanocomposites for possible endovascular treatment. The nanocomposites have been built by infiltrating CNTs into the SMPU in ethanol via ultrasonication. Experimental tests were performed to characterize the porous nanocomposites and to identify key parameters, such as the average pore size, density, porosity, and electrical resistivity. The shape recovery stimulus has been achieved by introducing a resistive-heating mechanism paving the way to new biomedical devices to treat ICAs using a catheter-based endovascular procedure.

3D graphene foams are also becoming very promising candidates to supply settings for mimicking “in vivo” environments, allowing effective cell attachment, proliferation, and differentiation due to their properties [23–26]. In [27] the authors discussed the overcoming of some limitations in the bio-medical field in conventional tissue engineering strategies by introducing 3D graphene foams. Typical limitations are the origination of inflammatory responses owing to scaffold biodegradation or insufficient cell migration [28, 29]. On the other hand, surfaces, structures, and biomaterials with 3D graphene foams having nanoscale features not only can induce cell migration, adhesion, proliferation, and differentiation, but also have the potential to mimic the natural microenvironment of cells.

Concerning other contributions on OSMFs as cell attachment and proliferation, Xie et al. [30] have developed polyurethane/hydroxyapatite-based shape-memory polymer foam as a scaffold substrate to facilitate bone regeneration. The authors have evaluated the minimally invasive delivery and the self-fitting behavior of the OSMF showing its feasibility in the treatment of bone defects “in vivo”. Good results have been obtained with easy implantation into lab art bone defects in a compact shape. The “in vivo” activation of the shape-memory effect allows the foam to self-match the boundary of bone defects. Micro-computed tomography has shown that bone ingrowth initiated bringing to a successful vascularization and bone remodeling.

OSMFs are currently under investigation in the biomedical field also for gastro-retentive drug delivery systems and wound dressings. In this context, Song et al. [31] have investigated comprehensive morphological, physical, and shape-memory characterization of biocompatible shape-memory polymer blend foams composed of thermoplastic polyurethane (TPU) and polylactic acid (PLA). The TPU/PLA blend compositions have been 80/20, 65/35, and 50/50 in wt%. Shape memory property has been based on the dynamic contractible porous structure of the foams with a recovery force in a typical range of OSMFs.

In the last years, the bio-absorbability aspects of OSMFs have been increasing their attractiveness in the biomedical field for the potential simplification in the secondary removal procedures.

In [32], the authors proposed an innovative OSMF based on polyhydroxybutyrate-hydroxyvalerate (PHBV). PHBV is a natural origin microbial polyester that presents non-toxicity, biocompatibility, and biodegradability that makes it suitable for biomedical applications. The authors developed a very simple way to produce PHBV foams: the polymer has been dissolved in chloroform (30 wt%) and then infiltrated in a packed bed of urea particles (particle size 0.84–2.35 mm). A syringe has been used as mold; after infiltration, the solvent has been left to evaporate in air and then the urea preform has been dissolved by immersion of distilled water. Furthermore, shape-memory tests have been carried out on PHBV samples providing a shape recovery of about 100% on 30% compressed samples with a linear dependence of the recovery stress on the temperature.

Biodegradable shape-memory polymer foams have also been treated in [33]. Hydrolytically and oxidatively biodegradable OSMFs by reacting polyols (triethanolamine or glycerol) with 6-aminocaproic acid or glycine have been used to generate foaming monomers with degradable ester bonds. A cross-linked OSMF structure has been obtained with excellent shape recovery within the time of 8 min. Triethanolamine-based ester-containing foams have shown interconnected porous structures along with increased mechanical strength. These biodegradable OSMFs with low shape-memory activation temperature for human body applications have shown very promising features for a hemostatic device; they can be mainly used on rapid interventions, and also as a drug-delivering tissue scaffold.

The application of OSMFs certainly needs to develop specific sterilization processes without reducing or influencing their shape-memory properties. Most sterilization methods need high temperatures or high humidity to efficiently reduce the bioburden of the device, but the environment has to be strongly controlled after device fabrication. OSMFs foams are very sensitive to heat flux and moisture exposures that can lead to a premature activation or changes in glass transition temperature. In this context, Muschalek et al. [34] have discussed two potential sterilization methods for the polyurethane shape-memory embolic foams: non-traditional ethylene oxide (ntEtO) gas sterilization and electron beam irradiation (e-beam). This last method has shown the best results, due to lower moisture absorption during sterilization and significant molecular changes (e.g., oxidation that could alter long-term stability and performance).

13.2 OSM Foams and Composites for Space

Shape-memory polymers (SMPs) can register a meta-stable deformation and can restore the equilibrium deformation if an external stimulus is applied. Thermal-responsive shape-memory polymers are the most common; they can fix a meta-stable shape by cooling below a transition temperature (which is typically the glass transition temperature T_g) [35]. Upon reheating to above T_g , polymer chains reorganize, and recovery of the initial shape is performed. In a typical thermo-mechanical cycle of a SMP (Fig. 13.1), starting from an equilibrium shape, the sample is heated at a temperature above T_g ; then stresses are applied to change its shape, and the sample is left to cool under constraints down to room temperature (memory stage). After cooling, loads can be removed with minimal changes in the applied deformation. In order to recover the first equilibrium shape, the sample has to be heated again above T_g without any applied load (recovery stage). If constraints are used, loads will be exerted on them. After full-shape recovery, other shape changes are not possible only by heating. For this reason, SMPs are considered one-way systems. Nevertheless, if

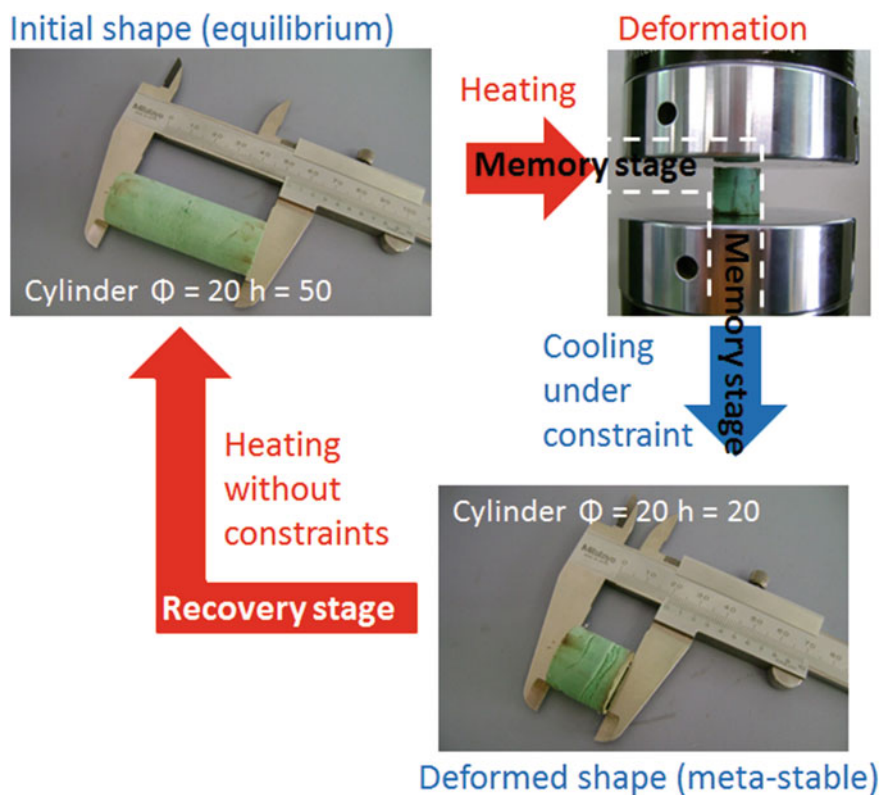


Fig. 13.1 Typical thermo-mechanical cycle for a SMP foam

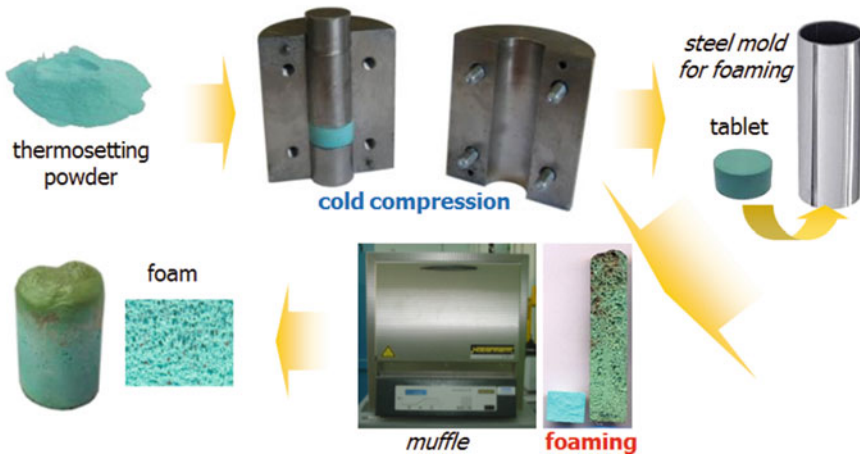


Fig. 13.2 Solid-state foaming process

other thermo-mechanical cycles are applied, the shape-memory (SM) behavior will be observed again with minimal alteration.

Shape-memory properties depend on the molecular structure of polymers but it can be exalted by microstructural features. Foaming is an efficient way to tailor SMP properties. Due to reduced mechanical stiffness and strength but enhanced compressibility, foams can be highly deformed to freeze non-equilibrium shapes. In the beginning, most of the studies on SMP foams were performed on thermosetting polyurethanes [12], but more recently, epoxies have also been considered as an alternative [13]. Innovation in foam processing leads to new materials and structures which can show enhanced shape-memory behavior. The “solid-state foaming” is a process that is easier than conventional foaming methods and provides homogeneous closed-cell structure with high mechanical properties [36]. The process is depicted in Fig. 13.2: thermosetting powders are used to make solid tablets by cold compression. These tablets are inserted into metallic molds to be heated into a muffle furnace at a very high temperature, around 300 °C. A mold release is interposed between tablet and mold to avoid sticking. Due to heating, resin starts to boil, but contemporarily, polymerization occurs and bubbles are frozen into the foam structure. No blowing agent or additive is used for foaming, and commercial thermosetting resins can be processed without any additional treatment, both epoxy-based [36] and polyester-based [37].

Solid-state foaming is an efficient technique to produce epoxy-based SMP foams that are very rigid at room temperature, and turn spongy after glass transition. Over T_g , they can be packed up to the full collapse of foam pores, with minimal damages. By cooling under constraints, the compacted structure is fixed with very low residual forces on constraints. The initial foam shape is rapidly recovered by further heating.

SMP epoxy foams show total recovery of the initial equilibrium shape and ability also during multiple memory-recovery cycles [38]. In the absence of constraints,

foams recover the equilibrium shape with a rate depending on the applied temperature. Generally, a temperature of about 130 °C is suggested to reduce the recovery time.

Composite foams can be manufactured by solid-state foaming by mixing fillers with uncured resin powders before tablet compaction. In the case of montmorillonite (MMT), as filler, SMP epoxy foams exhibited higher recovery loads and better dimensional stability during recovery [39]. Small amounts of graphene or multi-walled carbon nanotubes (MWCNTs) enhance the functional and structural behavior of foams [40]. Recovery loads increase and recovery times reduce significantly.

Composite structures can also be manufactured by using SMP foams as the core for composite sandwiches with remarkable self-repairing properties [41]. SMP composites (SMPCs) are very attractive because of the ability to combine structural performances of composite materials with the functional behavior of SMPs. However, apart from the sandwich structure with a SM core, the shape-memory behavior can be provided to a SMPC using its matrix or by adding a SMP interlayer [42]. SM carbon-fiber composites are produced by means of commercial thermosetting prepregs with epoxy matrix [43]. These materials by themselves do not exhibit any significant SM behavior which is added during lamination by using additional SM interlayers between adjacent prepreg plies.

From the beginning, SMPs and SMPCs have been developed for possible application in space because of the possibility of compressing shapes on the Earth before the launch in orbit and expanding the structures in space. Other possible uses are related to the ability to freeze elastic stresses into the material and relax during heating. Exerted recovery loads can be used in new-concept actuators or safety systems.

Conceptual prototypes of actuators and Space devices with SMPs and SMPCs are shown in Fig. 13.2. The active element of the SMP actuator was epoxy foam by solid-state foaming, with a cylindrical shape (diameter of 16 mm, length of 100 mm). During the memory stage, 30% compression strain was applied to reach a maximum actuation load of 50 N. The actuator can recover the full initial strain with a maximum stroke of 30 mm but the actuation load decreases by increasing the recovered strain. This SMP actuator is limited by the fact to be one-way but it has the big advantage of a very low actuation rate (Fig. 13.3).

Thanks to the flexibility of composite manufacturing technology, many objects with different shapes and functions can be produced. SMPCs can be used for deploying solar sails, solar panels, satellite structures, antennas, for grabbing devices and all other devices where volume reduction is necessary before flight or movements are necessary in orbit.

13.2.1 Principles of SMP and SMPC Recovery

Understanding basic principles of SM behavior for foams and composites is fundamental to design experiments and devices. The best way is to measure forces during a thermo-mechanical cycle or a part of it. Figure 13.4 shows a foam sample between



Fig. 13.3 Conceptual prototypes of actuators and space devices with SMPs and SMPCs

the compression platens of a universal testing machine. At equilibrium, this foam, by solid-state foaming, presents a cylindrical shape with a diameter of 20 mm, a height of 50 mm, and a density of 0.37 g/cm^3 , which corresponded to a porosity ratio of 74%. Its memory step was performed by confining in a mold with a cylindrical cavity to avoid buckling. At the end of the memory step, a compressive strain of 60% was applied for a porosity ratio of 36%.

Due to the memory step, 38% of sample porosity is lost but it can be recovered by heating. In Fig. 13.4, the sample at the end of the memory step with the height of 20 mm is shown between the compression platens but without any additional constraint. The upper platen is put in contact with the top sample surface with a minimal preload. Subsequently, the platen is fixed, and the sample is heated by a hot air gun. Because of heating, the foam starts to recover but the platens prevent its height recovery; therefore, loads are exerted on the platens and can be measured by the testing machine.

During heating, the load increases as molecular mobility is used to defrost stresses of the memory step. A maximum is reached and is kept constant for a long time (about 2 min). However, due to heating, the elastic modulus of the foam reduces and, in

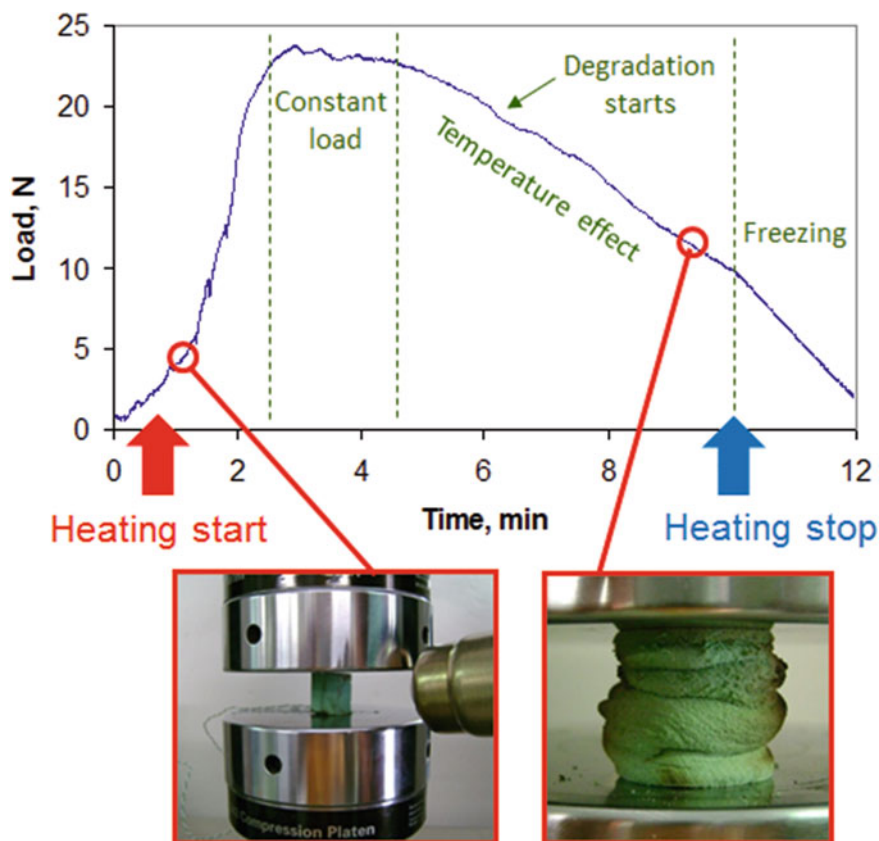


Fig. 13.4 Recovery loads of a SMP foam

turn, the sample rigidity. As a consequence, exerted loads start to decrease. Because of the long heating time, the degradation effects start with a further reduction of foam stiffness. At the end of the heating phase, at a very long time, the foam stiffness is so low that buckling occurs, and cracks can propagate into the structure. On turning off the hot air gun, the sample starts to cool, but the sample stiffness is not recovered because of crack propagation. By applying a low compressive strain in the memory step, buckling and crack propagation can be avoided. In this case, during cooling, the load starts to increase again up to a new plateau.

Temperature is responsible for stress recovery and elastic modulus decrease. Because of softening, stresses reduce as well. These phenomena are balanced after the curve maximum when a constant load is observed. Subsequently, material softening prevails, and recovery load reduces. At the maximum, a recovery load of about 23 N was reached in the test for the pressure of 0.74 bar.

Figure 13.5 reports the shape-memory behavior of a composite sample. A 2-ply carbon fiber composite sheet has been used in a bending configuration. The SMP

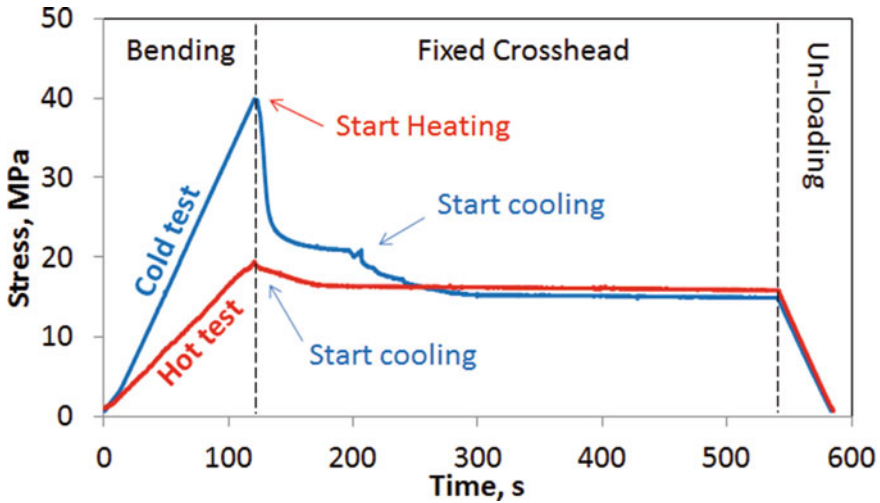


Fig. 13.5 Recovery loads of a SMPC sample

interlayer was interposed between the adjacent plies before prepreg curing. The final size of the sample was $100 \times 30 \times 0.6 \text{ mm}^3$. Buckling does not occur in composite laminates and both memory and recovery steps can be performed under the universal testing machine. Other complex thermo-mechanical cycles can be performed on the same sample as shown in Fig. 13.5. Two different tests were used, namely the hot and cold tests. In the hot test, the sample was heated to a temperature of about 120°C . Subsequently, bending starts at 1 mm/min with a span of 80 mm up to a maximum displacement of 2 mm . At this point, the testing machine crosshead was fixed and heating was stopped. Because of cooling, the composite increases its stiffness but contemporarily a part of elastic stresses is frozen by the SMP interlayer. For this reason, a peak is visible at the beginning of the cooling step and a plateau is reached. In the following unloading step, the plateau stress is lost by the sample elastic deformation and only a small amount of frozen stresses remain in the deformed sample.

In the cold test, the sample is initially at room temperature, and therefore, a higher stress peak is reached after the displacement of 2 mm . In the following stage with fixed crosshead, heating is applied up to reaching a temperature of 120°C . Elastic stresses reduce because of the stiffness reduction with temperature. Subsequently, heating is stopped, and the composite continues to reduce stresses during cooling. A plateau is reached also in this case, which is perfectly superimposed with the hot test plateau. In a perfect SM material, the stress curve decreases down to zero, but SMPC are stiffer than SMP and large elastic stresses are always present in the thermo-mechanical cycle. At the end of both tests, a residual middle-point flecion of 1.3 mm results (65% of the total applied displacement). By further heating, the displacement can be recovered. The number of frozen stresses into the SMPC can be calculated by the difference between the peak stress and the plateau stress of the

curves of Fig. 13.5, being dependent on the applied temperature. The value of the plateau stress by itself gives an evaluation of the elastic stresses which cannot be frozen by the SMP interlayer. Best SMPCs present high peak stress and very low plateau stress.

13.2.2 Experimental Set-Up for Experiments in Microgravity

Performing shape-recovery tests of SMP and SMPC in microgravity is very important to show the ability of these materials of working in the Space environment. Nevertheless, it is very complex because of the high times necessary for a full shape evolution. Microgravity tests can be made in orbit on the International Space Station (ISS) or in orbital unmanned flights, but other problems arise. Because of heating and possible emissions, tests have to be confined to an insecure environment. Energy supply can be critical if high currents or voltages would be necessary. The required volume of the experiment, before and after shape recovery, has to be limited to reduce issues during launch and operation in spacecraft. In the end, the cost of the experiment must be reduced at least in the first feasibility phases. For these reasons, an autonomous device was designed and built.

The experiment unit (EU) for in-orbit shape recovery tests consisted of the sample housings, the heater and the heating plate, thermal and optical sensors. All these elements were confined into the EU walls to make a heating chamber. This EU is shown in Fig. 13.6, it was purchased by the Italian Space Agency, and was provided by Kayser Italia. The EU was used for two different missions, where some details on the SM samples were changed. The heating plate consisted of an aluminum alloy disk (50 mm diameter) where all the samples had to be arranged by proper housings. The small disk diameter was selected to lower the overall system weight and volume. Three thermocouples were placed in the bottom of the aluminum plate, from the side of the heater, to measure temperature during heating. The temperature was settable between 90 °C and 120 °C for a settable time which was limited by the energy supplying system. In order to reduce thermal flow from the heating system to the EU external walls, it was thermally insulated using plastic spacers. The bottom and lateral external walls of the EU were also thermally insulated by foams which also provided mechanical insulation. The EU top wall was made of polycarbonate.

The sample housings were directly mounted on the heating plate to guarantee the best thermal conduction. They can be changed in successive experiments to study different recovery configurations. Apart from temperature data loggers, several additional sensors were placed into the EU and they could be changed in future missions as well in dependence on the experimental needs. In the performed tests, optical sensors were used to measure the height recovery of SMP foams. Moreover, a digital camera was used to acquire the shape evolutions during heating.

In order to make the EU an autonomous system, it was placed into a modified BOKON container which was previously developed for the different space missions.

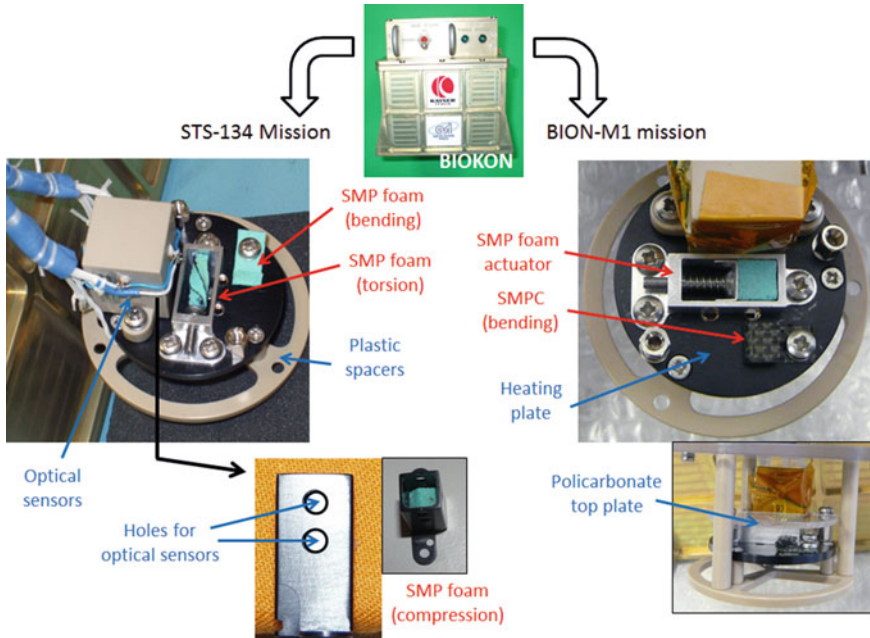


Fig. 13.6 Experimental set-up for in-orbit shape recovery experiments

It was composed of a top case, with the front panel and the battery, and a lower volume, containing the EU and the data acquisition system.

13.2.3 In-Orbit Experiments

Two experiments on shape recovery of SMPs and SMPCs have been carried out in orbit. The first (called “I-FOAM”) was made on the ISS on the 22nd of May 2011, during the last mission of the Space Shuttle Endeavour in the STS-134 Mission. The second, called “RIBES/FOAM2” was performed on the 20th of April 2013 during the BION-M1 mission of the Soyuz spacecraft [5].

I-FOAM experiment focused on SMP foams by solid-state foaming. Samples were manufactured by using a commercial epoxy resin (3 M Scotchkote 206 N) which is a one-part, heat curable, thermosetting coating for metals. Precursors (20 mm diameter, 10 mm height) were pressed at room temperature in a cylindrical stainless-steel mold up to the pressure of 130 MPa, with a packing rate of 10 mm/min, and a holding time of 1 min. Foaming was performed at 320 °C for 8 min by using a cylindrical stainless-steel mold with an inner diameter equal to the precursor diameter (20 mm). After foam cooling, each sample was machined to have the desired shape. The final foam density was about 0.36 g/cm³ with a foaming ratio close to 4.

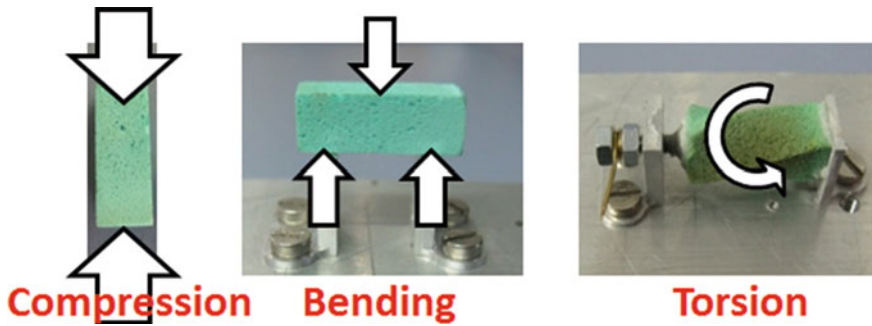


Fig. 13.7 Loading configurations for SMP foams

The ISS experiment had to exploit shape recovery from different configurations, as much as possible with the limit of the system size. Three loading conditions during storing were selected (compression, flexure, and torsion), according to previous on-Earth experimentation [2]. The actuation load was measured as a function of the loading configurations shown in Fig. 13.7. Results showed that loading configuration influences the maximum actuation load, the actuation start temperature, and load-temperature curve. In the compression configuration, the highest actuation load was measured: about 6.3 N by using a small block ($8 \times 8 \times 20 \text{ mm}^3$, less than 0.45 g) with a compressive strain of 55%.

The loading configurations of Fig. 13.7 were used as references also for the SMP samples of the I-FOAM experiment within the limits imposed by the EU (Fig. 13.6), mainly related to the volume of samples and housings, and the required energy supply [4].

The sample for the compression configuration was not changed, being about $8 \times 8 \times 10 \text{ mm}^3$ after the application of 60% of strain. It was placed into a rectangular box with three holes along with its height for the optical sensors. This box was made of aluminum alloy to improve sample heating. This foam sample was the only one that had to recover the shape by moving its free end far from the heating plate. The bending configuration was obtained starting from a flat foam sample ($20 \times 10 \times 2 \text{ mm}^3$) which was folded on itself for a length of 5 mm. In the end, the torsion configuration was made by twisting a foam block ($4 \times 4 \times 16 \text{ mm}^3$) along its height with 180° angle. The flat bent foam was fixed at one end by a screw, whereas the twisted sample was placed into a proper housing which allowed sample rotation.

In the RIBES/FOAM2 experiment, only two configurations were repeated (compression and bending), whereas the housing of the torsion configuration was used to place a small SMP actuator [3]. For this actuator, a spring (3 mm in diameter, 10 mm in length) was used to evaluate the load exerted during shape recovery. A camera acquisition allows extracting the spring displacement and, in turn, the applied force. For this reason, the spring was preliminarily characterized and stiffness of $0.580 \pm 0.001 \text{ N/mm}$ resulted. It was not expected that heating conditions would significantly reduce the spring stiffness because of the poor contact with the

heating plate and the low applied temperature (less than 120 °C). The foam block used for the actuator had an initial size of $8 \times 8 \times 14 \text{ mm}^3$ and was deformed along with its height with a 50% of strain during the memory step.

For the first time, in the RIBES/FOAM2 experiment, a SMPC sheet was also fabricated for the space experiment and used for the bending configuration. The composite laminate was manufactured in a hot parallel plate press by using the same epoxy resin of the SMP foams. Two layers of dry carbon fiber fabric were joined using the SMP interlayer, and a $24 \times 10 \times 0.4 \text{ mm}^3$ composite sheet resulted. Molding was carried out at low pressure (5 MPa), at the temperature of 150 °C for a molding time of 15 min. The direct contact between the composite sheets and the press plates was avoided by using two polyamide flat molds. The SMPC was post-cured in the oven for 1 h at 150 °C. In the memory step, 180 °C folding was performed with a bending diameter of 2.5 mm.

13.2.4 *Experimental Results in Microgravity*

In the I-FOAM experiment, the maximum temperature was limited to a nominal value of 100 °C and a maximum allowable value of 110 °C due to safety problems on ISS. A further limitation was imposed also to the maximum time for the experiment, 1 h from the system switch-on by the astronaut. These conditions were critical for the sample recovery as the glass transition of the cured epoxy resin is close to this value (about 100 °C), and foam samples have bad thermal diffusivity. These limitations were absent in the RIBES/FOAM2 experiment, being performed on an unmanned flight. Therefore, the recovery temperature was set to 120 °C but another issue occurred. Because of launch operations, a long time passed from the system switch-on and the beginning of the test. Even if the system was operating at the minimum energy consumption (related to the internal clock), consistent energy was spent before the experiment start.

Figure 13.8 shows a comparison between the average temperature of the aluminum plate for both experiments. The maximum temperature difference measured by the thermocouples was 1.11 °C for I-FOAM and 1.67 for RIBES/FOAM2.

Heating was more efficient in the first experiment (I-FOAM) and a maximum temperature of 109.7 °C was reached after 30 min. After this time, the system was switched off and data acquisition was stopped. Despite the fewer limitations, a similar temperature was reached in the RIBES/FOAM2 experiment (111.2 °C, only 1.4% more) but in a longer time, 46 min. In the second experiment, the system acquisition continued also during the cooling phase up to the full battery consumption.

The comparison of the heating chamber before and after the flight is shown in Fig. 13.9 for both experiments. Remarkable changes in the sample shape are visible for all the configurations, apart from compression, being the sample covered with the housing of the optical sensors. Nevertheless, the compression configuration gave bad results in the I-FOAM experiment and that was a reason for repeating it in RIBES/FOAM2. In fact, during the first on orbit experiment the optical sensors

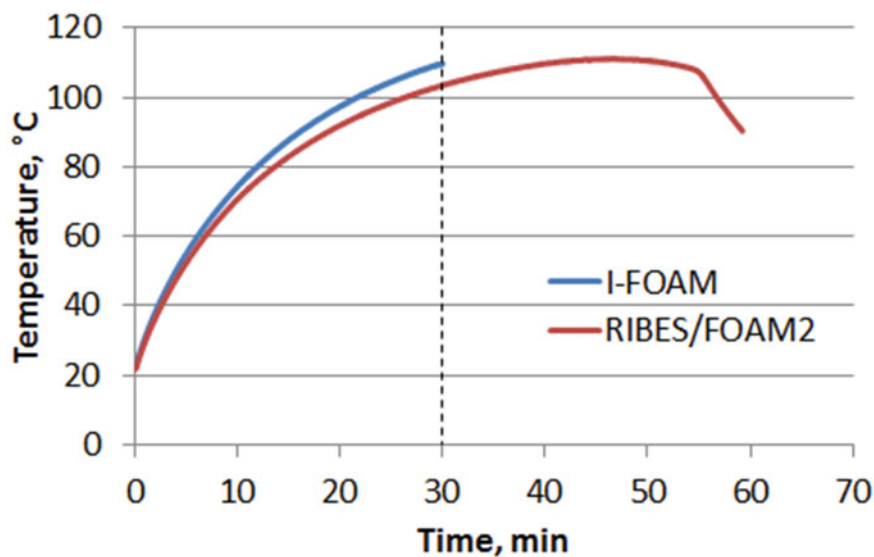


Fig. 13.8 Heating curves in microgravity experiments

mounted on the sample housing did not measure any shape recovery. Height recovery was about 10%, therefore, enough to activate only the first sensor. Better results were found for the bending configuration which reached 72% of recovery (e.g., an angular rotation of 130°), and for the torsion configuration with 71% of recovery (128° of angular rotation). These values (over 70%) were acceptable because of the limited applied temperature of 110°C and were comparable with on-Earth preliminary experiments. Thanks to the camera acquisition, it was observed that sample recovery in the torsion configuration began after 25 min when the plate temperature reached 110°C .

The poor behavior of the compression configuration in the I-FOAM experiment depended on the sample distortion during height recovery. Due to the non-uniformity of heat flow and non-perfect matching between the deformed foam and its housing, the sample free end rotated at the beginning of shape recovery and friction forces were generated. These forces constrained the foam and stopped shape evolution. In RIBES/FOAM2, attention was paid to reduce gaps between the deformed sample and its housing, and good results were found also for the compression configuration. The three optical sensors registered the shape recovery in the RIBES/FOAM2 experiment: the first after 34 min at 106.9°C , and the last after 48 min at 111.2°C . The block recovered 88% of the initial length maintaining the initial section entirely unaltered.

The SMPC laminate behaved very well too. Shape recovery started after 20 min; that was the lowest activation time from all the samples of both experiments. Because of the highest thermal conductivity and the lowest thickness, the SMPC exhibit a rapid shape evolution. The residual bending angle was evaluated to be 18.2° after the flight with shape recovery of about 90%, the highest in microgravity experiments.

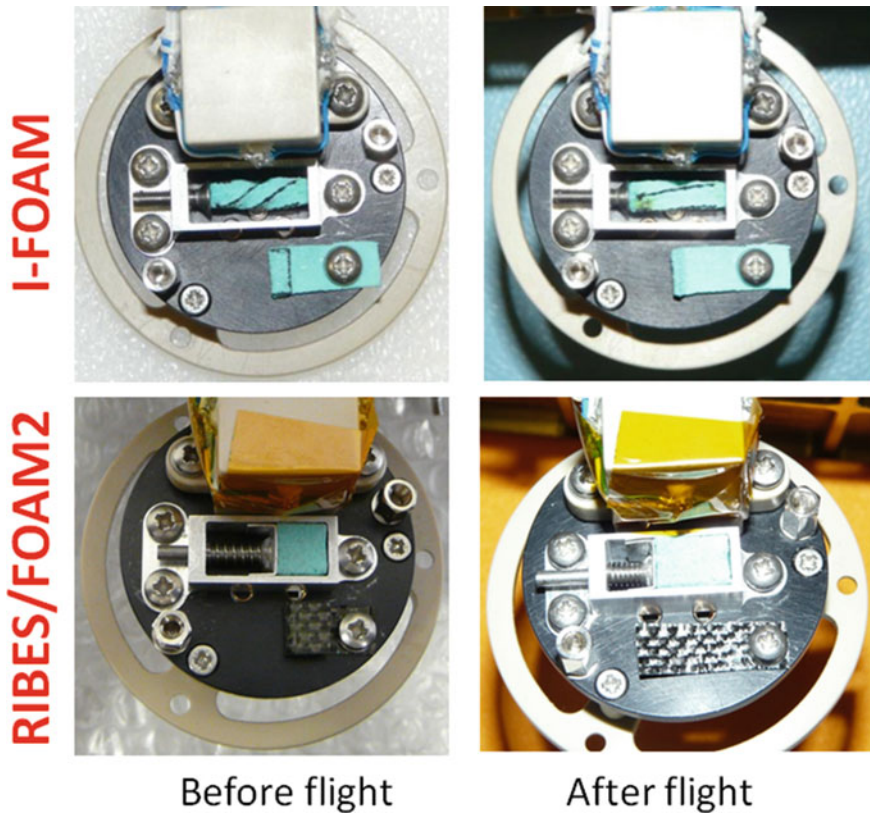


Fig. 13.9 Experimental system before and after the flight in the two experiments

Shape recovery can be used for actuation. In the RIBES/FOAM2 experiment, the calibrated spring preloaded the foam sample into its housing. The preload was 1.16 N and was originated by a displacement of 2 mm. This force tended to prevent the length recovery of the foam block. Actuation started after 33 min and arrived at the maximum displacement of 3.65 mm during the experiment. Images from the camera were acquired also during the first 5 min of cooling when important changes were still occurring. A final recovery of 76% was reached, in line with results from I-FOAM, despite the applied preload which was absent on I-FOAM samples.

Generally, a better recovery was obtained in the FOAM2 experiment. This was due to the longer heating time, about 25 min more, whereas the maximum applied temperature was comparable and the heating rate lower. In the RIBES/FOAM2 experiment, a temperature higher than 100 °C was applied for almost 30 min. Nevertheless, full recovery was not achieved again because of discussed limitations in energy supply. On the other hand, full recovery is not fundamental for technical application as shown by the behavior of the SMP actuator. Thermal properties of the samples and geometrical details of housings played an important role in the experiments above

all in terms of delay time from the heating start and the beginning of shape change. Figure 13.10 shows images from the onboard camera after 1 min and 30 min from the heating start for both experiments. The bent foam shows a very small displacement in comparison with the SMPC.

After 30 min, the torsion configuration is at the beginning of its shape recovery, whereas the actuator is still at its initial deformation. Most of the deformation will occur for all the samples in the following time. Figure 13.11 shows the behavior of

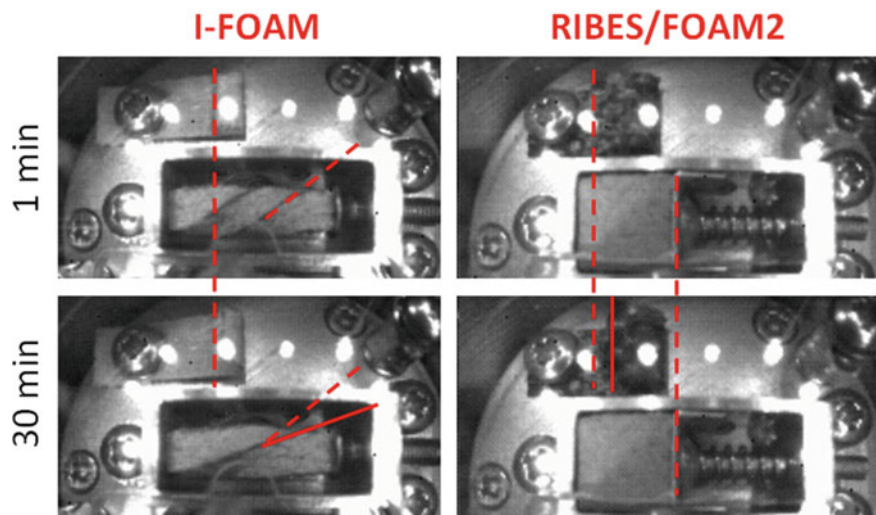


Fig. 13.10 Images from the onboard camera of SMP and SMPC samples

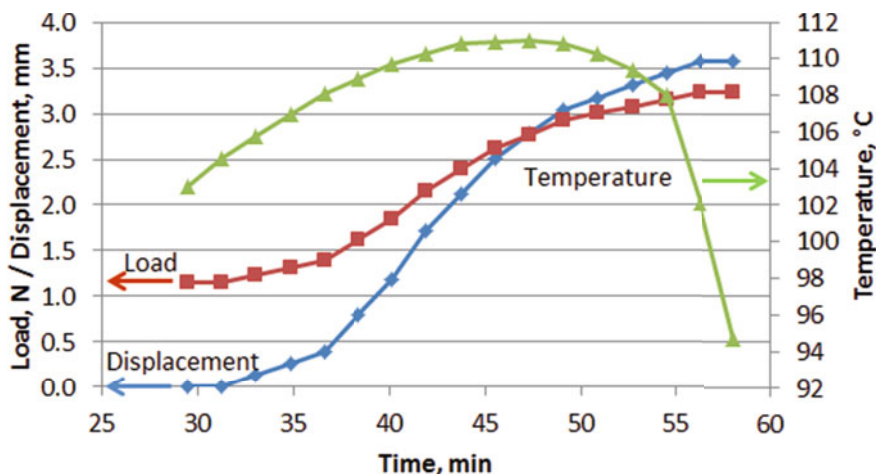


Fig. 13.11 Behavior of the SMP actuator in the RIBES/FOAM2 experiment

the SMP actuator in terms of load and displacement during the time. The heating plate temperature is superimposed for comparison. The load and displacement curves of Fig. 13.11 are a sigmoidal function of the time. The sigmoidal trend is typical for many polymer transitions. After the initial induction time, values increase and an inflection point occurs, in the end, a plateau is reached. A delay is also present between plate heating and shape recovery. The actuation load continues to increase also when the temperature starts to decrease. The maximum actuation load is reached 10 min after the temperature peak.

Making a comparison between the two blocks of the RIBES/FOAM2 experiment, in the compression configuration and the actuator, the final recovery of the former was 1 mm longer. The third optic sensor was activated after 48 min, 11 min before the maximum of the activation load and in correspondence of the temperature peak. Moreover, the optical sensors registered the sample recovery in the time range between 34.3 min and 47.7 min. The recovery rate decreases from 0.74 mm/min (between the first two sensors) to 0.32 mm/min (between the last two sensors). The average rate is 0.45 mm/min. In the same time intervals, the recovery rate of the actuator is 0.15 and 0.23 mm/min, respectively, with an average of 0.22 mm/min. The reduction of the recovery rate depends on the applied load of the spring, the effect of which is stronger than the effect of the contact with the heating plate, which is better for the actuator. Results are very interesting as they show that high shape recovery and loads can be obtained also with a single plate heating if an appropriate housing is adopted.

13.3 Future Trends for 4D Printing

In the future, the last achievements on the use of shape memory polymer foams in space and biomedicine will be integrated with the concepts of 4D printing. In this optic, some recent studies seem particularly interesting. 3D printing [44] has opened, in the last five years, the possibility to overcome multiple limitations of traditional subtractive processes. 3D printing can produce on-demand complex geometries, with high mechanical and electrical performances and are highly personalized. In addition, with very fast production time and minimizing wastes of raw materials. 3D-printed structures are gradually acquiring other properties, such as the shape-memory effect largely discussed in this work. The technological transition from 3D printing to 4D printing aims at introducing the capability of 3D printed materials and structures to change their configuration over time. OSMFs and shape memory polymers find their natural application in this context [45]. 4D printed OSMFs can also overcome the lack of flexibility and customization of traditional processes for foams manufacturing. Traditional molds can be replaced with a fast additive process, without requiring secondary machining operations to create the desired shape.

4D printed foams and polymers are treated in many contributions. Shape-memory polymers find an extensive application with fiber reinforcement [46] by directly printing glassy shape-memory polymer fibers in an elastomeric matrix. 4D printed

origami metamaterials have been proposed by Tao et al. [47], while in [48], a smart re-entrant honeycomb shape reconfigurable, self-deployable, mechanically tunable, and reusable has been presented.

Invernizzi et al. [49] investigated 4D printable polymer structures with shape-memory and self-healing properties. The proposed material is photo-crosslinked and printed via DLP technology [50] obtained combining polycaprolactonedimethacrylate (PCLDMA) macro-monomers with methacrylates bearing 2-ureido-4[1H]-pyrimidinone motifs (UPyMA). Samples have shown remarkable shape-memory and self-healing abilities both for surface and bulk damage with an activation temperature of about 80 °C.

In 2016, Senatov et al. [51] proposed a polylactide (PLA)/15 wt% hydroxyapatite (HA) porous scaffolds using 3D printing by fused filament fabrication [44]. Mechanical properties, structural characteristics, and shape-memory effect have been studied. The average pore size and porosity of the scaffolds were 700 μm and 30 vol%, respectively. The work has shown that PLA/15%HA porous scaffolds exhibit a shape recovery of 98% with a direct heating up to 80 °C. The authors proposed an application of this porous structure as a self-fitting implant for small bone defect replacement, thanks to the shape-memory effect.

Mu et al. [52] developed a printing process based on photocurable poly(ethylene glycol) diacrylate resin mixed with salt particles. The authors combined a DLP 3D printing process [50] with the salt leaching method to print porous polymeric components. The printing process has been based on a rotating blade that sweeps the resin onto a printing piston that moves gradually downward permitting the layer's deposition. A salt leaching follows the printing, taking 10 min to 6 h in dependence on the size of the object. A final step in an oven at 80 °C for two hours ends the foams manufacturing. Multiple shape-memory tests have been performed by using a hot plate at 70 °C; a recovery time of 2 min has been observed.

Amato et al. [53] have investigated a new additive manufacturing process called "direct bubble writing" [54] for foam production. Gas-filled bubbles with tunable size and porosities have been obtained, thanks to the injection of pressurized gas through the core of a core-shell nozzle with a co-flowing outer shell fluid (aqueous or organic inks). The material exhibited a very accessible T_g of 40 °C. In this context, a simple shape recovery test has been performed on a 3D printed flower that deploys completely floating on warm water at 60°C in 10 s.

13.4 Conclusion

In this chapter, the promising OSMF applicability in the biomedical and space field has been discussed. OSMFs have big potential to be used mainly as light actuators, expandable and self-deployable structures, and environmental-sensitive structures.

In the space field, the applicability under microgravity conditions is the premise for future applications in space. Dealing with SMPs and SMPCs, the effect of microgravity on shape recovery and related forces is negligible but microgravity affects

heat transfer, and shape recovery is dominated by heat transfer. Strong limitations for designing the heating system were, therefore, posed by microgravity for the difference in heat transfer on Earth and on-orbit.

For further experimentations, the main problem to solve is increasing the size of prototypes, due to volume restrictions of payloads of space missions. Results from on-orbit experiments have highlighted the complexity in developing SMP and SMP-based devices. Another important aspect that has to be studied to allow future Space applications of these classes of materials, is evaluating their behavior in an open-Space environment, which could affect their stability and functionality. Sample recovery could happen in orbit, because of direct heating from the sun or heat transfer from the surrounding platform. Moreover, aging effects could occur in terms of mass loss and material degradation (cross-linking, chain polymer break, delamination, and embrittlement). In this case, space exposure could fix the temporary shape, and recovery would be impossible.

Finally, the possibility to manufacture OSMFs by 4D printing could open new scenarios for in-space manufacturing and colonization missions.

References

1. Santo L (2016) Shape-memory polymer foams. *Prog Aerosp Sci* 81:60–65
2. Quadrini F, Santo L, Squeo EA (2012) Shape-memory epoxy foams for space applications. *Mat Lett* (69):20–23
3. Santo L, Quadrini F, Mascetti G, Dolce F, Zolesi V (2013) Mission STS-134: results of shape-memory foam experiment. *Acta Astron* 91:333–340
4. Santo L, Quadrini F, Squeo EA, Dolce F, Mascetti G, Bertolotto D, Villadei W, Ganga PL, Zolesi V (2012) Behavior of shape-memory epoxy foams in microgravity: experimental results of STS-134 mission. *Microgravity Sci Technol* 24:287–296
5. Santo L, Quadrini F, Ganga PL, Zolesi V (2015) Mission BION-M1: results of RIBES/FOAM2 experiment on shape-memory polymer foams and composites. *Aerosp Sci Technol* 40:109–114
6. Quadrini F (2014) Polymer matrix composites with shape-memory properties. *Mat Sci For* 783–786:2509–2516
7. Babaevskii PG, Kozlov NA, Devicheva OV (2015) The influence of the component composition on the glass transition temperature and open porosity of shape-memory polyester urethane foam. *Plast Mas* 5–6:43–47
8. L. Santo GM, Quadrini TF (2015) Manufacturing of a shape-memory polymer actuator. In: *Proceedings of the ASME 2015 international manufacturing science and engineering conference MSEC2015*. Charlotte, North Carolina, USA
9. Santo L, Quadrini F, Bellisario D (2016) Shape-memory composite antennas for space applications. *Mat Sci Eng* (161)
10. Santo L, Quadrini F, Accettura A, Villadei W (2014) Shape-memory composites for self-deployable structures in aerospace applications. *Proc Eng* 88:42–47
11. Sokolowski W, Tan S, Willis P, Pryor M, Shape-memory self-deployable structures for solar sails. In: *Proceedings of SPIE—the international society for optical engineering*, p 7267
12. Tobushi H, Okumura K, Endo M, Hayashi S (2014) Thermomechanical properties of polyurethane-shape-memory polymer foam. *J Intell Mater Syst Struct* 12:283–287
13. Di Prima MA, Lesniewski M, Gall K, McDowell DL, Sanderson T, Campbell D (2007) Thermo-mechanical behavior of epoxy shape-memory polymer foams. *Smart Mater Struct* 16:2330–2340

14. Meents EP, Barnell TJ, Cable KM, Margraf TW, Havens E (2009) Self-healing reflexive composite structures for marine environments. In: Proceedings of 2009 international sampe symposium and exhibition, vol 54. Baltimore, MD, United States. Code 79037, p 16
15. Santo L, Quadri F (2015) Shape-memory composite sandwich with self-healing properties for marine applications. In: 20th international conference on composite materials. Copenhagen
16. John M, Li G (2010) Self-healing of sandwich structures with a grid stiffened shape-memory polymer syntactic foam core. *Smart Mat Struct* (19):7
17. Zhang P, Ogunmekan B, Ibekwe S, Jerro D, Pang SS, Li G (2015) Healing of shape-memory polyurethane fiber-reinforced syntactic foam subjected to tensile stress. *J Intell Mat Syst Struct* 17:1–10
18. Kashyap D, Gaur S, Kanagaraj S (2020) Development of hybrid shape-memory polyurethane composites for endovascular applications. *Mat Today Commun* (22):100751
19. Landsman TL, Bush RL, Glowczwski A, Horn J, Jessen SL, Ungchusri E, Diguette K, Smith HR, Sayyeda MH, Nash D, Jr. Clubb FJ, Maitland DJ (2016) Design and verification of a shape-memory polymer peripheral occlusion device. *J Mech Behav Biomed Mat* (63):195–206
20. Boyle AJ, Landsman TL, Wierzbicki MA, Nash LD, Hwan W, Miller MW, Tuzun E, Hasan SM, Maitland DJ (2016) In vitro and in vivo evaluation of a shape-memory polymer foam-overwire embolization device delivered in saccular aneurysm models. *J Biomed Mat Res Part B App Biomater* (7):104
21. Wang J, Luo J, Kunkel R, Liu Y, Bohnstedt B, Lee CH (2018) Biomedical devices using shape-memory polymer foams for treatment of intracranial aneurysms. In: Proceedings of ASME 2018, international mechanical engineering congress and exposition. IMECE2048–86120
22. Wang J, Luo J, Kunkel R, Saha M, Bohnstedt N, Lee C-H, Liu Y (2019) Development of shape-memory polymer nanocomposites foam for treatment of intracranial aneurysms. *Mat Lett* 250:38–41
23. Harrison RH, St-Pierre J-P, Stevens MM (2014) Tissue engineering and regenerative medicine: a year in review. *Tiss Eng Part B: Rev* 20:1–16
24. Langer R, Vacanti J (2016) Advances in tissue engineering. *J Ped Surg* (51):1
25. Webber MJ, Khan OF, Sydlik SA, Tang BC, Langer RA (2015) A perspective on the clinical translation of scaffolds for tissue engineering. *Biomed Eng* (43):3
26. Del Bakhshayesh AR, Annabi N, Khalilov R, Akbarzadeh A, Samiei M, Alizadeh E, Alizadeh-Ghods M, Davaran S, Montaseri A (2018) Recent advances on biomedical applications of scaffolds in wound healing and dermal tissue engineering. *Artif Cells Nanomed Biotechnol* (46):691–705
27. Amani H, Mostafavi E, Arzaghi H, Davaran S, Akbarzadeh A, Akhavan O, Pazoki-Toroudi H, Webster TJ (2019) Three-dimensional graphene foams: synthesis, properties, biocompatibility, biodegradability, and applications in tissue engineering. *ACS Biomater Sci Eng* 5(1):193–214
28. Hsu SH, Huang GS (2013) Substrate-dependent Wnt signaling in MSC differentiation within biomaterial-derived 3D spheroids. *Biomater* 34(20):4725–4738
29. Chen G, Qi Y, Niu L, Di T, Zhong J, Fang T, Yan W (2015) Application of the cell sheet technique in tissue engineering. *Biomed Repo* 3(6):749–757
30. Xie R, Hu J, Hoffmann O, Zhang Y, Ng O, Qin T, Guo X (2018) Self-fitting shape-memory polymer foam inducing bone regeneration: a rabbit femoral defect study. *Biochem Biophys Acta (BBA)—Gen Subj* (1862)4:936–945
31. Song JJ, Chang HH, Naguib HE (2015) Design and characterization of biocompatible shape-memory polymer (SMP) blend foams with a dynamic porous structure. *Polymer* 56:82–92
32. Quadri F, Bellisario D, Santo L, Del Gaudio C, Bianco A (2013) Shape-memory foams of microbial polyester for biomedical applications. *Pol-PI Tech Eng* 52:599–602
33. Jang LK, Fletcher GK, Monroe MB, Maitland DJ (2020) Biodegradable shape-memory polymer foams with appropriate thermal properties for hemostatic applications. *J Biomed Mater Res A* 108(6):1281–1294
34. Muschalek R, Nash L, Jones R, Hasan SM, Keller BK, Monroe MBB, Maitland DJ (2017) Effects of sterilization on shape-memory polyurethane embolic foam devices. *J Med Device* 11(3):0310111–0310119

35. Ratna D, Karger-Kocsis J (2008) Recent advances in shape-memory polymers and composites: a review. *J Mater Sci* 43:254–269
36. Quadrini F, Squeo EA (2008) Solid-state foaming of epoxy resin. *J Cell Plast* 44:161–173
37. Lucignano C, Squeo EA, Guglielmotti A, Quadrini F (2011) Recycling of waste epoxy-polyester powders for foam production. *Int J Manuf Mat Mech Eng* 1:10–20
38. Squeo EA, Quadrini F (2010) Shape-memory epoxy foams by solid-state foaming. *Smart Mat Struct* 19:105002
39. Quadrini F, Santo L, Squeo EA (2012) Solid-state foaming of nano-clay-filled thermoset foams with shape-memory properties. *Pol-Pl Tech Eng* 51:560–567
40. Santo L, Tedde GM, Quadrini F, Mutlay I (2015) CNT and graphene filled shape-memory foams by solid state foaming. *Key Eng Mat* 651–653:719–725
41. Santo L, Quadrini F, De Chiffre L (2013) Forming of shape-memory composite structures. *Key Eng Mat* 554–557:1930–1937
42. Santo L, Quadrini F, Bellisario D, Ciampoli L (2015) Self-repairing behavior of shape-memory composites. *App Mech Mat* 809–810:453–547
43. Santo L, Quadrini F, Bellisario D (2016) Multilayered composite plates with shape-memory properties. *Key Eng Mat* 699:1–7
44. Gibson I, Rosen DW, Stucker B (2010) Additive manufacturing technologies. Springer, New York
45. Ligon SC, Liska R, Stampfl J, Gurr M, Mulhaupt R (2017) Polymers for 3D printing and customized additive manufacturing. *Chem Rev* 117(15):10212–10290
46. Ge Q, Qi JH, Dunn ML (2013) Active materials by four-dimension printing. *App Phys Lett* 103:131901
47. Tao R, Ji L, Li Y, Wan Z, Hu W, Wu W, Liao B, Ma L, Fang D (2020) 4D printed origami metamaterials with tunable compression twist behavior and stress-strain curves. *Comp Part B: Eng* 201:108344
48. Ji L, Hu WB, Tao R, Liao B, Wan Z, Wu W, Xi L, Fang D (2020) Compression behavior of the 4D printed reentrant honeycomb: Experiment and finite element analysis. *Smart Mat Struct* 29(11)
49. Invernizzi M, Turri S, Levi M, Suriano R (2018) 4D printed thermally activated self-healing and shape-memory polycaprolactone-based polymers. *Eur Pol J* 101:169–176
50. Invernizzi M, Natale G, Levi M, Turri S, Griffini G (2016) UV-assisted 3D printing of glass and carbon fiber-reinforced dual-cure polymer composites. *Materials* 9(7):583
51. Senatov FS, Niaza KV, Yu M, Zadorozhnyy MY, Maksimkin AV, Kaloshkin SD, Estrin YZ (2016) Mechanical properties and shape-memory effect of 3D-printed PLA-based porous scaffolds. *J Mech Behav Biomed Mater* 57:139–148
52. Mu X, Bertron T, Dunn C, Qiao H, Wu J, Zhao Z, Saldana C, Qi HJ (2017) Porous polymeric materials by 3D printing of photocurable resin. *Mater Horiz* 4(3)
53. Amato DN, Amato DV, Sandoz M, Weigand J, Patton DL, Visser CW (2020) Programmable porous polymers via direct bubble writing with surfactant-free inks. *ACS Appl Mater Interfaces* 12(37):42048–42055
54. Visser CW, Amato DN, Mueller J, Lewis JA (2019) Architected polymer foams via direct bubble writing. *Adv Mater* 31(46):1904668

Chapter 14

Combination of Shape-Memory Polymers and Metal Alloys



**Jyoti Prasad Gogoi, Sunita Barman, Utpal Jyoti Mahanta,
Muni Raj Maurya, Sreedevi Paramparambath, Sadiya Waseem,
Kishor Kumar Sadasivuni, and John-John Cabibihan**

14.1 Introduction

The changing capability of high-performance polymers to become sensitive to new physical or chemical environmental conditions provides a class termed smart polymers, stimuli-responsive polymers or functional polymers, and shape-memory polymers (SMPs). Extensive research on SMPs are carried out in the last few years due to its possibility of various interesting and significant applications. The range of applications of such materials is vast, covering medical, industrial, electronics, textiles, and others, and development across all these fields is continuing in laboratories around the globe. Successful commercial utilization of SMPs has begun many years ago. Even before the discovery of the term shape-memory effect (SME) [1], the applications of water shrinkable and heat shrinkable SMPs were found in history. The noteworthy discovery of solid-phase transformation in shape-memory alloy (SMA) by Swedish physicist O'lander in 1932 was the beginning where he demonstrated plastic deformation of gold-cadmium alloys upon cooling and regain its original

J. P. Gogoi (✉)

Department of Physics, D.K.D. College, Dergaon 785614, Assam, India

S. Barman

Department of Physics, Assam Kaziranga University, Jorhat 785006, India

U. J. Mahanta

Department of Physics, Sibsagar College, Joysagar 785640, India

M. R. Maurya · S. Paramparambath · K. K. Sadasivuni

Center for Advanced Materials, Qatar University, PO Box, 2713 Doha, Qatar

M. R. Maurya · J.-J. Cabibihan

Mechanical and Industrial Engineering Department, College of Engineering, Qatar University, PO Box, 2713 Doha, Qatar

S. Waseem

Advanced Carbon Products, CSIR-NPL, New Delhi, India

configuration when heated [2]. Literature review credits the discovery of SME in polymers to Chang and Read in 1932 [3]. Towards the 1960s, SMPs began to receive extensive industrial recognition because of the rapid development of Polyethylene polymers. Unique and special properties like flexibility, biocompatibility, etc., along with the scope of tailoring [4] have promoted SMPs to receive significant attraction from both industrial and academic researchers. However, to improve the properties through tailoring possibilities, composites and blends of SMPs are prepared. The improved properties can be featured as improvement in mechanical properties with improved shape recovery stress, reduction in shape recovery induction time by enhanced thermal conductivity, development of novel polymer/polymer blends with SME, tunable property to temperature switch, and producing efficient shape-memory materials sensitive to electromagnetic, optical and humid conditions. Further, SMP composites and blends demonstrate new properties suitable for different applications and are different from conventional SMPs [5]. Because of such increasing shape-memory properties of SMPs they might exceed those of SMAs. There are numerous kinds of SMPs and can be classified based on the type of external stimuli responsible for SME. The four basic categories of SMPs are thermo-responsive SMPs (SME attained via temperature variation), chemo-responsive SMPs (SME attained via a change in the chemical environment or as a result of a chemical reaction), mechano-responsive (SME attained via application of external stress or pressure), and photo-responsive (SME attained via exposure to light without apparent temperature fluctuation) [1]. Examples of four usually used engineering polymers that can demonstrate the SME include polytetrafluoroethylene, polylactide, ethylene–vinyl acetate, and Polyurethanes.

14.2 Shape-Memory Polymers

As implied in the name, shape-memory material has a “memory” of its shape. Materials possess SME if they can restore their permanent shape after deformation in some way and fixed into a temporary shape. They can return to their original shape under a particular external stimulus. This stimulus may be heat or light. This capability is recognized as the SME [1, 6] and can occur in alloys known as SMAs, and in polymers as SMPs, SME is also possible in shape-memory hybrids (SMHs). These 3 sets of materials being intelligent, responsive, and able to control some external stimuli belong to the category of “smart materials”. The shape of the material is affected by the application of some exterior stimuli like temperature, stress, moisture, a field in terms of electric or magnetic, pH, light, or chemical compound. Thermally induced SME is extremely common in cases where the recovery occurs in compliance with a certain critical temperature [7]. SMPs are an exciting field of polymer development. In real meaning, SMPs can ‘remember’ what geometry they had and can ‘requite’ to that previous geometry when some stimuli like heat, light, immersion in water, and electric or magnetic fields, etc., are applied. That is SMPs are materials that can

be deformed to a temporary geometry and then can be brought to the previous non-deformed geometry by applying a stimulus. The special chemical structure present in SMPs helps to return to an original state from a deformed state. The external stimuli responsible for this mechanism usually generate heat within the polymer. Polymers can occur in two states, either a uniformly organized crystalline state where it bears rigid and relatively strong structure or a randomly scattered amorphous state where it allows relatively soft and flexible structure. On the other hand, SMPs can have a semi-crystalline structure, i.e., both the states crystalline and amorphous can occur at the same time and usually at room temperature [8]. The mechanism or the ways behind achieving this ‘memory’ effect have different names such as dual-state mechanism, partial transition mechanism, and dual component mechanism. Considering the glass transition temperature (T_g) some of these mechanisms may be explained. T_g is the temperature where polymer changes state from one state to another. SMPs have two of these glass transition temperatures while changing states from an initial crystalline (rigid) state to an amorphous (flexible) state. The initial crystalline state is rigid, and the polymer segments are motionless in this state, the polymer will tend to return to this state when exposed to stimuli. State changes occur when the SMPs become heated, i.e., when the temperature is raised, the free rotation about the polymer segment bonds makes the possible transformation of SMPs from a crystalline state to an overall amorphous state. The reason behind this is that within the polymer material three types of segments hard segments, crystalline domains, and amorphous domains of soft segments always exist. However, only two of these three segments, i.e., amorphous and crystalline domains of the soft segments are the segments that lengthen or elongate, i.e., deformed, while the hard segments do not get deformation.

But, in SMPs material in their deformed state, the polymer chain segments which have been deformed by the external stress will prevent themselves from shrink backing into their original state. This is accomplished by ‘reversible net points’ which serve as molecular switches. The SMP goes back to its original state when the second glass transition temperature is attained. This return to the initial state may be due to the tendency of physical systems to want to return to a state of most disorder and most randomness, which is facilitated by an increase in the mobility of the polymer chains due to the addition of temperature. During stretching, polymer first place goes from a random alignment state of the chains to a little less random state, i.e., the SMP will desire to return to the less ordered original state and this happens because of the increase in the mobility of the constituent parts of the polymer at this stage and due to the interactions within the semi-crystalline structure of the polymer.

14.2.1 Molecular Origin of Shape-Memory Effect in Polymers

SMPs may be regarded as a stimulus-sensitive switch-operated polymer network system having elastic behavior [9]. SMPs networks are composed of molecular switches and net points to establish the original shapes of the networks which may have a chemical or physical origin. Figure 14.1 represents the overall architecture of SMPs. Domains connected to the peak thermal transition temperature serve as net, whereas domains with the second-highest thermal transition chain segments serve as molecular switches. The occurrence of dissimilar domains (i) a hard or a permanent domain and (ii) a soft or a switching domain is accountable for shape-memory consequences in SMPs. The hard and soft segments act as a turning point for shape recovery and absorbing applied stress to the material, respectively. A polymer comprising of two different domains morphology showcases physical cross-linking. The hard section is liable for withholding the permanent shape of the SMP. Deformation of a polymer to a needed extent takes place at a certain temperature on heating and the particular temperature is termed as switching temperature (T_s) and that may be glass transition temperature (T_g) or a melting point (T_m) of switching segments. On further heating of the polymer above the (T_s), the oriented chains of the polymer in the network reinstate the randomly oriented subunits of the polymer to the original shape. However, the polymer must have elevated strain fixity and strain recovery

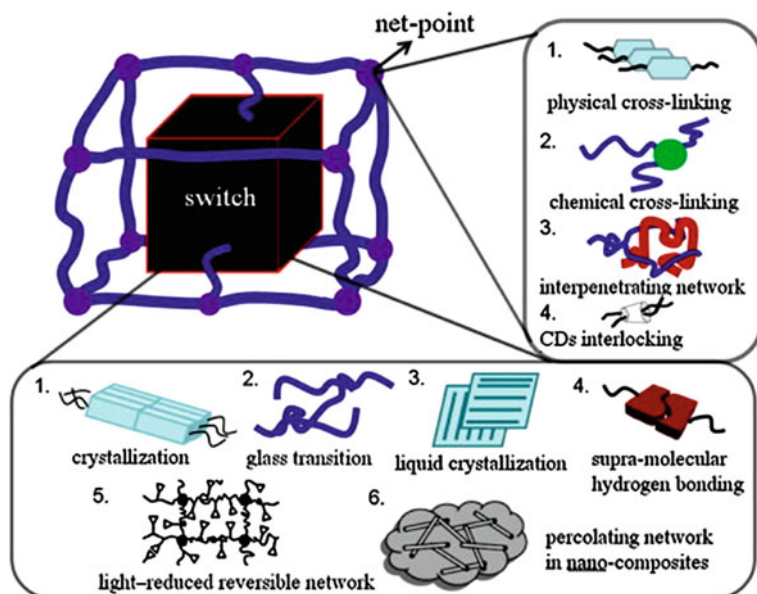


Fig. 14.1 The overall architecture of SMP. Reproduced with permission from [9]. Copyright, © 2010 The Royal Society of Chemistry

rates. Moreover, the SME of the polymers also depends on the applied strain or rate of deformation and its extent, and to have good shape recovery ratios the speed deformation should enhance with a decrease in strain [10]. However, the necessary recovery stress for SMPs depends on the factors such as minimum stretching rate, maximum stretching temperature, and stretch ratio.

14.2.2 Properties of Shape-Memory Polymers

SME is an imposed property of the material, i.e., not an inherent property. SME in the polymer may be the result of polymer functionalization. The original permanent form of polymer material is deformed and brought into a temporary form in a process called programming. The polymer regains its original form when exposing to external stimuli. These processes, deforming, and regaining can be repeated numerous times [6]. Programming normally results in two SMEs One-way SME (OW-SME) and Two-way SME (TW-SME) (Fig. 14.2). One-way SME is generally dependent on material's property where the material can remember only one shape (original). Alternatively, in Two-way SME material, it can memorize two distinct geometry, one at low and the other at high temperature, i.e., the material belonging to this group exhibits SME twice, one during heating and the other during cooling. This inherent bidirectional SME can also be realized without applying an external force [5]. The

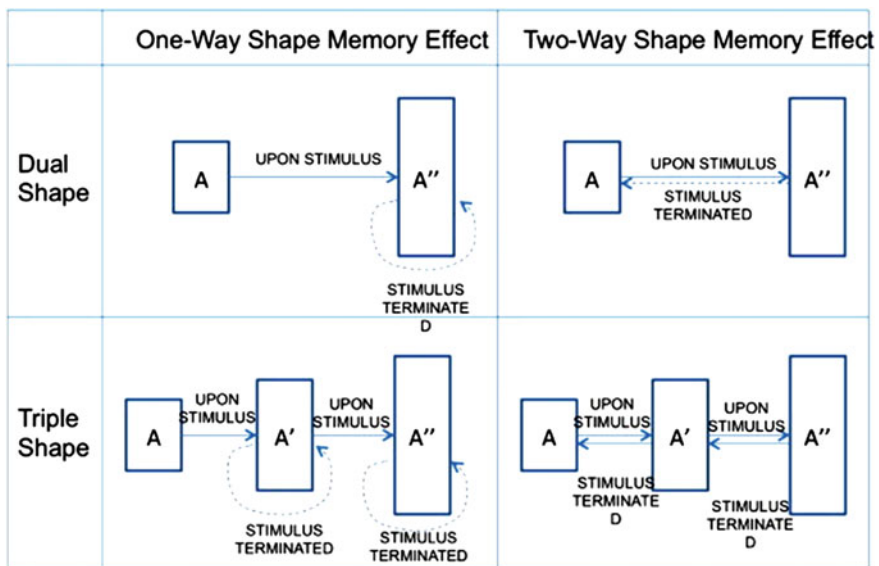


Fig. 14.2 SMPs shape-memory functionality. Reprinted from [6] Copyright © (2012) with permission from Elsevier Ltd.

polymeric material's capability to remember its parent shape is described by the quantity called strain recovery rate (R_r) and the capability of the switching segment to repair the deformation is described by the quantity called strain fixity rate (R_f) (extent of temporary shape). Moreover, transition temperature (T_{trans}), maximum recovery stress (σ_m), and maximum recoverable strain (ε_m) are also important parameters that are to be considered in describing SMEs in a polymeric material [10, 11].

When a polymer sample is deformed through several thermo-mechanical cycles (SM cycles) by applying stress for constant strain (ε_m) and then cooled by removing load (stress) and other constraints, a recovery of strain (ε_u) arises due to stored strain energy. The material is then subjected to a temperature above the switching temperature (T_s) to regain equilibrium shape. The complete thermo-mechanical cycle is called the SM cycle. The (R_r) and (R_f) for such N th cycles can be described by Eqs. 14.1 and 14.2 [12, 13].

$$R_r(N) = \frac{\varepsilon_m - \varepsilon_p(N)}{\varepsilon_m - \varepsilon_p(N-1)} \quad (14.1)$$

$$R_f(N) = \frac{\varepsilon_u(N)}{\varepsilon_m} \quad (14.2)$$

Using shape fixity ratio and Shape recovery ratio, SME can be explained as.

Shape fixity ratio,

$$R_f = 1 - \frac{E_r}{E_g} \quad (14.3)$$

Shape recovery ratio,

$$R_r = \frac{1 - f_{IR}}{\left[\left(1 - \frac{E_r}{E_g} \right) f \alpha \right]} \quad (14.4)$$

Here, $f\alpha$ is the strain when $T \gg T_r$ (recovery temperature) and f_{IR} is the viscous flow strain. E_g is the glassy modulus, which provides the polymeric material with high geometry fixity under instantaneous cooling and removing strain. On the other hand, the rubbery modulus E_r provides high elastic recovery at elevated temperatures. The requirements of polymer material for an easy shaping at $T \gg T_s$ (switching temperature) are the higher value of elasticity ratio $\frac{E_g}{E_r}$ and resistance to the deformation at $T \ll T_s$. The SMP needs to fulfill the above requirements for effective shape-memory applications.

To determine R_f and R_r , a shape-memory cycle (SMC) for the material is performed. The change that occurs in sample dimension is measured manually and using measured data and Eqs. (1) and (2) R_r and R_f can be calculated. Further, mechanical testing equipment with a climate chamber is used to evaluate (ε_m). Other shape-memory parameters in SMC can be precisely measured using such a thermo-mechanical analyzer [10].

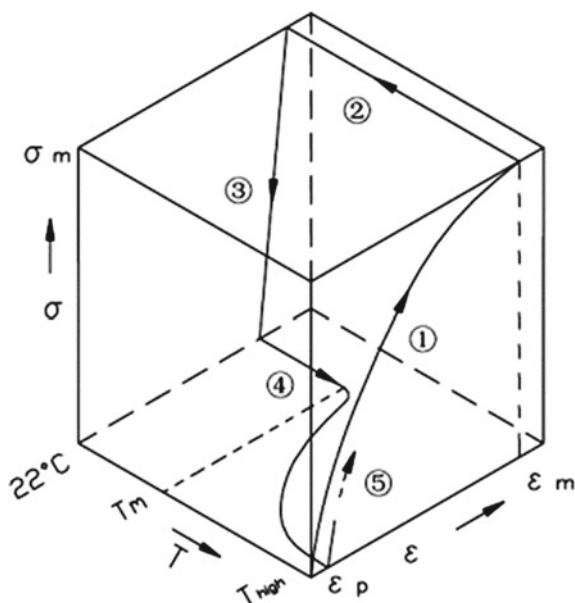


Fig. 14.3 Thermo-mechanical cycle of SMP. Reproduced with permission from [14]. Copyright © 2007, Wiley Periodicals, Inc.

14.2.3 Mechanism of Thermally Induced SMPs

Figure 14.3 shows the 3D plot of strain against force and temperature to illustrate a characteristic thermo-mechanical cycle of a thermo-sensitive SMP [14]. When the material is comparatively soft (stage 1) application of load at a high temperature results in easy deformation of the polymer material. The shape of the material is retained during subsequent unloading or cooling (stage 2). If the recovery of the polymer material is resisted by any other means, then the work done against the constraints is stored as latent strain energy in the sample (stage 3, 4). This stored energy is released from the sample when heating above the T_g or T_m . Regions of SME as illustrated in the 3D diagram may vary for different SMPs depending on their particular applications [6, 14].

14.2.4 Mechanism of Light-Induced SMPs

Through the integration of reversible photo-reactive molecular switches into the material architecture, the mechanism of light-induced stimulation in SMPs is accomplished and in the process acids like cinnamylidene acetic acid or cinnamic acid, moieties are integrated [15]. These incorporating groups act as light-triggered

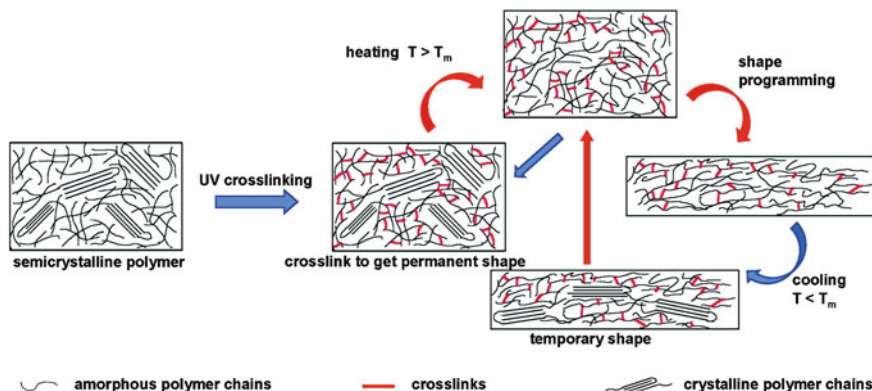


Fig. 14.4 Schematic of light-induced structural changes in the polymer. Reprinted with permission from [15]. Copyright © 2012 American Chemical Society

switches [6, 16]. Such moieties (in SMPs) in presence of light stimulus of appropriate wavelength initiate an additional reaction between them which leads to the formation of a cyclobutane-ring to promote cross-linking of covalent bonds. However, exposure to the light of different wavelengths may cause the splitting of the recently created bonds (Fig. 14.4).

14.2.5 Applications of Shape-Memory Polymers

There are numerous potential applications for SMPs. Some of the important properties of SMPs for which such polymer find potential applications in the fields of research and industry are lightweight, cost-effective recyclability, shape recovering ability for a broad range of stimuli, chemical stability, easy processing, biocompatibility, and biodegradability, etc. There are already a series of applications in use in the physical world, and it is expected that the range of applications will continue to rise. Some of the important fields of applications of SMPs are as follows: One of the first reported industrial applications of SMPs in the industry was with Heat Shrinkable Tubes (HSTs) used for insulation of wires; facilitate abrasion resistance and protection from the industrial environment. They are also used in connections, joints, and terminals in electrical works [17].

Robotics: Shape-memory foams are used in robotics to provide a soft grip when gripping objects. Foams can be cooled to harden and make a shape adaptive grip.

Automobile Industry: Modern vehicles employ several sensors and actuators due to the demand for efficient, more comfortable, and safer vehicles. SMPs are used in repairing of denting of the car by applying temperature. SMPs may also prove to be extremely useful in aircraft that would morph during flight, such as wings that change shape.

Construction industry: Shape-memory foams are used to seal window frames. Incorporating SMPs into existing building structures offers the potential to improve environmental performance and building envelope structures. Widespread research is being done on kinetic buildings [18].

Textile Industry: SMPs find wide application in textile industries due to stimulus–response triggered by temperature, light, pH, and moisture to obtain properties like moisture or temperature management, wound monitoring, etc. Also application in automotive seatbelts is found using SMP fibers which can absorb kinetic energy thereby ascertain the safety issues, wearable electronic devices, smart curtains, and orthopaedic smart textiles as corrective aids [19].

Biomedical applications: There are various potential applications of SMPs in the field of medical science. Some significant biomedical applications of SMPs include targeted drug delivery, tissue engineering, self-healing sutures, etc. [20–22]. SMP-based catheters get soften at human body temperature and possibly lessen the threats for soft tissue damage at the time of surgical delivery [21]. Other biomedical applications consist of biodegradable self-expanding and drug-eluting stents, implants for the treatment of obesity, coronary grafts, self-fitting vascular, and custom-built orthopaedic devices.

14.3 Shape-Memory Alloy

SMA makes up the group of smart materials and exhibits properties like SME and superelasticity that enables its applications in adaptive structures [23]. The initial reports considering the discovery of SMAs were started in the year 1890 through the finding of martensite in steel. Later, the reversible transformation of martensite was related and testified to the concept of thermoelastic martensitic transformation [24]. SMA was first revealed in 1932 [25], and the specific word “shape-memory” was introduced in 1941 [26]. The significance and the requirements of SMAs for major technical and engineering applications were not immediately realized, till the discovery of the SME in an equiatomic nickel-titanium (NiTi) alloy (Nitinol) [27]. The detection of Nitinol enhanced the research interest of scientists in SMAs. The beneficiaries of this technology are in various applications, such as mechanical engineering fields, automobile [28, 29], aerospace [30], micro-electromechanical systems (MEMS) [31], robotics [32], biomedical [33], and textile industries [34]. While metal alloys like copper-based and iron-based SMAs, such as Cu–Al–Ni, Cu–Zn–Al, and Fe–Mn–Si are cost-effective but NiTi-based SMAs are the desirable majority of applications. Another kind of SMA, known as ferromagnetic-SMA (FSMA), responds underneath strong magnetic fields. Nonetheless, every material is particularly meant for specific applications. The enhanced fatigue life and cost linked with the material systems make them a potential candidate for various engineering applications. Moreover, SMAs have reached the pinnacle of research for some previous decades owing to endlessly rising applications in different fields like structural engineering, robotics, and aerospace. All these fields require highly functional and lightweight

SMA. These materials can distort shape at the martensite phase which is at low temperature and to recover at elevated temperatures (austenite phase). The rise in temperature causes shape recovery even beneath high stress hence results in the formation of high actuation energy densities. Super elasticity is defined as a substantial retrieval of strain subject to deformation at different temperatures. Furthermore, SMAs can captivate and disintegrate mechanical energy while exposed to mechanical cyclic stressing via a reversible change in hysteretic shape [35–37]. The SMA can be used either way (i) individually or (ii) as reinforcement in composites subject to the requirements. The commercially available SMAs are found in the various form of foils, springs, ribbons, rods, wires, rods, and even foams [38]. SMA reinforced polymer composites showcasing high-performance such as Kevlar fiber, glass fiber, and carbon fiber have been tested and used successfully. The notion of SMA-based hybrid composite was primarily suggested by Rogers et al. [39]. In the initial stages, these hybrid materials were developed by reinforcing the SMA wires/strips in the epoxy matrix. The major application areas of these hybrid composites are creep control in structures shape, impact damage, acoustic properties, vibration control, and position control [40–42]. The latest research is performed keeping in mind the designing and creation of SMA embedded polymer composites.

14.3.1 Phase Transformation in Shape-Memory Alloys

SMAs have different crystal structures according to the two phases and therefore different properties within the distinct operating temperature range. The two different phases of SMAs can exist in three different crystal structures (i.e., austenite, detwinned martensite, and twinned martensite) and six possible transformations (Fig. 14.5) [43, 44]. The transformation from one structure to the other is known as martensitic transformation, and it is occurred by shear lattice distortion. Each martensitic crystal can have a different orientation direction, called a variant. At higher temperatures, austenite crystal structure (generally cubic) is stable, but martensite crystal structure (tetragonal, orthorhombic, or monoclinic) is stable towards lower temperatures. During heating, transform occurs in SMA from martensite into the austenite phase. The temperature at which austenite transformation begins is known as austenite-start-temperature (A_s) and the temperature at which this transformation ends is termed austenite-finish-temperature (A_f). Transformation into the austenite crystal structure (i.e., tendency to regain permanent shape by contraction) starts when SMA is heated above austenite-start-temperature (A_s). This transformation can exist still under high external stress, and this leads to the presence of high actuation energy densities [45]. On the other hand, the reverse transformation to the martensite (product phase) from austenite (parent phase), which forms the basis for the unique behavior of SMAs, begins while SMA is cooling to the martensite start-temperature (M_s) and the process continues till the martensite-finish-temperature (M_f) is reached [46]. The transformation from austenite to several martensitic variants is termed the forward transformation. The maximum temperature at which the

therefore, OW-SMA can be regarded as more reliable and cost-effective. The third one is pseudoelasticity or superelasticity. The term pseudoelasticity describes both superelastic behavior and so-called rubber-like behavior [54]. Here, the SMA relapses to its permanent shape after applying external loading at temperatures between A_f and M_d , without the application of thermal activation. The pseudoelastic performance of SMAs is connected with stress-induced transformation, which leads to strain production upon loading and following strain recovery during unloading at temperatures above A_f . A pseudoelastic thermo-mechanical loading path normally begins at an adequately high temperature where stable austenite exists, then develops a state under an applied load to which detwinned martensite is stable, and finally returns to the austenitic phase when returned to the zero-stress state. The reversible phase transformation explained by a thermo-mechanical loading path is termed as the superelastic behavior. The rubber-like effect is special conduct of the martensite phase only and happens to owe to the reversible reorientation of martensite [49]. The SME is a solid-phase transition between martensitic and austenitic crystal structures [55–58] without diffusion. However, there are other transformations such as rhombohedral (R-phase), bainite [55, 59], and the ‘rubberlike behavior’ in the martensite stage [60, 61], associated with SME and are not discussed in the present work in detail. Presently, SMA actuators are effectively employed in actuation and low-frequency vibration [62]. Currently, research has been carried out to promote the qualities of SMAs, by developing the material compositions [63–67] to attain a broader working temperature range, and improved material stability, in addition, to get better the material response, better mechanical design, controller systems, and fabrication processes. Consequently, to a large extent organized and systematic research is required to promote the effectiveness of SMAs [68, 69] by enhancing bandwidth, fatigue life, and stability [70].

14.3.3 *Types of Shape-Memory Alloys*

SMA with high transformation temperatures provides a novel group of SMAs termed high-temperature shape-memory alloys (HTSMAs). These materials have transformation temperatures above 100 °C. HTSMAs are prepared by incorporating ternary elements such as zirconium, gold, hafnium, platinum, and palladium to NiTi, and transformation temperatures can be tuned from 100 to 800 °C [55, 71, 72]. Since the actuation energy is disseminated through magnetic fields and is not obstructed by the relatively slow heat transfer mechanism Magnetic SMAs (MSMAs), usually termed ferromagnetic SMAs (FSMAs) can actuate at higher frequencies (up to 1 kHz) [73]. FSMAs are appropriate to bridge the technical gaps between SMAs and magnetostrictive materials and are an alternative for valve and motor applications [74] (Fig. 14.6).

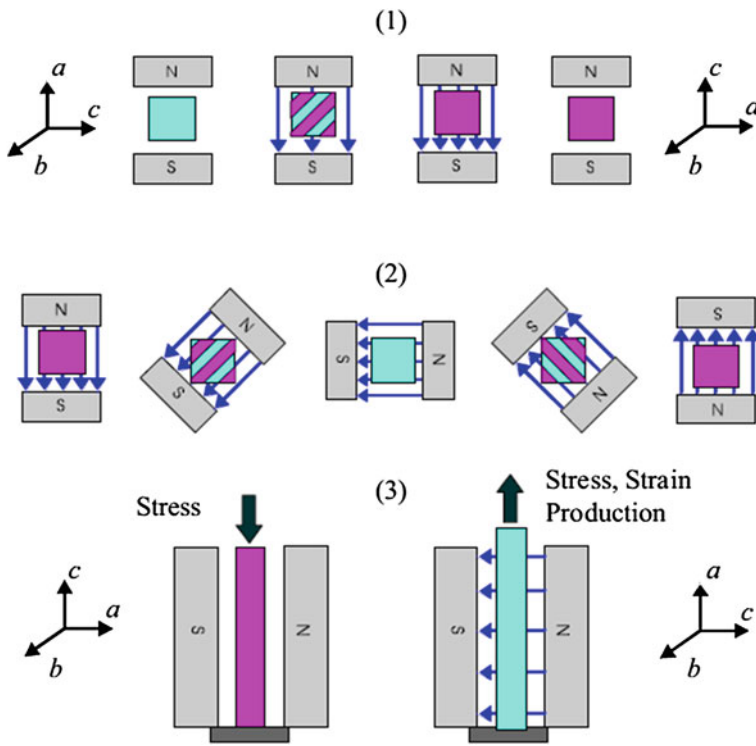


Fig. 14.6 MSMA element in (1) unidirectional, (2) rotating magnetic field, and (3) in the actuator. Reprinted from [73]. Copyright © (2016) with permission from Elsevier Inc.

14.3.4 Properties of Shape-Memory Alloys

The yield strength of SMAs is less when compared to conventional steel, but the yield strength of some compositions is higher than plastic or aluminum. The copper-based and NiTi-based SMAs are regarded as engineering materials. These compositions can be engineered to almost any shape and size. However, metals are not cost-effective and the processing of them to utilize in SMAs design is difficult and expensive. Consequently, these materials find applications where the SME can be utilized (in actuation). Another property is that in SMAs maximum of recoverable plastic strain can be induced, and these alloys can hold maximum recoverable strain without permanent damage.

14.3.5 Applications of Shape-Memory Alloy

In resolving engineering difficulties in different industries, engineers have utilized the exceptional properties of SMAs. SMAs have drawn immense attention in numerous fields of application with a broad range from medical implants and fixtures to surgical instruments, aerospace, and naval [75–78]. In the aerospace industry, SMA technology has extended its application to the areas of spacecraft, rotorcraft, fixed-wing aircraft, etc. The combination of unique characteristics of SMAs, viz., pseudoelastic characteristics and shape-memory together with the biocompatibility of Ni–Ti make SMA a potential applicant for medical applications. These exceptional qualities have promoted SMA in developing several medical components such as orthodontic wires, filters, stents, and devices for minimally invasive surgery along with orthodontic, cardiovascular, orthopaedic, and surgical instrument applications [49]. A broad range of applications of SMAs has been found in automobiles for actuation, sensing, and impact absorption. The pseudoelastic property of SMAs offers an efficient means for impact absorption on armor vehicles and dissipates vibrations [79, 80]. Various other fields incorporate SMAs. In the oil industry, SMA is used in releasing devices and protecting units for drilling equipment. Day-to-day life applications such as rice cookers and coffee makers have also included SMAs. In the air conditioner, SMA has also been integrated to adjust the temperature of the air. Sports and garments knitting industries have also used SMAs to manufacture their products [49]. Researchers are still trying to remove problems and limitations related to the applications of SMAs by developing efficient SMAs.

14.4 Review on Shape-Memory Alloy and Polymer Composites

Andreas Lendlein et al. [81] argued in a review article on thermo-responsive SMPs which talks about the one-way polymer effect, i.e., increasing the temperature of SMP above T_{trans} which prompts SME. The cooling of the polymer below transition temperature again leads to solidification, with no permanent change in shape observed. Change in shape and structure occurs by an alteration in temperature and is called thermally induced SME. Ghosh et al. [82] discussed the multifunctional smart material system (MSMS) made by the arrangement of thermally responsive SMA and SMP. The transformation temperatures of SMP are adjusted such that $M_f < T_g < A_s$ to attain multi-state smart bias systems having various stiffness. The number of SMA reinforcements is found by equating the stiffness $K_{SMA}^{\text{austenite}} = K_{SMP}^{\text{rubbery}}$. Additionally, specific volume fractions of each constituent were recognized to surpass issues like debonding owing to large differences in stiffness of the constituent's material. Billah et al. [83] reported the corrosion-free hybrid RC column and compared it with SS reinforced columns under the influence of earthquake loading. The adeptness of the hybrid reinforcement's concrete structures was proven based on bridged permanent

deformation, energy dissipation capacity, and adequate ductility. The results affirmed that in comparison to conventional SS reinforced columns, residual displacement was reduced to 87% when SMA is used in the plastic hinge zone. Hosoda et al. [86] anticipated the material design and SME of NiMnGa-FSMA/epoxy, which is a composite of polymer matrix and FSMA particles. Nonetheless, the shape memory properties are subjective to the internal defects, creep deformation of the matrix, and volume fraction. Presently, the maximum shape recovery strain is nearly 0.4% for the constant stress tests through thermal cycles and 2% for tensile stress-strain tests. Zhang et al. [85] studied an effectual method for enhancing the interfacial bonding between epoxy matrix and nickel-titanium SMA fibers via the addition of nitric acid dipping and layering the silica nanoparticles coating. Experimental results propose the likelihood of effectually uplifting the strength of the interfacial bond amid nickel-titanium SMA and epoxy matrix. The research discloses a decrease in both strength indices (load-carrying and tensile modulus) with an increase in the duration of acid treatment. The pull-out tests show that silica nano-coating is effective in elevating the interfacial shear strength. Particularly, the maximum enhancement was marked by dipping the SMA fiber in HNO₃ solution for 8 h before the nanoparticle coating. Parameswaranpillai et al. [86] have dedicated their study to thermal analysis and its associated properties of high-performance SMPs and their composites in various length scales. Fathi et al. [87] explored the SMA wire loading effect on the interfacial properties of SMA/epoxy composite. With the increase in the rate of loading rate of SMA from 0.3 mm/min to 400 mm/min a lowering of 5.5% is observed in the tensile strength and a 70% enhancement was noticed in the interfacial strength. Yazik et al. [88] reported the thermal properties of SMP composite loaded with different amounts of multi-walled carbon nanotubes. The results showed that improved dispersion was obtained in the SMEP with 1.5% MWCNT's. The upgradation in shape recovery in SMEP was obtained with the inclusion of 1.0% and 1.5% MWCNTs. It was also seen that the inclusion of MWCNT's reduced the T_g and thermal stability of the SMP nanocomposites. Katsiropoulos et al. [89] fabricated Ni-Ti wires loaded epoxy/Kevlar composites and analyzed the effect of the existence of the superelastic phase on the damping characteristics. It was observed that the damping factor of the composite can be engineered by properly choosing the pre-tension level and volume fraction of the attachments. Ashir et al. [90] inspected the friction spinning technology to develop the hinged fiber embedded fabrics with tailored SMA hybrid yarns. SMAs are integrated into the fabrics in a single step, using weaving technology which is a fully automatic process. The test results indicated that by elevating the hinged width from 50 to 150 mm, the extreme deformation of composite became thrice from 9.6 to 29.8 mm. The opposite trend was seen when the distance between two SMA hybrid yarns increases. An increment in distance from 10 to 25 mm caused a decline of the largest deformation from 19.5 to 9.5 mm in the composite. The thermal expansion performance of arbitrarily distributed curvy carbon nanotube (CNT) integrated SMP nanocomposite was reported by Aghdam et al. [91]. They fabricated the representative volume element of the model with CNT and SMP and their inter-phase was obtained through Van der Waals interactions. They showed a significant reduction in the coefficient of thermal expansion of the polymer nanocomposites

with the inclusion of carbon nanotubes. Composites having haphazardly oriented curly CNTs exhibit a linear rise and nanocomposites with straight CNTs showed a nonlinear increase in the coefficient of thermal expansion with temperature. Moreover, more integration of CNT in SMP nanocomposites reduced the coefficient of thermal expansion of composites. The study also revealed the results of inters phase characteristics (adhesion exponent, thickness) on the thermal expansion performance of SMP nanocomposite consisting of randomly distributed carbon nanotubes. They also carried out a study on the longitudinal and transverse coefficient of thermal expansion of ordered CNT-included SMP nanocomposite. The study was forwarded by Aghdam et al. by developing a novel formulation (micromechanical) to forecast the thermal conductivities of CNT- SMP nanocomposites [92]. The study pointed out the effective means of dissipation of heat through the alignment of carbon nanotubes into the SMP nanocomposites besides the thermal loading. A nonlinear decline in the axial thermal conductivity is observed with the increase in waviness (curviness) of CNT along with the rapid rise of transverse direction thermal conductivity of the nanocomposite. However, the axial thermal conductivity of the nanocomposites (CNT-SMP) is not influenced by the cross-sectional form of an array type of CNT, interfacial thermal resistance, whereas the transverse thermal conductivity of composites is affected by interfacial thermal resistance. Their investigation on the behavior of thermal conductivity of the developed composites finds important applications in the field of biological micro-electro-mechanical systems and temperature sensing elements. Another theoretical and experimental study was made on the performance composites such as SMAHCs (SMAH Composites) and thermoplastics to inform aeronautical importance by Guida et al. [93]. The composite used in their study regarding mechanical characterization was thermoplastic resin included carbon layers composed of fabric hybridized with SMA. They have revealed the high energy-absorbing ability of experimented samples through low-velocity impact experimentation of the composite sample and finally, results are simulated and confirmed using numerical models. The inclusion of SMAHCs in the investigation is to enhance energy absorption as well as impact the performance of the studied composite. The process of hybridization modifies mechanisms of energy absorption of the specimen by reforming the low-velocity impacts response for the integrated material specimen. The material on which they worked was aimed to use in designing aeronautical structural parts to fulfill the problem of bird collision and the mathematical results of the study had promised the purpose. Aghamirzadeh and his co-workers also researched composite derived from randomly oriented short hollow glass fibers (ROSHGFs) and SMA strips to study experimentally healing efficiency in a high strain test [94]. The study revealed an effective healing development obtained one week later from the initial strain. They experimentally determined healing process efficiency in terms of pre-strain percentage with different compositions of the SMA strips and found the strips with 2% pre-strains provide excellent results compared to any other pre-strains percentage composites. They investigated the healing efficiency of various samples having pre-damaged SMA and specimen without the SMA strips. The researchers have pointed out that the factors on which the healing performance of experimented specimens depended are energy absorption of the SMA strips, shear

strength (interfacial) between the SMA strips and the composite and shutting down of crack because of revival forces. In research conducted by Pan et al. [95], theoretically explained SME and mechanical belongings of sphere-shaped particle reinforced SMP composite considering as a representative volume element employing an adsorption algorithm. They searched for thermo-mechanical properties of composites prepared through the inclusion of elastic glass globules in an SMP matrix exploiting a linear viscoelastic model. It was revealed that the addition of fillers in the matrix promoted the regaining stress and elastic behavior (modulus elasticity) of the composites. Further, it was found that more inclusion of fillers reduces the shape fixity ratio of composites; however, this property is retained with composites of low reinforcers inclusion. They concluded the possibility of tuning elastic activities utilizing glass bead fillers in the proposed SMP by preserving SME character.

An article published by Zhenqing Wang and his fellow workers [96] described the possibility of improvement of SME in SMPs and composites through a study on their thermo-mechanical responses and proposed a statistical approach to narrate the SME of various substances. In the study, a thermo-mechanical activity of SMP was carried out by introducing a '4' element model two for elastic deformation and one each for flow behavior and strain of polymers. The study concluded that the possibility of modification of haphazard allocation of a chain of a polymer taking into account chain combination form, the geometry of the border condition, and inner inclusion. And recommended such a polymer chain can be controlled using reinforcers and peripheral limitations in composites and films, respectively, of polyurethane. However, the results of the study indicated that SME simply could increase by rising cross-link density in samples for a better elastic response. In another article by Yarali et al. [97], they mathematically investigated the thermo-mechanical response of SMP nanocomposite under considerable strains through the inclusion of coiled CNT. They reported that increasing the weight percentage of fillers in the composite up to a certain amount (0.6%) promoted the effective stress in the specimen significantly. This paper predicted a relation of spring length of the coiled CNT with the regaining strain and informed the later increases with spring length up to about eight percent. It has also been predicted that significant stress can be applied parallel to the coiled CNT direction compared to its perpendicular direction since coiled CNT bears a definite orientation in the composite, but the strain revival was independent of such orientation. In research conducted by Hassanzadeh-Aghdam and his co-workers [98] searched longitudinal and transverse elastic coefficient of CNT (carbon nanotube) reinforced SMP nanocomposites and investigated the dependence of weight percentage of inclusion, temperature, diameter, and kind of distribution of CNT in the matrix together with interphase dependent factors namely thickness and adhesion exponent. The study predicted that the elastic properties of CNT integrated SMP nanocomposites were found to be enhanced with the thickness of interphase or reduced with the adhesion exponent. Ameduri et al. [99] focused their study on the experimental functionality test, prototyping, and modeling of a smart actuator based on SMP technology. They worked on potential aerospace applications of shape-memory polymer composite. Krishan Kumar Patel

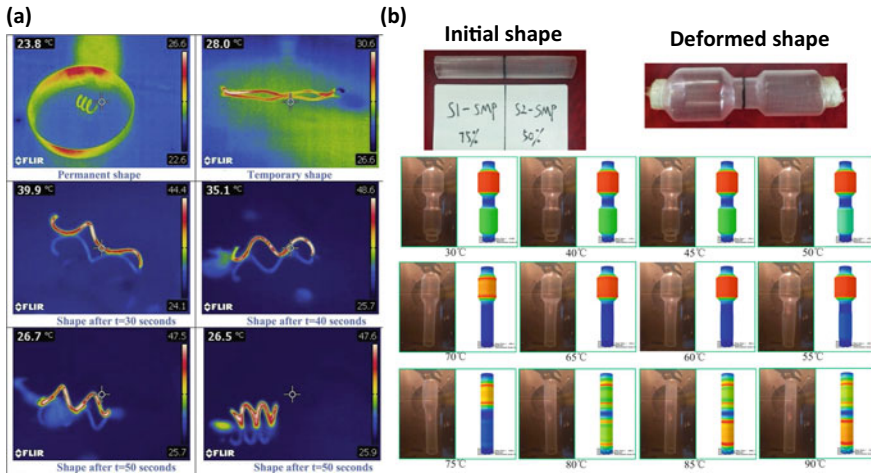


Fig. 14.7 **a** Microwave-induced shape recovery test at 2.45 GHz. Reprinted from [100] Copyright © (2019) with permission from Elsevier Ltd. **b** Double bottle-shaped SMP, initial and deformed shapes along with sequential shape recovery stages. Reprinted from [102] Copyright © (2019) with permission from Elsevier Ltd.

and his co-researchers [100] studied the thermo-responsive behavior of composites using microwave prepared through ex-situ polymerization of shape-memory thermoplastic polyurethane (SMPTU) with the incorporation of multi-wall carbon nanotubes (MWCNT) at different proportions in the matrix of SMPTU (Fig. 14.7a). They found considerable development in mechanical properties and shape-memory after the addition of MWCNT fillers into the matrix of SMPTU during the preparation of composites along with the increase of required elastic properties such as restoring force, elongation, and stretching strengths up to more than 100% compared to the composites of the only SMPTU. The study also concluded that the insertion of MWCNT in the composites improved the glass transition temperature (T_g) of the composites. The research was carried out to investigate microwave-induced shape-memory behavior on the proposed nanocomposite by utilizing the high absorption of microwave radiation of MWCNT to fulfill the requirement of fast heating, remote actuating, sensing, and for use in wireless devices. However, microwave-induced SME highly is dependent on microwave frequency and concentration of fillers MWCNT. A research article written by Ruoxuan Liu et al. [101] discussed the role of loading rate and level on thermosetting SMP while studying their thermo-mechanical behavior in an experimental investigation. The study reveals that at a temperature lower than the glass transition temperature (T_g) such polymer acts like rubbery material during stress experiments and a cyclic loading situation results in a large shape fix ratio. However, the job of loading level and rate are significant only at the starting and finishing of shape revival courses of the studied polymer. The researchers conclude that the recovery speed of material depends on their deformation corresponding to temperature T_g , higher revival speed is seen for materials getting

deformation at a temperature lesser than T_g than those in which deformation occurred at a temperature higher than T_g . They also pointed out that continuous stressing and un-stressing helped the sample to obtain the rubbery condition at a lower temperature for improved shape recovery performance. In an article, Du et al. [102] informed the preparation of a fragmented styrene-based triple-SMP of two different compositions of SMP having different glass transition temperatures T_g . They performed the characterization of thermo-mechanical belongings of both constituting materials through examining thermal expansion, multi-frequency scanning, tensile and shape-memory behavior of materials. The study announced dual-shape-memory behavior of more than 95% together with maximum shape fixity and shape recapturing ratios while conducting four-stair thermo-mechanical series of experiments. Further, triple SME is expected from both (SMP1 & SMP2) of the ingredient materials through the preparation of triple-SMP in a range of temperature 30 to 90° C (Fig. 14.7b). The discussed model regarding triple shape regaining nature was in beneficial agreement with the constitutive models announced by Liu and generalized Maxwell.

Researchers also lastly displayed applications of triple-SME actions in two programmable structures. Furthermore, Tobushi et al. stated the study on deformation and regaining stress of prepared composite consisting of both SMA and polymer [103]. They revealed two classes of SMA strips exhibiting SME and superelasticity and to remember their round shape heat stimulus was used. Fabrication of composites (SMA and SMP) had been completed by sandwiching already assembled oppositely facing round SMA strips in between sheets of SMP. Such produced material composites can find applications in the production of the belt by considering suitable aspects. Utilizing the SME and SE behavior of the SMA strips two-way bending deformation is obtained in the fabricated shape-memory composite while raising and lowering the temperature of the composite. It has also been observed that the belt constructed from such composite when subjected to heat application in its best condition then recovery stress improves during heating and lowers during cooling, and it is dependent on the two-way properties of the composite. The study pointed out the possibility of developing high-functional SMP composites from the mixture of SMA & SMP with a variety of phase transformations. In another study made by Amaël Cohades and co-workers explored high-level impact damage healing on heat treatment when wires made of SMA were used in repairing or sealing cracks in plates fabricated from glass fiber-reinforced polymer (FRP) in an epoxy-polycaprolactone matrix [104]. The report thus indicates a solution towards the need for sufficient durability of composite against matrix micro-cracking from impact. The developed composites show promising compressive strengths with complete regaining ability from large impact damage incidents without any supports. The above encouraging results of the study are due to the united properties of both epoxy-PCL healing matrix and SMA wires in closing cracks caused by moderate impact (energy around 17 J) however above that energy impact large deformations take place with consequent breakage of fiber. Research on SMA is also enriched by researcher Wang et al. and they observed the interfacial behavior of nickel-titanium (Ni-Ti) SMA fiber-reinforced vinyl ester resin composites [105]. They prepared SMA fibers coated with Al_2O_3 nanoparticles and silane coupling agent KH-550. A study was carried

out to reveal the performance of interface in presence of nanoparticle content for the composites of various wt% of Al_2O_3 contents. The result was that a little raise in the strength of adhesion together with the problem of small dispersion of the nanoparticles on the fiber surface introduces defects. However, a considerable rise in the strength of adhesion is reported among the Ni–Ti fiber and the vinyl ester resin matrix while the surface of fiber was transformed with a silane coupling agent and also assisted in the dispersion of Al_2O_3 nanoparticles on fiber surface. The report also stated that maximum adhesion strength was achievable for combinations transformed with 3 wt.% of both KH550 and Al_2O_3 . Hao et al. [106] engineering team designed SMA hybrid fiber-reinforced polymer composite embedded with two perpendicular layers of superelastic SMA wires. The study found that SMA hybrid laminates can bear more weight than laminates with plain wires because of the SMA wires' superior weight-bearing capabilities. It is understood by those who have experience in the field that the wire is damaged by the martensite process which causes less energy to be left in the wire to cause damage in the hybrid layer. Ruixu et al. [107] reviewed a 3-D finite element analysis of SMA and then combined them in new ways. SMA study was done by Khalili and his colleagues [108], where the equivalent fiber properties of randomly oriented EMM (epoxy methyl methacrylate) reinforced polymers were compared to the Mori–Tanaka process to model the elastic properties of the material. It is found that wires with a high aspect ratio are used in composite materials which increases the elastic modulus by 20%. Wang, Enhao et al. [109] fabricated SMA Ni–Ti fiber-reinforced Ti–Al laminated composites containing approximately 41 volume percent Ti and approximately 2.5 volume percent NiTi. The novel SMA laminated composite is a material with high strength (compressive strength of over 1,100 MPa) and high plasticity (a material that will deform over 5%/day) which means that this class of laminated composites are a new type of material. Wang et al. [110] chose glass/epoxy composite materials bonded with SMA wires (Fig. 14.8). Two glass/epoxy composites were tested, one glass/epoxy and glass/epoxy composite with SMA wires. The glass/epoxy with SMA wires was found to have higher fatigue endurance than the glass/epoxy composite. The fact that the SMA deformation reduces the rate of matrix cracking means that the composite is less likely to crack and therefore last longer. Song et al. [111] studied series of models for SMA and SMP with thermo-mechanical tests. The study concluded that the proposed novel-shaped composite shape-memory model was able to predict general trends of the thermo-mechanical behavior of the shape-memory composites. Yongkun Wang et al. [112] research the influence of the Fe_3O_4 nanoparticles content on the magnetic behavior, fracture morphology, mechanical properties, and thermal properties and of (styrene-*b*-butadiene-*b*-styrene) copolymer low-density polyethylene composites. It utilizes homogeneously dispersed Fe_3O_4 nanoparticles combined with SBS and LLDPE that ensure excellent conductive heat transfer and magnetically responsive SME, respectively, when subjected to an alternating magnetic field. These serve as good/flexible functional fillers in stretchable/flexible low-dimensional systems/materials. When Fe_3O_4 nanoparticles were put under alternating magnetic fields, the particles with appropriate size returned to the shape they maintained when

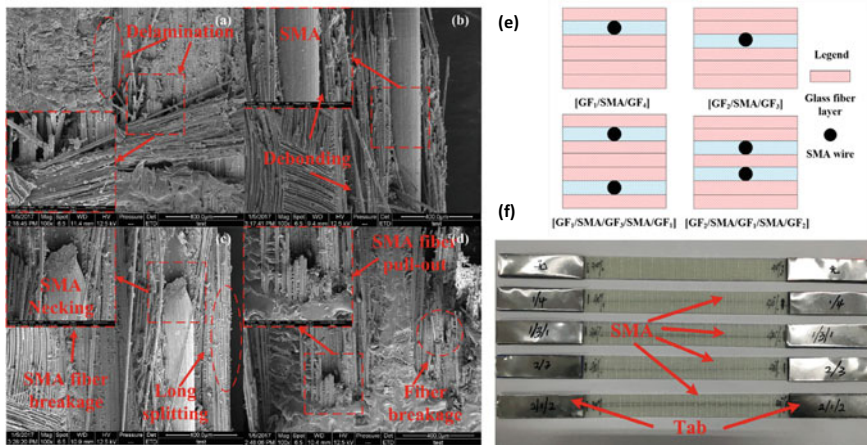


Fig. 14.8 a–d SEM images of the fatigue failure modes of SMA composites e Stacking chain of hybrid composite. f SMA composites samples with SMA wires. Reprinted from [110] Copyright © (2017) with permission from Elsevier Ltd.

exposed to consecutive magnetic fields varying from $f = 60$ kHz to $f = 120$ kHz along with a magnetic field strength of $H = 21.2$ kA m⁻¹.

Shen et al. [113] examined three sets of soft actuators that can be manipulated with an electrical current and an adjustable temperature. This Nafion-based ionic polymer-metal composite system is able of providing complex motions by utilizing several actuators in a coordinated manner under AC bias and simultaneous temperature stimulus (Fig. 14.9). Daghash et al. [114] have studied the cycling behavior of thermoset composite materials made with high-strength metal-reinforced thermoset polymer. Tensile tests were performed to investigate the physical properties of the composite, accounting for the stress levels, to serve as a good reference. The fatigue resistance of an SMA-FRP was investigated in depth. By using scanning electron microscopy, the researchers observed the microstructure of the fractured surfaces to better answer the question “Why did it collapse?” Tests show that SMA embedded composites can fully restore large strains and attain an ultimate tensile strain of 10–11%. Adding a large amount of fiber greatly improved the superplastic properties of the composite material. As a strain multiplied by amplification, energy dissipation and equivalent viscous damping increased [e.g., fatigue], while the secant modulus decreased [a.k.a. strain hardening]. The strain hardening will propagate in the composite’s behavior under cyclic loading. The liquefaction of the strengthening material was taken under the same strain (higher liquefaction rate) with a sudden change in the secant modulus, so it may slow down. In many SMA-FRP composites, the continuous overloading of the composite by cross-linking of the fiber resulted in the accumulation of residual amounts of deformation in the material, which in turn suppressed the properties of the composite and caused it to fail after many load cycles. It was found that the 9.9% infill material had little residual stress and 82 percent of the infill material could be

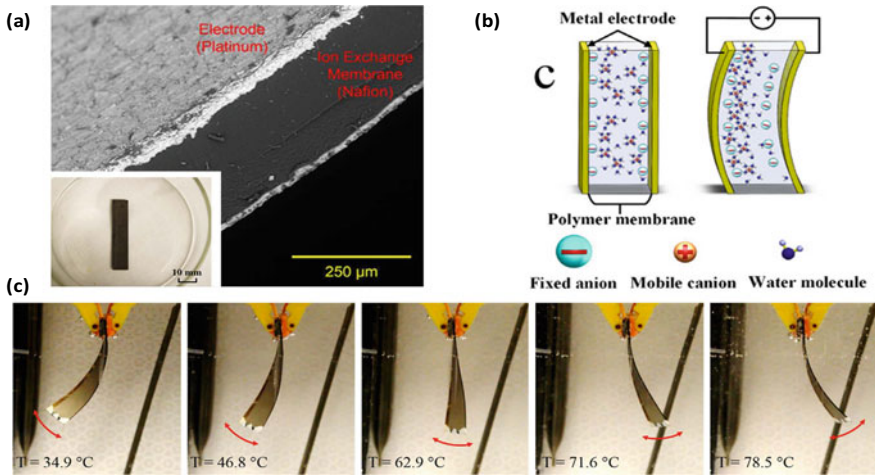


Fig. 14.9 a–b Nafion-based ionic polymer-metal composite cross-section SEM image and schematic showing ionic polymer membrane sandwiched between two electrodes, respectively. c Composite actuator underwater at the temperature range of 22–90 °C and a sinusoid AC voltage of 3.7V at 1 Hz frequency. Reproduced from [113], originally published under a CC BY 4.0 license, <https://doi.org/10.1038/srep31110>. Copyright © 2016, Qi Shen et al.

recovered during the combinations of the cyclic loading. The panel of judges determined that SMA consisted of various components that bound together to form an adhesive. It is important to incorporate SMA fibers into the epoxy composite materials. This allows the material to absorb transverse bending energy and direct force. This results in increased strength and stiffer material.

Pulla et al. [115] developed SMA particles using a simulation of the material properties of the globular particles. The SMP matrix is modeled with Ogden strain energy function, and the SMA filler is modeled with the Lagoudas' model. These two models are used to calculate the material composition and how that leads to different responses. A simulated version of the SMA-SMP composites is created with specific amounts of content and is simulated at a temperature from 18 °C to 55 °C. The surface of the gel stiffens as temperature rises, and the newly added strength of SMP adds to the surface of the gel and greatly increases its strength. It is claimed that SMA is more effective than conventional fillers because it has unique temperature-responsive mechanical and microstructure properties. Guo et al. [116] developed chopped carbon fiber-reinforced TPI through a novel process and aimed to improve its mechanical properties. SMP composite was fabricated with carbon fiber weight fractions from 5 to 13%. The data demonstrate that the rate at which the shape returns to the original shape decreases as the filler weight fraction increases. Cold temperatures increase stress fracture, but as the percentage of carbon fibers increases, fracture stress decreases. Young's modulus is largest at 7% with a sharp phase transition at 40 °C. As the number of cycles continues to increase, the stress level rapidly increases, and then reaches a relatively stable stress level that

remains consistent even when cyclic loading occurs. When put under the greatest stress, the 7wt percent specimen reaches its point of maximum stress three times the level of the other specimens. The strain increases as the number of cycles/repetitions increases. When certain levels of stress are reached, the stress level remains constant. No detectable strain was found in 9% of samples, and the lowest detectable strain was 50% less than that of the control. Dawood et al. [117] investigated the bond strength of nitinol SMA wires to carbon fiber-reinforced polymers to determine how well these materials bond together (CFRP). Forty-five different samples were tested up to failure. In the experiments, two different mechanisms of debonding were observed. One type resulted from radioisotope, while the other did not. There are two critical lengths for embedment: $L(d, \sigma)$ and $L(d, \varepsilon)$. To investigate the stresses and lengths required of the wires to transform, they will be evaluated. A 12.7 mm gauge wire was used to test wires with a diameter of 0.47 mm, 0.66 mm, and 0.89 mm, respectively. The method used to measure $L(d, \varepsilon)$ was found to be 12.7, 25.4, and 50.8 mm. Kang et al. [118] investigated the interfacial adhesion properties among the titanium alloy and SMP composite. The surface treatment of the titanium alloy with a silane coupling agent enhances the chemical bond with the metal and plastic. The blade was enhanced by the addition of CNT, PBE, and a microscopic amount of carbon nanotubes. Nji et al. [119] investigate the healing of structural-length scale damage via incorporation of thermoplastic SMP-based particulate as additives. They are trying to achieve a physiological change without damaging the cellular framework. By filling cracks with epoxy, the cracking is stopped, and the material used to repair is reduced. The study shows that planar stabilized composite can be used to heal on a small scale and maintain structural integrity on a large scale. As low as three percent, can achieve meaningful structural-length scale damage healing, and with less sacrifice of structural strength than competing technologies. It can be used to repair cracks in concrete and is comprised of small amounts of thermoplastic additives. The reduced width of the crack due to the confined shape and the copolyester help in reducing the bending load. The behavior of the polystyrene SMP shows how polystyrene improves the stiffness and toughness of a copolymer. The fracture strength of composites decreases with an increase in the content of copolyester. The shape recovery rate with polyethylene with copolyester films is lower.

14.5 Conclusion

In summary, comprehensive detail about shape-memory polymers (SMPs) and shape metal alloys (SMAs) in terms of shape-memory effect has been presented. The mechanism of shape-memory and various types of shape-memory under different external stimuli has been discussed in detail. The application of SMPs and SMAs in different fields is highlighted. Further, recent progress of combined SMPs and SMAs composites with design feasibility and fabrication by various methods has been covered in depth.

Acknowledgements This work was supported by an NPRP grant from the Qatar National Research Fund under the grant number NPRP12S-0131-190030. The statements made herein are solely the responsibility of the authors.

References

1. Wu X, Huang WM, Zhao Y, Ding Z, Tang C, Zhang J (2013) Mechanisms of the shape-memory effect in polymeric materials. *Polymers* 5:1169–1202. <https://doi.org/10.3390/polym5041169>
2. Jani JM, Leary M, Subic A, Gibson MA (2014) A review of shape-memory alloy research, applications and opportunities. *Mater Des* (1980–2015) 56:1078–1113. <https://doi.org/10.1016/j.matdes.2013.11.084>
3. Chang LC, Read TA (1951) Plastic deformation and diffusionless phase changes in metals—the gold-cadmium beta phase. *Trans AIME* 189:47. <https://doi.org/10.1007/BF03398954>
4. Humbeeck JV (2001) Shape-memory alloys: a material and a technology. *Adv Eng Mater* 3:837. <https://doi.org/10.1002/1527-2648>
5. Meng Q, Hu J (2009) A review of shape-memory polymer composites and blends. *Compos Part A Appl Sci Manuf* 40:1661–1672. <https://doi.org/10.1016/j.compositesa.2009.08.011>
6. Hu J, Zhu Y, Huang H, Lu J (2012) Recent advances in shape-memory polymers: structure, mechanism, functionality, modeling and applications. *Prog Polym Sci* 37:1720–1763. <https://doi.org/10.1016/j.progpolymsci.2012.06.001>
7. Ratna D, Karger-Kocsis J (2008) Recent advances in shape-memory polymers and composites: a review. *J Mater Sci* 43:254–269. <https://doi.org/10.1007/s10853-007-2176-7>
8. Shape Memory Polymers—A Complete Guide. <https://www.bpf.co.uk/plastipedia/applications/shape-memory-polymer.aspx>
9. Hu JL, Chen SJ (2010) A review of actively moving polymers in textile applications. *J Mater Chem* 20:3346–3355. <https://doi.org/10.1039/B922872A>
10. Thakur S, Hu J (2017) Polyurethane: a shape-memory polymer (SMP). Aspects of polyurethanes. In: Yilmaz F (ed) *In TechOpen*, vol 27. London, UK, pp 53–71
11. Zhao Q, Qi HJ, Xie T (2015) Recent progress in shape-memory polymer: New behavior, enabling materials, and mechanistic understanding. *Prog Polym Sci* 49:79–120. <https://doi.org/10.1016/j.progpolymsci.2015.04.001>
12. Kim BK, Lee SY, Xu M (1996) Polyurethanes having shape-memory effects. *Polymer* 37:5781–5793. [https://doi.org/10.1016/S0032-3861\(96\)00442-9](https://doi.org/10.1016/S0032-3861(96)00442-9)
13. Kunzelman J, Chung T, Mather PT, Weder C (2008) Shape-memory polymers with built-in threshold temperature sensors. *J Mater Chem* 18:1082–1086. <https://doi.org/10.1039/B718445J>
14. Meng Q, Hu J, Zhu Y, Lu J, Liu Y (2007) Polycaprolactone-based shape-memory segmented polyurethane fiber. *J Appl Polym Sci* 106:2515–2523. <https://doi.org/10.1002/app.26764>
15. Garle A, Kong S, Ojha U, Budhlall B (2012) Thermoresponsive semicrystalline poly(ϵ -caprolactone) networks: exploiting cross-linking with cinnamoyl moieties to design polymers with tunable shape-memory. *ACS Appl Mater Inter* 4:645–657. <https://doi.org/10.1021/am2011542>
16. Lendlein A, Jiang H, Jünger O, Langer R (2005) Light-induced shape-memory polymers. *Nature* 434:879–882. <https://doi.org/10.1038/nature03496>
17. Kong D, Xiao X (2017) Rigid high temperature heat-shrinkable polyimide tubes with functionality as reducer couplings. *Sci Rep* 7:1–10. <https://doi.org/10.1038/srep44936>
18. Li J, Duan Q, Zhang E, Wang J (2018) Applications of shape-memory polymers in kinetic buildings. *Adv. Mater Sci Eng.* <https://doi.org/10.1155/2018/7453698>
19. Hu J, Meng H, Li G, Ibekwe SI (2012) A review of stimuli-responsive polymers for smart textile applications. *Smart Mater Struct* 21:053001. <https://doi.org/10.1088/0964-1726/21/5/053001>

20. Liu C, Qin H, Mather PT (2007) Review of progress in shape-memory polymers. *J Mater Chem* 17:1543–1558. <https://doi.org/10.1039/B615954K>
21. Ward MA, Georgiou TK (2011) Thermoresponsive polymers for biomedical applications. *Polymers* 3:1215–1242. <https://doi.org/10.3390/polym3031215>
22. Wong Y, Kong J, Widjaja LK, Venkatraman SS (2014) Biomedical applications of shape-memory polymers: how practically useful are they? *Sci China Chem* 57:476–489. <https://doi.org/10.1007/s11426-013-5061-z>
23. Wayman CM (1990) Duerig TW (1990) An introduction to martensite and shape memory. Butterworth-Heinemann, Engineering Aspects of Shape-Memory Alloys(UK), pp 3–20
24. Kurdyumov GV, Khandros LG (1949) On the thermoelastic equilibrium on martensitic transformations. *InDokl Akad Nauk SSSR* 66:211–214
25. Ölander A (1932) An electrochemical investigation of solid cadmium-gold alloys. *J Am Chem Soc* 54:3819–3833. <https://doi.org/10.1021/ja01349a004>
26. Vernon LB, Vernon HM (1941) Process of manufacturing articles of thermoplastic synthetic resins. U S patent US 2(234):993
27. Buehler WJ, Gilfrich JV, Wiley RC (1963) Effect of low-temperature phase changes on the mechanical properties of alloys near composition TiNi. *J Appl Phys* 34:1475–1477. <https://doi.org/10.1063/1.1729603>
28. Stoeckel D (1990) Shape-memory actuators for automotive applications. *Mater Des* 11:302–307. [https://doi.org/10.1016/0261-3069\(90\)90013-A](https://doi.org/10.1016/0261-3069(90)90013-A)
29. Bellini A, Colli M, Dragoni E (2009) Mechatronic design of a shape-memory alloy actuator for automotive tumble flaps: a case study. *IEEE Trans Industr Electron* 56:2644–2656
30. Hartl DJ, Lagoudas DC (2007) Aerospace applications of shape-memory alloys. *Proc Inst Mech Eng, Part G: J Aerosp Eng* 221:535–552. <https://doi.org/10.1243/09544100JAERO211>
31. Fujita H, Toshiyoshi H (1998) Micro actuators and their applications. *Microelectron Eng* 29:637–40. [https://doi.org/10.1016/S0026-2692\(98\)00027-5](https://doi.org/10.1016/S0026-2692(98)00027-5)
32. Furuya Y, Shimada H (1991) Shape-memory actuators for robotic applications. *Mater Des* 12:21–28. [https://doi.org/10.1016/0261-3069\(91\)90088-L](https://doi.org/10.1016/0261-3069(91)90088-L)
33. Petrini L, Migliavacca F (2011) Biomedical applications of shape-memory alloys. *J Metall.* <https://doi.org/10.1155/2011/501483>
34. Van Langenhove L, Hertleer C (2004) Smart clothing: a new life. *Int J Cloth Sci Tech.* <https://doi.org/10.1108/09556220410520360>
35. Kakeshita T, Saburi T, Kindo K, Endo S (1997) Effect of magnetic field and hydrostatic pressure on martensitic transformation and its kinetics. *Jpn J Appl Phys* 36:7083. <https://doi.org/10.1143/JJAP.36.7083>
36. Sozinov A, Likhachev AA, Lanska N, Ullakko K (2002) Giant magnetic-field-induced strain in NiMnGa seven-layered martensitic phase. *Appl Phys Lett* 80:1746–1748. <https://doi.org/10.1063/1.1458075>
37. Chernenko VA, Besseghini S, Müllner P, Kostorz G, Schreuer J, Krupa M (2007) Ferromagnetic shape-memory materials: underlying physics and practical importance. *Sens Lett* 5:229–233. <https://doi.org/10.1166/sl.2007.085>
38. Fabrizio Q, Loredana S, Anna SE (2012) Shape-memory epoxy foams for space applications. *Mater Lett* 69:20–23. <https://doi.org/10.1016/j.matlet.2011.11.050>
39. Rogers C, Liang C, Jia J (1989) Behavior of shape-memory alloy reinforced composite plates. I-Model formulations and control concepts. In: 30th structures, structural dynamics and materials conference, p 1389. <https://doi.org/10.2514/6.1989-1389>
40. Paine JS, Rogers CA (1994) Improved impact damage resistance in adaptive shape-memory alloy hybrid composite materials. *Smart Struct Mater 1994: Smart Struct Intell Syst* 2190:402–409. <https://doi.org/10.1117/12.175200>
41. Jang BK, Kishi T (2005) Thermomechanical response of TiNifiber-impregnated CFRP composites. *Mater Lett* 59:2472–2475. <https://doi.org/10.1016/j.matlet.2005.03.027>
42. Jang BK, Kishi T (2006) Mechanical properties of TiNifiber impregnated CFRP composites. *Mater Lett* 60:518–521. <https://doi.org/10.1016/j.matlet.2005.09.027>

43. Sun L, Huang WM (2009) Nature of the multistage transformation in shape-memory alloys upon heating. *Met Sci Heat Treat* 51:573. <https://doi.org/10.1007/s11041-010-9213-x>
44. Guo YB, Klink A, Fu C, Snyder J (2013) Machinability and surface integrity of Nitinol shape-memory alloy. *Cirp Ann-Manuf Technol* 62:83–86. <https://doi.org/10.1016/j.cirp.2013.03.004>
45. Lagoudas DC (2008) Shape-memory alloys: modeling and engineering applications. Springer Science & Business Media. <https://doi.org/10.1007/978-0-387-47685-8>
46. Buehler WJ, Gilfrich JV, Wiley RC (1963) Effect of low-temperature phase changes on the mechanical properties of alloys near composition TiNi. *J Appl phys* 34:1475–1477. <https://doi.org/10.1063/1.1729603>
47. Duerig TW, Pelton AR (1994) Ti-Ni shape-memory alloys. *Mater Prop Handb: Titan Alloy* 1:1035–1048
48. Jani JM, Subic A, Gibson MA (2014) A review of shape-memory alloy research, applications and opportunities. *Mater Des* 1980–2015(56):1078–1113. <https://doi.org/10.1016/j.matdes.2013.11.084>
49. Kumar PK, Lagoudas DC (2008) Introduction to shape-memory alloys. *Shape-Memory Alloys* 1–51. https://doi.org/10.1007/978-0-387-47685-8_1
50. Machado LG, Savi MA (2003) Medical applications of shape-memory alloys. *Braz J Med Biol Res* 36:683–691. <https://doi.org/10.1590/S0100-879X2003000600001>
51. Mantovani D (2000) Shape-memory alloys: properties and biomedical applications. *52:36–44*. <https://doi.org/10.1007/s11837-000-0082-4>
52. Duerig T, Pelton A, Stöckel DJ (1999) An overview of nitinol medical applications. *Mater Sci Eng: A* 273:149–160. [https://doi.org/10.1016/S0921-5093\(99\)00294-4](https://doi.org/10.1016/S0921-5093(99)00294-4)
53. Ma J, Karaman I, Noe BD (2010) High temperature shape-memory alloys. *Int Mater Rev* 55:257–315. <https://doi.org/10.1179/095066010X12646898728363>
54. Otsuka K, Wayman CM (1999) Shape-memory materials. Cambridge University Press
55. Funakubo H, Kennedy JB (1987) Shape-memory alloys. Gordon and Breach, xii+ 275, 15 x 22 cm, Illustrated
56. Delaey L (2006) Diffusionless transformations. *Mater Sci Tech*. <https://doi.org/10.1002/9783527603978.mst0392>
57. Otsuka K (1998) Mechanism of shape-memory effect and superelasticity. *Shape Memory Mater* 27–48
58. Buehler WJ, Wang FE (1968) A summary of recent research on the nitinol alloys and their potential application in ocean engineering. *Ocean Eng* 1:105–120. [https://doi.org/10.1016/0029-8018\(68\)90019-X](https://doi.org/10.1016/0029-8018(68)90019-X)
59. Tadaki T, Otsuka K, Shimizu K (1988) Shape-memory alloys. *Annu Rev Mater Sci* 18:25–45. <https://doi.org/10.1146/annurev.ms.18.080188.000325>
60. Ren X, Otsuka K (1997) Origin of rubber-like behaviour in metal alloys. *Nature* 389:579–582. <https://doi.org/10.1038/39277>
61. Otsuka K, Ren X (2001) Mechanism of martensite aging effects and new aspects. *Mater Sci Eng: A* 312:207–218
62. Baz AJ, Imam K, McCoy J (1990) Active vibration control of flexible beams using shape-memory actuators. *J Sound Vib* 140:437–456. [https://doi.org/10.1016/0022-460X\(90\)90760-W](https://doi.org/10.1016/0022-460X(90)90760-W)
63. Choon TW, Salleh AS, Jamian S, Ghazali MI (2007) Phase transformation temperatures for shape-memory alloy wire. *World Academy of Science, Engineering and Technology*, p 25
64. Ren J, Liew KM (2005) Meshfree modelling and characterisation of thermomechanical behaviour of NiTi alloys. *Eng Anal Boundary Elem* 29:29–40. <https://doi.org/10.1016/j.enganabound.2004.09.004>
65. Wada K, Liu Y (2005) Shape recovery of NiTi shape-memory alloy under various pre-strain and constraint conditions. *Smart Mater Struct* 14:S273. <https://doi.org/10.1088/0964-1726/14/5/016>
66. Wang ZG, Zu XT, Feng XD, Zhu S, Bao JW, Wang LM (2004) Characteristics of two-way shape-memory TiNi springs driven by electrical current. *Mater Des* 25:699–703. <https://doi.org/10.1016/j.matdes.2004.02.022>

67. Wang ZG, Zu XT, Feng XD, Lin LB, Zhu S, You LP, Wang LM (2003) Design of TiNi alloy two-way shape-memory coil extension spring. *Mater Sci Eng, A* 345:249–254
68. Duerig TW, Stockel D (1990) Keeley A (1990) Actuator and work production devices. Butterworth-Heinemann, *Engineering Aspects of Shape-Memory Alloys(UK)*, pp 181–194
69. Hirose S, Ikuta K, Umetani Y (1988) Development of shape-memory alloy actuators. Performance assessment and introduction of a new composing approach. *Adv Robot* 3:3–16. <https://doi.org/10.1163/156855389X00145>
70. Karhu M, Lindroos T (2010) Long-term behaviour of binary Ti–49.7 Ni (at.%) SMA actuators—the fatigue lives and evolution of strains on thermal cycling. *Smart Mater Struct* 19:115019. <https://doi.org/10.1088/0964-1726/19/11/115019>
71. Lindquist PG, Wayman CM (1990) Shape-memory and transformation behavior of martensitic Ti–Pd–Ni and Ti–Pt–Ni alloys. Butterworth-Heinemann. *Eng Aspects Shape-Memory Alloys (UK)* 1990:58–68
72. Thoma PE, Boehm JJ (1999) Effect of composition on the amount of second phase and transformation temperatures of Ni_xTi_{90-x}Hf₁₀ shape-memory alloys. *Mater Sci Eng, A* 273:385–389. [https://doi.org/10.1016/S0921-5093\(99\)00303-2](https://doi.org/10.1016/S0921-5093(99)00303-2)
73. Aaltio I, Sozinov A, Ge Y, Ullakko K, Lindroos VK, Hannula SP (2016) Giant magnetostrictive materials, reference module in materials science and materials engineering. Elsevier
74. Henry CP (2002) Dynamic actuation properties of Ni–Mn–Ga ferromagnetic shape-memory alloys (Doctoral dissertation, Massachusetts Institute of Technology). <http://hdl.handle.net/1721.1/8442>
75. Liang C, Davidson FM, Schetky LM, Straub FK (1996) Applications of torsional shape-memory alloy actuators for active rotor blade control: opportunities and limitations. *Smart Struct Mater 1996: Smart Struct Integr Syst* 2717:91–100. <https://doi.org/10.1117/12.239049>
76. Garner LJ, Wilson LN, Lagoudas DC, Rediniotis OK (2000) Development of a shape-memory alloy actuated biomimetic vehicle. *Smart Mater Struct* 9:673. <https://doi.org/10.1088/0964-1726/9/5/312>
77. Ilyin AA, Sysolyatin PG, Gunter VE, Dergilev AP, Didin MA, Sysolyatin SP, Makarova IA (1997) The use of superelastic shape-memory implants in temporo-mandibular joint surgery. In: *Proceedings of the first international symposium on advanced biomaterials (ISAB)*. Montreal, Canada, p 177
78. Brailovski V, Trochu F (1996) Review of shape-memory alloys medical applications in Russia. *Bio-Med Mater Eng* 6:291–298. <https://doi.org/10.3233/BME-1996-6406>
79. Paine J, Rogers C (1994) High velocity impact response of composites with surface bonded nitinol-SMA hybrid layers. *J Intell Mater Syst Struct* 5:530–535
80. Barnes B, Brei D, Luntz J, Browne A, Strom K (2006) Panel deployment using ultrafast SMA latches. *ASME Int Mech Eng Congress Expos* 47659:273–280. <https://doi.org/10.1115/IMECE2006-15026>
81. Lendlein A, Kelch S (2002) Shape-memory polymers. *Angewandte Chemie Int Edn* 41:2034–2057. <https://doi.org/10.1002/1521-3773>
82. Ghosh P, Rao A, Srinivasa AR (2013) Design of multi-state and smart-bias components using shape-memory alloy and shape-memory polymer composites. *Mater Des* 44:164–171. <https://doi.org/10.1016/j.matdes.2012.05.063>
83. Billah AM, Alam MS (2012) Seismic performance of concrete columns reinforced with hybrid Shape-Memory Alloy (SMA) and fiber reinforced polymer (FRP) bars. *Constr Build Mater* 28:730–742. <https://doi.org/10.1016/j.conbuildmat.2011.10.020>
84. Hosoda H, Takeuchi S, Inamura T, Wakashima K (2004) Material design and shape-memory properties of smart composites composed of polymer and ferromagnetic shape-memory alloy particles. *Sci Technol Adv Mater* 5:503. <https://doi.org/10.1016/j.stam.2004.02.009>
85. Zhang Y, Mi C (2020) Strengthening bonding strength in NiTi SMA fiber-reinforced polymer composites through acid immersion and Nanosilica coating. *Compos Struct* 239:112001. <https://doi.org/10.1016/j.compstruct.2020.112001>
86. Parameswaranpillai J, Siengchin S, George J, Jose S (2020) Shape-memory polymers, blends and composites. Springer, Singapore. <https://doi.org/10.1007/978-981-13-8574-2>

87. Fathi H, Shokrieh MM, Saeedi A (2020) Effect of tensile loading rate on interfacial properties of SMA/polymer composites. *Compos B Eng* 183:107730. <https://doi.org/10.1016/j.compositesb.2019.107730>
88. Yazik MM, Sultan MT, Shah AU, Norkhairunnisa M (2020) Effect of MWCNT content on thermal and shape-memory properties of epoxy nanocomposites as material for morphing wing skin. *J Therm Anal Calorim* 139:147–158. <https://doi.org/10.1007/s10973-019-08367-6>
89. Katsiropoulos CV, Pappas P, Koutroumanis N, Kokkinos A, Galiotis C (2020) Improving the damping behavior of fiber-reinforced polymer composites with embedded superelastic Shape-Memory Alloys (SMA). *Smart Mater Struct* 29:025006. <https://doi.org/10.1088/1361-665X/ab6026>
90. Ashir M, Nocke A, Hanke U, Cherif C (2020) Adaptive hinged fiber reinforced plastics with tailored shape-memory alloy hybrid yarn. *Poly Compos* 41:191–200. <https://doi.org/10.1002/pc.25359>
91. Hassanzadeh-Aghdam MK, Ansari R, Darvizeh A (2019) Thermal expanding behavior of carbon nanotube-shape-memory polymer nanocomposites. *Mech Adv Mater Struct* 26:1858–1869. <https://doi.org/10.1080/15376494.2018.1452320>
92. Hassanzadeh-Aghdam MK, Ansari R (2019) Thermal conductivity of shape-memory polymer nanocomposites containing carbon nanotubes: a micromechanical approach. *Compos B Eng* 162:167–177. <https://doi.org/10.1016/j.compositesb.2018.11.003>
93. Guida M, Sellitto A, Marulo F, Riccio A (2019) Analysis of the impact dynamics of shape-memory alloy hybrid composites for advanced applications. *Materials* 12:153. <https://doi.org/10.3390/ma12010153>
94. Aghamirzadeh GR, Khalili SM, Eslami-Farsani R, Saeedi A (2019) Experimental investigation on the smart self-healing composites based on the short hollow glass fibers and shape-memory alloy strips. *Poly Compos* 40:1883–1889. <https://doi.org/10.1002/pc.24953>
95. Pan Z, Huang R, Liu Z (2019) Prediction of the thermomechanical behavior of particle reinforced shape-memory polymers. *Poly Compos* 40:353–63. <https://doi.org/10.1002/pc.24658>
96. Wang Z, Chang M, Kong F, Yun K (2019) Optimization of thermo-mechanical properties of shape-memory polymer composites based on a network model. *Chem Eng Sci* 207:1017–29. <https://doi.org/10.1016/j.ces.2019.07.022>
97. Yarali E, Baniassadi M, Baghani M (2019) Numerical homogenization of coiled carbon nanotube reinforced shape-memory polymer nanocomposites. *Smart Mater Struct* 28:035026. <https://doi.org/10.1088/1361-665X/ab02b6>
98. Hassanzadeh-Aghdam MK, Mahmoodi MJ, Ansari R, Darvizeh A (2019) Interphase influences on the mechanical behavior of carbon nanotube–shape-memory polymer nanocomposites: a micromechanical approach. *J Intell Mater Syst Struct* 30:463–478. <https://doi.org/10.1177/1045389X18812704>
99. Ameduri S, Ciminello M, Quadrini F, Santo L (2019) Shape-memory polymer composite actuator: modeling approach for preliminary design and validation. *Actuators* 8:51. <https://doi.org/10.3390/act8030051>
100. Patel KK, Purohit R (2019) Improved shape-memory and mechanical properties of microwave-induced shape-memory polymer/MWCNTs composites. *Mater Today Commun* 20:100579. <https://doi.org/10.1016/j.mtcomm.2019.100579>
101. Liu R, Li Y, Liu Z (2019) Experimental study of thermo-mechanical behavior of a thermosetting shape-memory polymer. *Mech Time-Depend Mater* 23:249–266. <https://doi.org/10.1007/s11043-018-9377-0>
102. Du H, Liu L, Zhang F, Leng J, Liu Y (2019) Triple-shape-memory effect in a styrene-based shape-memory polymer: characterization, theory and application. *Compos Part B: Eng* 173:106905. <https://doi.org/10.1016/j.compositesb.2019.106905>
103. Tobushi H, Hayashi S, Sugimoto Y (2009) Two-way bending properties of shape-memory composite with SMA and SMP. *Materials* 2:1180–1192. <https://doi.org/10.3390/ma2031180>
104. Cohades A, Hostettler N, Pauchard M, Plummer CJ, Michaud V (2018) Stitched shape-memory alloy wires enhance damage recovery in self-healing fibre-reinforced polymer composites. *Compos Sci Tech* 161:22–31. <https://doi.org/10.1016/j.compscitech.2018.03.040>

105. Wang Z, Liu Y, Lv H, Yang B (2018) Enhancement of interface performance between shape-memory alloy fiber and polymer matrix using silane coupling agent KH550 and Al₂O₃ nanoparticles. *Poly Compos* 39:3040–3047. <https://doi.org/10.1002/pc.24308>
106. Li H, Liu J, Wang Z, Yu Z, Liu Y, Sun M (2018) The low velocity impact response of shape-memory alloy hybrid polymer composites. *Polymers* 10:1026. <https://doi.org/10.3390/polym10091026>
107. Xu R, Bouby C, Zahrouni H, Zineb TB, Hu H, Potier-Ferry M (2018) 3D modeling of shape-memory alloy fiber reinforced composites by multiscale finite element method. *Compos Struct* 200:408–19. <https://doi.org/10.1016/j.compstruct.2018.05.108>
108. Khalili SM, Saeedi A (2017) Determination of the elastic properties of randomly oriented Shape-Memory Alloy (SMA) discontinuous wires reinforced epoxy resin. *Compos Struct* 180:148–60. <https://doi.org/10.1016/j.compstruct.2017.08.007>
109. Wang E, Tian Y, Wang Z, Jiao F, Guo C, Jiang F (2017) A study of shape-memory alloy NiTi fiber/plate reinforced (SMAFR/SMAPR) Ti-Al laminated composites. *J Alloy Compd* 696:1059–1066. <https://doi.org/10.1016/j.jallcom.2016.12.062>
110. Wang Z, Xu L, Sun X, Shi M, Liu J (2017) Fatigue behavior of glass-fiber-reinforced epoxy composites embedded with shape-memory alloy wires. *Compos Struct* 178:311–319. <https://doi.org/10.1016/j.compstruct.2017.07.027>
111. Song JJ, Chen Q, Naguib HE (2016) Constitutive modeling and experimental validation of the thermo-mechanical response of a shape-memory composite containing shape-memory alloy fibers and shape-memory polymer matrix. *J Intell Mater Syst Struct* 27:625–41. <https://doi.org/10.1177/1045389X15575086>
112. Wang Y, Ye J, Tian W (2016) Shape-memory polymer composites of poly (styrene-*b*-butadiene-*b*-styrene) copolymer/liner low density polyethylene/Fe₃O₄ nanoparticles for remote activation. *Appl Sci* 6:333. <https://doi.org/10.3390/app6110333>
113. Shen Q, Trabia S, Stalbaum T, Palmre V, Kim K, Oh IK (2016) A multiple-shape-memory polymer-metal composite actuator capable of programmable control, creating complex 3D motion of bending, twisting, and oscillation. *Sci Rep* 6:1–11. <https://doi.org/10.1038/srep24462>
114. Daghash SM, Ozbulut OE (2016) Characterization of superelastic shape-memory alloy fiber-reinforced polymer composites under tensile cyclic loading. *Mater Des* 111:504–512. <https://doi.org/10.1016/j.matdes.2016.09.034>
115. Pulla SS, Karaca HE, Lu YC (2016) Numerical design of shape-memory polymer composites with temperature-responsive SMA fillers. *Compos B Eng* 96:287–294. <https://doi.org/10.1016/j.compositesb.2016.04.044>
116. Guo J, Wang Z, Tong L, Lv H, Liang W (2015) Shape-memory and thermo-mechanical properties of shape-memory polymer/carbon fiber composites. *Compos A Appl Sci Manuf* 76:162–171. <https://doi.org/10.1016/j.compositesa.2015.05.026>
117. Dawood M, El-Tahan MW, Zheng B (2015) Bond behavior of superelastic shape-memory alloys to carbon fiber reinforced polymer composites. *Compos B Eng* 77:238–247. <https://doi.org/10.1016/j.compositesb.2015.03.043>
118. Kang JH, Siochi EJ, Penner RK, Turner TL (2014) Enhanced adhesive strength between shape-memory polymer nanocomposite and titanium alloy. *Compos Sci Technol* 96:23–30. <https://doi.org/10.1016/j.compscitech.2014.03.003>
119. Nji J, Li G (2012) Damage healing ability of a shape-memory-polymer-based particulate composite with small thermoplastic contents. *Smart Mater Struct* 21:025011. <https://doi.org/10.1088/0964-1726/21/2/025011>

Chapter 15

Devices and Sensors Based on Additively Manufactured Shape-Memory of Hybrid Nanocomposites



Vinayak Adimule, Santosh S. Nandi, and B. C. Yallur

15.1 Introduction

Smart materials especially polymers or nanoparticles embedded into the polymers generally called by the name shape-memory polymers (SMPs) undergo several temporary modifications in their structure by reformation under the influence of external forces such as heat, light, magnetic field, and electric field [1–3]. In recent years SMPs find many applications in the fields of aerospace, nanoengineering, nano-electronics, biosensors, structural materials, in the textile industry due to the modified properties like lightweight materials, high capacity to withstand stress and strain, temperature and tuneable glass transition temperature, pressure and electricity [4–6]. The SMPs possessing porous nature find more computable with their unique behaviour under the influence of external fields with reduced density, elongation ability, and surface structural modifications find applications in aerospace, biomedical and bioengineering fields [7–10]. Most of the SMPs consist of doped nanomaterials of rare earth to the cyclic polymers such as fullerenes, dendrimers, P3OT, and P3BT [11, 12]. The nanomaterial doped SMPs have heat temperature switching below and above the T_g . The physical state of the doped SMPs generally becomes soft and rubbery kind with rigid and stiff nature [13–15]. The structural configuration of porous SMPs varied by subjecting to heat temperature above the glass transition temperature (T_g) or below. The porous SMPs thus obtained possess

V. Adimule (✉)

Department of Chemistry, Angadi Institute of Technology and Management (AITM), Savagon Road, Belagavi 591108, Karnataka, India

S. S. Nandi

Chemistry Section, Department of Engineering Science and Humanities, KLE Dr M. S. Sheshgiri College of Engineering and Technology, Udhyambagh, Belagavi 590008, Karnataka, India

B. C. Yallur

Department of Chemistry, M S Ramaiah Institute of Technology, Bangalore 560054, Karnataka, India

variable electrical and electronic properties, lightweight smart transistors, light actuators, and biosensors [16, 17]. P. Haworth et al. [18] discussed the applications of high performance of Y doped BSCF porous smart materials for their phase transformation and the confirming high release of oxygen and oxygen-non stoichiometry. Soboyejo, W. O. et al. reported the development of high-temperature ceramics for aerospace applications and thermostructural applications [19]. In the year 2009, Alexander A. Ishchenko elaborately carried out experimentations in the field of the effect of photonic and molecular design for the dye-doped polymers for modern light-sensitive material for photonic applications [20]. CheikhCissé reported the elasto-caloric effect of CuAlBe shaped-memory effects for the quantitative phase-field modeling [21]. Yu Ying Clarrisa Choong et al. [22] experimentally determined high fixity, robust mechanical degradation of the 4D printed parts polymers using stereolithography. Ly et al. [22] designed and developed fused shape-memory polymers deposition modeling for 4D printing technologies. Amelia Yilin Lee et al. [23] reported the reviews on the reversibility of the 3D printed shape-memory polymers and their use in actuation and high rate of reversibility in 4D printing methods. Highly stretchable, self-healing 3D printing SMPs possessing elasticity towards 4D printing have been reported by Xiao Kuang et al. in the year 2018 [24]. Self-repairing graphene/polymer nanocomposites reported by Christopher IgweIdumah et al. showed the coatings and shape-memory polymeric material is among the most prospective smart materials [25]. Jinsong Leng et al. 2020 reported the Ag@CNF-based nanocomposite plays a quick and low-voltage-triggered electrical-responsive shape-memory behavior, creating a great aspirant for printing electroactive devices [26]. In the present research Y (3 wt. %, 5 wt. %, and 15 wt. %) were doped into the P3BT (poly-3-butyl thiophene) (1 molar wt. ratio) and the synthesized materials were primarily investigated for SEM, XRD, and XPS analysis for the effective detection of impurity and the change in the morphology of the crystal structure. However, the modified Y NPs doped P3BT was tested for shape reformation, sensors, and actuation mechanism under the influence of the forces and the results showed great enhancement in the actuation, recovery, flexible Tg and can be employed for the thin film transistors. The modified SMPs revealed greater electrical and electronic properties and can be effectively used in biosensor and biomedical applications.

15.2 Materials and Methods

The SMP containing Y (3 wt. %, 5 wt. %, and 15 wt. %) were doped into the P3BT(poly-3-butyl thiophene) (1 molar wt. ratio) that were prepared by purchasing Y_2O_3 powder from Sigma-Aldrich India and P3BT was purchased from Fluka India with a purity of $\geq 99.9\%$ Triethanolamine (TEA, 99.0%), and CTAB (cetyl trimethyl ammonium bromide, $\geq 99.0\%$). Were purchased from Sigma-Aldrich India. All materials were used as received. Other reagents and solvents like sodium hydroxide, ethanol, methanol, acetic acid, HCl, H_2SO_4 , and NH_4OH were procured from Spectro chem, Sigma Aldrich chemicals. Morphology of the SMPs investigated by using

SEM–EDS instrument was fitted with Zeiss ultra 55 with EsB. X-ray diffraction (XRD) spectrophotometer of Y doped P3BT SMPs was carried out using an instrument from Rigka Smart Lab with Cu–K α Radiation ($\lambda = 0.1542$ nm) operating at 50 kV. Austin CHI model D 630 instrument is used for CV spectral analysis, and Specord 210 plus is used for optical absorptivity investigation. I–V characteristics were performed using Keithley Instrument (1500 B series).

The SMP containing Y (3 wt. %, 5 wt. %, and 15 wt. %) were doped into the P3BT (poly-3-butyl thiophene) (1 molar wt. ratio) that were prepared by purchasing Y_2O_3 powder from Sigma-Aldrich India, P3BT was purchased from Fluka India with the purity of $\geq 99.9\%$ Triethanolamine (TEA, 99.0%), and CTAB (cetyl trimethyl ammonium bromide, $\geq 99.0\%$) were purchased from Sigma-Aldrich India. All materials were used as received. Other reagents and solvents like sodium hydroxide, ethanol, methanol, acetic acid, HCl, H_2SO_4 , and NH_4OH were procured from Spectrochem, Sigma Aldrich chemicals. Morphology of the SMPs investigated by using an SEM–EDS instrument fitted with Zeiss ultra 55 with EsB. X-ray diffraction (XRD) spectrophotometer of Y doped P3BT SMPs carried out using an instrument from Rigka Smart Lab with Cu–K α Radiation ($\lambda = 0.1542$ nm) operating at 50 kV. Austin CHI model D 630 instrument is used for CV spectral analysis, and SPECORD 210 plus is used for optical absorptivity investigation. I–V characteristics were performed using Keithley Instrument (1500 B series).

15.2.1 *Synthesis of Solid and Porous SMPs*

Different wt. % of Y (3, 5, and 15) were taken in RB flask, added with P3BT (1 mol) under acidic conditions with constant stirring. The reaction mixture (RM) was kept at 100 °C for 5–6 h, the bubble formation was removed or minimized by $N_2(g)$ purging into RM. NaOH/ NH_4OH aqueous solution added drop-wise, the precipitate was flitted and dried The powdered solid was taken into a beaker, under constant stirring sonicated for 24 h to dissolve P3BT organic polymer. Schematically reactions are explained in Fig. 15.1. After dissolution porous Y-P3BT SMPs NC was dried in a vacuum oven at 40 °C for 36 h, H_2O and other volatiles were removed, the SMP NS was brought to RT for 1 h. After natural cooling to RT, fully cured solid SMPs were taken out, subjected for solidification, sealed to protect from oxygen and other gases in the environment.

SMP containing Y-NPs and P3BT in solution form prepared and the entire content was freezed at -5 °C for 24 h under vacuum. Figure 15.2 depicts the incorporation of Y nanoparticles with the P3BT polymeric chain in different wt. the ratio of the filler loadings during the formation of SMPs. Template of different wt. % of Y_2O_3 in the P3BT slows down the reaction rate presence of vacuum helped in accelerating the condensation of Y^{3+} ions into the surface matrix of poly-3-butyl thiophene. The entire mass was subjected to curing in an oven with a temperature lesser than the freezing around maintained at 130 °C for 10 h.

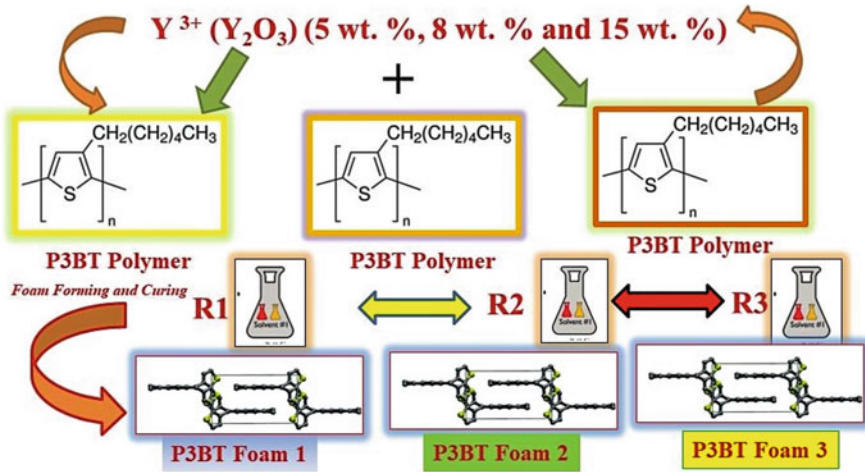


Fig. 15.1 Schematic reaction representation of the doping of Yttrium (Y^{3+} ions) into the poly-3-butyl thiophene polymer and subsequent formation of the SMPs

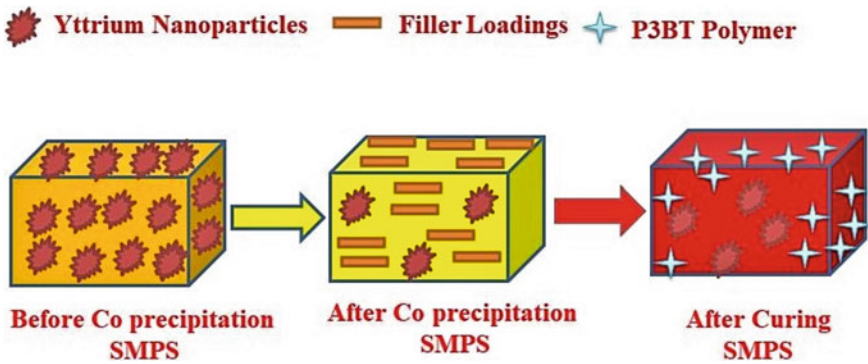


Fig. 15.2 Schematic of doping method of Y to P3BT polymer and subsequent conversion into SMPs **a** Before co-precipitation of SMPs **b** After co-precipitation of SMPs with filler loadings **c** SMP foam after curing process

15.3 Experimental

15.3.1 Characterization

Pre-procedural method for the characterization of the different wt. % of Y doped P3BT was carried out on a hotplate where the materials were heated at 70 °C for 2 min and the SMPs recovery rate was investigated after the quick cooling process. The procedure is repeated to understand the stability of the SMPs at various Tg values. Mechanical properties of Y doped (15 wt. %) with P3BT SMP foams were

tested by the Instron 5969 universal testing system with a thermal chamber. The cyclic compression was carried out for the different wt. % of Y doped P3BT nano-matrix for the T_g values ranging from 40 °C to 180 °C with increments of ($T_g + 10$) °C. All the Y-P3BT SMPs foams were preheated in a thermal chamber for 30 min to minimize the heat effect.

15.3.2 Fabrication of 4Dprinted Y/P3BT Nanocomposites

The different wt. % (5, 8, 15) Y was doped to P3BT and dissolved in octanol and ethanol mixtures and made in the form of ink and mixed with a glass rod for 30 min, transferred to a syringe which is mounted on the 4D printer to execute the printing process. The post-curing process (Fig. 15.3) was carried out after the printing of Y-P3BT NCs and brought back to room temperature with a decrease in temperature of 10 °C/h (Fig. 15.3).

The scaffolds thus printed and fabricated reduce the time from 130 h to 40 min as compared with the processing time in other methods [27, 28]. Al plate coated with PTFE over fiberglass fabric sheet was chosen as the base for printing. The fabric

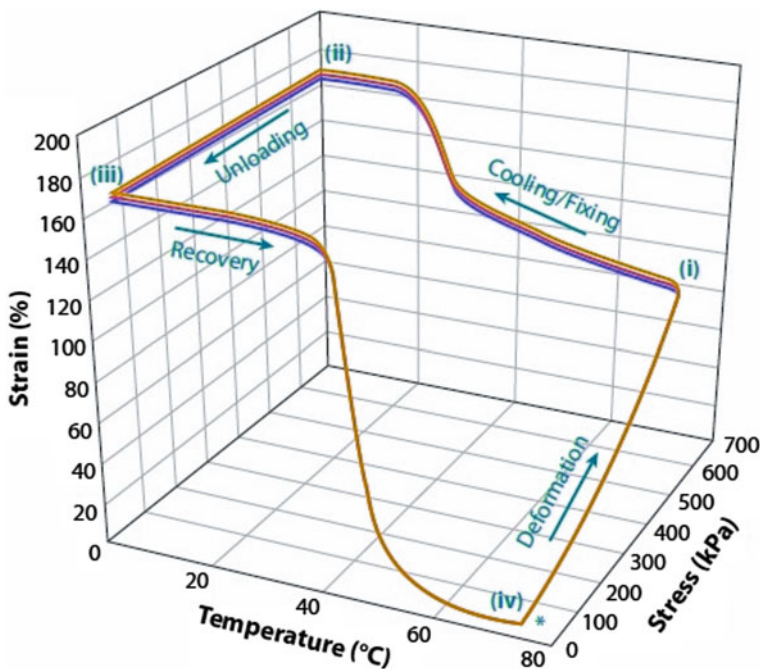


Fig. 15.3 Graphical representation of the uncoiling and recoiling of the pure P3BT with Y doped P3BT under different stress conditions at different temperatures

sheet becomes nonsticky to the ink and can be easily removed during the printing process. In the printing process, the amount of material transferred was more than 2 g and the time was set at 0 s, for every 4–5 min the quality of the Y-P3BT printing was recorded. However, the heat generated by the printing facilitated the curing process. The weight fraction of 2 wt. % Y-P3BT forms viscous ink material and could not be easily squeezed and it was carried out by adjusting the printing speed.

15.3.3 SEM Morphological Analysis

SEM analysis was performed to evaluate the grain, grain size, boundary distance, inter-pole diameter, and the average size of the pure P3BT (Fig. 15.4a, b, c, d materials).

The conductivity of the doped and undoped materials was increased by spluttered deposition which prevents the charging in SEM recording. With the help of SEM images, an average pore size of SMP foams was analyzed by Image J software and illustrated in Figure. SEM micrographs of pure P3BT and Y-P3BT were shown in Fig. 15.4a, b, c, d, respectively. The SMPs form cubic type structures which were observed for the 1D and 2D configurations. An average distribution of the grains is ~ 75 nm, with rods of ~ 25 μm in length and an average diameter of ~ 100 nm,

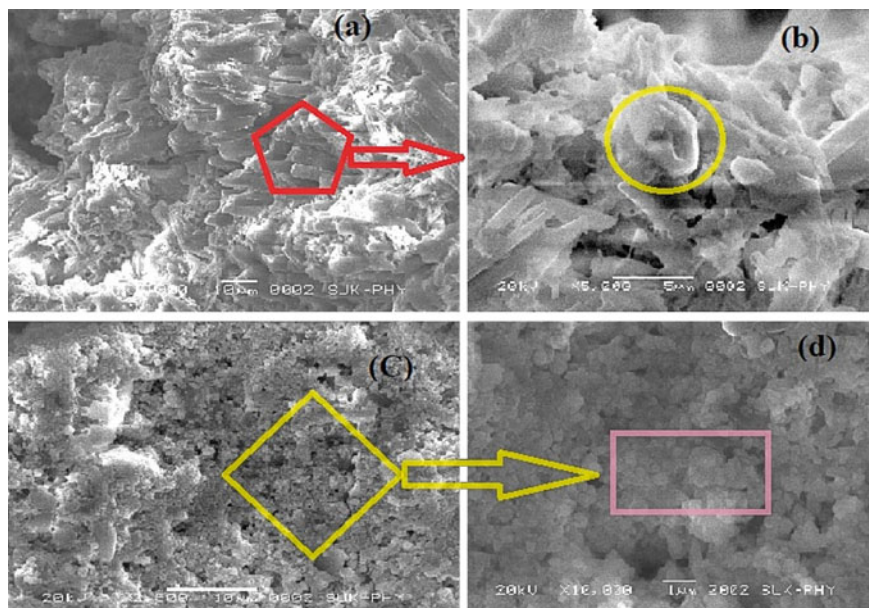


Fig. 15.4 a SEM images of pure P3BT SMPs (fabricated); b SEM images of 5 wt. % of Y doped P3BT; c 8 wt. % of Y-P3BT; d 15 wt. % Y-P3BT

~65 nm, ~80 nm, respectively (Fig. 15.4b, c, d) for 5 wt. %, 8 wt. %, and 15 wt. % of Y doped P3BT [29]. The nanorods (NRs) average grain diameter for 15 wt. % of Y doped P3BT hybrid NCs are ~50 nm, ~135 nm, ~155 nm, ~170 nm, respectively [30]. The heavily doped nanocomposites form the nano-matrix overfilled with fillers of Y and the crystal morphology considerably changes and doped Y undergoes particle agglomeration inside the polymeric molecules. Intergranular layers are clear for the P3BT doped with yttrium, as the wt. % of Y increases a regular rod-like structure formed into the crystal layers, interboundaries of grain particles develop on the P3BT surface, large numbers of interspaces are formed because of the formation of Y_2O_3 oxide layer as the Y doping increases on the P3BT surface which are responsible for enhanced electrical and electronic characteristics, sensor characteristics gas diffusion, transportation and conduction in nanostructures.

15.3.4 Thermo Gravimetric Analysis

Thermal stability, percentage of weight loss, flexibility, glass transition temperature variation, molecular durability and the morphological change in the crystal nature of the pure P3BT and Y-P3BT hybrid nanocomposites were investigated by TGA analysis. Pure P3BT SMPs do not vary much with an increase in temperature and become flattened from 100 °C to almost 800 °C. However, 15 wt. % of Y doped P3BT SMPs started to lose their weight after 250 °C with 20% of weight loss observed when the SMP heated beyond 400 °C with observable almost 10% subsequent weight loss observed beyond 600 °C [31]. The decomposition behavior of 4D printed Y-P3BT nanocomposites materials which investigated TGA with their thin films is shown in Fig. 15.5.

15.3.5 XPS Analysis of Pure and Y-P3BT SMPs

X-ray Photoelectron spectroscopy was carried out to explore the elemental and chemical composition of pure P3BT SMPs and Y-P3BT SMPs in the crystal lattice. Obtained XPS data have been deconvoluted with the background curve during validation of the individual peaks with respect to P3BT SMP polymer Fig. 15.6a for O1s and C1s for P3BT with binding energies laying in between 250 and 600 eV, for 15 wt. of Y doped P3BT small C1s peak at 380 eV observed. After deconvoluting the spectra, 4 pairs of peaks as illustrated in Fig. 15.6b, c have been observed. The first pair of peaks observed at binding energies 285.2 eV and 288.4 eV corresponding to 5 wt. % of Y overlay with pure P3BT SMPs, and the second pair appeared at 289.4 eV and 289.8 eV corresponding to elemental Y with 15 wt. % of Y-P3BT (Y 3d_{3/2} and Y 3d_{5/2} peaks). Chemical composition has been confirmed by XPS [32], which confirms the good incorporation of yttrium oxide into P3BT SMPs and the

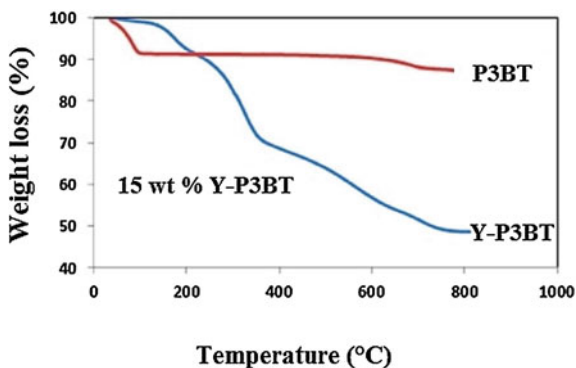


Fig. 15.5 Thermogravimetric analysis of the different wt. % of Y-P3BT with pure P3BT SMPs. The different wt. % of Y doped P3BT material was subjected for TGA to understand the morphological crystal change due to heat, their stability, and decomposition of the yttrium nano-matrix. Around 12% weight loss was incurred for the 8 wt. % of Y-P3BT and 15 wt. % of Y-P3BT material before it reaches the temperature of 250 °C. The exact decomposition temperature was around 290 °C with appropriate weight loss of the material where considerable weight loss of the nanocomposites appeared sharply. The weight loss becomes stable to leave out the Y-P3BT material and the fraction of Y left out in P3BT results in the smaller amount of let weight fractions

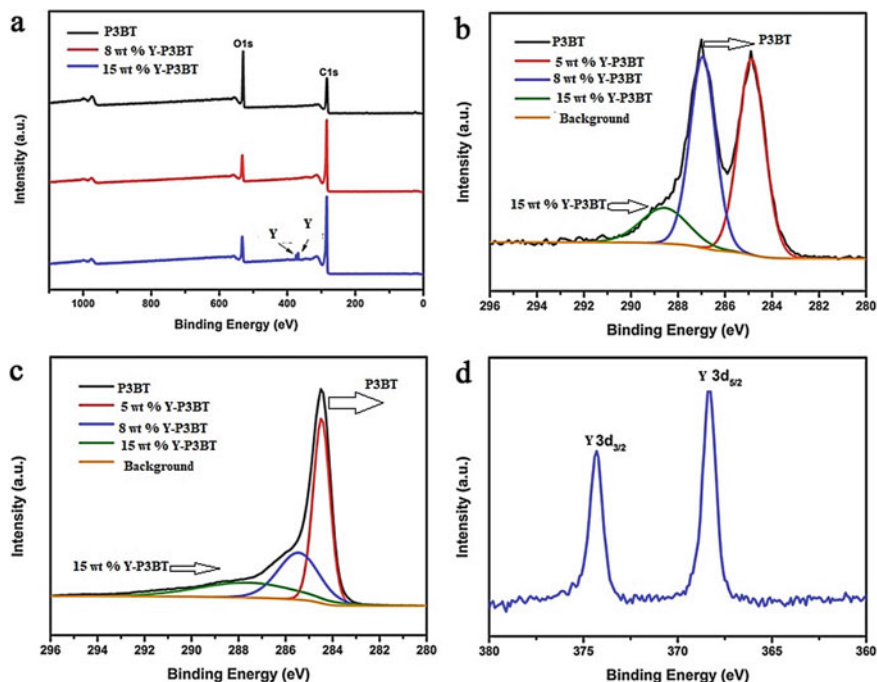


Fig. 15.6 a XPS spectrum of the pure P3BT SMPs and 8 wt. %, 15 wt. % of Y-P3BT peaks; b and c overlay of the 5 wt. %, 8 wt. % and 15 wt. % of Y-P3BT with background SMPs; d Incorporation of Y 3d_{3/2}, Y 3d_{5/2} peaks observed at binding energies 362 eV and 374 eV, respectively

presence of the hydroxyl group on the surface. Figure 15.6 illustrates the elemental and chemical composition of pure P3BT and Y-P3BT SMPs.

15.3.6 XRD- Spectroscopic Analysis

X-ray diffraction (XRD) patterns of the pure P3BT and Y-P3BT SMPs are correlated in Fig. 15.7. XRD patterns observed with no extra peaks of Y or Y_2O_3 and diffraction peaks of both SMPs match well with JCPDS file No (20–1412 for Y and 41–1105 for Y_2O_3) SMPs. The relative shift in the Bragg's peak towards the lower 2θ value of Y-P3BT was examined with the help of JCPDS file No of 10–454 for CdS/P3BT SMPs. The peaks for Y-P3BT corresponding to planes (101), (111), (121), (211), (221), (200), (201), (112), (103), (202), (213), (210), (211), (204) at $2\theta = 23.1^\circ$, 26.7° , 28.4° , 32.4° , 34.2° , 35.5° , 36.14° , 41.8° , 42.87° , 43.4° , 44.3° , and 44.8° well-matched with JCPDS card 16–0334 for $NaYF_4$ /P3BT SMP materials [33, 34] (Table 15.1).

Fig. 15.7 XRD pattern of the 15 wt. % of Y-P3BT SMPs

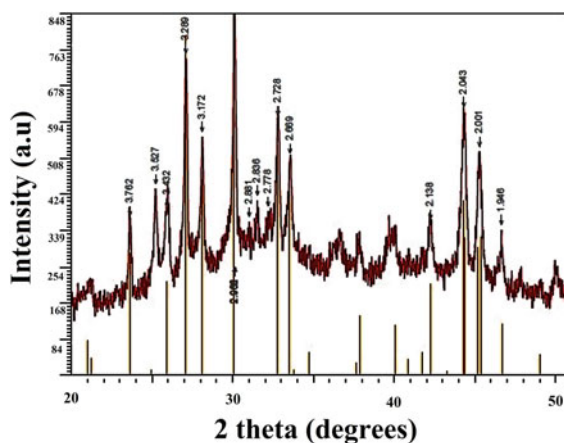


Table 15.1 XRD patterns and peak values of Y-P3BT SMPs

Nanostructures	Crystalline Phase	XRD Peak Intensities	Peak Intensity Relative to (112)	Size of the Crystal (Scherrer method)
		(111) (121)	(211) (002)	(220)(112)
Pure P3BT SMPs	Cubic	949 1240	2131 48.2	57.8 100 34
Y Doped P3BT SMPs	Cubic/Hexagonal (D)	735 875	1470 51.8	55.2 100 28

(D) deformed cubic shape

15.4 Results and Discussions

15.4.1 Density of CNT/SMP Nanocomposite Foams

Densities of Y/P3BT SMPs NS vary and are dependent on the Y size in the cavity of the nano-matrix and their densities increase with the increase in the concentration of Y impurity (5 wt. % and up to 15 wt. %). The low dense SMP material resulted as a result of Y insertion into the polymeric surface of P3BT and the size of the SMP confines to a cubic configuration which intern capable of dissolving more Y nanomaterials. The densities of the SMPs were 1.487 g/cm^3 and 1.0124 g/cm^3 , respectively. By referring to the literature evidence of SMP 4D smart materials, the high porous SMP foam possesses a high compressive capability and can be used for sensor characteristic studies.

15.4.2 I-V Electrical Characterization of Y Doped Poly-3-Butyl Thiophene (5, 8, 15 Wt. % of Y_2O_3)

The effect of weight fraction of yttrium nanomaterial opened to air forms Y_2O_3 which was varied from 5.0 wt. % to 15.0 wt. % studied for the 4D printing performance with an interval of 5 wt. % on the electrical resistivity of 4D printed Y-P3BT nanocomposite hybrid polymer scaffold [35–37] and their architecture of the electrical properties is illustrated in Fig. 15.8.

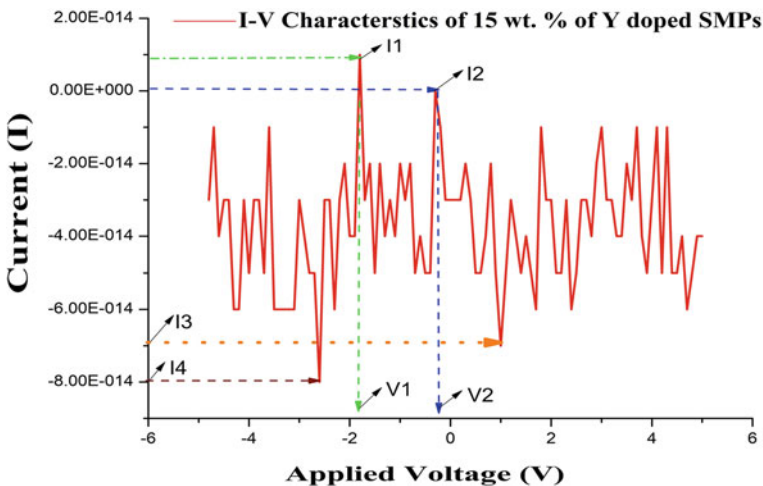


Fig. 15.8 I–V curve of the 15 wt. % of Y doped P3BT material with low and high dips in applied current and applied voltage

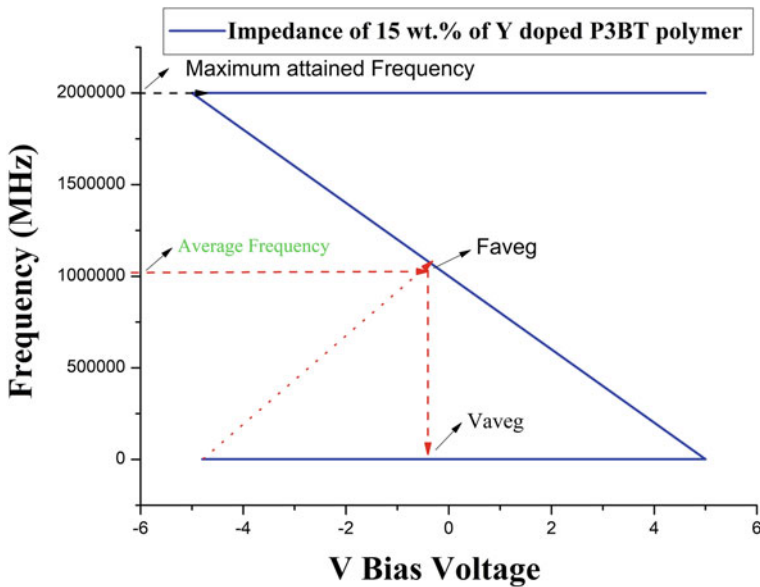


Fig. 15.9 Impedance measurement of 15 wt. % of Y-P3BT materials with varying frequency versus Bias voltage

The poorer conductivity would be the main reason for the displacement of the doped Y nanoparticles in the P3BT polymeric chain as shown in the I-V curve Fig. 15.9. When the weight fraction of Y was above a critical value of 15 wt. %, the electrical conductivity became larger instantly.

15.4.3 Impedance Measurements

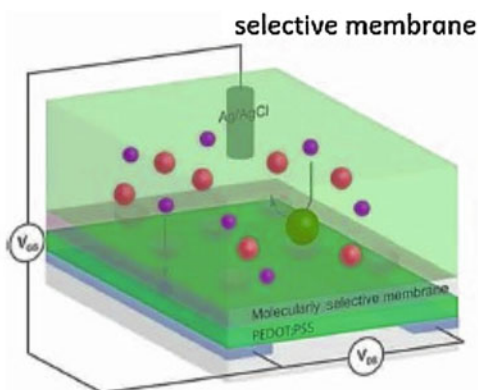
15.4.4 Procedure for 4D Printing and 4D Optimization

See Table 15.2.

Table 15.2 Bias Voltage, Impedance, and Admittance of Y doped P3BT SMPs

Bias Voltage [V]	Impedance [Ω] $\times 10^3$	Admittance [S/m] $\times 10^{-10}$
-0.5	6,025,667	1.659
0.8	9,900,941	1.010
1.2	5,508,601	1.815
2.1	4,366,929	2.289

Fig. 15.10 Typical architecture of the 15 wt. % of Y-P3BT sandwiched between glass and ITO and Ag/AgCl as a reference electrode for sensor characteristics



Architecture of Fabricated Y-P3BT

15.4.4.1 Sensor Characteristics of Y Doped Poly-3-Butyl Thiophene

MOS device consisting of PEDOT: PSS layer consisting of indium tin oxide coated over a glass substrate and top of which Y-P3BT membrane was kept separating the electrolyte and PEDOT: PSS gated with an Ag/AgCl reference electrode. Laser patterned micro-capillary channel is used for sample acquisition, ITO surface allow flexibility, the main part of sensor performance achieved by different wt. % of Y doping into P3BT polymer. Working principle of the functionalization device with conducting surfaces between the gate electrode and the channel in MOS device fabrication is shown in Fig. 15.10.

By employing different solutes and solvents (90 mM NaCl, 10 mM NaCl, 5 mM NH_4Cl , and 0.1 mM MgCl_2) for optimization of the sensor device, we investigated key factors such as the effect of solvent and change in the morphology of the SMPs during the fabrication of the Y doped P3BT thin film membrane. Usually, porogenic solvents lead to more surface area of the polymer with a high amount of vapor pressure. Dichloromethane showed better performance over the rest of the solvents (methanol, acetonitrile, etc.) and obtained results are reproducible.

15.4.4.2 SMPs of Y-P3BT as Thin Film Transistors and Light Actuators

Keithley 1500 B series and Image J software were used for measuring the output characteristics, transfer characteristics, and I-V related characteristics of the Y doped P3BT nanomaterials. All voltammetric measurements were carried out using a BioLogicSP-200 potentiostat. The sensitivity and selectivity (Figs. 15.11 and 15.12) in the response of pure and Y doped P3BT nanostructure [38–41] to chloroform were carried out with the 0–3000 ppm of gas concentration.

The selectivity and sensitivity of doped Y NS are compared with that of pure P3BTSMPs of NS. The quick recovery time, response time, and sensitivity of NS

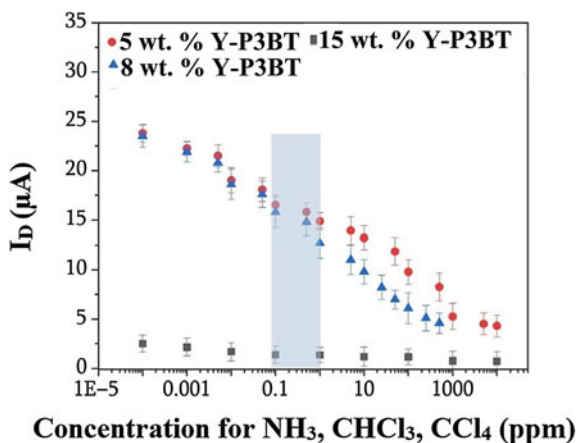


Fig. 15.11 Graph illustrating the variation of the drain current versus concentration of the gases with fabricated different wt % of Y doped P3BT SMPs

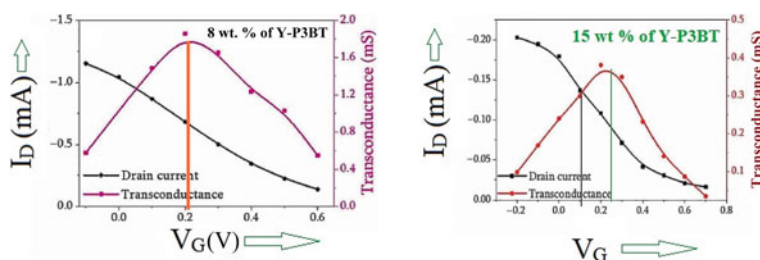


Fig. 15.12 Representing the drain-source current versus voltage gain for sensor characteristics of 8 wt. % of Y-P3BT with 15 wt. % of Y-P3BT SMPs for the effective sensing of ammonia, chloroform, and carbon tetrachloride molecules

increase with the increase in the chloroform concentration up to 100 ppm as can be understood with the I-V related characteristics of Y doped SMPs as shown in Table 15.2 (Table 15.3).

Nanostructures prepared in the form of thin films are exposed to chloroform vapors and the selectivity, response, and sensitivity of the nanostructures reached to maximum and flat curve is obtained upon completion of the experimentation thin films that were exposed to fresh air and the recovery response time was noted. Sun Y et al. reported the various factors responsible for the sensor performance of the NS and their device fabrication methods [42]. Kaur et al. reported the change in morphology, crystal nature, optical properties, and acetone gas sensing applications of WO_3 doped with Y-P3BT nanocomposites [43]. Shaikh et al. discussed the effect of doping Sr impurity into the SnO_2 thin films and experimentally demonstrated the effective sensing performance of the NPs towards ethanol vapors [44]. Figure 15.9 indicates the selective response-time graph of undoped and Y doped P3BT NS

Table 15.3 Comparison of I-V characteristics values (current, voltage, resistance, conductance, and power dissipation) of Y-P3BT thin films

Current [I]	Voltage [V]	Resistance [Ω]	Conductance [S/m]	Power Dissipation [W] $\times 10^{-5}$
1.35×10^{-5}	0.3	22,268.57	4.490×10^{-5}	0.4
2.16×10^{-5}	0.5	23,099.81	4.329×10^{-5}	1.07
2.20×10^{-5}	0.55	24,972.64	4.004×10^{-5}	1.20
1.19×10^{-5}	0.75	62,967.53	1.588×10^{-5}	0.89
5.66×10^{-5}	1	176,527.5	5.664×10^{-5a}	0.56
4.67×10^{-5}	1.25	267,974.7	3.732×10^{-6}	0.58
4.57×10^{-5}	1.5	328,320.2	3.045×10^{-6}	0.68
4.85×10^{-5}	2	412,435.8	2.424×10^{-6}	0.97
5.25×10^{-5}	3	571,262.1	1.750×10^{-6}	1.57
5.34×10^{-5}	3.3	617,448	1.619×10^{-6}	1.76
5.50×10^{-5}	4	727,207.9	1.375×10^{-6}	2.19
5.04×10^{-5}	5	992,475.1 ^b	1.007×10^{-6}	2.52 ^c

^a (observed highest conductance); ^b (highest resistance recorded), and ^c (highest Power dissipation factor)

($R_{\text{pure}} = 1034 \text{ k}\Omega$. $R_{\text{Y/P3BT}} = 668 \text{ k}\Omega$) sensor response at 100 ppm of chloroform concentration (Fig. 15.13) showed greater response with the varying concentration of the volatile gas.

Results obtained for the undoped and Y doped P3BT NS thin films show greater recovery, response time for chloroform concentration [45, 46]. The undoped P3BT

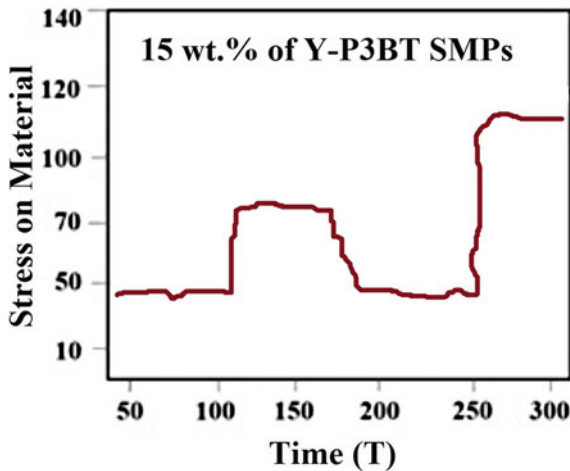


Fig. 15.13 Variation of the stress on the 15 wt. % of Y-P3BT SMPs versus Time elapsed showing quick recovery of the highly doped shape-memory polymeric material

SMPs and Y doped nano-microstructures acting as sensors showed response and recovery time of 26/ 25 s, 18/14 s, respectively (Tables 15.4 and 15.5).

Table 5.6 represents a comparison of the response and recovery rates of the Y doped P3BT SMPs with various volatile gases.

Table 15.4 Comparison of sensitivity values of various reacting gases, their response, and recovery rates of Y doped P3BT SMPs

Function of Volatile Gases	λ (nm)	λ (nm)	Response (s) Absorption	Recovery (s) Emission
NH ₄	480	520	58	87
CHCl ₃	700	610	18	14
CH ₃ OH	410	545	32	20
CH ₃ COCH ₃	360 ^a	455	29	26
CH ₄	485	555	35	32
H ₂ S	580	640	37	28
CH ₂ = CH ₂	525	595	20	24

^a (Minimum absorption of radiation occurred in the spectrum)

Table 15.5 Response, response time, and recovery time of the different wt. % of Y doped P3BT SMPs

Serial No	Materials	Response	Response time (s)	Recovery time (S)
1	Pure P3BT	51	42	42
2	5 wt. % Y-P3BT	38	28	29
3	10 wt. % Y-P3BT	40	26	27
4	15 wt. % Y-P3BT	24	26	25

Table 15.6 Comparison of different, typical smart materials used in 4D printing

Material	Input stimulus	Output response	Applications
Polymeric gel	pH change	pH change	Artificial
Electro-rheological fluid	Electrical signal	Viscosity change	Torsional steering
Pyroelectric material	Temperature	Electric signal	Personnel sensor
Polymer	Humidity change	Capacity	Humidity sensor
Self-healing materials	Force	Force	Smartphone chassis
Smart metal alloys	Temperature	Shape	Motor actuators
Dielectric elastomers	Voltage	Strain	Robotics
Varistor (e.g., Bidoped ZnO)	Voltage	Resistance	Surge protector
Piezoelectric material	Deformation	Electric signal	Active noise device

15.5 Conclusion

Nano-crystalline materials of Y doped P3BT SMPs NS (5 to 15 wt. %) synthesized by co-precipitation method, CV, XRD, SEM, UV–Visible spectroscopic investigations are carried out to understand the crystal size, morphology, optical absorptivity, and redox potentials of the Y-P3BT SMPs. Further nanomaterials of Y-P3BT SMP were studied for I-V and impedance measurements. XRD patterns reveal agglomerated tetragonal crystal structure transformed from the monoclinic structures compared and agree with the JCPDS file. The size of the nanoparticle was ~35 nm and ~50 nm, respectively, whereas the average grain boundary distance was ~70 nm. I-V, impedance recorded for the 15 wt. % showed a nonlinear relationship with the applied current and a considerable increase in the power output, admittance, and surface conductivity was observed for the pelletized samples. The voltage was varied from 0.3 V to 5 V and non-linearity of the I-V curve and Impedance curve was observed during experimentation. Upon increase in the Y wt. percentage above 15 wt. % power output decreases due to overloading of filler concentration in the SMP nanostructures. The response and sensitivity of the 15 wt % of Y doped P3BT nanostructures towards chloroform were 25 s/26 s and response and recovery time was 18 s/14 s, respectively. Present investigation can be used for doping rare-earth NCs to prepare SMPs for useful electrical and electronic applications. Present investigation can be used for doping rare-earth NCs to prepare SMPs for useful electrical and electronic applications.

Acknowledgements Authors are thankful to CENSE, IISc Bangalore, MSRIT, Bangalore and Mangalore University, Mangalore for necessary experimentations and characterizations.

Authors Contributions Dr Vinayak Adimule contributed to Design and synthesis of Y doped P3BT SMPs, purification and book chapter preparations, submission. Mr Santosh S Nandi contributed to fabrication, I-V, C-V, and sensor characteristics studies. Dr Yallur BC contributed to the SEM, XRD, XPS, Density measurements of the Y doped SMPs.

Compliance with Ethical Standards

Conflicts of Interest All authors declare that they don't have any conflicts of interest.

All the authors declare that the above research does not involve any human or animal participants as informed consent.

Availability of Data and Materials Not Applicable.

Code Availability Not Applicable.

References

1. Ernie H, Emily AS, Tong TH (2005) Light-activated shape-memory polymers and associated applications. *Smart Mater Struct*
2. Ly ST, Kim JY (2017) 4D printing—fused deposition modeling printing with thermal-responsive shape-memory polymers. *Int J Pr Eng Man-Gt* 4:267–272
3. Jinlian H, Yong Z, Huang H, Jing L (2012) Recent advances in shape-memory polymers: structure, mechanism, functionality, modeling and applications. *Prog Polym Sci* 37:1720–1763
4. Jinsong L, Xin L, Yanju L, Shanyi D (2011) Shape-memory polymers and their composites: stimulus methods and applications. *Prog Mater Sci* 56:1077–1135
5. Muhammad YR, Mathias A, Lars F, Bernd W (2007) Thermal, electrical and magnetic studies of magnetite filled polyurethane shape-memory polymers. *Mater Sci Eng, A* 444:227–235
6. Leng JS, Lan X, Liu YJ, Du SY, Huang WM, Liu N, Phee SJ, Yuan Q (2008) Electrical conductivity of thermo responsive shape-memory polymer with embedded micron sized Ni powder chains. *Appl Phys Lett* 92:014104
7. Hasan SM, Nash LD, Maitland DJ (2016) Porous shape-memory polymers: design and applications. *J Polym Sci Part B: Polym Phys* 54:1300–1318
8. Ward S, Pooja S, Thomas SW, Duncan JM (2010) Biomedical applications of thermally activated shape-memory polymers. *J Mater Chem* 20:3356–3366
9. Mohadeseh Z, Molamma P, Prabhakaran NP, Seeram R (2019) Thermally-induced two-way shape-memory polymers: Mechanisms, structures, and applications. *Chem Eng J* 374:706–720
10. Fenghua Z, Yuliang X, Yanju L, Jinsong L (2020) Nano/microstructures of shape-memory polymers: from materials to applications. *Nanoscale Horiz* 5:1155–1173
11. Lyudmila MB, Zinaida BS (2011) Dendrimers as encapsulating, stabilizing, or directing agents for inorganic nanoparticles. *Chem Rev* 111:5301–5344
12. Elmira B, Yakov E, Margarita G (2013) Nanocomposites based on polyurethanes and carbon nanoparticles: preparation, properties and application. *J Mater Chem A* 1:6509–6529
13. Chun-Sheng Z, Qing-Qing N, Shao-Yun F, Ken K (2007) Electromagnetic interference shielding effect of nanocomposites with carbon nanotube and shape-memory polymer. *Compos Sci Technol* 67:2973–2980
14. Julie M, Pratheep KA, Stephen JE, Rafeedah R, Stuart J, Rowan E, Johan F, Christoph W (2011) bioinspired mechanically adaptive polymer nanocomposites with water-activated shape-memory effect. *Macromolecules* 44:6827–6835
15. Madbouly SA, Lendlein A (2009) Shape-memory polymer composites. In: Lendlein A (eds) *Shape-memory polymers: advances in polymer Science*, p 226
16. Haibao L, Kai Y, Yanju L, Jinsong L (2010) Sensing and actuating capabilities of a shape-memory polymer composite integrated with hybrid filler. *Smart Mater Struct* 19:6
17. Xiaoming F, Farhad K, Vahid R, Mariyappan S, Masoud L, Jacek J, Robert WC, Eugene T, Balaji P (2015) MoS₂ actuators: reversible mechanical responses of MoS₂-polymer nanocomposites to photons. *Nanotechnology* 26
18. Haworth P, Smart S, Glasscock J, Diniz da Costa JC (2012) High performance yttrium-doped BSCF hollow fibre membranes. *Sep Purif Technol* 94:16–22
19. Soboyejo WO, Obayemi JD, Annan E, Ampaw EK, Daniels L, Rahbar N (2015) Review of high temperature ceramics for aerospace applications. *Open J Adv Mater Res* 1132:385–407
20. Alexander AI (2009) Photonics and molecular design of dye-doped polymers for modern light-sensitive materials. *Pure Appl Chem* 80:1525–1538
21. Cheikh C, Mohsen AM (2020) On the elastocaloric effect in CuAlBe shape-memory alloys: a quantitative phase-field modeling approach. *Comput Mater Sci* 183
22. Ying Y, Clarrisa C, Saeed M, Hengky E, Jun W, Pei-Chen S (2017) 4D printing of high-performance shape-memory polymer using stereo lithography. *Mater Des* 126:219–225
23. Ly ST, Kim JY (2017) 4D printing—fused deposition modeling printing with thermal-responsive shape-memory polymers. *Int J Precis Eng Manuf Green Tech* 4:267–272
24. Amelia YL, Jia A, Chee KC (2017) Two-way 4D printing: a review on the reversibility of 3D-printed shape-memory materials. *Engineering* 3:663–674

25. Xiao K, Kaijuan C, Conner KD, Jiangtao W, Vincent CFL, Jerry HQ (2018) 3D printing of highly stretchable, shape-memory, and self-healing elastomer toward novel 4D printing. *ACS Appl Mater Interfaces* 10(8):7381–7388
26. Christopher II, Odera SR (2020) Recent advancement in self-healing graphene polymer nanocomposites, shape-memory, and coating. *Polym Plast Technol Eng Mater* 59:1167–1190
27. Hongqiu W, Xavier C, Ivonne ON, Yahya A, Kambiz C, Uttandaraman S, Yanju L, Jinsong L, Daniel T (2019) Direct 3D Printing of hybrid nanofiber-based nanocomposites for highly conductive and shape-memory applications. *ACS Appl Mater Interfaces* 11:24523–24532
28. Wei Z, Fenghua Z, Jinsong L, Yanju L (2019) Personalized 4D printing of bio inspired tracheal scaffold concept based on magnetic stimulated shape-memory composites. *Compos Sci Technol* 184
29. Zhou Y, Huang WM, Kang SF (2015) From 3D to 4D printing: approaches and typical applications. *J Mech Sci Technol* 29:4281–4288
30. Zhengwang H, Nitin S, Tao X, Yang-Tse C, Zach HJ (2011) Remote controlled multishape polymer nanocomposites with selective radiofrequency actuations. *Adv Mater* 23:3192–3196
31. Qingyu P, Hongqiu W, Yuyang Q, Zaishan L, Xu Z, Fan X, Jinsong L, Xiaodong H, Anyuan C, Yibin L (2016) Shape-memory polymer nanocomposites with a 3D conductive network for bidirectional actuation and locomotion application. *Nanoscale*. 8:18042–18049
32. Santosh KY, Hye JY, Jae WC (2013) Click coupled graphene for fabrication of high-performance polymer nanocomposites. *Polym Phys* 51:39–47
33. Shaobing Z, Xiaotong Z, Xiongjun Y, Jianxin W, Jie W, Xiaohong L, Feng B, Ming Y (2007) Hydrogen bonding interaction of Poly(D, L-Lactide)/hydroxyapatite nanocomposites. *Chem Mater* 19:247–253
34. Liu Y, Ying L, Guang Y, Xiaotong Z, Shaobing Z (2015) Multi-stimulus-responsive shape-memory polymer nanocomposite network cross-linked by cellulose nanocrystals. *ACS Appl Mater Interfaces* 7:4118–4126
35. Amirian M, Nabipour C, Sui A (2012) Enhanced shape-memory effect of poly(L-lactide-co- ϵ -caprolactone) biodegradable copolymer reinforced with functionalized MWCNTs. *J Polym Res* 19:9777
36. Chengjun Z, Liwu L, Wenfeng B, Yanju L, Jinsong L (2020) 4D printed electro-induced continuous carbon fiber reinforced shape-memory polymer composites with excellent bending resistance. *Compos B Eng* 194
37. Yang L, Wei Z, Fenghua Z, Xin L, Jinsong L, Shuang L, Xinqiao J, Chase C, Baozhong Sun, Bohong G, Tsu-Wei C (2018) Shape-memory behaviour and recovery force of 4D printed laminated Miura-origami structures subjected to compressive loading. *Compos B Eng* 153:233–242
38. Sun Y, Wan Y, Nam R (2019) 4D-printed hybrids with localized shape-memory behaviour: implementation in a functionally graded structure. *Sci Rep* 9:18754
39. Tianzhen L, Tianyang Z, Yongtao Y, Fenghua Z, Liwu L, Yanju L, Jinsong L (2017) Stimulus methods of multi-functional shape-memory polymer nanocomposites: a review. *Compos Part A Appl Sci Manuf* 100:20–30
40. Tong M, Liwu L, Xin L, Yanju L, Jinsong L (2018) Shape-memory polymers for composites. *Compos Sci Technol* 160:169–198
41. Zhilong S, Zeru W, Baocun W, Zhen L, Songman X, Wenkai Z, Haoxiong Y, Min L, Zhao H, Jianfeng Z, Fei Y, Huan L (2016) Sensitive room-temperature H₂S gas sensors employing SnO₂ quantum wire/reduced graphene oxide nanocomposites. *Chem Mater* 28:1205–1212
42. Harper M, Guoqiang L (2013) A review of stimuli-responsive shape-memory polymer composites. *Polymer* 54:2199–2221
43. Wei Z, Liwu L, Fenghua Z, Jinsong L, Yanju L (2019) Shape-memory polymers and their composites in biomedical applications. *Mater Sci Eng* 97:864–883
44. Chougule MA, Dalavi DS, Sawanta M, Patil PS, Moholkar AV, Agawane GL, Kim JH, Shashwati S, Patil VB (2012) Novel method for fabrication of room temperature polypyrrole–ZnO nanocomposite NO₂ sensor. *Measurement* 45:1989–1996

45. Yung C, Wong B, Chin A, Haseeb AS, Aainaa AB, Yew HW (2019) Conducting polymers as chemi resistive gas sensing materials: a review. *J Electrochem Soc* 167:3
46. Oliveira J, Correia V, Castro H, Martins P, Lanceros MS (2018) Polymer-based smart materials by printing technologies: improving application and integration. *Addit Manuf* 21:269–283
47. Mahyar PS, Mahbod A, Mina N, Arian A, Parham D, Vahabodin G, Beniamin Z (2019) Deep focusing on the role of microstructures in shape-memory properties of polymer composites: a critical review. *Eur Polym J* 117:280–303

Chapter 16

Recent Developments on 4D Printings and Applications



Deepalekshmi Ponnamma, M. Sai Bhargava Reddy, Muni Raj Maurya, Omkar Kulkarni, Manikant Paswan, Kishor Kumar Sadasivuni, Mithra M. M. Nair Geetha, and Mariam Ali Al-Maadeed

16.1 Introduction

Additive manufacturing (AM) innovation allows makers, research wannabes, and individual clients to create custom 3D objects via computer-aided design [1, 2]. Thanks to its highly customizable nature and ease in printing complex 3D geometries [3]. Conventional AM technologies are designed to produce static structures using a single material, which is not capable of fulfilling the demands of dynamic functions needed for applications such as adaptive wind turbines, self-folding packaging, and soft grippers for surgery. This kind of dynamic transformation incorporation in the object fabricated with AM gave the advent to the fourth printing dimension. This idea of additional dimension introduced a new branch of AM and is known as four-dimensional (4D)-printing. 4D printing includes the idea of progress inside the printed design with time, by the action of any external stimuli [4]. 4D printing is furthermore alluded to as dynamic origami [5], 4D bioprinting, and shape-transforming frameworks [6] that utilizes equal strategies of 3D printing to make three-dimensional objects. Along with other new technologies, such as artificial intelligence, quantum computing, and autonomous mobile robots, 4D printing is in the stage of development triggering and is expected to reach its mainstream over the time of 10 years [7].

D. Ponnamma (✉) · M. R. Maurya · K. K. Sadasivuni · M. M. M. Nair Geetha · M. A. Al-Maadeed
Center for Advanced Materials, Qatar University, Doha, Qatar

M. Sai Bhargava Reddy
Center for Nanoscience and Technology, Institute of Science and Technology, Jawaharlal Nehru Technological University, Telangana State, Hyderabad 500085, India

O. Kulkarni · M. Paswan
Department of Mechanical Engineering, National Institute of Technology, Jamshedpur, India

16.2 Steps in 4D Printing

4D printing can be quoted as an advancement of the 3D printed object in property, shape, and functionality terms [8]. It is time-dependent, printer-independent, and predictable. There are key viewpoints to be satisfied for 4D printing that include the incorporation of stimuli-responsive composite materials in the framework of the 3D printed material [9]. Next is the stimulus that will act on the 3D printed object which will interact with the shape-memory elements of structure and result in deformation that leads to the formation of a new shape. For further exploration of how 4D printing occurs, we'd like to review the building blocks that make and complete the 4D printing. These include choosing the appropriate 3D printer, smart material selection [10], stimuli to be applied, mathematical modeling, and selection of the interaction mechanism. There are many prophecies about 4D printing, and these elements are fundamentals of 4D printing, as shown in Fig. 16.1 [9].

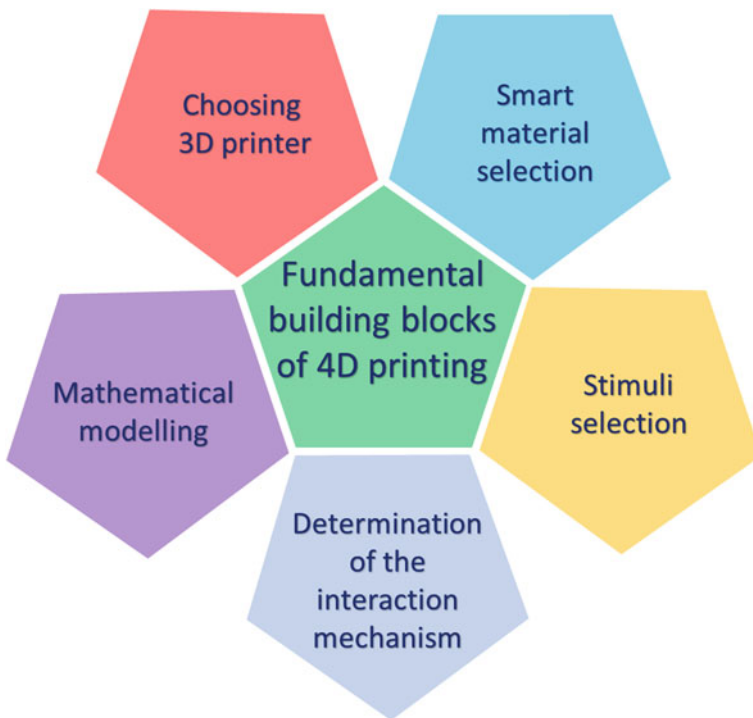


Fig. 16.1 Major steps involved in 4D printing

16.2.1 Choosing 3D Printer

4D printing is the extended branch of AM where the 3D printed object undergoes structural deformation with time upon exposure to external stimuli like temperature, current, magnetic field, water, etc. Thus, it is essential to understand the concept of 3D printing which is one of the essential parts of 4D printing. Generally, a 4D printed structure is made by consolidating a shape-memory material in the matrix of 3D printing material. There are more than 50 AM technologies that can be classified into seven categories that include direct energy deposition, sheet lamination, binder jetting, material jetting, powder bed fusion, VAT photo-polymerization process, and material extrusion as Polyjet 3D printers. The choice of the 3D printing technology majorly depends on the type of shape-memory material and geometrical resolution of the 3D printed objects. Thus, 3D printing is significant for creating shape-memory structures with 3D geometry [11, 12].

16.2.2 Smart Material Selection

Stimulus-responsive element is one of the first essential parts of 4D printing. Shape-memory materials (SMM) are an important class of functional compounds. These materials exhibit robust mechanical properties. Smart materials can be made with unique physical properties at low cost, by adding fillers, such as minerals, ceramics, and metals or even air. The addition of fillers in the matrix of smart materials can provide mechanical reinforcement, unique optical properties, enhanced electrical conductivities, high electrical breakdown, and strength. Stimulus-responsive materials are regularly characterized into a few sub-classifications and are characterized by numerous attributes that incorporate self-detecting, responsiveness, shape-memory, and multifunctionality. In AM, material structures are isolated into single and multi-material structures [5] (Fig. 16.2).

16.2.3 Stimuli Selection

A stimulus acts as a catalyst to activate the modifications of shape, property, and usefulness of a printed structure. The most common 4D printing stimuli are temperature, gravity, light, magnetic field, wind, and electric current. SMM undergoes two unique stages, which include “programming” and “recovery”. These materials demonstrate the ability to regain or remember a material’s original shape, either using a mechanical deformation or by with and without the stimulus. Thus, depending on the type of recovery, SMM is classified into (i) one-way SMM; which have one permanent and one temporary shape. (ii) Two-way SMM; these materials show the reversible transition between temporary shapes. (iii) Multiple-way SMM, which

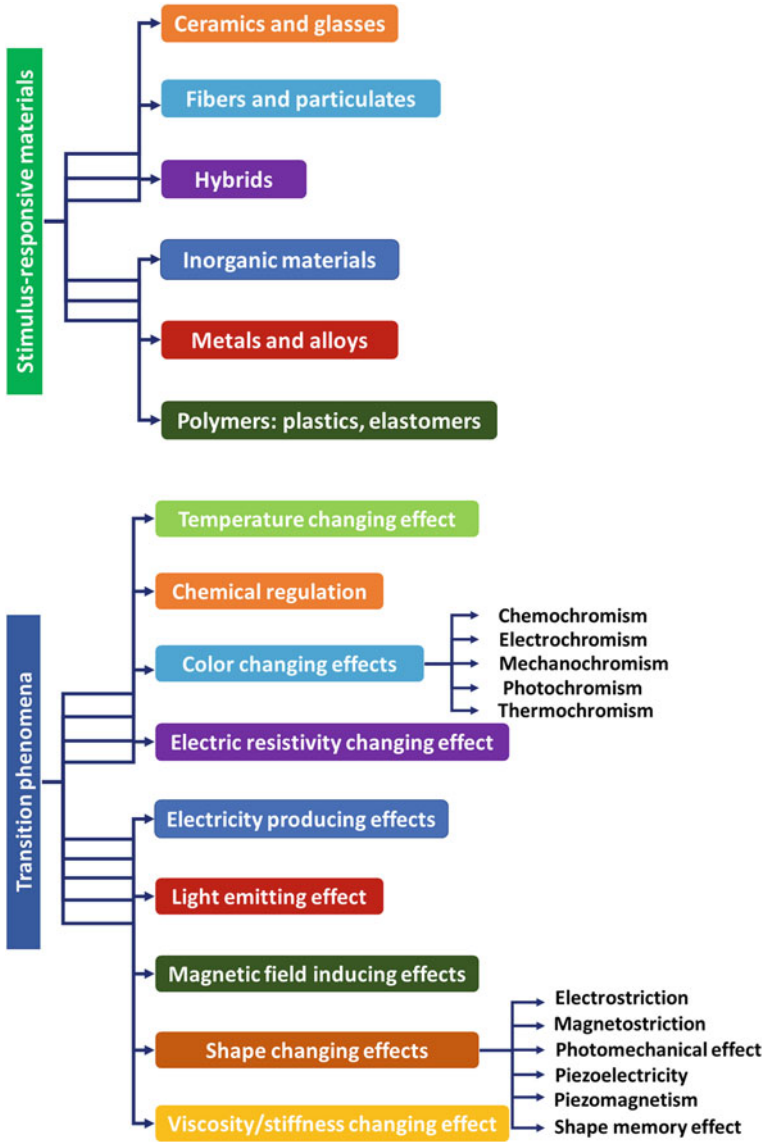


Fig. 16.2 One possible classification of smart materials

possesses one permanent and multi temporary shapes. The type of external stimulus used to trigger the shape deformation mainly depends on the physical and chemical properties of the material as well as the targeted application. As a result, based on the

type of stimuli that SMM responds to, they are classified as thermo-responsive, moisture responsive, electro responsive, photoresponsive, magneto responsive materials [13].

16.2.4 Determination of the Interaction Mechanism

Sometimes, the predefined state of a 4D printed structure isn't straightforwardly accomplished by just exposing the SMM to the stimulus. The stimulus should be applied in a definite framework for a specific period that triggers the interaction mechanism within the materials and results in shape deformation [14, 15]. One of the most commonly studied interaction behaviors is thermomechanics [16]. The 3D printed object is exposed to thermal treatment during this mechanism, and thus the smart material undergoes structure memory impact. It consists of a 4-step cycle. To begin with, the object at a high temperature is deformed by an external force; thereafter, the temperature is brought down in presence of external force; followed by this, the load is gradually removed at lowered temperature, and in this way, the ideal shape is accomplished; lastly, the main shape is slowly restored by heating the structure. To understand these predetermined shape changes it is necessary to incorporate mathematical models that can foresee explicit interactions mechanisms that permit shape deformation under the external stimulus.

16.2.5 Mathematical Modeling

Mathematical modeling finds extensive application in the fields of physics, chemistry, and biomedical sciences. Mathematical modeling is generally carried out to assess properties sensitive to the position, configuration, and shape deformation. Since many properties of interest in the study of SMM are dynamic, mathematical modeling offers an obvious advantage. Mechanisms of deformation and phase transformation, phenomena related to superplasticity and mass transport, measurement of transport coefficients, and other time-dependent processes are well-suited for mathematical modeling. Numerical and theoretical models [17–19] are assessed and created to decide the associations between four center components: final shape, material geometry, stimulus, material properties and be categorized into the forward and reverse protocol (Fig. 16.3). To simulate or control the shape-shifting sequences during a constrained process, computer-aided software is the best tool. The reasons why mathematical modeling is crucial are recorded beneath:

- (1) It is required to anticipate the structure advancement in the wake of printing after some time.
- (2) For theoretical models, mathematical modeling is opted to eliminate crashes among parts of the object during the self-assembly activity.

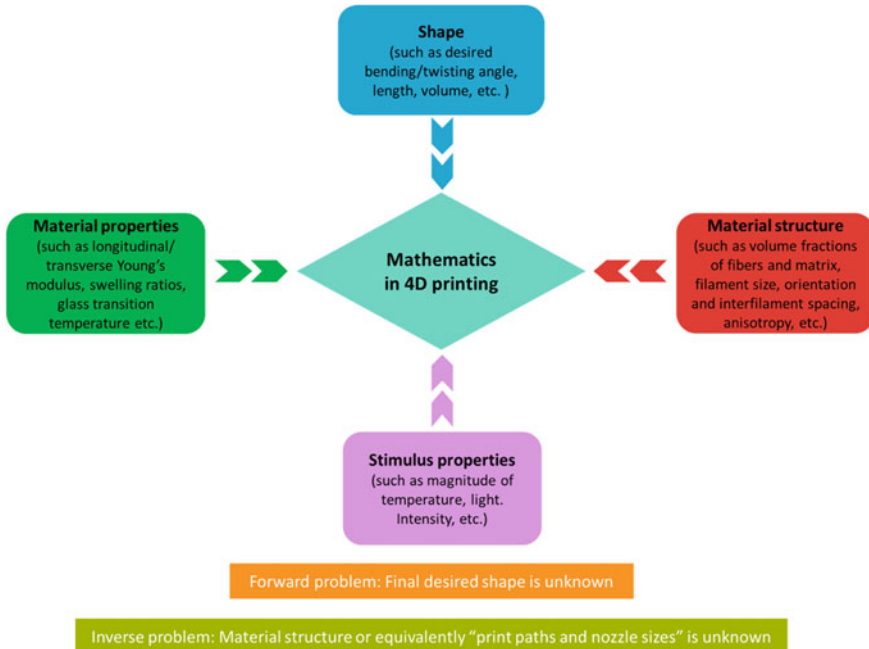


Fig. 16.3 4D printing mathematical model

(3) Decreases the measure of experimentation tests.

In general, mathematical modeling often tends to act as a bridge between theoretical models and empirical studies. In order to discover new systems exhibiting shape-memory effect and to upscale existing systems, simulations will play an important role.

16.3 3D Printing Versus 4D Printing

4D printing is a new technique, in which customized material systems or multi-material structures can be printed with the ability to transform shape over time, directly off the print bed. The transformation over time was described as the fourth dimension, stressing that printed geometries are no more static structures; instead, they can transform independently and are active. 4D printing is also recognized as additive manufacturing technology where material with varying properties or stimuli-responsive composite material-based physical objects is printed by laying down successive layers appropriately. The printed objects respond to the manually applied stimuli or from the environment, leading to a chemical or physical transformation of the state, over time. Later researchers redefined the definition as 3D-printed

objects that show intended desired property, shape, or functionality transformation with exposure to a predetermined stimulus. Thus, the basic difference between a 3D printer and a 4D printer is that the objects created with a 3D printer can be rigid or flexible. In a 3D printer, the dimensions of the thing depend on the dimensions of the printer. A 4D printer can produce a structure that's much larger than the printer's dimensional limitations [20]. Further, these differences will be explored in a detailed manner:

16.3.1 Materials

The major difference between 3 and 4D printing originates from the type of material incorporated to produce the 3D object. In 3D printing, the printing material is subjected to phase deformation prior to printing and undergoes layer-by-layer deposition to form the 3D object having fixed geometrical constraints. This is a lot of like an elastic band that can be extended yet goes to its unique structure [21]. On the other hand, in 4D printing, 3D objects designed using shape-memory materials can exhibit geometrical transformation under the presence of stimuli. The smart materials can be entirely produced using expandable materials or might be associated with expandable components. When these 3D printed objects having expandable components get exposed to specific stimuli, they change shape that can be a contraction, expansion, twisting, forward or reverse movement, etc. Such types of smart materials incorporate hydrogel, which is fit for engrossing a huge amount of water and polymeric material that can come back to its unique shape from a distorted state [21].

16.3.2 Material Size

In the case of 3D printing, the size of the printed object relies on the size of the printer. Whereas objects exhibiting 4D printing properties permanent shape is constrained to the printer dimension, but their deformed shape can surpass the geometrical limits of the printer incorporated to print the object. This can be visualized by a simple example of level cardboard and a collapsed cardboard. In 3D printing, you should legitimately print a collapsed cardboard, though, through 4D printing, you just need to create a level object that later changes itself into a collapsed cardboard.

16.3.3 Methods of Manufacturing

3D printing is layer-by-layer deposition of material to print the targeted shapes. 3D printing is enhancing the ability to print a variety of intricate, complex structures. The reality is equipping the ability to print simple or complex structures that are intricate

and prototypes on-demand with accuracy and precision. Though not cost-effective for mass production, it could save time and capital. The reception of these techniques is due to their capability in offering the choice to design and improvise with a variety of materials to produce unique shapes. These common 3D-printing strategies can be classified into seven categories that include direct energy deposition, sheet lamination, binder jetting, material jetting, powder bed fusion, VAT photo-polymerization process, and material extrusion [22, 23]. 4D printing is a next-generation version of 3D printing, which has the potential to realize self-repair, self-assembly, and multi-functionality. 4D printing feeds on technology related to 3D printing, with an extra feature of getting transformed overtime under external stimuli. Some of the distinct differences between 3 and 4D printing were represented in Table 16.1.

Table 16.1 3D versus 4D printing

Division	3D Printing	4D Printing
Materials	Thermoplastics such as ABS, metals and alloys, biomaterials and gels, and nanomaterials	Smart materials such as SMP, SMA, self-assembled materials, hydrophilic polymers, and biomaterials
Material programmability	Not possible	Materials properties and functions are programmable with a specific exposure sequence and time of stimulus, and the spatial orientation of material in the desired final product
Design	3D digital information	Transformation of 3D digital information
Printer	3D printers such as stereolithography, selective laser sintering, extrusion	Smart 3D printer (modified nozzle, laser, binder), multi-material 3D printer (solid/liquid, nanocomposite)
Application field	Toys, automobiles, health care, aerospace, etc	Areas requiring smart materials with a different transition such as mechanical shape deformation or color change upon heating, etc.
Benefits	Off the shelf, technology is widely available and implementable	Adds 'smart' functionality to 3D printed materials, including actuation and sensing functions. The disruptive platform can be used to invent novel products and devices with a wide range of applications in different industry sectors

16.4 Materials Used in 4D Printing

4D printing is built on the pillars of SMM and 3D printing. SMM undergoes significant macroscopic deformation upon the application of an external stimulus. In particular shape-memory alloys (SMAs) respond to heat by changing their shape, i.e., the thermally induced shape-memory effect has witnessed its importance in industry and research has been actively conducted for more than thirty years. On the other hand, pure shape-memory polymers (SMPs) exhibit lower modulus and recovery forces, when compared to SMAs. These materials are suitable potential alternatives for SMAs due to their flexibility, lightweight, biocompatibility, and high-strain capacities for a variety of advanced applications in ergonomic products and biomedical devices. However, for efficient high strength and high recovery force-related applications, SMPs are not suitable. Recently to overcome these issues, materials with specific performance have been reinforced as fillers into SMPs. These nanofiller impregnated SMPs composite shows extraordinary mechanical deformation and shape recovery. The incorporation of above-mentioned SMM in 3D printing for generating 3D structures that undergoes shape deformation under external stimuli enabled the emergence of 4D printing. The stimuli could be external pressure, power, attractive fields, temperature, synthetics, chemicals, hydrostatic pressure, and atomic radiation. The related variable physical properties may be shape, firmness, thickness, viscosity, or damping [24–28]. Smart materials are arranged into different classifications:

Piezoelectric materials: When exposed to an electrical charge or variety in voltage, piezoelectric material will experience mechanical change and the reverse way around.

Magnetostrictive materials: When exposed to an attractive field, and the other way around, these materials will experience a change and actuate mechanical strain.

Rheological materials: These are in a fluid stage which may turn right away through the apparatus of an electrical or attractive charge. By and large, a rheological material is a material that can change its physical state rapidly in response to a stimulus.

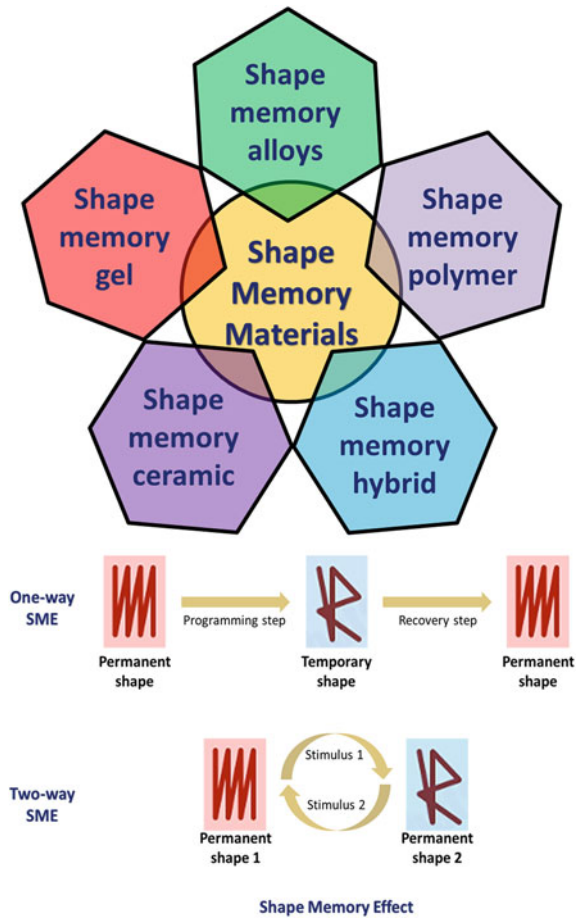
Thermo-responsive material: Thermal responsivity is the capacity of a material to change properties in light of temperature changes. They are additionally called temperature-responsive materials.

Electrochromic materials: Electrochromic is the capacity of a material to change its optical properties when voltage is applied across it.

Apart from classifying smart materials based on their response to the stimulus, smart materials (especially materials that have the shape-shifting capability) can also be characterized into two sub-classes: shape-changing materials and shape-memory materials. A shape-changing material changes its shape when a stimulus is applied and comes back to its parent shape in the absence of the stimulus. This kind of change is restricted to basic relative adjustments, for example, direct volume extension and shrinkage. Usually, in 4D printing technology, structures were designed to display one-way transformation, which means that structures need to be programmed (temporary shape setting by human interference) before every single cycle of stimulus.

Thus, the need to eliminate the manual interaction to achieve two way or reversible 4D printing arises. This kind of two-way reversibility can be realized by employing materials which can respond to an external stimulus and attain their parent properties back, by exposing to another external stimulus. This allows reversibility into 4D printed parts where the phenomenon is fully dependent on the external stimuli. Further, it eliminates the necessity of reprogramming, which is time-consuming. Moreover, after every recovery, the structure can be reused, which allows its usage over continuous cycles. Conventionally, this type of reversibility is termed “two-way memory” since it allows the two permanent shapes of material [29]. Figure 16.4 illustrates the one-way (irreversible) shape-memory and two-way (reversible) shape-memory effect. Reversibility or repeatability is referred to as the capability of 4D printed objects to replicate the complete cycle without any significant alteration to the permanent shape or fracture.

Fig. 16.4 Shape-memory materials and the differences between one-way and two-way SME



Shape-memory alloys (SMAs) are a well-known shape-transforming smart material (under temperature stimulus) that has two stages: martensite stage and austenite stage (high temperature). SMA shows a change in shape with an external stimulus such as response to heat. Upon cooling, SMAs transform from austenite phase to martensite phase. The martensite phase is comparably soft and easily deformable, whereas the austenite phase develops at higher temperatures and is stronger. Structural phase transformation of SMAs materials is known as martensitic transformation. Moreover, heating of alloy above its transformation temperature range results in its transformation from martensitic phase to austenite. A remarkable point is in the austenite phase metal that retains memory and “remembers” pre-deformation shape [30]. Nitinol is the most well-known case of an SMA with a structure of nickel and titanium, has discovered prominence in the car, aviation, biomedical, mechanical autonomy, and delicate incitation ventures.

Another class of smart materials that are picking up prevalence are shape-memory polymers (SMPs) [31]. SMPs are lightweight (or low dense), high in shape recoverability (recoverability strain). As well they have many advantages that include the ease with processing and modifying the physical properties, such as transition temperature, stiffness, biodegradability, ease of functional grading, programmability, and controllable recoverability. Moreover, SMPs can recall a lasting shape and change to a brief shape when presented to various outer stimuli, for example, temperature, pressure, water, pH levels, and magnetic field. Various SMAs/SPMs used in 4D printing for a particular area of application have been noted in Table 16.2.

16.5 Multi Materials or Composites in 4D Printing

In 4D printing, different materials generally should be embedded into a solitary and single printed geometry. This multi-material geometry can be a blend of various SMM or a composite of SMM and ordinary materials. The single-material geometry is ought to consistently be manufactured with a smart material. Furthermore, the gradient distribution of a solitary material implies that the thickness of the structure is distinctive in different areas. This anisotropy can produce shape deformation, for example, bending, twisting, and contraction [32].

Shape-memory composites networks are composed of molecular switches and net points to establish the original shapes of the networks which may have a chemical or physical origin. The occurrence of dissimilar domains (i) a hard or a permanent domain and (ii) a soft or a switching domain is accountable for shape-memory consequences in shape-memory composites. The hard and soft segments act as a turning point for shape recovery and absorbing applied stress to the material, respectively. The material comprising of two different domains morphology showcases physical cross-linking. The hard section is liable for withholding the parent shape of the object. Deformation of a shape-memory composites to a needed extent takes place at a certain temperature on heating and the particular temperature is termed as switching temperature (T_s) and that may be glass transition temperature (T_g) or a

Table 16.2 Some of the 4D printing materials for a particular area of use

S. No	4D printed materials	Use in a particular area
1	Hydrophilic acrylate monomers	Used in folds, Multiple hinges, and curls from a flat sheet
2	Tangoblack and Verowhite	Used in a box, Hinges, plane, etc
3	TPU (Thermoplastic polyurethane elastomer)	Used for Grips, foldable flowers
4	Makerbot Company's PLA	for heat shrinkable pattern transformations
5	Pattern transformations (Heat-shrinkable)	Used in hydrogel-based sensors, valves
6	Accura 60's Shape-memory epoxy	Used in micro claw, active springs
7	Methacrylate based monomers and crosslinkers	Used in Springs, grippers, stents
8	Dimplex MM-4520 pellets, Acrylonitrile butadiene styrene	Used in ABS ball joint robotic arm or SMP
9	Hydrogel composite ink	for biomedical devices, tissue engineering, soft robotics
10	co-epoxy polyacrylate particles when dispersed in epoxy resin	Used in actuators and hinges
11	poly(ethylene glycol)diacrylate (PEGDA)	Gripper, Origami, 3D Electronic device
12	Polyurethane elastomer, Polyurethane Hydrogel	Origami Structures
13	Cotton derived pulp linters, montmorillonite, Sodium carboxymethyl cellulose (CMC-Na/CMC),	Shape morphing structure
14	Nanoclay, nanofibrillated cellulose, glucose, glucose oxidase, N, N-dimethylacrylamide	Biomimetic architectures
15	Epoxy diacrylate oligomer, Polyethylene, Vinyl Caprolactam,	Self-folding grids
16	Ni-Ti Powder	for Truss structures, actuators, bone reconstruction, and medical implants
17	Polyether based polyurethane	Used in hydrogel Hinges, box
18	A mix of poly(hydroxyalkanoates) and poly(lactic acid) along with recycled wood fibers	Used in actuators, Hinges
19	poly(2 - vinyl-pyridine)(P2VP)	Used in flow-regulating devices, catalytic supports
20	Semicrystalline methacrylate PCL (Poly(ϵ -caprolactone))	Used in medical equipment
21	Semicrystalline thermoplastic PLA pellets	Used in medical devices
22	Incorporated carbon nanofibers	Used in medical devices and conductive hinges
23	PolyvinylSiloxane, polyurethane	Used in mechanical Metamaterials

(continued)

Table 16.2 (continued)

S. No	4D printed materials	Use in a particular area
24	Digital materials and Verowhite Plus	For tensegrity deployable structures

melting point (T_m) of switching segments. On further heating of the shape-memory composites above the (T_s), the oriented chains of the polymer in the network reinstate the randomly oriented subunits of the polymer to the original shape. However, the composites should have elevated strain recovery rates and strain fixity. The necessary recovery stress for shape-memory composites depends on the factors such as minimum stretching rate, maximum stretching temperature, and stretch ratio.

16.6 4D Printing in Production

Generally, an appropriate distribution of different materials forming a single composite material is used for 4D printing objects. The synergetic effect of materials properties, such as thermal expansion coefficient and swelling ratio, results in shifting behavior, transforming to a new desired shape. Therefore, to fabricate the simple and complex geometry of these smart materials 3D printing is essential. They are the most essential properties of 4D printing materials that are self-repair, multifunctionality, and self-assembly.

16.6.1 Self-Repair

The possibility of self-assembling is regularly used for self-dismantling. The correction of error and self-repairing capacity of 4D fabricated items show colossal points of interest concerning reusability and reusing. Self-healing hydrogels and self-healing pipes are some of the likely applications [33, 34].

16.6.2 Self-Assembly

Self-assembling structures are frequently produced with the help of 4D printing, particularly for combat areas or for use in space. Also, a few demerits in architectural research and trials are frequently expelled with the capacities of self-assembling 4D printed structures. Self-constructing structures are widely used for different purposes like in the manufacturing of containers, safe boxes, and lockers [15, 34].

16.6.3 Multifunctionality

Multifunctional or versatile frameworks are another element of 4D printing. This can reduce the number of parts incorporated in the structure. Multi-useful and self-versatile 4D printed tissues and 4D-printed customized clinical gadgets, as tracheal stents, are other captivating utilizations of multifunctionality [34, 37]. A wide variety of materials are utilized in 4D printing and by controlling the fabric orientation, it's also possible to program the desired shape.

16.7 Production of SMAs by 3D Printing

SMAs are popular smart materials in the industry. Selective laser melting (SLM) and Polyjet printing are usually used to make complex models of nickel-titanium (Ni-Ti) SMA [35]. In SLM printing, a laser beam is employed to sinter the material powder and then rolled to produce the final shape. The process is similar to laser melting, except that instead of heating material above the melting point the material is heated below the melting point to allow particle fusion. Ni-Ti SMA powder is especially used in these cases. The predefined complex shapes are frequently structured utilizing computer-aided design software [36]. A layer of powder is spread with a roller or wiper. The texture is reinforced by dissolving each layer of powder to the past layer utilizing the laser that follows the arranging of the cut item. The intelligence of the smart materials isn't enough for the manufacturing of 4D printed materials. 4D printing production is highly dependable on the printability of the shape-memory material. If the SMM can't be printed, the 4D structure can't be made. Numerous investigations used a rheology modifier (thickeners or viscosity modifiers) for extrusion-based printing to supply a material viscosity. Accordingly, the sacrificial agents, cross-linking and photoinitiator are the few different areas that are required to be considered for the right material printability.

16.8 Applications of 4D Printing

Integration of SMM in 4D printing has opened the possibility of systems for self-healing self-assembly and changes in material properties. 4D printing will change "mechanical transmission + engine drive" mode to the drive method of a smart material. A diverse range of intelligent materials for 4D printing innovation is being investigated. Currently, the deformation mode and the incentive methods of the smart materials for 4D printing are restricted. The general applications of 4D printed materials can be divided into two subcategories: (1) demonstrated applications (2) potential applications. Demonstrated applications are those which have proven their working

in lab experiments, such as bio-origami, origami structures, artificial crampon potential structure, smart valve, 4D nano printing, adaptive metamaterials, laser-based cell printing, smart gripper, stent, adaptive scaffolds, smart key-lock connectors, and adaptive joints. Potential applications are those applications that have the potential or capacity to be able to get the desired work done. Smart textiles, drug delivery systems, self-healing hydrogels, self-assembly at huge scales and in unfavorable conditions, adaptive pipes, tissue engineering, self-repairing structures, soft robots, and using contour crafting for the construction on mars are some of the applications that researchers see potential in 4D printing.

16.8.1 4D Printing Applications in the Medical Field

4D printing is an evolution of 3D printing, a revolutionary technique for manufacturing advanced medical devices and implants according to the patient's progress, using smart materials. Patient data is collected by scanning techniques and printed by 4D printing technology using layer-by-layer processing. The implant will change form based on the time of development of the human body. It has an excellent capacity to manufacture stents and organs that can change the shape of time as required. This research will help save the patient's lives and offer a safer alternative to serious organ shortages. There are thrilling opportunities for tissue manipulation and smart implants. 4D Printing has tested its technology to configure smart multi-material medical printing to easily display different body parts in a 3D printed model. This addresses the question of ventilation for babies with a direct fit and a complete genetic balance with the configuration of the liver, kidney, and heart and the greater versatility of the materials that are printed. 4D printing conveniently produces a range of advanced medical instruments and equipment and has amazing possibilities for printing skin grafts including original colors. It is used for complex surgery with a strong success rate and to save the patient's life.

4D printing development is leading a massive shift in the healthcare industry, such as organ manufacturing, tissue engineering, and the self-assembling of human biomaterials. Biomedical stents, splints, bioprinting, and orthodontic equipment are developed as per human development. In the future, this new technology should be more useful and can continue to build infinite possibilities in the medical industry [37, 38]. Thanks to its complicated and patient-specific structure, the manufacturing of a stent involves several procedures. 4D printing allows it possible to easily produce personalized stents. The shape-memory feature of the stent makes it possible to reduce the surgical interference of the implantation by first printing the stent to the ideal ultimate diameter and then optimizing the stent to a smaller radius for simplicity of implantation and accurate positioning. Upon implantation, the stent returns to its initial diameter at body temperature. Geometry is a crucial feature for therapeutic devices like splints in which the alignment of the system to the subject is important for the proper functioning of the system. Nevertheless, in situations in which the growth of the subject is important, traditionally designed biomedical instruments

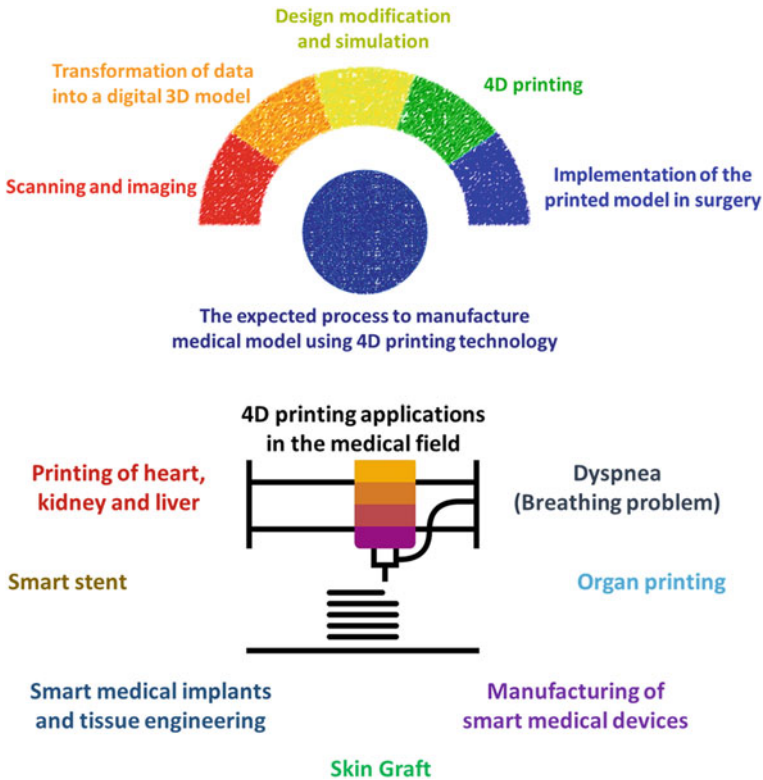


Fig. 16.5 4D printing methodology in the medical field and their potential applications

have difficulty in adjusting to growth over time. 4D printing of such instruments may make it possible to alter the shapeshift due to growth. Figure 16.5 illustrates the ideal methodology employed during 4D printing in the medical field and some of the potential applications in the field.

16.8.2 4D Bioprinting or the Utilization of 4D Printing in Tissue and Organ Recovery

Bioprinting is an energizing possibility in the clinical field. Bioprinting can be characterized as additive manufacturing of 3D tissues and organs utilizing biomaterials, cells, and biological molecules. 3D printing is advancing into an unrivaled biomanufacturing innovation since 4D printing, during design fabrication involves a time-dependent dynamic process that is believed to further revolutionize the current fabrication processes of tissue and organs. Engineered or synthetic tissues, which can overlap and be controlled remotely by light, were manufactured by printing structures

containing hundreds or thousands of conveying watery droplets that are programmed and arranged in patterns. These kinds of structures, with numerous communicating compartments and dynamic shape evolving abilities, are rendered more closely and accurately resembling living life forms. These structures could be improved to take after living cells by adding the capacity to synthesize protein from epitomized DNA. Additionally, the improvement of smart and profoundly biocompatible materials for 4D printing is turning into an active exploration zone [39].

16.8.3 4D Printing for Pharmaceuticals

4D printing is still to be used in the pharmaceutical drug delivery system field. Nevertheless, smart materials have also been implemented in the field, producing bio-adhesive tools that react to pH with the precise targeting of sites of the GI tract, or perhaps remotely operated ‘micro-robots engineered to administer chemotherapy specifically to a tumor location. As a consequence, prior creativity of smart materials is expected to serve as a guide to the eventual acceptance of 4D printing throughout the field. It would open the way to produce therapeutics that integrates the precision of additive manufacturing mostly with sophisticated kinetics of smart materials. While 3D printing is now in development, even within the pharmaceutical industry, the switch to 4D appears easy. While utilizing smart materials as raw material, it can establish drug delivery innovations that may modify and adjust the reaction to various situations inside the gastrointestinal tract. By achieving, such ‘smart drugs’ will enable the highly selective release of drugs [40] shown in Fig. 16.6 which can be tailored both for the clinical condition of every particular patient. 3D printing also needs a lot of progress and then it will be commercially feasible, although it will be prudent to look forward to the future because 4D printing is expected to materialize faster than one would expect [41].

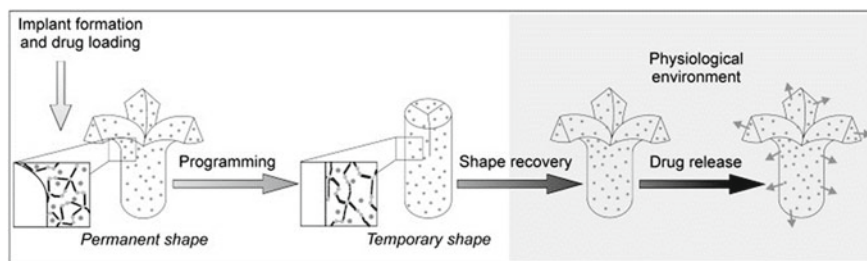


Fig. 16.6 The smart drug release system. Reprinted from [40] Copyright © (2009) with permission from Elsevier B.V.

16.8.4 Usage of 4D Printing for Applications in Space

A model where 4D printing could be utilized in the long in a pre-customized way is that by using opting DPR (deployable panel radiator), with two DPRs being obliged on each satellite. At first during dispatch, the DPR is stored, and sent to orbit once by the usage of a single-axis mechanism which thereby fuses adaptable piping for cooling of liquids. Most regular deployable gadgets are profoundly sophisticated, containing various linkages, pivots, and engines, which eventually go with the significant expense and substantial structures. Ongoing advancements in 4D printed materials offered to ascend to lightweight, reasonably less expensive materials equipped for different deformations without any degradation occurring. The usefulness of 4D printing permits materials to interface and adjust to evolving conditions. In space, to print precisely what's required in remote places on a frequently required basis spares weight (particularly on starting dispatch) and likely misuse of materials [42]. 4D printing can also be used in soft robotics to fabricate shape-changing pneumatic and hydraulic actuators.

16.8.5 4D Printed Multi-stable Metamaterials

Because the physical structure of micro-structural components dictates the features of the mechanical metamaterials, the design and behaviors of the metamaterials are permanent without the potential to modify and change. 4D printing technique can be used to build spatially tunable, physically deployable, and mechanically modifiable lightweight metamaterials. Using a technique of modern micro-additive processing and a thermo-responsive shape-memory polymer that experiences a drastic shift in modulus of elasticity, and lightweight structural metamaterials with successful stiffness could be changed more than a hundred times. The 4D printed SMP multi-stable metamaterial also has a shape-memory feature that during the deformation process can recall any shape and can be self-driven to extend [43]. Mechanical metamaterials printed in 4D can see a wide variety of applications including controllable shock-absorbing frameworks, aerospace flexible and flexible systems, soft robotics, and implantable biomedical microdevices [44].

16.8.6 Textiles and Fashion Ware Applications of 4D Printing

To build practical, flexible, and active properties in fabrics, the goal was to take upon the concept of “4D printing.” The fashion wares were introduced specifically for foot wares, jewelry, and textiles with the style of 4D printing to ease the user from its flexible setting or necessity configuration as shown in Fig. 16.7. Many experimental material studies were carried out using 3D printing to investigate how to finish a

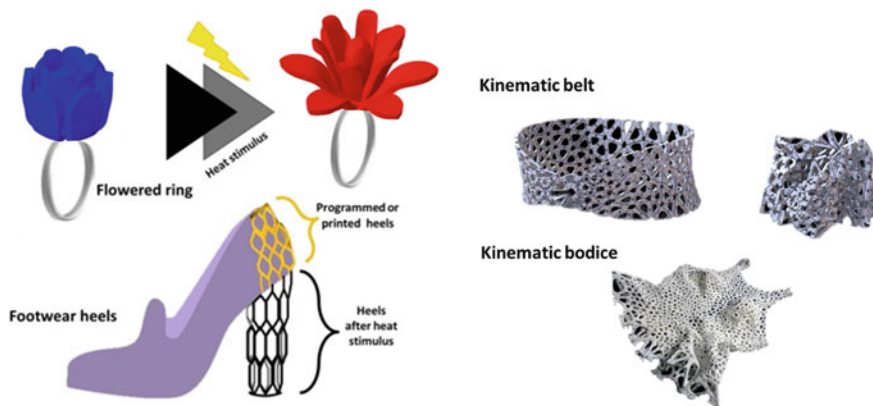


Fig. 16.7 4D printed fashion ware and textiles

textile surface with a 3D imprint to create a particular movement. It was achieved by a tailored blend of fabric tension and a 3D Geometric model, and often a “smart” print filament that can recall its shape. Due to this mix of materials, the whole cloth surface embraces the printed material’s shape-memory and material knowledge, enabling us to determine accurate patterns of movement that it executes separately in reaction to such temperature changes. It prints the model geometry that makes it a permanent shape. However, one of the first approaches which enabled a formal variation in time to be applied to a 3D printed object (4D printing) was cinematics or even the science which explores the movement of bodies in a period. Kinematics is used in these dresses to print complicated 3D constructs, consisting of several rigid components, which are fused tightly. These constructs, taking advantage of computational models, may be folded back into itself to minimize their thickness during the printing process [45, 46].

16.8.7 *Soft Robotics*

4D printing reflects a significant industrial paradigm change of single-function fixed systems to dynamically embedded, interactive structures. Direct printing of dynamic structures has a broad range of applications, such as sensors and actuators and robotics with numerous benefits (e.g., design flexibility, low material costs) [47]. Soft robotics is a modern robotics approach wherein hard and rigid structures are substituted by fluid and versatile materials to imitate processes that function in living organisms, which are critical to performing complex, dynamic activities. Nevertheless, little work has been documented in the direct printing of soft robotics. Just a few SMMs have been effectively printed owing to the limited history of 4D printing, such as shape thermo-responsive polymers with comparatively low actuation strains (up to ~8%). These soft robots have different sensors and actuators installed in them. One

of the most significant actuators in soft robotics is the dielectric elastomer actuator (DEA), which acts as a capacitor with an elastomer layer sandwiched between two compatible electrodes, producing distortion under the electric field. DEA is generally used more like an “artificial muscle” to imitate mammalian muscles because of its high strain and energy density capacity to generate massive strains (~200%). Dielectric elastomer actuator (DEA) is selected as the actuator for soft robotics to achieve broad movement [48]. SMMs are essential for smart 4D-printed robotic actuators. In terms of their morphological transformations, there are two forms of SMMs: one way and two-way shape-memory materials. One-way SMMs experience a shape transformation on an external stimulus, such as temperature, that persists until the stimulus is removed. Conversely, a switching stimulus, basically a dynamic biomorphic process, helps two-way SMMs to transform reversibly into two separate types. The use of other products, such as magnetic or light-responsive micro and nanostructures, to shape 4D-printed composite components would also provide new possibilities in smart robotic actuators [49]. Soft robotic grippers built on shape-memory material [50] are exceptionally flexible and able to manage a wide variety of items as seen in Fig. 16.8 successful models of established 4D microstructures utilizing composite materials, liquid crystals and hydrogels have gained a foothold in recent years. Stimuli-responsive monomers were widely used in the processing of soft structures showing activity primarily guided by pH shifts in aqueous media or temperature. Liquid crystal-based compounds have already been investigated as qualified applicants for microscale operation and the first instances of basic micro-actuated robots [51].

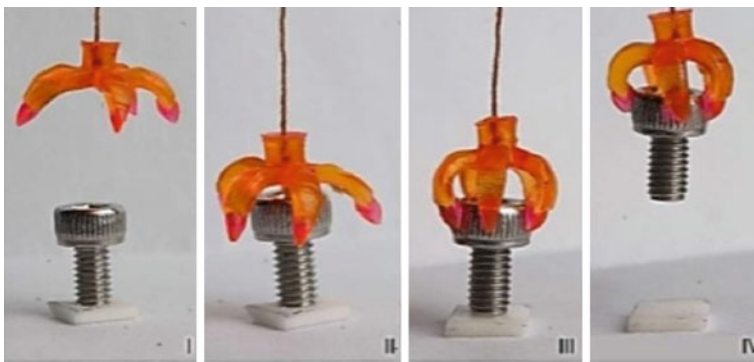


Fig. 16.8 Heat actuated soft robotic grippers. Reproduced from [50], originally published under a CC BY 4.0 license, <https://doi.org/10.1038/srep31110>. Copyright © 2016 Qi Ge et al.

16.8.8 Electronics Application of 4D Printing

Mechanical reformation provided by SMM improves the actuation and sensing capacities of the electronics industry (MEMS, NEMS, transistors, etc.) yet new and sophisticated electronics design with versatility as the cornerstone method captures the crucial role in research realms around the world. The superiority of electronics was further demonstrated by the dimension-transforming capabilities of 4D printing. The origami bending of the SMM has widened the scope of print-electronic entities by mobilizing or furnishing dynamics. Printed artifacts may be used in modular electronics by combining SMPs with conductive materials and illustrating potential uses in two forms of sensitive electrical devices. The developed electrical temperature sensor unit consists of a 3D-shaped-memory polymer-printed structure (Fig. 16.9a) on which the electrical contacts were inkjet-printed using silver nanoparticle ink (Fig. 16.9b). Figure 16.9c shows the purpose of the device: the provisional form is an open electrical circuit, and once the circuit is heated above the T_m , the circuit is closed, and the LED is illuminated. [55].

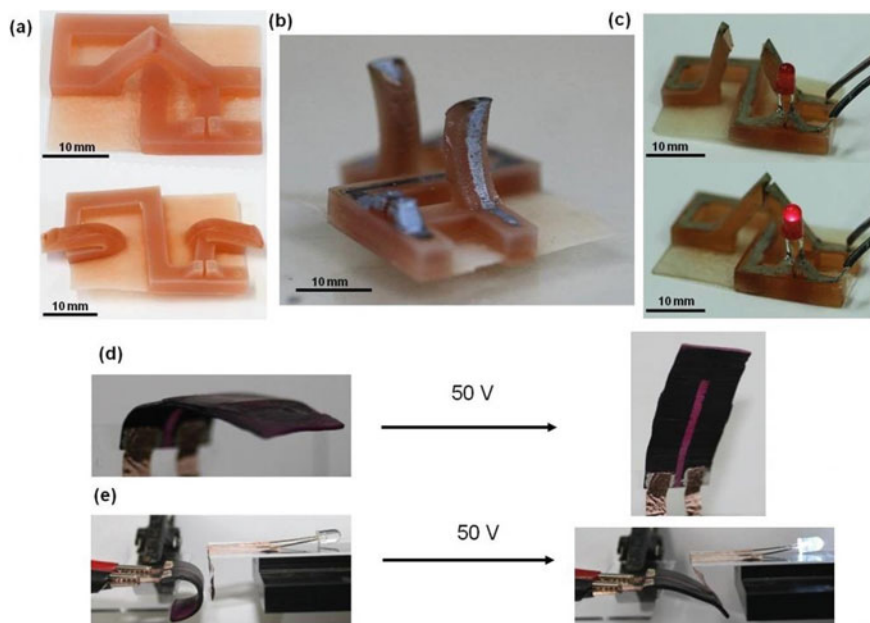


Fig. 16.9 Printed 3D electrical circuit made of shape-memory polymers, activated by heat. Reproduced with permission from [55]. Copyright © 2015 WILEY-VCH Verlag GmbH & Co. KGaA, Weinheim

16.8.9 4D Printing in the Military

The programmable problem would have a broad variety of uses in the military field. Designing military requirements including such 3D printing replacement parts in the field and designing programmable components that shape a full building with all the required materials, such as power, plumbing, and other technological structures because technology helps products to alter their appearance, military vehicles, automobiles, and fabrics will make it possible for them to adjust their camouflage. Military advances in 4D printing technologies will improve coating content in the automobile industry, which will alter the composition to deal with the humid atmosphere and corrosion. In the same way, the change of tires relies on the surface and environmental conditions.

16.8.10 Furniture and House Appliances

People might feel satisfaction when the flat-packed furniture is self-assembled, and the furniture can be used without any hassle. Likewise, the self-disassembly of furniture when shifting from one position is encouraging. Along with saving money, it might help citizens get rid of repetitive assembly procedures and errors.

16.8.11 4D Printing of Shape-Shifting Devices

Organisms, such as flowers and trees, include tissue combinations and microstructures that establish complex morphologies that can change shape over time in response to environmental stimuli. Origami is a popular Japanese artwork with an intricate folding chain that creates a graphical form. In-built origami is seen in plant leaves (curls or twists), berries, seeds, insects (fleeting of wings), and in the body proteins where an imaginative process of folding chronology is created, and can also be used in containers, market bags, solar devices, and other space science equipment [52]. The demand for origami architecture has increased since the advent of 4D printing and is now applied to space and medical science for self-constructing constructs from a purely static system with far-reaching uses and consequences for sophisticated devices, autonomous robots, UAVs, toys, and artificial intelligence [27]. Each of such exercise's pivots or smooth folds for complex motions are guided by electrical or stimulation.

Scientists at the Wyss Institute have imitated several complex form shifts such as those produced by tendrils, leaves, and flowers in reaction to variations in humidity or temperature using groundbreaking 4D-printed hydrogel composites. By aligning cellulose fibrils extracted from wood in arrangements that are projected in the 4D-printing phase using a specialized computational model, the composite ink encodes

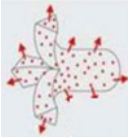


anisotropic swelling and rigidity features that can be patterned across the printing path. Using this technique, local swelling activities in water-immersed composites are programmable, resulting in complex and extremely repetitive shifts in form. In comparison, several hydrogel compounds can be used interchangeably, leading to various stimulus-responsive activities, whereas cellulose fibrils can be supplemented by other anisotropic fillers of choice, like conductive fillers. Such products can be used to produce medical instruments that take form while in touch with body fluids, as well as smart textiles, flexible construction materials, and innovative computer sensors and actuators.

Multifunctional composite materials could be added with a few stimuli to accomplish a few diverse reaction mechanisms in testing environmental situations [53]. To this date, 4D printing of metals includes predominant shape-memory alloys, while various publications have risen itemizing elective stimuli for polymers and composites. The newly augmenting mechanical advances permit the joining of metals and polymers in greater complex structures geometries [54]. The following stage could see the advancement of bigger scope printers consolidating additive manufacturing and mechanical autonomy, with multi-material printing. Likewise, the advancement of the nanoscale of these composites helps greatly in focusing on drug delivery for medication inside the body. Technology development trends of the 4D printing were represented in Table 16.3 along with some comments.

16.9 Conclusion



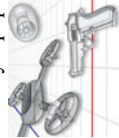
In summary, even though 4D printing has indicated extraordinary application potential and keeps on creating consideration, it is still in its early stages as an exploration territory. Later on, 4D printing requires innovative advances in different fields including modeling, software, chemistry, and mechanics. Self-assembling materials have been seriously read for a considerable length of time, yet just a little segment of these materials have been explored for 4D printing. Multi-responsive structures activated by different stimuli require more noteworthy endeavors and mastery. 4D printing is still at the concept development stage that has stepped forward in understanding the capacities of pre-programming matter which respond to different stimuli. The responsive materials can change aviation, clinical, and defense industries in the following decade.

Table 16.3 Applications of major Industries towards 4D printing

Industry	Field	Illustration of one of the field applications	Comments
Health care Including pharmaceutical	Implants, healthcare instruments, drug delivery carriers		<ul style="list-style-type: none"> • Reduce medical procedures and costs with medical 4D printing printouts • Self-assembled organs such as self-changing stents, splints, artificial bones, tissue, and organs, etc • Targeted drug delivery will effectively work on a specific targeted region and minimize the side effects
Electronics including soft robotics	Home and Industry appliances, MEMS, NEMS		<ul style="list-style-type: none"> • Smart and adaptive sensors fabrication using smart responsive materials 4D printing • A solar cell that can maximize shape conversion by adjusting shape according to the light quantity and the possibility of origami designs in space applications such as satellites and ISS
Transportation (automotive, aerospace, and aeronautical)	Machine parts, and their components		<ul style="list-style-type: none"> • Folding mechanisms, chassis, wheels, and various mechanical devices that change shape depending on the external environment • Aircraft that can recover on their own even if damaged during flight

(continued)

Table 16.3 (continued)

Industry	Field	Illustration of one of the field applications	Comments
Fashion ware	Clothing, design, toys, jewellery	Jewellery 	<ul style="list-style-type: none"> • Clothing that can respond to temperature, water, and light • Kinematic design wares that enable shape-shifting and color-changing ornaments and textiles, etc
Civil constructions	Construction materials and structures	Smart structures 	<ul style="list-style-type: none"> • Smart structures which respond to various physical effects and exhibit shape-shifting, color variations according to the environment • Rapid construction and self-assembling can be possible in these structures
Military	Safety equipment's, weapons, and carriers	Military equipment's 	<ul style="list-style-type: none"> • Camouflage like a chameleon and convert material by the refraction of light • 4D printing of radar absorbing structure based on gradient-refractive-index metamaterials • Aerial vehicles such as drones

Acknowledgements This work was supported by an NPRP grant from the Qatar National Research Fund under the grant number NPRP12S-0131-190030. The statements made herein are solely the responsibility of the authors.

References

1. Ngo TD, Kashani A, Imbalzano G, Nguyen KT, Hui D (2018) Additive manufacturing (3D printing): a review of materials, methods, applications and challenges. *Compos Part B-Eng* 143:172–196. <https://doi.org/10.1016/j.compositesb.2018.02.012>
2. Bak D (2003) Rapid prototyping or rapid production? 3D printing processes move industry towards the latter. *AssemAutom.* <https://doi.org/10.1108/01445150310501190>
3. Lipson H, Kurman M (2013) *Fabricated: the new world of 3D printing*. John Wiley & Sons
4. Lee JY, An J, Chua CK (2017) Fundamentals and applications of 3D printing for novel materials. *Appl Mater Today* 7:120–33. <https://doi.org/10.1016/j.apmt.2017.02.004>
5. Ge Q, Dunn CK, Qi HJ, Dunn ML (2014) Active origami by 4D printing. *Smart Mater Struct* 23:094007
6. Gladman AS, Matsumoto EA, Nuzzo RG, Mahadevan L, Lewis JA (2016) Biomimetic 4D printing. *Nat Mater* 15:413–8. <https://doi.org/10.1038/nmat4544>
7. Wu JJ, Huang LM, Zhao Q, Xie T (2018) 4D printing: history and recent progress. *Chin J Polym Sci* 36:563–575. <https://doi.org/10.1007/s10118-018-2089-8>
8. Kuang X, Roach DJ, Wu J, Hamel CM, Ding Z, Wang T, Dunn ML, Qi HJ (2019) Advances in 4D printing: materials and applications. *Adv Funct Mater* 29:1805290. <https://doi.org/10.1002/adfm.201805290>
9. Momeni F, Liu X, Ni J (2017) A review of 4D printing. *Mater Des* 122:42–79. <https://doi.org/10.1016/j.matdes.2017.02.068>
10. Leist SK, Zhou J (2016) Current status of 4D printing technology and the potential of light-reactive smart materials as 4D printable materials. *Virtual Phys Prototy* 11:249–262. <https://doi.org/10.1080/17452759.2016.1198630>
11. Deshmukh K, Houkan MT, AlMaadeed MA, Sadasivuni KK (2020) Introduction to 3D and 4D printing technology: State of the art and recent trends. *3D and 4D Printing of Polymer Nanocomposite Materials* 1:1–24. <https://doi.org/10.1016/b978-0-12-816805-9.00001-6>
12. Choi J, Kwon OC, Jo W, Lee HJ, Moon MW (2015) 4D printing technology: a review. *3D Printing Addit Manuf* 2:159–167. <https://doi.org/10.1089/3dp.2015.0039>
13. Zhang Z, Demir KG, Gu GX (2019) Developments in 4D-printing: a review on current smart materials, technologies, and applications. *Int J Smart Nano Mater* 10:205–224. <https://doi.org/10.1080/19475411.2019.1591541>
14. Manikandan N, Rajesh PK, Harish V (2021) An analysis of the methods and materials for 4-dimensional printing. *Mater. Today: Proc* 38:2167–2173. <https://doi.org/10.1016/j.matpr.2020.05.551>
15. Campbell TA, Tibbits S, Garrett B (2014) The programmable world. *Sci Am* 311:60–65
16. Ge Q, Dunn CK, Qi HJ, Dunn ML (2014) Active origami by 4D printing. *Smart Mater Struct* 23:094007. <https://doi.org/10.1088/0964-1726/23/9/094007>
17. Gladman AS, Matsumoto EA, Nuzzo RG, Mahadevan L, Lewis JA (2016) Biomimetic 4D printing. *Nat Mater* 15:413–418
18. Tobushi H, Hashimoto T, Hayashi S, Yamada E (1997) Thermomechanical constitutive modeling in shape-memory polymer of polyurethane series. *J Intell Mater Syst Struct* 8:711–718. <https://doi.org/10.1177/1045389X9700800808>
19. Rastogi P, Kandasubramanian B (2019) Breakthrough in the printing tactics for stimuli-responsive materials: 4D printing. *Chem Eng J* 366:264–304. <https://doi.org/10.1016/j.cej.2019.02.085>

20. Khare V, Sonkaria S, Lee GY, Ahn SH, Chu WS (2017) From 3D to 4D printing—design, material and fabrication for multi-functional multi-materials. *Int J Precis Eng Manuf-Green Technology* 4:291–9. <https://doi.org/10.1007/s40684-017-0035-9>
21. Vaezi M, Chianrabutra S, Mellor B, Yang S (2013) Multiple material additive manufacturing—Part 1: a review: this review paper covers a decade of research on multiple material additive manufacturing technologies which can produce complex geometry parts with different materials. *Virtual Phys Prototy* 8:19–50. <https://doi.org/10.1080/17452759.2013.778175>
22. Zhang YS, Yue K, Aleman J, Mollazadeh-Moghaddam K, Bakht SM, Yang J, Jia W, Dell’Erba V, Assawes P, Shin SR, Dokmeci MR (2017) 3D bioprinting for tissue and organ fabrication. *Ann Biomed Eng* 45:148–63. <https://doi.org/10.1007/s10439-016-1612-8>
23. Ly ST, Kim JY (2017) 4D printing—fused deposition modeling printing with thermal-responsive shape-memory polymers. *Int J Precis Eng Manuf-Green Technol* 4:267–72. <https://doi.org/10.1007/s40684-017-0032-z>
24. Choong YY, Maleksaeedi S, Eng H, Su PC, Wei J (2017) Curing characteristics of shape-memory polymers in 3D projection and laser stereolithography. *Virt Phys Prototy* 12:77–84. <https://doi.org/10.1080/17452759.2016.1254845>
25. Li Z, Loh XJ (2017) Four-dimensional (4D) printing: Applying soft adaptive materials to additive manufacturing. *J Mol Eng Mater* 5:1740003. <https://doi.org/10.1142/S2251237317400032>
26. Vaezi M, Chianrabutra S, Mellor B, Yang S (2013) Multiple material additive manufacturing—Part 1: a review: this review paper covers a decade of research on multiple material additive manufacturing technologies which can produce complex geometry parts with different materials. *Virtual Phys. Prototy* 8:19–50. <https://doi.org/10.1080/17452759.2013.778175>
27. Ge Q, Sakhaei AH, Lee H, Dunn CK, Fang NX, Dunn ML (2016) Multimaterial 4D printing with tailorable shape-memory polymers. *Sci Rep* 6:1–1. <https://doi.org/10.1038/srep31110>
28. Okuzaki H, Kuwabara T, Funasaka K, Saido T (2013) Humidity-sensitive polypyrrole films for electro-active polymer actuators. *Adv Funct Mater* 23:4400–4407. <https://doi.org/10.1002/adfm.201203883>
29. Breger JC, Yoon C, Xiao R, Kwag HR, Wang MO, Fisher JP, Nguyen TD, Gracias DH (2015) Self-folding thermo-magnetically responsive soft microgrippers. *ACS Appl Mater Interfaces* 7:3398–3405. <https://doi.org/10.1021/am508621s>
30. Pei E, Loh GH (2018) Technological considerations for 4D printing: an overview. *Progr Addit Manuf* 3:95–107. <https://doi.org/10.1007/s40964-018-0047-1>
31. Jani JM, Leary M, Subic A, Gibson MA (2014) A review of shape-memory alloy research, applications and opportunities. *Mater Des* 56:1078–1113. <https://doi.org/10.1016/j.matdes.2013.11.084>
32. Hager MD, Bode S, Weber C, Schubert US (2015) Shape-memory polymers: past, present and future developments. *Prog Polym Sci* 49:3–33. <https://doi.org/10.1016/j.progpolymsci.2015.04.002>
33. Yakacki CM, Saed M, Nair DP, Gong T, Reed SM, Bowman CN (2015) Tailorable and programmable liquid-crystalline elastomers using a two-stage thiol–acrylate reaction. *RSC Adv* 5:18997–19001. <https://doi.org/10.1039/C5RA01039J>
34. Taylor DL, in het Panhuis M (2016) Self-healing hydrogels. *Adv Mater* 28:9060–9093. <https://doi.org/10.1002/adma.201601613>
35. Whitesides GM, Grzybowski B (2002) Self-assembly at all scales. *Science* 295:2418–2421. <https://doi.org/10.1126/science.1070821>
36. Tibbitts S, McKnelly C, Olguin C, Dikovskiy D, Hirsch S (2014) 4D printing and universal transformation. *acadia14_539*
37. Khademhosseini A, Langer R (2016) A decade of progress in tissue engineering. *Nat Protoc* 11:1775–1781. <https://doi.org/10.1038/nprot.2016.123>
38. Khoo ZX, Liu Y, An J, Chua CK, Shen YF, Kuo CN (2018) A review of selective laser melted NiTi shape-memory alloy. *Materials* 11:519. <https://doi.org/10.3390/ma11040519>
39. Gustmann T, Neves A, Kühn U, Gargarella P, Kiminami CS, Bolfarini C, Eckert J, Pauly S (2016) Influence of processing parameters on the fabrication of a Cu–Al–Ni–Mn shape-memory

- alloy by selective laser melting. *Addit Manuf* 11:23–31. <https://doi.org/10.1016/j.addma.2016.04.003>
40. Javaid M, Haleem A (2019) 4D printing applications in medical field: a brief review. *Clin Epidemiol Glob Health* 7:317–321. <https://doi.org/10.1016/j.cegh.2018.09.007>
 41. Serpooshan V, Hu JB, Chirikian O, Hu DA, Mahmoudi M, Wu SM (2018) 4D printing of actuating cardiac tissue. In: *3D printing applications in cardiovascular medicine*, pp 153–162. <https://doi.org/10.1016/B978-0-12-803917-5.00008-0>
 42. Miao S, Castro N, Nowicki M, Xia L, Cui H, Zhou X, Zhu W, Lee SJ, Sarkar K, Vozzi G, Tabata Y (2017) 4D printing of polymeric materials for tissue and organ regeneration. *Mater Today* 20:577–591. <https://doi.org/10.1016/j.mattod.2017.06.005>
 43. Wischke C, Neffe AT, Steuer S, Lendlein A (2009) Evaluation of a degradable shape-memory polymer network as matrix for controlled drug release. *J Control Release* 138:243–250. <https://doi.org/10.1016/j.jconrel.2009.05.027>
 44. Firth J, Gaisford S, Basit AW (2018) A new dimension: 4D printing opportunities in pharmaceuticals. In: *3D printing of pharmaceuticals*, pp 153–162. https://doi.org/10.1007/978-3-319-90755-0_8
 45. Melly SK, Liu L, Liu Y, Leng J (2020) On 4D printing as a revolutionary fabrication technique for smart structures. *Smart Mater Struct* 29:083001. <https://doi.org/10.1088/1361-665X/ab9989>
 46. Tao R, Xi L, Wu W, Li Y, Liao B, Liu L, Leng J, Fang D (2020) 4D printed multi-stable metamaterials with mechanically tunable performance. *Compos Struct* 252:112663. <https://doi.org/10.1016/j.compstruct.2020.112663>
 47. Yang C, Boorugu M, Dopp A, Ren J, Martin R, Han D, Choi W, Lee H (2019) 4D printing reconfigurable, deployable and mechanically tunable metamaterials. *Mater Horiz* 6:1244–1250. <https://doi.org/10.1039/C9MH00302A>
 48. Web page of Nervous System about kinematics projects (2016). <http://n-e-r-v-o-u-s.com/projects/sets/kinematics>
 49. Rastogi P, Kandasubramanian B (2019) Breakthrough in the printing tactics for stimuli-responsive materials: 4D printing. *Chem Eng J* 366:264–304. <https://doi.org/10.1016/j.cej.2019.02.085>
 50. Garces IT, Ayranci C (2020) Active control of 4D prints: towards 4D printed reliable actuators and sensors. *Sens Actuators, A: Phys* 301:111717. <https://doi.org/10.1016/j.sna.2019.111717>
 51. Cai J (2016) 4D printing dielectric elastomer actuator based soft robots. <https://scholarworks.uark.edu/etd/1680>
 52. de Marco C, Pané S, Nelson BJ (2018) 4D printing and robotics. *Sci Robot* 3:287–294
 53. Spiegel CA, Hippler M, Münchinger A, Bastmeyer M, Barner-Kowollik C, Wegener M, Blasco E (2020) 4D printing at the microscale. *Adv Funct Mater* 30:1907615. <https://doi.org/10.1002/adfm.201907615>
 54. Zarek M, Layani M, Cooperstein I, Sachyani E, Cohn D, Magdassi S (2016) 3D printing of shape-memory polymers for flexible electronic devices. *Adv Mater* 28:4449–4454. <https://doi.org/10.1002/adma.201503132>
 55. Rus D, Tolley MT (2018) Design, fabrication and control of origami robots. *Nat Rev Mater* 3:101–112. <https://doi.org/10.1038/s41578-018-0009-8>

Chapter 17

Modern Approach Towards Additive Manufacturing and 4D Printing: Emerging Industries, Challenges and Future Scope



Pallav Gupta, Anbesh Jamwal, Sumit Gupta, and Vijay Chaudhary

17.1 Introduction

Sustainability in manufacturing processes is very important as it helps to reduce the carbon emission levels and consumption of natural resources. The other important measures for sustainability in manufacturing are recycling, less energy consumption, process optimization, and balance in sustainability dimensions [1]. Sustainability that plays an important role in the industries results in economic as well as environmental benefits [2]. Sustainability in any manufacturing process depends on the type of operational principle of that manufacturing process. Due to some technological and other limitations, conventional manufacturing processes fail to manufacture complex shapes and maintain sustainability in manufacturing [3]. Additive manufacturing with sustainability consideration is the promising choice to solve this issue. In the last few years development in the manufacturing sector has boosted the adoption of additive manufacturing technology in place of traditional manufacturing approaches [4]. Additive manufacturing is capable to produce complex shapes without an additional process while maintaining sustainability at the same time. In the additive manufacturing process, less waste scrap is generated as compared to the traditional manufacturing processes. As well, material selection in the additive manufacturing processes helps to maintain a balance between the economic and environmental aspects of sustainability [5]. However, still fewer studies are reported about the consideration of social aspects in additive manufacturing which is still a limitation in the field of additive manufacturing. Direct metal additive manufacturing processes are the most popular area these days in the field of additive manufacturing as

P. Gupta (✉) · S. Gupta · V. Chaudhary
Department of Mechanical Engineering, A.S.E.T., Amity University Uttar Pradesh, Noida, India
e-mail: pgupta7@amity.edu

A. Jamwal
Department of Mechanical Engineering, Alakh Prakash Goyal Shimla University, Shimla,
Himachal Pradesh, India

it is capable to generate and manufacture complex 3D shapes with minimal waste by the layer-by-layer fabrication using metallic materials [6]. This process is done with the help of computer-aided design manufacturing in which the first desired shape is generated in any designing software and then layer-by-layer fabrication is done with the help of 3D printers [7]. Life cycle assessment of additive manufacturing products is also an emerging area that helps to provide the guidelines for future research that how more improvements can be done in the area of additive manufacturing [8, 9]. Unlike the traditional additive manufacturing processes in which plastic-based materials are being used for fabrication direct additive manufacturing doesn't require any secondary process for metallic material processing [10–15]. Direct metal additive manufacturing helps to reduce the lead time in manufacturing as well as carbon emission which results in balancing of sustainability dimensions. In the early stages of the direct additive manufacturing process, it is used to fabricate only the aerospace and automobile sector components which are difficult to fabricate with the conventional manufacturing processes such as casting, squeeze casting, and powder metallurgy [16–19]. However, some authors have reported about the sustainability consideration in conventional manufacturing processes and how the industries can maintain sustainability while using conventional manufacturing processes for product development [20]. Advancement in the progress of the metal and ceramic materials research area has expanded the scope of direct additive manufacturing [21]. Nowadays, it is possible to fabricate lightweight composite materials for many engineering applications with direct metal additive manufacturing [22]. The layer-by-layer fabrication of complex engineering shapes with additive manufacturing has replaced the use of the conventional manufacturing process in industries [23]. The main promising merits of direct metal additive manufacturing over other manufacturing processes are discussed below.

- (a) Less manufacturing cost as compared to traditional manufacturing processes.
- (b) Less scrap generation as compared to other manufacturing processes, e.g., casting.
- (c) Faster production rate with less waste and minimal lead times.
- (d) It is easier to generate a complex shape which is difficult to generate by other manufacturing routes.
- (e) Helps to maintain all sustainability aspects. Hence, additive manufacturing process helps to achieve sustainability in business practices.

These are some of the advantages of additive manufacturing processes over traditional manufacturing processes. In the next section, we have discussed the processing techniques for additive manufacturing and various studies carried out on additive manufacturing in the last 20 years. This will help to frame the research gaps and provide future recommendations in the area of sustainable additive manufacturing.

17.2 Fabrication Processes for Additive Manufacturing and 4D Printing

In this section of the chapter, we have discussed different fabrication approaches for additive manufacturing processes. The different processes are discussed below.

17.2.1 Sheet Lamination Process (SLP)

Sheet lamination process is widely used for fabricating additive manufacturing products. Generally, sheet lamination process consists of two types of processes: Ultrasonic consolidation processes and laminated objective manufacturing processes. In this type of process, two-dimensional approaches are used in which metal sheet cutting, joining, and assembly are the main operations. Laser and CNC cutters are used in this process with respect to the CAD model [24].

17.2.2 Binder Jet Process

Binder Jet process is used for 3D printing. In this process, metallic powders are used to generate geometry. These powders are supplied with the help of a feeder. In this process, layer-by-layer fabrication is done for the generation of shape. This layer-by-layer construction is known as the green part. In some cases, sintering operations are also done to improve the structural and mechanical properties of the final shape. In this process, layer thickness varies from 0.14 mm to 0.45 mm with a building speed of a maximum of 24 mm/hr [25].

17.2.3 Powder Bed Fusion

In the powder bed fusion process, metallic powders are used via the feeders with the energy sources having high densities. It is found that waste is less in this process as compared to other processes. Slicing data is used for the layer-by-layer construction. Repeated powder feeding helps to create the final shape of the product. The building speed of the powder bed fusion process is 5–20cm³/hr. Figure 17.1 shows the powder bed fusion process [26].

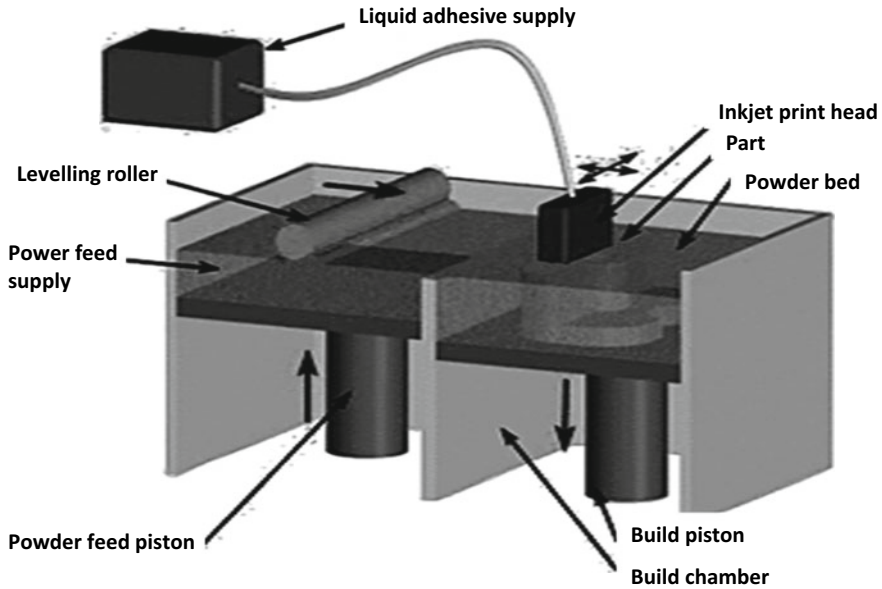


Fig. 17.1 Powder bed fusion process

17.2.4 Sintering Type Powder Bed Fusion Process

Both direct laser sintering and selective laser sintering techniques are the types used for the powder bed fusion process. In this process, the sintering process is done for the metallic powders using high-intensity lasers. Porosity for the process is around 30–35% which is having better volume densities among other processes. The working principle of this process is different from the direct metal laser sintering process. The building speed of this process is around 7 m/s which is high among other processes [27]. Figure 17.2 shows the sintering type powder bed fusion process.

17.3 Methodology

In this chapter, we have used the systematic literature review approach to map studies published in the area of additive manufacturing and sustainable additive manufacturing. Firstly, additive manufacturing practices in which review, conceptual or methodological approach being used is considered for study as it is impossible to map all the studies published in this area. The flowchart for the present study is discussed in Fig. 17.3:

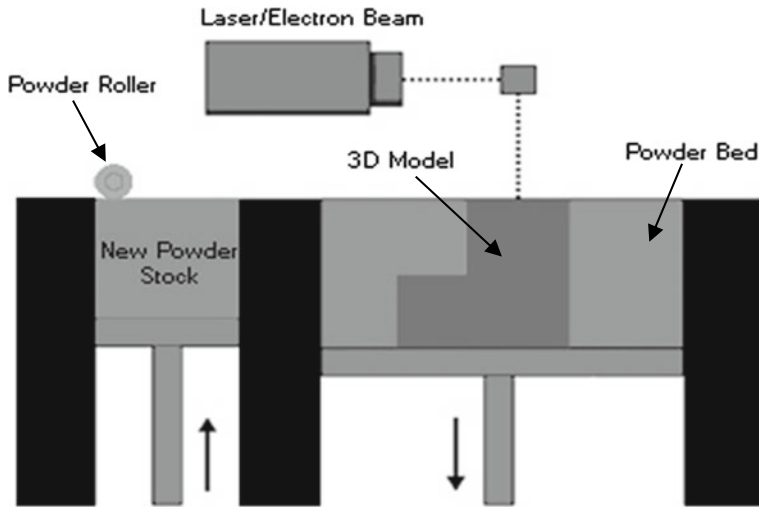


Fig. 17.2 Sintering type powder bed fusion process

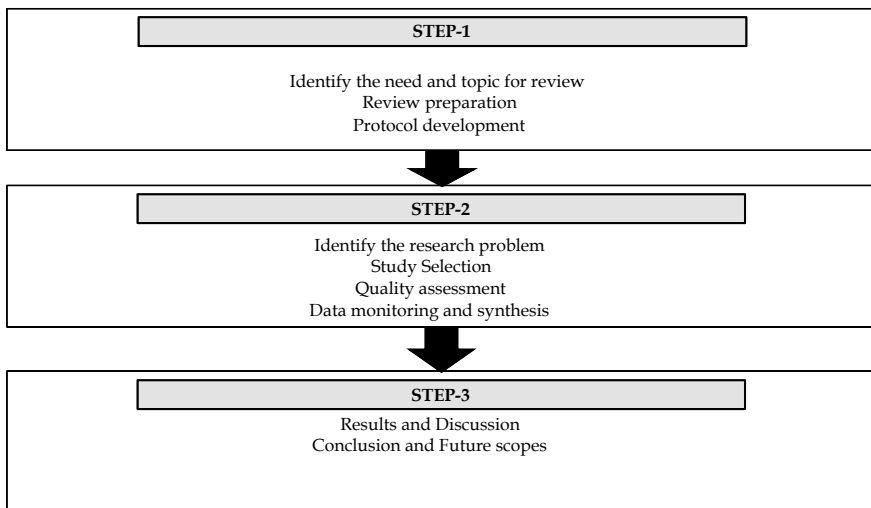


Fig. 17.3 Flow chart for study

17.4 Literature Review

In this book chapter, we have considered the previously published articles from reputed Journals/Conference series. The papers were extracted from the Google Scholar database. Google Scholar is the largest database which is having different types of article collection. By keeping quality work in our mind, we have only

considered articles from reputed publishers which are either indexed in the Scopus database or Web of Science database. Further, Table 17.1 represents the sources considered for the present work.

17.4.1 Top Authors Working on Sustainable Additive Manufacturing

From the dataset extracted from the Google Scholar database, we have found the top authors working in the area of sustainable additive manufacturing. In any research area, it is important to find the top contributors as it helps to map the studies in a particular research area in a better way. Table 17.1 shows the top 10 authors working on sustainable additive manufacturing. We found that “Priarone, P. C.” is the top contributor in this area with 8 publications which is followed by “Haapala, K. R.” and “Despeisse, M.” with 7 and 6 publications, respectively. Further, the remaining authors with their total publications in this area are shown in Table 17.1.

Table 17.1 Top Authors working in the area of sustainable additive manufacturing

Name of author	Total publications	Research area explored
Priarone, P. C.	8	Re-designing in additive manufacturing, Metal additive manufacturing, Energy efficiency modeling, Fused deposition modeling
Haapala, K. R.	7	Subtractive manufacturing, Environmental performance, Direct metal laser sintering, Energy efficiency, Impact assessment
Despeisse, M.	6	Resource efficiency, Sustainability issues, Value roadmaps, Circular economy, Impact assessment
Settineri, L.	6	Machining processes, Re-designing in additive manufacturing, Human health risks assessment, Energy efficiency
Junk, S.	5	Sustainable designing, Topology, Optimization, Lightweight designing, Additive fillers
Kellens, K.	5	Energy efficiency, Resource efficiency, Environmental assessment, Energy modeling
Kerbrat, O.	5	Sustainability, Predictive modeling, Selection methods, Customized tool
Li, L.	5	Environmental sustainability, Energy consumption, Machine learning approaches, Resource consumption
Li, T.	5	Cost analysis, Energy analysis, Impact assessment, Metal additive manufacturing, Health risk assessment
Liverani, A.	5	Sustainable designing, Metal additive manufacturing, Additive fillers, Risk assessment

17.4.2 Top Cited Articles in Sustainable Additive Manufacturing

It is impossible to access all the available literature for policymakers and academia. To better understand any particular research topic, it is necessary to read the quality articles. The no. of total citations on a particular article defines its quality. In this chapter, we have identified the top-cited articles in sustainable additive manufacturing which will help to understand the additive manufacturing concepts and the role of sustainability in this area. The topmost cited articles are shown in Table 17.2.

17.4.3 Top Countries Working on Sustainable Additive Manufacturing

In this study, we have identified the studies done in the different countries to investigate the research progress on additive manufacturing in different regions of the world. The top 10 countries working on sustainable additive manufacturing are shown in Table 17.3. It can be seen that the United States has most of the publications in this area which is followed by Germany. The reason is that, the United States and Germany are working on the Industry 4.0 implementation and additive manufacturing which is considered as a key technology for the adoption of Industry 4.0 practices. In the top 10 countries, we have found that only two developing nations China and India are working on sustainable additive manufacturing technologies.

17.4.4 Institute-Wise Research Progress in Sustainable Additive Manufacturing

In the institute-wise research progress, we have found that a total of 142 institutes from the different regions of the world are working on sustainable additive manufacturing. Most of the institutes are from the developed countries and are working collaboratively to promote the research area of sustainable additive manufacturing. In the top 10 institutes, “Politecnico di Torino” is the most active institute in this research area with 14 publications followed by “Cardiff University” with 10 publications. The remaining institutes with their total publications are listed in Table 17.4.

17.4.5 Journal-Wise Distribution

Journal-wise distribution of articles helps the authors to find the most productive journals in the particular research area. Also, this distribution helps to decide which

Table 17.2 Top 5 cited articles on sustainable additive manufacturing

Article Title	Name of Journal	Total citations	Research findings
“Additive manufacturing and sustainability: an exploratory study of advantages and challenges”	Journal of Cleaner Production	306	Additive manufacturing is creating opportunities for sustainability by improving closed-loop material flow and energy efficiency. Industries are focusing on eco-design and process design for additive manufacturing
“Additive manufacturing: A framework for implementation”	International Journal of Production Economics	284	Implementation of additive manufacturing practices affected by economic and environmental-related factors. Impact assessment is an emerging research area in additive manufacturing
“A wafer-based monocrystalline silicon photovoltaics road map: utilizing known technology improvement opportunities for further reductions in manufacturing costs”	Solar Energy Materials and Solar Cells	220	Opportunities for high-power solar cell are discussed. Advanced cell architecture needs initial investment and higher material costs
“Life cycle economic analysis of distributed manufacturing with open-source 3D printers”	Mechatronics	185	Open-source additive manufacturing printers help to promote the distributed manufacturing. With the ReRaps approach, half of the products can be manufactured in minimum time
“A comparison of energy consumption in bulk-forming, subtractive, and additive processes: Review and case study”	International Journal of Precision Engineering and Manufacturing-Green Technology	147	Energy consumption modeling is discussed. It is found that additive manufacturing techniques require less operational energy as compared to traditional manufacturing approaches

Table 17.3 Top Countries working on sustainable additive manufacturing

Name of Country	No. of Publications	Research areas explored
United States	179	Life cycle assessment of 3D printing, Recyclable polymers for additive manufacturing, Polylactic acids, and Biological fillers for additive manufacturing
Germany	68	Mechanical and other properties, 3D printing for membranes, Life cycle assessment, Metal additive manufacturing
United Kingdom	63	Life cycle assessment, Membrane development for water technologies, Life cycle analysis, Manufacturing, and characterization
Italy	58	Life cycle analysis, Impact assessment, Metal additive manufacturing, Process route developments, Automobile applications
China	50	Toys industry, Additive fillers, Manufacturing and characterization, Healthcare products, Architectural engineering, Energy consumption
India	45	Manufacturing and characterization, Impact assessment, Cost analysis, 3D designing, Product development for medical applications
France	27	Impact assessment, Sustainable material design, Metal additive manufacturing
Netherlands	22	Healthcare products, Engineering tools, Automobile, and Aerospace components development
Australia	21	Life cycle assessment, Metal additive manufacturing, Additive fillers, Mechanical characterization
Canada	21	Impact assessment, Material designing, Energy consumption

journal is suitable and matching their scope of work. “Journal of Cleaner Production” is the most productive journal with 36 articles followed by “Procedia CIRP” with 27 articles. Top 10 journal with their total publications in this area is shown in Table 17.5.

17.4.6 Top Keywords in Sustainable Additive Manufacturing

Keyword analysis helps to find new research areas. In most of the studies, keywords cluster analysis has been done to find the new research themes in the particular research area. In this study, we have identified the most used keywords in sustainable additive manufacturing. It is found that “3D Printers” is mostly used keyword with 342 occurrences followed by “Sustainable Development” with 297 occurrences. The remaining top keywords used in articles are shown in Table 17.6 with their occurrence.

Table 17.4 Top institutes working on sustainable additive manufacturing

Name of the Institute	Total Publications	Key Research areas explored
Politecnico di Torino	14	Metal additive manufacturing, Mechanical characterization
Cardiff University	10	Life cycle analysis, Metal additive manufacturing
CNRS Centre National de la Recherche Scientifique	9	Additive fillers, Sustainable routes for manufacturing, 3D designing, Healthcare applications
Oregon State University	9	Energy consumption modeling, Construction engineering, Metal additive manufacturing
Politecnico di Milano	9	Additive fillers, Manufacturing and characterization, Healthcare products, Architectural engineering, Energy consumption
The Ohio State University	9	Aerospace component development, Mechanical and environmental characterization, Process route development
University of California	8	Impact assessment, Energy cost analysis, Energy consumption modeling
Ku Leuven	8	Sustainable material design, Metal additive manufacturing
Alma Mater Studiorum, Universiti di Bologna	8	Manufacturing and characterization, Impact assessment, Product development for medical applications
Carnfield University	7	3D membranes for water technologies, Health care products, Process development

17.4.7 Content Analysis Based on Different Research Areas in Sustainable Additive Manufacturing

In industries from economic perspective sustainable additive manufacturing is highlighted in many studies. In past years, several authors have discussed the consideration of economic aspects of additive manufacturing. The Binder jet process is compared with the traditional manufacturing processes in studies. It is found that additive manufacturing processes with sustainability consideration consumes less energy as compared to other processes. It also helps to reduce the carbon emission levels generated from the different types of processes. The main characteristics of sustainable additive manufacturing are flexibility, minimal assembly operations, and complexity. Some studies have highlighted the use of cost analysis in their studies which indicates that Polyjet Printers have higher operating costs as compared to

Table 17.5 Journal-wise distribution of articles

Journal Name	Total no. of publications	Research areas highlighted
Journal of Cleaner Production	36	Selective laser sintering, Environmental assessment, Mechanical behavior, Energy efficiency models
Procedia CIRP	27	Aerospace industries, Laser powder bed fusion, Impact assessment, Total life cycle, Eco-designing
Procedia Manufacturing	23	Designing methods, Cost models, Impact assessment, Bio-inspired product designing, Simulations, Process development
Rapid Prototyping Journal	10	Decision-making approaches in metal additive manufacturing, Laser sintering, Process development, Sustainable designing
International Journal of Advanced Manufacturing Technology	8	Impact assessment, Life cycle analysis, Energy consumption models, Manufacturing, and characterization
ACS Sustainable Chemistry and Engineering	8	Impact assessment, Bio fillers, Additive filler development, Characterization
Additive Manufacturing	7	Process routes, Characterization, Fillers, Impact assessment, Simulations, Product designing
Construction and Building Materials	7	Construction materials, Additives for social use, Impact assessment, Cost analysis
International Journal of Precision Engineering and Manufacturing Green Technology	3	Metal additive 3D printing, Energy consumption models, Life cycle assessment, Process development
Journal of Intelligent Manufacturing	3	Process development, Energy cost analysis, Manufacturing and characterization, Product designing

other 3D printers. Now the industries are more focused on the adoption of FDM parts due to its lower operating and maintenance costs. It can be concluded that rapid prototyping manufacturing processes are the most economical processes for household item production. As a large number of research articles are available on sustainable additive manufacturing so we have considered articles only from reputed

Table 17.6 Top keywords in sustainable additive manufacturing

Most highlighted keywords	Keyword occurrence
3D printers	342
Sustainable development	297
Additive manufacturing	264
Additives	155
Sustainability	101
Life cycle	92
Environmental impact	69
Industrial research	60
Product design	59
Energy utilization	54

Publishers/Journals for content analysis. Table 17.7 shows the list of sources that have been considered for the content analysis.

Table 17.7 Journal considered for content analysis

Journal name	No. of papers considered in the study
Additive Manufacturing	10
Journal of Cleaner Production	8
Materials Today: Proceedings	8
Rapid Prototyping Journal	6
Physics Procedia	6
International Journal of Rapid Manufacturing	5
Journal of Engineering Manufacture	5
International Journal of Precision Engineering and Manufacturing Green Technology	5
CIRP Annals-Manufacturing Technology	4
Materials MDPI	3
Procedia Manufacturing	3
IOP Science conference series	3
CIRP Journal of Manufacturing Science and Technology	2
Procedia CIRP	2
Development	2
Energy Policy	2
Materials Today Communication	2
Virtual and physical prototyping	2
Mechatronics	1

The different studies which report about the consideration of economic aspects of additive manufacturing are discussed below.

The first study on the economic aspects was found in 2013 in which Wittbrodt et al. discussed the consideration of total cost and operation cost of the final fabricated product by additive manufacturing. In this study other costs like total energy consumption cost, time invested in the fabrication and filament costs were also considered. It is found that additive manufacturing processes are economical for the fabrication of household items [29]. In 2014, Gebler et al. considered the three sustainability aspects for additive manufacturing. The literature review considered from various databases leads to qualitative evolution. In the sustainability aspects, the main focus was on environmental and economic aspects rather than the social aspects. In the mathematical model, they have considered the GHG emission, total production cost, and total energy consumed in the fabrication. It is found that additive manufacturing processes have the potential to minimize carbon emission levels [30]. We found two studies from 2015 which report the economic consideration in additive manufacturing. Among them, Lindemann et al. developed an economic model for part selection of engineering needs with economic considerations. Economic aspects with their limitations in additive manufacturing were discussed in the study. It is concluded that economic aspects play an important role in part selection for additive manufacturing. It is also concluded that the proposed model can be used in different industry sectors [31]. In another study of economic aspects, Weller et al. investigated the various types of impacts and emissions generated from the additive manufacturing processes in an industry. Economic-based model for additive manufacturing is proposed with its characteristics and limitations. It is found that additive manufacturing processes are economical in nature, and it reduces the human efforts in assembly operations and minimizes the emissions to the environment [32]. In another study, Li et al. 2017 considers the economic aspects to identify the economic conditions for installed printers in manufacturing industries. In this study, cost analysis method is used with 99 indicators. It is concluded in the study that the FDM technique is suitable for economic aspects as compared to PolyJet Printers, but a better surface finish is found in PolyJet Printers [33]. Similarly in another study, Khorram et al. consideration has been made towards economic sustainability. Drivers for the additive manufacturing process are found in comparison to traditional manufacturing processes. Survey analysis is also done to assess the impact of drivers in manufacturing industries. It is found that additive manufacturing processes are only suitable for low volume production rather than high volume production [34]. These are some of the studies which discuss the consideration of economic aspects in the additive manufacturing processes.

17.5 Studies on Environmental Perspectives in Sustainable Additive Manufacturing

17.5.1 Energy Consumption-Related Studies

In industries from an environmental perspective sustainable additive manufacturing is highlighted in many studies. In past years several authors have discussed the consideration of environmental aspects of additive manufacturing.

The different studies which report about the consideration of economical aspects of additive manufacturing are discussed below.

From the environmental perspective, we have identified energy consumption-related studies in which environmental-related factors are considered. The first study was found in 2006 in which Mognol et al. investigated the role of environmental aspects in sustainable additive manufacturing. In the study, a part is fabricated with different positions and orientations. Total electricity consumption used in the fabrication process is noted down. In the study, specific recommendations were given to minimize the total energy consumption. It is found that with the reduction in total energy consumption, total production time in the fabrication process is also reduced [35]. Similarly, in 2011, Baumers et al. considered the total energy consumption in sustainable additive manufacturing processes on laser sintering process and found that energy consumption in additive manufacturing is dependent on the total production time [36]. Junk et al. investigated the effect of energy consumption variables on additive manufacturing and concluded that the FLM process requires more energy consumption for fabrication in comparison to the 3DP process [37]. Meteyer et al. proposed a mathematical model to evaluate the total energy consumption in which the binder jet process is used to fabricate the part. It is concluded that the proposed model can be beneficial for industries to estimate the total energy consumption and total cost of fabrication. However, we have also found some studies related to metal production in sustainable additive manufacturing [38]. In 2018, Jackson et al. proposed a mathematical model to calculate total energy consumption in metal additive manufacturing. It is found that during the fabrication process wire-based processes require less energy as compared to other manufacturing processes which helps to maintain sustainability [39]. One more study highlights the consideration of energy variables in the additive manufacturing processes. In another study, Liu et al. studied the effect of total energy consumption in metal additive manufacturing. In the study, life cycle assessment of fabricated parts is also done to calculate the environmental impacts due to electricity consumption [40].

17.5.2 Design Aspect-Related Studies

In the other studies, we have identified studies related to design optimization in sustainable additive manufacturing. In this area, we have considered one study which

considers the design aspects to maintain environmental sustainability in additive manufacturing. In 2010, Hao et al. investigated the role of design parameters in some experimental studies done for additive manufacturing. It is found that products fabricated with sustainability consideration are based on specific design parameters which are light in weight as compared to traditional manufacturing processes. It is also found that less energy is consumed as compared to other techniques [41].

17.5.3 Environmental Aspect-Related Studies

In environmental-related studies, various authors have compared different additive manufacturing processes, i.e., EBM, SLS, and 3DP.

In these studies, the use of regression modeling is also reported to find the interrelationship between the different variables related to the production time and design variables. It is also found that better decision support systems in additive manufacturing processes help to reduce the environmental impacts. In future studies, MCDM techniques, i.e., AHP [42], Fuzzy-AHP [43], ANP [44], ISM [45], and other techniques can be used to prioritize the different attributes. We have found 4 related studies to this area which are discussed below.

The first study in this area is found in 1999 where Luo et al. have proposed a conceptual model based on different additive manufacturing strategies in rapid prototyping technologies. Each process in this study is divided into the different life cycle stages which helps to calculate the environmental impact generated at each stage of the fabrication process. It is concluded that the proposed model can be used to compare the different rapid prototyping processes to assess the environmental impacts [46]. In 2006, Drizo et al. reviewed the different environmental impacts generated from the additive manufacturing processes. Various evaluation methods of environmental impacts are discussed based on available literature survey. Harmful effects from these environmental issues are also discussed in the study with some barriers [47]. In 2016, Vimal et al. investigated a study on the selection of environmental conscious rapid prototyping processes without reduction in the structural and mechanical properties. A model is built, based on analytical network process and fuzzy logic [48]. In 2018, Garcia et al. investigated the environmental sustainability concepts in additive manufacturing processes. With the literature survey, it is found that most of the studies have been found in the area of energy consumption and life cycle assessment. Advantages and limitations of additive manufacturing processes as compared to other manufacturing processes are also discussed with the help of a comprehensive literature survey [49].

17.5.4 Life Cycle Assessment-Related Studies

Life cycle assessment plays an important role in additive manufacturing. It is essential to assess the various environmental impacts generated from additive manufacturing processes. These impacts can be generated from the cutting fluids, material consumption, and waste material generation. In the past few years, various studies have been done in additive manufacturing which reports about the use of Life cycle assessment in additive manufacturing to assess the environmental impacts. These studies are discussed below.

The first study on Life cycle assessment in sustainable additive manufacturing is reported in 2010 where Sreenivsan et al. investigated the environmental impacts of additive manufacturing processes with life cycle assessment. The data is collected for the total energy consumed in the fabrication process in the additive manufacturing industry. Life cycle assessment is done to assess the environmental impacts of the additive manufacturing process. It is found that the SLS process is having less emission generation during the fabrication process as compared to other processes [50]. In 2013, Kreiger et al. assess the environmental impacts with the life cycle assessment for a product fabricated with the 3D printer. Two processes are compared in the study to assess the environmental impacts. It is found that the direct metal additive manufacturing process is having lesser environmental impacts as compared to the 3DP process [51]. In 2015, Burkhart et al. assessed the environmental impacts of the additive manufacturing process in an additive manufacturing industry. A framework is proposed to the manufacturing industry based on life cycle assessment to reduce the environmental impacts. In the study powder bed fusion process and other processes were compared to assess the environmental impacts. It is found that the powder bed fusion process has few carbon emission levels as compared to other processes [52]. In 2016, Paris et al. investigated the environmental impacts through LCA for both traditional manufacturing processes and additive manufacturing processes. The study of turbine manufacturing is considered in a turbine manufacturing industry. A LCA-based framework is proposed to assess the environmental impacts. It is found that energy consumption plays an important role in the development of additive manufacturing research areas [53]. In 2017, Paris and Mandil proposed LCA-based framework for a product manufactured by additive manufacturing process without considering the recycling phase. A study on both conventional and traditional manufacturing processes is compared with additive manufacturing processes. It is found that a combined approach of traditional manufacturing and additive manufacturing will be beneficial to reduce the environmental impacts [54]. Similarly, Kafara et al. investigated the environmental emissions from sustainable additive manufacturing with LCA. Life cycle assessment is done for the four different phases of the fabrication of a product. It is concluded that additive manufacturing processes are more economical and produce fewer emissions as compared to traditional manufacturing processes [55]. In 2018, Ma et al. proposed a life cycle assessment-based model for manufacturing industries in which environmental assessment of sustainable 3D parts is done with GABi software. It is found that additive manufacturing processes

produce fewer emissions and is more economical than other manufacturing routes. It is also concluded that this process is suitable for aluminum alloys in generating complex shapes with sustainability considerations. These are some studies that report the consideration of life cycle assessment-based models in additive manufacturing processes [56].

17.6 Application Areas of Additive Manufacturing

During the evolution of additive manufacturing, no one thought that this technology will revolutionize the industries to the next industrial shift. The advancements in rapid prototyping technologies have accelerated the adoption of additive manufacturing technologies in the present time [57–61]. There are some main application areas of additive manufacturing products which are discussed below.

17.6.1 *Aerospace Applications*

Additive manufacturing products are widely used in the aerospace industries due to its ability to fabricate complex shapes with metals, e.g., titanium. Additive manufacturing technologies have increased the productivity of aerospace industries in the last few years. The key contributions of additive manufacturing to aerospace industries are discussed below.

1. Product lead time has decreased by 30–70% by using additive manufacturing technologies in aerospace industries [62].
2. It helps to reduce the manufacturing cost as compared to traditional manufacturing processes by 45%.

Figure 17.4 shows the different application areas of additive manufacturing in aerospace industries.

17.6.2 *Medical Applications*

Additive manufacturing technologies are also used in medical applications. Complex anatomical parts can be easily manufactured by additive manufacturing technologies [63]. Also, this technology has helped during the COVID-19 for ventilator and gloves manufacturing [64–68]. There are many other application areas in medical engineering that make additive manufacturing promising technology for the fabrication of products. Figure 17.5 shows the application of additive manufacturing in the medical sector.



Fig. 17.4 Aerospace applications of additive manufacturing

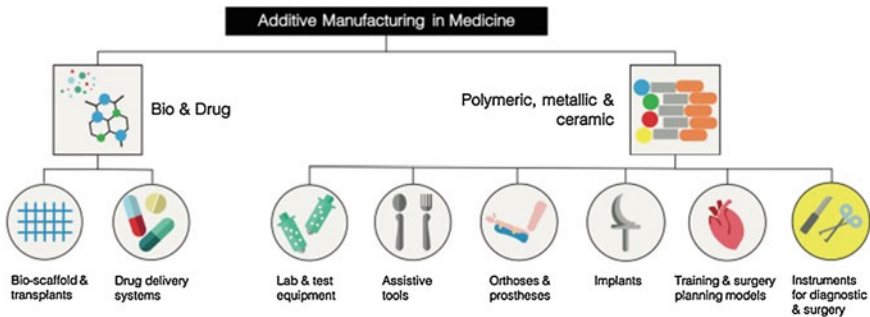


Fig. 17.5 Application of additive manufacturing in the medical sector

17.6.3 Architectural Applications

As we know that the architecture and jewelry industry has been changed in the last few years. Now the customers are focusing on the customized products which require high manual operations and efforts [69]. It also consumes a lot of time for complex shapes generation. But the use of additive manufacturing technologies has changed the market scenario by reducing the costs and time [70].

17.7 Research Gaps and Future Scope

Additive manufacturing technologies are still facing many challenges from both business and technical points of view. These challenges are discussed below.

17.7.1 Business Challenges for Additive Manufacturing Technology

1. Generally, additive manufacturing technologies are having higher machine costs as compared to the traditional manufacturing processes. These processes are suitable only for customized batch production or prototype development.
2. In additive manufacturing processes, the processing cost and material costs are relatively high as compared to traditional manufacturing processes.
3. Additive manufacturing is the emerging technology of Industry 4.0 which requires an initial investment for technology. Availability of required machines with adequate technology integration is a major problem in developing nations.

These are some of the challenges for additive manufacturing adoption in developing economies from the business point of view.

17.7.2 Challenges Related to the Technical Perspective

There are some of the technical challenges on which industries are still struggling. The major challenges related to the technical perspective are as follows:

1. Generally, the fabrication methods for the additive manufacturing processes are different from the traditional manufacturing processes which require advanced technological solutions and methods.
2. Each fabrication method is only suitable with a different machine or 3D printers which influence the adoption of additive manufacturing practices.
3. Metallic powders used for fabrication of product is highly influencing factor. It is found that the quality of metallic powder influences the mechanical and structural properties of additive manufacturing products.

We found that very few studies are related to the consideration of social perspective in additive manufacturing. Although additive manufacturing is indeed the key technology for the adoption of Industry 4.0 practices, to maintain sustainability in the business practices it is necessary to balance all the aspects of sustainability in the business practices. Social and environmental perspectives are still an emerging research area in additive manufacturing because very few studies have been found in this area. A detailed survey on the development of sustainability index is still a limitation and emerging research area that can be explored in future studies.

Sustainable model development for material consumption, energy consumption, and environmental impacts can be addressed in future studies for different fabrication processes.

17.8 Conclusion

In the present chapter, we have followed the comprehensive literature survey methodology for mapping the research progress of the additive manufacturing or sustainable additive manufacturing processes. In this study, we have considered the Google Scholar database for the article extraction. 3D printing technology for printing 3D objects has become popular which is based on the controlled layer deposition of printable materials. The development in additive manufacturing in the last two years has made several research scopes in the development of Industry 4.0. 4D printing allows a user to build a shape by integrating the dimensions of time. The development in synthetic smart materials, deformation mechanisms, novel printers, and mathematical modeling has enhanced the research area of 4D printing. We found that a detailed survey on the development of sustainability index is still a limitation and emerging research area that can be explored in future studies. Also, in the present study, we have considered a limited number of articles for the systematic literature review which can be extended by addressing the bibliometric analysis and considering the major databases like Scopus and Web of sciences in future studies. Sustainable model development for material consumption, energy consumption, and environmental impacts can be addressed in future studies for different fabrication processes.

References

1. Jamwal A, Agrawal R, Gupta S, Dangayach GS, Sharma M, Sohag MAZ (2020) Modelling of sustainable manufacturing barriers in pharmaceutical industries of Himachal Pradesh: an ISM-Fuzzy Approach. In: Proceedings of international conference in mechanical and energy technology. Springer, Singapore, pp 157–167
2. Jamwal A, Agrawal R, Sharma M, Dangayach GS, Gupta S (2021) Application of optimization techniques in metal cutting operations: a bibliometric analysis. *Mater Today: Proc* 38(1):365–370
3. Panda B, Paul SC, Hui LJ, Tay YWD, Tan MJ (2017) Additive manufacturing of geopolymer for sustainable built environment. *J Clean Prod* 167:281–288
4. Diegel O, Singamneni S, Reay S, Withell A (2010) Tools for sustainable product design: additive manufacturing. *J Sustain Dev* 3(3):68–75
5. Sanchez-Rexach E, Johnston TG, Jehanno C, Sardon H, Nelson A (2020) Sustainable materials and chemical processes for additive manufacturing. *Chem Mater* 32(17):7105–7119
6. Vidakis N, Petousis M, Maniadi A, Koudoumas E, Vairis A, Kechagias J (2020) Sustainable additive manufacturing: mechanical response of acrylonitrile-butadiene-styrene over multiple recycling processes. *Sustainability* 12(9):3568

7. Godina R, Ribeiro I, Matos F, Ferreira B T, Carvalho H, Peças P (2020) Impact Assessment of Additive Manufacturing on Sustainable Business Models in Industry 4.0 Context. *Sustainability* 12(17):7066
8. Jamwal A, Mittal P, Agrawal R, Gupta S, Kumar D, Sadasivuni KK, Gupta P (2020) Towards sustainable copper matrix composites: manufacturing routes with structural, mechanical, electrical and corrosion behaviour. *J Compos Mater* 54(19):2635–2649
9. Majeed A, Zhang Y, Ren S, Lv J, Peng T, Waqar S, Yin E, A big data-driven framework for sustainable and smart additive manufacturing. *Robot Comput-Integr Manuf* 67:102026
10. Nayim STI, Hasan MZ, Seth PP, Gupta P, Thakur S, Kumar D, Jamwal A (2020) Effect of CNT and TiC hybrid reinforcement on the micro-mechano-tribobehaviour of aluminium matrix composites. *Mater Today: Proc* 21(3):1421–1424
11. Kumar A, Arafath MY, Gupta P, Kumar D, Hussain CM, Jamwal A (2020) Microstructural and mechano-tribological behavior of Al reinforced SiC–TiC hybrid metal matrix composite. *Mater Today: Proc* 21(3):1417–1420
12. Sohag MAZ, Gupta P, Kondal N, Kumar D, Singh N, Jamwal A (2020) Effect of ceramic reinforcement on the microstructural, mechanical and tribological behavior of Al–Cu alloy metal matrix composite. *Mater Today: Proc* 21(3):1407–1411
13. Jamwal A, Seth PP, Kumar D, Agrawal R, Sadasivuni KK, Gupta P (2020) Microstructural, tribological and compression behaviour of Copper matrix reinforced with Graphite–SiC hybrid composites. *Mater Chem Phys* 251:123090
14. Jamwal A, Prakash P, Kumar D, Singh N, Sadasivuni KK, Harshit K, Gupta P (2019) Microstructure, wear and corrosion characteristics of Cu matrix reinforced SiC–graphite hybrid composites. *J Compos Mater* 53(18):2545–2553
15. Bandil K, Vashisth H, Kumar S, Verma L, Jamwal A, Kumar D, Gupta P (2019) Microstructural, mechanical and corrosion behaviour of Al–Si alloy reinforced with SiC metal matrix composite. *J Compos Mater* 53(28–30):4215–4223
16. Tamjid E, Bohloulou M, Mohammadi S, Alipour H, Nikkhah M (2020) Sustainable drug release from highly porous and architecturally engineered composite scaffolds prepared by 3D printing. *J Biomed Mater Res, Part A* 108(6):1426–1438
17. Garg P, Jamwal A, Kumar D, Sadasivuni KK, Hussain CM, Gupta P (2019) Advance research progresses in aluminium matrix composites: manufacturing and applications. *J Mater Res Technol* 8(5):4924–4939
18. Nayim STI, Hasan MZ, Jamwal A, Thakur S, Gupta S (2019) Recent trends & developments in optimization and modelling of electro-discharge machining using modern techniques: a review. In: *AIP conference proceedings*, vol 2148, No. 1. AIP Publishing LLC, p. 030051
19. Rocheton B, Segonds F, Laverne F, Hesam PN, A human centered sustainable additive manufacturing tool for early design stages. *Comput-Aided Des Appl* 18(2):258–271
20. Melugiri-Shankaramurthy B, Sargam Y, Zhang X, Sun W, Wang K, Qin H (2019) Evaluation of cement paste containing recycled stainless steel powder for sustainable additive manufacturing. *Constr Build Mater* 227:116696
21. Agrawal R, Vinodh S (2019) State of art review on sustainable additive manufacturing. *Rapid Prototyp J* 25(6):1045–1060
22. Singh R, Kumar R, Farina I, Colangelo F, Feo L, Fraternali F (2019) Multi-material additive manufacturing of sustainable innovative materials and structures. *Polymers* 11(1):62
23. Agrawal R, Vinodh S (2019) Application of total interpretive structural modelling (TISM) for analysis of factors influencing sustainable additive manufacturing: a case study. *Rapid Prototyp J* 25(7):1198–1223
24. Wong KV, Hernandez A (2012) A review of additive manufacturing. *Int Sch Res Not*, Article ID 208760
25. Frazier WE (2014) Metal additive manufacturing: a review. *J Mater Eng Perform* 23(6):1917–1928
26. Ngo TD, Kashani A, Imbalzano G, Nguyen KT, Hui D (2018) Additive manufacturing (3D printing): a review of materials, methods, applications and challenges. *Compos B Eng* 143:172–196

27. Singh S, Ramakrishna S, Singh R (2017) Material issues in additive manufacturing: a review. *J Manuf Process* 25:185–200
28. Huang SH, Liu P, Mokasdar A, Hou L (2013) Additive manufacturing and its societal impact: a literature review. *Int J Adv Manuf Technol* 67(5–8):1191–1203
29. Wittbrodt BT, Glover AG, Laureto J, Anzalone GC, Oppliger D, Irwin JL, Pearce JM (2013) Life-cycle economic analysis of distributed manufacturing with open-source 3-D printers. *Mechatronics* 23(6):713–726
30. Gebler M, Uiterkamp AJS, Visser C (2014) A global sustainability perspective on 3D printing technologies. *Energy Policy* 74:158–167
31. Lindemann C, Reiher T, Jahnke U, Koch R (2015) Towards a sustainable and economic selection of part candidates for additive manufacturing. *Rapid Prototyp J* 21(2):216–227
32. Weller C, Kleer R, Piller FT (2015) Economic implications of 3D printing: Market structure models in light of additive manufacturing revisited. *Int J Prod Econ* 164:43–56
33. Li Y, Linke BS, Voet H, Falk B, Schmitt R, Lam M (2017) Cost, sustainability and surface roughness quality—a comprehensive analysis of products made with personal 3D printers. *CIRP J Manuf Sci Technol* 16:1–11
34. Niaki MK, Nonino F, Palombi G, Torabi SA (2019) Economic sustainability of additive manufacturing. *J Manuf Technol Manag* 30(2):353–365
35. Mognol P, Lepicart D, Perry N (2006) Rapid prototyping: energy and environment in the spotlight. *Rapid Prototyp J* 12(1):26–34
36. Baumers M, Tuck C, Bourell DL, Sreenivasan R, Hague R (2011) Sustainability of additive manufacturing: measuring the energy consumption of the laser sintering process. *Proc Inst Mech Eng, Part B: J Eng Manuf* 225(12):2228–2239
37. Junk S, Côté S (2012) A practical approach to comparing energy effectiveness of rapid prototyping technologies. In: *Proceedings of AEPR'12, 17th European forum on rapid prototyping and manufacturing*
38. Meteyer S, Xu X, Perry N, Zhao YF (2014) Energy and material flow analysis of binder-jetting additive manufacturing processes. *Procedia Cirp* 15:19–25
39. Jackson MA, Van Asten A, Morrow JD, Min S, Pfeifferkorn FE (2018) Energy consumption model for additive-subtractive manufacturing processes with case study. *Int J Precis Eng Manuf-Green Technol* 5(4):459–466
40. Liu ZY, Li C, Fang XY, Guo YB (2018) Energy consumption in additive manufacturing of metal parts. *Procedia Manuf* 26:834–845
41. Hao L, Raymond D, Strano G, Dadbakhsh S (2010) Enhancing the sustainability of additive manufacturing. In: *5th international conference on responsive manufacturing - green manufacturing (ICRM 2010)*. pp 390–395
42. Gautam N, Ojha MK, Swain P, Aggarwal A, Jamwal A (2019) Informal investigation of fourth-party and third-party logistics service providers in terms of Indian context: an AHP approach. In: *Advances in industrial and production engineering* Springer, Singapore, pp 405–413
43. Singh PL, Sindhwani R, Dua NK, Jamwal A, Aggarwal A, Iqbal A, Gautam N (2019) Evaluation of common barriers to the combined lean-green-agile manufacturing system by two-way assessment method. In: *Advances in industrial and production engineering*. Springer, Singapore, pp 653–672
44. Jamwal A, Patidar A, Agrawal R, Sharma M (2020) A fuzzy multicriteria methodology for selection among solar PV adoption barriers in India. In: *Electronic systems and intelligent computing*. Springer, Singapore, pp 521–531
45. Sohag MAZ, Kumari P, Agrawal R, Gupta S, Jamwal A (2020) Renewable energy in bangladesh: current status and future potentials. In: *Proceedings of international conference in mechanical and energy technology*. Springer, Singapore, pp 353–363
46. Luo Y, Leu MC, Ji Z (1999) Assessment of environmental performance of rapid prototyping and rapid tooling processes. In: *Proceedings of solid freeform fabrication symposium*, pp 783–792
47. Drizo A, Pegna J (2006) Environmental impacts of rapid prototyping: an overview of research to date. *Rapid Prototyp J* 12(2):64–71

48. Vimal KEK, Vinodh S, Brajesh P, Muralidharan R (2016) Rapid prototyping process selection using multi criteria decision making considering environmental criteria and its decision support system. *Rapid Prototyp J* 22(2):225–250
49. Garcia FL, da Silva Moris VA, Nunes AO, Silva DAL (2018) Environmental performance of additive manufacturing process—an overview. *Rapid Prototyp J* 24(7):1166–1177
50. Sreenivasan R, Bourell D (2010) Sustainability study in selective laser sintering- an energy perspective. *Minerals, Metals and Materials Society/AIME*, 420 Commonwealth Dr., P. O. Box 430 Warrendale PA 15086 USA.[np]
51. Kreiger M, Pearce JM (2013) Environmental life cycle analysis of distributed three-dimensional printing and conventional manufacturing of polymer products. *ACS Sustain Chem Eng* 1(12):1511–1519
52. Burkhart M, Aurich JC (2015) Framework to predict the environmental impact of additive manufacturing in the life cycle of a commercial vehicle. *Procedia Cirp* 29:408–413
53. Paris H, Mokhtarian H, Coatanéa E, Museau M, Ituarte IF (2016) Comparative environmental impacts of additive and subtractive manufacturing technologies. *CIRP Ann* 65(1):29–32
54. Paris H, Mandil G (2017) Environmental impact assessment of an innovative strategy based on an additive and subtractive manufacturing combination. *J Clean Prod* 164:508–523
55. Kafara M, Süchting M, Kemnitzer J, Westermann HH, Steinhilper R (2017) Comparative life cycle assessment of conventional and additive manufacturing in mold core making for CFRP production. *Procedia Manuf* 8:223–230
56. Ma J, Harstvedt JD, Dunaway D, Bian L, Jaradat R (2018) An exploratory investigation of additively manufactured product life cycle sustainability assessment. *J Clean Prod* 192:55–70
57. Dalawai SP, Aly MAS, Latthe SS, Xing R, Sutar RS, Nagappan S, Liu S (2020) Recent advances in durability of superhydrophobic self-cleaning technology: a critical review. *Progress Organic Coat* 138:105381
58. Ponnamma D, Guo Q, Krupa I, Al-Maadeed MAS, Varughese KT, Thomas S, Sadasivuni KK (2015) Graphene and graphitic derivative filled polymer composites as potential sensors. *Phys Chem Chem Phys* 17(6):3954–3981
59. Sadasivuni KK, Saha P, Adhikari J, Deshmukh K, Ahamed MB, Cabibihan JJ (2020) Recent advances in mechanical properties of biopolymer composites: a review. *Polym Compos* 41(1):32–59
60. Ponnamma D, Sadasivuni KK, Grohens Y, Guo Q, Thomas S (2014) Carbon nanotube based elastomer composites—an approach towards multifunctional materials. *J Mater Chem C* 2(40):8446–8485
61. Deshmukh K, Houkan MT, AlMaadeed MA, Sadasivuni KK (2020) Introduction to 3D and 4D printing technology: State of the art and recent trends. In: *3D and 4D printing of polymer nanocomposite materials*. Elsevier, pp 1–24
62. Sadasivuni KK, Ponnamma D, Rajan M, Ahmed B, Al-Maadeed MAS (eds) (2019) *Polymer nanocomposites in biomedical engineering*. Springer, Berlin
63. Sadasivuni KK, Cabibihan JJ, Deshmukh K, Goutham S, Abubasha MK, Gogoi JP, Rao KV (2019) A review on porous polymer composite materials for multifunctional electronic applications. *Polym-Plast Technol Mater* 58(12):1253–1294
64. Agrawal S, Jamwal A, Gupta S (2020) Effect of COVID-19 on the Indian economy and supply chain. Preprints, 2020050148. <https://doi.org/10.20944/preprints202005.0148.v1>
65. Sinha MS, Bourgeois FT, Sorger PK (2020) Personal protective equipment for COVID-19: distributed fabrication and additive manufacturing. *Am J Public Health* 110(8):1162–1164
66. Srinivasan R, Mian A, Gockel J, Luehrmann LM (2020) Additive manufacturing and how 3D printing is fighting COVID-19. Shelter-in-Place (SiP) Lecture Series. <https://corescholar.libraries.wright.edu/mme/487>
67. Arora PK, Arora R, Haleem A, Kumar H (2021) Application of additive manufacturing in challenges posed by COVID-19. *Mater Today: Proc* 38(1):466-468
68. Manero A, Smith P, Koontz A, Dombrowski M, Sparkman J, Courbin D, Chi A (2020) Leveraging 3D printing capacity in times of crisis: recommendations for COVID-19 distributed manufacturing for medical equipment rapid response. *Int J Environ Res Public Health* 17(13):4634

69. Kumar YR, Deshmukh K, Sadasivuni KK, Pasha SK (2020) Graphene quantum dot based materials for sensing, bio-imaging and energy storage applications: a review. *RSC Adv* 10(40):23861–23898
70. Ponnamma D, Chirayil CJ, Sadasivuni KK, Somasekharan L, Yaragalla S, Abraham J, Thomas S (2013) Special purpose elastomers: synthesis, structure-property relationship, compounding, processing and applications. In *Advances in elastomers I*. Springer, Berlin, pp 47–82

Correction to: Characterization Techniques for Shape-Memory Alloys



Praveen K. Jain, Neha Sharma, Rishi Vyas, and Shubhi Jain

Correction to:

Chapter 2 in: M. R. Maurya et al. (eds.), *Shape Memory Composites Based on Polymers and Metals for 4D Printing*, https://doi.org/10.1007/978-3-030-94114-7_2

In the original version of the book, Few lines are missed to insert in Introduction section.

Missing lines have been updated in the “Chapter 2, Characterization Techniques for Shape-Memory Alloys”.

The chapter and book have been updated with the changes.

The updated version of this chapter can be found at https://doi.org/10.1007/978-3-030-94114-7_2